The Pennsylvania State University

The Graduate School

College of Engineering

DEVELOPMENT OF UNCERTAINTY METHODOLOGY FOR COBRA-TF VOID DISTRIBUTION AND CRITICAL POWER PREDICTIONS

A Dissertation in

Nuclear Engineering

by

Fatih Aydogan

Submitted in Partial Fulfillment
of the Requirements
for the Degree of

Doctor of Philosophy

May 2008

The dissertation of Fatih Aydogan was reviewed and approved* by the following:

Lawrence Hochreiter
Professor of Nuclear Engineering
Dissertation Advisor
Co-chair of Committee

Kostadin Ivanov
Professor of Nuclear Engineering
Co-chair of Committee

John Mahaffy
Professor of Nuclear Engineering

Turgay Ertekin
Professor of Petroleum & Natural Gas Engineering

Kurshad Muftuoglu
Principal Engineer
GE-Hitachi Nuclear Energy Americas Company
Wilmington, NC
Special Member

Jack Brenizer
Professor of Nuclear Engineering
Head of the Department of Nuclear Engineering

*Signatures are on file in the Graduate School

ABSTRACT

Thermal hydraulic codes are commonly used tools in licensing processes for the evaluation of various thermal hydraulic scenarios. The uncertainty of a thermal hydraulic code prediction is calculated with uncertainty analyses. The objective of all the uncertainty analysis is to determine how well a code predicts with corresponding uncertainties. If a code has a big output uncertainty, this code needs further development and/or model improvements. If a code has a small uncertainty, this code needs maintenance program in order to keep this small output uncertainty. Uncertainty analysis also indicates the more validation data is needed.

Uncertainty analyses for the BWR nominal steady state and transient scenarios are necessary in order to develop and improve the two phase flow models in the thermal hydraulic codes. Because void distribution is the key factor in order to determine the flow regime and heat transfer regime of the flow and critical power is an important factor for the safety margin, both steady state void distribution and critical power predictions are important features of a code. An uncertainty analysis for these two phenomena/cases provides valuable results. These results can be used for the development of the thermal hydraulic codes that are used for designing a BWR bundle or for licensing procedures.

This dissertation includes the development of a particular uncertainty methodology for the steady state void distribution and critical power predictions. In this methodology, the PIRT element of CSAU was used to eliminate the low ranked uncertainty parameters. The SPDF element of GRS was utilized to make the uncertainty methodology flexible for the assignment of PDFs to the uncertainty parameters. The developed methodology includes the uncertainty comparison methods to assess the code precision with the sample-averaged bias, to assess the code spreading with the sample-averaged standard deviation and to assess the code reliability with the proportion of specimens among the sample with a bias lower than the experimental uncertainty. Besides, the rankings of dominant phenomena are observed with the second comparison method (sensitivity

analysis). Simple Random Sampling, Order Statistics, Richardson Extrapolation are some of the methods that are in the developed methodology. This uncertainty methodology was implemented for the COBRA-TF predictions. The uncertainty and sensitivity results are presented in the dissertation.

TABLE OF CONTENTS

LIST OF FIGURES

LIST OF TABLES

ACKNOWLEDGEMENTS

This is very hard to remember all the people that have helped me to achieve this success. If your name is not listed, be sure that that my gratitude is not less than for those listed below. At the beginning of this section, I need to say that I am very appreciative to our Creator for everything I have achieved so far. I hope he continues to help me all the time and blesses me through all my life.

First, I would like to thank my advisor, Dr. Lawrence Hochreiter for everything that he has done for me. I could not have found a better advisor and guru for my graduate study. His interest on my research for providing high-quality work has made a deep impression on me. I owe him lots of gratitude for having me shown this way of research. He taught me to trust myself. He could not even realize how much experience I have earned with him and I am sure I will keep learning from him. Besides of being an excellent supervisor, Larry was as close like a big brother to me and more importantly such a good close friend that a person can hardly find.

I am very thankful to Dr. Kostadin Ivanov, for the guidance and support he has provided throughout the course of this work. Today I would not graduate without his help and encouragement. Thanks for never giving up on me. I will do my best to improve my skills that he made me realize.

I would like to thank my thesis committee, Dr. John Mahaffy, Dr. Turgay Ertekin and Dr. Kurshad Muftuoglu for their sincere efforts to guide me through all these years. I need to express my sincere thanks to Dr. Kurshad Muftuoglu for his help during my internship in Westinghouse Electric Company and for his help to develop uncertainty methodology and to implement the methodology. I am thankful to Dr. John Mahaffy for his thoughtful guidance. I am grateful to Dr. Ertekin for his help and guidance. I would like to thank the United States Nuclear Regulatory Commission (US-NRC) for their financial support during my PhD years.

Lots of people have helped me during the whole course of this study. Current and previous members of the Reactor Thermal-Hydraulics Group (Sule, Jeff, James, Douglas, Robert, all the others) and Reactor Dynamics and Fuel Management Group (Alim, Serkan, James, Maria, Boyan, Peter, Vuyani, Nadedja, Shadi, all the others), I believe as a privilege to work with you guys. I am very happy that I have come here to meet with you. To all my friends, Fatih, Zafer, Nuriddin, Isa, Elif, Armagan, Sinem, Danisman, Sacit, Nesrin, Ahmet, Caglan and all the others. I thank you guys for helping me get through the difficult times. To my sweetheart, Sena, you are my inspiration. My acknowledgement would not be completed without expressing my appreciation to your support, your help, your patience, and your encouragement. I would not have achieved this much in a year without you,.

I am forever indebted to my parents, Ismet and Mukadder Aydogan for their love. Words are not enough to express my feelings to you. You have been always with me and I know you will be till the end of time. It is the God's biggest gift to me for having such a wonderful parents like you. Thank you for all the things that you have done for me. I would thanks also to my brother, Ramazan Aydogan, to my sisters Ayse Togay and Nurgul Aydogan for their support. Finally I would like grateful to my Grandmother, Munise Sakar and Grandfather Fikri Sakar. I know you are watching me up there. I will never ever let you down. Rest in Peace.

Chapter 1

INTRODUCTION

Thermal hydraulic codes are commonly used tools in licensing processes for the evaluation of various thermal hydraulic scenarios. The results of code predictions are generally subjected to some uncertainties. The reasons of these uncertainties are generally given as [1]:

- model limitations;
- approximations in the numerical solution;
- nodalization;
- homogenization approaches;
- imperfect knowledge of boundary and initial conditions.

The uncertainties of the thermal hydraulic code predictions are evaluated using an uncertainty analysis method. Two types of uncertainty analyses are generally defined in the literature. The first uncertainty analysis [2] is defined as the difference between the code prediction and measurement. This analysis provides bias information. The second uncertainty analysis is defined as the code prediction uncertainty according to measurement uncertainties [3]. The uncertainties of the model parameters are sometimes accounted in addition to measurement uncertainties. The objective of all these uncertainty analyses is to determine how well a code predicts with corresponding uncertainties. If a code has a big output uncertainty, this code needs further development and/or model improvements and may give unreliable predictions but the code predictions are reliable. If a code has a small uncertainty, this code needs maintenance program in order to keep this small output uncertainty. Uncertainty analysis also identifies where more validation data is needed.

Wickett and Yadigaroglu [4] provided three reasons about the need of uncertainty analysis for the thermal hydraulic codes. These reasons are briefly given as,

1. Licensing and safety
    - The objective is to move from licensing based on conservative evaluation models to the use of "best estimate" calculations with uncertainty estimates. This was the prime motivation for development of uncertainty analysis methods. Besides, uncertainty analysis allows more realistic estimates of the safety margins of nuclear power plants.
2. Accident management
    - Uncertainty analysis makes it clear where more information is needed to define improved Emergency Response Guidelines (ERGs).
3. Research prioritization
    - Uncertainty analysis could help identifying correlations and code models that need the most improvement and development.
    - It can also identify areas where more data are needed.
    - It could make the code development and validation more cost-effective.
    - It helps to evaluate and to improve the quality of a computer code.

- It can be used to define the point at which a code has been sufficiently developed.
- It can also be used to identify whether new versions of the codes are real improvements or not.

Because of the reasons given above, in uncertainty analysis of a thermal hydraulic code is one of the essential steps that have to be done to evaluate the code for different types of problems/scenarios. Thus, various uncertainty analyses have been applied to different thermal hydraulic codes.

Especially in the last decade, various uncertainty analysis methods have been applied to a range of thermal hydraulic codes for specific thermal hydraulic scenarios. For example,

- Westinghouse automated statistical treatment of uncertainty methodology on AP1000 best estimate large break LOCA [5]
- AREVA's realistic large break LOCA analysis methodology [6]
- Uncertainty and sensitivity analyses of the Kozloduy pump trip test using coupled thermal–hydraulic 3D kinetics code [1].

Most of the uncertainty analyses are based on Loss of Coolant Accident (LOCA) scenarios in order to determine the performance of the Emergency Core Cooling Systems (ECCS) according to the Nuclear Regulatory Commission (NRC) Regulatory Guide

1.157 [7]. In addition to the LOCA scenario, other scenarios which include commonly operated commercial nuclear power plants help also to evaluate the code’s performance.

The majority of the constructed commercial nuclear power plants in the world are either Pressurized Water Reactor (PWR) or Boiling Water Reactor (BWR) type. Although PWR consists of single phase flow in the reactor, Boiling Water Reactor includes two phase flow. Because of two phase flow, a BWR has more flow regimes in its reactor than a PWR has. The models for two phase flow in the thermal hydraulic codes still need development and improvement in order to predict the two phase flow behavior accurately. Thus, to predict the flow behavior of two phase flow is much more difficult than the flow behavior of single phase flow. In other words, uncertainty analyses of the BWR steady state nominal and transient condition scenarios are necessary in order to develop and improve the two phase flow models in the thermal hydraulic codes. Two important cases for a BWR cases are the steady state void distribution in the BWR bundle, which affects the reactor power distributions, and steady state critical power predictions, which affect the BWR thermal limit:

- Void distribution or void fraction inside the BWR bundle is the key factor in order to determine the flow regime and heat transfer regime of the flow as well as the reactor power distribution. A code has to predict void distribution accurately in order to predict the flow and heat transfer regimes correctly.

- Critical power is the power that demonstrates the dry-out occurrence of the liquid film on the heated rod. Thus, critical power is an important factor for determining the safety margin and determining the plant thermal limits.

Both steady state void distribution and critical power predictions are important features for a code. Thus, an uncertainty analysis for these predictions will provide valuable results. These results can be used for the development of the thermal hydraulic codes that are used for designing a BWR bundle or for a licensing procedure of a best-estimate subchannel code.

This dissertation focuses on the uncertainty analysis on the void distribution and critical power predictions of one of the commonly used thermal hydraulic codes, COBRA-TF [8, 9]. COBRA-TF (COolant Boiling in Rod Arrays-Two Fluid) code is a sub-channel analysis code and NRC accepts COBRA-TF as a licensed code to be used for the safety analyses. The COBRA-TF (3D Module) is based on a two-fluid, three field representation of two phase flow. The three fields are a vapor field, a continuous liquid field, and an entrained liquid drop field. COBRA-TF is a verified and validated code so that an uncertainty analysis can be performed by using this code. COBRA-TF can predict the void distribution and critical power, dry-out locations. In order to determine the uncertainty of the void distribution and critical power, a detailed study is needed using a detailed void distribution and critical power database, such as, the Nuclear Power

Engineering Cooperation (NUPEC) BWR Full-Size Fine-Mesh Bundle Test (BFBT) [10] database.

The NUPEC BFBT [10] database provides detailed full size fine mesh bundle test data for BWR. Part of this BFBT [10] database has been made available for the international benchmark activity entitled as the Organisation for Economic Co-operation and Development (OECD)/NRC BWR BFBT [10]. This international project is officially approved by the Japan Ministry of Economy, Trade, and Industry (METI), NRC, and endorsed by the OECD/NEA. The BFBT test facility is able to simulate the high-pressure, high temperature fluid conditions found in BWRs. The test facility has the capability for a full range of steady-state testing over BWR operating conditions. Because two types of void distribution measurement equipments were employed (an X-ray CT scanner and an X-ray densitometer) in BFBT facility, the BFBT database provides detailed void distribution database. Also, the thermocouples were located at three elevations to measure detailed critical power and dry-out locations.

This dissertation will develop a methodology to evaluate the uncertainties of the COBRA-TF void distribution and critical power predictions using the NUPEC BWR BFBT benchmark database. The main contributions and uniqueness of the dissertation are given as,

- The development and analysis of the uncertainty predictions of the void distributions are based on subchannels as well as the bundle,

- The development and analysis of the uncertainty predictions of the critical power and dry-out elevation,
- The developed and implemented uncertainty analyses methodology includes the assessment of the uncertainties with the detailed BFBT void distribution and critical power database from the NUPEC Benchmark Program. These databases are used for the comparisons.
- The uncertainty analyses are applied to COBRA-TF, a well-established best-estimate subchannel code.

Since uncertainty analysis accounts for COBRA-TF model uncertainties in addition to boundary condition uncertainties, Chapter 2 describes COBRA-TF models as well as the conservation equations. Besides, this chapter provides the main conservation equations' assumptions that were used for the derivation of them.

Chapter 3 includes the literature review of the uncertainty methods. These methods were classified. Because sampling uncertainty methodology among classified methods is more commonly used in the nuclear field, some applications of sampling uncertainty methodology were also described.

Because experimental database was used in the uncertainty comparison methods, the selected experimental database (OECD/NRC BFBT) was described in Chapter 4. This chapter describes the test facility, BWR bundle, experimental database and measurement methods.

Chapter 5 describes the developed uncertainty methodology for the particular cases (steady state void distribution and critical power for BWR). This methodology utilizes some elements from GRS and CSAU (described in Chapter 3). Besides, some new elements were added to this methodology.

The implementation of the uncertainty methodology to the steady state void distribution and critical power was described in Chapter 6. This chapter includes comparison results. First of them is the uncertainty comparison results. Uncertainty results provide the average prediction, average bias, maximum bias, standard deviation and coverage ratio information. Second one is the sensitivity results. Sensitivity results are the comparison between prediction results due to phenomenon change and nominal prediction results. Sensitivity provides which phenomena are the dominant ones and their rankings.

1.1. References

1. Salah, A. B. et. al., 2006, Uncertainty and sensitivity analyses of the Kozloduy pump trip test using coupled thermal–hydraulic 3D kinetics code, Nuclear Engineering and Design 236 1240–1255

2. Duke Power Company, 1996, Duke Power Company Thermal-Hydraulic Statistical Core Design Methodology, BWU-Z CHF Correlation

3. Wickett, T. , et al., 1998, Report of the uncertainty methods study for advanced best estimate thermal hydraulic code applications, NEA/CSNI/R(97)35

4. Wickett, A.J., Yadigaroglu, G., 1994, Report of a CSNI workshop on uncertainty analysis methods, NEA/CSNI/R(1994)20/VOL1

5. Frepoli, C. et. al., 2005, AP1000 Best estimate large break LOCA analysis performed with the Westinghouse Automated statistical treatment of uncertainty method (ASTRUM), ICONE13-50115, Beijing, China

6. Martin, R. P. and O'Dell, L. D., 2005, AREVA's realistic large break LOCA analysis methodology," Nuclear Engineering and Design 235 1713–1725

7. U.S. Nuclear Regulatory Commission, Regulatory Guide 1.157 (Task RS 701-4), Best Estimate Calculations of Emergency Core Cooling Performance

8. Analysis of FLECHT-SEASET 163-Rod Blocked Bundle Data Using COBRA-TF, NRC/EPRI/ Westinghouse Report No:15, NUREG/CR-4166 EPRI NP-4111 WCAP-10375

9. COBRA/TRAC - A Thermal-Hydraulics Code for Transient Analysis of Nuclear Reactor Vessels and Primary Coolant Systems, NUREG/CR-3046 PNL-4385 Vol.1

10. Neykov, B., Aydogan, F., Hochreiter, L., Ivanov, K., Utsuno, H., Fumio, K., Sartori , E., Martin, M., 2005, NUPEC BWR Full-Size Fine-Mesh Bundle Test (BFBT) Benchmark *Volume I: Specifications,* NEA/NSC/DOC(2005)5

Chapter 2

COBRA-TF (RBHT)

This chapter provides the conservation equations and models of COBRA-TF [1, 2]. In order to provide best estimate thermal hydraulic analysis of a light water reactor (LWR) for design basis accidents and probable transients, Pacific Northwest Laboratory developed the COBRA-TF computer code [3]. COBRA-TF represents a two-fluid, three-field (continuous liquid, continuous vapor and entrained liquid drop) representation of two-phase flow [4].

For heat transfer from and within the solid structures in contact with the fluid, a finite-difference and semi-implicit numerical technique on an Eulerian mesh is used to solve conservation equations for each of the three fields.

2.1 Conservation Equations for the Three-Field Model of Two-Phase Flow

Two phase flows consist of two fluids which are separated by moving phase interfaces. Material properties are not changed continuously across these interfaces. For each phase, a separate set of conservation equations and constitutive relations are used. Interaction equations are used to connect each phase's equations.

Two fluid phasic conservation equations are given in Equation 2.1 - 2.3 for conservation of mass, momentum and energy respectively. The assumptions that are used for the phasic conservation equations are listed as:

- Volumetric heat generation in the fluid is neglected
- Radiation heat transfer is limited to
    - rod to drop

  - rod to steam

- In all phases, the pressure is the same
- Gravity is the only body force
- In the enthalpy formulation of the energy equation, the viscous dissipation is neglected

Conservation of Mass

$$\frac{\partial}{\partial t}(\alpha_k \rho_k) + \nabla(\alpha_k \rho_k \underline{\mathrm{U}}_k) = \Gamma_k \tag{2.1}$$

Rate of change mass + Rate of mass efflux = Rate of mass transfer to phase k from the other phases

Conservation of Momentum

$$\frac{\partial}{\partial t}(\alpha_k \rho_k \underline{\mathrm{U}}_k) + \nabla(\alpha_k \rho_k \underline{\mathrm{U}}_k \underline{\mathrm{U}}_k) = \alpha_k \rho_k \underline{g} - \alpha_k \nabla \mathrm{P}$$

$$+ \nabla\left[\alpha_k (\underline{\underline{\tau}}_k + \underline{\underline{\mathrm{T}}}_k^{\mathrm{T}})\right] + \underline{\mathrm{M}}_k^{\Gamma} + \underline{\mathrm{M}}_k^{d} \tag{2.2}$$

Rate of change of momentum + Rate of efflux of momentum = Gravity force + Pressure gradient force

+ Viscous and turbulent forces + Momentum exchange due to mass transfer to phase k + Interfacial drag force

Conservation of Energy

$$\frac{\partial}{\partial t}(\alpha_k \rho_k h_k) + \nabla(\alpha_k \rho_k h_k \underline{\mathrm{U}}_k) = -\nabla\left[\alpha_k (\underline{0}_k + \underline{q}_k^{\mathrm{T}})\right] + \Gamma_k h_k^i + q_{\mathrm{I}_k}^{"} + \alpha_k \frac{\partial \rho}{\partial t} \tag{2.3}$$

	Rate of change of enthalpy	+	Rate of efflux of enthalpy	=	Conduction and turbulent heat flux
+	Energy exchange due to mass transfer to phase k	+	Interfacial heat transfer	+	Pressure work

The definitions of Table 2.1 have been used in this chapter.

Table 2.1. The Definitions of the Parameters Used in Conservation Equations

Parameter	**Explanation**
α_k	Average k-phase void fraction
ρ_k	Average k-phase density
$\underline{U}_k$	Average k-phase velocity
Γ_k	Average rate of mass transfer to phase k from the other phases
$\underline{g}$	Acceleration of gravity
P	Average pressure
$\underline{\underline{\tau}}_k$	Average k-phase viscous stress tensor (stress deviator)
$\underline{\underline{T}}_k$	k-phase turbulent (Reynolds) stress tensor
$\underline{\underline{M}}_k^{\Gamma}$	Average supply of momentum to phase k due to mass transfer to phase k
$\underline{M}_k^{d}$	Average drag force on phase k by the other phases
h_k	Average k-phase enthalpy
$\underline{Q}_k$	Average k-phase conduction vector
$\underline{q}_k^{T}$	k-phase turbulent heat flux
h_k^{i}	Surface average enthalpy of phase k
Pw	Wetted perimeter
σ	Surface tension
v	Vapor
l	Continuous liquid
e	Entrained liquid
Γ'''	Average rate of vapor generation per unit volume
η	the fraction of the total vapor generation coming from the entrained liquid
S'''	Average net rate of entrainment per unit volume
$\underline{\tau}'''_{I_{vy}}$	Average drag force per unit volume by the vapor on y phase
$\underline{\tau}'''_{I_{wy}}$	The force exerted by the wall on phase y
$\underline{\underline{\sigma}}_y$	The fluid-fluid viscous stress tensor for phase y
Q'''_{wy}	The wall heat transfer rates per unit volume to the phase y
$\underline{q}_y$	The fluid-fluid conduction vector for the phase y

Table 2.1. The Definitions of the Parameters Used in Conservation Equations (Cont.)

$\underline{M}^d$	Interfacial momentum exchange
$\underline{M}^\Gamma$	The momentum exchange due to mass transfer
q'''_{I_k}	Interfacial heat transfer for phase k
A'''_I	The average interfacial area per unit volume
H	The surface heat transfer coefficient
K_I	The interfacial friction coefficients
S	The net mass entrainment rate
k_σ	The mass transfer coefficient
NB	Nucleate boiling
FC	Forced convection

COBRA-TF uses three continuity equations, three momentum equations, and two energy equations in the three-field formulation. The reason of the usage of a single energy equation for the combined continuous liquid and liquid droplet fields is both fields are assumed to be at the same temperature.

The three-field models are used the following assumptions to derive from Equation 2.1 through 2.3:

1. Within the entrained phase, the turbulent stresses and turbulent heat flux are neglected.
2. The viscous stresses have two components (wall shear and fluid-fluid shear). In the entrained liquid phase, the fluid-fluid shear is neglected.
3. The conduction heat flux term has two components (wall term and a fluid to fluid conduction). The fluid-fluid conduction term is neglected in the entrained liquid.
4. All mass entering or leaving a phase interface is at saturation.

After applying all these assumptions and required substitutions, the three-field conservation for COBRA-TF are:

Conservation of Mass (3 equations)

$$\frac{\partial}{\partial t}(\alpha_V \rho_V) + \nabla(\alpha_V \rho_V \underline{U}_V) = \Gamma'''$$
$$\frac{\partial}{\partial t}(\alpha_\ell \rho_\ell) + \nabla(\alpha_\ell \rho_\ell \underline{U}_\ell) = -\Gamma_\ell''' - S''' \tag{2.4}$$
$$\frac{\partial}{\partial t}(\alpha_e \rho_\ell) + \nabla(\alpha_e \rho_\ell \underline{U}_e) = -\Gamma_e''' + S'''$$

Conservation of Momentum (3 equations)

$$\frac{\partial}{\partial t}(\alpha_v \rho_v \underline{U}_v) + \nabla(\alpha_v \rho_v \underline{U}_v \underline{U}_v) = -\alpha_v \nabla \mathrm{P} + \alpha_v \rho_v \underline{g}$$
$$+ \nabla\left[\alpha_v(\underline{\underline{\sigma}}_v + \underline{\underline{T}}_v^T \alpha_\ell\right] + \underline{\tau}_{wv}''' - \underline{\tau}\mathrm{I}_{ve}''' + (\Gamma'''\underline{U})$$
$$\frac{\partial}{\partial t}(\alpha_\ell \rho_\ell \underline{U}_\ell) + \nabla(\alpha_\ell \rho_\ell \underline{U}_\ell \underline{U}_\ell) = -\alpha_\ell \nabla P + \alpha_\ell \rho_\ell \underline{g} \tag{2.5}$$
$$+ \nabla[\alpha_\ell(\underline{\underline{\sigma}}_\ell + \underline{\underline{T}}_\ell^T)] + \underline{\tau}_{ve}''' - (\Gamma_\ell'''\underline{U}) - (S'''\underline{U})$$
$$\frac{\partial}{\partial t}(\alpha_e \rho_\ell \underline{U}_e) + \nabla(\alpha_e \rho_\ell \underline{U}_e \underline{U}_e) = -\alpha_e \nabla P + \alpha_e \rho_\ell \underline{g} + \underline{\tau}_{we}''' + \underline{\tau}\mathrm{I}_{ve}'''$$
$$-(\Gamma_e'''\underline{U}) + (S'''\underline{U})$$

Conservation of Energy (2 equations)

$$\frac{\partial}{\partial t}(\alpha_v \rho_v h_v) + \nabla(\alpha_v \rho_v h_v \underline{U}_v) = -\nabla[\alpha_v(\underline{q}_v + \underline{q}_v^T)] + \Gamma''' h_g + q_{\mathrm{I}\,v}''' + Q_{wv}''' + \alpha_v \frac{\partial \rho}{\partial t}$$

$$\frac{\partial}{\partial t}[(\alpha_\ell + \alpha_e)\rho_\ell h_\ell] + \nabla(\alpha_\ell \rho_\ell h_\ell \underline{U}_\ell) + \nabla(\alpha_e \rho_\ell h_\ell \underline{U}_e)$$
$$= -\nabla[\alpha_\ell(\underline{q}_\ell + \underline{q}_\ell^T)] - \Gamma''' h_f + q_{\mathrm{I}}''' + Q_{w\ell}''' + (\alpha_\ell + \alpha_e)\frac{\partial \rho}{\partial t} \tag{2.6}$$

For each computational cell structure, the flow regime is defined from the properties and flow conditions. Normal flow regime is given in this section because of dissertation scope. Figure 2.1 and 2.2 demonstrate the normal two phase flow regime and corresponding map respectively.

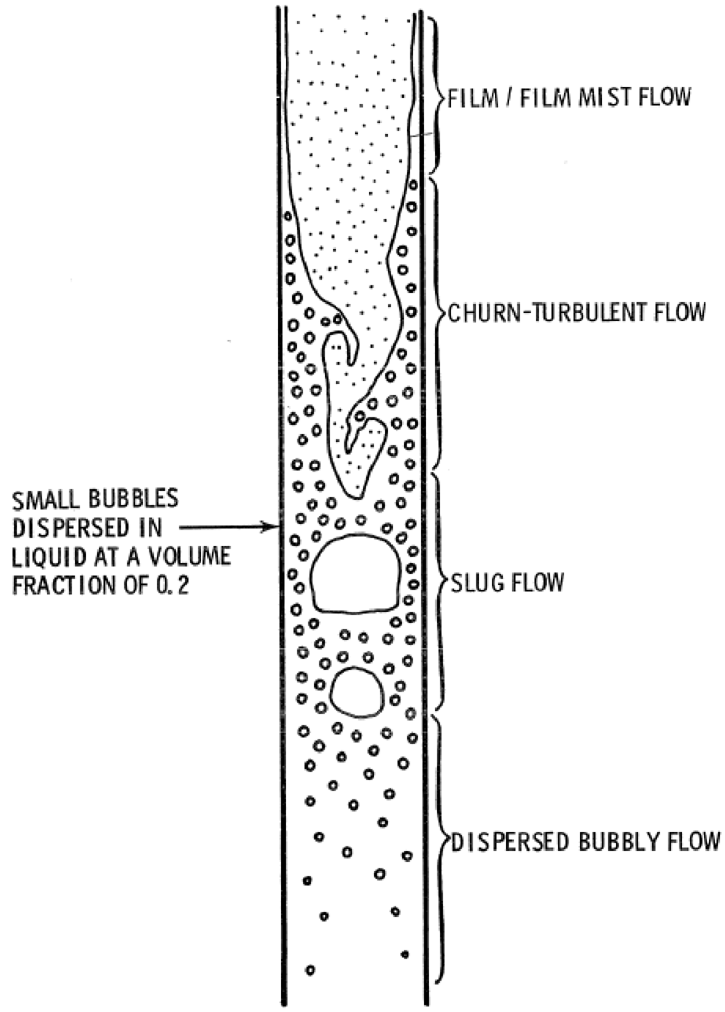

Figure 2.1. Normal Two Phase Flow Regimes

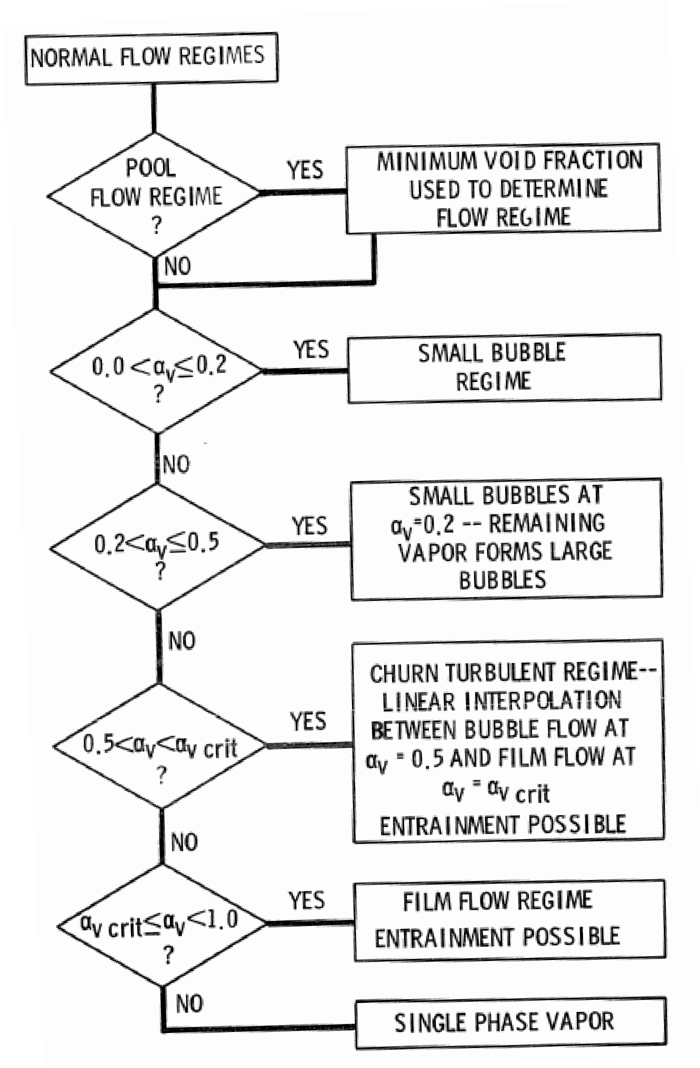

Figure 2.2. Normal Flow Regime Selection Logic

2.2 Physical Models

Closure of the conservation equations need physical models for the models:

- the mass exchange among the three fields at the phase interfaces,
- the exchange of momentum at the interfaces,
- the drag forces at solid boundaries,

- the viscous stress,
- turbulence terms in the continuous fields,
- the entrainment rate.

Interfacial Mass Transfer

The model for interfacial mass transfer is given as,

$$\Gamma''' = \frac{-q_{\mathrm{I}}^{M'}{}_{\ell} - q_{\mathrm{I}}^{M'}{}_{v}}{h_{fg}} \tag{2.7}$$

where

$$q'''_{\mathrm{I}_k} = HA'''_{\mathrm{I}}(T_s - T_k) \tag{2.8}$$

The vapor generation has four components:

1. Superheated liquid (SHL)
2. Subcooled liquid (SCL)
3. Superheated vapor (SHV)
4. Subcooled vapor (SCV)

Table 2.2 and Table 2.3 demonstrate interfacial heat transfer correlations for the various flow regimes.

Table 2.2. Interfacial Heat Transfer Coefficients

Mode of Heat Transfer	Correlation (Btu/hr-ft^2-F)	Flow Regime
H_{SHV}	1.0×10^4	Bubble
	$(2.0+0.74\,\mathrm{Re}_v^{0.5}\,\mathrm{Pr}_v^{1/3})\dfrac{k_v}{D_H}$	Large bubble
	$\dfrac{f_I}{2}\rho_v C_{\rho_v}\lvert\underline{\cup}_{v\ell}\rvert \mathrm{Pr}_v^{-2/3}$	Film
	$(2.0+0.74\,\mathrm{Re}_d^{0.5}\,\mathrm{Pr}_v^{1/3})\dfrac{k_v}{2r_d}$	Drop
	$(2.0+0.74\,\mathrm{Re}_v^{0.5}\,\mathrm{Pr}_v^{1/3})\dfrac{k_v}{D_H}$	Liquid chunk, inverted annular
H_{SCV}	1.0×10^4	All regimes
H_{SHL}	$\dfrac{1}{\sqrt{x}}\left(\dfrac{k_\ell\lvert\underline{\cup}_{v\ell}\rvert}{r_b}\rho_\ell C_{p\ell}\right)^{1/2}$	Bubble
	1.0×10^5	Large bubble, liquid chunk and inverted annular
	$1.925\rho_\ell C_{\rho_\ell}\lvert\underline{\cup}_\ell\rvert/(\mathrm{Re}_f^{2/3}\,\mathrm{Pr}_\ell^{2/3}$ $for\,\mathrm{Re}_f < 1000$ $0.2701\rho_\ell C_{\rho_\ell}\lvert\underline{\cup}_\ell\rvert/(\mathrm{Re}_f^{0.38}\,\mathrm{Pr}_\ell^{2/3}$ $for 1000 \le \mathrm{Re}_f$ *and* $2.Ok_\ell/\sigma$	Film
	$C\dfrac{\pi^2}{3}\dfrac{k_\ell}{r_A}(C=2.7)$	Drop

Table 2.3. Interfacial Heat Transfer Area Per Unit Volume

Mode of Heat Transfer	Correlation (Btu/hr-ft^2-F)	Flow Regime
H_{SCL}	$\frac{1}{\sqrt{\pi}}\left(\frac{k_\ell \lvert \underline{\cup}_{v\ell} \rvert}{r_b}\sigma_\ell C_{\rho_\ell}\right)^{1/2}$	Bubble, large bubble
	$1.925\rho_\ell C_{\rho_\ell} \lvert \cup_\ell \rvert /(\mathrm{Re}_f^{2/3}\ \mathrm{Pr}_\ell^{2/3}$ *for* $\mathrm{Re}_f < 1000$ $0.2701\rho_\ell C_{\rho_\ell} \lvert \cup_\ell \rvert /(\mathrm{Re}_f^{0.38}\ \mathrm{Pr}_\ell^{2/3}$ *for* $1000 \le \mathrm{Re}_f$	Film
	$C\frac{\pi^2}{3}\frac{k_\ell}{r_d}(C = 2.7)$	Drop, liquid chunk, inverted annular

where

$$
\begin{aligned}
\mathrm{Re}_v &= \frac{D_H \rho_v \lvert \underline{\cup}_{v\ell} \rvert}{\mu_v} \\
\mathrm{Re}_b &= \frac{2r_b \rho_\ell \lvert \underline{\cup}_{v\ell} \rvert}{\mu_{m_b}} \quad \mu_{m_b} = \mu_\ell (1-\alpha_v)^{-2.5}\frac{(\mu_v + 0.4\mu_\ell)}{(\mu_v + \mu_\ell)} \\
\mathrm{Re}_d &= \frac{2r_d \rho_v \lvert \underline{\cup}_{ve} \rvert}{\mu_{m_b}} \quad \mu_{m_b} = \mu_v \alpha_v \frac{-2.5(\mu_\ell + 0.4\mu_v)}{(\mu_v + \mu_\ell)} \\
\mathrm{Re}_f &= \frac{D_\mathrm{H} \rho_\ell \lvert \underline{\cup}_\ell \rvert}{\mu_\ell}
\end{aligned}
\tag{2.9}
$$

$$f_\mathrm{I} = 0.005(1 + 75\alpha_\ell) \tag{2.10}$$

Interfacial Drag Force

The average interfacial drag forces per unit volume for different phases are given in Equation 2.11 and 2.12.

$$\underline{\tau}\mathrm{I}_{v\ell}''' = \mathrm{K}_{\mathrm{I}_{v\ell}} \underline{\mathrm{U}}_{v\ell} \tag{2.11}$$

$$\underline{\tau}\mathrm{I}_{ve}''' = \mathrm{K}_{\mathrm{I}_{ve}} \underline{\mathrm{U}}_{ve} \tag{2.12}$$

The interfacial friction coefficients are defined for different flow regimes as given below:

$$\mathrm{K}_{\mathrm{I}_{v\ell}} = 0.375 \frac{C_{D_b}}{r_b} \alpha_v \rho_\ell \left| \underline{\mathrm{U}}_{v\ell} \right| \qquad \text{(for bubble flow regime)} \tag{2.13}$$

$$\mathrm{K}_{\mathrm{I}_{ve}} = 0.375 \frac{C_{D_d}}{r_d} \alpha_e \rho_\ell \left| \underline{\mathrm{U}}_{ve} \right| \qquad \text{(for drop flow regime)} \tag{2.14}$$

$$\mathrm{K}_{\mathrm{I}_{v\ell}} = 2.0 \frac{f_\mathrm{I}}{D_H} \sqrt{\alpha_v} \rho_v \left| \underline{\mathrm{U}}_{v\ell} \right| \qquad \text{(for film flow regime)} \tag{2.15}$$

$$\mathrm{K}_{\mathrm{I}_{v\ell}} = 2.0 \frac{f_\mathrm{I}}{D_H} \sqrt{\alpha_\ell} \rho_v \left| \underline{\mathrm{U}}_{v\ell} \right| \qquad \text{(for inverted annular flow regime)} \tag{2.16}$$

where

Drag coefficient on a bubble correlation of Ishii [5] is given by

$$C_{D_b} = \frac{24}{\mathrm{Re}_b}(1.0 + 0.1\,\mathrm{Re}_b^{0.75}) \tag{2.17}$$

$$\mathrm{Re}'_b = 2r_b\rho_\ell(1-\alpha_v)\left|\underline{\cup}_{v\ell}\right| / \mu_m \tag{2.18}$$

Equation 2.19 shows Wallis [6] interfacial friction factor.

$$f_\mathrm{I} = f_S\left\{1 + 1400F[1 - \exp(-\frac{1}{G}\frac{(1+1400F)^{3/2}}{13.2F}]\right\} \tag{2.19}$$

where

$$G = \frac{\rho_\ell g D_H}{\rho_v u_v^2 f_S}$$

$$F = \frac{m^+}{\mathrm{Re}_v^{0.9}}\frac{\mu_\ell}{\mu_v}\sqrt{\frac{\rho_v}{\rho\ell}} \tag{2.20}$$

$$m^+ = [(0.707\,\mathrm{Re}_\ell^{0.5})^{2.5} + (0.0379\,\mathrm{Re}_\ell^{0.9})^{2.5}]^{0.40} \tag{2.21}$$

$$f_S = 0.046\,\mathrm{Re}_v^{-0.20} \tag{2.22}$$

Drag coefficient of a droplet is same as the drag coefficient of a bubble except the Re_d. Re_d is defined as given in Equation 2.9.

Wall Drag Force

Equation 2.23 shows the single phase friction factor for phase k.

$$\left.\begin{array}{ll} f_k = 64/\mathrm{Re}_k & \text{for laminar} \\ f_k = \max(1.691/\mathrm{Re}_k^{-0.43},\ 0.117\,\mathrm{Re}_k^{-0.14}) & \text{for turbulent} \end{array}\right\} \quad (2.23)$$

Entrainment Rate

Entrainment rate (Equation 2.24) is defined as the net mass entrainment rate of liquid drops from the continuous liquid phase.

$$S_{\mathrm{E}} = (\alpha_\ell - \alpha_{\ell\, crit})\rho_\ell \left|\cup_\ell\right| \mathrm{A} \quad (2.24)$$

where

$$\alpha_{\ell\, crit} = (1 - \alpha_{v\, crit}) \quad (2.25)$$

$$\alpha_{v\, crit} = 1.0 - 4.0 C_1 \sigma / \rho_v \left|\underline{\cup}_v - \underline{\cup}_\ell\right|^2 D_{\mathrm{H}} \quad (2.26)$$

C_1: The constant containing the effects of wave shape and amplitude on the surface tension force a pressure force.

De-entrainment in Film Flow

De-entrainment in film flow is defined as the deposition of droplets on the liquid film. The drops so that droplets stick to the liquid film because of transverse velocity produced by the random turbulent motions. Equation 2.27 shows the Cousins [7] de-entrainment rate.

$$S_{DE} = k_\sigma \Delta C \mathrm{P}_W \Delta x \quad (2.27)$$

where

$$\Delta C = \frac{\alpha_e \rho_\ell}{\alpha_e + \alpha_v} \tag{2.28}$$

$$k_\sigma = \max\left\{3.0491\times10^{12}\sigma^{5.3054}, 12.491\sigma^{0.8968}\right\} \tag{2.29}$$

De-Entrainment on Grid Spacers

There are two assumptions about the de-entrainment on grid spacers:

1. If a droplet is on the projection of grid spacer, this droplet impinges on grid spacer and de-entrains.
2. The amount of de-entrainment is equal to the amount of entrainment.

Equation 2.30 shows the de-entrainment.

$$S_{DE} = 0.15\alpha_e \rho_\ell \left|\mathrm{U}_e\right| \mathrm{A} \tag{2.30}$$

Wall heat transfer coefficients

Wall heat transfer coefficient is defined in Equation 2.31.

$$\mathrm{H_w} = \max\left(0.23\frac{k_\ell}{D_H}\left(\frac{G_\ell D_H}{\mu_\ell}\right)^{0.8}(\mathrm{Pr}_\ell)^{0.4}, 7.86\frac{k_\ell}{D_H}\right) \tag{2.31}$$

Nucleate boiling

COBRA-TF uses CHEN heat transfer coefficient (Equation 2.32) [8].

$$\mathrm{H_{CHEN}} = \mathrm{H_{SPL}} + \mathrm{H_{NB}} \tag{2.32}$$

where

$$\mathrm{H}_{SPL} = 0.023F\left(\frac{k_f}{D_H}\right)\mathrm{Re}^{0.8}\,\mathrm{Pr}^{0.4} \tag{2.33}$$

where

S = suppression factor

Tw = wall surface temperature

Pw = saturation pressure corresponding to T_w

F=Reynolds number factor

Re=Reynolds number= $\frac{(1-\times)GD_H}{\mu_f}$ (2.34)

Pr=Prandtl number

$$F = \begin{cases} 1.0; x_{tt}^{-1} < 0.1 \\ 2.34(x_{tt}^{-1} + 0.213)^{0.736}; x_{tt}^{-1} > 0.1 \end{cases} \tag{2.35}$$

$$x_{tt}^{-1} = (\frac{x}{1-x})^{0.9} (\frac{\rho_f}{\rho_g})^{0.5} (\frac{\mu_g}{\mu_f})^{0.1} \tag{2.36}$$

$$S = \begin{Bmatrix} [1+0.12(\text{Re}'_{TP})^{1.14}]^{-1}; \text{Re}'_{TP} < 32.5 \\ [1+0.42(\text{Re}'_{TP})^{0.78}]^{-1}; 32.5 < \text{Re}'_{TP} < 50.9 \\ 0.1; \text{Re}'_{TP} > 50.9 \end{Bmatrix} \tag{2.37}$$

$$\text{Re}'_{TP} = (1 \times 10^{-4}) \text{Re}\, F^{1.25} \tag{2.38}$$

$$\text{H}_{NB} = 0.00122 S[\frac{k_f^{0.79} C_{\rho_f}^{0.45} \rho_f^{0.49} g_c^{0.25}}{\sigma^{0.5} \mu_f^{0.29} h_{fg}^{0.24} \rho_g^{0.24}}](T_w - T_f)^{0.24} (P_w - P)^{0.75} \tag{2.39}$$

Sub-cooled nucleate boiling

The Chen correlation [8] is used for the subcooled region.

$$q'' = q''_{FC} + q''_{NB} \tag{2.40}$$

$$q''_{NB} = \text{H}_{NB}(T_w - T_f) \tag{2.41}$$

$$q''_{FC} = 0.023(\frac{k_\ell}{D_H})\mathrm{Re}^{0.8}\,\mathrm{Pr}^{0.4}(T_w - T_\ell) \tag{2.42}$$

Turbulent Mixing

Mixing term produces energy and momentum transfer without inter-subchannel mass transfer. In the original COBRA-TF source code, the fluctuating cross flow between subchannels i and j for gap k has defined as given in Equation 2.43.

$$W_k^{'} = \beta.S_k.\overline{G}_{ij} \tag{2.43}$$

where

W'_k = fluctuating cross flow

β = mixing coefficient

S_k = intersubchannel gap width of gap k

= channel averaged mass flux

Rogers' [9] mixing Stanton number and non-dimensional mixing parameter are given in Equation 2.44 and 2.45 respectively.

$$M_{ij} = \frac{W'_{ij}}{G_i c} \tag{2.44}$$

$$\lambda_{ij} = \frac{2M_{ij}\,\mathrm{Re}_i^{1-m}}{\left[1+\left(\frac{d_{e_j}}{\partial_{e_i}}\right)^{\frac{3m}{2-n}}\right]\frac{d_{e_i}}{d}} = K'\frac{d}{2_{ij}} \tag{2.45}$$

where

c: clearance between elements

d: fuel element diameter

d_e: subchannel equivalent diameter

m: empirical exponent of Reynolds number

n: empirical exponent of Reynolds number in friction factor equation

w'_{ij}: mixing flow rate per unit length between subhcannels i and j

z_{ij}: “mixing distance” between subhcannels i and j

λ_{ij}: non-dimensional mixing parameter

Critical heat flux correlation

Critical heat flux correlation determines the power including the departure nucleate boiling or dry-out of liquid film. Biasi [10] correlation is defined as given below,

$$q''_{B1}=(5.9695x10^6)\ G^{-1/6}\ (F(P)\ G^{-1/6} - X)\ D_H^{-n} \qquad \text{(for low quality)} \tag{2.46}$$

$$q''_{B2}=(11.98x10^6)\ H(P)\ (1-X)\ D_H^{-n}\ G^{-1/6} \qquad \text{(for high quality)} \tag{2.47}$$

where

q”: Critical heat flux

G: Mass flux

D_H: Hydraulic diameter

x: Quality

n: 0.6 if $D_H < 1cm$: n: 0.4 if $D_H \geq 1cm$

$F(P) = 0.7249 + 0.099\ P\ \exp(-0.032\ P)$

$H(P) = -1.159 + 0.149\ P\ \exp(-0.019\ P) + 8.99\ P\ (10+P^2)^{-1}$

2.3. References

1. Wickett, T. , et al., 1998, Report of the uncertainty methods study for advanced best estimate thermal hydraulic code applications,” NEA/CSNI/R(97)35

2. A.J. Wickett, G. Yadigaroglu Agust, 1994, Report of a CSNI workshop on uncertainty analysis methods, NEA/CSNI/R(1994)20/VOL1

3. Analysis of FLECHT-SEASET 163-Rod Blocked Bundle Data Using COBRA-TF, NRC/EPRI/ Westinghouse Report No:15, NUREG/CR-4166 EPRI NP-4111 WCAP-10375

4. COBRA/TRAC- A Thermal-Hydraulics Code for Transient Analysis of Nuclear Reactor Vessels and Primary Coolant Systems, NUREG/CR-3046 PNL-4385 Vol.1

5. Ishii, M., Zuber, N., 1979, Drag Coefficient and relative velocity in bubbly, droplet or particulate flows, AIChE Journal, Vol 25, No. 5

6. Wallis, G. B., 1970, Annular two-phase flow, part-I: simple theory, Journal of Basic Engineering

7. Cousins, L. B. , Denton, W. H. and Hewitt, G. F., 1965, Liquid mass transfer in annular two phase flow, Paper C4 presented at the Symposium on two-phase flow volume 2, , p. 401-430

8. CHEN, J.C., 1966, Correlation for boiling heat transfer to saturated fluids in convective flow, I&EC Process Design and development, Vol 5 No. 3

9. Rogers, J.T. and Rosehart, R.G., 1972, Mixing by turbulent interchange in fuel bundles. Correlations and inferences, AIChE-ASME Heat Transfer Conference, 72-HT-53

10. Biasi, L.,et. al., 1967, Studies on burnout part 3. A new correlation for round ducts and uniform heating and its comparison with world data, Energia Nucleare, vol. 14. N.9.

Chapter 3

UNCERTAINTY ANALYSIS METHODS

A mathematical model is a series of equations, input factors, parameters, and variables that characterize the process being investigated. A model's input is subject to many sources of measurement and model uncertainty (because of measurement sensors' accuracy and absence of information and poor or partial understanding of the driving forces and mechanisms). Uncertainty and Sensitivity Analysis offer valid tools for characterizing the uncertainty associated with a model.

Uncertainty and Sensitivity Analysis can be used to determine:

1. The model resemblance with the process under study
2. The quality of model definition
3. Factors that mostly contribute to the output variability

Uncertainty is the estimation of scatter in a measurement or in a prediction [1, 2, 3]. If a model's output result propagates as a function of "uncertain" input parameters, propagation of uncertainty is the effect on the output results of the input uncertainties. In other words, uncertainty analysis quantifies the variation of the results for given uncertainty variation of input parameters. Mainly, the variables that have uncertainties due to measurement limitations (e.g. instrument precision) and model accuracy produces an output within an uncertainty bound.

Sensitivity analysis (SA) is the study of how the response of a model can quantitatively be apportioned to different sources of input variations [4, 5, 1]. Thus, sensitivity analysis is closely linked to uncertainty analysis (UA). Although sensitivity analysis just focuses on one uncertainty input's effect, uncertainty analysis focuses on the output's uncertainty by using all uncertainty inputs to observe the cross effects of them.

Verification and Validation are the assessment of accuracy and reliability of simulations [6, 7, 8, 9]. Oberkampf [9] separates verification into two groups:

1. **Code verification** is assessment of the reliability of the software coding.

2. **Solution verification** is assessment of the numerical accuracy of the computational model.

Validation is defined as physical modeling accuracy of a computational simulation by comparing with experimental data.

Briefly, **Verification** is the process of the set of mathematical equations has been correctly translated into computer code; **Validation** is the process of the selected code or calculation method is suitable for the specific analysis purpose by comparing experimental data [10].

Because verification and validation terms have elements similar to uncertainty and sensitivity analysis, it is possible to confuse verification and validation with the uncertainty analysis. This dissertation focuses on uncertainty analysis for void distribution and critical power, not verification and validation analyses.

Uncertainty and sensitivity analysis (UA and SA) can be performed by several possible procedures, such as, sampling methods, sensitivity testing, analytical methods, and computer algebra based methods [11]. In this chapter, these methods are briefly described with giving references.

3.1 Analytical Methods

Opposite of sampling methods, analytical uncertainty methods need to access to the original models. This method uses one of the given techniques to obtain uncertainty bounds:

1. Re-formulation of original model using stochastic algebraic differential equations

2. Differentiation of model equations and subsequent solution of a set of auxiliary sensitivity equations.

The analytical methods need accessing of the governing model equations. Because these methods may include writing additional computer codes for the solution of the auxiliary equations, application of this method may be impractical. Reformulating an existing computational model developed by others could require prohibitive amounts of resources for most of the uncertainty analysis applications. Therefore, this method is rarely applied in the nuclear industry.

Some of the analytical methods are listed as,

(a) Coupled and decoupled direct methods,

(b) Spectral based stochastic finite element method,

(c) Green's function method,

(d) Differential analysis methods.

3.1.a Coupled/Decoupled Direct Method

Coupled/Decoupled direct method (CDDM) uses the differentiation of the model equations and the sensitivity equations. In Coupled Direct Method, the sensitivity equations are then solved along with the original model equations [12]. In Decoupled Direct Method, the sensitivity equations and the model equations are solved together [12]. On the other hand, the sensitivity and model equations are solved separately in Decoupled Direct Method [13, 14].

The advantageous of decoupled method are the computational efficiency and stability of the solution.

3.1.b Spectral Based Stochastic Finite Element Method

Spectral Based Stochastic Finite Element Method uses stochastic processes representation including a series expansion. Galerkin's method or operator expansion is used for the solution of this method [15].

3.1.c Green's Function Method

Differentiating a model's equations provide the model's sensitivity equations in this model. These sensitivity equations and a series of Green's functions are solved. Although Green's function method decreases the number of equations to be solved [16, 17], decoupled method is more efficient method than Green's function method.

3.1.d Differential Analysis Methods

Neuman expansion [18, 19] or perturbation theory [18, 20] is used in Differential Analysis Method. Neuman expansion may not be applicable to every model because it uses inverse function of the model. The Perturbation Method uses small perturbations of the model parameters to observe the model output change. Perturbation has a limitation because of perturbations' smallness.

3.2 Computer Algebra Based Methods

This method manipulates the computer code and estimate the uncertainty and sensitivity of model outputs with respect to model inputs. Computer Algebra Based Methods do not need to access the model structure or the model equations. This method uses pattern algorithms to generate a derivative code by using the model code as a black box. For instance, Worley [21] and Bischof [22] defined ADGEN and ADIC software packages by using computer algebra method respectively.

3.3 Sensitivity Testing Methods

The sensitivity method is used to see the effect of one input's change on the predicted output. Measuring the robustness of the model is the target of sensitivity testing methods by testing if the model response changes significantly after changing the model parameters. Roselle [23], Sistla [24], Vieux [25] and Vanderperk [12] used this approach for different applications.

Even though these sensitivity methods give information regarding the change of the model or the parameters in the model, output uncertainty including cross-effects of all input uncertainty parameters cannot be obtained since calculations vary the input parameters one at a time.

3.4 Sampling Methods

One of the most common uncertainty analysis methods is sampling-based method because modifying the model equations is not required in sampling method model [26].

For the combination of factor values sampled with some probability distribution, uncertainty analysis is performed by executing the model repeatedly by using the combination of sampled values generated with probability distribution functions. The steps of the sampling methods are generally listed as,

1. Specify the target function (the function on which the uncertainty analysis will be applied),
2. Select the input of interest,
3. Appoint a probability distribution function (PDF) to the selected inputs,
4. Generate an input sampling matrix with that PDF(s),
5. Evaluate the model and compute the distribution of the target function,
6. Select and run a method in order to calculate the uncertainty bound.

Monte Carlo [27, 28], Latin Hypercube [29], Fourier Amplitude Sensitivity Test (FAST) [30] and Reliability Based Methods [31] are some of the sampling method techniques.

3.5. Uncertainty Analysis Methods in Nuclear Industry

General information and classifications of the uncertainty analysis methods have been provided above. In nuclear field, various uncertainty analysis methods have been developed to complement the code predictions through the quantification of the uncertainty margins, for instance, UMAE (Uncertainty Methodology based on Accuracy Extrapolation), AEAT (AEA Technology), CEA (Commissariat à L'énergie Atomique), GRS (Gesellschaft fur Anlagen-rUnd Reaktorsicherheit) and CSAU (Code Scaling Applicability and Uncertainty) methods [32, 33].

The uncertainty analysis elements of the CSAU and GRS were utilized to develop the uncertainty methodology used in this dissertation. These two methods were briefly described below:

3.5.1. CSAU (The Code Scaling, Applicability and Uncertainly) Methodology

US Nuclear Regulatory Commission developed the Code Scaling Applicability and Uncertainty methodology to quantify the uncertainty in a complex phenomenon [32, 33]. CSAU is one of the common sensitivity analysis methods and it includes the given features:

- **Scaling** is one of the uncertainty components. Because there is a scale difference between test facilities and a full scale nuclear power plant, this feature is used to account the uncertainty due to scaling.
- **Accident scenario** is defined at the beginning of the methodology so that

this method can be applied to a specific accident scenario.

- **Uncertainty evaluation** can be used to quantify the uncertainties of the calculated results.
- **Ranking** is performed in the phenomena identification and ranking table (PIRT). PIRT defines the important phenomena that affect the selected scenario. Then, the important phenomena are ranked based on having the most significant effect on the scenario. Therefore, CSAU just uses the important phenomena for the uncertainty evaluation.

The CSAU methodology (Figure 3.1) has 14 primary steps, which are grouped in 3 main key elements [32, 33]:

1. *Requirements and capabilities:* To determine the code's applicability to the particular scenario and to identify potential limitations, scenario modeling requirements are identified and compared against code capabilities in this element (from step 1 to 6).

2. *Assessment and Ranging of parameters:* Code capabilities to calculate important processes to the scenario are assessed in this element (from step7 to 10).

3. *Sensitivity and Uncertainty Analysis:* Uncertainty and sensitivity analysis is performed in this element (from step 11 to 14).

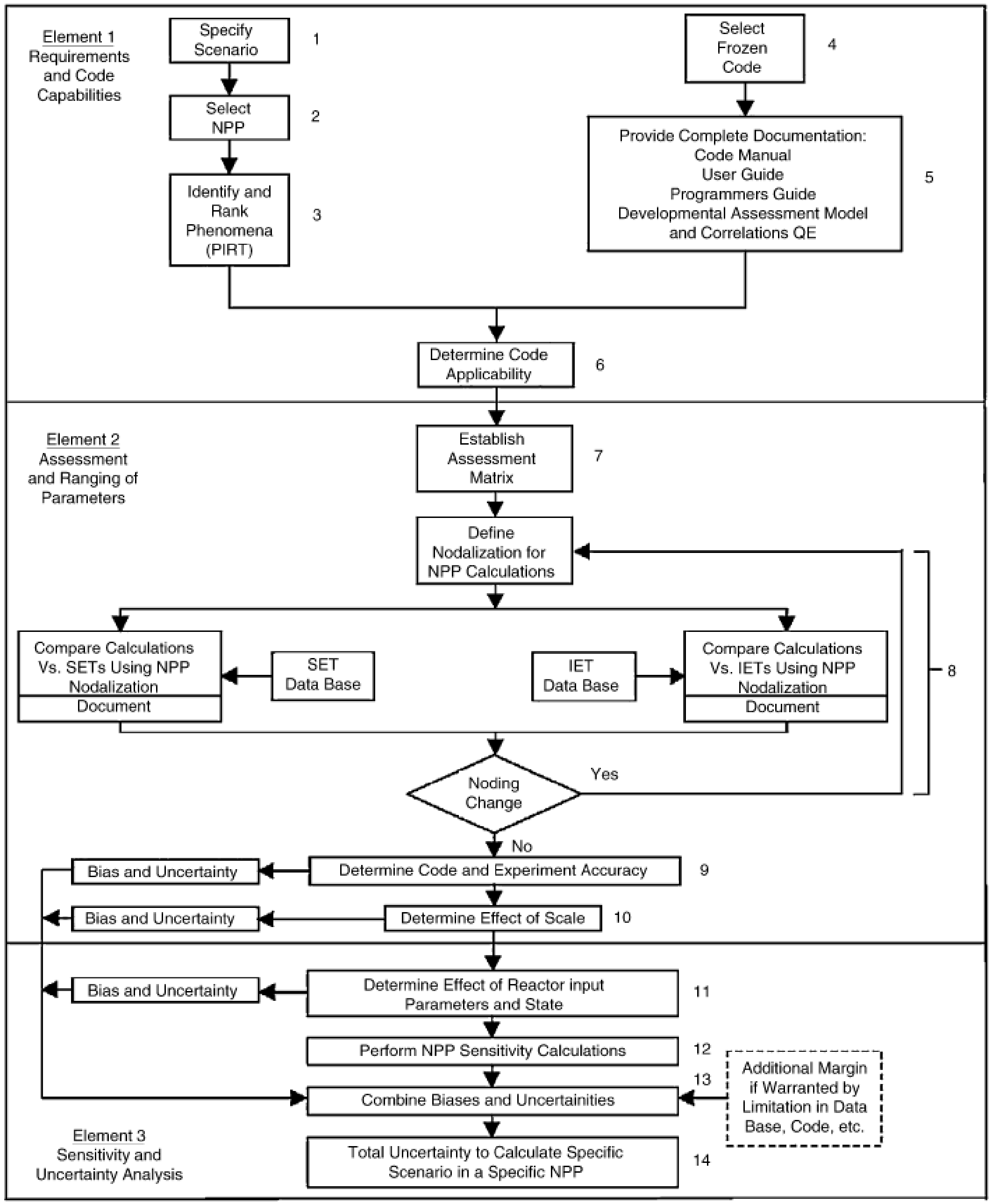

Figure 3.1. CSAU (Code Scaling, Applicability and Uncertainty Evaluation) Flow Diagram

3.5.2. GRS (Gesellschaft fur Anlagen-rUnd Reaktorsicherheit) Methodology

The GRS method (Figure 3.2) for uncertainty and sensitivity analysis considers the effect of uncertainty of input parameters on the calculation results [32, 33]. GRS method two main elements:

1. Integral test: The scenario, important phenomena selection and ranking, probability distribution function assignments to the uncertainty parameters and finally the uncertainty analyses are in this element.

2. Plant transient: This is full size power transient uncertainty analyses using the integral test element. The dominant phenomena selection, assignment of probability distribution functions and the uncertainty analyses are in this element.

Because only the integral test element is in the scope of the dissertation, the steps of this element are described below briefly:

- An integral test including the scenario of interest is selected. (Steps 1,2 and 3).
- Decision on significant phenomena and corresponding computer code models (Steps 4 and 5) (Similar to CSAU).
- Initial conditions, boundary conditions and model parameters, which potentially contribute to the uncertainty in the code predictions for the chosen tests, are selected (Step 6 to 7).

- Probability density functions or subjective probability distribution functions (SPDFs) are identified for each identified uncertain parameters (Step 8 and 9). Although CSAU just includes PDFs, GRS includes both PDFs and SPDFs.

- Key parameters are chosen for the uncertainty analyses (Step 10) (Similar to CSAU).

- According to the SPDFs or PDFs and quantified dependencies for each code run, a set of random values of each uncertain parameter are selected.

- Wilks' [34] formula provides the minimum number of code calculations for a given tolerance limit. The number of code calculations does not change with the number of input uncertainty parameters or any assumption about the distribution of the result. It just depends on the chosen tolerance limits.

- Code runs are performed with these parameter values (Step 11).

- Quantitative statement of the combined influence of the quantified input uncertainties on the code results is derived.

- To see if the calculated uncertainties bracket the data, calculated uncertainty intervals are compared with measured integral test data. Sensitivity studies provide the ranking of important uncertainty parameters.

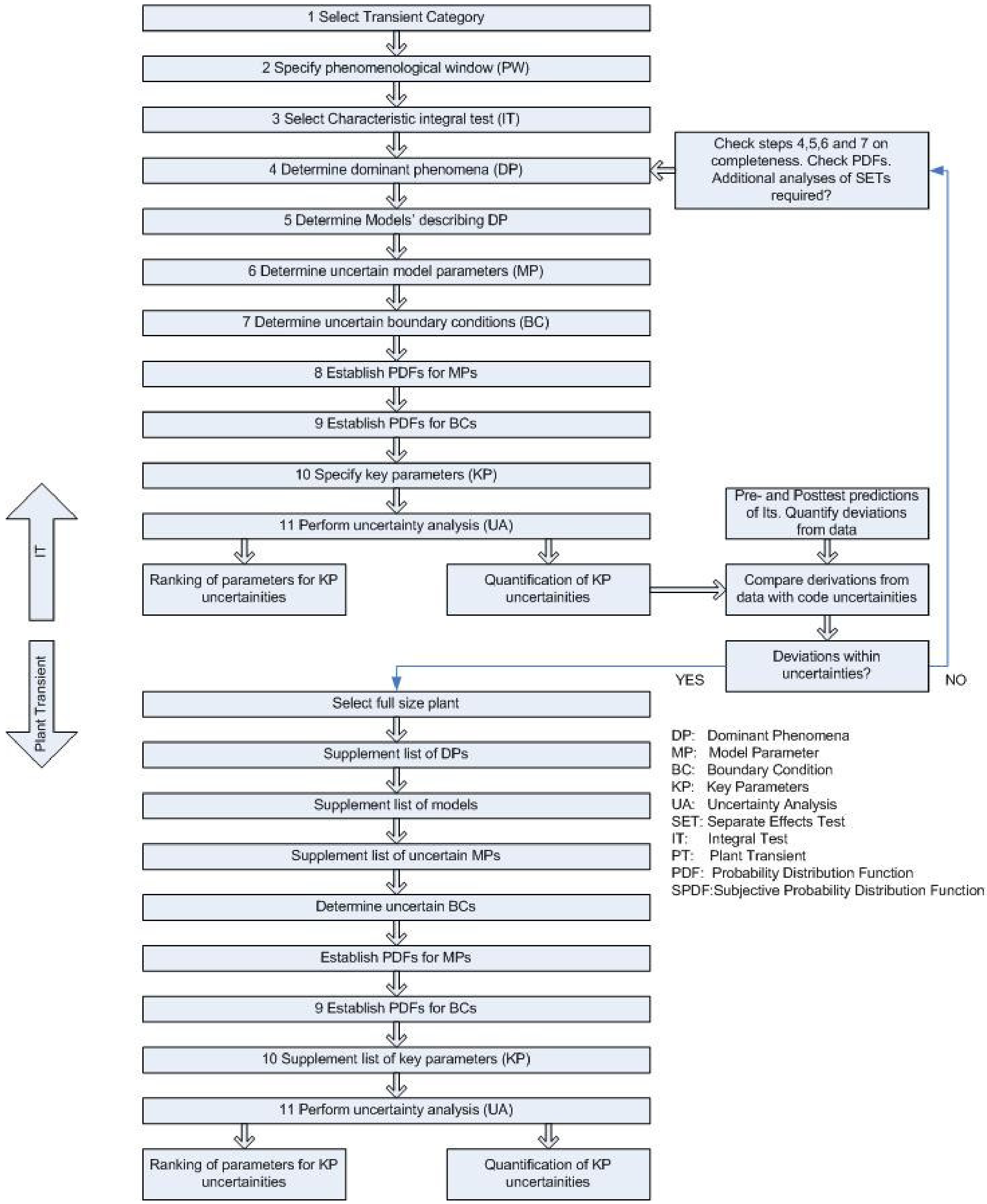

Figure 3.2. GRS Flow Diagram

3.6. References

1. Wheeler, A. J., Ganji, A. R., 1996, Introduction to Nuclear Engineering Experimentation, Prentice Hall

2. Hochreiter, L., 2006, Thermal-Hydraulics Uncertainties As Applied to DNB Analysis and Best-Estimated LOCA Calculations, ACE Uncertainty Workshop, North Carolina State University

3. Dixon, W. J. and Massey, F. J., 1957, Introduction to Statistics Analysis, McGraw-Hill Book Company, Inc.

4. Saltelli, A., Chan, K. and Scott, E.M., 2000, Sensitivity Analysis, WILEY publication

5. Saltelli, A. et. al., 2004, Sensitivity Analysis in Practice. A Guide to Assessing Scientific Models, John Wiley & Sons publishers.

6. Roache, P.J., 1998, Verification and Validation in Computational Science and Engineering, Hermosa Publishers, p. 403-412

7. http://www.personal.psu.edu/faculty/j/h/jhm/470/lectures/VandV/VandV.html

8. Oberkampf, W. L., Trucano, T. G. and Hirsch, C., 2002, Verification and validation for modeling and simulation in computational science and engineering applications- Foundations for verification and validation in the 21st century workshop.

9. Ghezzi, C., Jazayeri, M., Mandrioli, D., Fundamentals of Software Engineering, Prentice Hall, ISBN 0-13-099183-X

10. Greyvenstein, G. P., Niekerk, W. M. K. and Labuschagne, J. T. , 2006, Verification and validation of the HTGR systems CFD code Flownex, Jan P. Ravenswaay, Nuclear Engineering Design

11. Isukapalli, S. S., 1999, Uncertainty Analysis of Transport-Transformation Models, PhD thesis, Rutgers, The State University of New Jersey

12. Vanderperk, M., , 1997, Effect of model structure on the accuracy and uncertainty of results from water quality models. Hydrological Processes., 11(3):227-239

13. Tomovi'c, R. and Vukobratovi'c, M., 1972. General Sensitivity Theory. Elsevier, New York

14. Dunker, A. M., 1984, The decoupled direct method for calculating sensitivity coefficients in chemical kinetics. *Journal of Chemical Physics*, 81(5):2385-2393

15. Prokopakis, G. J., 1993, Decoupled direct method for the solution of ordinary boundary value problems. Applied Mathematical Modelling., 17(9):499-503

16. Villadsen, J. and Michelsen, M. L.. 1978, Solution of Differential Equation Models by Polynomial Approximation. Prentice-Hall, Englewood Cliffs, New Jersey

17. Doughtery, E. P. and Rabitz, H., 1979, A computational algorithm for the Green's function method of sensitivity analysis in chemical kinetics. International Journal of Chemical Kinetics, 11:1237-1249

18. Doughtery, E. P., Hwang, J. T. and Rabitz H., 1979, Further developments and applications of the Green's function method of sensitivity analysis in chemical kinetics. International Journal of Chemical Kinetics, 71(4):1794-1808

19. Adomian, G., 1980, Applied stochastic processes. In G. Adomian, editor, Stochastic System Analysis, pages 1-17. Academic Press, New York

20. Tatang, M. A., 1992, Combined Stochastic and Deterministic Approach in Solving Stochastic Differential Equations". Master's thesis, Carnegie Mellon University

21. Worley, B. A., Pin, F. G., Horwedel, J. E. and Oblow, E. M., 1989, ADGEN - ADjoint GENerator for computer models. Technical Report ORNL/TM-11037, Oak Ridge National Laboratory

22. Bischof, C. H., Roh, L. and Maueroats, A. J.. 1997, ADIC - an extensible automatic differentiation tool for ANSI-C. Software-Practice & Experience., 27(12):1427-1456

23. Roselle, S. J., 1994, Effects of biogenic emission uncertainties on regional photochemical modeling of control strategies. Atmospheric Environment., 28(10):1757-1772

24. Sistla, G., Rao, S.T. and Godowitch, J., 1991, Sensitivity analysis of a nested ozone air quality model. roceedings of the AMS/AWMA Joint Conference on Applications of Air Pollution Modeling and Its Applications, New Orleans, LA

25. Vieux, B. E., and Needham, S., 1993, Nonpoint-pollution model sensitivity to grid-cell size. Journal of Water Resources Planning & Management-ASCE., 119(2):141-157

26. http://en.wikipedia.org/wiki/Sensitivity_analysis

27. Kalos, M. H. and Whitlock, P. A., 1986, Monte Carlo Methods : Basics. John Wiley & Sons, New York

28. Fishman, G. S., 1996, Monte Carlo : Concepts, Algorithms, and Applications. Springer Verlag, New York

29. Loh, W. L., 1996, On Latin Hypercube Sampling. *Annals of Statistics.*, 24(5):2058-2080

30. Helton, J. C., 1993, Uncertainty and sensitivity analysis techniques for use in performance assessment for radioactive waste disposal. P. 327-367

31. Karamchandani, A., , 1992, C. A. Cornel. Sensitivity estimation within first and second order reliability methods. Structural Safety, 11(2):95-107

32. Wickett, T. , et al., 1998 "Report of the uncertainty methods study for advanced best estimate thermal hydraulic code applications," NEA/CSNI/R(97)35

33. Wickett, A.J. and Yadigaroglu, G., 1994, Report of a CSNI workshop on uncertainty analysis methods, NEA/CSNI/R(1994)20/VOL1

34. Wilks, S.S., 1941, Determination of Sample Sizes for Setting Tolerance Limits, The Annals of Mathematical Statistics, Vol.12, p. 91-96

Chapter 4

BWR FULL SIZE FINE MESH BUNDLE TEST (BFBT) DATABASE

Although there are different databases that we can use for uncertainty analysis, there is only one database that includes detailed full size fine mesh bundle test data for a BWR Bundle. This database is NUPEC BWR BFBT database. Part of this BFBT database has been made available for an International Benchmark Activity entitled as the OECD/NRC BFBT Benchmark. This international project is officially approved by the Japan Ministry of Economy, Trade, and Industry (METI), US Nuclear Regulatory Commission (NRC), and endorsed by the OECD [1].

BFBT database provides detailed BWR void distribution [2] and critical power data. Therefore, BFBT database will be used as a basis for the uncertainty analysis for the COBRA-TF void distribution and critical power predictions [3, 4, 5, 6].

In the scope of this dissertation, the sampling uncertainty method is applied to COBRA-TF in order to estimate the uncertainty range of the steady state void distribution predictions as well as steady state critical power predictions by comparing the predictions to the BFBT database. In the BFBT database, steady state void distribution and steady state critical power data are available in the Phase I-Exercise 1 and Phase II-Exercise 1 respectively.

The BFBT test facility is able to simulate the high-pressure, high temperature fluid conditions found in BWRs. An electrically-heated rod bundle has been used to simulate a full scale BWR fuel assembly. Figure 4.1 shows a diagram of the test loop. The main structural components are made of stainless steel (SUS304). De-mineralized water is used as a cooling fluid. The maximum operating conditions for the facility are 10.3 MPa in pressure, 315 °C in temperature, 12 MW in test power, and 75 t/h in flow rate. The test facility has the capability for a full range of steady-state testing over BWR operating conditions and can also simulate time-dependent characteristics of complex BWR operational transients. Water is circulated by the circulation pump (1) and the coolant flow rate is controlled by the three valves (3) of different sizes. The inlet fluid temperature for the test section (5) is controlled by a direct-heating tubular pre-heater (4). Sub-cooled coolant flows upward into the test bundle (5), where it is heated and becomes a two-phase mixture. The steam is separated from the steam-water mixture in the separator (7) and is condensed using a spray of sub-cooled water in the steam drum (8). The condensed water is then returned to the circulation pump (1). The system pressure in both steady and transient state is controlled by spray lines (9), which have four different-sized valves. The pressurizer (6) controls the system pressure when the test assembly power is low. The spray pump (10) forces a spray into the steam-drum after water is cooled with two air-cooled heat exchangers (11). Based on this diagram, the test loop was operated covering the full range of BWR steady-state operating conditions.

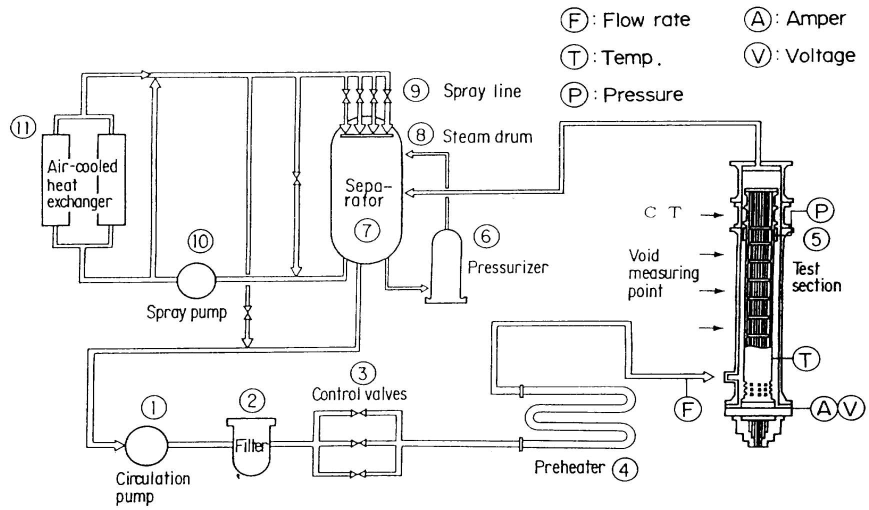

Figure 4.1. System Diagram of Test Facility for NUPEC Rod Bundle Test Series

The test section, shown in Figure 4.2, consists of a pressure vessel, a simulated flow channel, and electrodes. The simulated full-scale BWR fuel assembly was installed within the vessel. Two bundle types, a current 8×8 type and a high burn-up 8×8 type, were simulated. Here it should be noticed that the terminology “current 8×8 design” refers to the late 1980s when the NUPEC BFBT database was collected. The dimensions for the different rod bundle arrays are summarized in Table 4.1. Each rod in the test assembly is indirectly electrically heated to simulate a reactor fuel rod. The cladding, the insulator, and the heater were made of inconel, boron nitride, and nichrome, respectively.

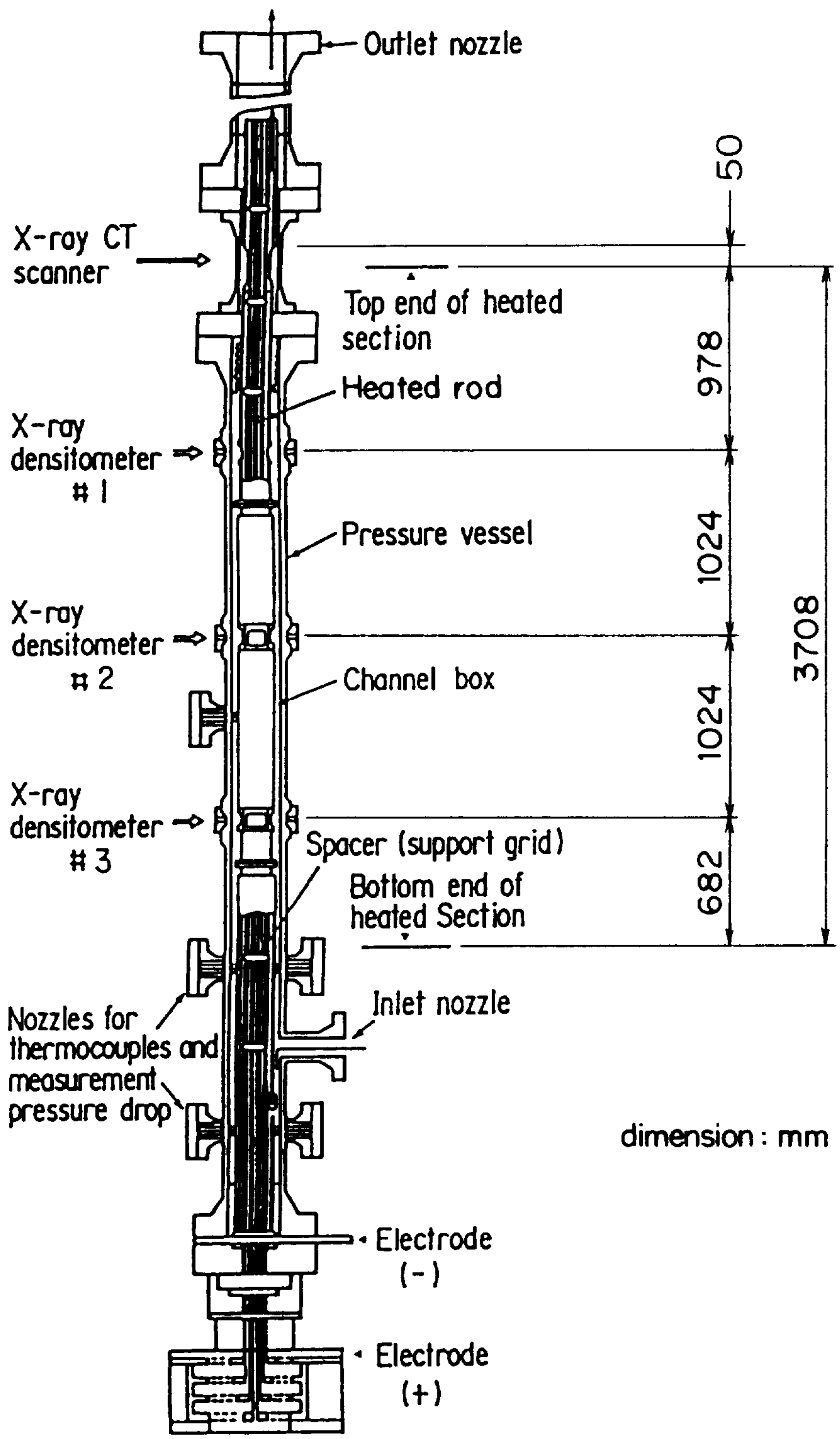

Figure 4.2. Cross-sectional View of Test Section

Table 4.1. Dimensions of BWR Test Bundles

Items	**Current**	**High Burnup**
	8x8	**8x8**
Number of fuel rods	62	60
Outer diameter (mm)	12.3	12.3
Heated length (m)	3.7	3.7
Number of water rods (mm)	2	1
Outer diameter of water rod (mm)	15	34
Rod pitch (mm)	16.2	16.2
Width of channel box	132.5	132.5
Number of spacers	7	7
Spacer type	Grid	Ferrule

The void distribution and critical power measurement methods that are used in the BFBT are briefly discussed below.

4.1. Void Distribution Measurement Methods

As shown in Figure 4.3 (a), two types of void distribution measurement systems were employed: an X-ray CT scanner and an X-ray densitometer.

Under steady-state conditions, fine mesh void distributions were measured using the X-ray CT scanner, which was located 50 mm above the heated length. The measurement system and the location are shown in Figure 4.3 (a). The system consists of an X-ray tube and 512 detectors. Figure 4.3 (b) shows the void fraction measuring section, where the pressure vessel was made of titanium (Ti). The channel wall and the cladding of the heater rods at this location are made of beryllium (Be) to minimize X-ray attenuation in the structure. In order to avoid the effect of the two-phase flow fluctuations, the collection of projection data was repeated and the results were time-averaged. The attained spatial resolution was as small as 0.3 mm × 0.3 mm.

The X-ray CT scanner is also used for transients void measurements called chordal averaged void fraction measurements. During the transient the X-ray CT scanner is not rotated but fixed. The data called “CT Chordal Averaged Void Fraction” is the value averaged over nine separate measurements at different bundle cross-section locations, taken during nine repetitions of the same transient.

The X-ray densitometer measurements were performed at three axial elevations. The channel box was made of beryllium (Be) and the heater rods had beryllium cladding of the same diameter as the Inconel portion of the heater rod. Figure 4.4 shows the void measurement directions of the X-ray densitometer. The chordal averaging is done from west to east (or x direction) and the order of data collection is from north to south (or y direction, y=1 to 9).

Figure 4.5 demonstrates the void fraction measurement methods.

The cross-sectional averaged transient void distributions were measured with the X-ray densitometer at different axial positions. During the transient void measurements the X-ray densitomer was fixed (not rotated) at a given axial position (Figure 4.4). The measurement was repeated nine times with changing the radial location of the densitometer at a fixed axial location along the heated length. The data is called "DENsitometer Chordal Averaged Void Fraction". The DEN chordal averaged void fraction is the value averaged over these nine measurements.

The CT-scanner X-ray beam is scanned over an object. An outline of the CT scanner principle is shown in Figure 4.3 (c). When scanning, the fan-shaped X-ray beam is attenuated by the object and the attenuated beam is measured by the detectors. The X-ray intensity data recorded by the detectors is called the projection data. The complete 360^o projection data are obtained for the object.

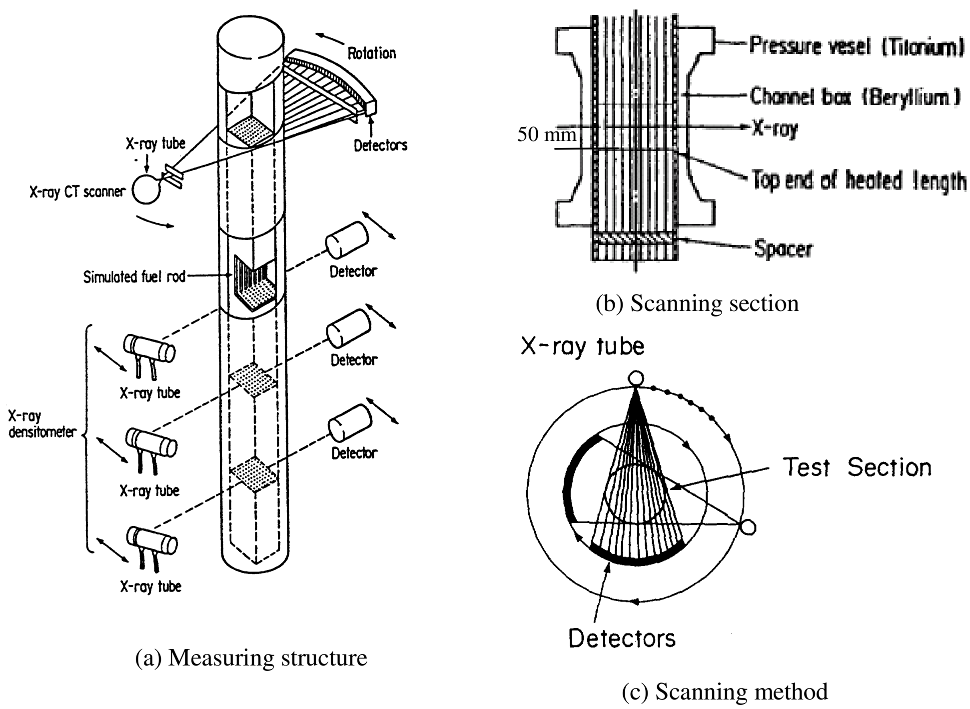

(a) Measuring structure

(b) Scanning section

(c) Scanning method

Figure 4.3. Void Fraction Measurement System

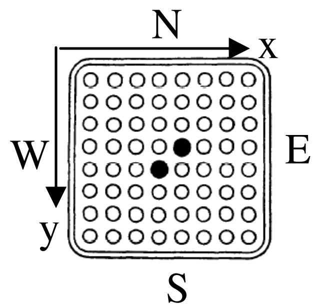

Figure 4.4. Void Fraction Measurement Directions

All void fraction signals from the detectors are calibrated using a signal from a reference detector to improve the signal-to-noise ratio.

Before performing actual void fraction measurements, position coordinates are calibrated at room temperature with the test section empty. They are then repeated with the section filled with water and at operating temperature with non-boiling water. Frequent measurements through a standard absorber are made to correct any electronic drift.

Absolute and differential pressures were measured using diaphragm transducers. The inlet flow rate was measured using turbine flow meter. The inlet sub-cooling was measured using double thermistors. The heater rods surface temperatures were monitored at positions just upstream of the spacers by chromel-alumel thermocouples, which were located in the heater rod cladding. The thermocouples have a diameter of 0.5 mm.

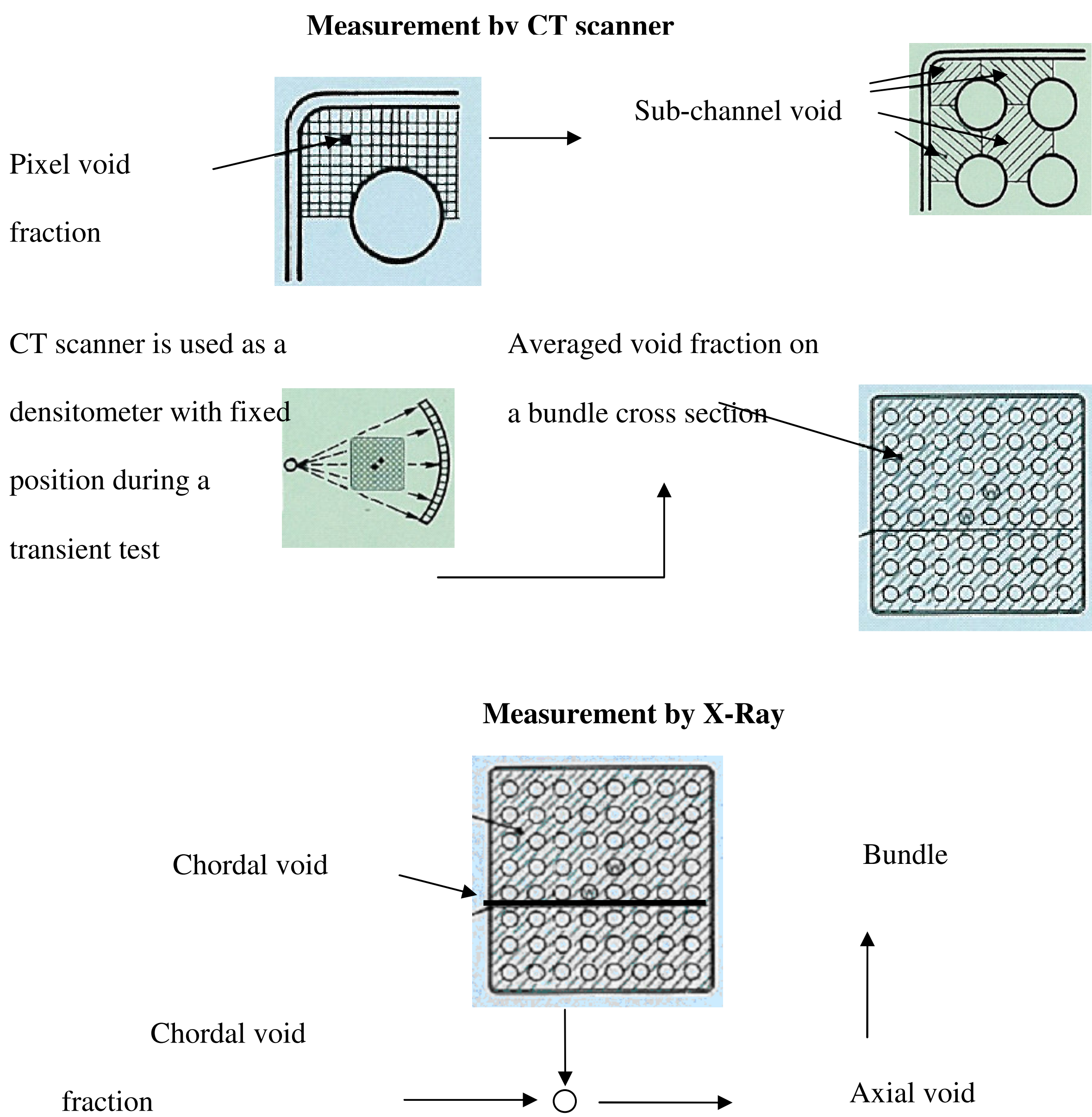

Figure 4.5. Void Fraction Measurement Methods

Table 4.2 shows the estimated measurement accuracy. Three types of void fraction measurements were carried out: a local void fraction on a 0.3 mm × 0.3 mm square pixel element; a sub-channel-averaged void fraction, which is averaged over more than 400 pixel elements; and a cross–sectional averaged void fraction, which is averaged over more than 10^5 pixel elements. The accuracy of these void fraction measurements depends on the photon statistics of the X-ray source, the detector non-linearity, and the accuracy of the known fluid condition (temperature and pressure) measurements.

Table 4.2. Estimated Accuracy of Main Process Parameters for Void Distribution Measurements

Quantity	Accuracy
Pressure	1%
Flow	1%
Power	1.5%
Inlet fluid temperature	1.5 Celsius
X-ray CT scanner	
• Local void fraction	8%
• Sub-channel void fraction	3%
• Cross-sectional void fraction	2%
Spatial resolution	0.3 mm × 0.3 mm
Scanning time	15 seconds
X-ray densitometer	
• Sampling time	Max. 60 seconds

Five different types of bundle assembly design with different combinations of geometries and power shapes were tested in the void distribution experiments. BWR steady state and transient conditions were simulated.

Two types of BWR assemblies are simulated in a full length test facility, a current 8×8 fuel bundle and an 8×8 high burn-up bundle. In total, five test assembly configurations with different geometry and power profiles were utilized for the void distribution and critical power measurements.

Table 4.3 summarizes the assembly types (Type 0 to Type 4) used in the void distribution measurements.

Table 4.3. Test Assembly and Radial Power Distribution for Void Distribution Measurements

Test assembly No.	0	1	2	3	4
Fuel Type	Current use 8x8 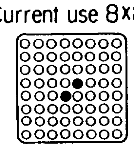				High burnup 8x8 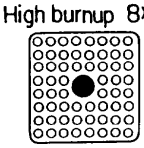
Planar power profile	Uniform	Simulated design profile	Simulated design profile	Simulated design profile	Simulated design profile
Axial power profile	Uniform	Cosine	Half-cosine	Inlet peak	Uniform
Heated length	Full	Full	Half	Full	Full
Axial powe distribution (Axial → Power)	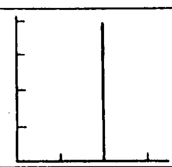	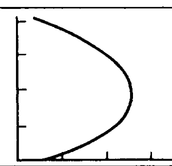	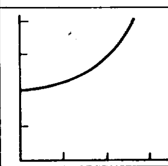	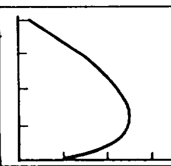	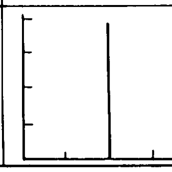

The *test assembly type 0* (as given in Table 4.3) has uniform radial and axial power distributions. Three sub-types of test bundle 0, namely 0-1, 0-2, and 0-3, were used to examine the effects of radial power distribution on the void fraction distribution by varying the number of unheated rods among them. The radial arrangements of heated and unheated rods are shown in Figure 4.6. Test assembly 0-1 simulates a current BWR fuel assembly and has two unheated rods. Test assemblies 0-2 and 0-3 have four and nine unheated rods, respectively. Two water channels (rods) are present in all of these three sub-type test assemblies and they are counted as unheated rods.

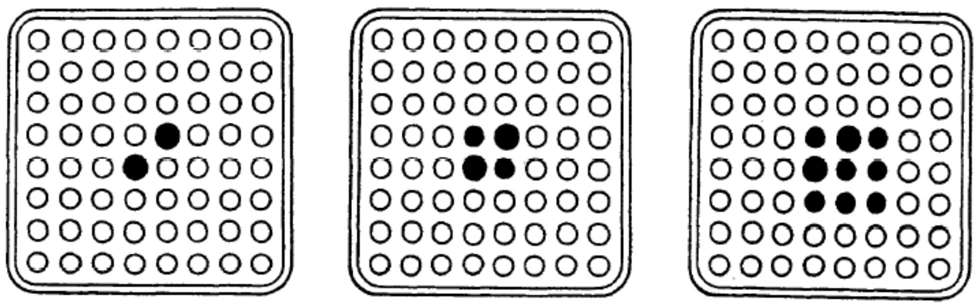

(a) 0-1 (b) 0-2 (c) 0-3

○ : Heated rod ● : Unheated rod

Figure 4.6. Unheated Rods Arrangements in Test Assembly Type 0

Test assembly types 1, 2, and 3 are like assembly type 0-1 with two unheated rods, but with different axial heated length and different axial power shapes. These bundles have a design-simulated radial power profile.

Figure 4.7 shows the cross-sectional view of the heated rod. The rod is single-ended, grounded electrical heater rod, which represents the nuclear fuel rod. The original geometry of the electrical heater is spiral coil. This geometry treatment does not affect the steady state calculation. For the transient the thermal time constant may affect the results. Therefore in addition to the demonstrated geometrical data, a thermal time constant of about 5 seconds is specified as a reference value. The cladding, the insulator, and the heater are made of inconel, boron nitride, and nichrome, respectively. Gaps between heater, insulator and cladding could be assumed zero contact. The heated rod surface temperature is measured by chromel-alumel thermocouples. Individual cladding thermocouples are embedded in the cladding surface. Axially, they are positioned mainly just upstream of the spacers. Each heated rod is joined to an X-ray transmission section, which has the same diameter as the heated rod but the cladding is made of beryllium (Be) for case of X-ray transmission.

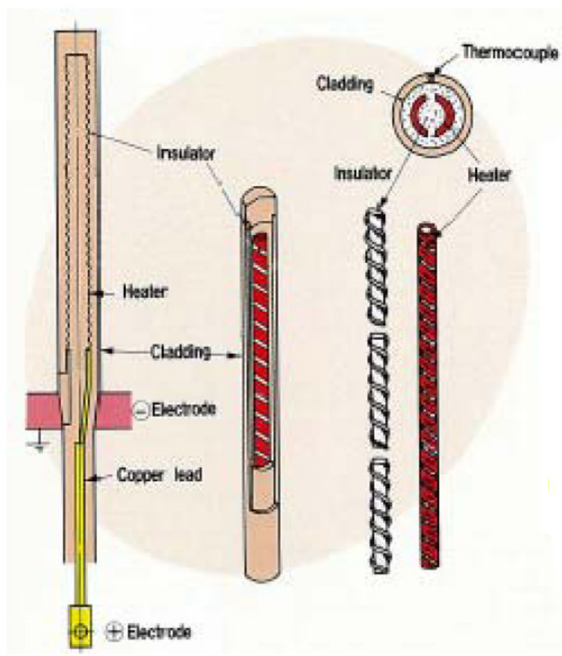

Figure 4.7. Cross Sectional View of Heater Rod

Spacer grids are used to support fuel rods in nuclear reactor fuel assemblies. These grids interact with the flow and heat transfer in a number of ways. It is known that they generally have a beneficial effect on critical heat flux (CHF) in typical nuclear reactor assemblies. However, the obtained enhancement depends on the geometrical characteristics of the spacer grids as well as on the parameter range in terms of pressure, local mass velocity, and quality. Spacer grids decrease the flow cross sectional area locally and thereby increase the local pressure drop and heat transfer coefficients. They may have special geometrical features to promote turbulence, the effect of which may propagate further downstream. Spacer grids may provide a larger surface area on which to collect the entrained liquid droplets, which may cause increase in the local fluid film flow rate under sub-CHF conditions and may lead to rewetting of the fuel rod cladding under post-CHF conditions.

There are two types of spacers used in the NUPEC BFBT experiments - ferrule type and grid type. The grid type spacers are applied to the 8x8 assemblies (assembly types 0, 1, 2, and 3). The ferrule type is applied to the high burn-up 8x8 assemblies (assembly types 4, C2A, C2B and C3).

Table 4.4 gives test matrix of steady state void distribution measurements.

Table 4.4. Test Matrix of Steady-State Void Distribution Measurements

Assembly	Pressure (Mpa)	Inlet sub-cooling (kJ/kg)	Flow rate (t/h)	Exit quality (%)						No. of data
				2	5	8	12	18	25	
0-1	1.0	50.2	10	X	X	X	X	-	-	13
			30	X	X	X	X	-	-	
			55	X	X	W	X	-	-	
	3.9		10	X	X	X	X	X	X	19
			30	X	X	X	X	X	X	
			55	X	X	X	X	X	W	
	7.2	20.9	45	-	X	-	X	-	-	36
		50.2	10	X	X	X	X	X	X	
			20	X	X	X	X	X	X	
			30	X	X	X	X	X	X	
			55	W	E1	W	E1	W	E1	
			70	X	X	X	X	X	-	
		126	55	-	X	-	X	-	-	
	8.6	50.2	10	X	X	X	X	X	X	18
			30	X	X	X	X	X	X	
			55	X	X	X	X	W	-	
0-2	3.9	50.2	55	X	X	X	X	X	W	28
	7.2		10	X	X	X	X	X	X	
			30	X	X	X	X	X	X	
			55	W	E1	W	E1	W	E1	
			70	X	X	X	X	X	-	
	8.6		55	X	X	X	X	W	-	

X: test case, W: duplicated test case, E1: exercise 1 case, E2: exercise 2 case, E4: exercise4 case

Table 4.4. Test Matrix of Steady-State Void Distribution Measurements (Cont.)

Assembly	Pressure (Mpa)	Inlet sub-cooling (kJ/kg)	Flow rate (t/h)	Exit quality (%)						No. of data
0-3	3.9	50.2	55	X	X	X	X	X	W	28
	7.2		10	X	X	X	X	X	X	
			30	X	X	X	X	X	X	
			55	W	E1	W	E1	W	E1	
			70	X	X	X	X	X	-	
	8.6		55	X	X	X	X	W	-	
1	1.0	50.2	10	X	X	X	X	-	-	13
			30	X	X	X	X	-	-	
			55	X	E4	W	X	-	-	
	3.9		10	X	X	X	X	X	X	19
			30	X	X	X	X	X	X	
			55	X	E4	X	X	X	W	
	7.2	20.9	45	-	X	-	X	-	-	36
		50.2	10	X	E4	X	X	X	X	
			20	X	E4	X	X	X	X	
			30	X	X	X	X	X	X	
			55	W,E4	E1, E4	W	E1, E4	W	E1, E4	
			70	X	E4	X	X	X	-	
		126	55	E4	X	-	X	-	-	
	8.6	50.2	10	X	X	X	X	X	X	18
			30	X	X	X	X	X	X	
			55	X	E4	X	X	W	-	

X: test case, W: duplicated test case, E1: exercise 1 case, E2: exercise 2 case, E4: exercise 4 case

Table 4.4. Test Matrix of Steady-State Void Distribution Measurements (cont'd)

Assembly	Pressure (Mpa)	Inlet sub-cooling (kJ/kg)	Flow rate (t/h)	Exit quality (%)						No. of data
				2	5	8	12	18	25	
2	3.9	50.2	10	X	X	X	X	-	X	14
			30	X	X	X	X	-	-	
			55	X	X	X	X	-	-	
	7.2		10	X	X	X	X	-	X	23
			20	X	X	X	X	-	X	
			30	X	X	X	X	-	X	
			55	X	X	X	W	-	-	
			70	X	X	X	-	-	-	
	8.6		10	X	X	X	X	-	X	13
			30	X	X	X	X	-	-	
			55	X	X	W	-	-	-	
3	3.9	50.2	55	X	X	X	X	X	W	28
	7.2		10	X	X	X	X	X	X	
			30	X	X	X	X	X	X	
			55	W	X	W	X	W	X	
			70	X	X	X	X	X	-	
	8.6		55	X	X	X	X	W	-	
4	1.0	50.2	10	X	X	X	X	-	-	13
			30	X	X	X	X	-	-	
			55	X	X	W	X	-	-	
	3.9		10	X	X	X	X	X	X	19
			30	X	X	X	X	X	X	
			55	X	X	X	X	X	W	
	7.2	20.9	45	-	X	-	X	-	-	36
		50.2	10	X	X	X	X	X	X	
			20	X	X	X	X	X	X	
			30	X	X	X	X	X	X	
			55	W,E2	E1,E2	W	E1,E2	W	E1,E2	
			70	X	X	X	X	X	-	
		126	55	-	X	-	X	-	-	
	8.6	50.2	10	X	X	X	X	X	X	18
			30	X	X	X	X	X	X	
			55	X	X	X	X	W	-	

X: test case, W: duplicated test case, E1: case for exercise 1, E2: case for exercise 2

For the uncertainty analysis, the selection of the experiments from the experimental cases is given in Chapter 6.

4.2. Critical Power Measurement Methods

The test loop used for the void distribution measurements (Figure 4.1 and 4.2) was also utilized for the critical power measurements. The test loop was operated under normal BWR operational conditions.

The full scale test bundle, simulating the 8x8 high burn-up fuel, was installed in the test section. Three combinations of radial and axial power shapes were tested:

1) Beginning of cycle radial power pattern/cosine axial power shape (the so-called C2A pattern);

2) Middle of cycle radial power pattern/cosine axial power shape (C2B pattern);

3) Beginning of cycle radial power pattern/inlet peaked axial power shape (C3 pattern).

The individual radial and axial power distributions for all three combinations are discussed in the void distribution section of the current chapter.

The critical power was measured by slowly increasing the bundle power while monitoring the individual heater rod thermocouple signals. The critical power was defined when the peak rod surface temperature became 14^{o}C higher than the steady-state temperature level before the dry-out occurred. The dry-out was observed in the peak power rod located at the peripheral row adjacent to the channel box. The boiling transition was always observed just upstream of the spacer. The estimated accuracies of the major process parameters were equivalent to those in the void measurement tests as listed in Table 4.2.

Figure 4.8 describes the definition of thermocouple position. Each thermocouple position is identified as follows: Rod No. – Axial location – Rotational angle. For example 16 – B – 270

The rod surface temperature was also monitored at several locations as depicted in Figures 4.9 to 4.11.

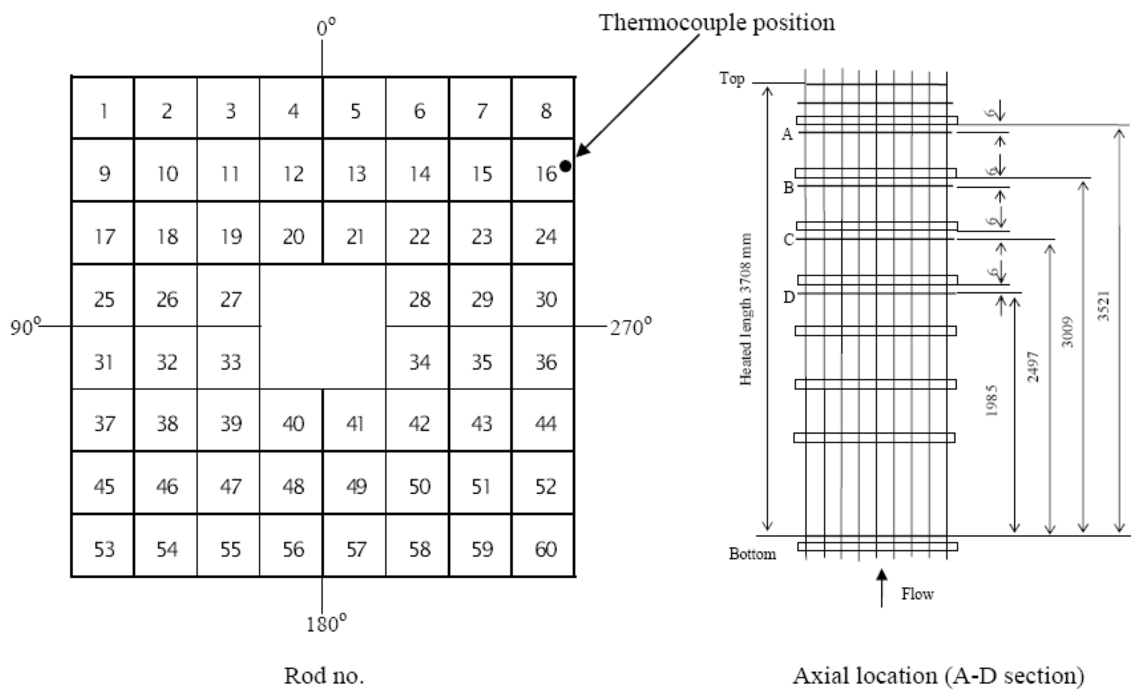

Figure 4.8. Definition of Thermocouple Position

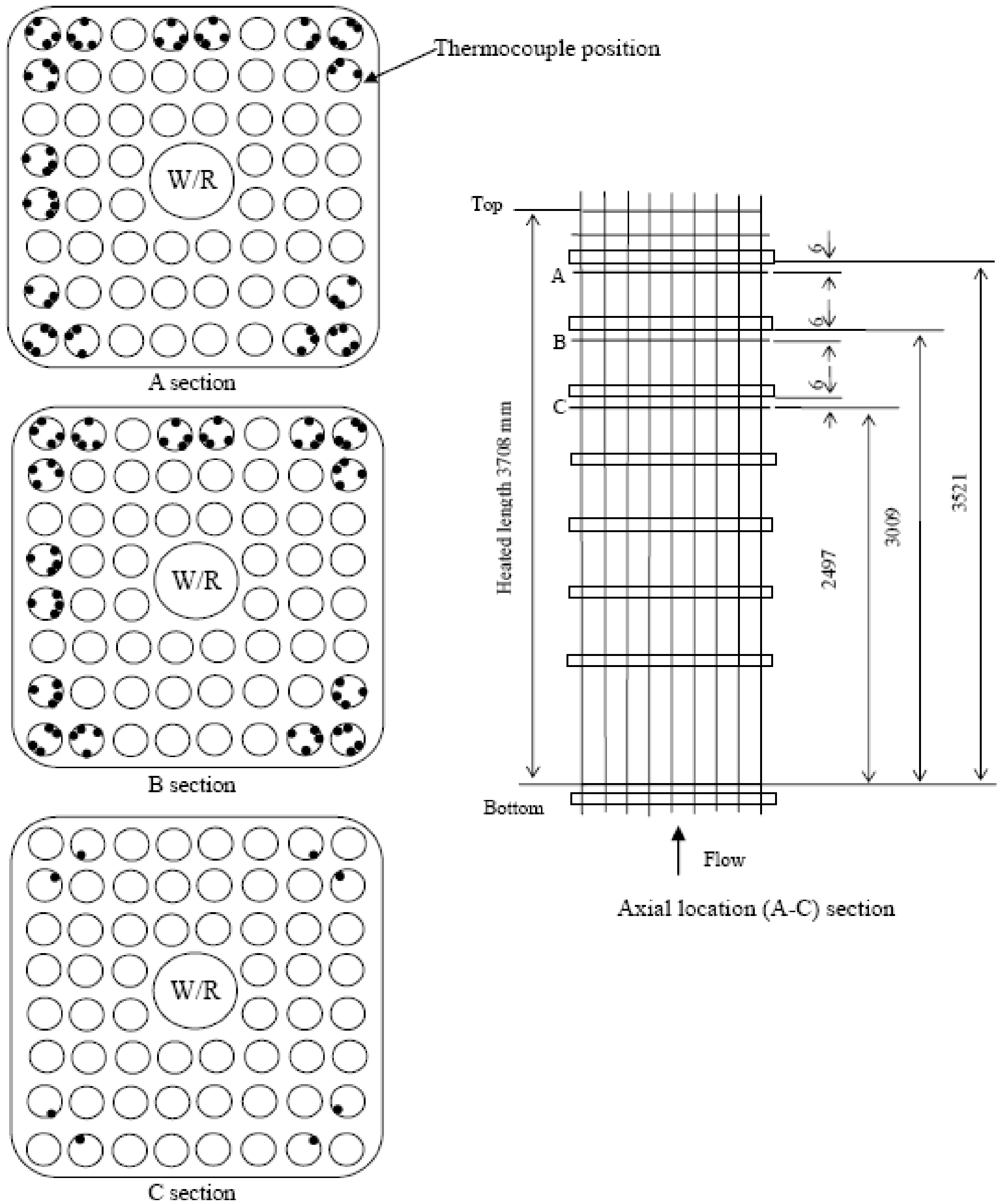

Figure 4.9. Locations of Thermocouples for Critical Power Measurement (C2A)

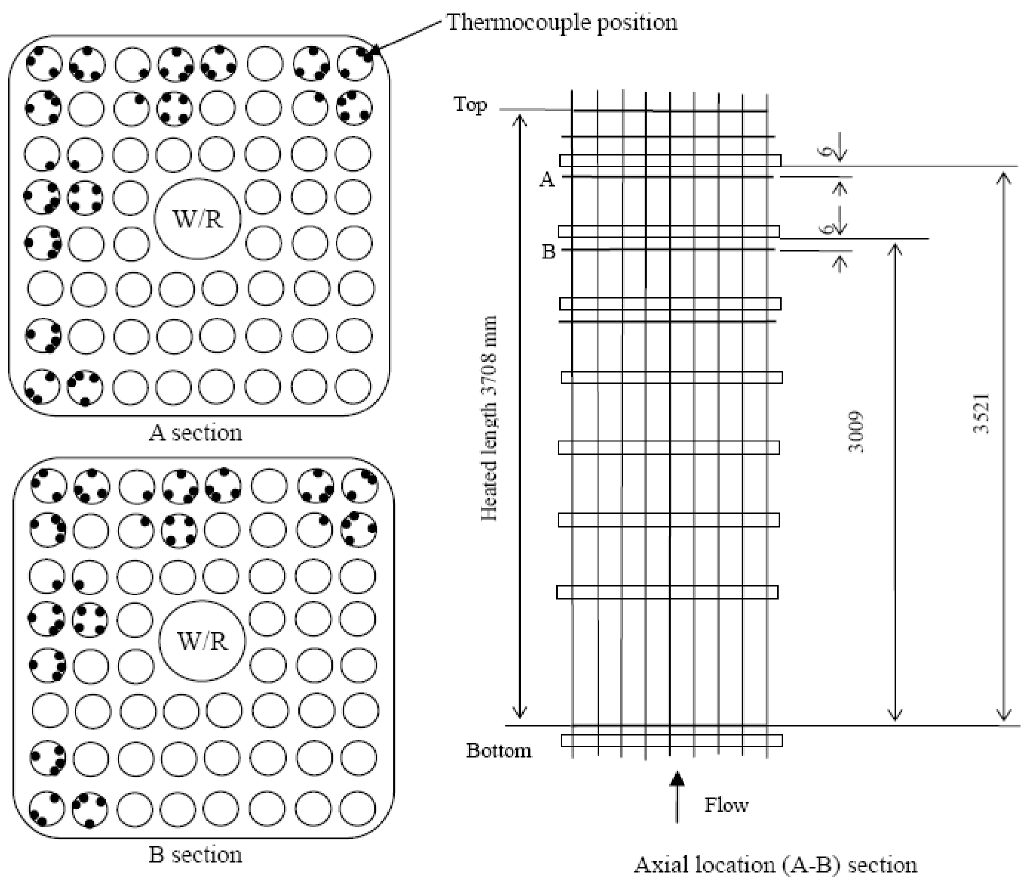

Figure 4.10. Locations of Thermocouples for Critical Power Measurement (C2B)

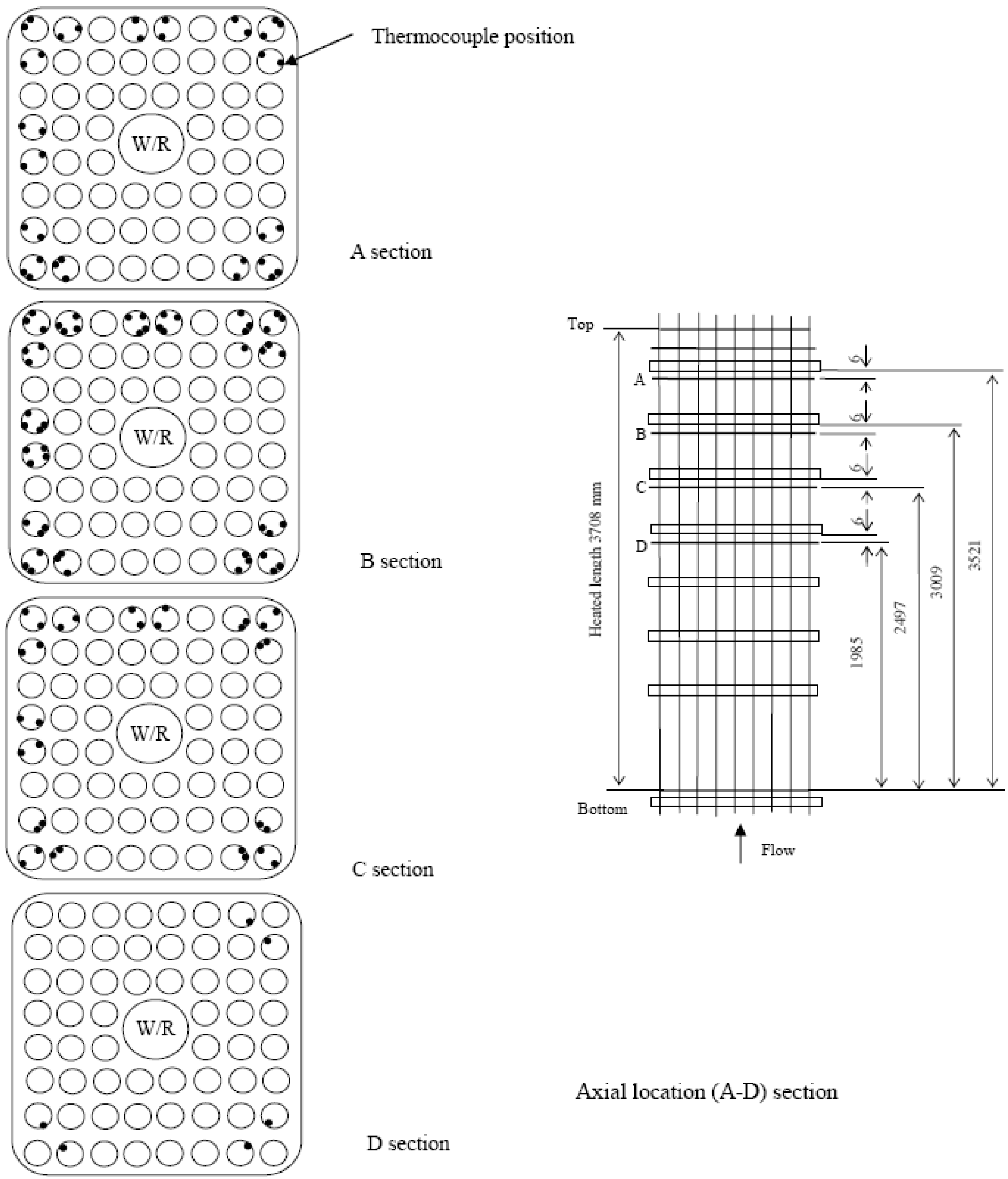

Figure 4.11. Locations of Thermocouples for Critical Power Measurement (C3)

Table 4.5 demonstrates the test matrix of steady state critical power measurements.

Table 4.5. Test Matrix of Steady State Critical Power Measurements

Assembly	Pressure (MPa)	Flow rate (t/h)	Inlet sub-cooling (kJ/kg)					No. of data
			25	50	84	104	126	
C2A	5.5	20	X	E1,W	X	-	X	20
		45	X	E1	X	-	X	
		55	E1,W	E1,W	E1,W	-	E1	
		65	X	E1	X	-	X	
	7.2	10	X	X	X	X	X	35
		20	X	E1,W	X	X	X	
		30	X	E1	X	X	X	
		45	X	E1	X	X	X	
		55	E1,W	E1,W	E1	E1,W	E1	
		60	X	E1	X	X	X	
		65	X	E1	X	X	X	
	8.6	20	X	E1,W	X	-	X	20
		45	X	E1	X	-	X	
		55	E1,W	E1,W	E1,W	-	E1	
		65	X	E1	X	-	X	
C2B	7.2	10	X	X	X	X	X	36
		20	X	E1	X	X	X	
		30	X	E1	X	X	X	
		45	X	E1	X	X	X	
		55	E1	E1,W	E1	E1	E1	
		60	X	E1	X	X	X	
		65	X	E1	X	X	X	
C3	7.2	10	X	X	X	X	X	36
		20	X	E1	X	X	X	
		30	X	E1	X	X	X	
		45	X	E1	X	X	X	
		55	E1	E1,W	E1	E1	E1	
		60	X	E1	X	X	X	
		65	X	E1	X	X	X	

X: test case, W: duplicated test case, E1: exercise 1 case

For the uncertainty analysis, the selection of the experiments from the experimental cases are given in Chapter 6.

There are three types of assemblies in the steady state critical power exercise. These are C2A, C2B and C2C. The axial and radial power profiles of these are shown in Table 4.6.

Table 4.6. Test Assemblies and Power Distributions for Critical Power Measurements

Test Item	**Critical Power Test**		
Test Assembly	C2A	C2B	C3
Fuel Type	High Burn-up 8x8		
Axial Power Profile	Cosine	Cosine	Inlet Peak
Radial Power Shape	A	B	A

A- Simulation pattern for beginning of operation

B- Simulation pattern for middle of operation

Because C2A is selected for the uncertainty analysis for critical power, only A type of radial distribution is demonstrated in Figure 4.12.

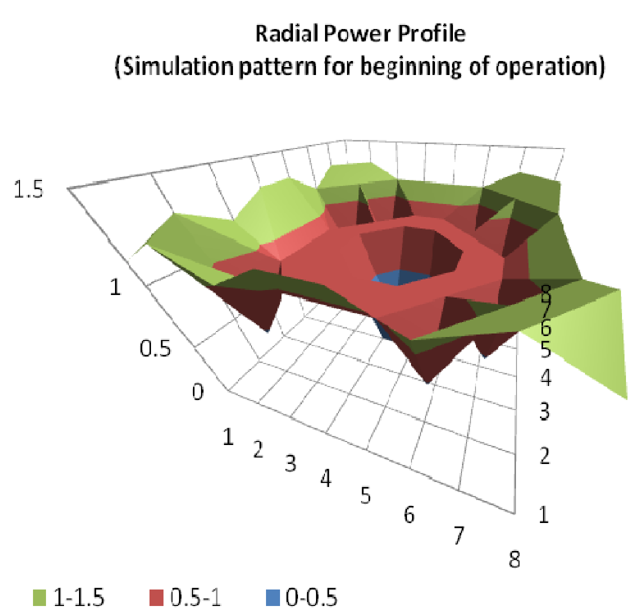

Figure 4.12. A Type of Radial Profile

Figure 4.13 demonstrates the cosine shape axial power distribution.

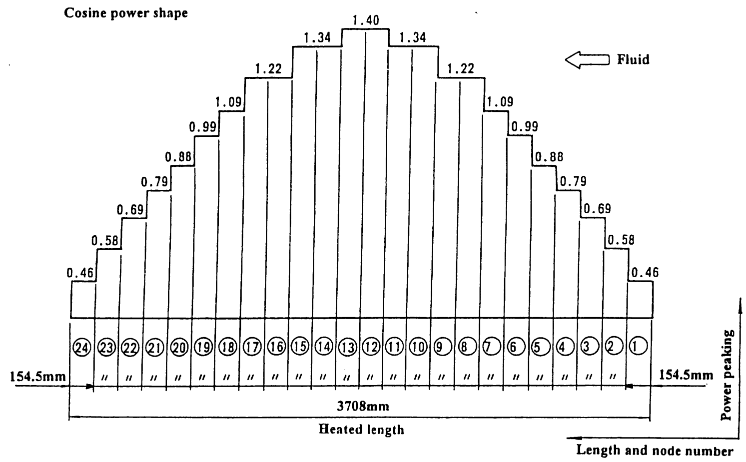

Figure 4.13. Cosine Shape Axial Power Distribution Pattern for Critical Power Measurements

4.3. References

1. Neykov, B., Aydogan, F., Hochreiter, L., Ivanov, K., Utsuno, H., Fumio, K. , Sartori, E., Martin, M., 2005, NUPEC BWR Full-Size Fine-Mesh Bundle Test (BFBT) Benchmark Volume I: Specifications, , NEA/NSC/DOC(2005)5

2. Aydogan F. et. al. 2006, Evaluation of the subchannel code COBRA-TF for the prediction of BWR fuel assembly void distribution, ICONE 14-89174, 14th International Conference on Nuclear Engineering, Florida

3. Aydogan, F., L. Hochreiter, K., Ivanov, M., Martin, H., Utsuno, E., Sartori, 2007, NUPEC BWR Full Size Fine Mesh Bundle Test (BFBT) BENCHMARK Volume II:

Uncertainty and Sensitivity Analyses of Void Distribution and Critical Power-Specification, NEA/NSC/DOC(2007)21

4. Aydogan, F. et al. 2007, Phenomena Idenditification Ranking Table for BWR Steady State Void Distribution, (254), Nureth-12 International Conference, 2007

5. Aydogan, F. et al., 2007, Phenomena Idenditification Ranking Table for BWR Steady State Critical Power, (255), Nureth-12 International Conference, 2007

6. Aydogan, F. et al., 2007, Overview and Status of the OECD/NRC BFBT Benchmark Activities, (138), Nureth-12 International Conference, 2007

Chapter 5

DEVELOPMENT OF UNCERTAINTY METHODOLOGY

In the past, various uncertainty analysis methods have been exclusively developed and implemented for the Loss of Coolant Accidents (LOCA) in nuclear thermal hydraulics field. The new phenomena to be examined are the steady state void distribution in the BWR bundle as well as the steady state critical power. The selected phenomena for BWRs have been already discussed in the introduction chapter. Therefore, this chapter just provides the details of the particular uncertainty methodology used to analyze these phenomena.

The sampling methodology selected to be used as discussed in Chapter 3. The main reasons for this selection is that sampling method is applicable to any computational tool, without modifications of the codes. The analyses are based on the statistical variation of model input parameters and the uncertainty margins could be obtained for any output parameter of the code.

Some of the CSAU and GRS's elements are also used for the development of proposed uncertainty methodology (Figure 5.1) that is selected and implemented for the uncertainty analysis of steady state void distribution and critical power. The developed uncertainty methodology has 26 elements. The definitions of elements are given below:

1. **Specify Scenario**: Identify the problem through specification of the event scenario/case. The scenario or case is described with this element.

2. **PIRT**: Phenomena Identification Ranking Table is defined with this element. The United States Nuclear Regulatory Commission (US NRC) developed Phenomena Identification Ranking Table (PIRT) concept for assessing the relative importance of individual phenomena (models or correlations) met to determine safety margins in operating reactors [1, 2, 3, 4, 5]. Even though USNRC developed PIRT as part of the Code Scaling, Applicability and Uncertainty (CSAU) methodology for the Emergency Core Cooling System (ECCS) Performance applied to quantify Reactor Safety Margins for the LOCA by the vendors, such as, Westinghouse [5] and AREVA [3], PIRT is a good test to identify which phenomena are the most important for a given scenario.

Although the CSAU and the GRS methods have similar elements for the determination of significant phenomena affecting the output uncertainty parameters, the CSAU has the PIRT ranking feature and the GRS method does not. USNRC showed how independent expert groups could also define PIRTs. Thus, the CSAU's PIRT is selected for the particular uncertainty methodology.

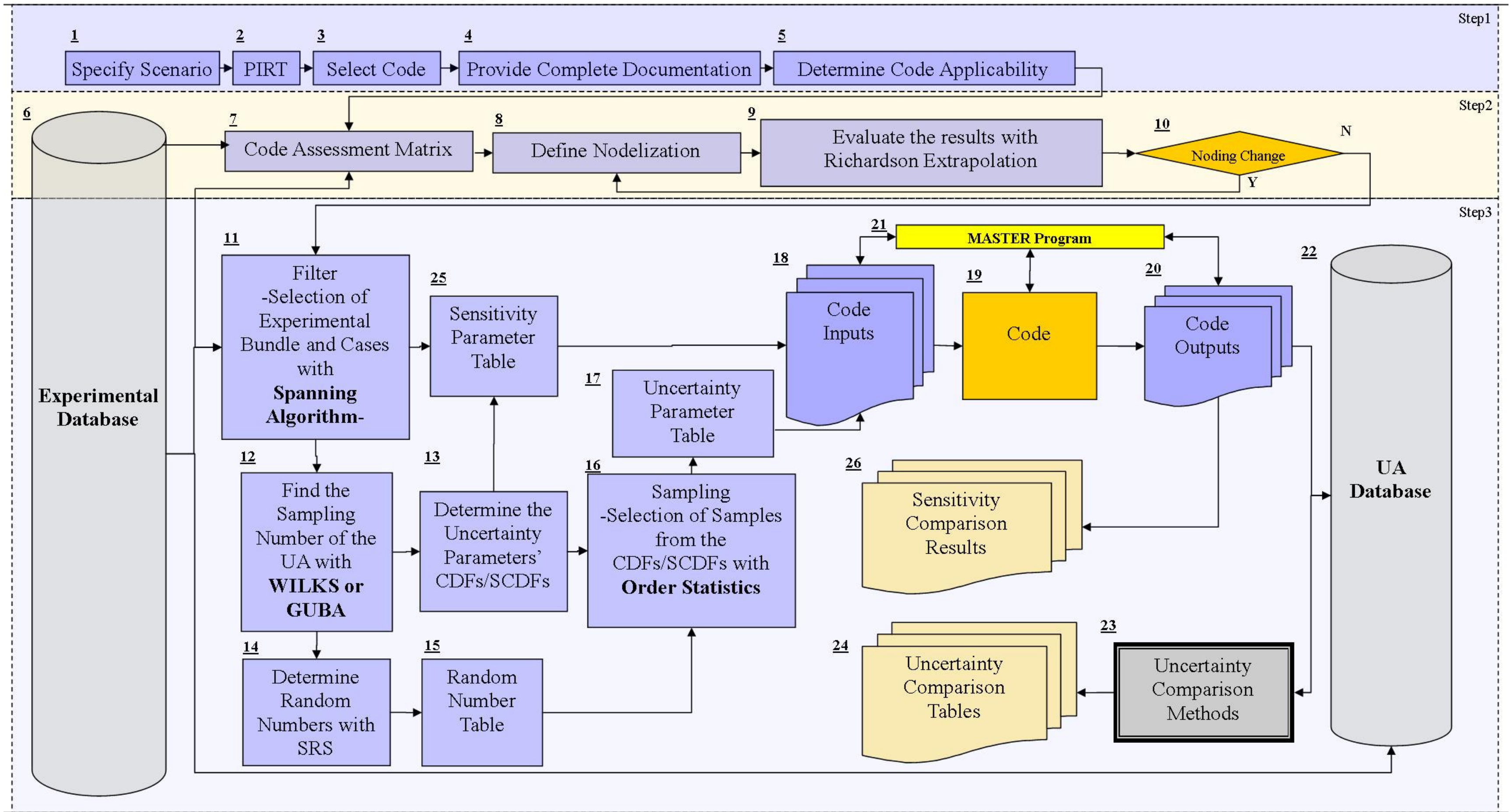

Figure 5.1. Proposed Uncertainty Methodology Flow Chart

3. **Select Code**: The code is selected with this element. The selected code has to provide solutions for the selected scenario/case.

4. **Provide Complete Documentation**: This element provides the code's description and the manual of the code.

5. **Determine Code Applicability**: Whether the code is applicable or not for the selected case is confirmed by this element.

6. **BFBT Experimental Database**: This is the experimental database used to compare with predicted result to provide comparisons.

7. **Code Assessment Matrix**: Some of the experimental cases are selected. These experimental cases are used for the nodding optimization.

8. **Define Nodding**: Experimental facility is modeled with a number of nodes. The bigger number of the nodes, the longer process time of the code runs. Therefore, the objective uses to define the minimum number of nodes needed to correctly capture the phenomena and prevent any numerical instability.

9. **Evaluate the Results with Richardson Extrapolation**: Richardson extrapolation [6] is a sequence acceleration method, used to improve the rate of convergence of

a sequence. Richardson Extrapolation is used to help for the optimization of the the node numbers. Richardson extrapolation formula is given in Equation 5.1.

$$\varepsilon = \frac{f_2 - f_1}{r^p - 1} \tag{5.1}$$

where

$$r = h_{i+1} / h_i \tag{5.2}$$

and

$$p = \ln\left(\frac{f_{i+2} - f_{i+1}}{f_{i+1} - f_i}\right) / \ln(r) \tag{5.3}$$

ε is the discretization error,

f_i is the function output,

i is the node ID,

h is the axial mesh size.

10. **Noding Change**: If nodding change is necessary, define the nodes again and evaluate the results with Richardson extrapolation. If not, the nodding is optimized.

11. **Filter**: There are many different experimental conditions and bundle types used in the experimental database. The objective of filtering is to decrease the number of bundle types and experimental cases for using in the uncertainty analysis. Since a sampling uncertainty analysis method requires a sampling matrix for each

experimental case, running all these sampling matrixes by computer codes requires a tremendous amount of time. To decrease the process time, element of filtering selects the bundle type and the number of experimental cases among experimental data.

Selection of the appropriate bundle type provides flexibility to the analyst. For instance, a database includes pressure drop, void distribution, transient and critical data. However, the database may just provide pressure drop data for two types of bundle and the same database may just provide void distribution data for other types of bundle, etc. Therefore, the criterion of bundle type selection is to select a bundle type that is involved as many cases/scenarios in the database as possible, such that a range based of experimental data exists for that bundle.

Selection of the cases is the second step of the filtering. Because each experimental case has different boundary conditions, uncertainty analyses of different experimental cases will produce different uncertainty results. Thus, selection of the cases affects the uncertainty results. The criteria of experimental case selection are given as,

- Cover the experimental database boundary conditions to represent the experimental database,
- Limit the number of the selected experimental cases with four to decrease the process time,

- Select such different experimental cases that uncertainties of the selected cases are increased.

Spanning algorithm was developed to meet the selection criteria. This algorithm has five steps:

1. Select the output uncertain parameter,
2. Select the independent parameters in the database,
3. Find the minimum and maximum values of output uncertain parameter,
4. Sort the data with the independent parameters,
5. Select the cases including the maximum number of independent parameters' values.

Select the case including the minimum independent parameters' values.

12. **Find the Sampling Number of the Uncertainty Analysis with using either the WILKS method or the GUBA method:** The number of the samples for a sampling uncertainty method is one of the essential elements. If the number of the samples is a small number, the output uncertainty may not be obtained. Because the number of the samples is proportional with the processing time, the number of the samples is desired to be small in order to decrease the CPU time. Therefore, there is an optimum sampling number. Two formulas are discussed in this section. One of them is given by Wilks [7] and the other one is by Guba [8]. The formula

by Wilks is given below as:

$$\beta=(1-\gamma)^N \tag{5.4}$$

where

β: confidence level

γ: tolerance level

N: number of the samples

By substituting γ=95/100 and β= 95/100, the number of the cases (N) is found to be 59 for one output parameter. Wilks gives a conservative estimate of the 95% value at a confidence level of 95%. The Wilks formula is defined only for one output parameter. If the problem includes more than one uncertain output parameter, an extension of the Wilks approach by Guba[8] method should be used as:

$$\beta=\sum_{j=0}^{N-p}\frac{N!}{(N-j)!\,j!}\gamma^{j}(1-\gamma)^{N-j} \tag{5.5}$$

where

β: confidence level

γ: tolerance level

N: number of the samples

p: number of the outcomes

GUBA calculates the number of the samples for the given confidence and tolerance values for more than one uncertainty outputs.

13. **Determine the Uncertainty Parameters' CDFs/SCDFs**: This element assigns a Cumulative Distribution Function (CDF) or Subjective Cumulative Distribution Functions. Although CSAU use PDFs and GRS use PDFs or SPDFs, the proposed uncertainty methodology uses CDF/CDFs. Before the discussion of the usage of CDF/CDFs. PDF, SPDF, CDF are defined below:

A **probability density function (PDF)** is a function, $f(x)$, which describes normalized probability of the input variable (x) given as below.

$$\int_{-\infty}^{+\infty} f(x)dx = 1 \qquad (5.6)$$

where

$0 \leq f(x) \leq 1$ for all values of x

For the input variable (x) within the range $a \leq x \leq b$, several classical probability density functions f(x) can be defined as shown in Table 5.1.

Table 5.1. Definitions of the Probability Definition Functions

PDF	**Features**	**Definition**	**Equation Number**
Uniform	-	$f(x) = 1 / (b - a)$	(5.7)
Triangular	Shape parameter c with $a \leq c \leq b$	$f(x) = 2 (x - a) / (b - a) (c - a)$ if $a \leq x \leq c$ $f(x) = 2 (b - x) / (b - a) (b - c)$ if $c \leq x \leq b$	(5.8) (5.9)
Exponential	Location parameter γ Scale parameter λ	$f(x) = \lambda \exp[-\lambda (x - \gamma)]$	(5.10)
Normal	Mean value μ Standard deviation σ	$f(x) = \exp[-(x-\mu)^2 / 2\sigma^2] / \sigma(2\pi)^{1/2}$	(5.11)
Log normal	Mean value of logarithms μ Standard deviation of logarithms σ	$f(x) = \exp[-(\ln(x)-\mu)^2 / 2\sigma^2] / (x\sigma(2\pi)^{1/2})$	(5.12)

The reason for the SPDF's usage is to provide flexibility to the analyst when a PDF is difficult to obtain or could not be obtained. At this case, an expert defines SPDFs with engineering experience. In the particular methodology, CDFs and SCDFs are used instead of PDFs and SPDFs. The mathematical definition of the CDF is given in equation 5.13 and 5.14 for continuous and discrete PDFs respectively:

$$CDF(x <= X) = \int_{0}^{X} f(x)dx \tag{5.13}$$

$$CDF(x <= X) = \sum_{i=1}^{N} f(x_i)dx \tag{5.14}$$

where

f(x) is the PDF for the variable of interest.

The behaviour of the CDF depends on the expression for the PDF. For instance, CDF is a linear function if PDF is a flat function as given in Equation 5.7. CDF/SCDF are used in the proposed methodology in order to apply Order Statistics.

14. **Determine Random Numbers with SRS**: A Simple Random Sample (SRS) is a subset of random numbers chosen from a larger set. Each number is chosen randomly and entirely by chance. Each individual number has the same probability of being chosen at any stage during the sampling process [9]. Simple Random Sampling is one of the common sampling methods. This method is easy to implement and to explain [10]. The selected numbers by SRS is called as pre-samples. They are between zero and one. The number of the pre-samples has already calculated by 12th element.

15. **Random Number Table**: The results of 14th element (pre-samples) are recorded into the random number table.

16. Sampling with Order Statistics: Order Statistics [11] is used to pick the sample elements by using CDFs/SCDFs of uncertainty parameters. The mathematical model of the order statistics is given below.

Let $X_1, X_2, \ldots, X_n$ be the absolutely continuously distributed random variables, and $X_{(1)}, X_{(2)}, \ldots, X_{(n)}$ be the corresponding order statistics.

Let f(x) be the probability density function and F(x) be the cumulative distribution function of X_i. Then the probability density of the k^{th} statistic can be found as follows [12].

$$
\begin{aligned}
f_{x_{(k)}}(x) &= \frac{d}{d_x} F_{x_{(k)}}(x) = \frac{d}{d_x} P(X_{(k)} \le x) = \frac{d}{dx} P(at\ least\ k\ of\ the\ Xs\ are \le x) \\
&= \frac{d}{dx} P(\ge k\ success\ in\ n\ trials) = \frac{d}{dx} \sum_{j=k}^{n} \binom{n}{j} P(X_1 \le x)^j (1 - P(X_1 \le x))^{n-j} \\
&= \frac{d}{dx} \sum_{j=k}^{n} \binom{n}{j} F(x)^j (1 - F(x))^{n-j} \\
&= \sum_{j}^{n} \binom{n}{j} (j(F(x)^{j-1} f(x)(1 - F(x))^{n-j} + F(x)^j (n-j)(1 - F(x))^{n-j-1}(-f(x))) \\
&= \sum_{j=k}^{n} (n\binom{n-1}{j-1} F(x)^{j-1} (1 - F(x))^{n-j} - n\binom{n-1}{j} F(x)^j (1 - F(x))^{n-j-1}) f(x) \\
&= n\ f(x) \left(\sum_{j=k-1}^{n-1} \binom{n-1}{j} F(x)^j (1 - F(x))^{(n-1)-j} - \sum_{j=k}^{n} \binom{n-1}{j} F(x)^j (1 - F(x))^{(n-1)-j} \right) \\
&= n\ f(x) \binom{n-1}{k-1} F(x)^{k-1} (1 - F(x))^{(n-1)-(k-1)} \\
&= \frac{n!}{(k-1)!(n-k)!} F(x)^{k-1} (1 - F(x))^{n-k} f(x))
\end{aligned}
\tag{5.15}
$$

Figure 5.1 demonstrates the usage of CDF for sampling. After the number of the samples is defined by either the Wilks or the Guba formula, pre-samples are generated with SRS. All these random pre-samples are used for sampling. The corresponding value of CDF's x-axis to a pre-sample is called as a sample. CDF/SCDF is used to calculate the corresponding samples to the random numbers as shown in Figure 5.2.

Random Generated Number with SRS (Pre-samples)

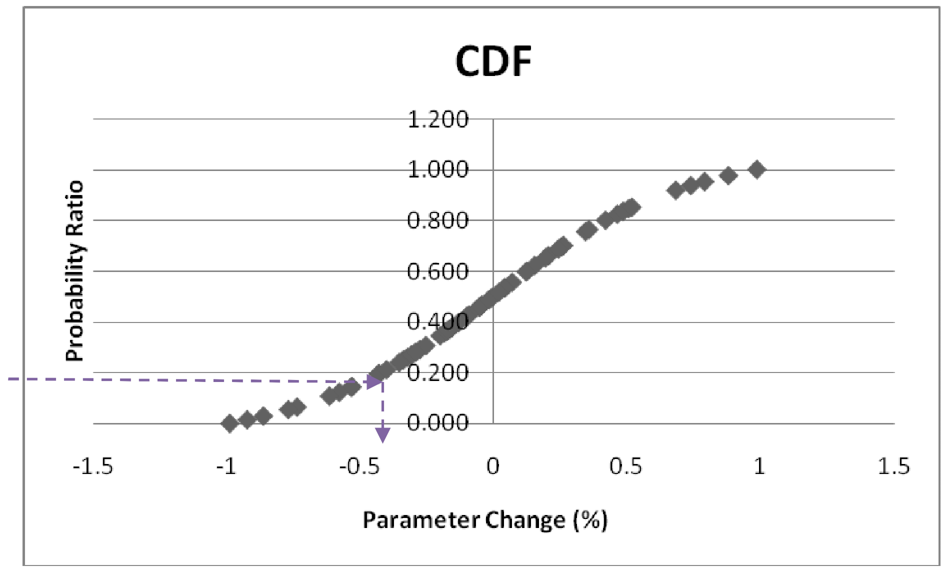

Figure 5.2. Representation of CDF Usage for Sampling

17. Uncertainty Parameter Table: 14th element of the methodology generates the samples of uncertainty parameters in terms of percentage change. All the uncertainty parameters' samples are recorded inside uncertainty parameter table. These numbers are used by the code input.

18. **Code Inputs**: Code input is formatted file used by the code to produce the output. Because the code input generally has to be in a special format, the uncertainty parameters have to be processed and inserted into the code input with the appropriate format.

19. **Code:** Code is the computer program that is used for the uncertainty analysis. For this approach, COBRA-TF (RBHT) is used in Chapter 6.

20. **Code Outputs:** Code outputs include not only the necessary information that is used for the uncertainty analysis, but also includes other useful information. Therefore, the code input has to be processed to extract necessary uncertainty data.

21. **Master Program:** Master program manages the code, code inputs and code outputs. The tasks of this element are given as,
    a. It makes necessary changes on the input file names,
    b. It runs the code with the appropriate input,
    c. When the code complete its run, Master program takes the outputs and renames their filenames,
    d. Master program repeats step a, b and c until it completes running all the inputs,

e. Finally, it produces a report including the information of files failed and successfully run.

22. **UA Database**: UA database contains all the predicted and measured uncertainty data that will be used for the uncertainty comparison methods.

23. **Uncertainty Comparison Methods**: To generate the uncertainties of the predicted results and compare them with the measured results, uncertainty comparisons are designed with the given criteria below [13]:

- To assess the code precision with the sample-averaged bias
- To assess the uncertainty propogation with the sample-averaged standard deviation
- To assess the code reliability with the proportion of specimens among the sample with a bias lower than the experimental uncertainty.

To accomplish these assessments, this element calculates the given parameters below:

- Mean value:

  The average of code predictions

- The individual relative bias:

  Each sample's bias between prediction and measurement

- The mean relative bias:

Average of sample's bias between prediction and measurement

- The maximum bias:

  The maximum bias between prediction and measurement

- The standard deviation:

  The standard deviation of the predictions

- The coverage ratio:

  The ratio of samples that are in the measurement uncertainty range

For a series of N individual assessments by a code (x^{code}_n) of a output variable x, Table 5.2 demonstrates the statistical comparisons using experimental results.

Table 5.2. Definition of the Formulas Used in the Evaluation of the Uncertainty

Definition	Formula	Equation Number
The mean value	$x^{code} = \frac{1}{N}\sum_{n\leq N} x_n^{code}$	(5.16)
The individual relative bias	$\delta_n^{code} = \frac{x_n^{code} - x^{\exp}}{x^{\exp}}$	(5.17)
The mean relative bias	$\delta^{code} = \frac{1}{N}\sum_{n\leq N} \delta_n^{code}$	(5.18)
The maximum bias	$\varepsilon^{code} = \max\left\|\delta_n^{code}\right\|$	(5.19)
The standard deviation	$\sigma^{code} = \sqrt{\frac{1}{N}\sum_{n\leq N}(x_n^{code} - x^{code})^2}$	(5.21)
The coverage ratio is the proportion of individual assessments among the series with a relative bias lower than the ratio of experimental uncertainty $\varepsilon^{\exp}$	$R^{code} = \frac{card\left\{\delta_n^{code} \text{ with } \delta_n^{code} \leq \varepsilon^{\exp}\right\}}{N}$	(5.22)

24. **Uncertainty Comparison Tables**: This element contains all the uncertainty comparison tables. These tables are used to evaluate the uncertainty results.

25. **Sensitivity Parameter Table**: Sensitivity parameter table contains the uncertainty parameters and corresponding input uncertainties. This table is used to perform sensitivity analysis by changing one parameter at a time. This allows the analyst to see which uncertainty parameter significantly affects the output uncertainty parameter (or ranking of the input uncertainty parameters).

26. **Sensitivity Comparison Results**: All the sensitivity results are collected by this element so that an analyst can make conclusions by using them.

5.1. References

1. Holowach, M. J., 2000, The Development of a Reflood Heat Transfer Computational Package For Small Hydraulic Diameter Geometries, M.S. Thesis, The Pennsylvania State University

2. U.S. Nuclear Regulatory Commission, Regulatory Guide 1.157 (Task RS 701-4), Best Estimate Calculations of Emergency Core Cooling Performance

3. Martin, R. P., O'Dell, L. D., AREVA's realistic large break LOCA analysis methodology, Nuclear Engineering and Design 235 (2005) 1713-1725

4. USNRC Quantifiying Reactor Safety Margins NUREG/CR-5249, 1989

5. Boyack, B., 1995, AP600 Large-Break Loss-of-Coolant Accident Phenomena Identification and Ranking Tabulation, LA-UR-95-2718

6. Richardson, L. F., 1910, The approximate arithmetical solution by finite differences of physical problems including differential equations, with an application to the stresses in a masonry dam, Philosophical Transactions of the Royal Society of London, Series A 210: 307–357

7. Wilks, S.S., 1941, Determination of Sample Sizes for Setting Tolerance Limits, The Annals of Mathematical Statistics, Vol.12, p. 91-96

8. Guba, A., Makai, M., Lenard, P., 2003, Statistical aspects of best estimate method-I, Reliability Engineering and System Safety, Vol.80, 217-232

9. Yates, D., Moore, D. S., Starnes, D. S., 2007, The Practice of Statistics, W. H. Freeman publication, ISBN: 978-0716773092

10. Gaudier, F., Martin, M., 2006, Uncertainty Analysis: Application to Void Fraction Model, Presentation in OECD/NRC Benchmark based on BFBT , 3rd BFBT Workshop, Pisa Italy

11. Schotter, A. R., 1996, Microeconomics, Addison-Wesley Publication, ISBN: 0-673-99944-0, p. 458-462

12. http://en.wikipedia.org/wiki/Order_statistic

13. Aydogan, F., Hochreiter, L., Ivanov, K., Martin, M., Utsuno, H., Sartori, E., 2007, NUPEC BWR FULL_SIZE FINE-MESH BUNDLE TEST (BFBT) BENCHMARK Volume II: Uncertainty and Sensitivity Analyses of Void Distribution and Critical Power-Specification, NEA/NSC/DOC(2007)21

Chapter 6

UNCERTAINTY ANALYSIS SYSTEM

A particular uncertainty methodology was already described for the selected phenomena in Chapter 5. Chapter 6 provides the implementation of the particular uncertainty methodology to the selected two scenario/cases with COBRA-TF (RBHT) [1, 2]. Based on the selected phenomena, this chapter was divided into two main sections:

a. Implementation of particular uncertainty methodology to steady state void distribution prediction,

b. Implementation of particular uncertainty methodology to steady state critical power prediction.

6.1. Implementation of Particular Methodology to Steady State Void Distribution

Void distribution inside the BWR bundle is the key factor to determine the flow regime and heat transfer regime of the flow. A code has to calculate void distribution accurately for the prediction of the flow and heat transfer regimes correctly.

The implementation of particular uncertainty methodology to the steady state void distribution inside the BWR bundle for COBRA-TF prediction provides the uncertainty ranges of subchannel and bundle void fraction at the exit of BWR bundle. Besides, the ranking of the dominant phenomena affecting these void fractions are also obtained with this methodology. Therefore, 3 steps with 26 elements of the particular uncertainty methodology were applied to obtain the uncertainty and sensitivity results.

6.1.1. Step-1

1. **Specify Scenario**: The scenario/case is steady state void distribution inside the BWR bundle. This scenario/case is described with the subchannel and bundle void fractions at the exit of the BWR bundle because at the exit of the BFBT bundle, CT-scanner scanned the whole bundle and provided detailed void fraction measurements.

2. **PIRT**: PIRT for the selected scenario is given in Table 6.1. Two independent expert groups worked independently on the PIRT tables for void distribution [3]. First group members are given as:

   - Fatih Aydogan (The Pennsylvania State University),
   - Lawrence Hochreiter (The Pennsylvania State University),
   - Maria Avramova (The Pennsylvania State University)

   Second group members are given as:

   - James Spring (The Pennsylvania State University),
   - Jeffrey Lane (The Pennsylvania State University),

- Douglas Miller (The Pennsylvania State University).

The steps of the development of the PIRT tables are given as:

- The first group developed the PIRT tables and ranked them. Three rankings are used: low, medium and high. The more effect on the uncertainty output parameter, the higher ranking the input uncertainty parameter has.
- The second group members reviewed the PIRT tables and provided their comments.
- Finally, the first group finalized the PIRT tables according to the second group's reviews.

The two expert groups agreed with each other for most of the parameters except for a few uncertain parameters' ranks. Table 6.2 demonstrates the disagreement and final decision about the PIRT for the case of void distribution.

1st and 2nd expert groups were not informed about the accuracy of the uncertainty parameters and the thermal hydraulic code on which uncertainty analysis are applied. Therefore, there were only two criteria for expert groups:

i. Which phenomena are dominant for the void distribution of BWR bundle at the exit,

ii. How dominant are the selected phenomena?

Second criterion was used for ranking process.

Table 6.1. PIRT for Steady State Void Distribution in BWR Bundle

Boundary Condition Effect			
ID	Parameter	Ranking	Basis for Ranking
1	Initial vessel operating pressure	M	This parameter affects the saturation temperature. The ranking of this parameter has to be determined with sensitivity analysis
2	Flow rate in the bundle	H	This parameter is in the energy equation
3	Power	H	This parameter is in the energy equation
4	Inlet Flow Temperature	M	This parameter changes the inlet boundary condition. The ranking of this parameter has to be determined with sensitivity analysis

where L: Low, M: Medium, H: High

Table 6.1. PIRT for Steady State Void Distribution in BWR Bundle (Cont.)

Geometry Effect			
ID	Parameter	Ranking	Basis for Ranking
1	Wetted perimeter	L	This perimeter affects the friction factor
2	Sub-channel area	H	This parameter affects the mass flow rate
3	Nominal gap width	L	This parameter affect the lateral flow
4	The distance between the centers of channels	L	This parameter affect the lateral flow
5	Fraction of channel area blocked by grid	M	This parameter affects the pressure drop and the heat transfer. The ranking of this parameter has to be determined with sensitivity analysis
6	Grid Perimeter	M	This parameter is used to calculate spacer loss coefficient. The ranking of this parameter has to be determined with sensitivity analysis
7	Heated perimeter	H	This perimeter affects the heat flux and void distribution
8	Housing wetted perimeter	L	This perimeter affects the friction factor

where L: Low, M: Medium, H: High

Table 6.1. PIRT for Steady State Void Distribution in BWR Bundle (Cont.)

Model Parameter Effect – Hydraulics			
ID	Parameter	Ranking	Basis for Ranking
1	The loss coefficient for a gap -lateral-	M	This parameter affects the lateral flow in a bundle. The ranking of this parameter has to be determined with sensitivity analysis
2	The wall friction factor for the gap	L	This affects the pressure drop
3	The grid loss coefficient -axial-	M	This parameter affects the pressure drop in the bundle. The ranking of this parameter has to be determined with sensitivity analysis
4	The mixing coefficient	H	This parameter affects the lateral void distribution in the bundle
5	Equilibrium distribution weighing factor in void drift	H	This parameter affects the lateral void distribution in the bundle
Interfacial Mass Transfer			
6	Interfacial Friction Factor	H	This parameter affects the pressure drop
Interfacial Drag Force			
7	Drag Coefficient for bubble flow regime	M	The ranking of this parameter has to be determined with sensitivity analysis
8	Drag Coefficient for drop flow regime	M	The ranking of this parameter has to be determined with sensitivity analysis
9	Interfacial friction factor for film flow regime	H	This parameter affects the mass transfer between film flow and vapor.
Friction Factor in Wall Drag Force			
10	Single Phase Friction Factor in Wall Drag Force	L	This affects the pressure drop
11	Two Phase Friction Factor in Wall Drag Force	M	This affects the pressure drop. Because two phase pressure drop models have higher uncertainty, this parameter is ranked as M. The ranking of this parameter has to be determined with sensitivity analysis.

where L: Low, M: Medium, H: High

Table 6.1. PIRT for Steady State Void Distribution in BWR Bundle (Cont.)

Model Parameter Effect – Thermal			
ID	Parameter	Ranking	Basis for Ranking
Wall Heat Transfer Coefficient			
1	Single phase liquid	M	This parameter affects the heat transfer from wall to the fluid. The ranking of this parameter has to be determined with sensitivity analysis.
2	Subcooled nucleate boiling	M	This parameter affects the heat transfer from wall to the fluid. The ranking of this parameter has to be determined with sensitivity analysis.
3	Saturated boiling region	M	This parameter affects the heat transfer from wall to the fluid. The ranking of this parameter has to be determined with sensitivity analysis.
Entrainment/Deposition			
Entrainment in film flow			
4	Entrainment rate	M	The ranking of this parameter has to be determined with sensitivity analysis. This parameter has more importance in the post-CHF scenario.
De-Entrainment in film flow			
5	De-entrainment rate for film flow	M	The ranking of this parameter has to be determined with sensitivity analysis.
De-Entrainment on grid spacers			
6	S_{DE}	M	The ranking of this parameter has to be determined with sensitivity analysis.
Spacer grid enhancement for entrained phase (to create thicker liquid film)			
7	S_E	M	The ranking of this parameter has to be determined with sensitivity analysis.

where L: Low, M: Medium, H: High

Table 6.2. Comparison of Two Independent Expert Groups' Decisions about the PIRT Tables for the Void Distribution

Effect	Parameter(s)	First group's Decision	Second Group's Decision	Final Decision	Comments
Boundary Condition Effect	Inlet Temperature	L	M	M	Second group commented that if the inlet temperature is increased, exit temperature of the coolant changes for a fixed power.
Geometry Effect	All	Agreement	Agreement	-	-
Hydraulic Effect	Drag Coefficient for bubble flow regime	L	M	M	Second group commented that if lateral cross loss coefficient is increased, there will be no cross flow. In this case, void drift and mixing coefficient may not be effective in that case. Therefore, 2nd group's suggested to change its ranking to medium.
Hydraulic Effect	Interfacial friction factor in mass transfer and interfacial drag force	M	H	H	2nd group's suggested to change this parameter's ranking to High.
Thermal effect	All	Agreement	Agreement	-	-

3. **Select Code**: COBRA-TF (RBHT) was selected for this analysis because this code is capable of predicting void distribution inside a BWR bundle.

4. **Provide Complete Documentation**: Two NUREG's documents can be used for COBRA-TF (RBHT) documentation:

    a. COBRA/TRAC- A Thermal-Hydraulics Code for Transient Analysis of Nuclear Reactor Vessels and Primary Coolant Systems [2]

    b. Analysis of FLECHT-SEASET 163-Rod Blocked Bundle Data Using COBRA-TF [1].

5. **Determine Code Applicability:** COBRA-TF (RBHT) is capable of predicting void distribution inside a BWR bundle [1, 2].

6.1.2. Step-2

6. **Experimental Database**: This module provides the experimental void distribution database to the uncertainty analysis. Because the steady state test series were performed using thermal-hydraulic conditions that envelope BWR bundle geometrical, power shape and two-phase flow parameters of actual plant steady-state operation, there is a wide range of test conditions. The range of test conditions was as follows: pressure - 1 ÷ 8.6 MPa; flow rate - 284 ÷ 1988 kg/m^2-s; and exit quality – 1 ÷ 25%. In

total, 476 measurement points were included. The detailed information about the database is provided in Chapter 5.

BFBT void distribution database includes detailed void distribution data. The file format for each experiment is in the text format in BFBT database. Appendix-1 (in Section 6.4.1) shows the format of one example of this text file. Each file includes the experimental and process conditions. Both experimental and process conditions include the values of pressure, mass flow rate, inlet sub-cooling and power. The process conditions are selected for the uncertainty analysis because it includes the real values of the system parameters. As mentioned in Chapter 5, both the X-ray CT scanner and the X-ray densitometers were used in the experiments in order to measure void distribution. Because the CT-scanner scanned whole bundle and it is located at the exit of the bundle, CT-scanner values are used for the uncertainty analysis.

In addition to measured BFBT void distribution database, the accuracy of the BFBT database is important as well. NUPEC provided the accuracy of measured BFBT database and it is provided in Chapter 4.

7. **Code Assessment Matrix:** Code assessment matrix is the same matrix selected for the uncertainty analysis. This matrix was obtained with the Spanning Algorithm in the 11th element.

8. **Define Nodalization**: There is only one BWR bundle in the BFBT experimental database. Therefore, the optimized nodes were determined as:

    a. Axial nodes

    b. Time interval

The 9th element of the particular uncertainty analysis consists the analysis on axial nodes and time intervals.

9. **Evaluate the Results with Richardson Extrapolation**: This element consists of two nodalization processes:

    i. **Axial Node Optimization:** The number of the axial nodes on BWR bundle model was optimized in this analysis. The output pressure of the BWR bundle was compared as the function output in Richardson extrapolation [4]. Table 6.3 shows the discretization error for the axial node optimization.

Table 6.3 Discretization Error of Axial Node Optimization

Node ID (i)	Sequence of Three Mesh Space	Node Number	Discretization Error (ε)
3	f3(h3)	11	-
2	f2(h2)	17	-
1	f1(h1)	29	4.7E-7

Because calculated discretization error (4.7E-7) is much smaller than the measured pressure accuracy (1% of pressure which is 0.08MPa), 29 axial nodes was selected as the optimum number of the axial nodes.

The second step after optimization of the axial node number is the optimization of time interval.

ii. **Time Interval Optimization:** 9 axial nodes are used for the time interval optimization. This step is similar to axial node optimization. However, time intervals are used instead of axial node size in this step. Table 6.4 shows the discretization error for the time interval optimization.

Table 6.4 Discretization Error of Time Interval Optimization

Node ID (i)	Sequence of Three Mesh Space	Time Intervals in seconds (h_i)	Discretization Error (ε)
3	f3(h3)	0.04	-
2	f2(h2)	0.02	-
1	f1(h1)	0.01	2E-6

Because calculated discretization error (2E-6) is much smaller than the measured pressure accuracy (1% of pressure which is 0.08MPa), 0.01second is selected as the optimum value of the time interval.

Finally, 29 for optimized number of axial nodes and 0.01seconds for optimized time interval were determined. This configuration of the node length and time interval is used for the uncertainty analysis.

After nodalization was performed, the minimum required time for the steady state was calculated. The COBRA-TF model was run for 50seconds to see how many seconds is sufficient for the steady state runs. Figure 6.1 and 6.2 show the output pressure change with time and void fractions' change with time respectively. These results demonstrate that 5 seconds is sufficient for the steady state cases which are selected for the uncertainty analysis. These selected cases are discussed in the 11th element of the uncertainty analysis.

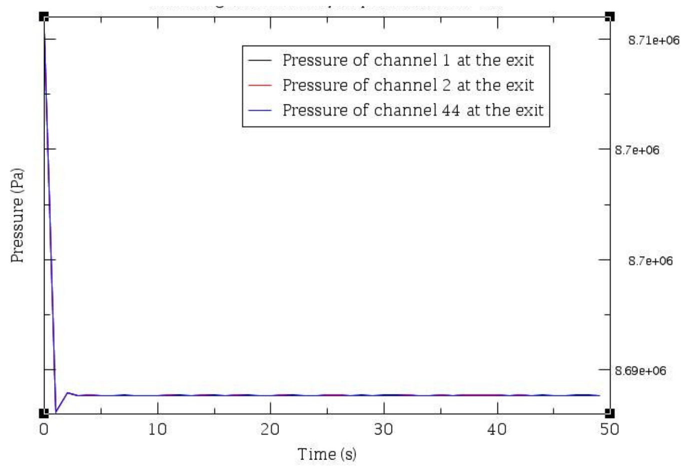

Figure 6.1. Output Pressure Change with Time

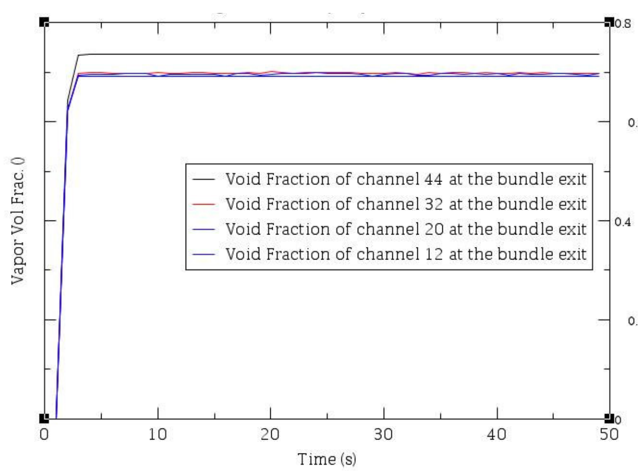

Figure 6.2. Subchannel Void Fraction Change with Time

10. Noding Change: There is no need to change node size after optimum node size met the error criteria given in 9^{th} element.

6.1.3. Step-3

11. Filter: This element has two components: selection of the bundle and selection of the experimental cases with Spanning Algorithm.

a. **Selection of Bundle Type**: Before the experimental case selection, bundle type has to be selected. NUPEC used different bundle types for various BFBT exercises. The bundle types used for the steady state void distribution, steady state critical power, steady state single and two phase pressure drop exercises were given in Table 6.5. Because bundle type 4 and C2A have the same geometry type, bundle type 4 was selected for the void distribution uncertainty analysis. One common geometry type selection provides a detailed analysis on different exercises, such as, void distribution, critical power, etc.

Table 6.5. The Bundle Types in BFBT Experimental Database

Phase	Exercises		Assembly ID
Void distribution	Steady state sub-channel		0-1
			0-2
			0-3
			1
			2
			3
			4
	Steady state microscopic		0-1
			0-2
			0-3
			1
			2
			3
			4
	Transient macroscopic		4
Critical power	Steady state	*Pressure drop*	C2A (single phase)
			C2A (for two phase)
		Critical power	C2A
			C2B
			C3
	Transient	*Critical Power*	C2A

b. **Selection of the Experimental Cases:** The desired experimental cases are the cases that span the whole experimental database. Therefore, Spanning algorithm was developed and used to select the experimental cases. The steps of the spanning algorithm applied to the steady state void distribution case:

1. **Select the dependent parameter**: One dependent parameter has to be defined in this step. Bundle void fraction was selected as the dependent parameter for the void distribution case.

2. **Select the independent parameters in the database:** Pressure, flow rate and inlet sub-cooling were selected as independent parameters. These parameters are the boundary conditions of the experimental cases.

   Figure 6.3, 6.4 and 6.5 show the experimental cases' distribution based on independent parameters (Pressure, flow rate and inlet sub-cooling) versus dependent parameter (bundle void fraction) respectively.

3. **Find the minimum and maximum values of output uncertain parameter:** All experimental cases are sorted based on dependent parameters' values. Red and brown points in Figure 6.3, 6.4 and 6.5 demonstrate the minimum and maximum points respectively.

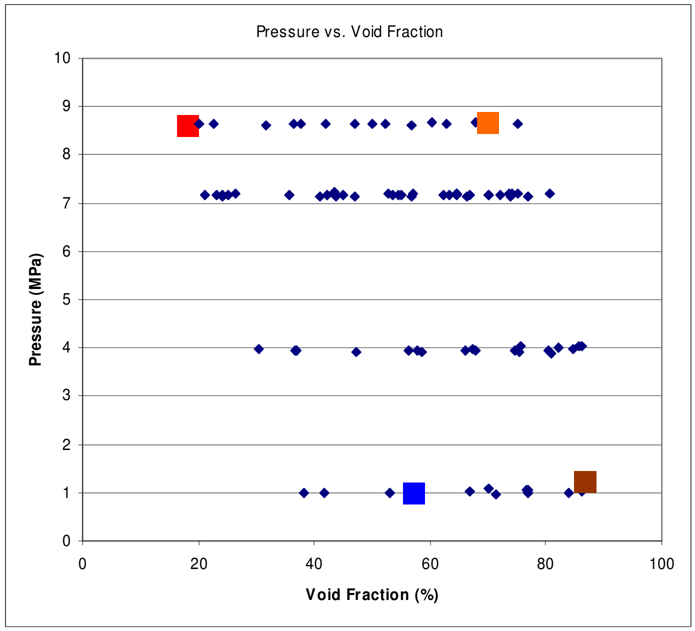

Figure 6.3. Pressure versus bundle exit void fraction for the void distribution scenario

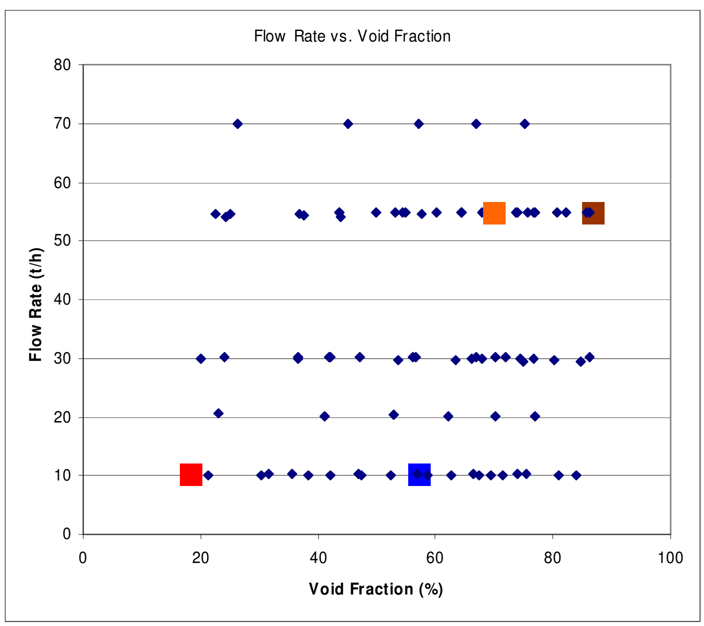

Figure 6.4. Flow rate versus bundle exit void fraction for the void distribution scenario

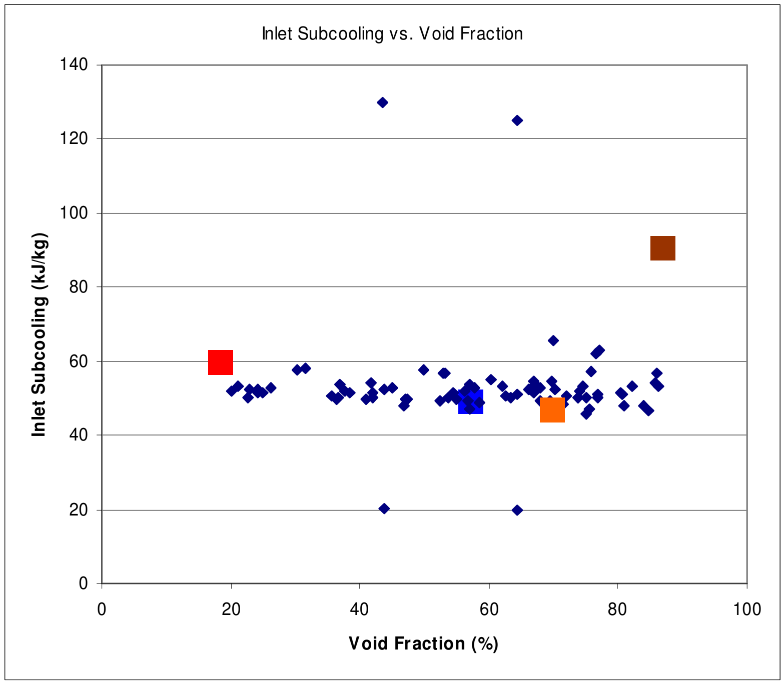

Figure 6.5. Inlet subcooling versus bundle exit void fraction for the void distribution scenario

4. **Sort the cases by using the independent parameters and select the cases:** Select the case including the maximum independent parameters' values. This case was the third selected case shown in orange color in Figure 6.3, 6.4 and 6.5. Sorted cases were used to select the 4th case including the minimum independent values. The 4th case is shown in blue color in Figure 6.3, 6.4 and 6.5. Table 6.6 summarizes the selected four cases for the void distribution.

Table 6.6. The Selected Cases for the Void Distribution

Experiment conditions	Void Fraction	Pressure (MPa)	Flow Rate (t/h)	Inlet Sub-cooling (kJ/kg)	Outlet Quality (%)	Place of the Selected Case in the Plots	Color of the selected case in Figure 6.3, 6.4 and 6.5
Test 4101-02	57.1	0.994	10.12	53.3	0.32	Bottom	Blue
Test 4101-13	86.8	1.224	55.01	92.5	4.46	Right	Brown
Test 4101-69	18.2	8.638	10.08	52.5	0.23	Left	Red
Test 4101-86	69.8	8.705	54.59	54.2	4.62	Top	Orange

12. **Finding the sampling number:** The uncertainty output is the void distribution at the BWR bundle exit. Therefore, the Wilks formula is used to obtain the number of the samples. β and γ values are commonly used as 95% in various uncertainty analyses [5, 6, 7] to provide two standard deviation distribution for a normal distribution. As a confidence and a tolerance level, 95% is an acceptable value for the US-NRC in the US-NRC- Regulatory Guide 1.157 [8].

    The number of the cases (N) was calculated as 59 by substituting γ=95/100 and β= 95/100 into the equation 5.4.

13. **Uncertainty parameters and corresponding CDFs/SCDFs:** PIRT includes four categories of dominant phenomena of steady state void distribution:

    i. Boundary condition effect,

    ii. Geometry effect,

iii. Hydraulic model parameter effect,

iv. Thermal model parameter effect.

The expert groups ranked some of the phenomena as low because they decided that these phenomena do not affect the output uncertainty parameter(s). Therefore, the low ranked parameters are discarded from the uncertainty analysis. The only important phenomena for the uncertainty analysis are medium and high ranked phenomena.

The boundary condition phenomenon effect includes two medium and two high ranked parameters. These parameters are operating pressure, flow rate, power and inlet flow temperature. All of them are used in the uncertainty analysis.

Geometry effect phenomenon includes only two medium and two highly ranked uncertain parameters. The medium ranked parameters are fraction of channel area blocked by grid and grid perimeter. Because spacer loss coefficient represents these parameters, spacer loss coefficient (in hydraulic effect table) was used instead of these parameters. Heated perimeter is high ranked perimeter but it is not used in the COBRA-TF input.

Hydraulic model effect phenomenon includes three high ranked parameters and five medium ranked parameters. The high ranked parameters are the mixing coefficient, equilibrium distribution weighing factor in void drift and interfacial friction factor. Void drift is accounted in COBRA-TF. When mixing coefficient is changed, both void drift and mixing coefficient are changed essentially. Therefore, mixing and interfacial friction factor are used in the uncertainty analysis. The medium ranked parameters are the loss coefficient (velocity head) for a gap, the grid loss coefficient (velocity head), drag coefficient for bubble flow regime, and drag coefficient for drop flow regime, interfacial friction factor for film flow regime and two phase friction factor. Two phase friction factor is not used in the 3 field COBRA-TF (RBHT) equations. Except two phase friction factor all the medium ranked parameters were selected for the uncertainty analysis.

The phenomenon of thermal model effect includes seven medium ranked parameters. These parameters are single phase liquid heat transfer coefficient, subcooled nucleate boiling heat transfer coefficient, saturated boiling region heat transfer coefficient, entrainment rate, de-entrainment rate for film flow, de-entrainment on grid spacers and spacer grid enhancement for entrained phase. Entrainment rate and de-entrainment rate models include de-entrainment on grid spacers and spacer grid enhancement for entrained phase models in COBRA-TF (RBHT). Therefore, single phase liquid heat transfer coefficient, subcooled nucleate boiling heat transfer coefficient, saturated boiling region heat transfer coefficient, entrainment rate and de-entrainment rate for film flow were selected for the uncertainty analysis.

After the uncertainty parameters were obtained, the CDFs/SCDFs of the uncertainty parameters were provided with the corresponding references: Figure 6.6 through 21 demonstrate the CDFs/SCDFs of pressure [10,11,12], mass flow rate [10,11,12], power [10,11,12], inlet temperature [10,11,12], flow area [13], gap loss coefficient [14], grid loss coefficient [15, 16], mixing coefficient [9], interfacial friction factor [17], drag coefficient for a bubble [18, 19], drag coefficient for a droplet [20], single phase heat transfer coefficient [21, 22, 23], subcooled nucleate boiling heat transfer coefficient [24], saturated boiling heat transfer coefficient [24], entrainment [25, 26] and de-entrainment [25, 27] respectively. CDFs/SCDFs were obtained with the comparison between a correlation and corresponding experimental data.

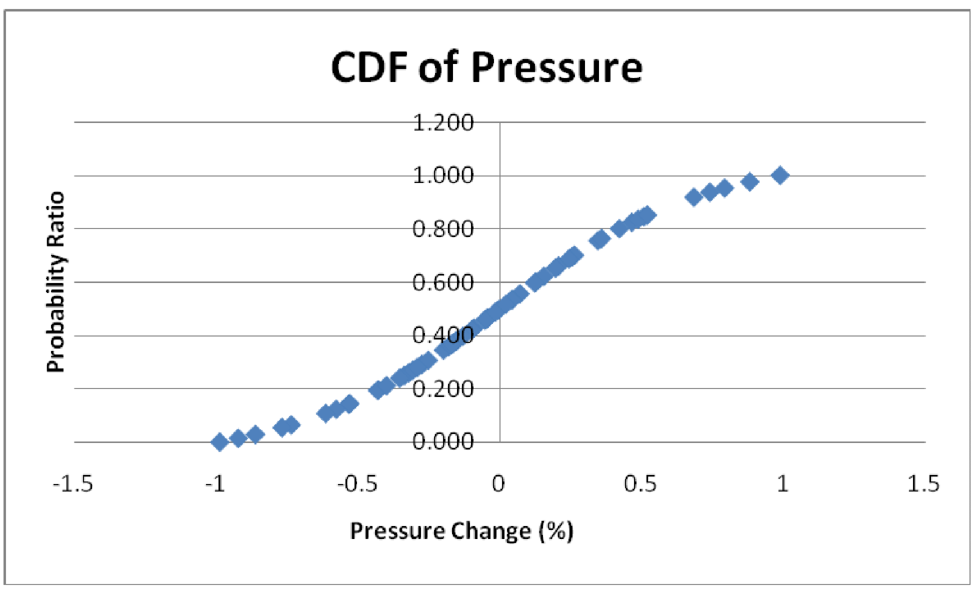

Figure 6.6. CDF/SCDF of Pressure

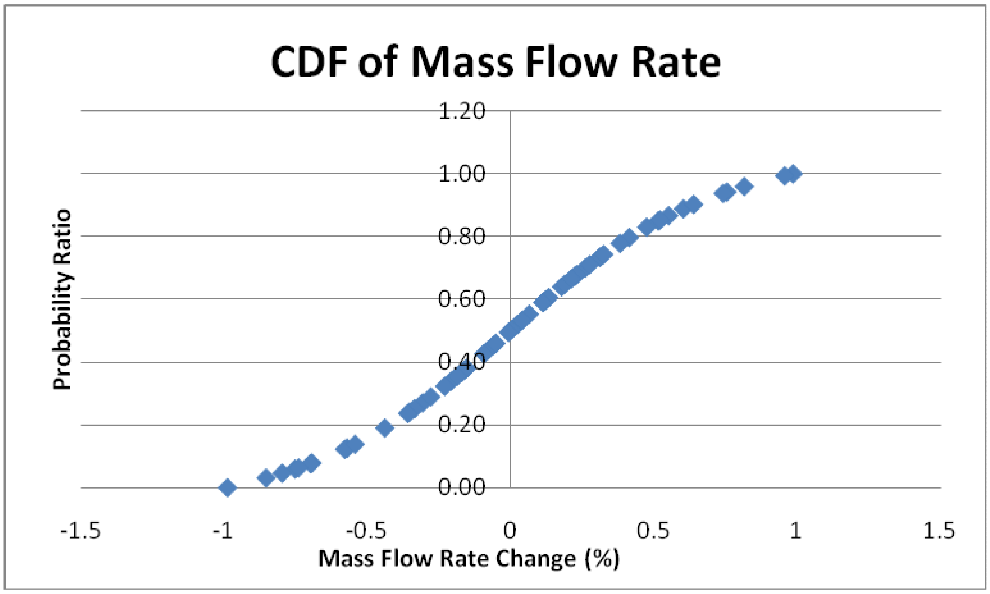

Figure 6.7. CDF/SCDF of Mass Flow Rate

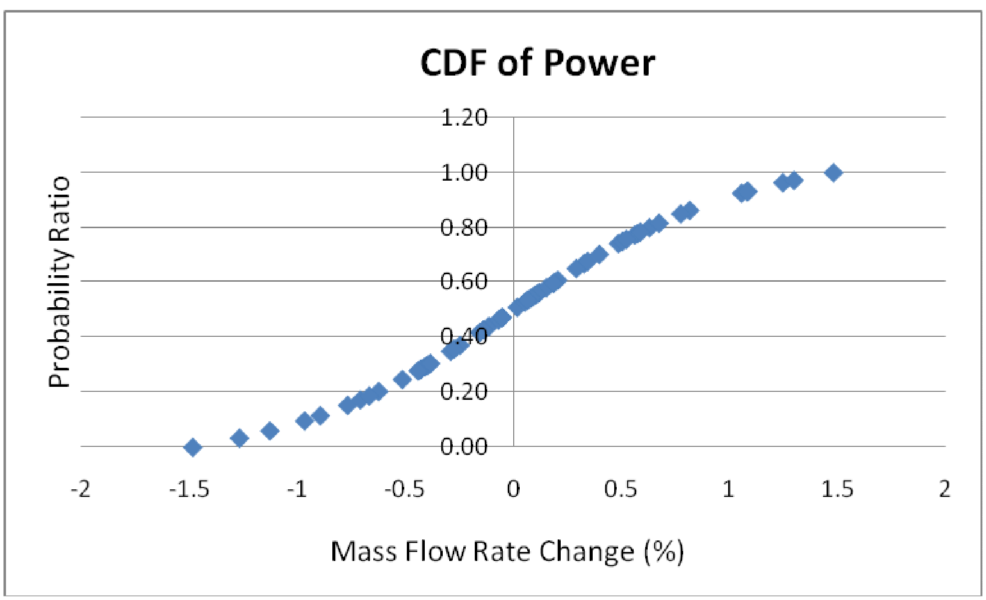

Figure 6.8. CDF/SCDF of Power

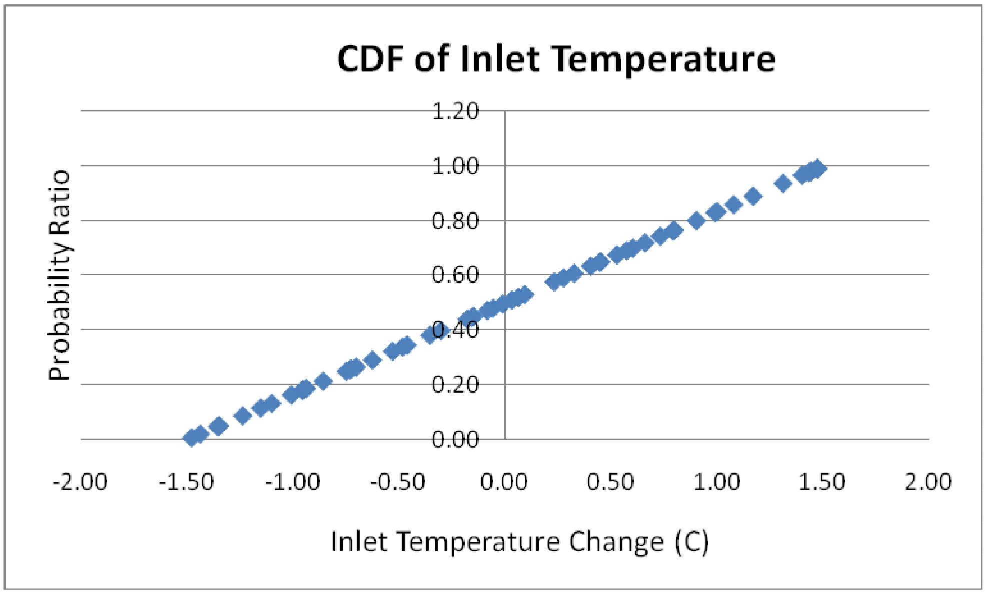

Figure 6.9. CDF/SCDF of Inlet Temperature

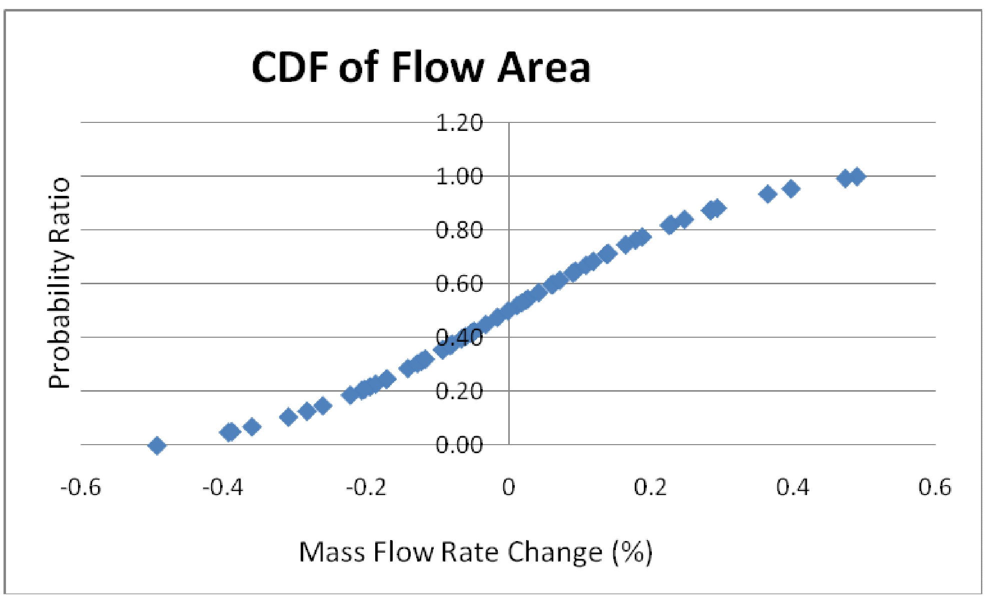

Figure 6.10. CDF/SCDF of Flow Area

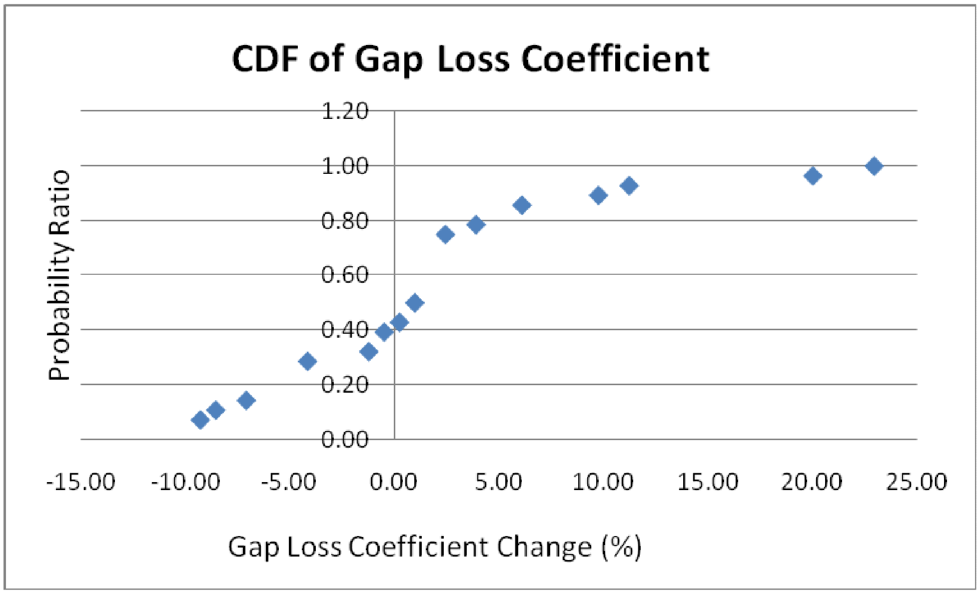

Figure 6.11. CDF/SCDF of Gap Loss Coefficient

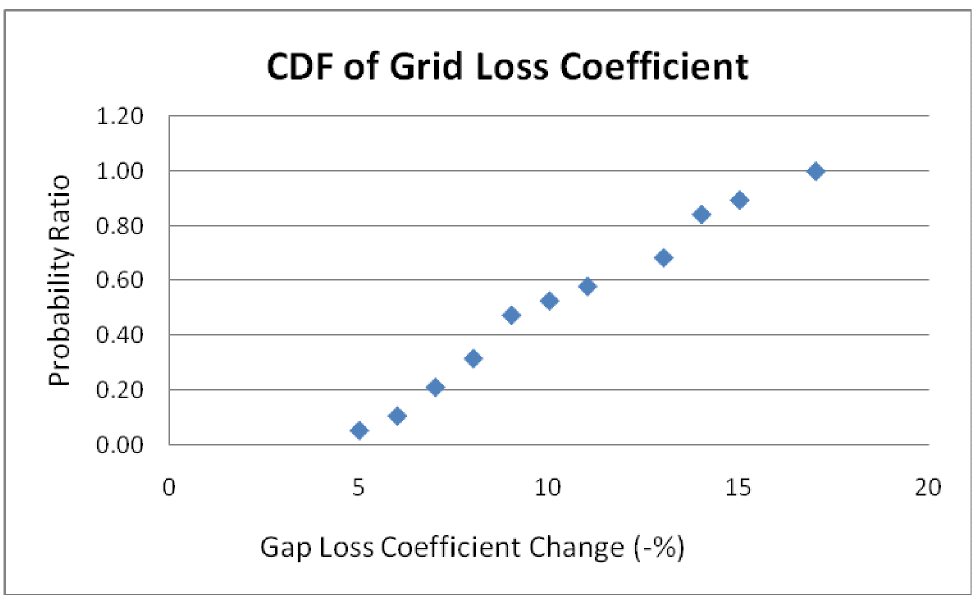

Figure 6.12. CDF/SCDF of Grid Loss Coefficient

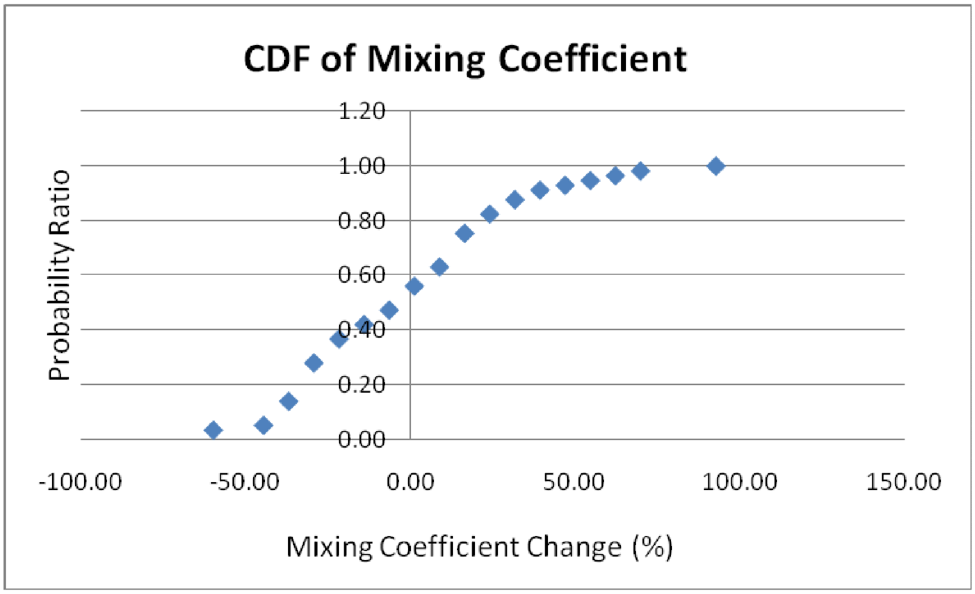

Figure 6.13. CDF/SCDF of Mixing Coefficient

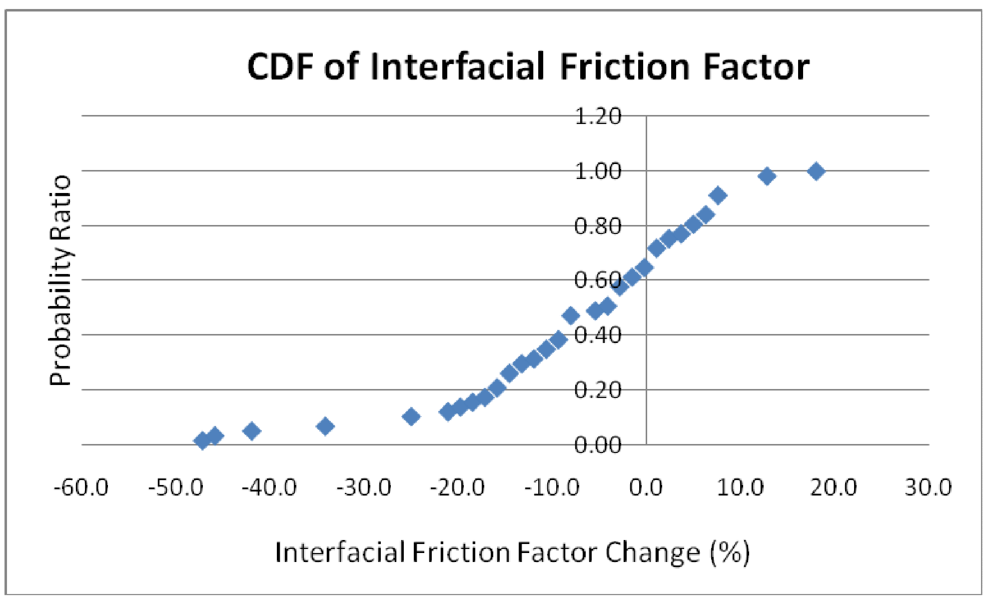

Figure 6.14. CDF/SCDF of Interfacial Friction Factor

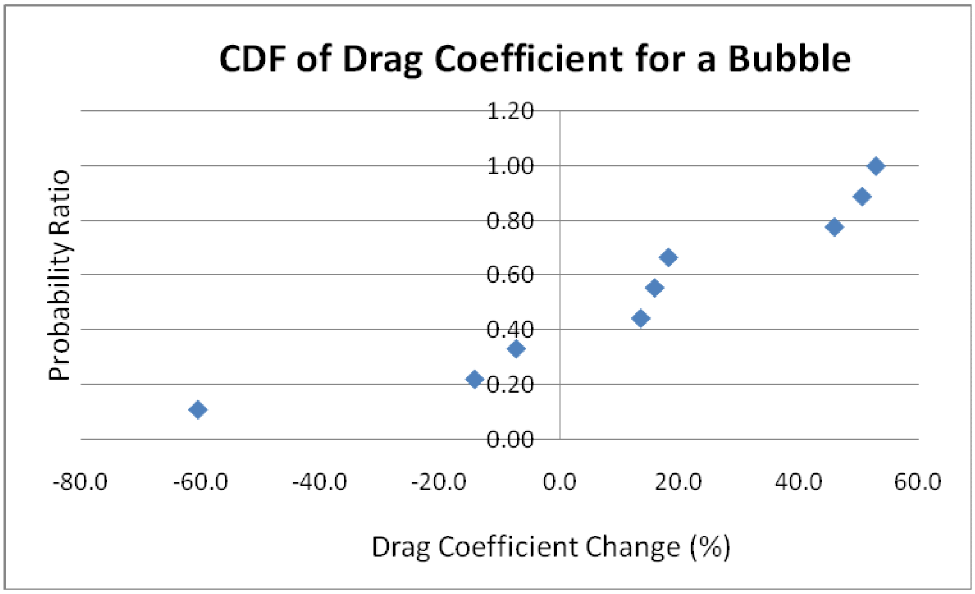

Figure 6.15. CDF/SCDF of Drag Coefficient for a Bubble

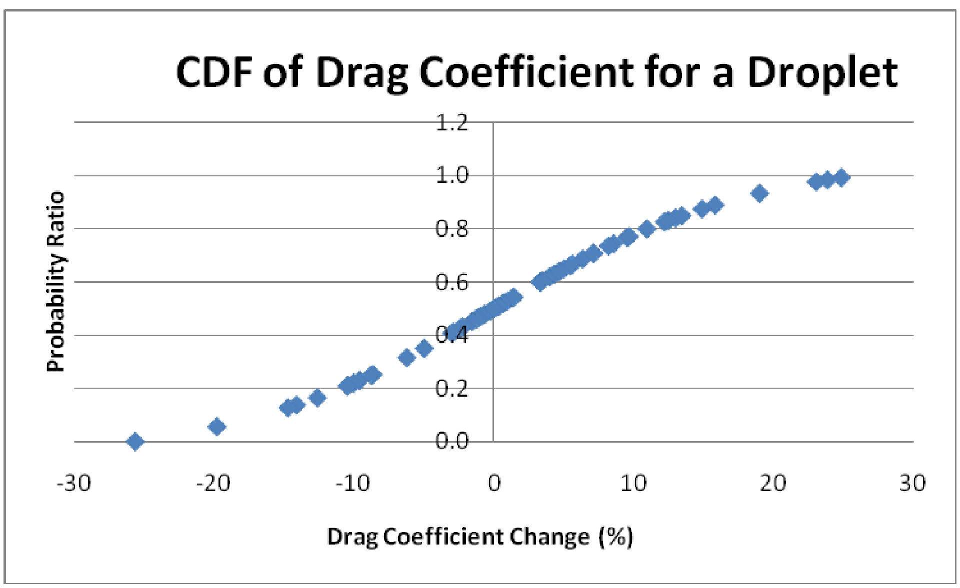

Figure 6.16. CDF/SCDF of Drag Coefficient for a Droplet

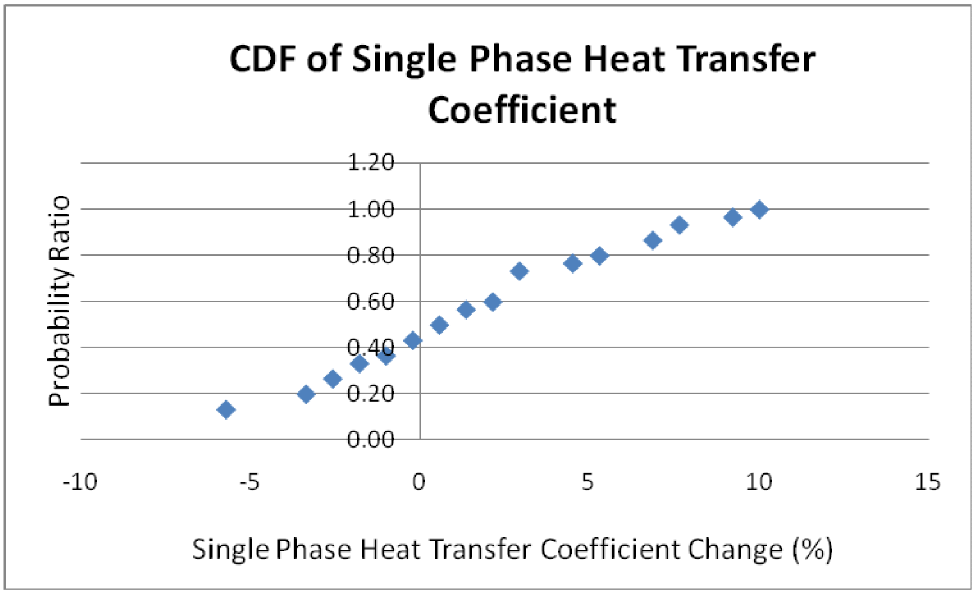

Figure 6.17. CDF/SCDF of Single Phase Heat Transfer Coefficient

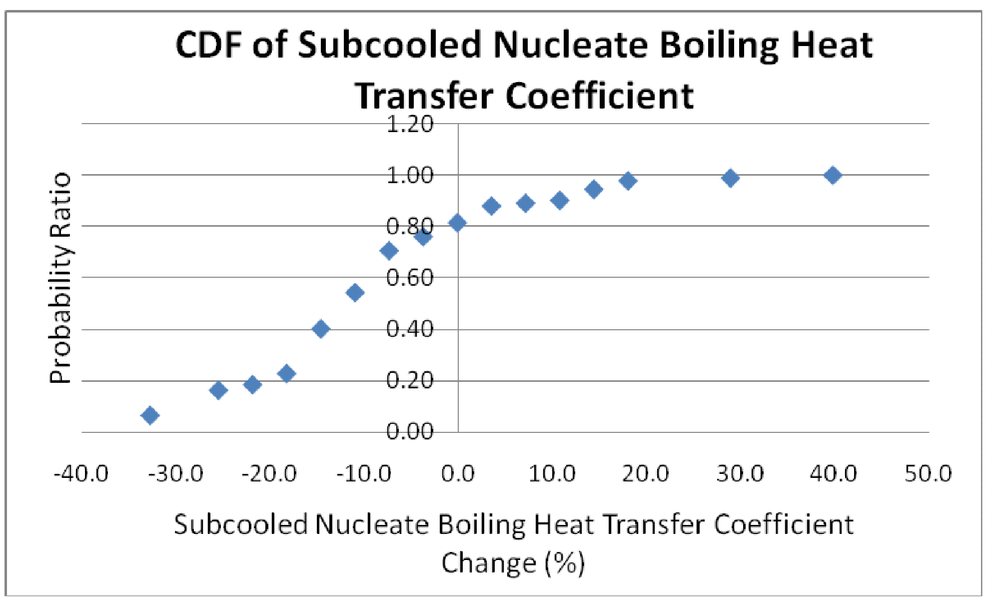

Figure 6.18. CDF/SCDF of Subcooled Nucleate Boiling Heat Transfer Coefficient

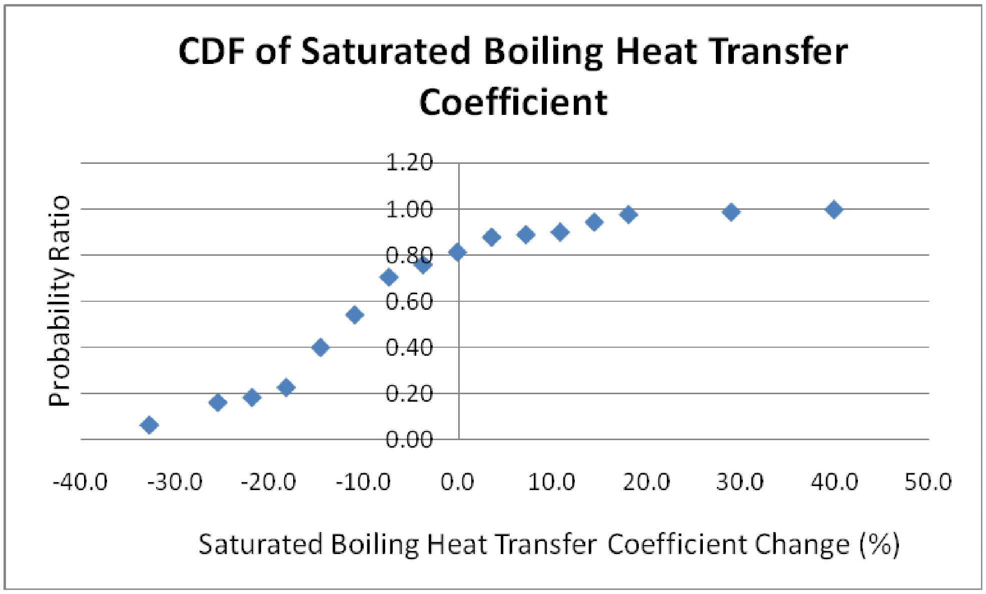

Figure 6.19. CDF/SCDF of Saturated Boiling Heat Transfer Coefficient

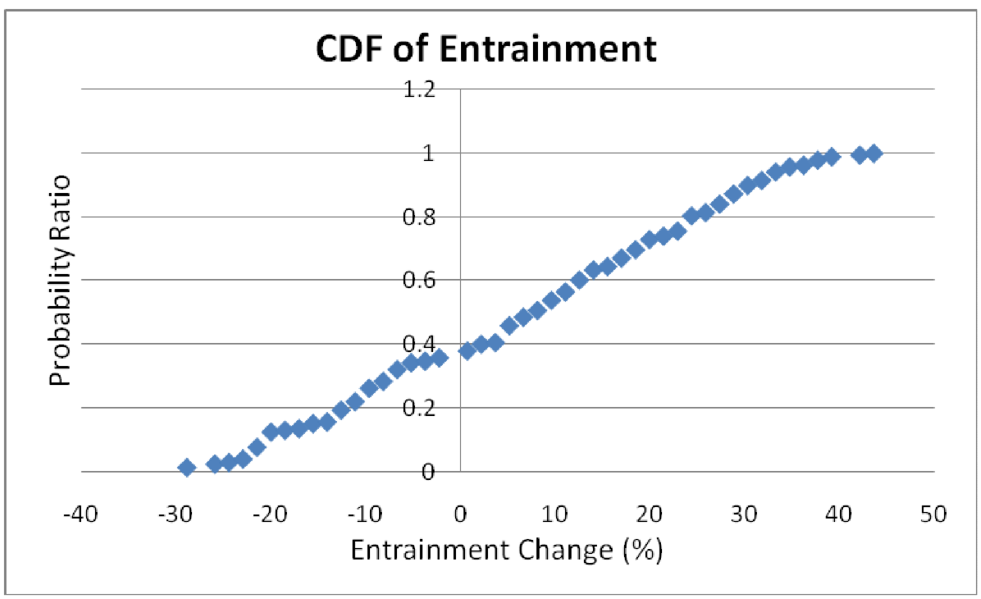

Figure 6.20. CDF/SCDF of Entrainment of Droplets

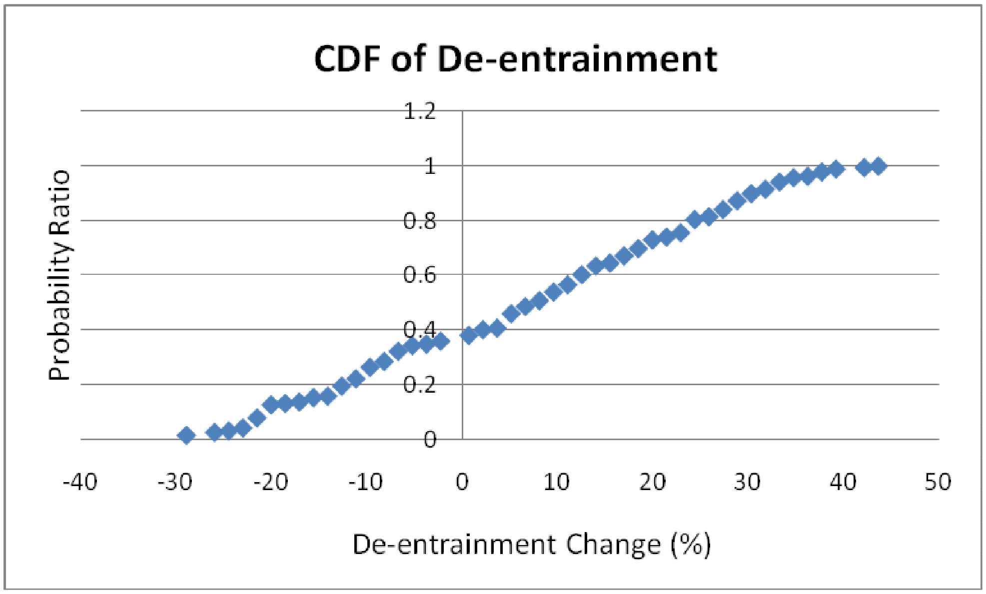

Figure 6.21. CDF/SCDF of De-entrainment of Droplets

14. **Determine Random Numbers with SRS:** Before assigning 59 random numbers to each uncertainty parameter, medium ranked uncertainty parameters have to be ranked as high or low due to CSAU [28, 29]. CSAU [28, 29] method suggests sensitivity analysis on the medium ranked parameters. However, the particular uncertainty methodology does not eliminate the medium ranked parameters. Therefore, 59 random numbers were generated for each medium and high ranked uncertainty parameter. Each number was independently generated. These numbers are used as the input to the Order Statistics Method.

SRS generated 59 random numbers, which are between 0 and 1 and assigned to each high and medium ranked uncertainty parameter. Each number generation was independent of the others. The generated random numbers are called pre-samples. Pre-samples are shown in Random Number Table in element 15.

15. **Random Number Table**: The results of 14th element, pre-samples, were recorded into the random number table (Table 6.7).

Table 6.7. Random (or Pre-sample) Table for Void Distribution

ID	Pressure	Flow rate	Power	Inlet Temperature	Flow Area	Gap loss Coefficient	Grid Loss Coefficient	Mixing Coefficient	fi	CDb	CDd	HTC_{single}	HTC_{sub}	HTC_{sat}	Entrainment	De-entrainment
1	0.60	0.13	0.86	0.16	0.36	0.57	0.21	0.61	0.45	0.82	0.41	0.49	0.71	0.59	0.14	0.97
2	0.06	0.73	0.20	0.48	0.36	0.36	0.47	0.60	0.66	0.56	0.93	0.86	0.74	0.26	0.41	0.06
3	0.14	0.24	0.51	0.26	0.82	0.50	0.75	0.84	0.80	0.88	0.51	0.66	0.92	0.81	0.28	0.72
4	0.14	0.83	0.00	0.97	0.42	0.98	0.31	0.29	0.78	0.30	0.47	0.53	0.16	0.04	0.04	0.38
5	0.47	0.64	0.56	0.98	1.00	0.70	0.30	0.37	0.79	0.70	0.60	0.50	0.60	0.76	0.78	0.18
6	0.56	0.60	0.61	0.99	0.42	0.40	0.75	0.85	1.00	0.95	0.77	0.36	0.12	0.35	0.82	0.60
7	0.62	0.08	0.70	0.76	0.93	0.97	0.57	0.77	0.81	0.20	0.16	0.39	0.21	0.71	0.30	0.55
8	0.20	0.19	0.96	0.80	0.65	0.94	0.67	0.37	0.48	0.54	0.62	0.56	0.00	0.65	0.55	0.65
9	0.38	0.44	0.47	0.45	0.54	0.95	0.44	0.59	0.62	0.33	0.65	0.70	0.25	0.73	0.65	0.42
10	0.46	0.59	0.60	0.50	0.21	0.38	0.31	0.52	0.43	0.71	0.63	0.57	0.22	0.44	0.71	0.63
11	0.19	0.55	0.35	0.13	0.57	0.36	0.73	0.50	0.77	0.17	0.54	0.67	0.72	0.82	0.61	0.86
12	0.01	0.85	0.93	0.02	0.22	0.51	0.40	0.12	0.70	0.60	0.47	0.33	0.93	0.78	0.87	0.63
13	0.25	0.87	0.78	0.99	0.77	0.12	0.88	0.05	0.00	0.85	0.06	0.42	0.76	0.40	0.69	0.60
14	0.00	0.85	0.30	0.70	0.64	0.16	0.89	0.62	0.75	0.93	0.21	0.70	0.17	1.00	0.49	0.22
15	0.60	0.12	0.15	0.45	0.25	0.87	0.25	0.61	0.44	0.18	0.48	0.61	0.23	0.37	0.15	0.69
16	0.70	0.70	0.93	0.51	0.11	0.09	0.93	0.58	0.81	0.51	0.49	0.69	0.35	1.00	0.88	0.50
17	0.53	0.52	0.29	0.47	0.45	0.03	0.52	0.20	0.76	0.80	0.14	0.50	0.20	0.51	0.65	0.34
18	0.36	0.89	0.55	0.98	0.71	0.12	0.17	0.69	0.49	0.30	0.53	0.87	0.36	0.80	0.71	0.10
19	0.43	1.00	1.00	0.53	0.13	0.63	0.62	0.56	0.08	0.26	0.83	0.90	1.00	0.54	0.68	0.78
20	0.46	0.14	0.67	0.32	0.60	0.16	0.51	0.76	0.48	0.40	0.45	0.36	0.51	0.47	0.43	1.00

where fi: interfacial friction factor, CDb: Drag Coefficient for a Bubble, CDd: Drag Coefficient for a Droplet, HTCsingle: Single Phase Heat Transfer Coefficient, HTCsub: Subcooled Nucleate Boiling Heat Transfer Coefficient, HTCsat: Saturated Boiling Heat Transfer Coefficient, Entrainment: Entrainment rate, De-entrainment: De-entrainment rate

Table 6.7. Random (or Pre-sample) Table for Void Distribution (Cont.)

ID	Pressure	Flow rate	Power	Inlet Temperature	Flow Area	Gap loss Coefficient	Grid Loss Coefficient	Mixing Coefficient	fi	CDb	CDd	HTCsingle	HTCsub	HTCsat	Entrainment	De-entrainment
21	0.80	0.90	0.58	0.01	0.15	0.05	0.53	0.67	0.73	0.92	0.98	0.46	0.17	0.72	0.43	0.29
22	0.03	0.03	0.44	0.25	0.87	0.50	0.23	0.27	0.93	0.81	0.25	0.34	0.73	0.00	0.80	0.07
23	0.70	0.37	0.46	0.05	0.52	0.86	0.78	0.00	0.33	0.49	0.69	0.52	0.61	0.47	0.17	0.48
24	0.66	0.43	0.85	0.21	0.48	0.69	0.51	0.55	0.52	0.37	0.42	0.90	0.34	0.31	0.55	0.50
25	0.42	0.00	0.29	0.72	0.29	0.75	0.30	0.24	0.70	0.92	0.99	0.75	0.46	0.74	0.94	0.70
26	0.26	0.67	0.65	0.98	0.54	0.92	0.75	0.82	0.73	0.52	0.00	0.95	0.85	0.65	0.56	0.77
27	0.12	0.60	0.53	0.29	0.76	0.64	0.30	0.46	0.80	0.65	0.64	0.88	0.29	0.31	0.00	0.95
28	0.38	0.96	0.60	0.99	0.41	0.81	0.63	0.72	0.49	0.83	0.77	0.68	0.99	0.82	0.86	0.03
29	0.11	0.37	0.43	0.18	0.42	0.40	0.96	0.41	0.20	0.23	0.23	0.47	0.58	0.67	0.71	0.14
30	0.46	0.27	0.56	0.52	0.23	0.20	0.96	0.70	0.84	0.46	0.71	0.55	0.26	0.99	0.41	0.87
31	0.95	0.99	0.30	0.67	0.75	0.82	0.12	0.72	0.93	0.66	0.89	0.54	0.43	0.72	0.08	0.37
32	0.53	0.53	0.80	0.99	0.25	0.89	0.15	0.62	0.53	0.73	0.71	0.55	0.90	0.63	0.37	0.77
33	0.29	0.74	0.54	0.83	0.84	0.76	0.92	0.80	0.41	0.48	0.52	0.68	0.74	0.33	0.52	0.66
34	0.98	0.50	0.42	0.44	0.99	0.55	0.40	0.36	0.70	0.18	0.32	0.34	0.64	0.71	0.78	0.07
35	0.92	0.34	0.28	0.12	0.00	0.33	0.36	0.54	0.11	0.84	0.41	0.50	0.60	0.61	0.40	0.14
36	0.35	0.71	0.74	0.77	0.31	0.51	0.57	0.24	0.60	1.00	0.66	0.42	0.12	0.70	0.42	0.68
37	0.65	0.25	0.03	0.65	0.71	0.56	0.00	0.46	0.50	0.23	0.74	0.82	0.85	0.60	0.25	0.73
38	0.82	0.45	0.17	0.18	0.42	0.55	0.10	0.45	0.41	0.77	0.84	0.77	0.68	0.63	0.70	0.30
39	0.76	0.80	0.54	0.63	0.19	0.32	0.07	0.85	0.61	0.27	0.46	0.68	0.12	0.65	0.40	0.31
40	0.27	0.38	0.54	0.94	0.05	0.38	0.62	0.07	0.79	0.10	0.54	0.50	0.70	0.53	0.06	0.53
41	0.31	0.29	0.19	0.86	0.87	0.35	0.46	0.36	0.50	0.19	0.43	0.00	0.41	0.76	0.64	0.85
42	0.28	0.32	0.93	0.59	0.71	0.06	0.25	0.82	0.28	0.16	0.25	0.99	0.47	0.85	0.68	0.51
43	0.50	0.50	0.12	0.38	0.38	0.91	0.07	0.73	0.94	0.83	0.67	0.98	0.45	0.75	1.00	0.42
44	0.85	0.06	0.28	0.61	0.30	0.22	0.30	1.00	0.43	0.41	0.83	0.40	0.72	0.39	0.26	0.65
45	0.21	0.46	0.47	0.69	0.60	0.19	0.78	0.38	0.51	0.69	0.22	0.60	0.25	0.67	0.42	0.53
46	0.36	0.36	0.77	0.89	0.88	0.60	0.66	0.46	0.90	0.85	0.98	0.56	0.55	0.67	0.92	0.93
47	0.37	0.74	0.75	0.26	0.61	0.18	0.76	0.22	0.82	0.17	0.50	0.41	0.69	0.30	0.35	0.74
48	0.05	0.68	0.37	0.34	0.67	0.30	0.72	0.69	0.73	0.24	0.13	0.82	0.76	0.48	0.52	0.91
49	0.84	0.24	0.97	0.35	0.05	0.54	0.23	0.61	0.75	0.74	0.52	0.47	0.63	0.19	0.86	0.30
50	0.94	0.61	0.36	0.58	0.50	0.84	0.43	0.95	0.96	0.20	0.80	0.38	0.98	0.50	0.50	0.25
51	0.69	0.65	0.68	0.09	0.82	0.92	0.19	0.44	0.81	0.41	0.85	0.72	0.68	0.37	0.89	0.85
52	0.24	0.08	0.31	0.27	0.32	0.65	0.56	0.31	0.82	0.60	0.51	0.83	0.30	0.50	0.99	0.90
53	0.37	0.05	0.10	0.65	0.68	0.51	0.40	0.53	0.44	0.50	0.88	0.31	0.55	0.57	0.87	0.72
54	1.00	0.67	0.43	0.05	0.40	0.21	0.72	0.37	0.56	0.26	0.50	0.94	0.17	0.44	0.60	0.99
55	0.40	0.94	0.06	0.74	0.53	0.23	0.63	0.27	0.83	0.26	0.60	0.32	0.44	0.51	0.38	0.70
56	0.85	0.78	0.78	0.05	0.21	0.62	0.65	0.46	0.13	0.09	0.21	0.70	0.55	0.70	0.65	0.18
57	0.49	0.06	0.76	0.40	0.37	0.23	0.74	0.65	0.56	0.34	0.74	0.65	0.41	0.60	0.60	0.84
58	0.76	0.59	0.82	0.83	0.07	0.53	0.18	0.92	0.72	0.71	0.60	0.76	0.83	0.96	0.85	0.80
59	0.52	0.94	0.25	0.19	0.95	0.30	0.65	0.80	0.70	0.45	0.35	0.33	0.45	0.70	0.95	0.46

where fi: interfacial friction factor, CDb: Drag Coefficient for a Bubble, CDd: Drag Coefficient for a Droplet, HTCsingle: Single Phase Heat Transfer Coefficient, HTCsub: Subcooled Nucleate Boiling Heat Transfer Coefficient, HTCsat: Saturated Boiling Heat Transfer Coefficient, Entrainment: Entrainment rate, De-entrainment: De-entrainment rate

16. **Sampling with Order Statistics:** CDFs/SCDFs of the uncertainty parameters and pre-samples have been obtained until 16th element. The inverse function values of the CDFs/SCDFs are the sample values. There are two methods to find the inverse function value of the CDF/SCDF:

    a. **Using inverse function of CDF/SCDF**: A mathematical function has to be defined to use the inverse function of CDF. This solution method's main disadvantage is the existence of function fitting's accuracy. In other words, a function is fitted to the CDF/SCDF data and this fitted function has an accuracy margin between function and data. This accuracy will change the uncertainty results.

    b. **Using interpolation between CDF/SCDF data points**: This method just uses the CDF/SCDF data points. If there is a pre-sample between two CDF/SCDF data points, interpolation is used to find the inverse function value by just using the data points. The interpolation formula was given in equation 6.1.

    $$x= (y-y_1)/(y_2-y_1)* (x_2-x_1) + x_1 \qquad (6.1)$$

    where

    x, x_1 and x_2 : x€ Real Numbers,

    $f(x)$: The function depend on x

    $y=f(x)$, $y_1=f(x_1)$, $y_2=f(x_2)$

Second method (using interpolation between CDF/SCDF data points) was selected not to create fitted function accuracy affecting uncertainty results. Samples were selected by using pre-samples and interpolation and shown in Table 6.8. Inlet temperature was converted to the inlet enthalpy to make the sample matrix appropriate to the COBRA-TF (RBHT) input deck.

Table 6.8. Sample Table for Void Distribution

ID	Pressure	Flow rate	Power	Inlet Enthalpy	Flow Area	Gap loss Coefficient	Grid Loss Coefficient	Mixing Coefficient	fi	CDb	CDd	HTC_{single}	HTC_{sub}	HTC_{sat}	Entrainment	De-entrainment
1	0.13	-0.57	0.82	-0.27	-0.09	1.42	-7.00	6.28	-8.49	47.54	-2.91	0.39	-6.84	-9.96	-16.91	36.89
2	-0.74	0.31	-0.62	-0.02	-0.09	-0.76	-8.98	5.34	-0.09	16.05	19.01	6.77	-4.99	-17.63	3.64	-22.17
3	-0.53	-0.35	0.02	-0.20	0.23	1.02	-13.42	25.61	4.66	50.04	0.33	2.50	12.36	-0.57	-8.40	19.57
4	-0.53	0.48	-1.48	0.37	-0.05	21.45	-7.95	-28.40	3.90	-9.34	-1.14	0.92	-25.61	-32.76	-22.99	0.51
5	-0.04	0.18	0.12	0.38	0.49	2.14	-7.85	-21.14	4.27	26.52	3.29	0.57	-9.74	-3.74	23.48	-13.40
6	0.07	0.12	0.21	0.39	-0.05	-0.41	-13.42	27.71	17.95	51.88	9.52	-1.16	-28.92	-15.65	26.23	12.39
7	0.15	-0.69	0.40	0.21	0.36	20.12	-10.83	18.33	5.02	-25.15	-12.65	-0.73	-19.92	-7.13	-7.66	9.92
8	-0.43	-0.44	1.25	0.24	0.09	14.08	-12.73	-22.03	-7.20	15.50	3.97	1.22	-32.76	-8.63	9.96	15.55
9	-0.15	-0.08	-0.05	-0.04	0.03	16.54	-8.79	4.16	-1.38	-7.34	5.01	2.74	-17.77	-5.73	15.70	3.84
10	-0.04	0.12	0.19	0.00	-0.21	-0.57	-7.95	-2.31	-8.84	30.16	4.31	1.53	-18.63	-13.65	19.18	13.84
11	-0.43	0.07	-0.29	-0.29	0.04	-0.76	-13.29	-4.19	3.63	-34.83	1.35	2.56	-6.64	0.15	12.81	28.21
12	-0.92	0.52	1.06	-0.38	-0.19	1.04	-8.53	-38.65	0.63	16.80	-0.96	-1.81	13.04	-2.75	28.69	13.91
13	-0.34	0.55	0.57	0.39	0.19	-7.99	-14.72	-49.51	-47.26	48.96	-19.84	-0.42	-3.54	-14.67	17.83	12.45
14	-0.99	0.52	-0.39	0.16	0.09	-6.80	-14.91	12.86	2.85	51.48	-10.46	4.15	-25.26	39.68	6.59	-10.90
15	0.12	-0.58	-0.77	-0.04	-0.17	7.56	-7.38	6.80	-8.57	-33.84	-0.67	2.22	-18.30	-15.30	-16.12	17.79
16	0.26	0.26	1.09	0.01	-0.31	-8.89	-15.67	2.76	5.02	14.93	-0.27	2.68	-15.69	39.78	29.40	7.49
17	0.04	0.03	-0.43	-0.02	-0.03	-9.27	-9.88	-33.76	2.43	46.78	-14.14	0.57	-20.33	-11.98	15.70	-5.39
18	-0.18	0.60	0.10	0.38	0.14	-7.94	-6.62	12.43	-6.26	-9.04	0.98	6.85	-15.41	-1.13	19.17	-20.91
19	-0.09	0.99	1.48	0.02	-0.28	1.75	-11.78	0.97	-31.07	-11.89	12.20	7.31	39.68	-11.01	17.66	23.67
20	-0.05	-0.54	0.33	-0.14	0.06	-6.68	-9.69	19.09	-7.58	-1.24	-1.57	-1.32	-4.99	-8.44	4.92	43.57
21	0.42	0.64	0.15	-0.39	-0.26	-9.27	-10.07	10.97	1.45	51.26	23.87	0.14	-23.81	-6.14	4.33	-8.05
22	-0.86	-0.85	-0.11	-0.20	0.28	1.02	-7.19	-29.92	8.65	47.29	-8.68	-1.67	-6.00	-32.76	24.20	-21.75
23	0.26	-0.17	-0.07	-0.36	0.01	6.62	-13.61	-59.87	-11.69	14.51	6.35	0.81	-9.52	-12.88	-13.51	5.91
24	0.21	-0.09	0.78	-0.23	-0.02	2.14	-9.69	-0.04	-4.01	0.34	-2.46	7.27	-15.86	-16.45	9.94	7.49
25	-0.10	-0.99	-0.41	0.18	-0.14	2.46	-7.85	-31.56	0.65	51.17	24.86	3.72	-13.05	-5.19	32.91	18.56

where fi: interfacial friction factor, CDb: Drag Coefficient for a Bubble, CDd: Drag Coefficient for a Droplet, HTCsingle: Single Phase Heat Transfer Coefficient, HTCsub: Subcooled Nucleate Boiling Heat Transfer Coefficient, HTCsat: Saturated Boiling Heat Transfer Coefficient, Entrainment: Entrainment rate, De-entrainment: De-entrainment rate

Table 6.8. Sample Table for Void Distribution (Cont.)

ID	Pressure	Flow rate	Power	Inlet Enthalpy	Flow Area	Gap loss Coefficient	Grid Loss Coefficient	Mixing Coefficient	f_i	CD_b	CD_d	HTC_{single}	HTC_{sub}	HTC_{sat}	Entrainment	De-entrainment
26	-0.32	0.23	0.29	0.38	0.03	11.07	-13.42	23.10	1.34	15.14	-25.69	8.40	1.86	-8.68	10.48	23.20
27	-0.58	0.12	0.05	-0.17	0.18	1.84	-7.85	-8.79	4.65	17.77	4.66	7.01	-17.05	-16.49	-28.96	33.59
28	-0.15	0.82	0.19	0.39	-0.06	4.61	-11.97	14.11	-5.71	48.12	9.68	2.62	25.66	-0.08	28.07	-25.50
29	-0.61	-0.16	-0.14	-0.26	-0.05	-0.27	-16.24	-15.93	-16.19	-13.84	-9.63	0.20	-10.16	-8.18	18.86	-16.92
30	-0.05	-0.31	0.11	0.02	-0.19	-5.95	-16.24	13.02	6.22	13.97	7.11	1.21	-17.67	33.98	3.49	28.52
31	0.79	0.96	-0.40	0.14	0.17	5.10	-6.14	14.26	9.20	17.96	15.81	1.07	-13.79	-6.36	-21.69	-0.26
32	0.04	0.04	0.63	0.39	-0.17	9.84	-6.43	7.47	-3.75	34.80	7.11	1.22	10.04	-9.01	-1.21	23.14
33	-0.28	0.31	0.08	0.26	0.25	2.84	-15.48	21.15	-9.07	14.26	0.65	2.61	-4.99	-16.17	8.48	16.31
34	0.88	0.00	-0.16	-0.05	0.47	1.32	-8.53	-22.43	0.70	-32.91	-6.24	-1.56	-8.95	-6.89	23.72	-21.81
35	0.68	-0.21	-0.43	-0.31	-0.49	-1.12	-8.28	-0.78	-23.55	48.40	-3.02	0.58	-9.74	-9.61	2.83	-17.80
36	-0.20	0.28	0.49	0.21	-0.12	1.06	-10.83	-31.70	-2.16	52.80	5.46	-0.33	-28.43	-7.52	3.97	17.22
37	0.20	-0.33	-1.27	0.12	0.14	1.38	-5.00	-8.74	-4.85	-13.74	8.55	5.77	2.07	-9.70	-10.16	20.11
38	0.46	-0.06	-0.71	-0.25	-0.05	1.30	-5.90	-10.09	-9.13	45.12	12.99	4.65	-7.90	-9.16	18.48	-7.73
39	0.35	0.42	0.07	0.11	-0.22	-1.34	-5.33	27.71	-1.87	-11.31	-1.25	2.62	-28.73	-8.67	1.89	-7.27
40	-0.31	-0.15	0.07	0.35	-0.39	-0.60	-11.78	-43.53	4.12	-60.47	1.41	0.52	-7.57	-11.43	-22.39	8.98
41	-0.25	-0.28	-0.67	0.29	0.29	-0.93	-8.91	-22.05	-4.88	-28.93	-2.26	-5.74	-14.42	-4.03	14.34	27.50
42	-0.29	-0.23	1.08	0.07	0.14	-9.27	-7.38	23.23	-13.88	-38.09	-8.79	9.78	-12.88	1.57	17.18	8.23
43	0.00	-0.01	-0.89	-0.10	-0.08	10.49	-5.33	14.89	9.36	48.04	5.60	9.46	-13.40	-4.51	43.57	3.93
44	0.51	-0.75	-0.44	0.09	-0.13	-5.50	-7.85	92.66	-8.82	7.32	12.46	-0.66	-6.50	-14.83	-9.72	15.53
45	-0.40	-0.05	-0.05	0.15	0.06	-6.10	-17.00	-20.20	-4.22	24.63	-10.06	2.15	-17.73	-8.24	3.92	9.03
46	-0.18	-0.19	0.56	0.31	0.29	1.61	-12.54	-8.82	7.29	49.05	23.07	1.29	-10.88	-8.18	31.89	32.63
47	-0.16	0.33	0.51	-0.19	0.07	-6.39	-13.48	-32.73	5.39	-34.77	0.00	-0.54	-7.79	-16.76	-4.60	21.76
48	-0.77	0.23	-0.25	-0.13	0.11	-3.32	-13.23	12.24	1.55	-13.05	-14.76	5.65	-3.94	-12.68	8.38	31.18
49	0.49	-0.36	1.30	-0.12	-0.39	1.22	-7.19	5.91	2.13	37.52	0.65	0.22	-9.03	-21.83	28.03	-7.72
50	0.74	0.13	-0.27	0.06	0.00	5.55	-8.72	56.66	10.91	-22.90	10.94	-0.81	18.60	-12.11	7.82	-10.23
51	0.24	0.19	0.34	-0.33	0.23	10.73	-6.81	-11.93	5.02	7.40	13.44	2.87	-8.00	-15.26	29.92	27.84
52	-0.35	-0.70	-0.38	-0.19	-0.12	1.89	-10.64	-27.23	5.39	16.83	0.33	5.89	-16.78	-12.14	41.04	30.58
53	-0.17	-0.80	-0.96	0.12	0.12	1.03	-8.53	-1.98	-8.64	14.78	14.89	-2.07	-10.85	-10.37	28.50	19.25
54	0.99	0.21	-0.14	-0.36	-0.07	-5.74	-13.23	-21.28	-3.27	-12.08	0.00	8.01	-23.73	-13.76	12.36	38.97
55	-0.13	0.76	-1.13	0.19	0.02	-5.19	-11.97	-29.83	5.76	-11.68	3.29	-1.95	-13.76	-11.76	-0.04	18.53
56	0.52	0.38	0.59	-0.36	-0.20	1.70	-12.35	-8.86	-20.37	-60.47	-10.50	2.71	-10.88	-7.52	15.52	-13.22
57	-0.02	-0.74	0.52	-0.08	-0.08	-5.27	-13.35	10.19	-3.20	-5.09	8.19	2.44	-14.39	-9.76	12.50	27.34
58	0.36	0.11	0.68	0.27	-0.36	1.19	-6.71	42.64	1.17	28.39	3.45	3.99	0.91	16.12	27.68	24.05
59	0.02	0.74	-0.51	-0.25	0.40	-2.72	-12.35	21.36	0.63	13.58	-5.00	-1.85	-13.43	-7.52	34.18	5.00

where fi: interfacial friction factor, CDb: Drag Coefficient for a Bubble, CDd: Drag Coefficient for a Droplet, HTCsingle: Single Phase Heat Transfer Coefficient, HTCsub: Subcooled Nucleate Boiling Heat Transfer Coefficient, HTCsat: Saturated Boiling Heat Transfer Coefficient, Entrainment: Entrainment rate, De-entrainment: De-entrainment rate

17. Uncertainty Parameter Table: Uncertainty parameter table (Table 6.9) is similar to sample table. Even though sample table demonstrates the percentage difference, uncertainty parameter table shows the ratio of the uncertainty parameters' change. The relationship between the ratio and percentage difference is given in equation 6.2. This ratio is used with new developed COBRA-TF Uncertainty Module. This module was described in the 18th, 19th and 20th element of the uncertainty system.

$$\text{(Uncertainty Parameter Ratio)} = \text{(Percentage Change of Uncertainty Parameter}+100)/100 \tag{6.2}$$

Table 6.9. Uncertainty Parameter Table for Void Distribution

ID	Pressure	Flow rate	Power	Inlet Enthalpy	Flow Area	Gap loss	Grid Loss	Mixing	fi	CDb	CDd	HTCsingle	HTCsub	HTCsat	Entrainment	De-entrainment
1	1.001	0.994	1.008	0.997	0.999	1.014	0.930	1.063	0.915	1.475	0.971	1.004	0.932	0.900	0.831	1.369
2	0.993	1.003	0.994	1.000	0.999	0.992	0.910	1.053	0.999	1.161	1.190	1.068	0.950	0.824	1.036	0.778
3	0.995	0.996	1.000	0.998	1.002	1.010	0.866	1.256	1.047	1.500	1.003	1.025	1.124	0.994	0.916	1.196
4	0.995	1.005	0.985	1.004	1.000	1.215	0.921	0.716	1.039	0.907	0.989	1.009	0.744	0.672	0.770	1.005
5	1.000	1.002	1.001	1.004	1.005	1.021	0.922	0.789	1.043	1.265	1.033	1.006	0.903	0.963	1.235	0.866
6	1.001	1.001	1.002	1.004	0.999	0.996	0.866	1.277	1.179	1.519	1.095	0.988	0.711	0.844	1.262	1.124
7	1.002	0.993	1.004	1.002	1.004	1.201	0.892	1.183	1.050	0.748	0.873	0.993	0.801	0.929	0.923	1.099
8	0.996	0.996	1.012	1.002	1.001	1.141	0.873	0.780	0.928	1.155	1.040	1.012	0.672	0.914	1.100	1.155
9	0.998	0.999	0.999	1.000	1.000	1.165	0.912	1.042	0.986	0.927	1.050	1.027	0.822	0.943	1.157	1.038
10	1.000	1.001	1.002	1.000	0.998	0.994	0.921	0.977	0.912	1.302	1.043	1.015	0.814	0.863	1.192	1.138
11	0.996	1.001	0.997	0.997	1.000	0.992	0.867	0.958	1.036	0.652	1.014	1.026	0.934	1.001	1.128	1.282
12	0.991	1.005	1.011	0.996	0.998	1.010	0.915	0.614	1.006	1.168	0.990	0.982	1.130	0.973	1.287	1.139
13	0.997	1.006	1.006	1.004	1.002	0.920	0.853	0.505	0.527	1.490	0.802	0.996	0.965	0.853	1.178	1.124
14	0.990	1.005	0.996	1.002	1.001	0.932	0.851	1.129	1.028	1.515	0.895	1.042	0.747	1.397	1.066	0.891
15	1.001	0.994	0.992	1.000	0.998	1.076	0.926	1.068	0.914	0.662	0.993	1.022	0.817	0.847	0.839	1.178
16	1.003	1.003	1.011	1.000	0.997	0.911	0.843	1.028	1.050	1.149	0.997	1.027	0.843	1.398	1.294	1.075
17	1.000	1.000	0.996	1.000	1.000	0.907	0.901	0.662	1.024	1.468	0.859	1.006	0.797	0.880	1.157	0.946
18	0.998	1.006	1.001	1.004	1.001	0.921	0.934	1.124	0.937	0.910	1.010	1.069	0.846	0.989	1.192	0.791
19	0.999	1.010	1.015	1.000	0.997	1.018	0.882	1.010	0.689	0.881	1.122	1.073	1.397	0.890	1.177	1.237
20	0.999	0.995	1.003	0.999	1.001	0.933	0.903	1.191	0.924	0.988	0.984	0.987	0.950	0.916	1.049	1.436
21	1.004	1.006	1.002	0.996	0.997	0.907	0.899	1.110	1.014	1.513	1.239	1.001	0.762	0.939	1.043	0.920
22	0.991	0.991	0.999	0.998	1.003	1.010	0.928	0.701	1.087	1.473	0.913	0.983	0.940	0.672	1.242	0.783
23	1.003	0.998	0.999	0.996	1.000	1.066	0.864	0.401	0.883	1.145	1.063	1.008	0.905	0.871	0.865	1.059
24	1.002	0.999	1.008	0.998	1.000	1.021	0.903	1.000	0.960	1.003	0.975	1.073	0.841	0.835	1.099	1.075
25	0.999	0.990	0.996	1.002	0.999	1.025	0.922	0.684	1.007	1.512	1.249	1.037	0.870	0.948	1.329	1.186
26	0.997	1.002	1.003	1.004	1.000	1.111	0.866	1.231	1.013	1.151	0.743	1.084	1.019	0.913	1.105	1.232
27	0.994	1.001	1.001	0.998	1.002	1.018	0.922	0.912	1.046	1.178	1.047	1.070	0.829	0.835	0.710	1.336

where fi: interfacial friction factor, CDb: Drag Coefficient for a Bubble, CDd: Drag Coefficient for a Droplet, HTCsingle: Single Phase Heat Transfer Coefficient, HTCsub: Subcooled Nucleate Boiling Heat Transfer Coefficient, HTCsat: Saturated Boiling Heat Transfer Coefficient, Entrainment: Entrainment rate, De-entrainment: De-entrainment rate

Table 6.9. Uncertainty Parameter Table for Void Distribution (Cont.)

ID	Pressure	Flow rate	Power	Inlet Enthalpy	Flow Area	Gap loss Coefficient	Grid Loss Coefficient	Mixing Coefficient	fi	CDb	CDd	HTCsingle	HTCsub	HTCsat	Entrainment	De-entrainment
28	0.998	1.008	1.002	1.004	0.999	1.046	0.880	1.141	0.943	1.481	1.097	1.026	1.257	0.999	1.281	0.745
29	0.994	0.998	0.999	0.997	1.000	0.997	0.838	0.841	0.838	0.862	0.904	1.002	0.898	0.918	1.189	0.831
30	1.000	0.997	1.001	1.000	0.998	0.940	0.838	1.130	1.062	1.140	1.071	1.012	0.823	1.340	1.035	1.285
31	1.008	1.010	0.996	1.001	1.002	1.051	0.939	1.143	1.092	1.180	1.158	1.011	0.862	0.936	0.783	0.997
32	1.000	1.000	1.006	1.004	0.998	1.098	0.936	1.075	0.962	1.348	1.071	1.012	1.100	0.910	0.988	1.231
33	0.997	1.003	1.001	1.003	1.002	1.028	0.845	1.211	0.909	1.143	1.007	1.026	0.950	0.838	1.085	1.163
34	1.009	1.000	0.998	1.000	1.005	1.013	0.915	0.776	1.007	0.671	0.938	0.984	0.910	0.931	1.237	0.782
35	1.007	0.998	0.996	0.997	0.995	0.989	0.917	0.992	0.764	1.484	0.970	1.006	0.903	0.904	1.028	0.822
36	0.998	1.003	1.005	1.002	0.999	1.011	0.892	0.683	0.978	1.528	1.055	0.997	0.716	0.925	1.040	1.172
37	1.002	0.997	0.987	1.001	1.001	1.014	0.950	0.913	0.951	0.863	1.086	1.058	1.021	0.903	0.898	1.201
38	1.005	0.999	0.993	0.997	0.999	1.013	0.941	0.899	0.909	1.451	1.130	1.046	0.921	0.908	1.185	0.923
39	1.003	1.004	1.001	1.001	0.998	0.987	0.947	1.277	0.981	0.887	0.987	1.026	0.713	0.913	1.019	0.927
40	0.997	0.998	1.001	1.003	0.996	0.994	0.882	0.565	1.041	0.395	1.014	1.005	0.924	0.886	0.776	1.090
41	0.997	0.997	0.993	1.003	1.003	0.991	0.911	0.779	0.951	0.711	0.977	0.943	0.856	0.960	1.143	1.275
42	0.997	0.998	1.011	1.001	1.001	0.907	0.926	1.232	0.861	0.619	0.912	1.098	0.871	1.016	1.172	1.082
43	1.000	1.000	0.991	0.999	0.999	1.105	0.947	1.149	1.094	1.480	1.056	1.095	0.866	0.955	1.436	1.039
44	1.005	0.992	0.996	1.001	0.999	0.945	0.922	1.927	0.912	1.073	1.125	0.993	0.935	0.852	0.903	1.155
45	0.996	0.999	0.999	1.002	1.001	0.939	0.830	0.798	0.958	1.246	0.899	1.021	0.823	0.918	1.039	1.090
46	0.998	0.998	1.006	1.003	1.003	1.016	0.875	0.912	1.073	1.490	1.231	1.013	0.891	0.918	1.319	1.326
47	0.998	1.003	1.005	0.998	1.001	0.936	0.865	0.673	1.054	0.652	1.000	0.995	0.922	0.832	0.954	1.218
48	0.992	1.002	0.998	0.999	1.001	0.967	0.868	1.122	1.015	0.870	0.852	1.057	0.961	0.873	1.084	1.312
49	1.005	0.996	1.013	0.999	0.996	1.012	0.928	1.059	1.021	1.375	1.007	1.002	0.910	0.782	1.280	0.923
50	1.007	1.001	0.997	1.001	1.000	1.055	0.913	1.567	1.109	0.771	1.109	0.992	1.186	0.879	1.078	0.898
51	1.002	1.002	1.003	0.997	1.002	1.107	0.932	0.881	1.050	1.074	1.134	1.029	0.920	0.847	1.299	1.278
52	0.996	0.993	0.996	0.998	0.999	1.019	0.894	0.728	1.054	1.168	1.003	1.059	0.832	0.879	1.410	1.306
53	0.998	0.992	0.990	1.001	1.001	1.010	0.915	0.980	0.914	1.148	1.149	0.979	0.891	0.896	1.285	1.192
54	1.010	1.002	0.999	0.996	0.999	0.943	0.868	0.787	0.967	0.879	1.000	1.080	0.763	0.862	1.124	1.390
55	0.999	1.008	0.989	1.002	1.000	0.948	0.880	0.702	1.058	0.883	1.033	0.980	0.862	0.882	1.000	1.185
56	1.005	1.004	1.006	0.996	0.998	1.017	0.877	0.911	0.796	0.395	0.895	1.027	0.891	0.925	1.155	0.868
57	1.000	0.993	1.005	0.999	0.999	0.947	0.866	1.102	0.968	0.949	1.082	1.024	0.856	0.902	1.125	1.273
58	1.004	1.001	1.007	1.003	0.996	1.012	0.933	1.426	1.012	1.284	1.034	1.040	1.009	1.161	1.277	1.241
59	1.000	1.007	0.995	0.997	1.004	0.973	0.877	1.214	1.006	1.136	0.950	0.982	0.866	0.925	1.342	1.050

where fi: interfacial friction factor, CDb: Drag Coefficient for a Bubble, CDd: Drag Coefficient for a Droplet, HTCsingle: Single Phase Heat Transfer Coefficient, HTCsub: Subcooled Nucleate Boiling Heat Transfer Coefficient, HTCsat: Saturated Boiling Heat Transfer Coefficient, Entrainment: Entrainment rate, De-entrainment: De-entrainment rate

18. **Code Inputs:** Only a few selected uncertainty parameters can be changed from an COBRA-TF (RBHT) input. These parameters are pressure, mass flow rate, inlet temperature (or enthalpy), power and subchannel flow area. Other parameters have to

be changed inside the COBRA-TF source code. Therefore, a new card inside the COBRA-TF input deck was designed and implemented. This card is called as uncertainty card (or Card-0). Figure 6.22 demonstrates the format of this card.

```
********************************************************************************
* INPUT DECK -FINAL-
* Assembly 4,
*  Case 4101-86,
*   A Type Radial Power
* F. AYDOGAN MARCH 2007
********************************************************************************
* Card 0 - Uncertainty Parameters -
*P1     P2      P3      P4      P5      P6      P7      P8      P9      P10
1.0     1.0     1.0     1.0     1.0     1.0     1.0     1.0     1.0     1.0
*P11    P12     P13     P14     P15     P16     P17     P18     P19     P20
1.0     1.0     1.0     1.0     1.0     1.0     1.0     1.0     1.0     641.
*  NORMAL CONDITIONS ---!!!---
*  P1:  initial vessel pressure
*  P2:  flow rate
*  P3:  power
*  P4:  inlet enthalpy
*  P5:  subchannel area
*  P6:  gap loss coeff.
*  P7:  grid loss coeff.
*  P8:  mixing coeff.
*  P9:  N/A
*  P10: interfacial friction factor
*  P11: drag coeff.for a bubble
*  P12: drag coeff.for a drop
*  P13: N/A
*  P14: single phase HTCliq.
*  P15: subcooled nucleate boiling HTC
*  P16: saturated boiling HTC
*  P17: Entrainment
*  P18: De-entrainment
*  P19: Critical power
*  P20: CASE #
********************************************************************************
* Main Problem Control Data *
********************************************************************************
*       ICOBRA
             0
*       DTSTEP         TIMET
             0           0.0
*         EPSO        OITMAX          IITMAX
          .001            10              40
```

Figure 6.22. Uncertainty Module in COBRA-TF Input

Card-0 was replaced at the beginning of COBRA-TF input deck so that one can easily change the uncertainty parameters without scrolling the file. Another advantage of this replacement is one can easily divide the COBRA-TF input deck into two sections: First section includes just the uncertainty parameters' ratios and second section is the standard COBRA-TF input deck [1]. Briefly, this format provides modularity.

Card-0 consists of uncertainty parameter ratios (defined in Equation 6.2) that corresponds to the following:

1. P1: Pressure
2. P2: Flow rate
3. P3: Power
4. P4: Inlet enthalpy
5. P5: Subchannel flow area
6. P6: Gap loss coefficient
7. P7: Grid loss coefficient
8. P8: Mixing coefficient
9. P10: Interfacial friction factor
10. P11: Drag coefficient for a bubble
11. P12: Drag coefficient for a droplet
12. P14: Single phase heat transfer coefficient
13. P15: Subcooled nucleate boiling heat transfer coefficient
14. P16: Saturated boiling heat transfer coefficient
15. P17: Entrainment

16. P18: De-entrainment

17. P19: Critical heat flux

9th and 13th parameters of this card are not used. 20th parameter is the arbitrarily unique number (or ID of the file).

The COBRA-TF input model includes 44 subchannels, 30 heater rods, 73 gaps and 6 different walls as shown in Figure 6.23. This chapter uses this subchannel map for all the subchannel analyses.

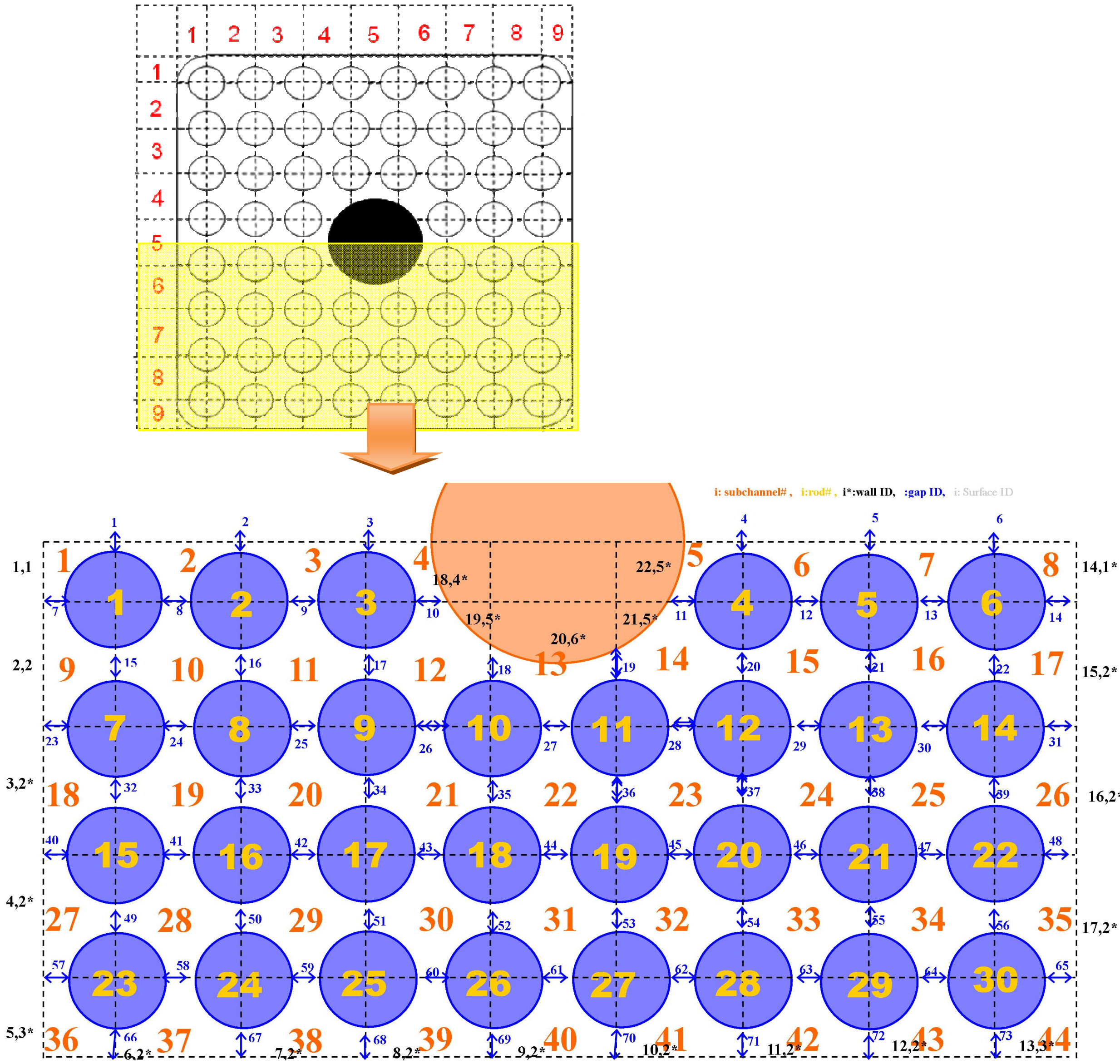

Figure 6.23. COBRA-TF Model

19. Code: This element describes the thermal hydraulics code, COBRA-TF. There are mainly two modifications in the COBRA-TF code:

a. **Implementation of the Rogers and Rosehart's mixing model** to make the code capable of handling the mixing phenomenon. Avramova [30] demonstrated verification and validation test results of this model to the COBRA-TF.

b. **Implementation of the uncertainty module** to read the uncertainty module (Card-0) and to process the uncertainty parameter ratios. To change an uncertainty parameter according to its uncertainty, this parameter is just multiplied with the corresponding uncertainty parameter ratio. For instance, if the pressure's uncertainty parameter ratio is 1.01, 1.01 is multiplied with the pressure variable inside the code. The steps of this code process are given in Figure 6.24.

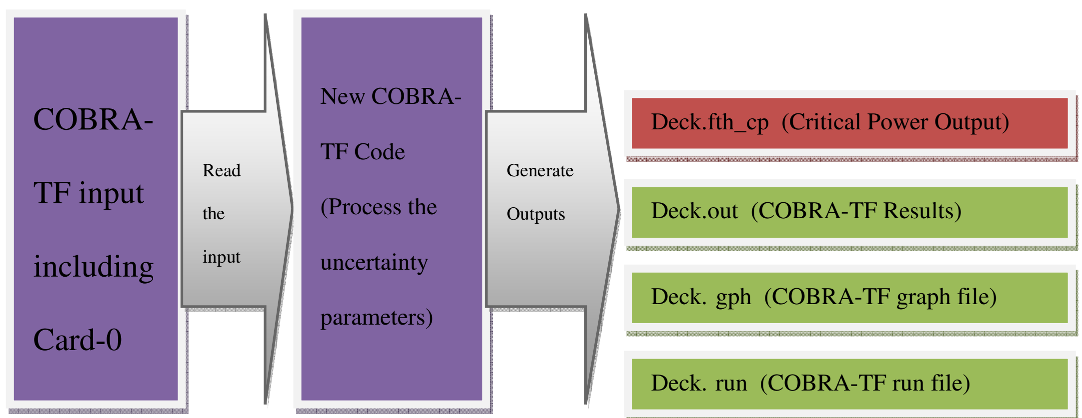

Figure 6.24. The Process of New COBRA-TF

New COBRA-TF code reads the new COBRA-TF input deck and multiplies the uncertainty parameter ratio with the corresponding parameter in addition to original COBRA-TF procedures. The source code of the process is given in Appendix-2 (in Section 6.4.2).

20. Outputs: This element is the code outputs. Original COBRA-TF produces three outputs:

Deck.out: in which, the code results,

Deck.run: in which, run status of the COBRA-TF,

Deck.gph: in which, graph file.

In addition to this original COBRA-TF output files, new COBRA-TF produces two more outputs:

Deck.fth_o: in which, the void distribution file including the subchannel, bundle void fractions (%) and uncertainty parameter ratios (Figure 6.25).

Deck.fth_cp: in which, the critical power file including the critical power information. The definition of this file was given in the critical power section of this chapter.

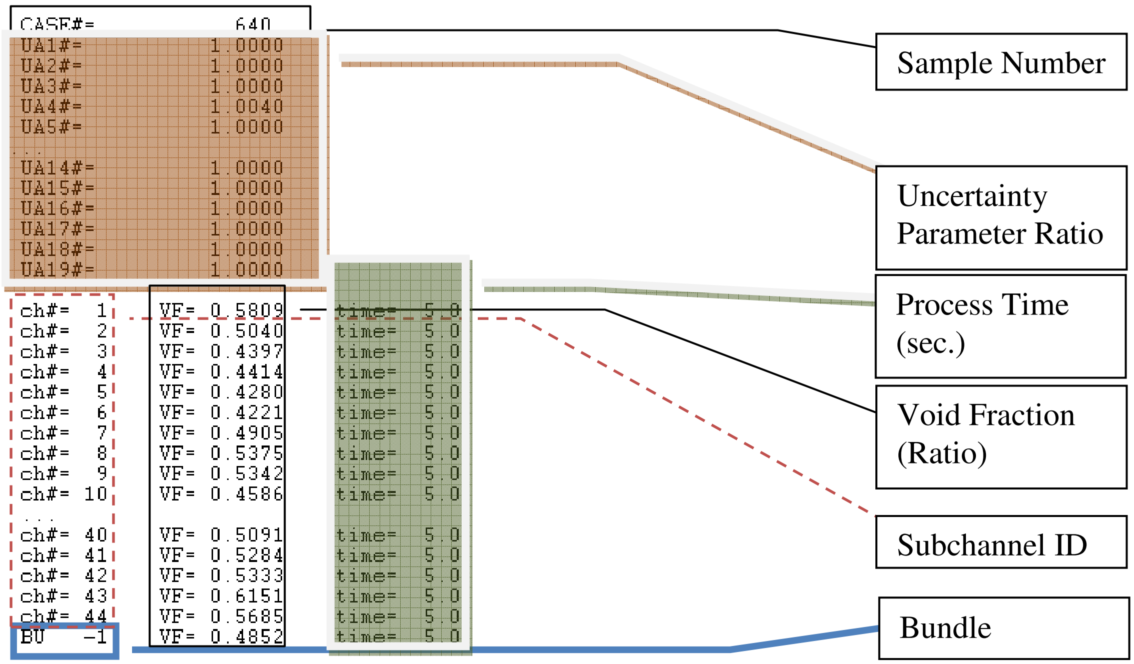

Figure 6.25. The Format of Void Distribution Output File (Deck.fth_o)

21. Master Program: Master program module manages the COBRA-TF runs and record to the Void Distribution Database. This program is one of the most required components of the system because there are many COBRA-TF inputs that have to be run. Therefore, Master program takes the inputs one by one, run and rename them. The process of the Master program is given in Figure 6.26.

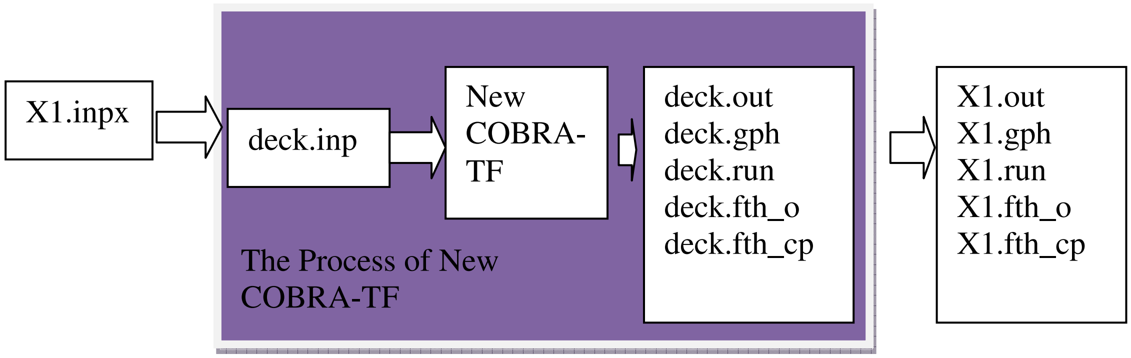

Figure 6.26. The process of Master program

Master was coded by using C++ programming language (Visual C++ 2005 Express Edition – version 8.0). The source code of the Master program is given in Appendix-3 (in Section 6.4.3).

22. **UA Database:** This element includes the predicted and measured data for uncertainty comparison formulas (given in Equation 5.16-22).

23. **Uncertainty Comparison Methods:** Uncertainty comparison methods have been already defined from equation 5.16 to 5.22 in Chapter 5. For these methods, the accuracy of the subchannel and bundle void fractions were obtained from the experimental database. The absolute accuracies of the measured subchannel void fraction and bundle are 3% and 2% respectively.

24. **Uncertainty Comparison Tables:** The results of the uncertainty equations were given in this element. Although four experimental cases have been selected, two

COBRA-TF cases (Test 4101-02 and Test 4101-13) failed. The reason is about the boundary conditions. If the pressure is increased, these cases run without any problem. Because of this failure, one new experimental case (Test 4101-55) was added to the experimental cases.

Table 6.10, 6.11, 6.12, 6.13 and 6.14 demonstrate the mean value of predicted, mean relative bias, maximum bias, predicted standard deviation and coverage ratio of subchannel void fraction by using Figure 6.23 COBRA-TF modeling map for test case 4101-86 respectively and Table 6.15 shows the bundle void fraction uncertainty values for the same test cases. The set of tables from 6.16 through 6.21 and 6.22 through 6.27 demonstrate the same comparisons for Test 4101-69 and Test 4101-55 respectively.

Table 6.10. Mean Value of Predicted Subchannel Void Fraction for Case Test 4101-86

	1	2	3	4	5	6	7	8	9
1	0.71	0.81	0.74	0.74	0.71	0.71	0.73	0.79	0.75
2	0.77	0.80	0.71	0.68	0.70	0.67	0.70	0.79	0.76
3	0.78	0.71	0.61	0.62	0.66	0.62	0.61	0.70	0.77
4	0.75	0.67	0.62	0.76	0.57	0.58	0.61	0.67	0.72
5	0.76	0.71	0.66	0.59		0.53	0.65	0.69	0.74
6	0.75	0.67	0.62	0.76	0.57	0.58	0.61	0.67	0.72
7	0.78	0.71	0.61	0.62	0.66	0.62	0.61	0.70	0.77
8	0.77	0.80	0.71	0.68	0.70	0.67	0.70	0.79	0.76
9	0.71	0.81	0.74	0.74	0.71	0.71	0.73	0.79	0.75

Table 6.11. Mean Relative Bias of Subchannel Void Fraction for Case Test 4101-86

	1	2	3	4	5	6	7	8	9
1	0.08	0.13	0.09	0.01	-0.05	-0.02	0.04	0.03	0.00
2	0.01	0.08	-0.04	-0.08	-0.03	-0.05	0.01	0.04	-0.01
3	0.06	-0.04	-0.10	-0.04	-0.01	-0.07	-0.09	-0.07	0.09
4	0.01	-0.05	-0.07	0.12	0.03	-0.07	-0.03	0.02	0.04
5	0.03	-0.04	-0.01	0.05		0.03	-0.04	-0.04	0.04
6	-0.01	-0.08	-0.11	0.12	0.07	-0.10	-0.08	0.02	0.04
7	0.06	-0.03	-0.12	0.03	0.04	-0.05	-0.10	0.01	0.03
8	0.00	0.10	0.02	-0.03	0.00	-0.04	0.00	0.10	-0.04
9	0.07	0.05	0.02	0.03	0.02	0.08	0.08	0.03	0.04

Table 6.12. Maximum Bias of Subchannel Void Fraction for Case Test 4101-86

	1	2	3	4	5	6	7	8	9
1	0.17	0.29	0.18	0.12	0.14	0.12	0.14	0.21	0.10
2	0.14	0.26	0.11	0.16	0.12	0.13	0.08	0.19	0.14
3	0.22	0.09	0.25	0.22	0.08	0.22	0.28	0.13	0.24
4	0.09	0.15	0.20	0.34	0.12	0.29	0.20	0.08	0.11
5	0.13	0.13	0.12	0.13		0.11	0.13	0.10	0.12
6	0.08	0.18	0.24	0.34	0.17	0.32	0.25	0.08	0.11
7	0.22	0.08	0.27	0.20	0.12	0.20	0.29	0.06	0.18
8	0.13	0.29	0.08	0.11	0.09	0.11	0.07	0.25	0.17
9	0.15	0.21	0.11	0.14	0.10	0.19	0.18	0.21	0.13

Table 6.13. Standard Deviation of Predicted Subchannel Void Fraction for Case Test 4101-86

	1	2	3	4	5	6	7	8	9
1	0.025	0.062	0.031	0.033	0.030	0.035	0.028	0.059	0.032
2	0.044	0.060	0.024	0.024	0.034	0.020	0.019	0.062	0.047
3	0.055	0.016	0.038	0.056	0.031	0.039	0.048	0.019	0.058
4	0.023	0.033	0.043	0.068	0.027	0.051	0.049	0.018	0.029
5	0.030	0.027	0.040	0.022		0.019	0.033	0.021	0.033
6	0.023	0.033	0.043	0.068	0.027	0.051	0.049	0.018	0.029
7	0.055	0.016	0.038	0.056	0.031	0.039	0.048	0.019	0.058
8	0.044	0.060	0.024	0.024	0.034	0.020	0.019	0.062	0.047
9	0.025	0.062	0.031	0.033	0.030	0.035	0.028	0.059	0.032

Table 6.14. The Coverage Ratio of Subchannel Void Fraction for Case Test 4101-86

	1	2	3	4	5	6	7	8	9
1	0.02	0.02	0.02	0.04	0.05	0.05	0.01	0.04	0.19
2	0.25	0.01	0.03	0.03	0.27	0.03	0.20	0.03	0.03
3	0.02	0.03	0.02	0.04	0.03	0.02	0.01	0.07	0.02
4	0.12	0.03	0.03	0.01	0.03	0.01	0.03	0.04	0.03
5	0.03	0.02	0.15	0.02		0.03	0.03	0.02	0.03
6	0.10	0.01	0.01	0.01	0.00	0.01	0.01	0.04	0.03
7	0.02	0.03	0.01	0.04	0.03	0.02	0.01	0.12	0.03
8	0.29	0.01	0.05	0.03	0.27	0.03	0.20	0.01	0.03
9	0.02	0.03	0.06	0.04	0.05	0.01	0.01	0.04	0.02

Table 6.15. The Uncertainty Results of Bundle Void Fraction for Case Test 4101-86

Mean of Predicted Void Fraction	Mean Relative Bias Uncertainty	Max Bias Uncertainty	Standard Deviation of Predicted Void Fraction	Coverage Ratio	Measured Void Fraction
0.694	-0.005	0.121	0.036	0.09	0.698

Table 6.16. Mean Value of Predicted Subchannel Void Fraction for Case Test 4101-69

	1	2	3	4	5	6	7	8	9
1	0.114	0.166	0.142	0.139	0.136	0.135	0.136	0.147	0.129
2	0.166	0.224	0.215	0.203	0.188	0.199	0.213	0.222	0.164
3	0.148	0.224	0.193	0.204	0.182	0.202	0.191	0.222	0.146
4	0.141	0.194	0.202	0.152	0.077	0.152	0.192	0.186	0.136
5	0.1198	0.2221	0.2087	0.0945		0.086	0.1839	0.228	0.124
6	0.141	0.1936	0.2018	0.152	0.077	0.1524	0.192	0.186	0.1355
7	0.148	0.224	0.193	0.204	0.1815	0.202	0.1912	0.2216	0.1461
8	0.166	0.224	0.215	0.203	0.1884	0.1994	0.213	0.222	0.1637
9	0.114	0.166	0.142	0.139	0.1359	0.1353	0.1362	0.1471	0.1286

Table 6.17. Mean Relative Bias of Subchannel Void Fraction for Case Test 4101-69

	1	2	3	4	5	6	7	8	9
1	0.26	0.17	0.15	0.03	0.01	-0.02	-0.12	-0.05	-0.02
2	0.07	-0.11	0.13	-0.06	-0.21	-0.07	-0.07	-0.18	-0.06
3	0.10	-0.01	-0.12	-0.04	-0.12	0.15	0.14	-0.01	0.01
4	-0.01	-0.14	0.02	-0.01	-0.23	0.04	-0.03	-0.10	0.07
5	-0.02	-0.04	-0.06	0.05		-0.07	0.05	0.02	-0.03
6	0.01	-0.07	0.03	0.04	0.04	-0.04	0.08	-0.09	0.01
7	-0.01	0.08	-0.04	0.03	0.06	0.05	-0.02	0.00	-0.11
8	0.12	0.08	-0.10	-0.07	-0.09	-0.05	0.08	-0.07	-0.03
9	0.12	-0.08	-0.09	0.05	-0.01	0.03	0.06	-0.09	-0.11

Table 6.18. Maximum Bias of Subchannel Void Fraction for Case Test 4101-69

	1	2	3	4	5	6	7	8	9
1	0.42	0.27	0.29	0.11	0.05	0.10	0.29	0.17	0.13
2	0.28	0.33	0.25	0.23	0.33	0.25	0.22	0.35	0.27
3	0.26	0.21	0.26	0.19	0.29	0.34	0.28	0.21	0.19
4	0.07	0.28	0.22	0.07	0.40	0.09	0.28	0.28	0.11
5	0.20	0.24	0.31	0.18		0.17	0.22	0.12	0.08
6	0.06	0.22	0.24	0.11	0.23	0.12	0.33	0.27	0.06
7	0.16	0.27	0.17	0.17	0.24	0.24	0.15	0.21	0.28
8	0.34	0.29	0.22	0.24	0.22	0.24	0.24	0.24	0.24
9	0.29	0.20	0.21	0.12	0.05	0.10	0.22	0.21	0.22

Table 6.19. Standard Deviation of Predicted Subchannel Void Fraction for Case Test 4101-69

	1	2	3	4	5	6	7	8	9
1	0.01	0.01	0.01	0.01	0.00	0.01	0.01	0.01	0.01
2	0.02	0.02	0.01	0.02	0.01	0.01	0.02	0.02	0.02
3	0.01	0.02	0.01	0.01	0.02	0.02	0.01	0.03	0.01
4	0.00	0.01	0.02	0.01	0.01	0.01	0.02	0.01	0.00
5	0.01	0.02	0.02	0.01		0.00	0.01	0.01	0.00
6	0.00	0.01	0.02	0.01	0.01	0.01	0.02	0.01	0.00
7	0.01	0.02	0.01	0.01	0.02	0.02	0.01	0.03	0.01
8	0.02	0.02	0.01	0.02	0.01	0.01	0.02	0.02	0.02
9	0.01	0.01	0.01	0.01	0.00	0.01	0.01	0.01	0.01

Table 6.20. The Coverage Ratio of Subchannel Void Fraction for Case Test 4101-69

	1	2	3	4	5	6	7	8	9
1	0.00	0.00	0.00	0.04	0.26	0.06	0.03	0.03	0.05
2	0.02	0.03	0.00	0.03	0.02	0.04	0.03	0.02	0.07
3	0.18	0.03	0.05	0.07	0.04	0.02	0.00	0.29	0.03
4	0.22	0.03	0.06	0.05	0.02	0.06	0.02	0.02	0.00
5	0.11	0.05	0.03	0.04		0.03	0.04	0.09	0.07
6	0.19	0.03	0.06	0.03	0.05	0.06	0.02	0.02	0.22
7	0.18	0.03	0.07	0.07	0.04	0.04	0.11	0.29	0.02
8	0.02	0.03	0.02	0.03	0.03	0.04	0.03	0.03	0.07
9	0.02	0.03	0.03	0.04	0.26	0.06	0.03	0.02	0.02

Table 6.21. The Uncertainty Results of Bundle Void Fraction for Case Test 4101-69

Mean of Predicted Void Fraction	Mean Relative Bias Uncertainty	Max Bias Uncertainty	Standard Deviation of Predicted Void Fraction	Coverage Ratio	Measured Void Fraction
0.179	-0.015	0.167	0.015	0.073	0.182

Table 6.22. Mean Value of Predicted Subchannel Void Fraction for Case Test 4101-55

	1	2	3	4	5	6	7	8	9
1	0.379	0.528	0.457	0.384	0.406	0.456	0.396	0.491	0.441
2	0.453	0.523	0.448	0.460	0.423	0.451	0.444	0.518	0.533
3	0.430	0.481	0.458	0.393	0.413	0.390	0.424	0.476	0.470
4	0.484	0.454	0.420	0.383	0.265	0.383	0.375	0.421	0.466
5	0.4655	0.4985	0.4277	0.3069		0.227	0.416	0.4618	0.4393
6	0.484	0.4544	0.42	0.383	0.265	0.3825	0.3754	0.421	0.4657
7	0.430	0.481	0.458	0.393	0.4131	0.3896	0.424	0.4763	0.4698
8	0.453	0.523	0.448	0.460	0.4232	0.4514	0.4435	0.5182	0.5327
9	0.379	0.528	0.457	0.384	0.4058	0.4563	0.3958	0.491	0.4408

Table 6.23. Mean Relative Bias of Subchannel Void Fraction for Case Test 4101-55

	1	2	3	4	5	6	7	8	9
1	0.16	0.11	0.06	-0.16	-0.11	0.04	-0.10	-0.06	0.13
2	-0.10	-0.02	-0.06	-0.07	-0.17	-0.07	-0.08	0.05	0.07
3	-0.01	-0.02	0.10	-0.06	-0.09	0.01	-0.03	-0.01	0.07
4	0.11	-0.08	0.04	0.10	0.01	0.21	0.05	-0.04	0.06
5	0.05	-0.01	0.00	0.06		-0.05	0.07	-0.02	0.00
6	0.01	-0.06	0.02	0.00	0.10	-0.01	0.06	0.03	0.09
7	0.07	-0.01	0.03	0.01	0.06	-0.05	-0.06	-0.03	0.03
8	0.02	-0.01	-0.03	0.00	0.01	-0.04	0.04	0.01	0.02
9	0.10	0.04	-0.02	-0.06	0.04	0.07	0.02	0.03	0.06

Table 6.24. Maximum Bias of Subchannel Void Fraction for Case Test 4101-55

	1	2	3	4	5	6	7	8	9
1	0.31	0.18	0.13	0.25	0.21	0.12	0.20	0.17	0.27
2	0.19	0.11	0.17	0.12	0.26	0.12	0.21	0.15	0.15
3	0.09	0.10	0.24	0.13	0.17	0.09	0.17	0.10	0.15
4	0.21	0.16	0.13	0.21	0.15	0.33	0.16	0.12	0.16
5	0.15	0.09	0.09	0.14		0.17	0.16	0.08	0.12
6	0.12	0.15	0.11	0.12	0.24	0.13	0.18	0.11	0.18
7	0.15	0.10	0.17	0.09	0.14	0.13	0.21	0.11	0.11
8	0.11	0.11	0.14	0.06	0.11	0.09	0.17	0.11	0.09
9	0.26	0.10	0.09	0.15	0.14	0.15	0.12	0.14	0.19

Table 6.25. Standard Deviation of Predicted Subchannel Void Fraction for Case Test 4101-55

	1	2	3	4	5	6	7	8	9
1	0.03	0.01	0.02	0.01	0.02	0.02	0.02	0.03	0.02
2	0.02	0.02	0.02	0.01	0.02	0.01	0.02	0.03	0.02
3	0.02	0.02	0.03	0.01	0.02	0.01	0.03	0.02	0.01
4	0.02	0.02	0.02	0.02	0.02	0.02	0.02	0.02	0.02
5	0.02	0.02	0.02	0.01		0.01	0.02	0.01	0.02
6	0.02	0.02	0.02	0.02	0.02	0.02	0.02	0.02	0.02
7	0.02	0.02	0.03	0.01	0.02	0.01	0.03	0.02	0.01
8	0.02	0.02	0.02	0.01	0.02	0.01	0.02	0.03	0.02
9	0.03	0.01	0.02	0.01	0.02	0.02	0.02	0.03	0.02

Table 6.26. The Coverage Ratio of Subchannel Void Fraction for Case Test 4101-55

	1	2	3	4	5	6	7	8	9
1	0.01	0.00	0.05	0.02	0.03	0.02	0.06	0.04	0.02
2	0.06	0.07	0.03	0.85	0.07	0.03	0.03	0.13	0.06
3	0.02	0.10	0.03	0.12	0.02	0.02	0.02	0.04	0.03
4	0.00	0.02	0.06	0.27	0.01	0.00	0.02	0.04	0.01
5	0.02	0.07	0.26	0.02		0.02	0.01	0.05	0.35
6	0.08	0.02	0.06	0.27	0.01	0.12	0.02	0.04	0.01
7	0.02	0.10	0.03	0.12	0.02	0.02	0.02	0.04	0.03
8	0.06	0.07	0.03	0.85	0.07	0.03	0.03	0.13	0.06
9	0.01	0.03	0.05	0.02	0.03	0.02	0.06	0.04	0.02

Table 6.27. The Uncertainty Results of Bundle Void Fraction for Case Test 4101-55

Mean of Predicted Void Fraction	Mean Relative Bias Uncertainty	Max Bias Uncertainty	Standard Deviation of Predicted Void Fraction	Coverage Ratio	Measured Void Fraction
0.438	0.000	0.085	0.020	0.112	0.438

25. **Sensitivity Parameter Table:** Sensitivity parameter table (Table 6.28) contains the uncertainty parameters and corresponding input uncertainties. Input uncertainties were determined with taking the maximum and minimum of each column in Table 6.9. This table is used to perform sensitivity analysis by changing one parameter at a time. This allows the analyst to see which uncertainty parameter significantly affects the output uncertainty parameter (or ranking of the input uncertainty parameters).

Table 6.28. Sensitivity Parameter Table for Void Distribution

ID	Pressure	Flow rate	Power	Inlet Enthalpy	Flow Area	Gap loss Coefficient	Grid Loss Coefficient	Mixing Coefficient	fi	CDb	CDd	HTCsingle	HTCsub	HTCsat	Entrainment	De-entrainment
Max	1.010	1.010	1.015	1.004	1.005	1.215	0.950	1.927	1.179	1.528	1.249	1.098	1.397	1.398	1.436	1.436
Min	0.990	0.990	0.985	0.996	0.995	0.907	0.830	0.401	0.527	0.395	0.743	0.943	0.672	0.672	0.710	0.745

where fi: interfacial friction factor, CDb: Drag Coefficient for a Bubble, CDd: Drag Coefficient for a Droplet, HTCsingle: Single Phase Heat Transfer Coefficient, HTCsub: Subcooled Nucleate Boiling Heat Transfer Coefficient, HTCsat: Saturated Boiling Heat Transfer Coefficient, Entrainment: Entrainment rate, De-entrainment: De-entrainment rate

26. Sensitivity Comparison Results: This element shows the sensitivity analysis results. The uncertainty parameter was changed based on sensitivity parameter table. The absolute maximum change of the void fraction is demonstrated in the sensitivity comparison results. In these results, one uncertainty parameter was changed once at a time and the void fraction is observed. Then, the percentage difference between the predicted and nominal predicted results were used in these plots. The formula of the percentage void fraction change is ((Predicted Void Fraction-Nominal Predicted Void Fraction)/Nominal Predicted Void Fraction*100). The subchannel IDs are the IDs that are used in the subchannel map as shown 11th element of uncertainty analysis.

Figure 6.27-6.70, Figure 6.72-6.115 and 6.117-6.160 show the subchannel void fraction sensitivity results for the case 4101-86, 4101-69 and 4101-55 respectively. Figure 6.71, 6.116 and 6.161 demonstrate the bundle void fraction sensitivity results for the case 4101-86, 4101-69 and 4101-55 respectively.

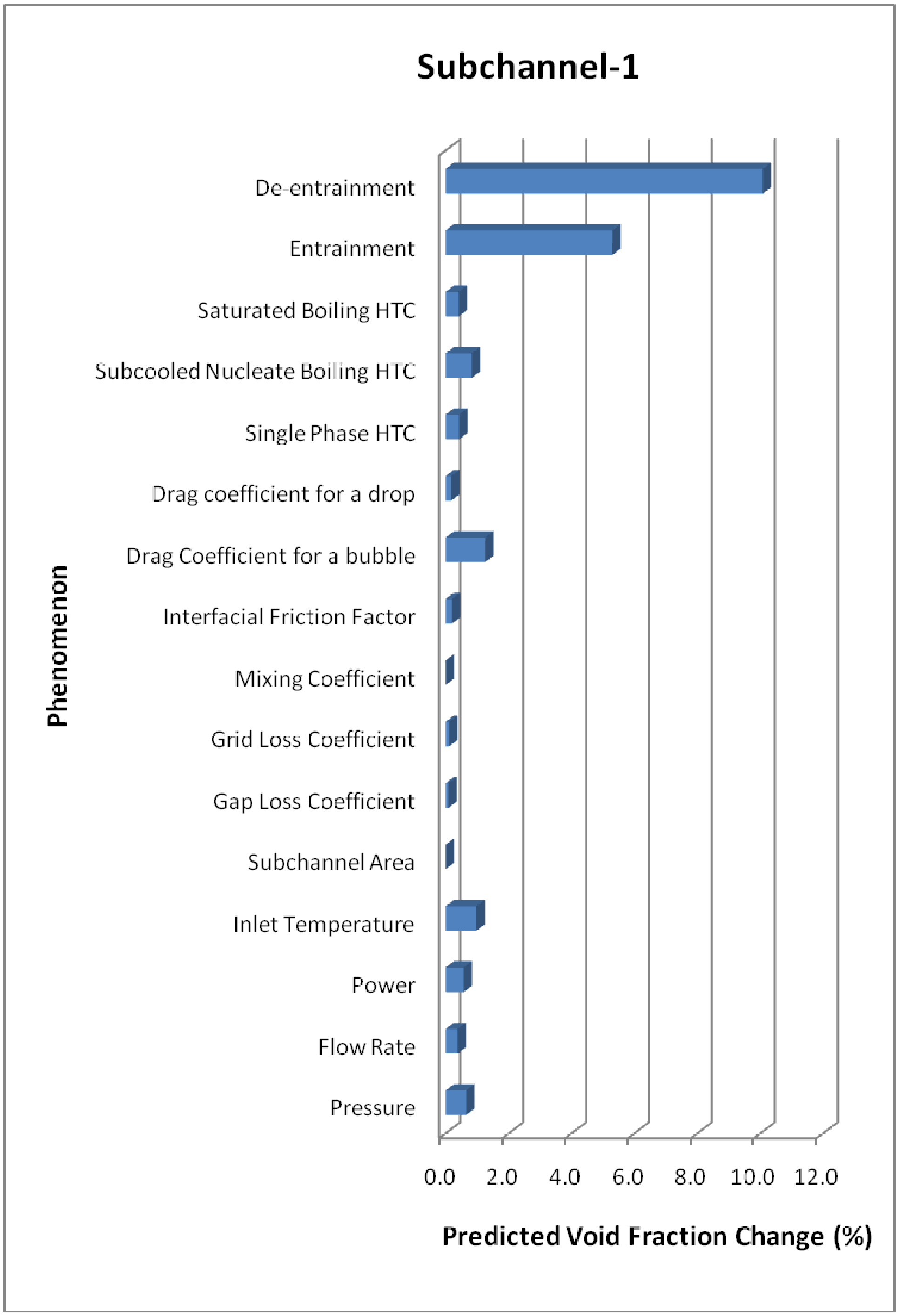

Figure 6.27. Predicted 1st Subchannel Void Fraction Change versus Phenomenon for Test 4101-86

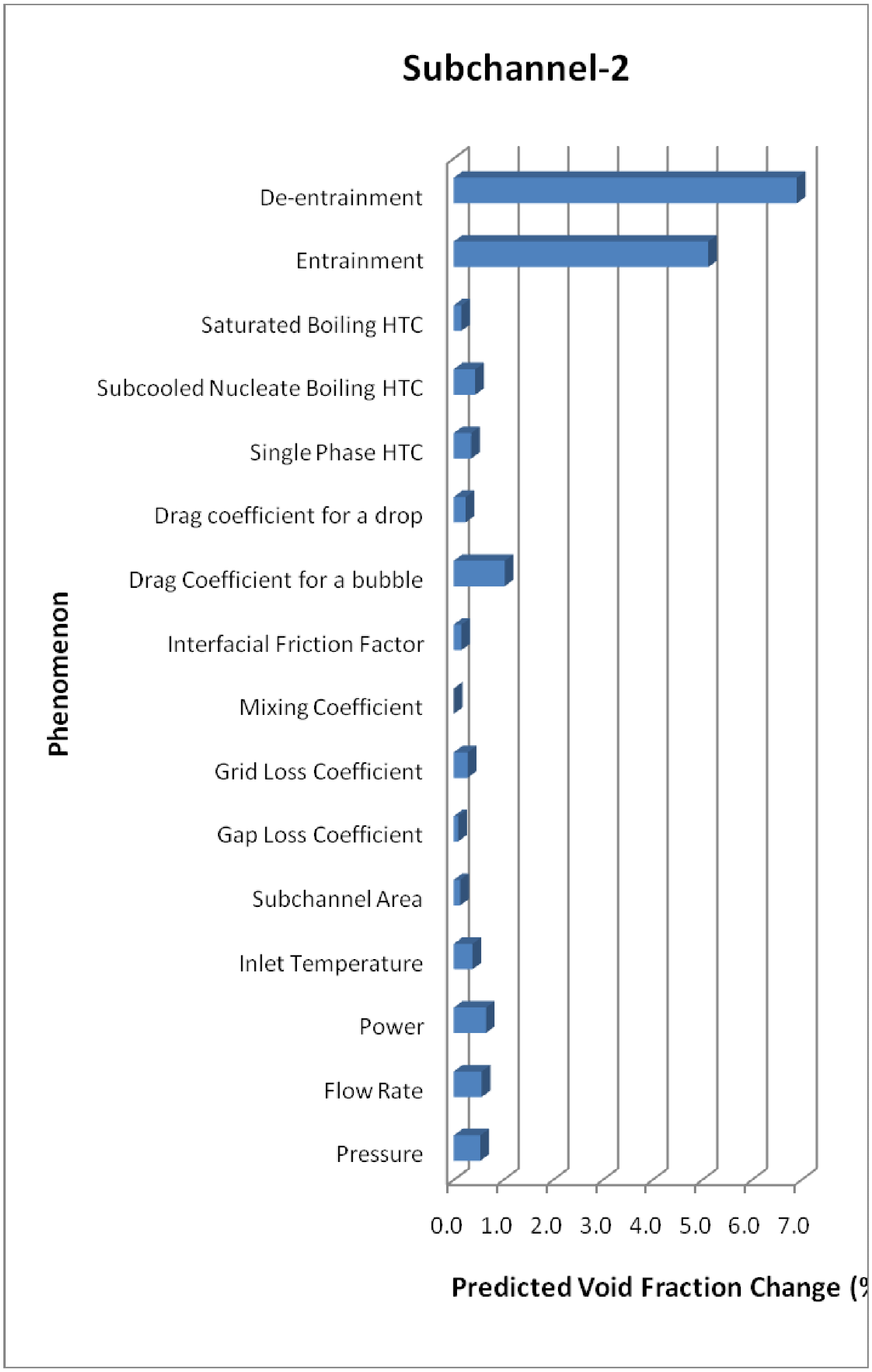

Figure 6.28. Predicted 2nd Subchannel Void Fraction Change versus Phenomenon for Test 4101-86

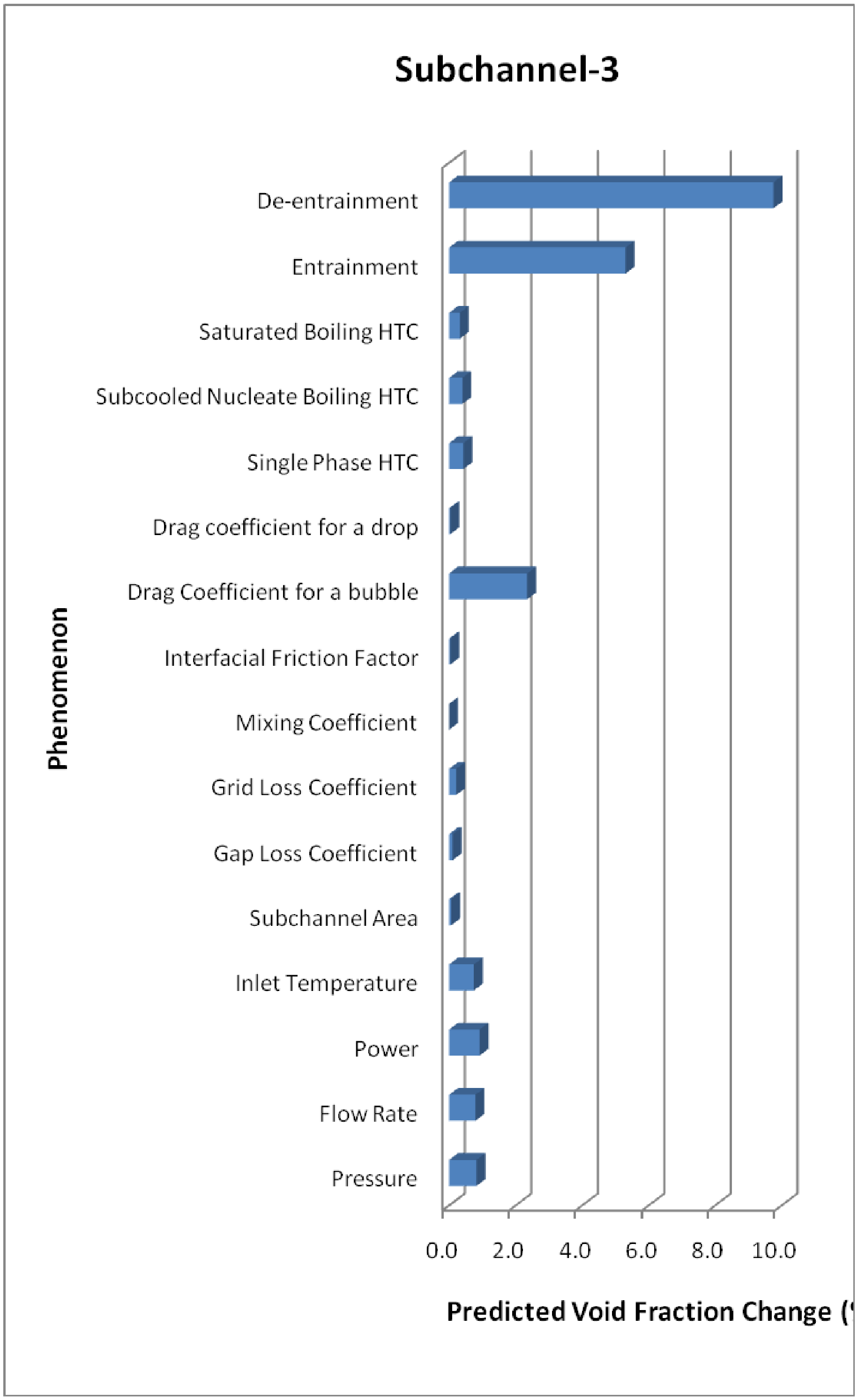

Figure 6.29. Predicted 3rd Void Fraction Change versus Phenomenon for Test 4101-86

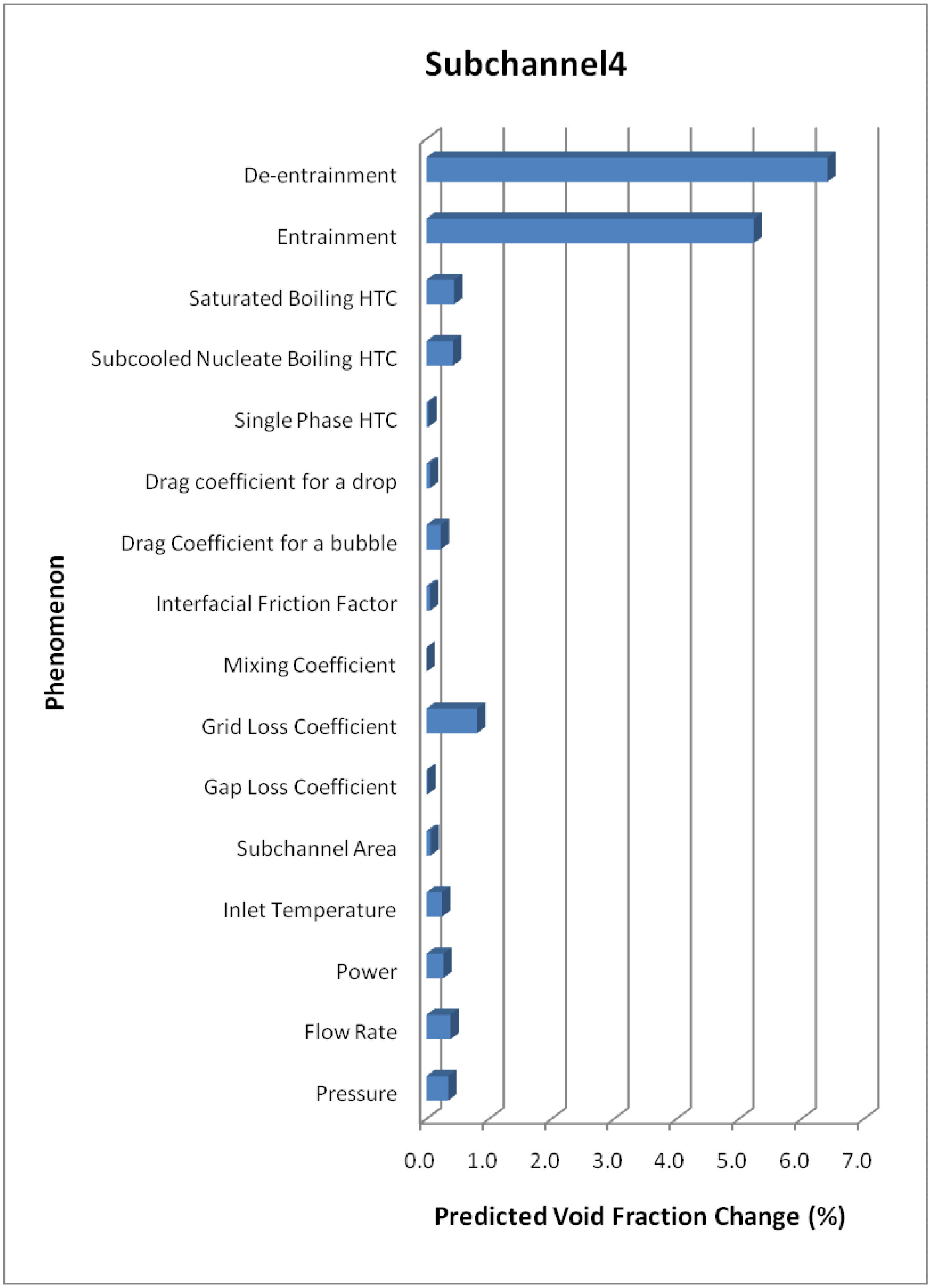

Figure 6.30. Predicted 4th Subchannel Void Fraction Change versus Phenomenon for Test 4101-86

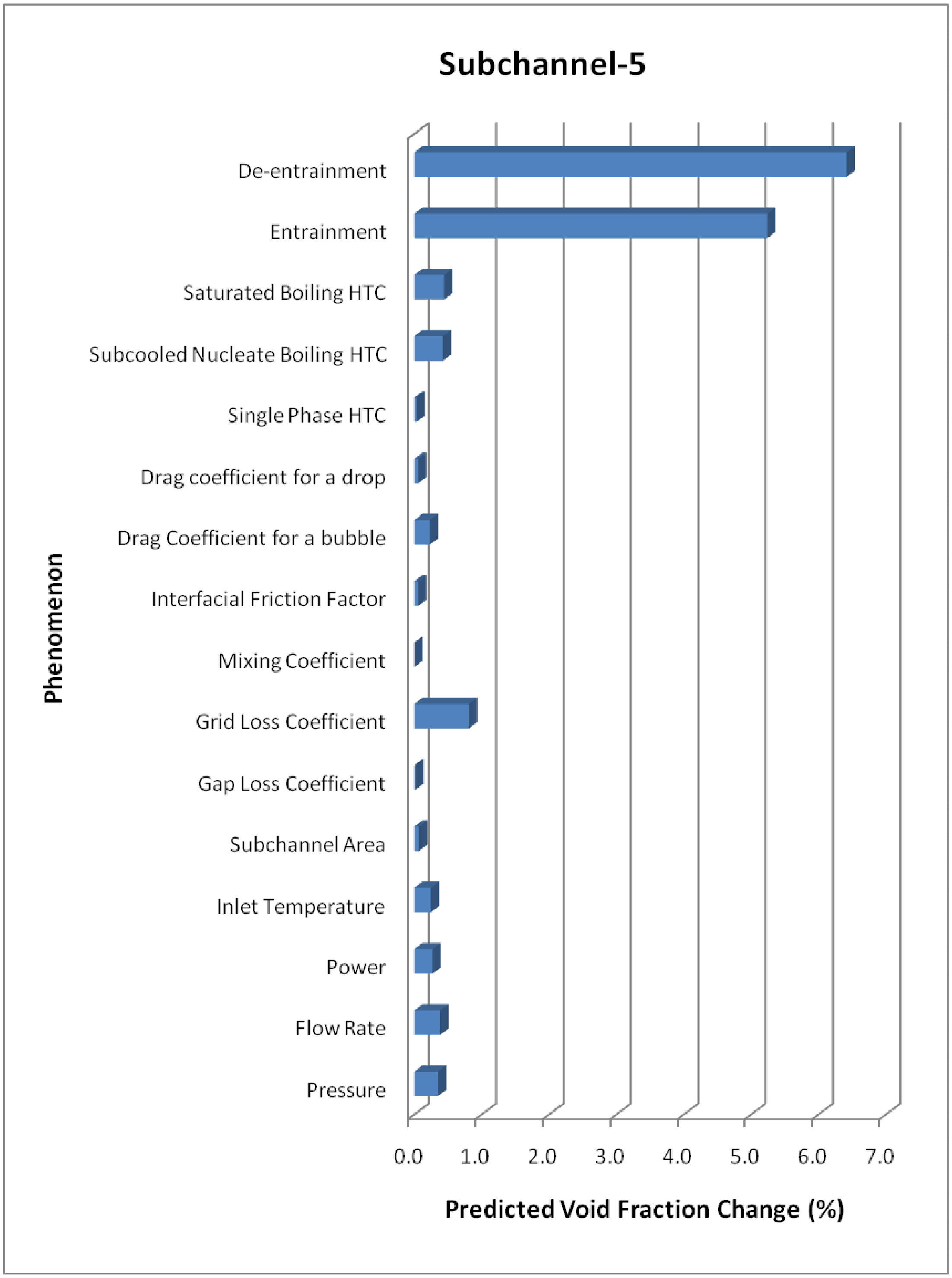

Figure 6.31. Predicted 5th Subchannel Void Fraction Change versus Phenomenon for Test 4101-86

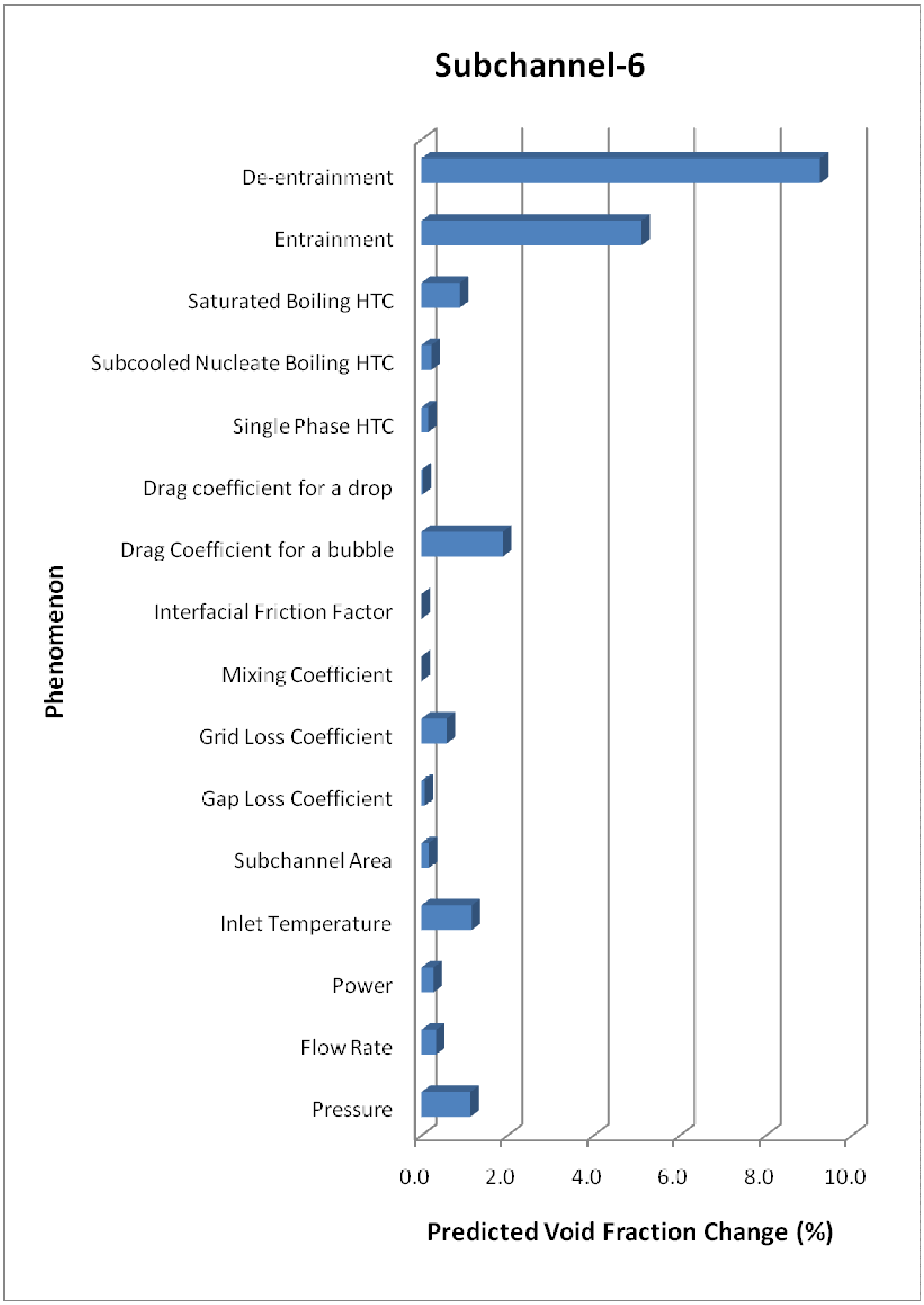

Figure 6.32. Predicted 6th Subchannel Void Fraction Change versus Phenomenon for Test 4101-86

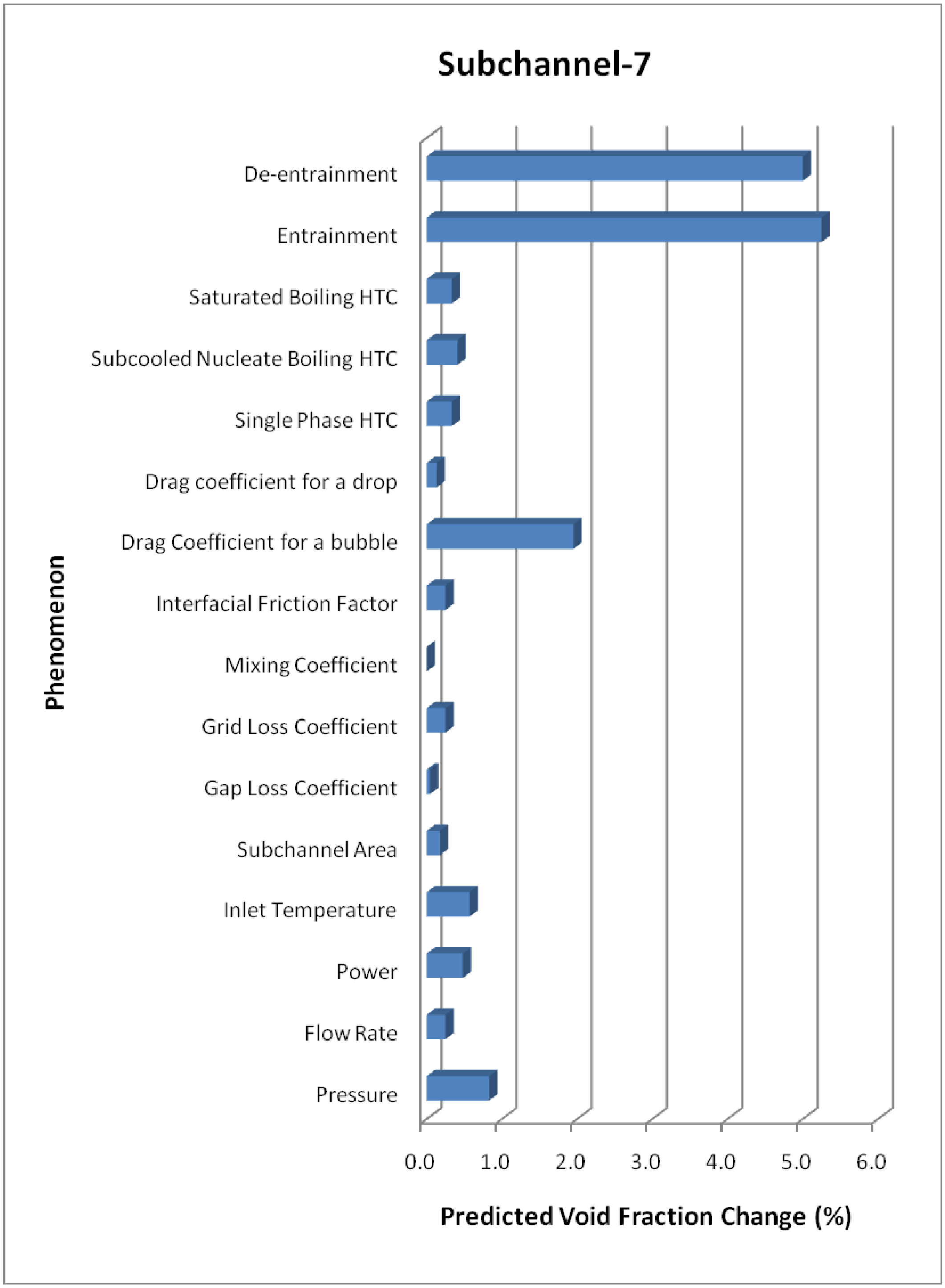

Figure 6.33. Predicted 7th Subchannel Void Fraction Change versus Phenomenon for Test 4101-86

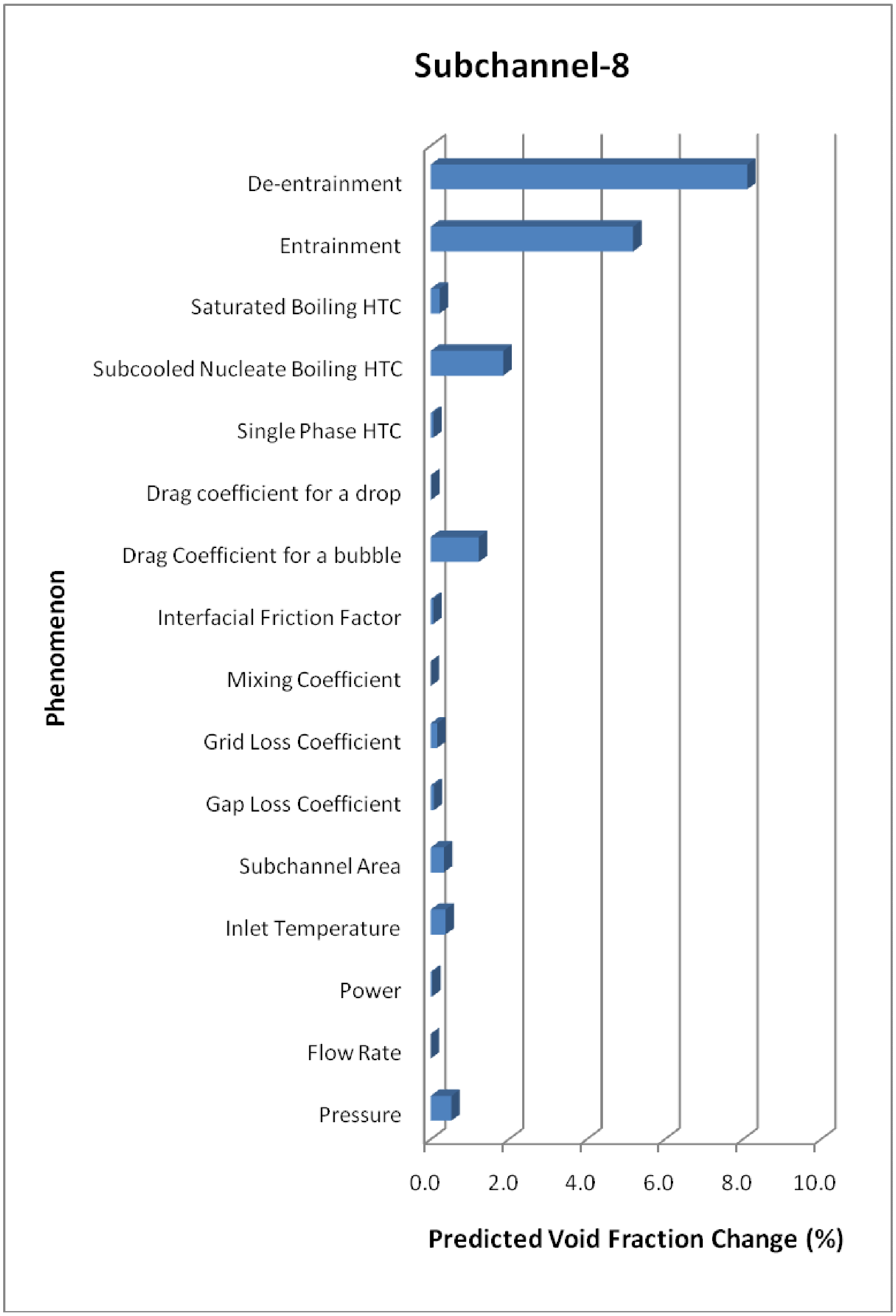

Figure 6.34. Predicted 8th Subchannel Void Fraction Change versus Phenomenon for Test 4101-86

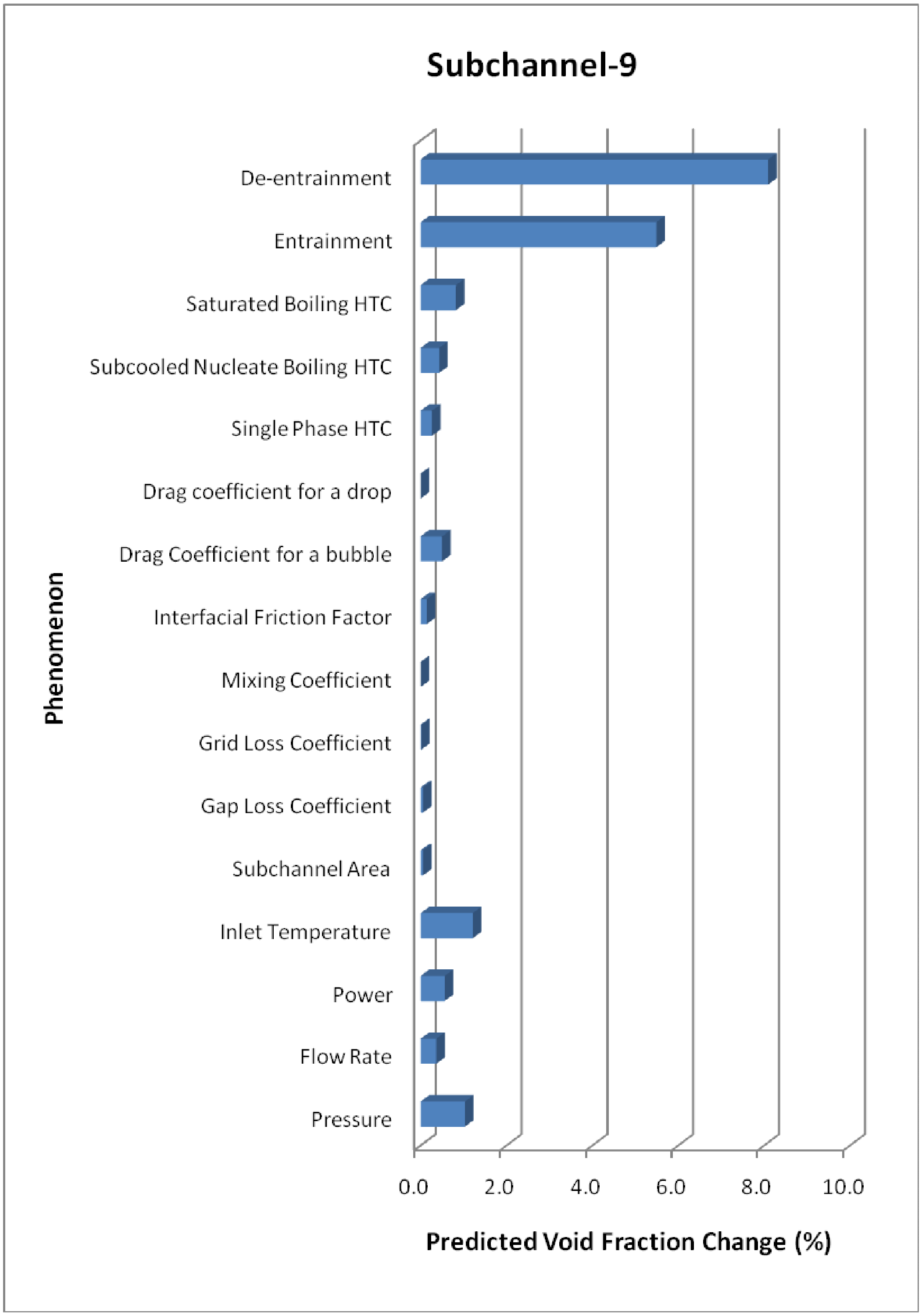

Figure 6.35. Predicted 9th Subchannel Void Fraction Change versus Phenomenon for Test 4101-86

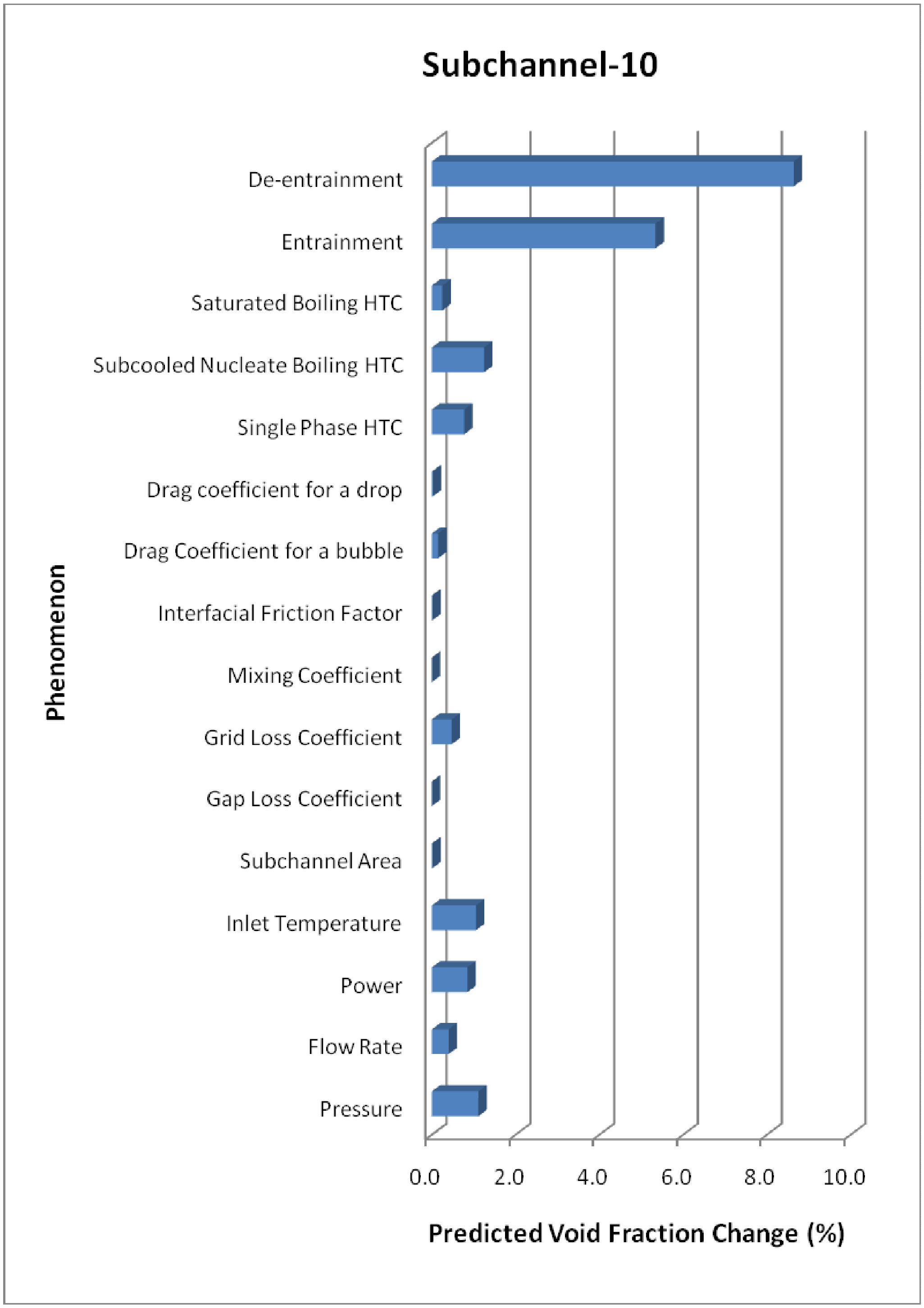

Figure 6.36. Predicted 10th Subchannel Void Fraction Change versus Phenomenon for Test 4101-86

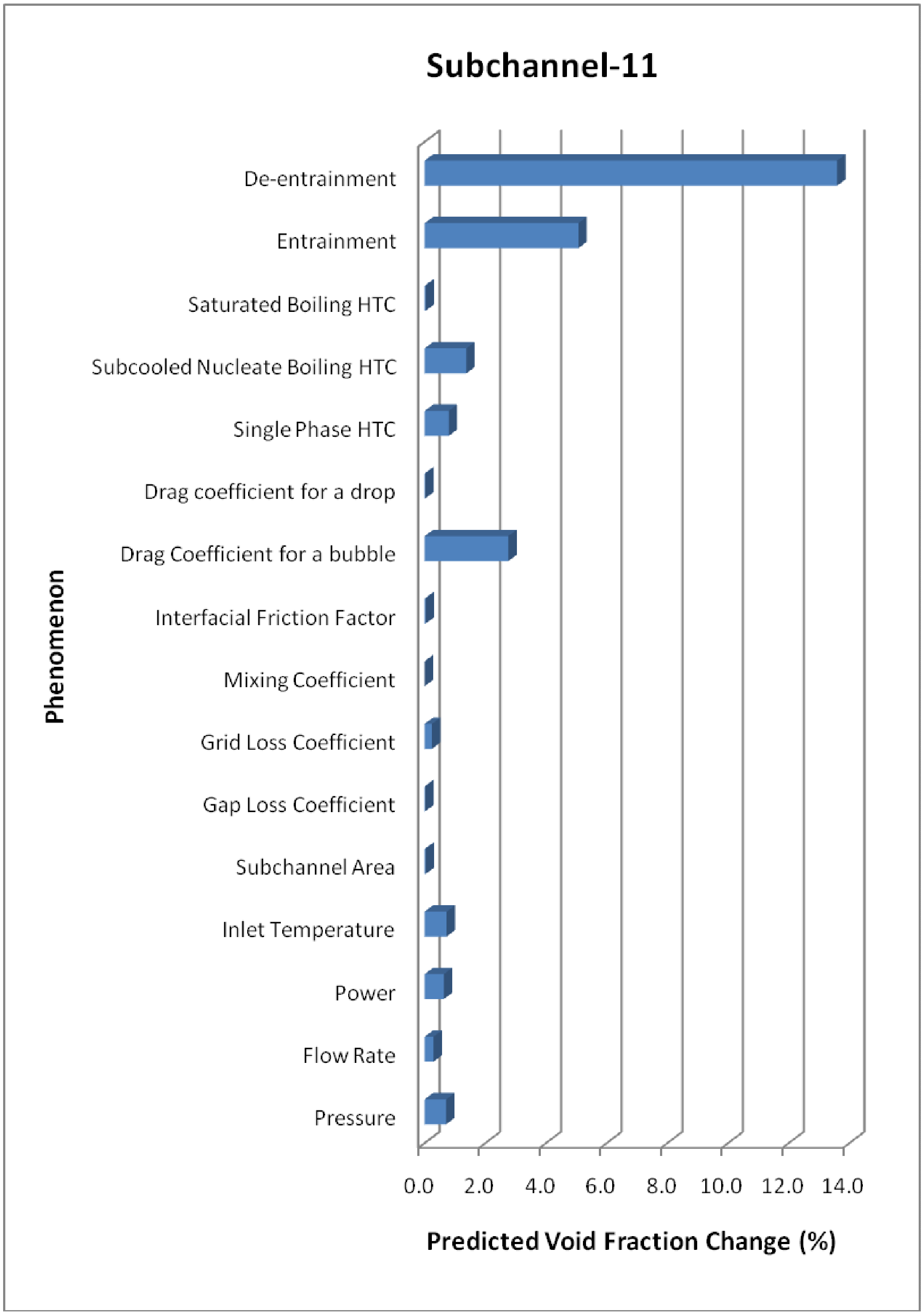

Figure 6.37. Predicted 11th Subchannel Void Fraction Change versus Phenomenon for Test 4101-86

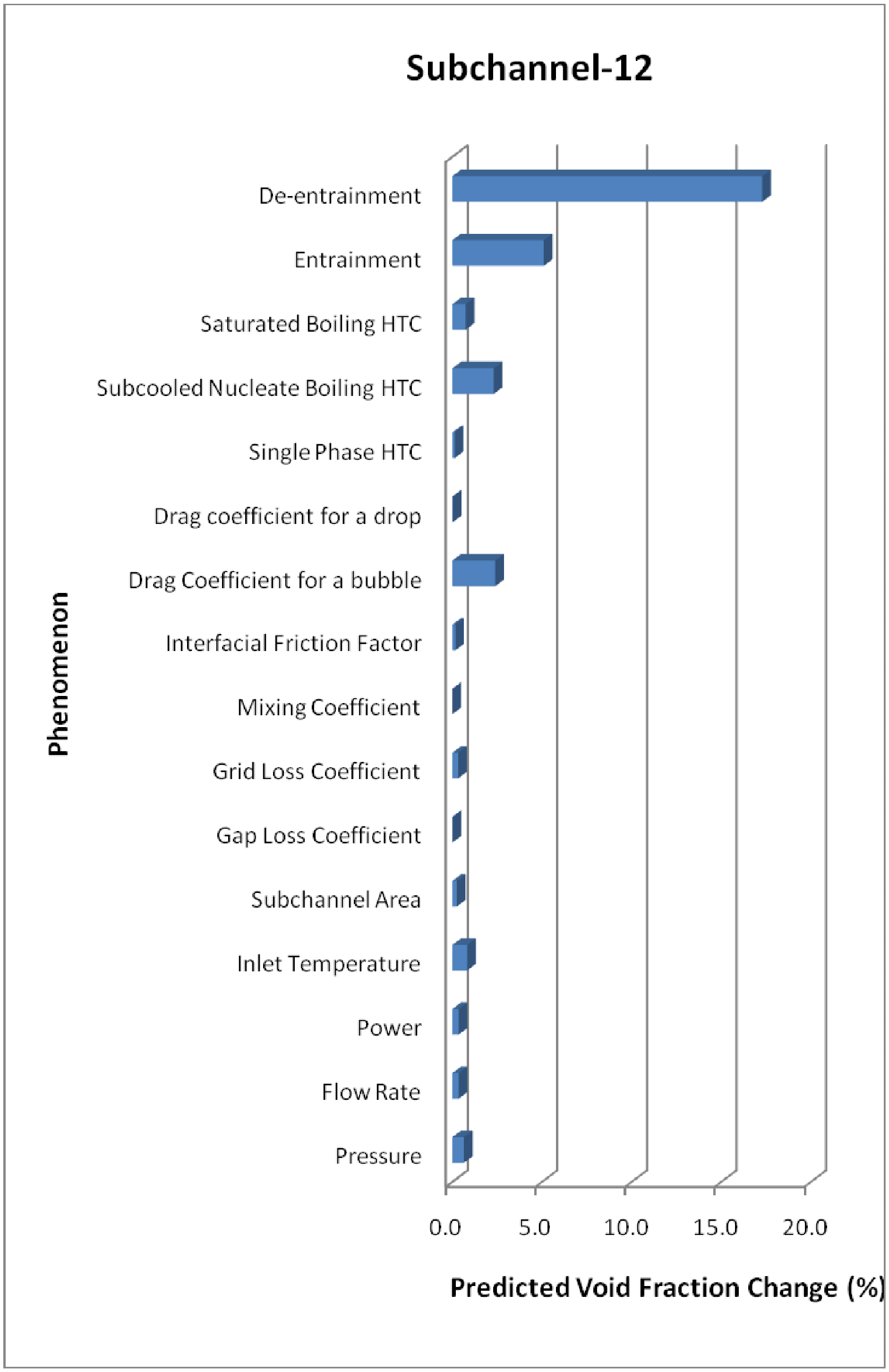

Figure 6.38. Predicted 12th Subchannel Void Fraction Change versus Phenomenon for Test 4101-86

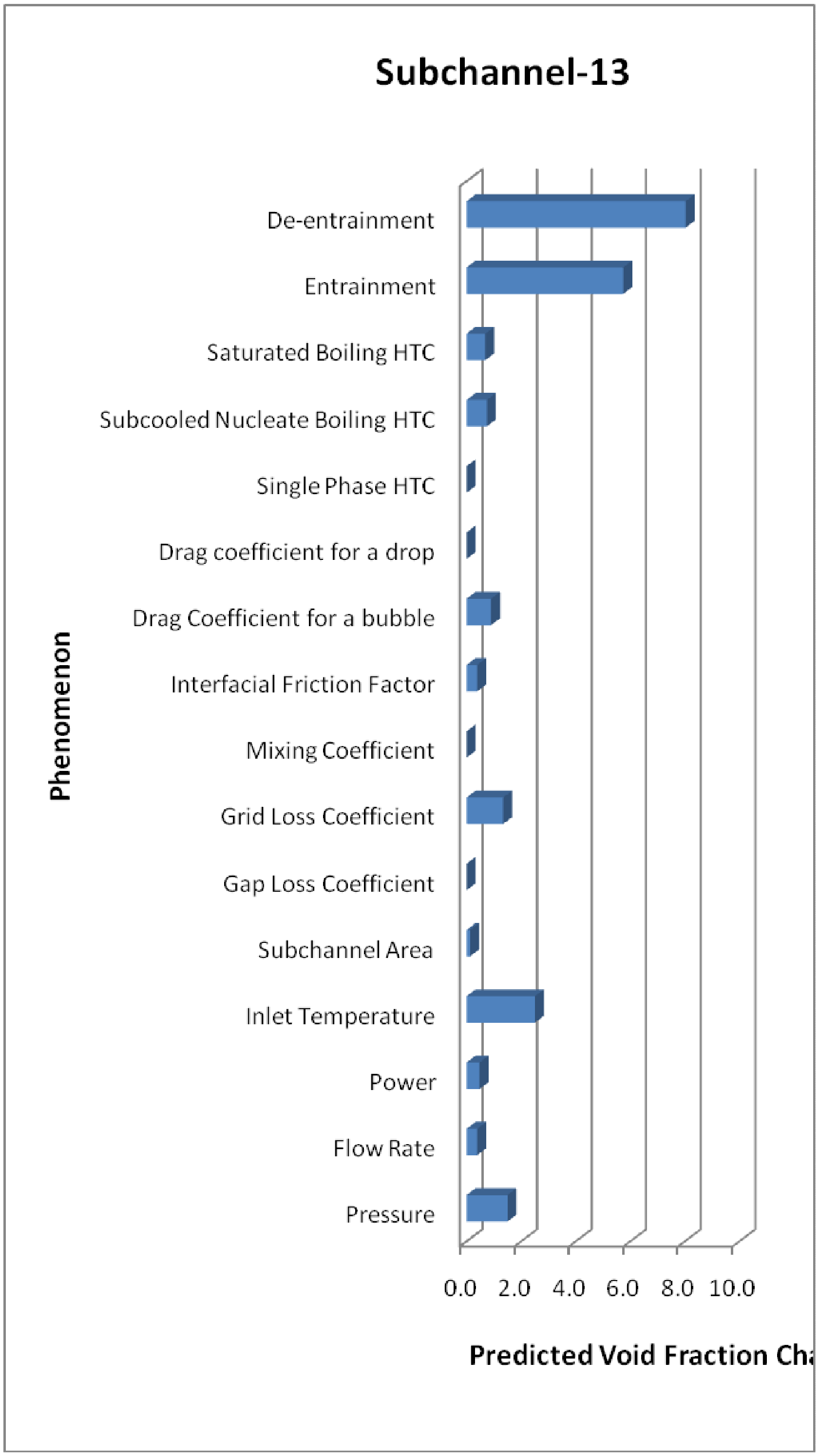

Figure 6.39. Predicted 13th Subchannel Void Fraction Change versus Phenomenon for Test 4101-86

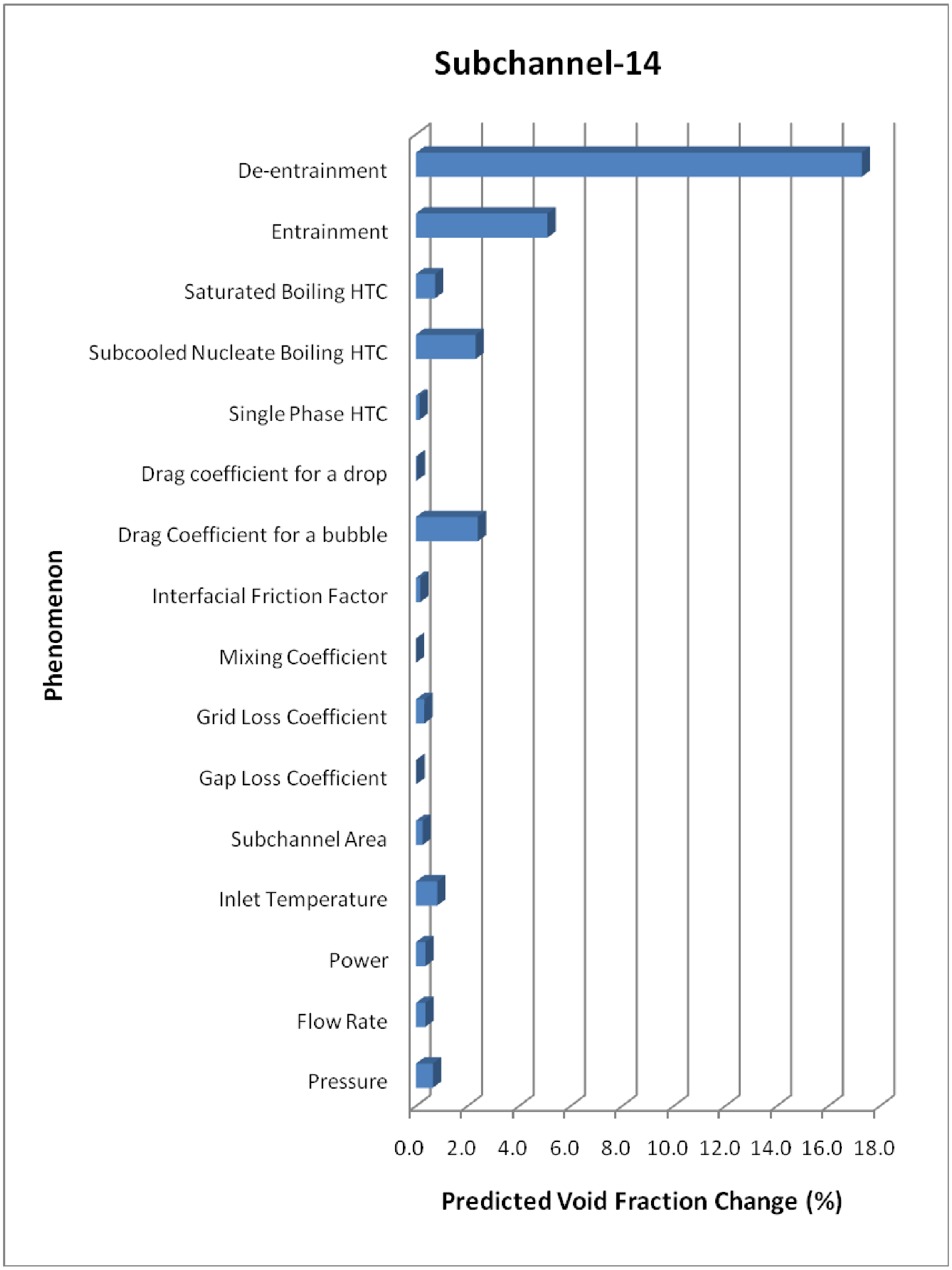

Figure 6.40. Predicted 14th Subchannel Void Fraction Change versus Phenomenon for Test 4101-86

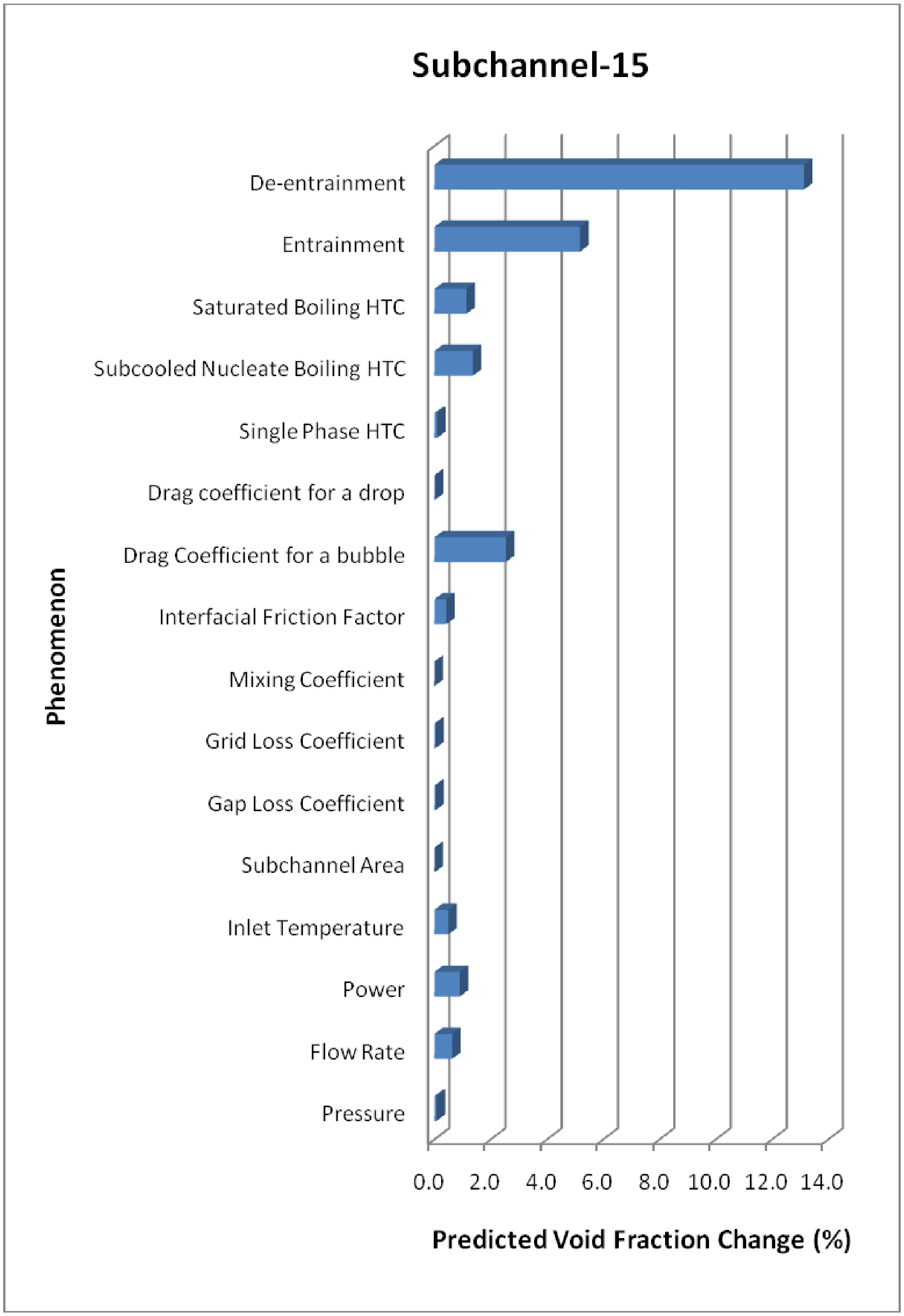

Figure 6.41. Predicted 15th Subchannel Void Fraction Change versus Phenomenon for Test 4101-86

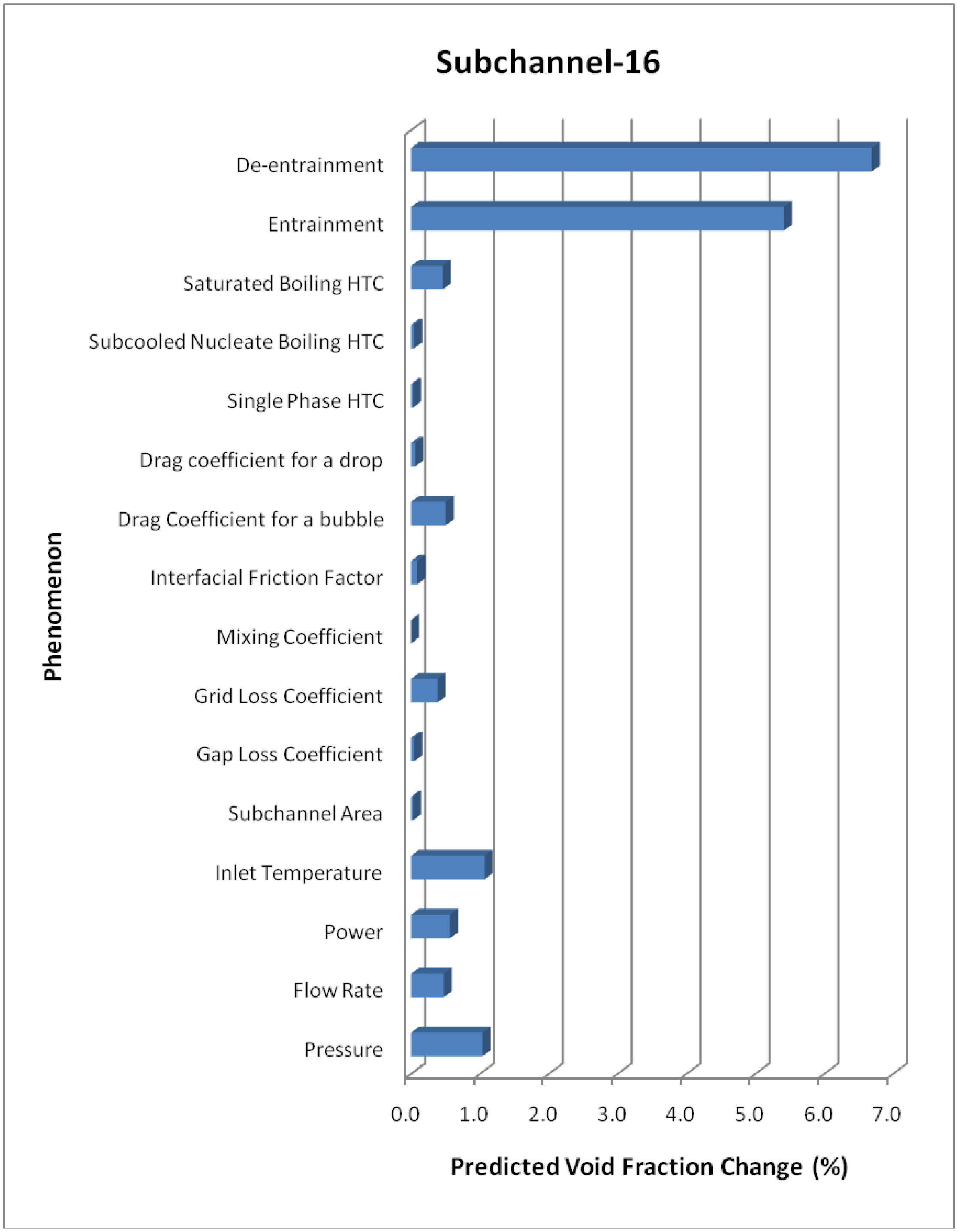

Figure 6.42. Predicted 16th Subchannel Void Fraction Change versus Phenomenon for Test 4101-86

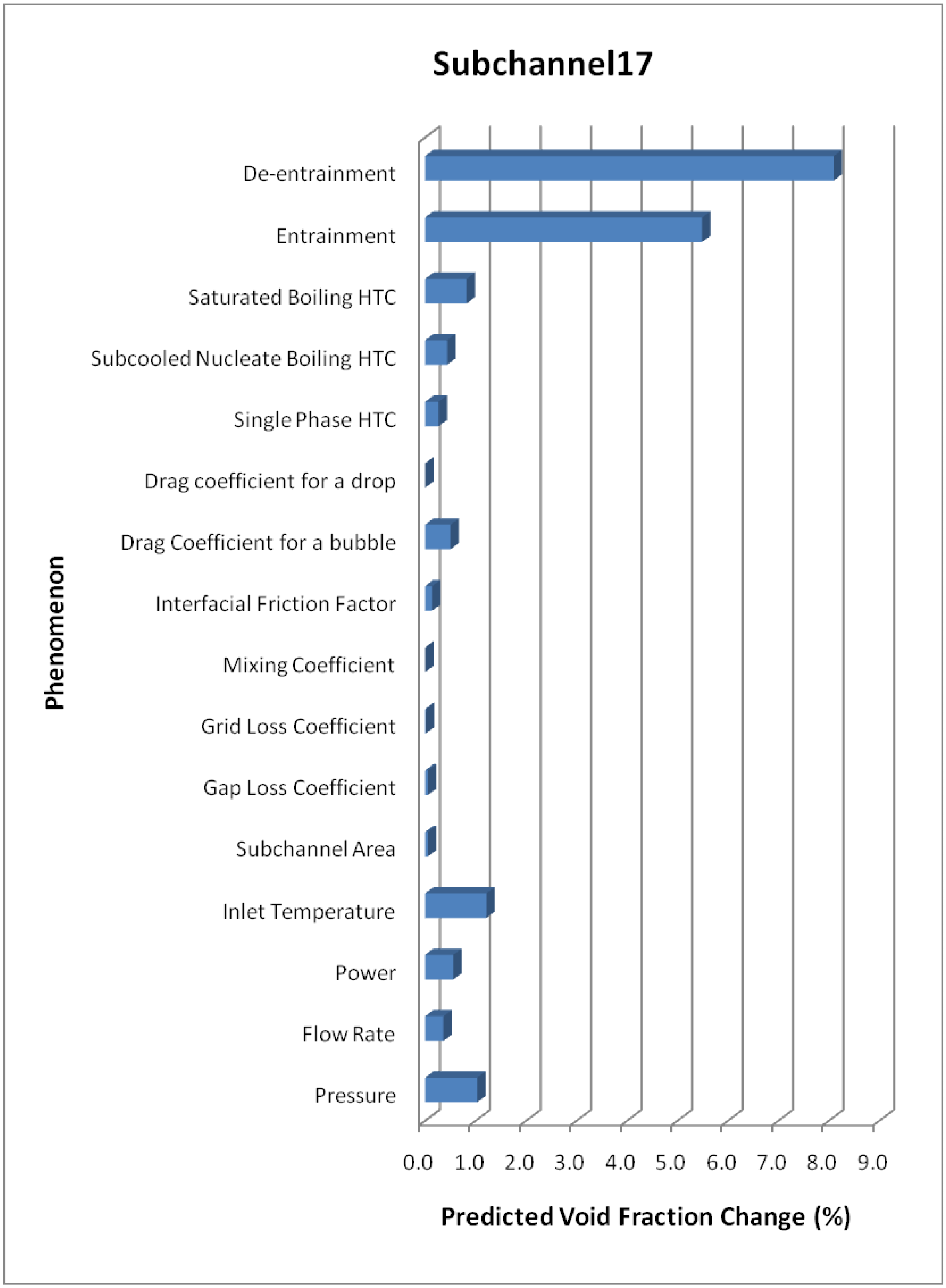

Figure 6.43. Predicted 17th Subchannel Void Fraction Change versus Phenomenon for Test 4101-86

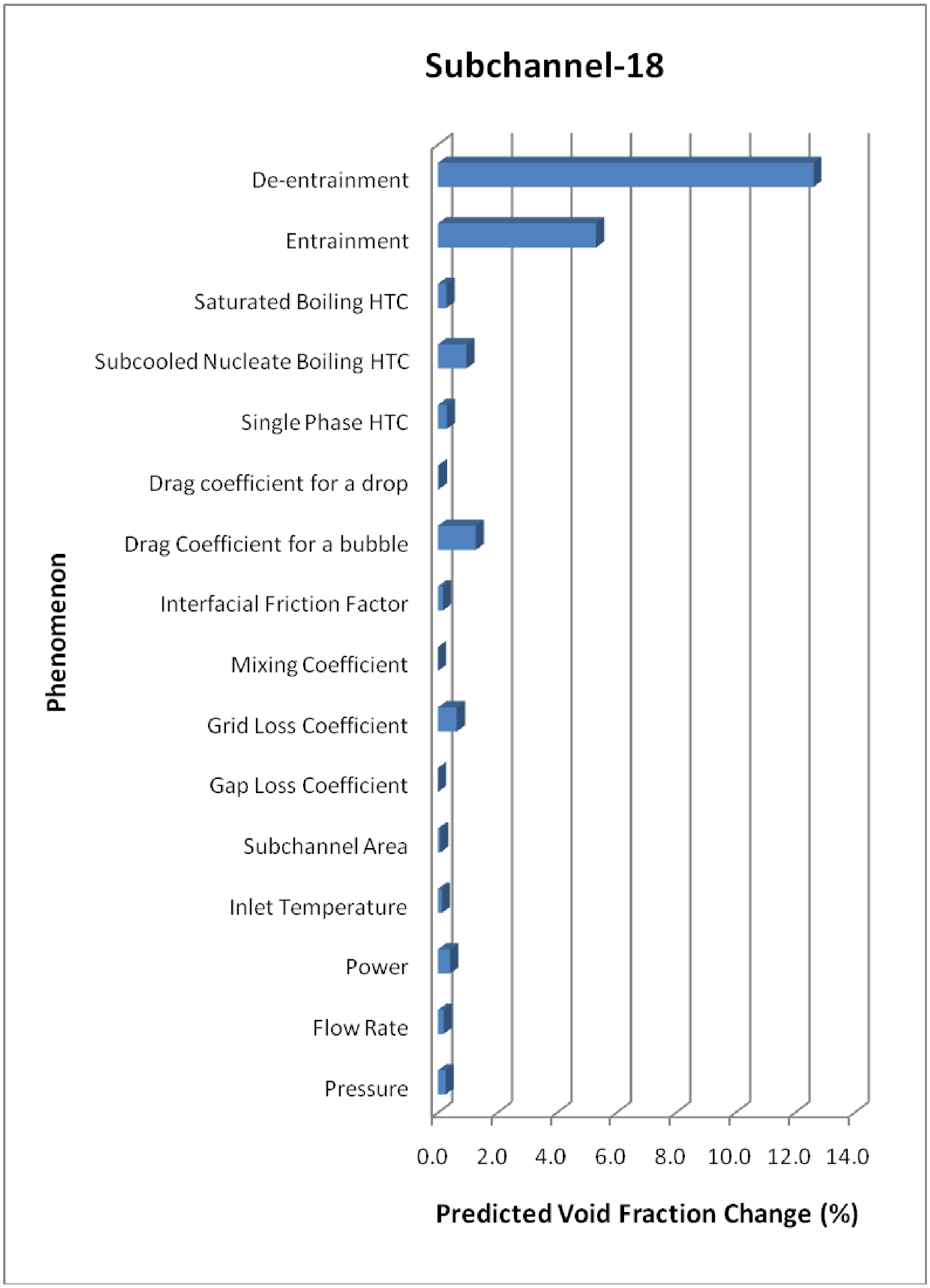

Figure 6.44. Predicted 18th Subchannel Void Fraction Change versus Phenomenon for Test 4101-86

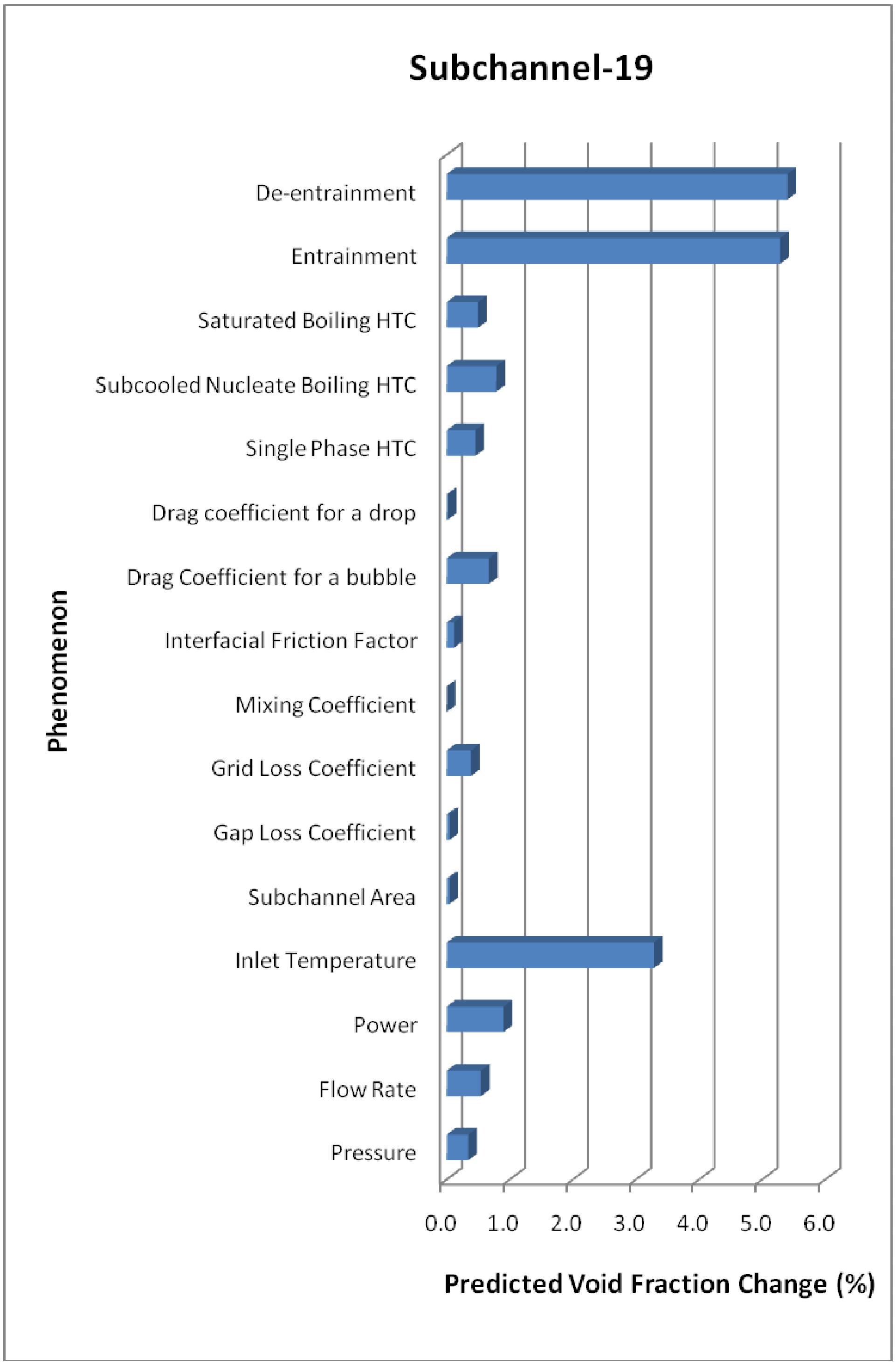

Figure 6.45. Predicted 19th Subchannel Void Fraction Change versus Phenomenon for Test 4101-86

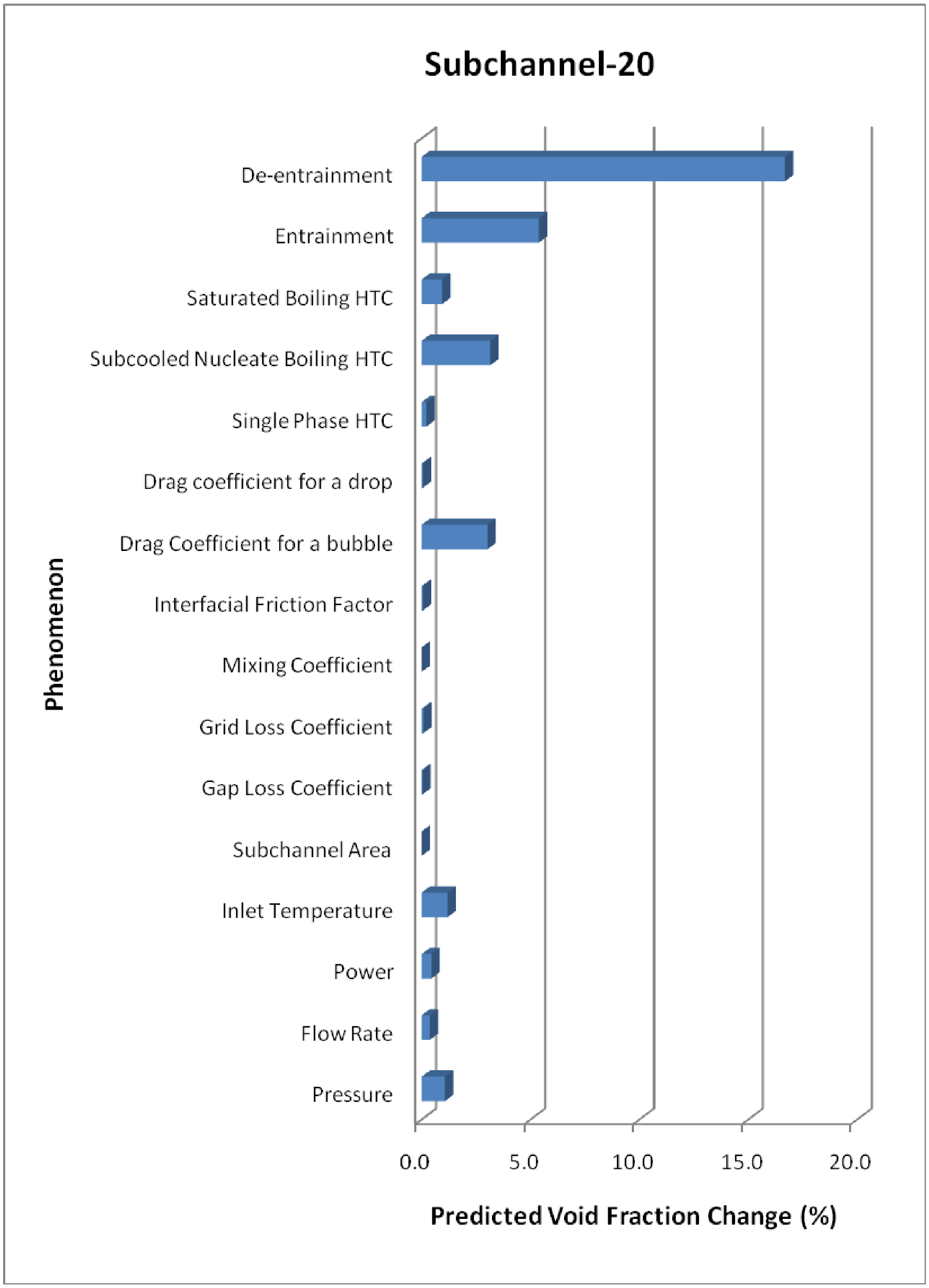

Figure 6.46. Predicted 20th Subchannel Void Fraction Change versus Phenomenon for Test 4101-86

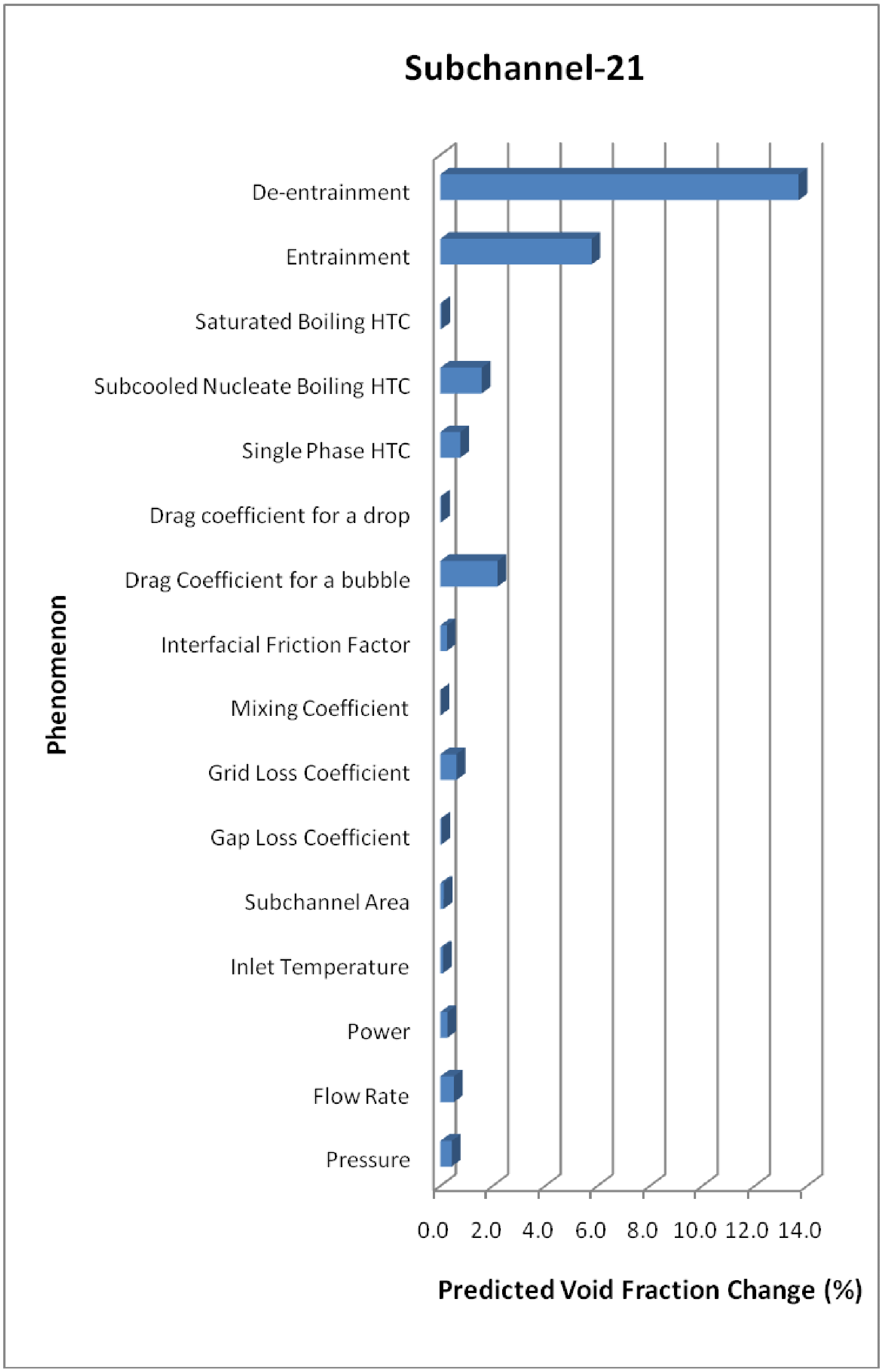

Figure 6.47. Predicted 21th Subchannel Void Fraction Change versus Phenomenon for Test 4101-86

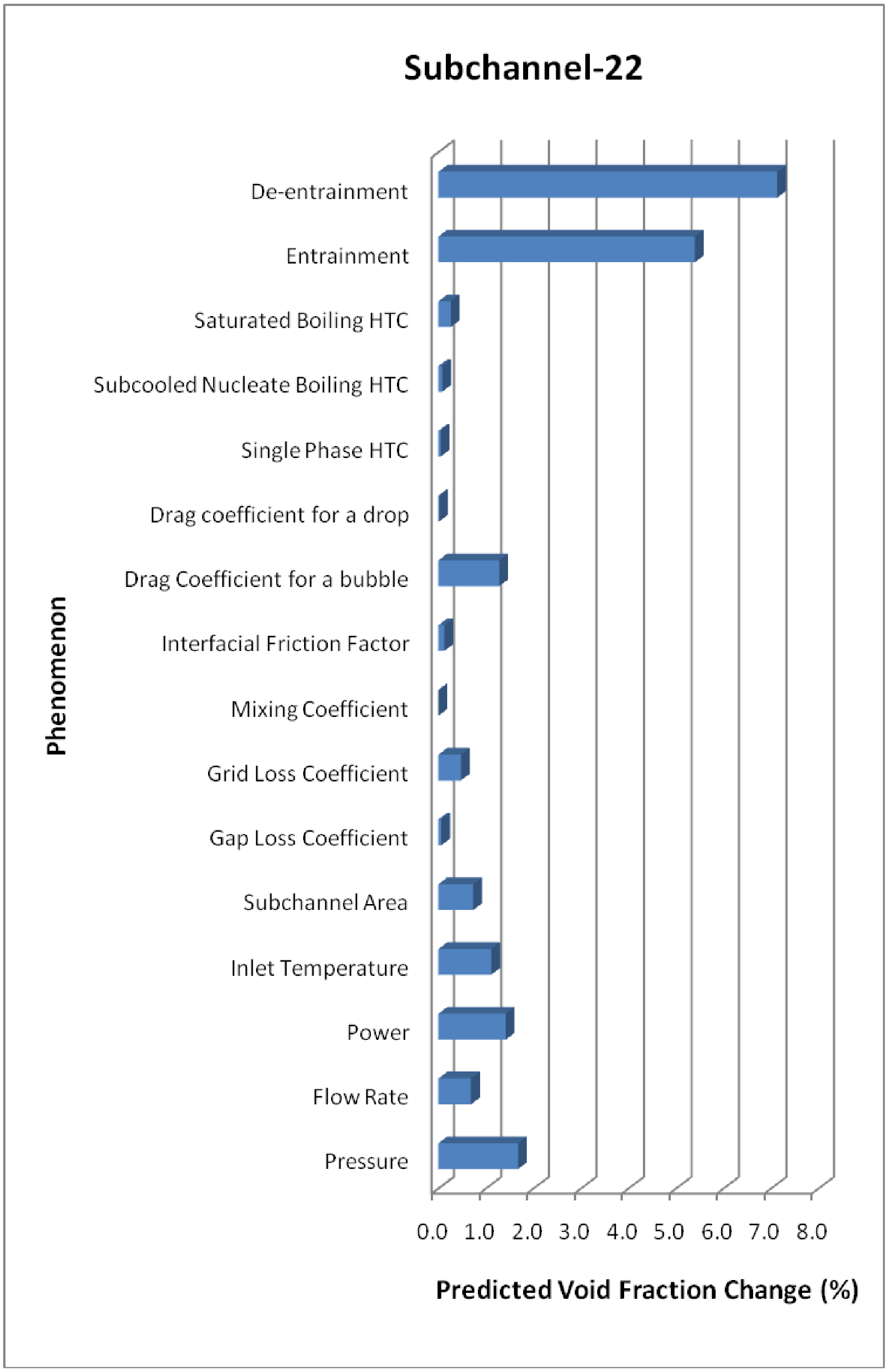

Figure 6.48. Predicted 22nd Subchannel Void Fraction Change versus Phenomenon for Test 4101-86

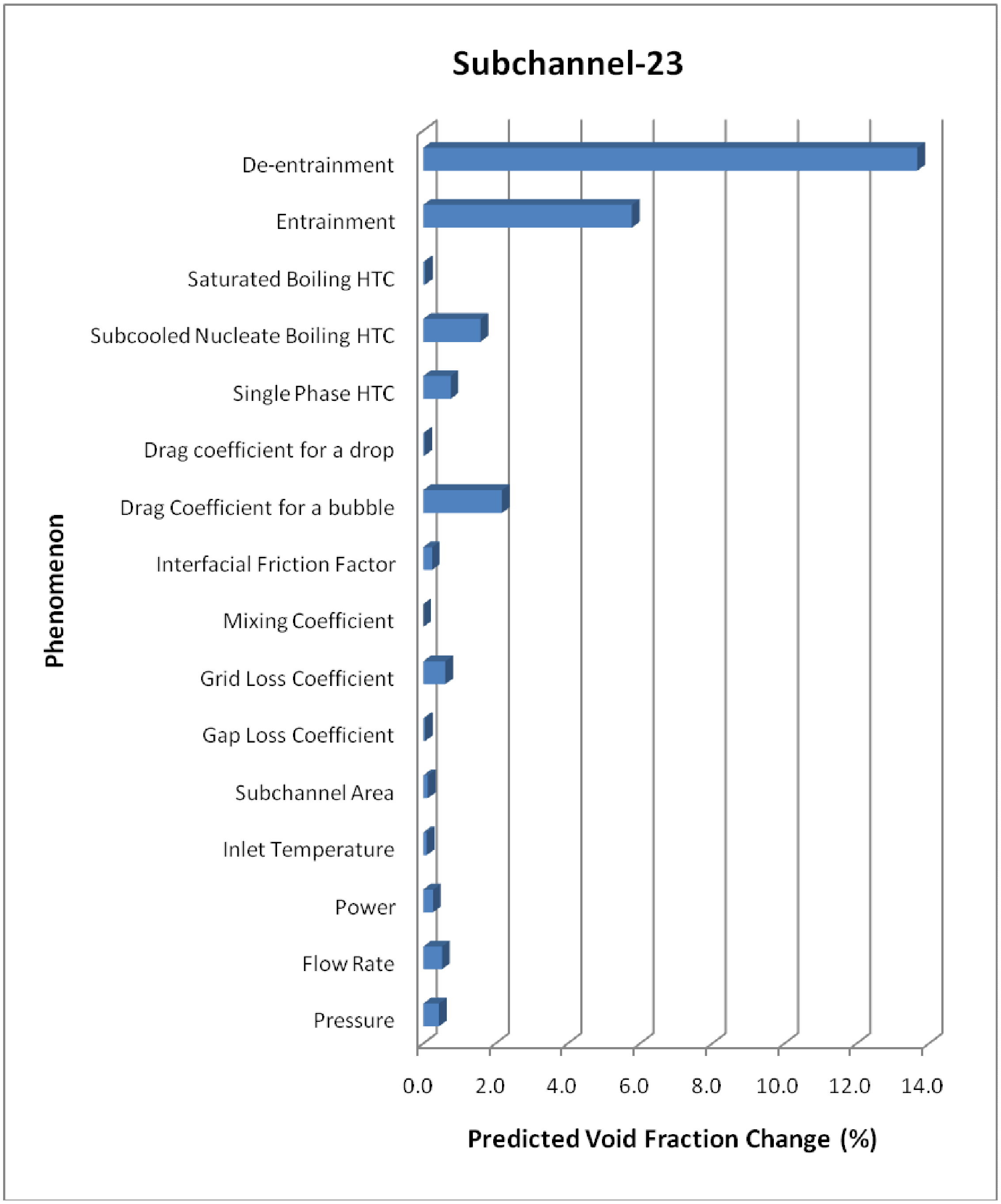

Figure 6.49. Predicted 23th Subchannel Void Fraction Change versus Phenomenon for Test 4101-86

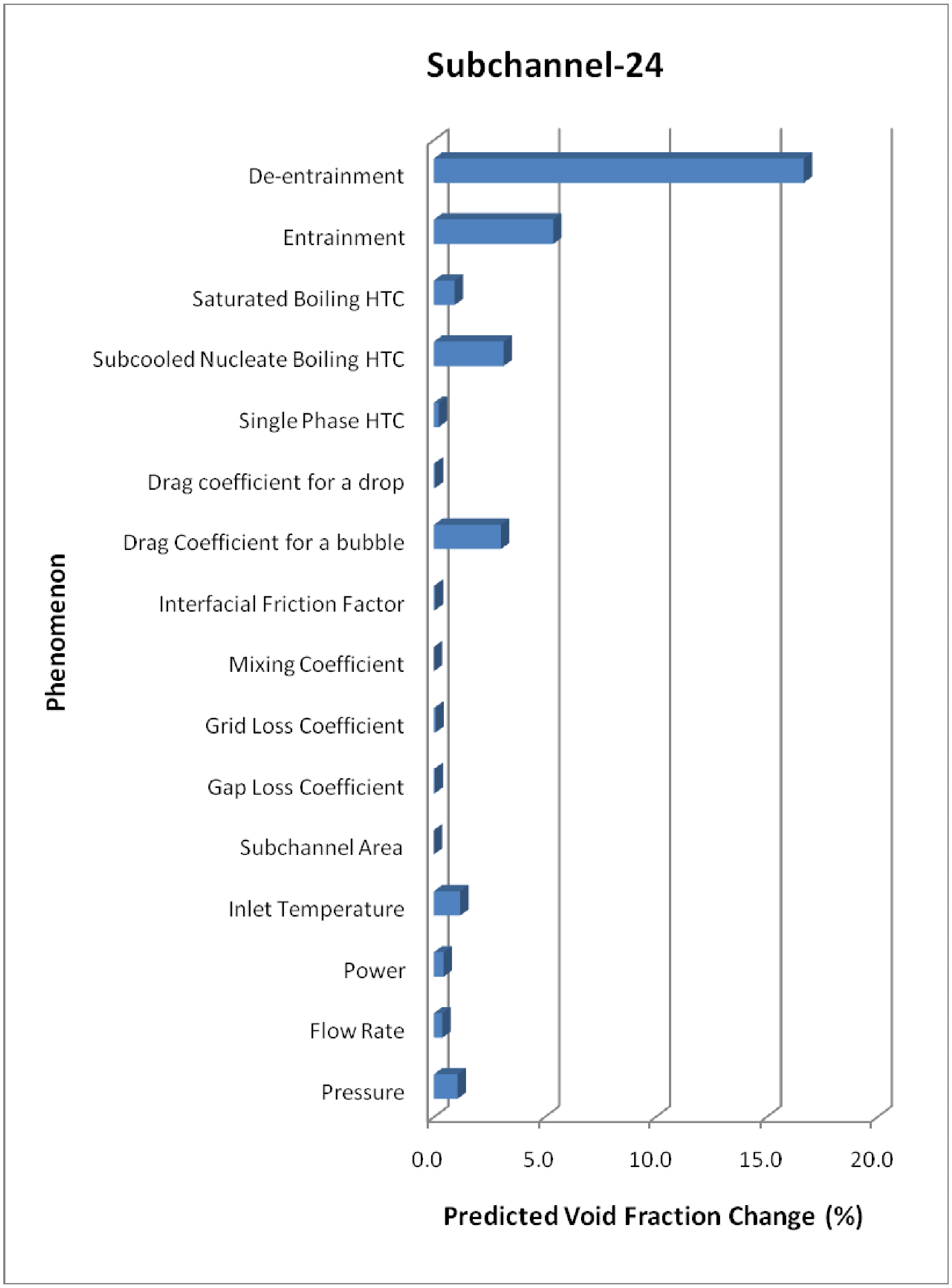

Figure 6.50. Predicted 24th Subchannel Void Fraction Change versus Phenomenon for Test 4101-86

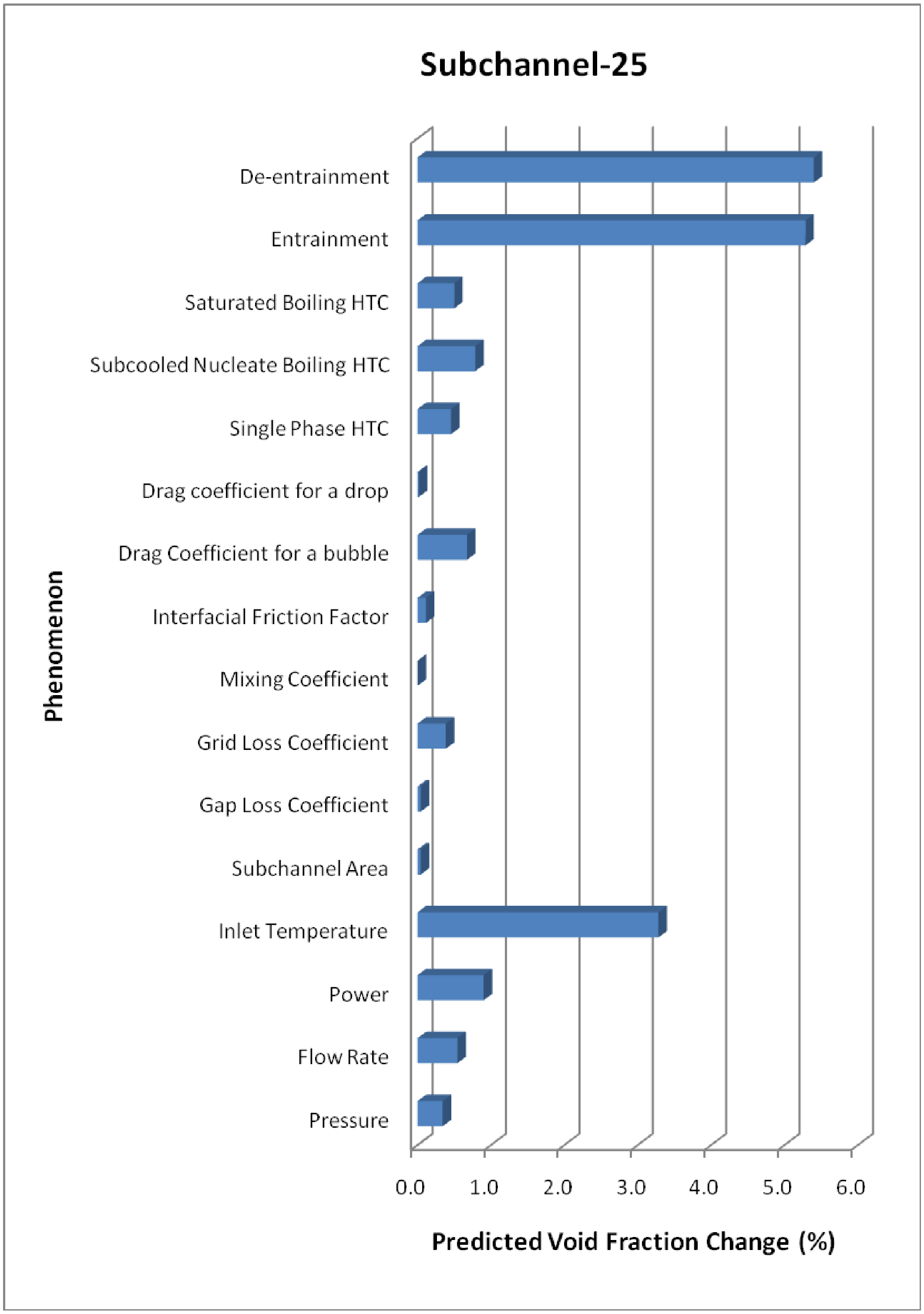

Figure 6.51. Predicted 25th Subchannel Void Fraction Change versus Phenomenon for Test 4101-86

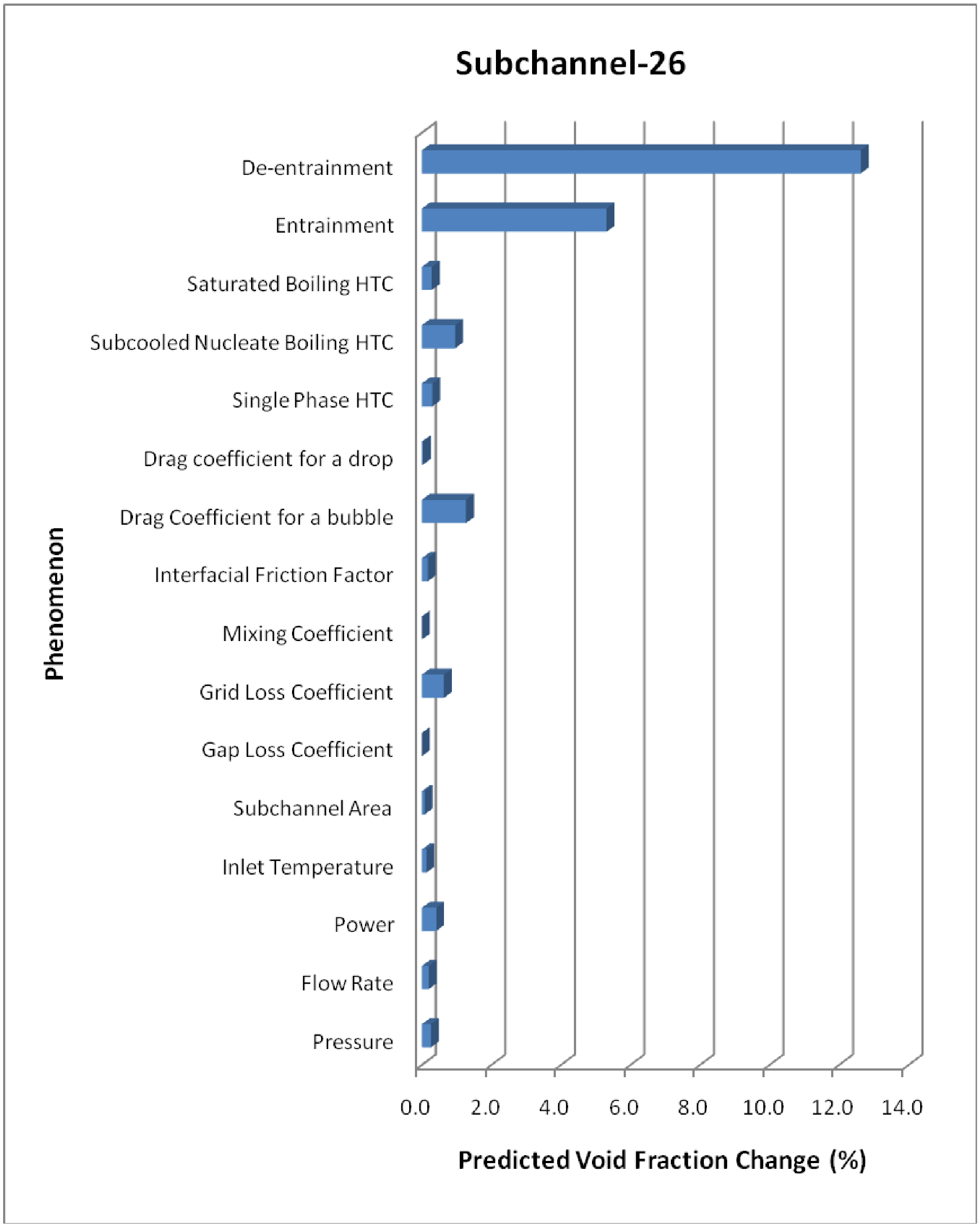

Figure 6.52. Predicted 26th Subchannel Void Fraction Change versus Phenomenon for Test 4101-86

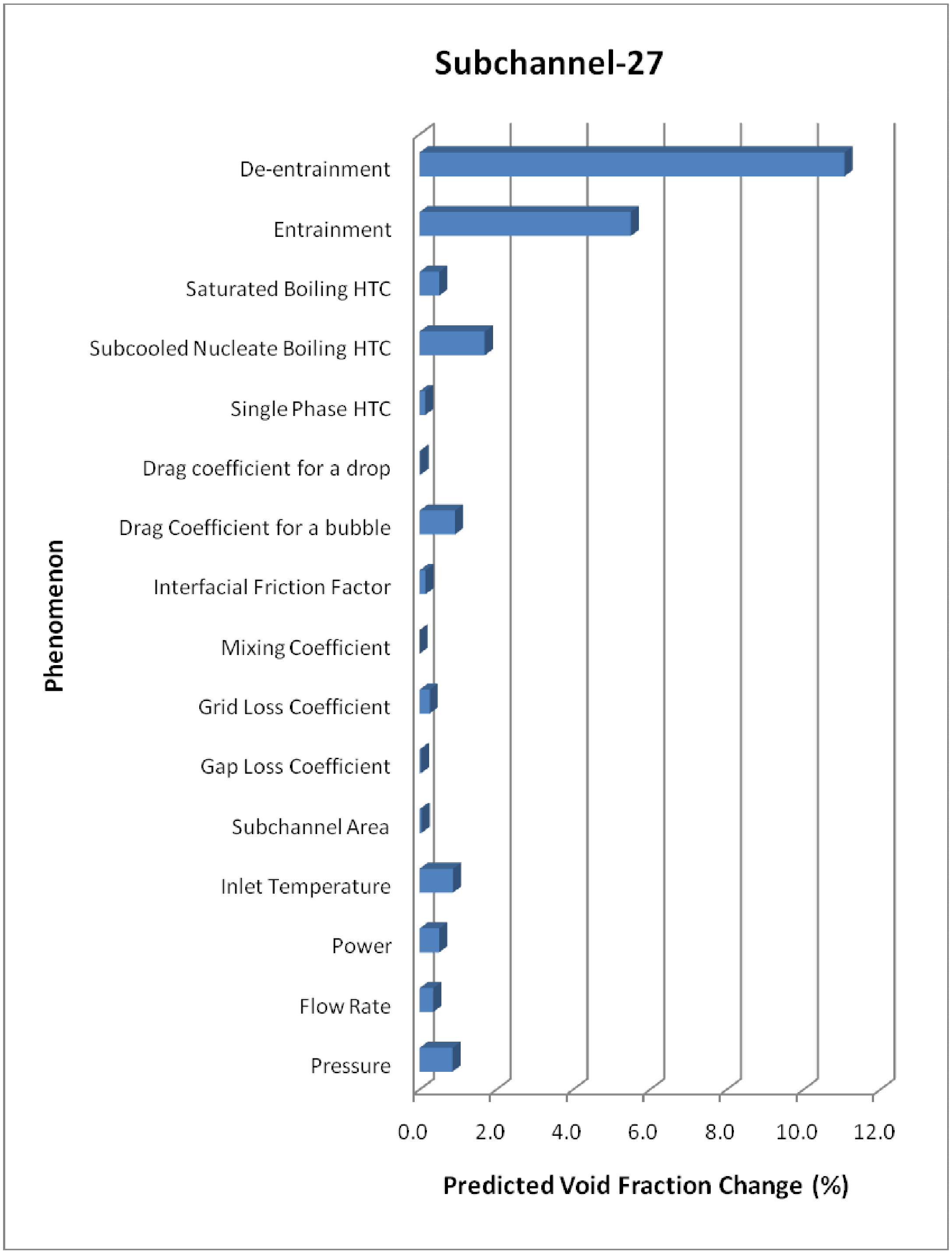

Figure 6.53. Predicted 27th Subchannel Void Fraction Change versus Phenomenon for Test 4101-86

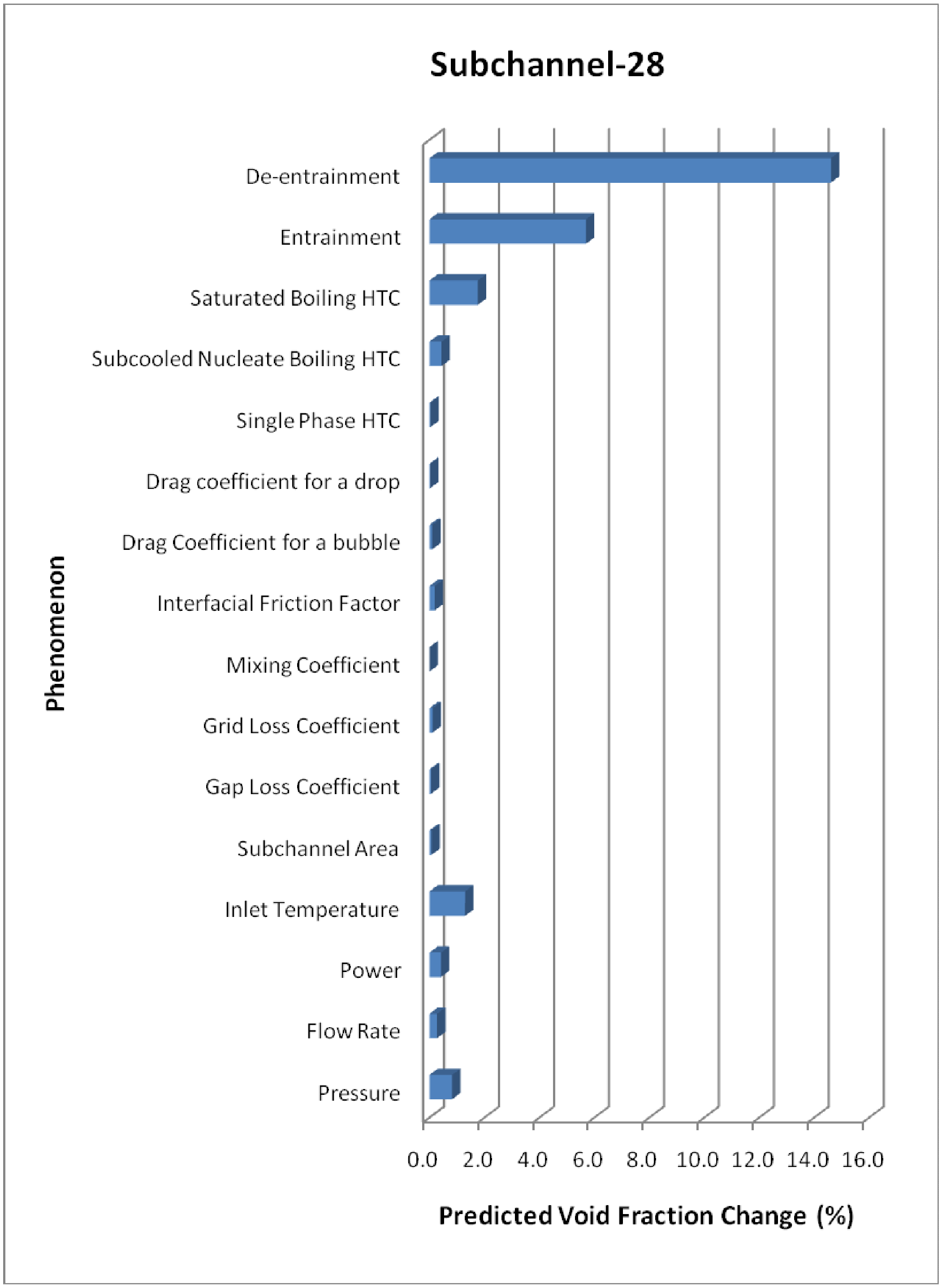

Figure 6.54. Predicted 28th Subchannel Void Fraction Change versus Phenomenon for Test 4101-86

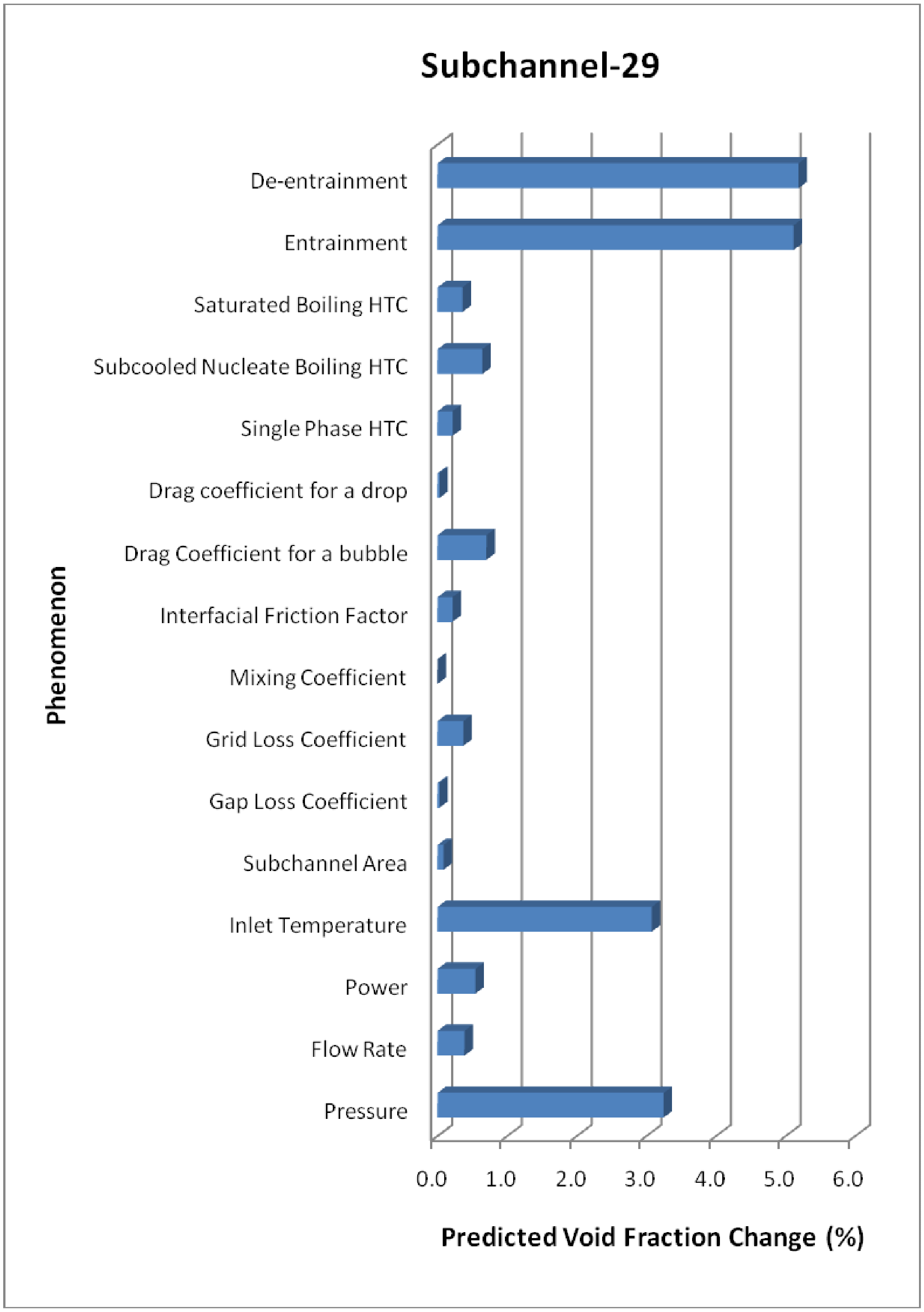

Figure 6.55. Predicted 29th Subchannel Void Fraction Change versus Phenomenon for Test 4101-86

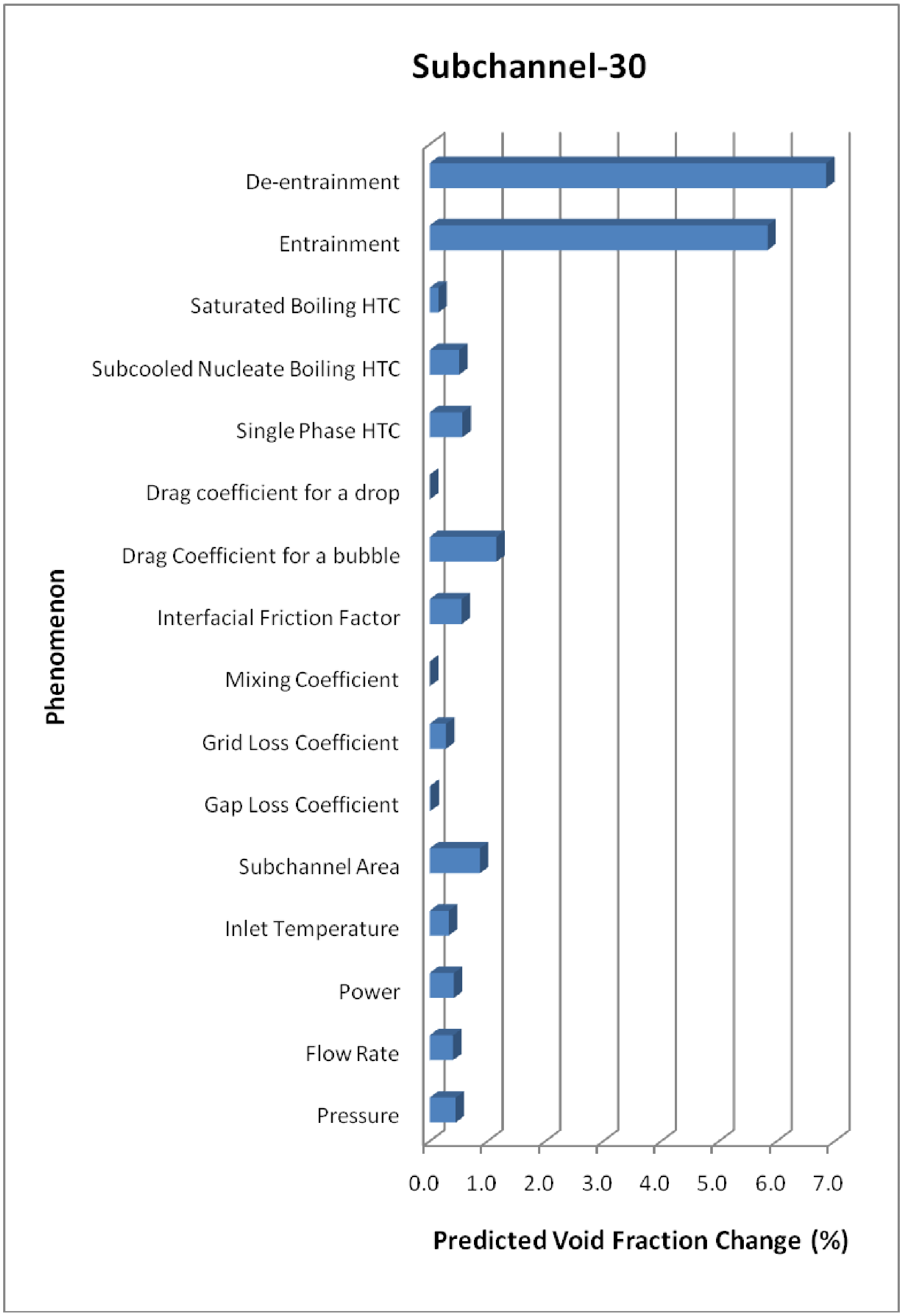

Figure 6.56. Predicted 30th Subchannel Void Fraction Change versus Phenomenon for Test 4101-86

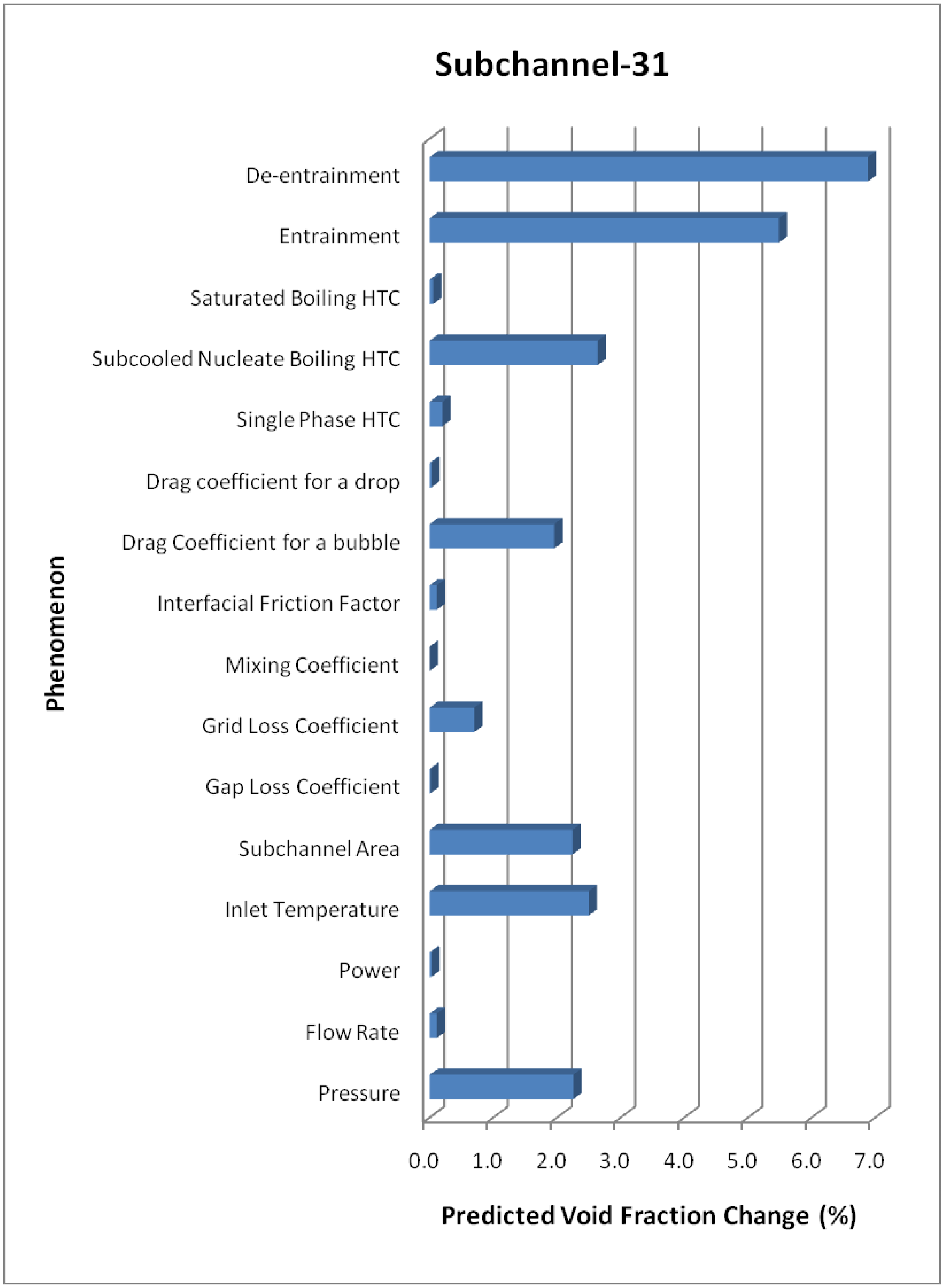

Figure 6.57. Predicted 31st Subchannel Void Fraction Change versus Phenomenon for Test 4101-86

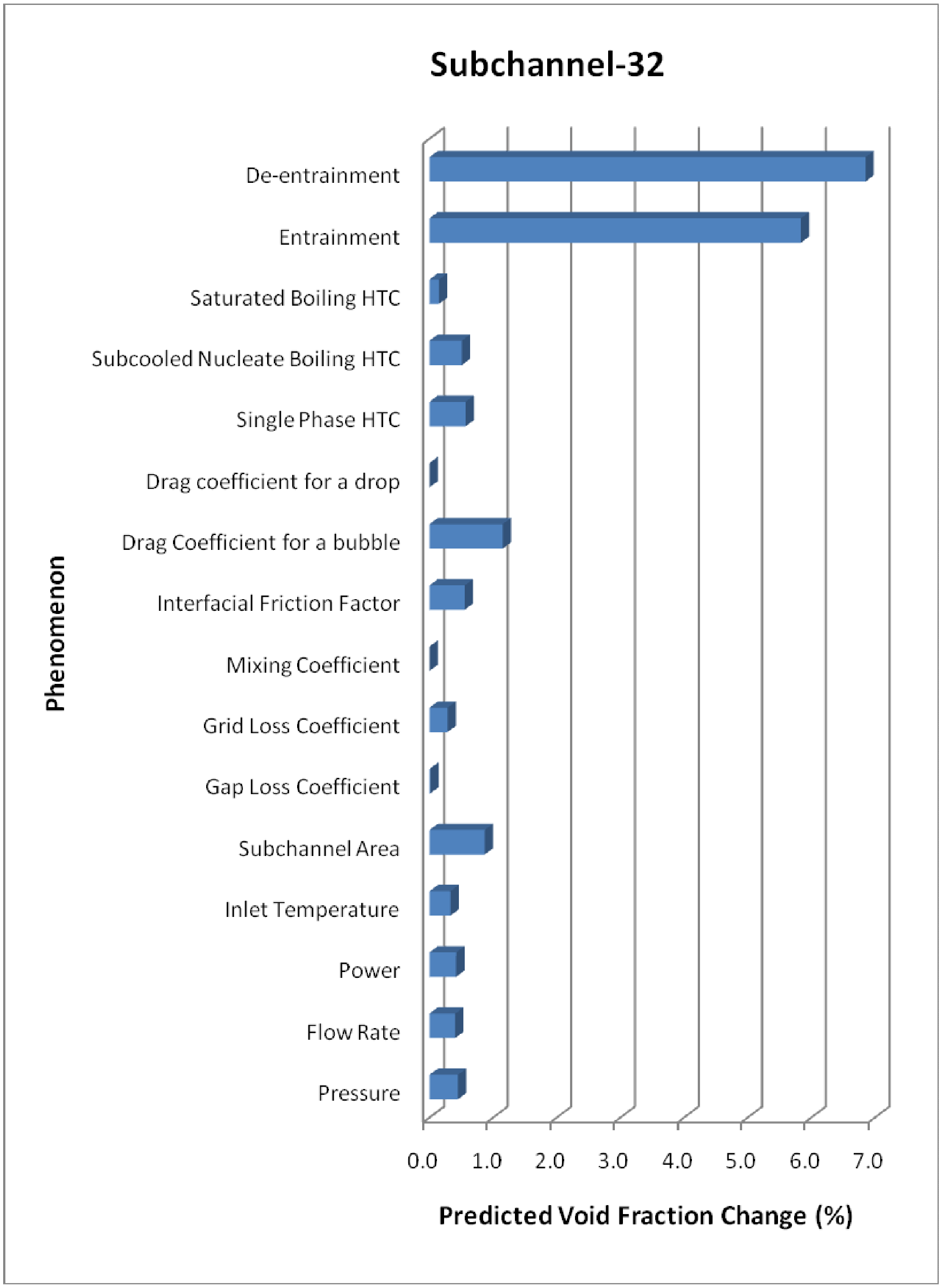

Figure 6.58. Predicted 32nd Subchannel Void Fraction Change versus Phenomenon for Test 4101-86

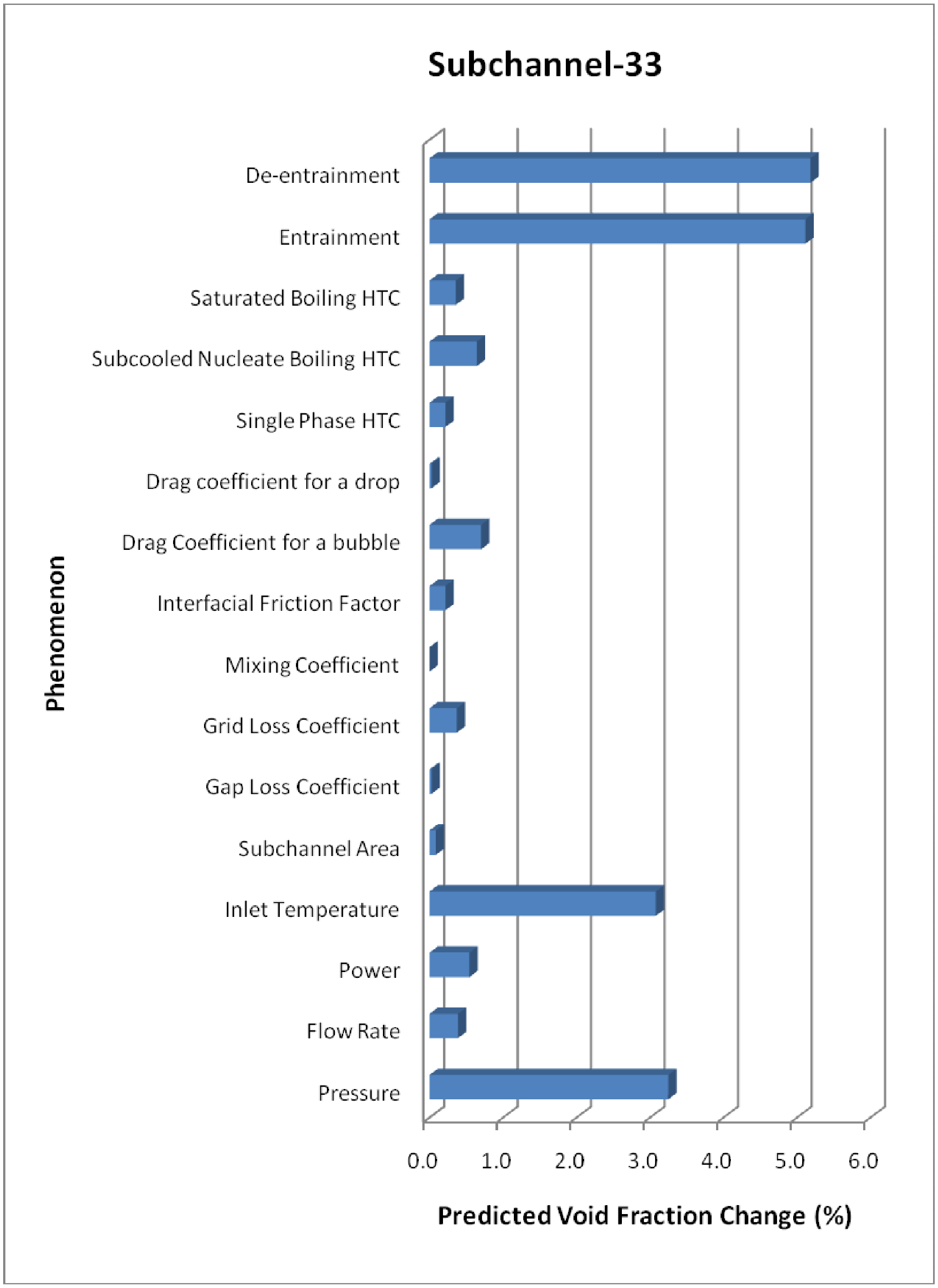

Figure 6.59. Predicted 33th Subchannel Void Fraction Change versus Phenomenon for Test 4101-86

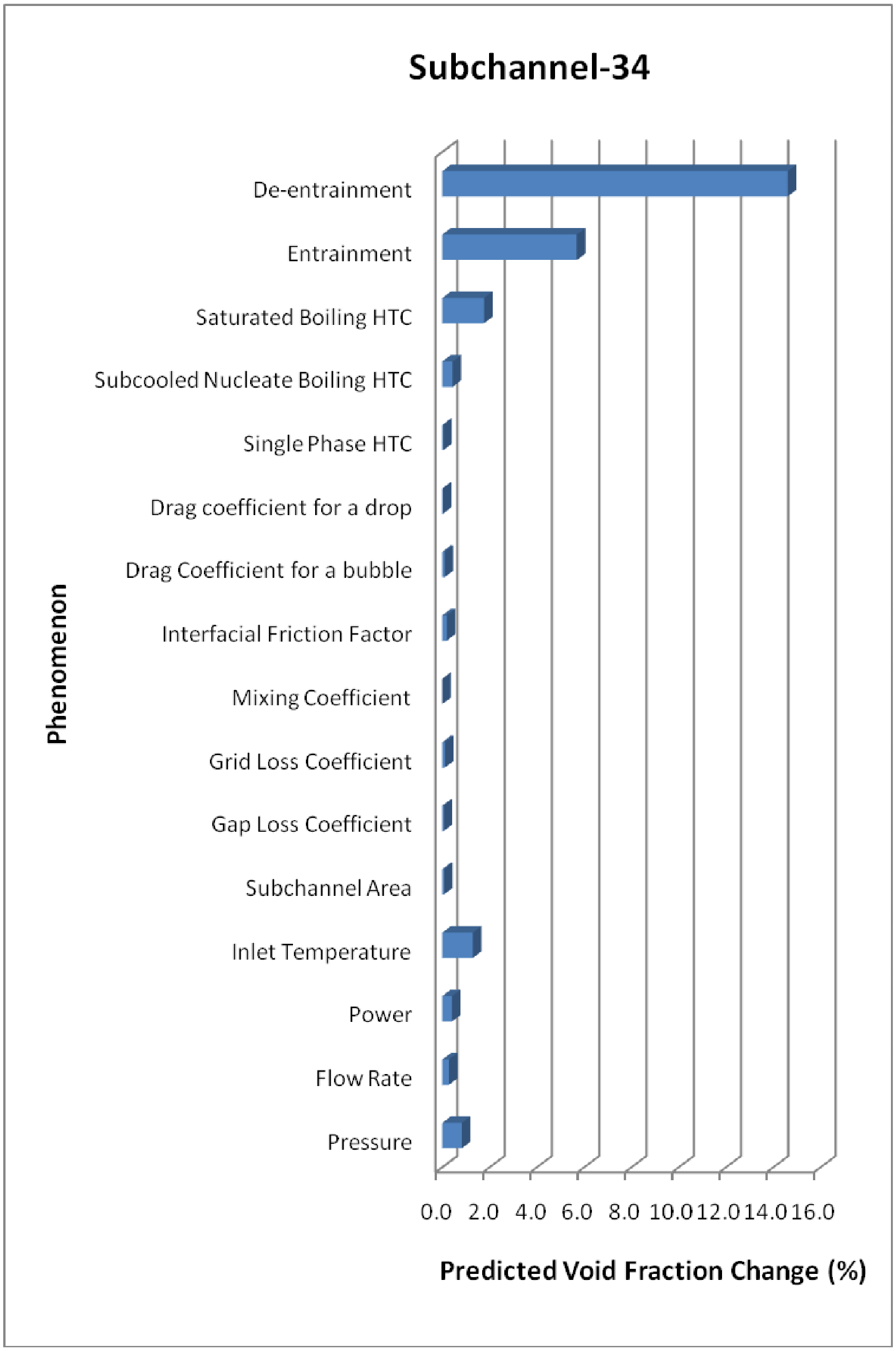

Figure 6.60. Predicted 34th Subchannel Void Fraction Change versus Phenomenon for Test 4101-86

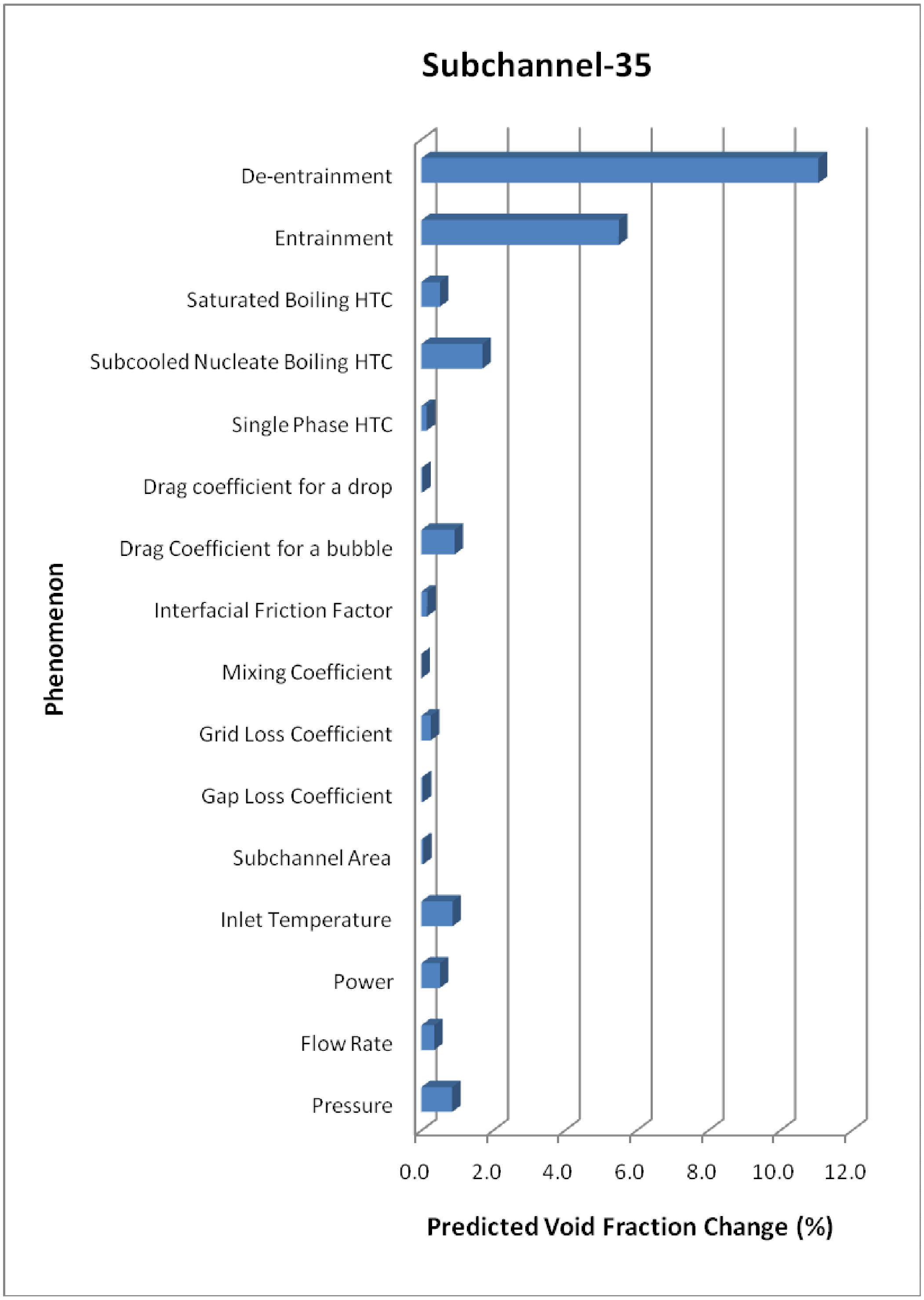

Figure 6.61. Predicted 35th Subchannel Void Fraction Change versus Phenomenon for Test 4101-86

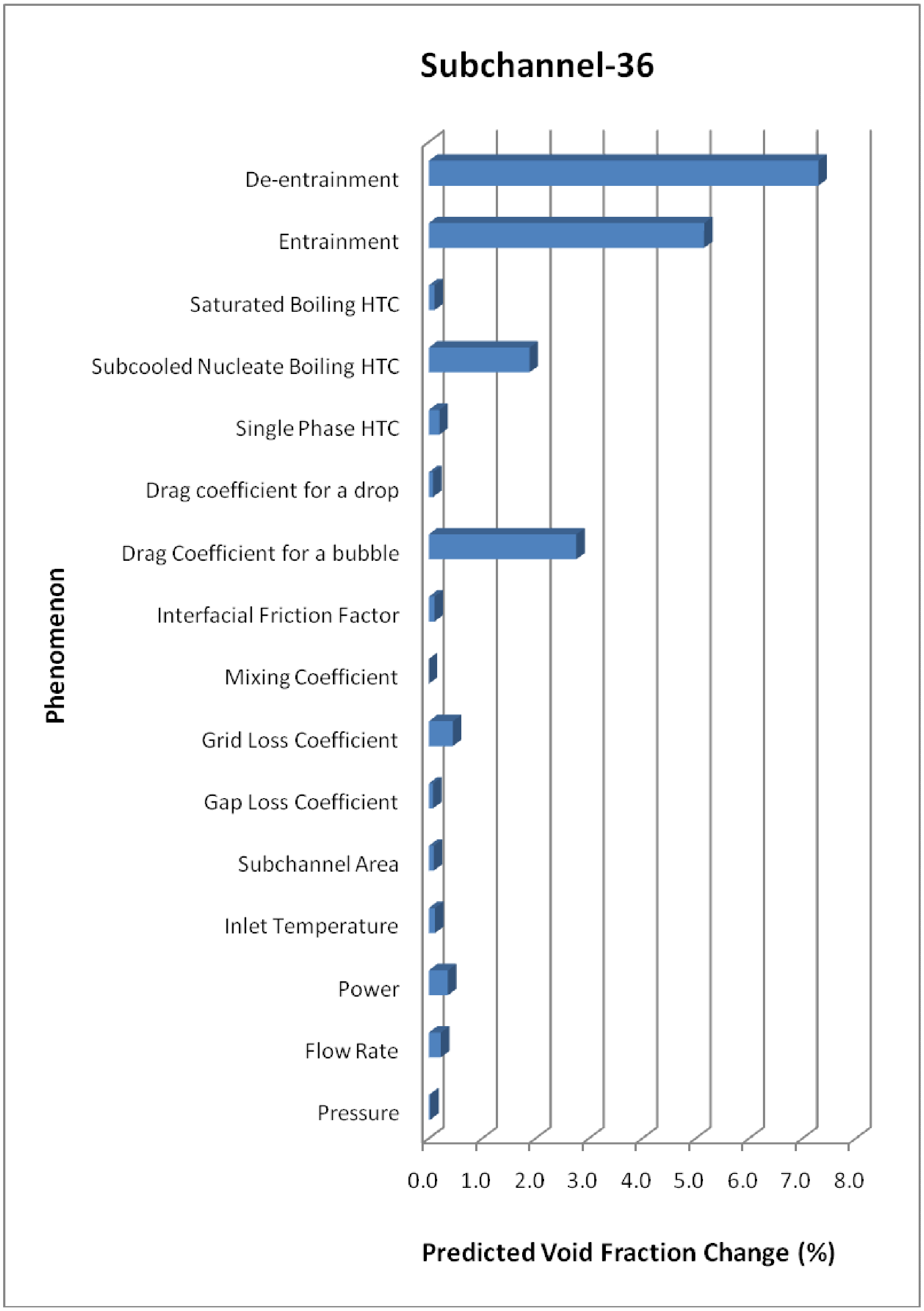

Figure 6.62. Predicted36th Subchannel Void Fraction Change versus Phenomenon for Test 4101-86

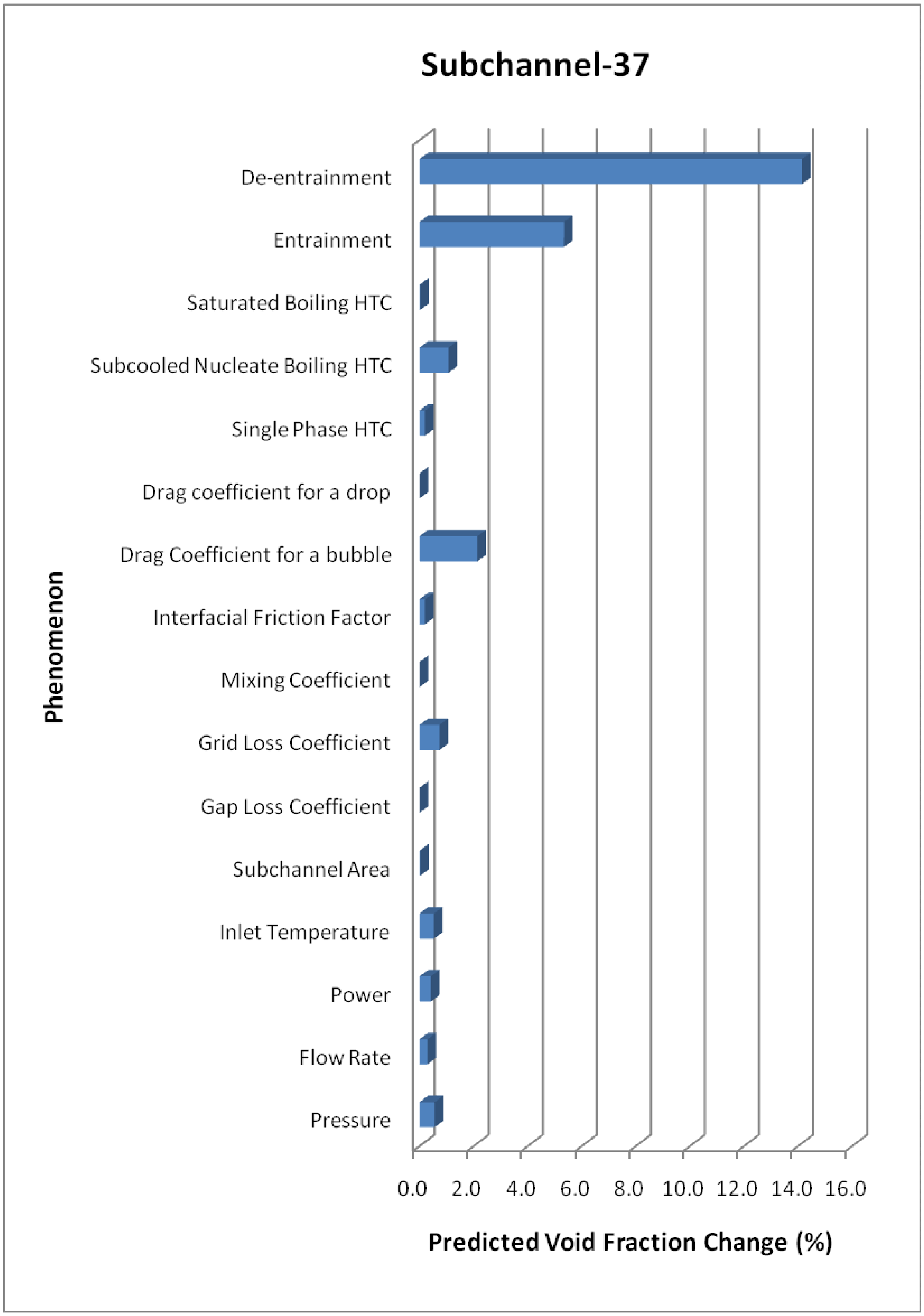

Figure 6.63. Predicted 37th Subchannel Void Fraction Change versus Phenomenon for Test 4101-86

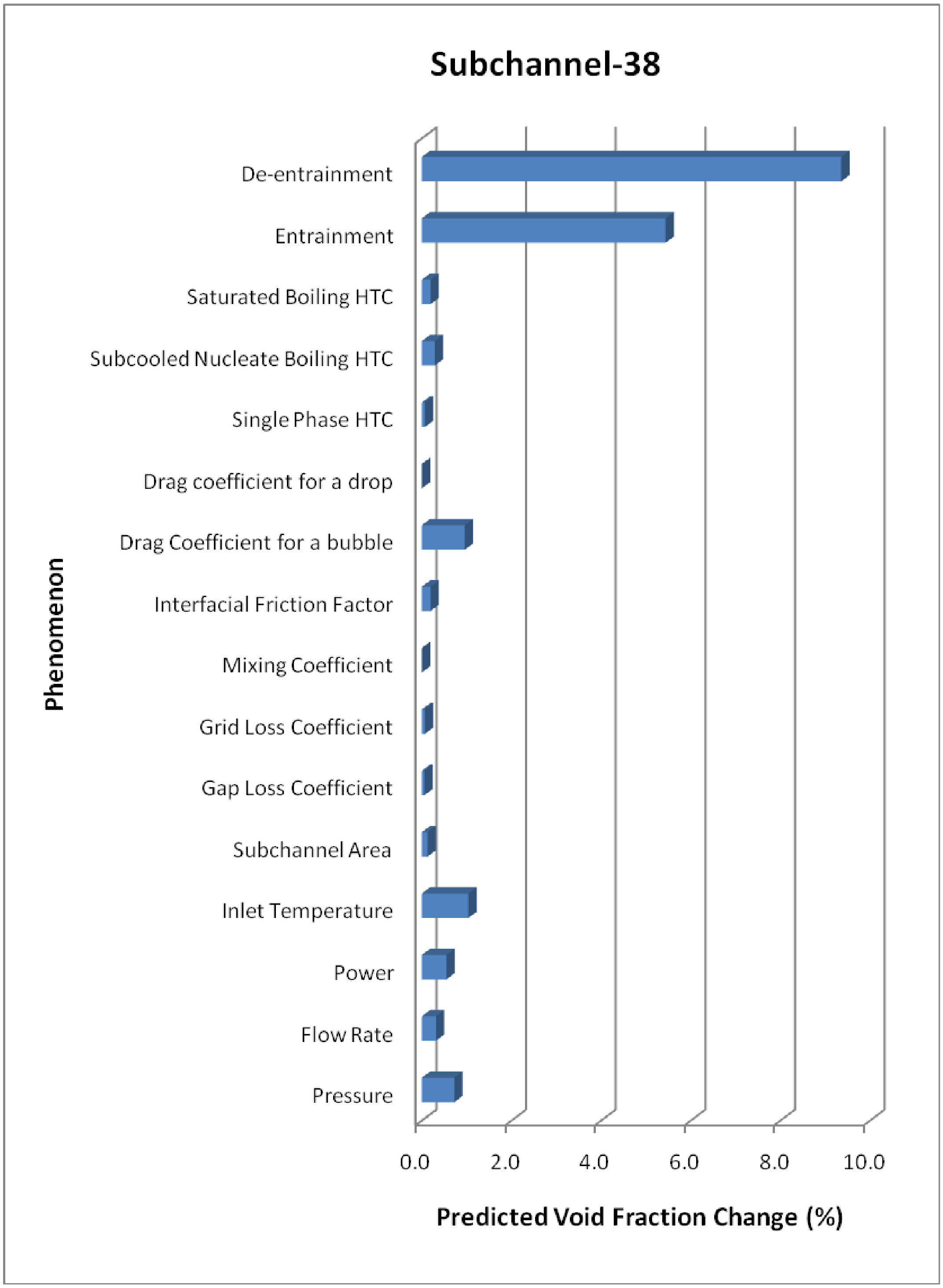

Figure 6.64. Predicted 38th Subchannel Void Fraction Change versus Phenomenon for Test 4101-86

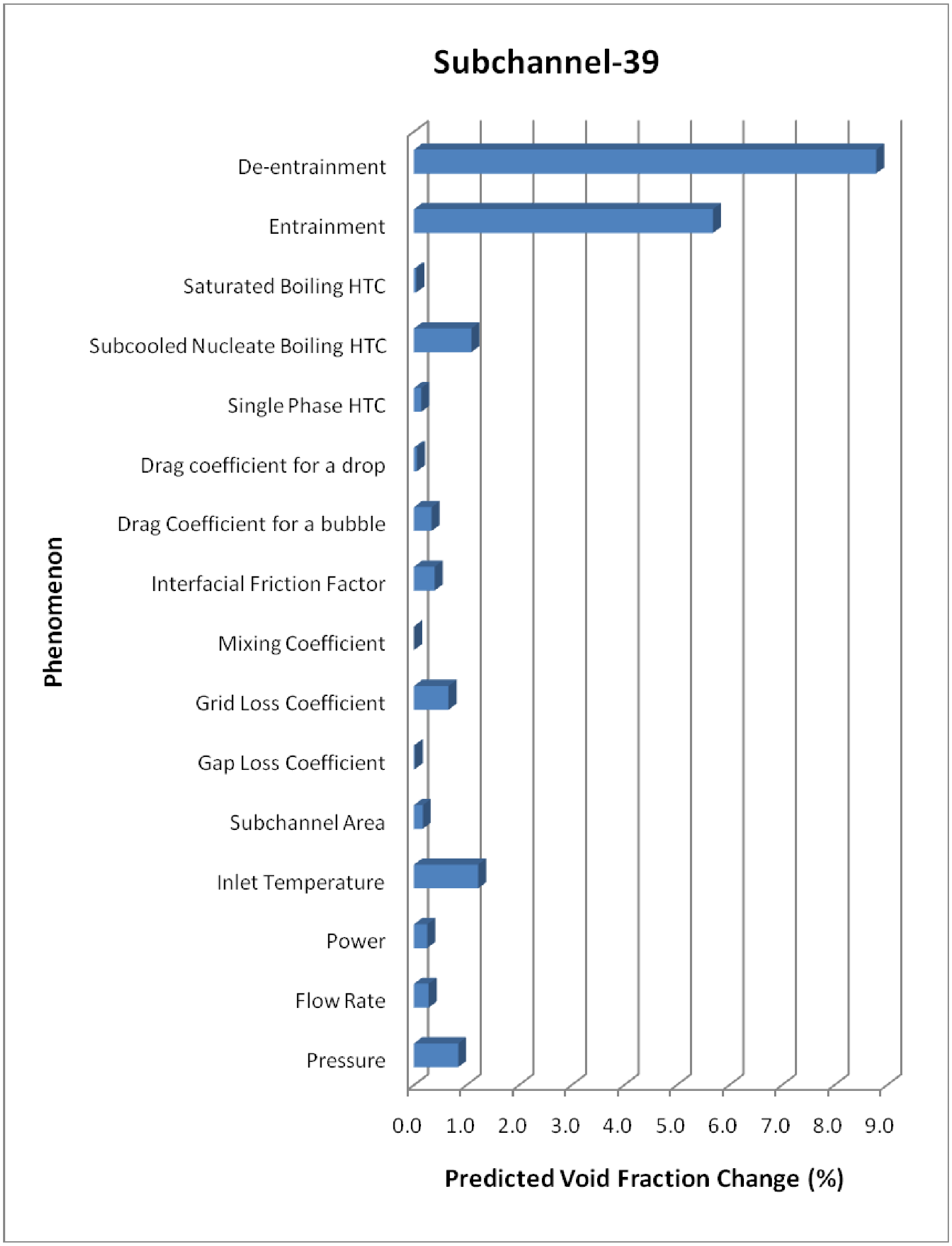

Figure 6.65. Predicted 39th Subchannel Void Fraction Change versus Phenomenon for Test 4101-86

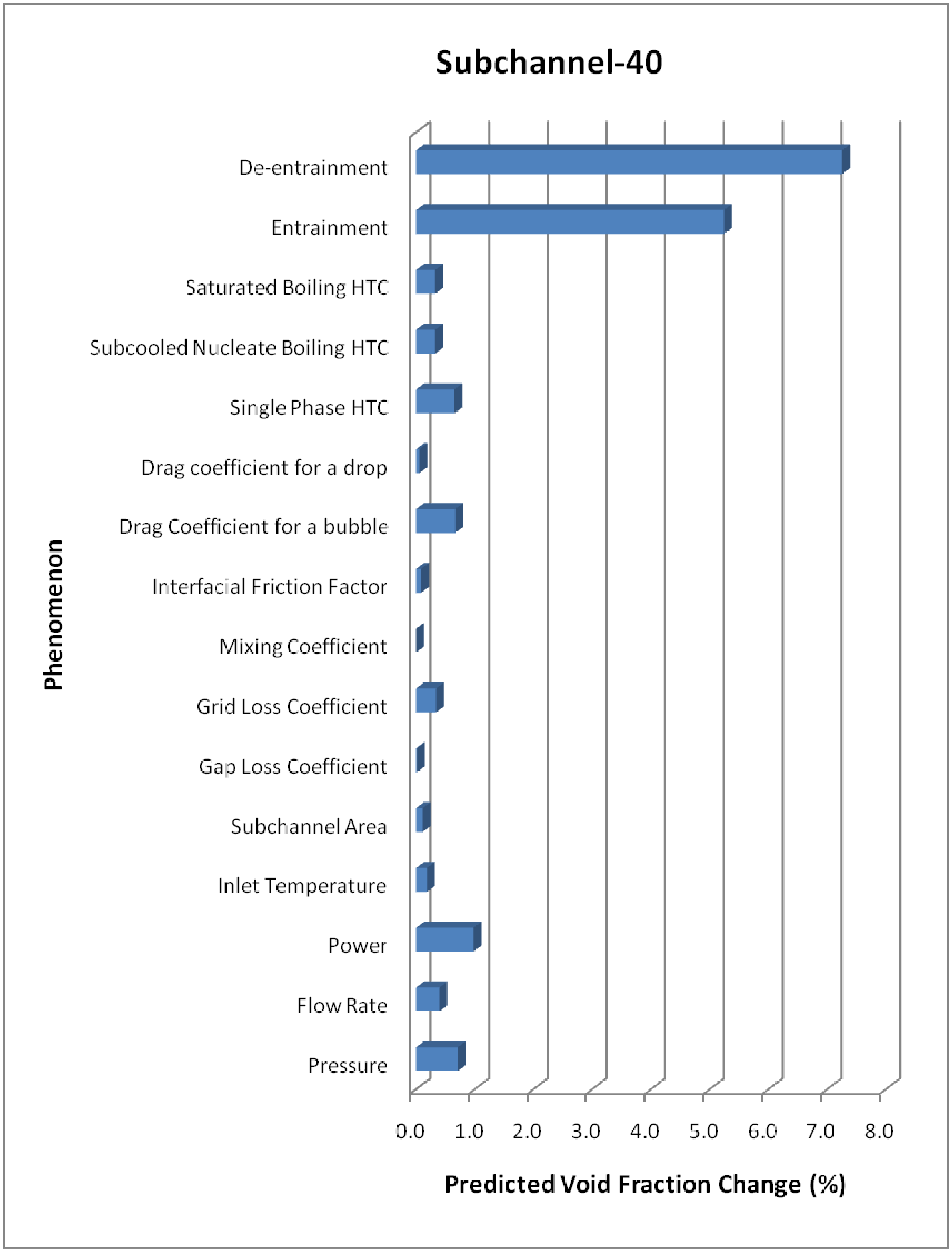

Figure 6.66. Predicted 40th Subchannel Void Fraction Change versus Phenomenon for Test 4101-86

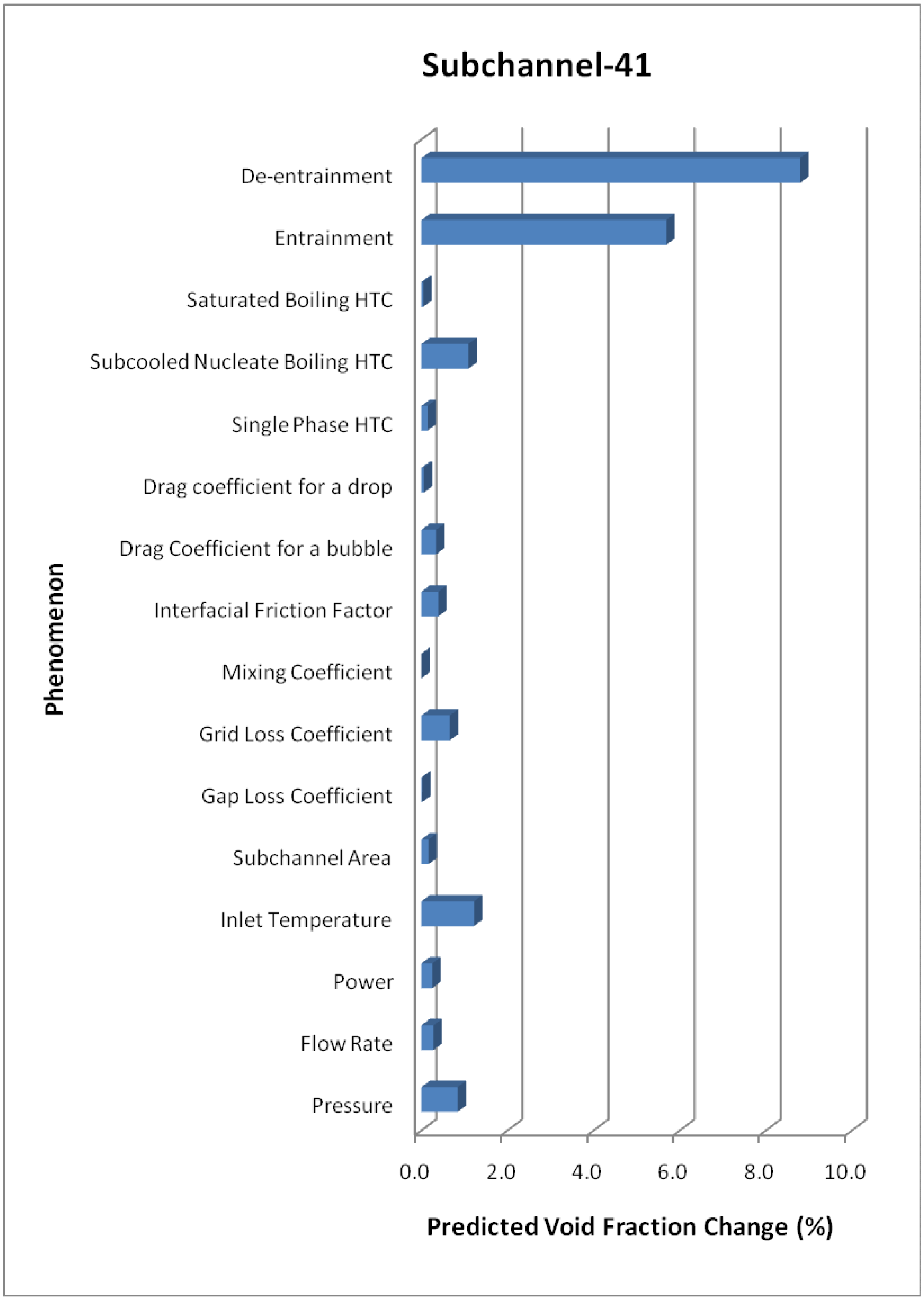

Figure 6.67. Predicted 41th Subchannel Void Fraction Change versus Phenomenon for Test 4101-86

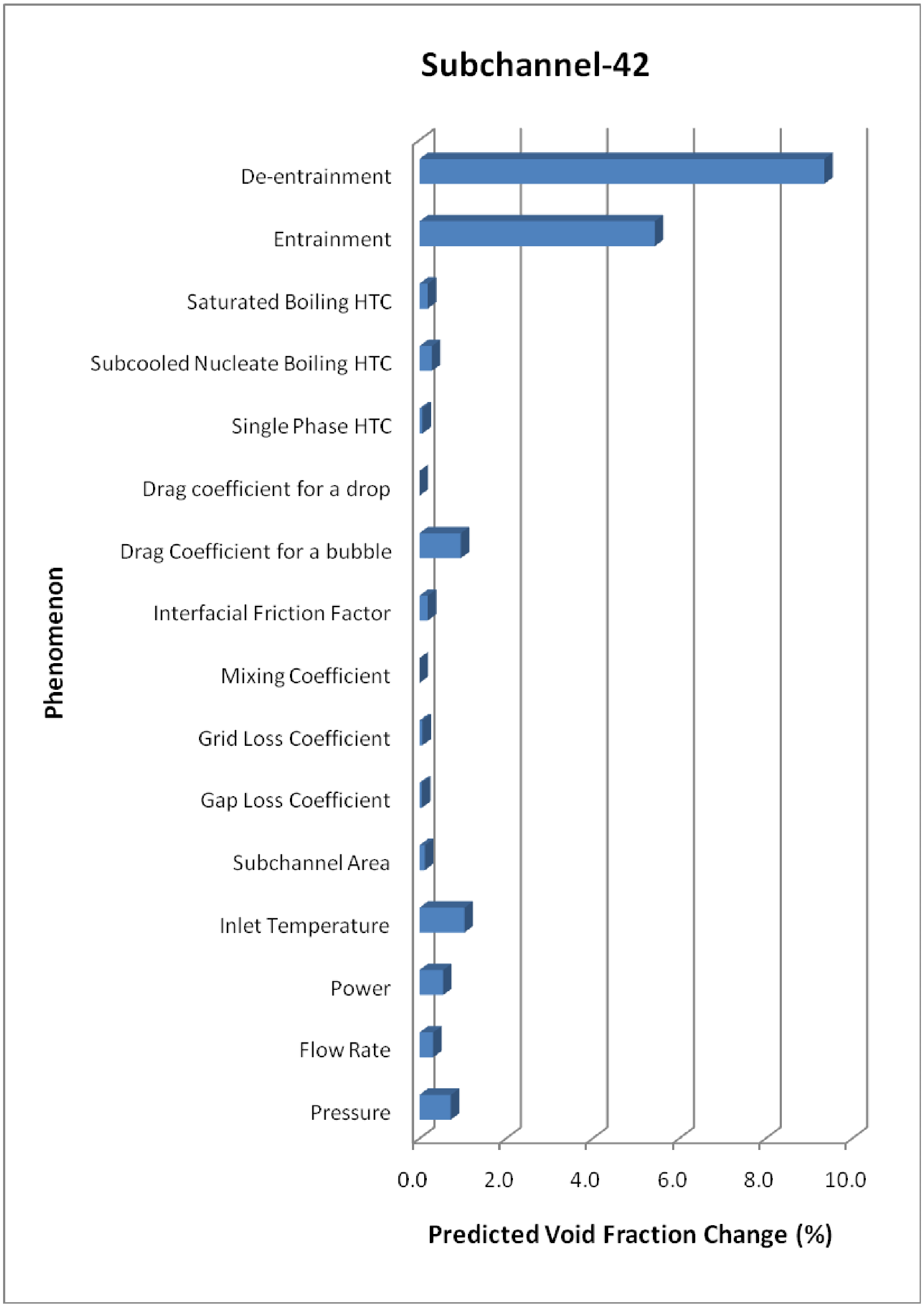

Figure 6.68. Predicted 42nd Subchannel Void Fraction Change versus Phenomenon for Test 4101-86

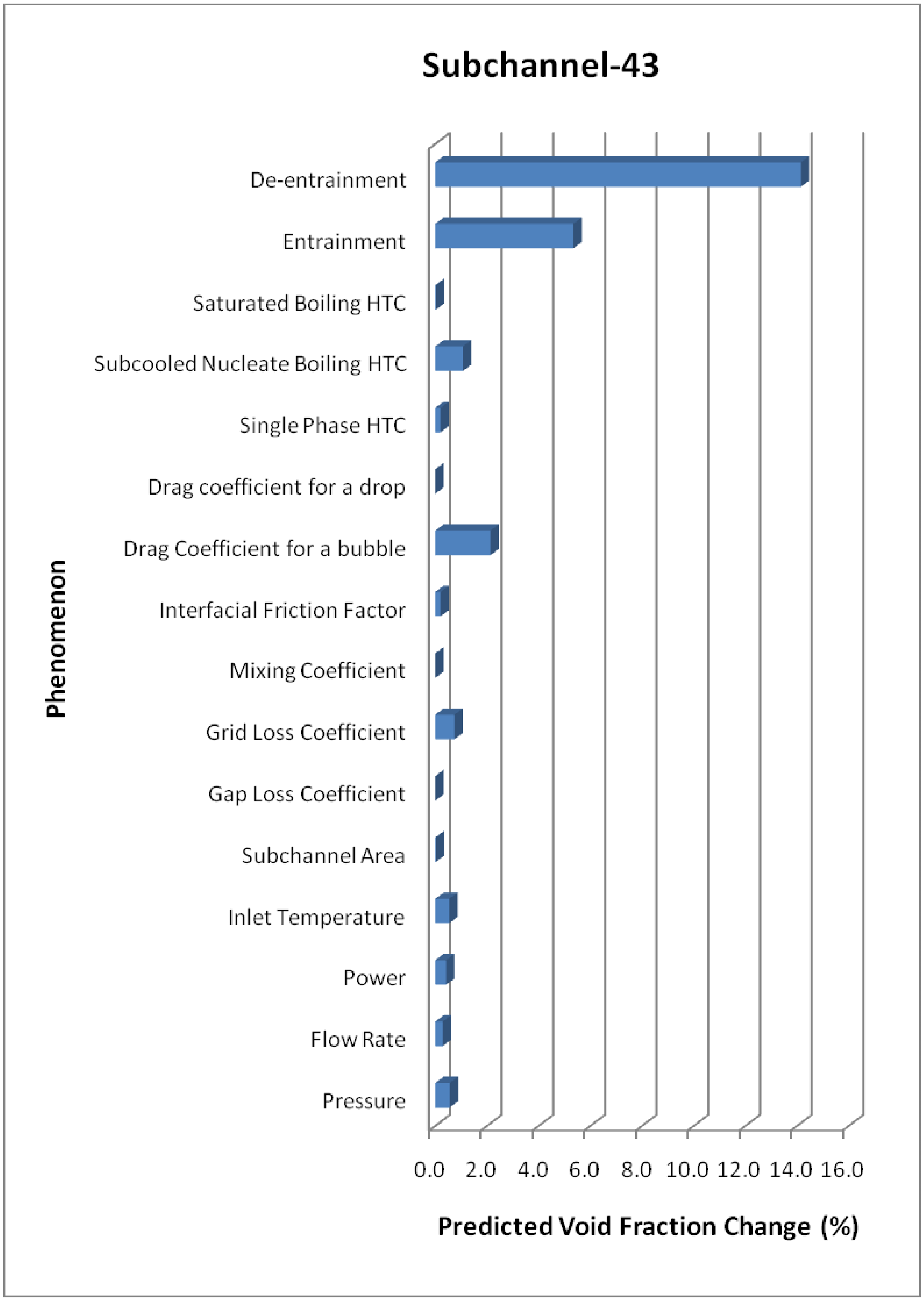

Figure 6.69. Predicted 43th Subchannel Void Fraction Change versus Phenomenon for Test 4101-86

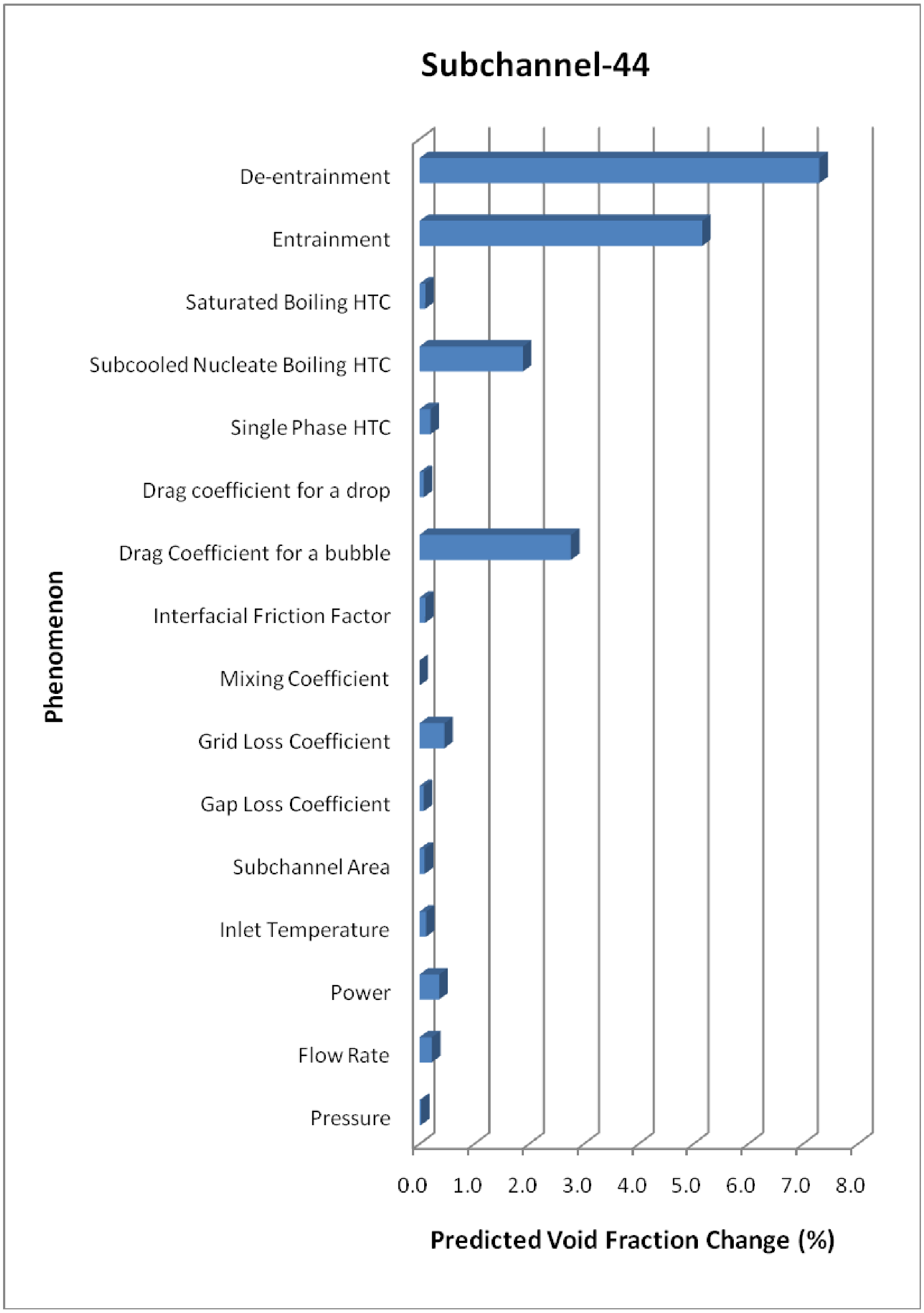

Figure 6.70. Predicted 44th Subchannel Void Fraction Change versus Phenomenon for Test 4101-86

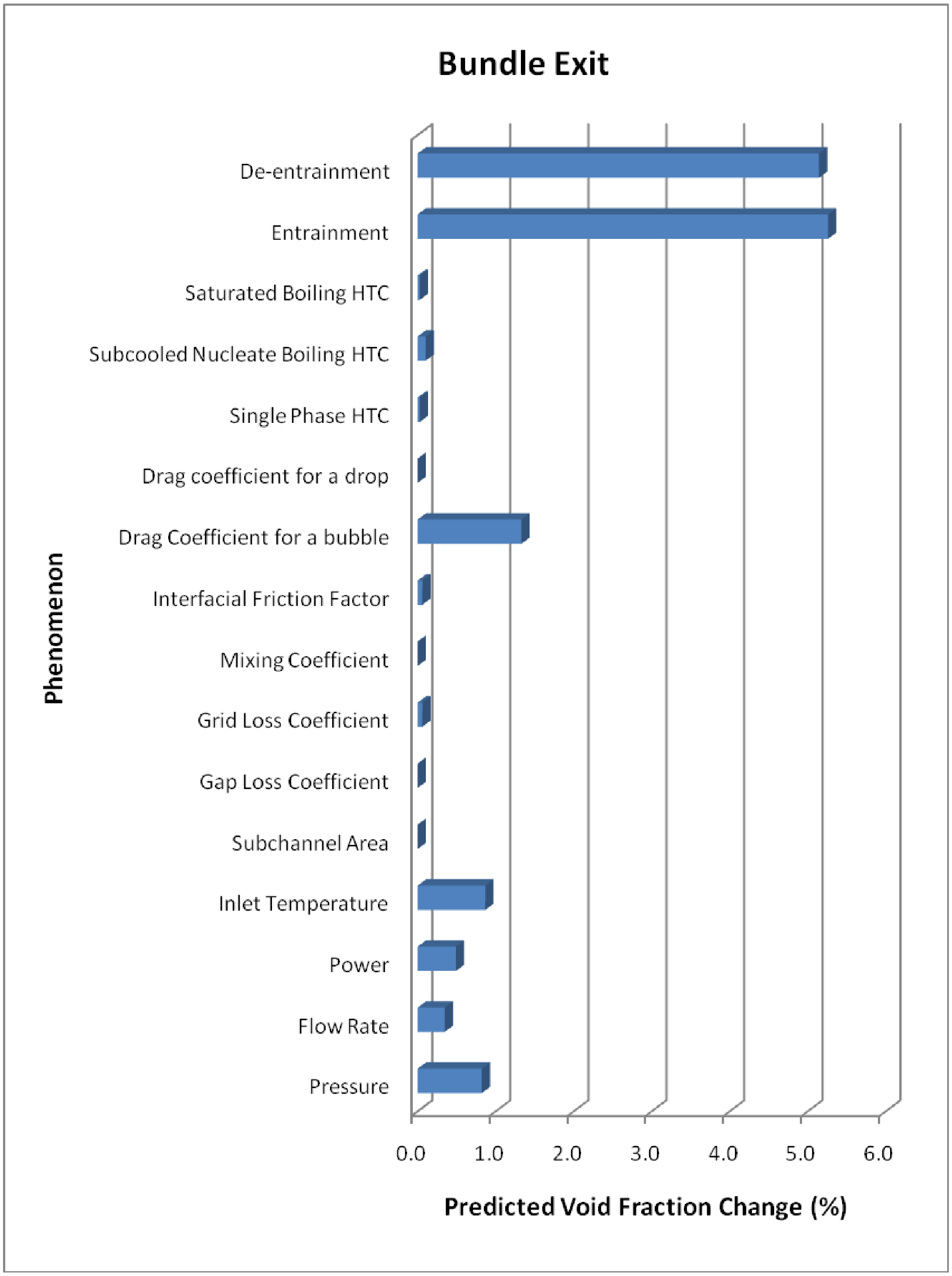

Figure 6.71. Predicted Bundle Void Fraction Change versus Phenomenon for Test 4101-86

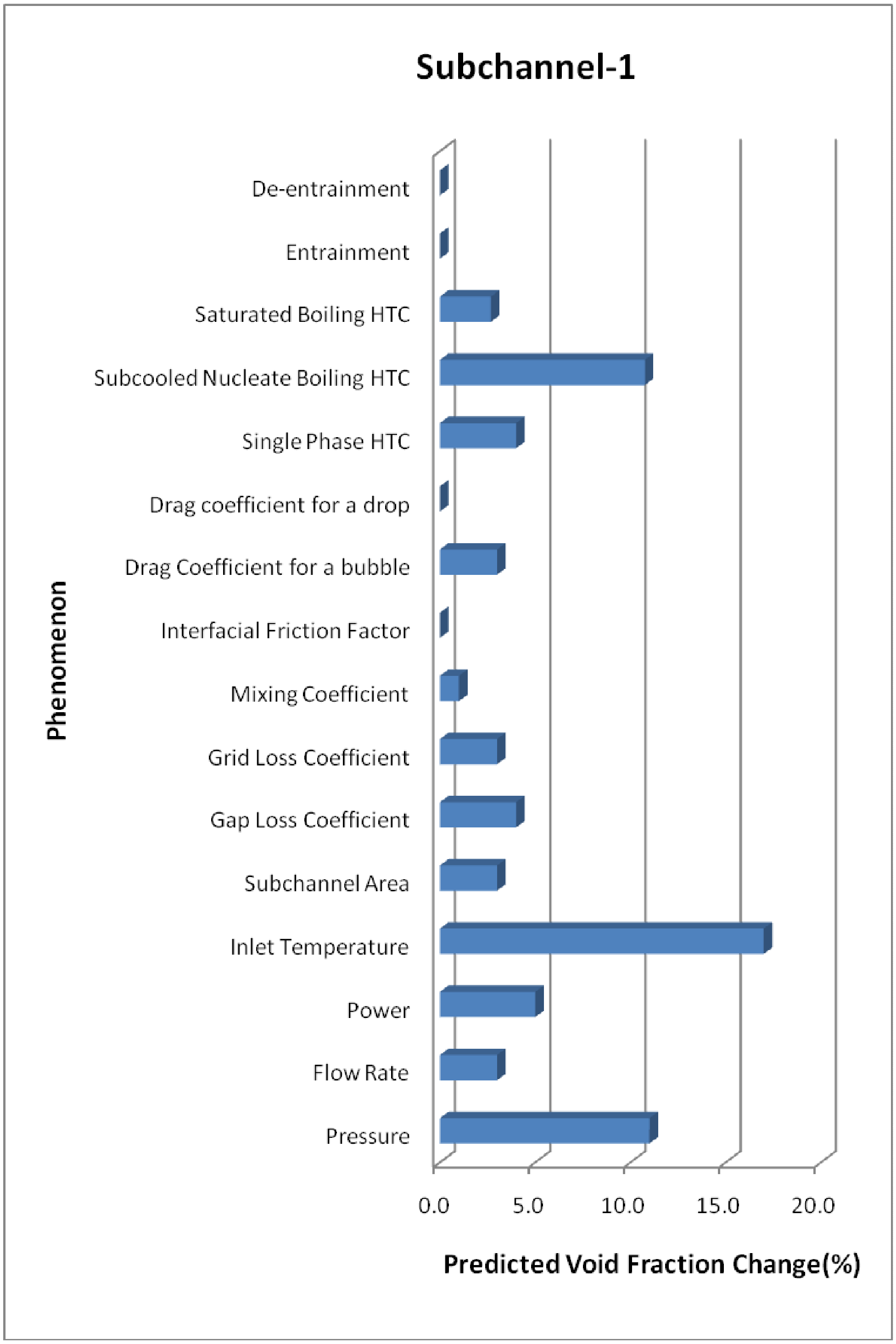

Figure 6.72. Predicted 1st Subchannel Void Fraction Change versus Phenomenon for Test 4101-69

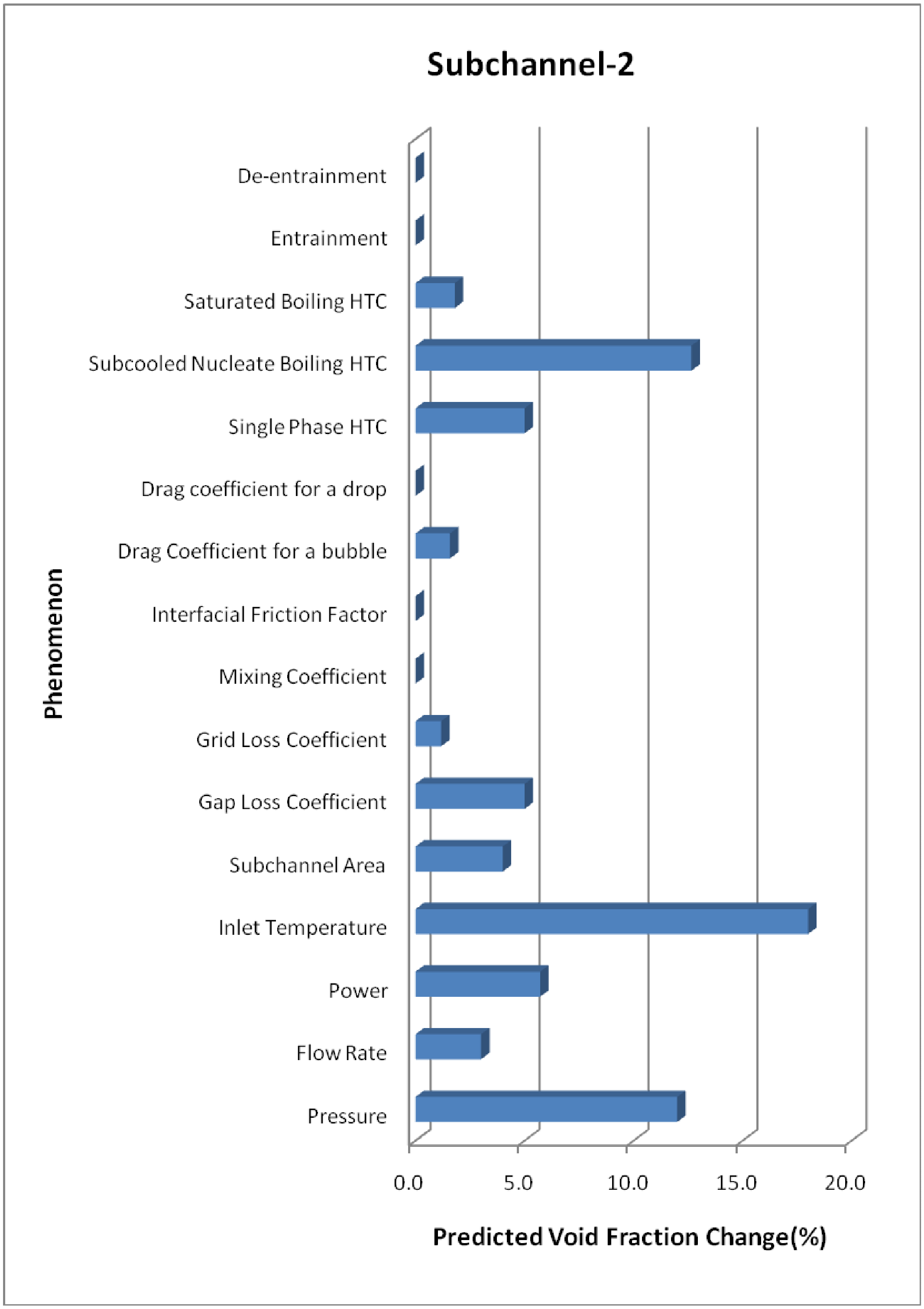

Figure 6.73. Predicted 2nd Subchannel Void Fraction Change versus Phenomenon for Test 4101-69

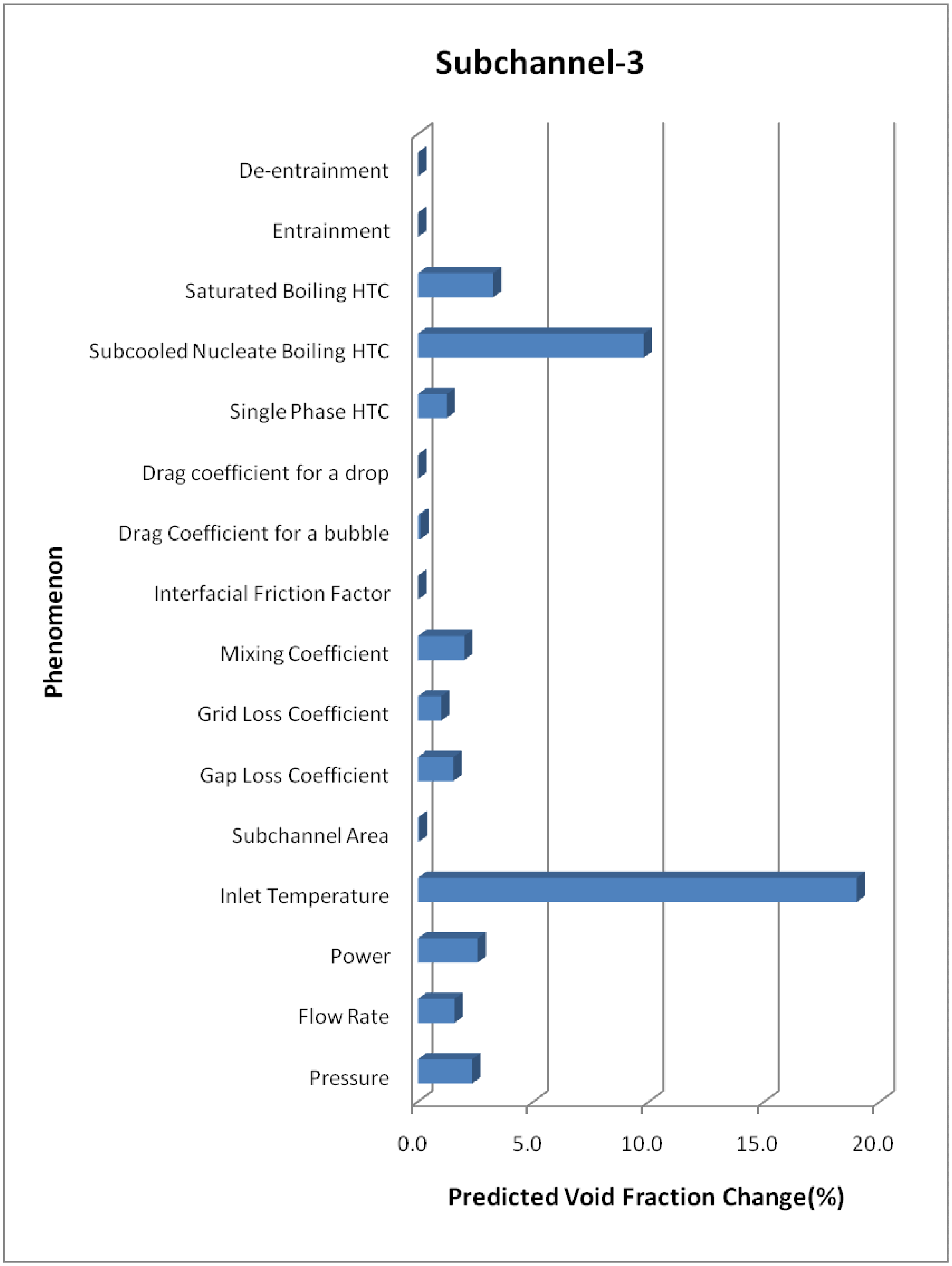

Figure 6.74. Predicted 3rd Subchannel Void Fraction Change versus Phenomenon for Test 4101-69

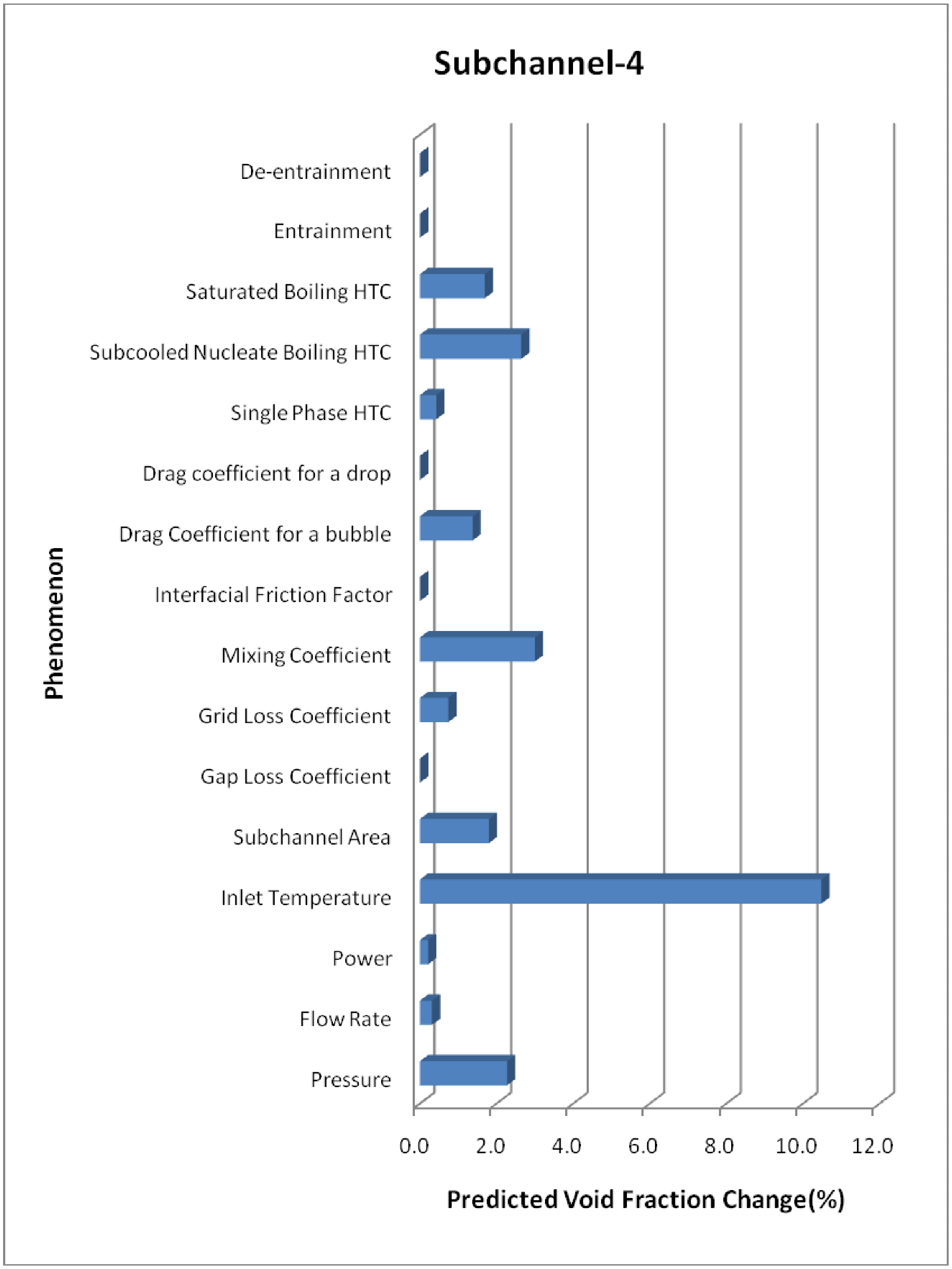

Figure 6.75. Predicted 4th Subchannel Void Fraction Change versus Phenomenon for Test 4101-69

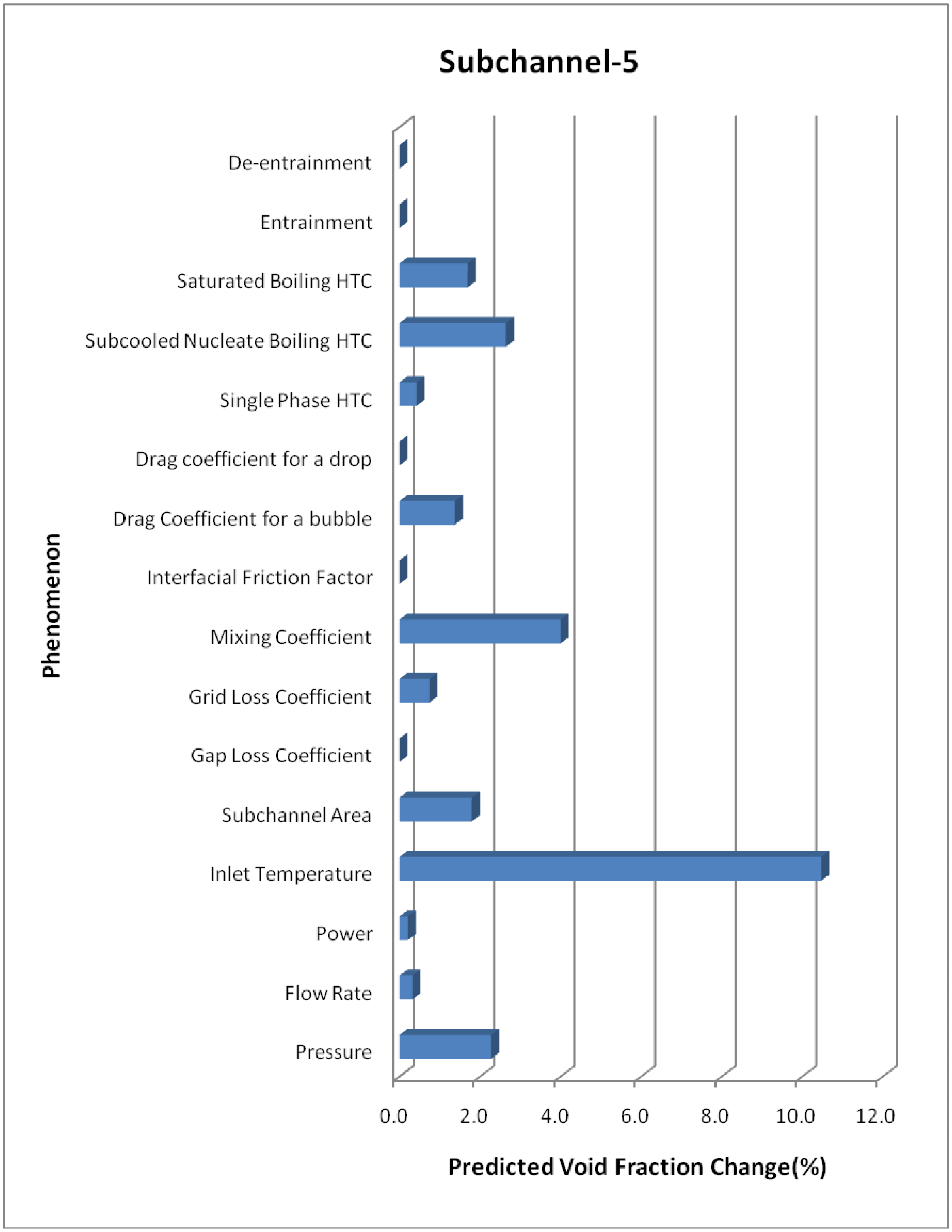

Figure 6.76. Predicted 5th Subchannel Void Fraction Change versus Phenomenon for Test 4101-69

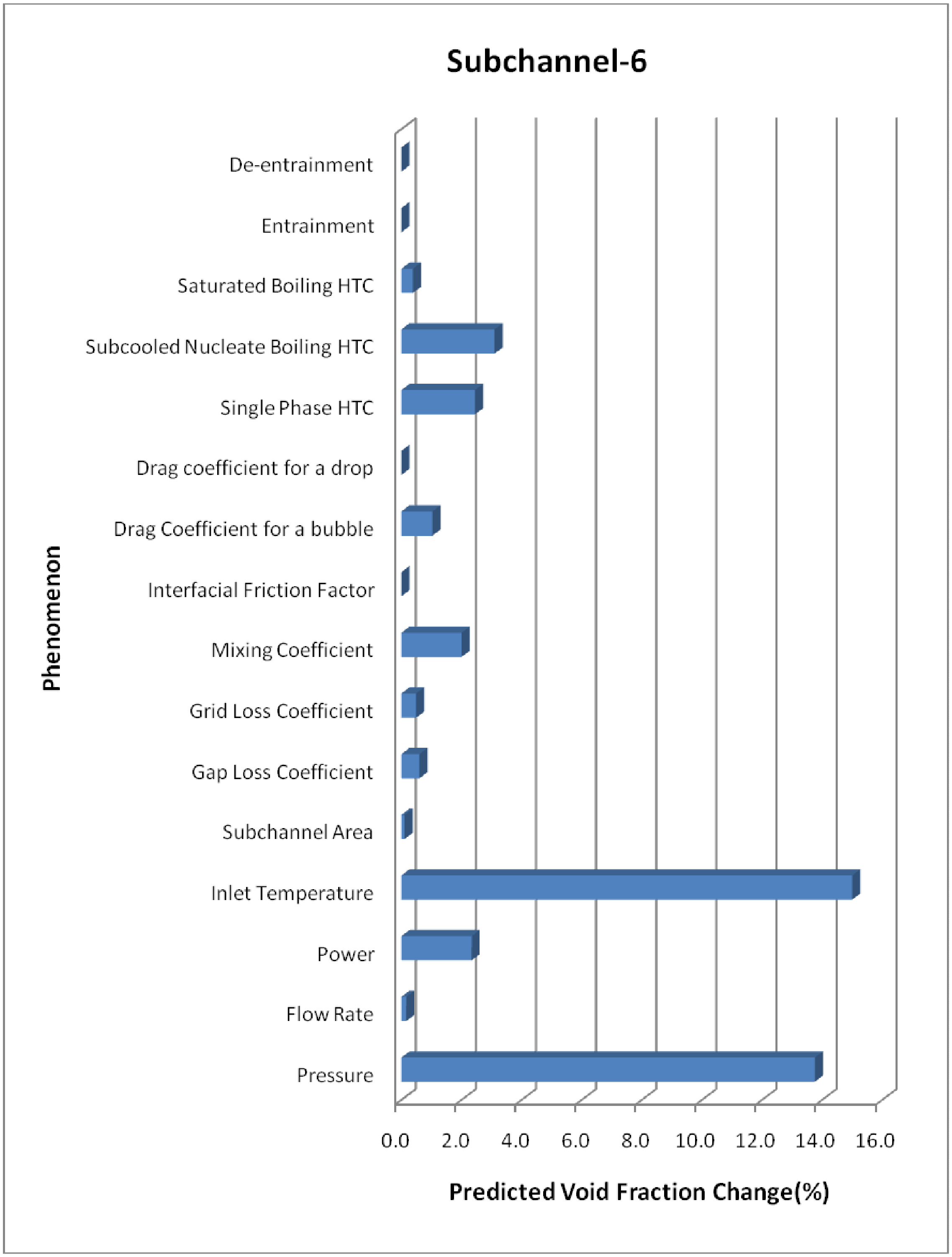

Figure 6.77. Predicted 6th Subchannel Void Fraction Change versus Phenomenon for Test 4101-69

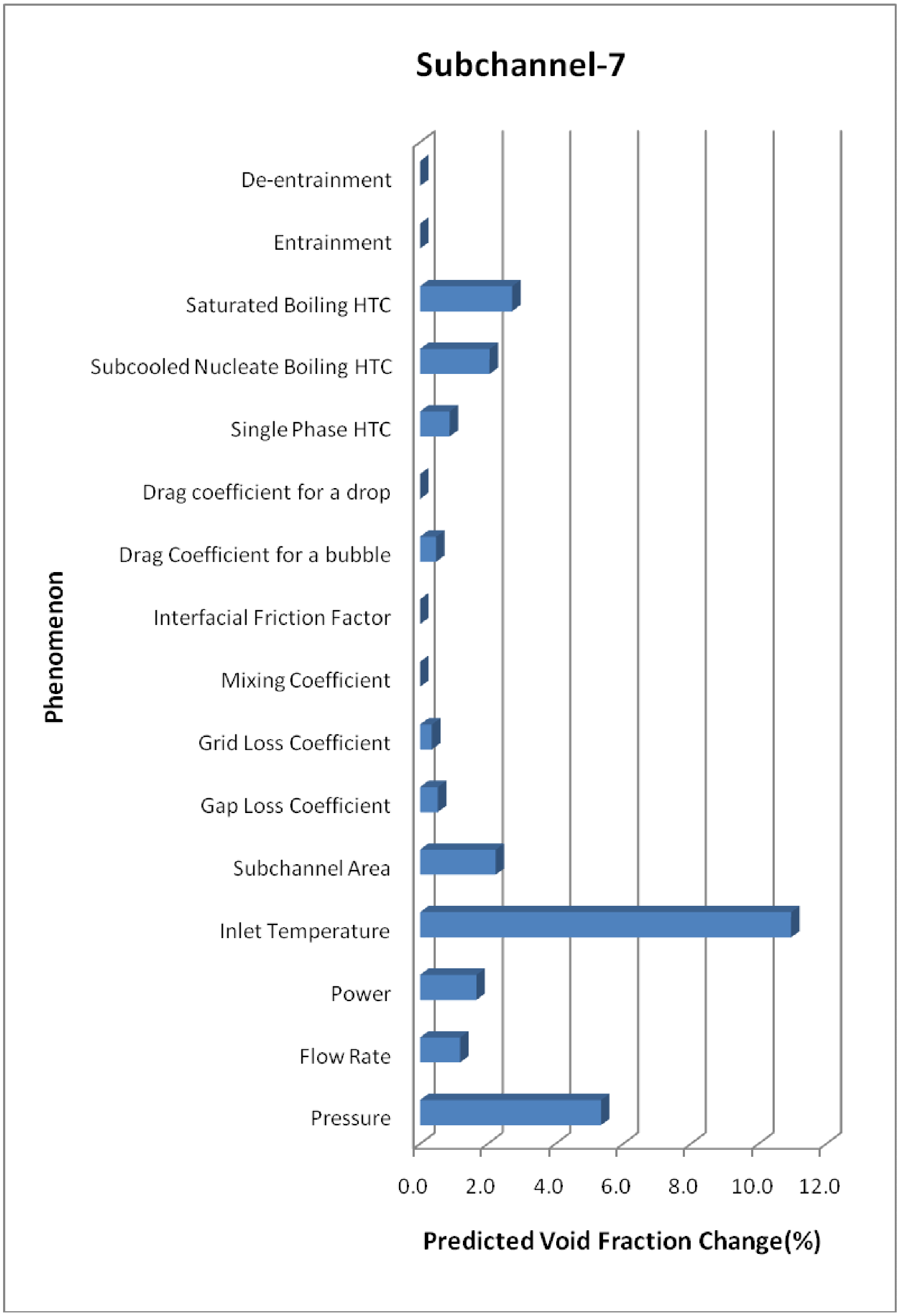

Figure 6.78. Predicted 7th Subchannel Void Fraction Change versus Phenomenon for Test 4101-69

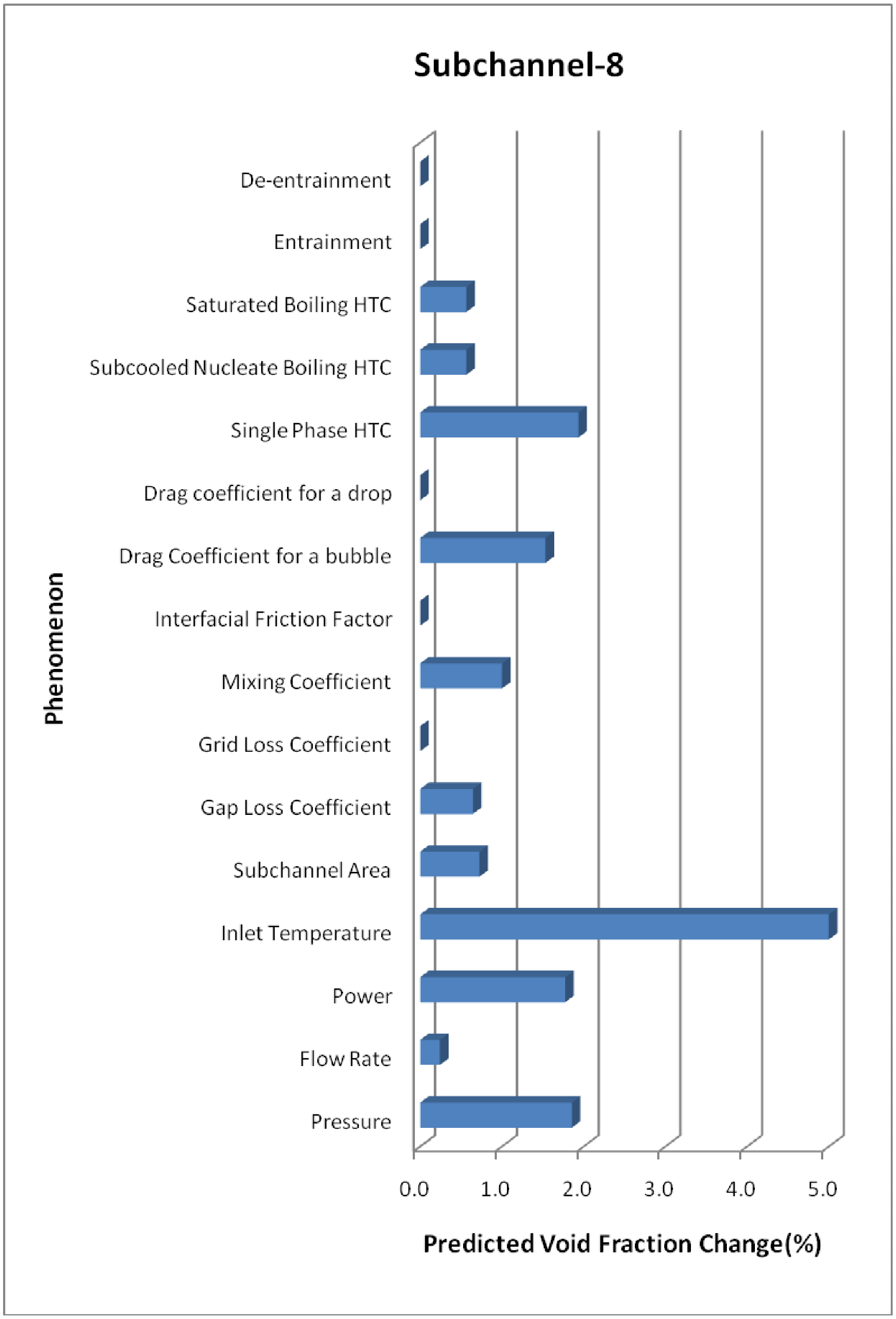

Figure 6.79. Predicted 8th Subchannel Void Fraction Change versus Phenomenon for Test 4101-69

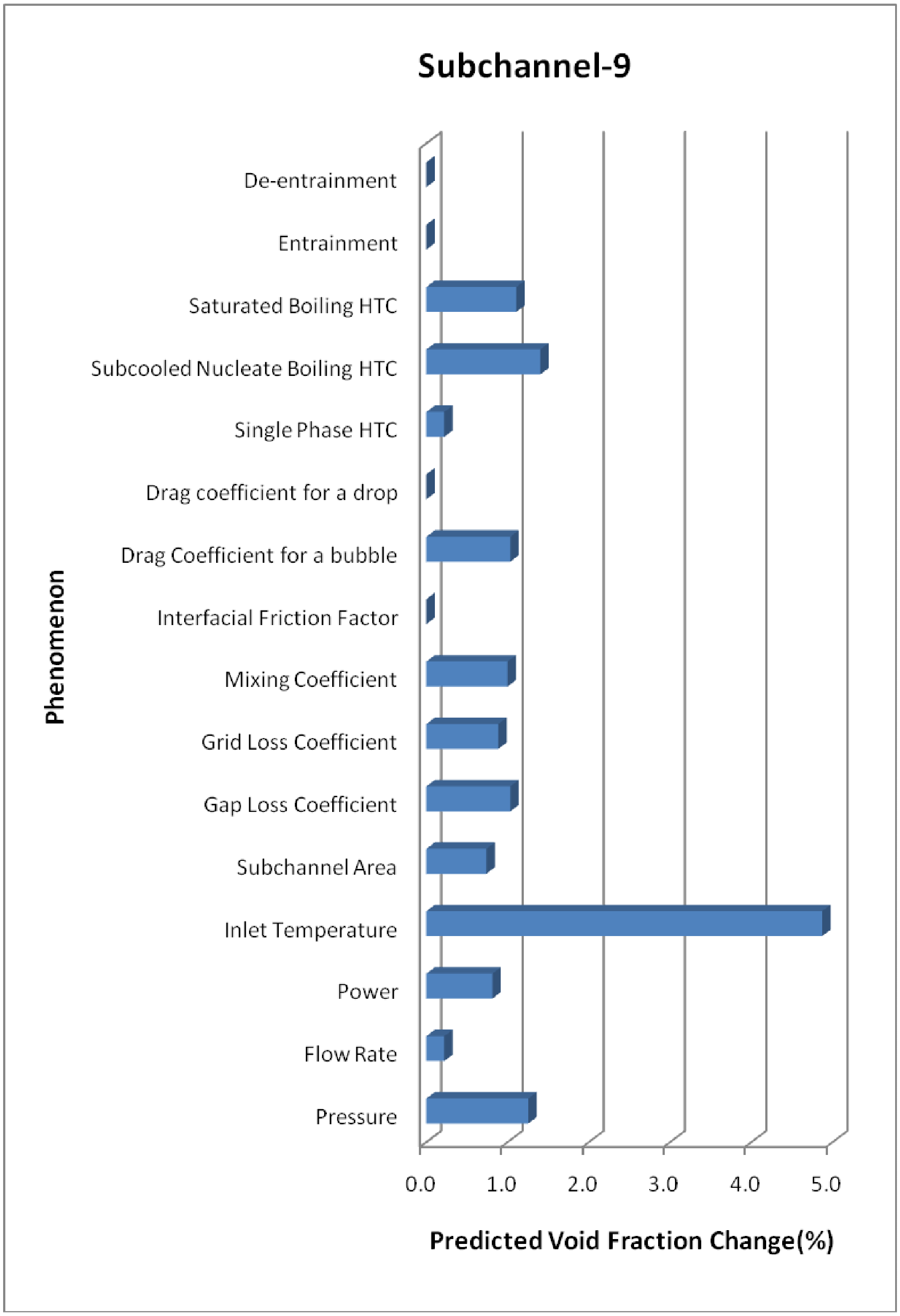

Figure 6.80. Predicted 9th Subchannel Void Fraction Change versus Phenomenon for Test 4101-69

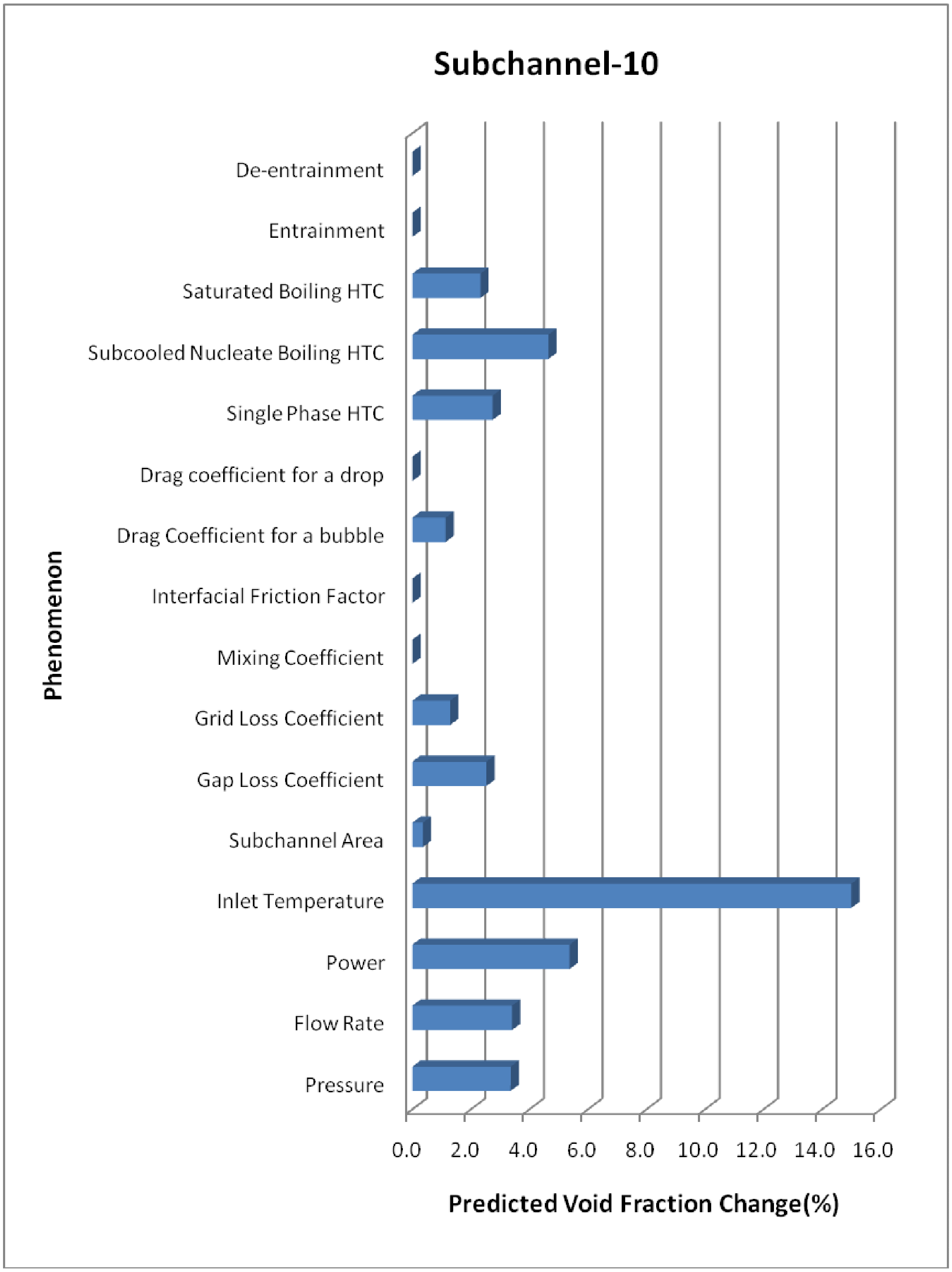

Figure 6.81. Predicted 10th Subchannel Void Fraction Change versus Phenomenon for Test 4101-69

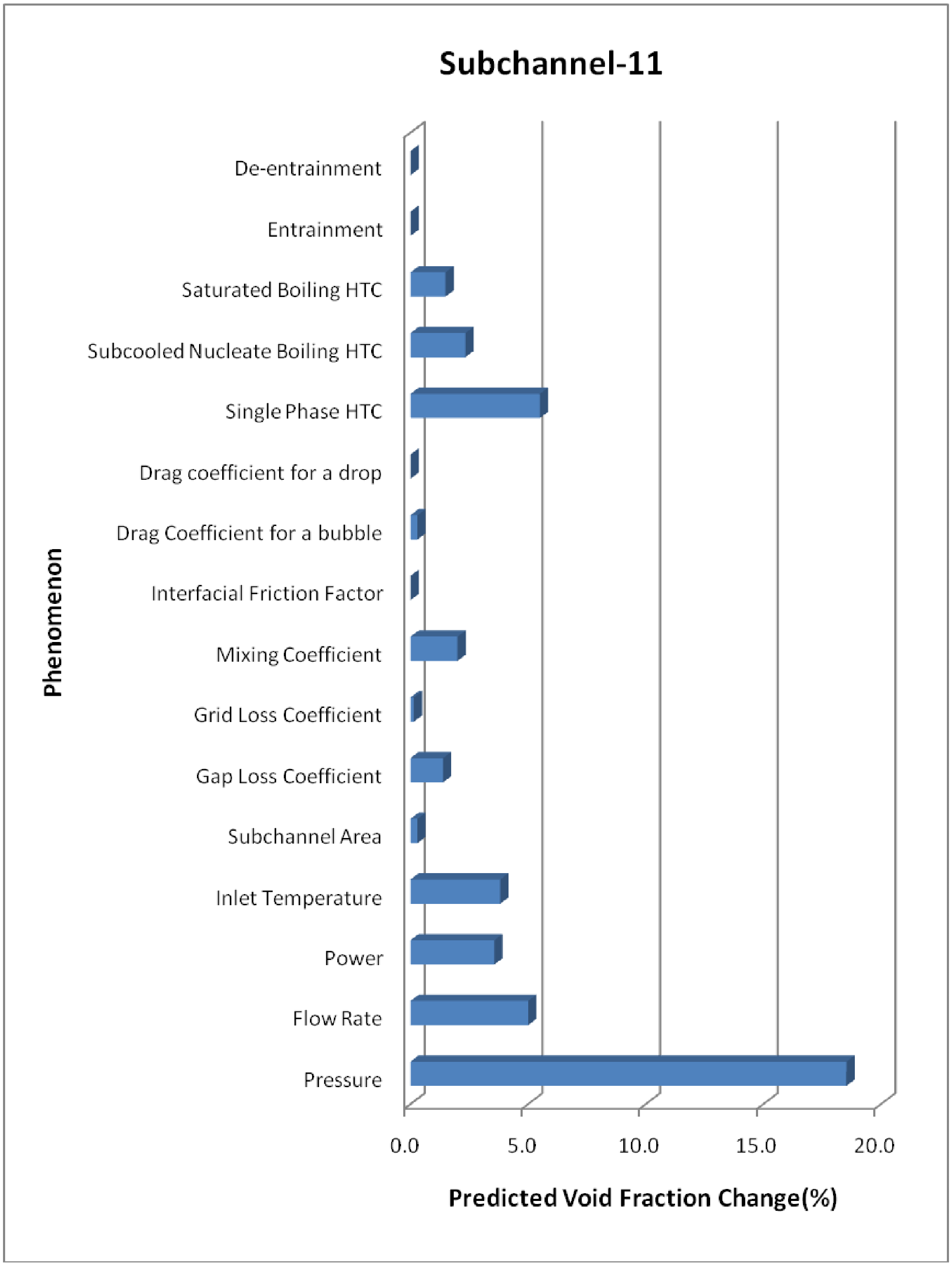

Figure 6.82. Predicted 11th Subchannel Void Fraction Change versus Phenomenon for Test 4101-69

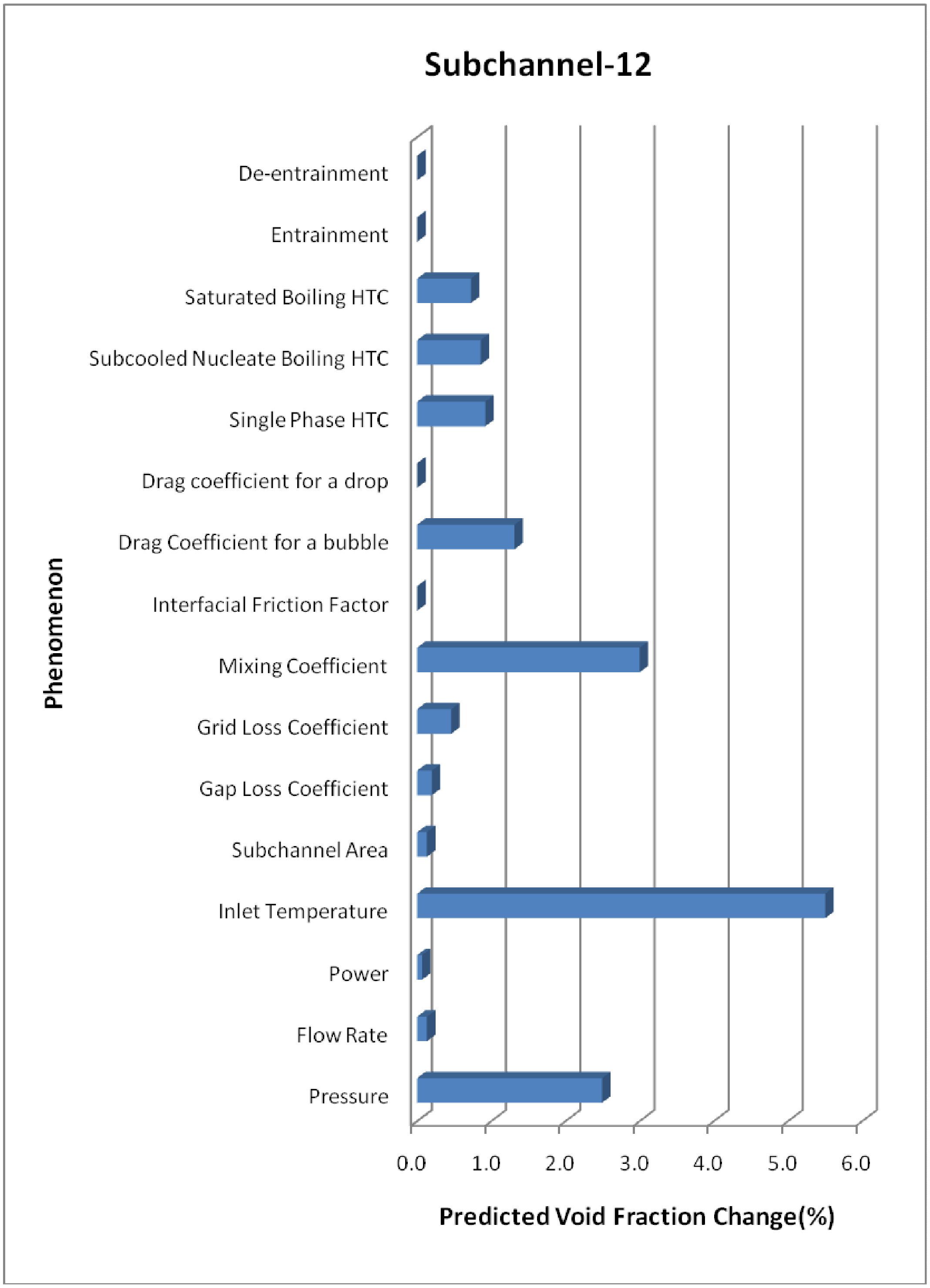

Figure 6.83. Predicted 12th Subchannel Void Fraction Change versus Phenomenon for Test 4101-69

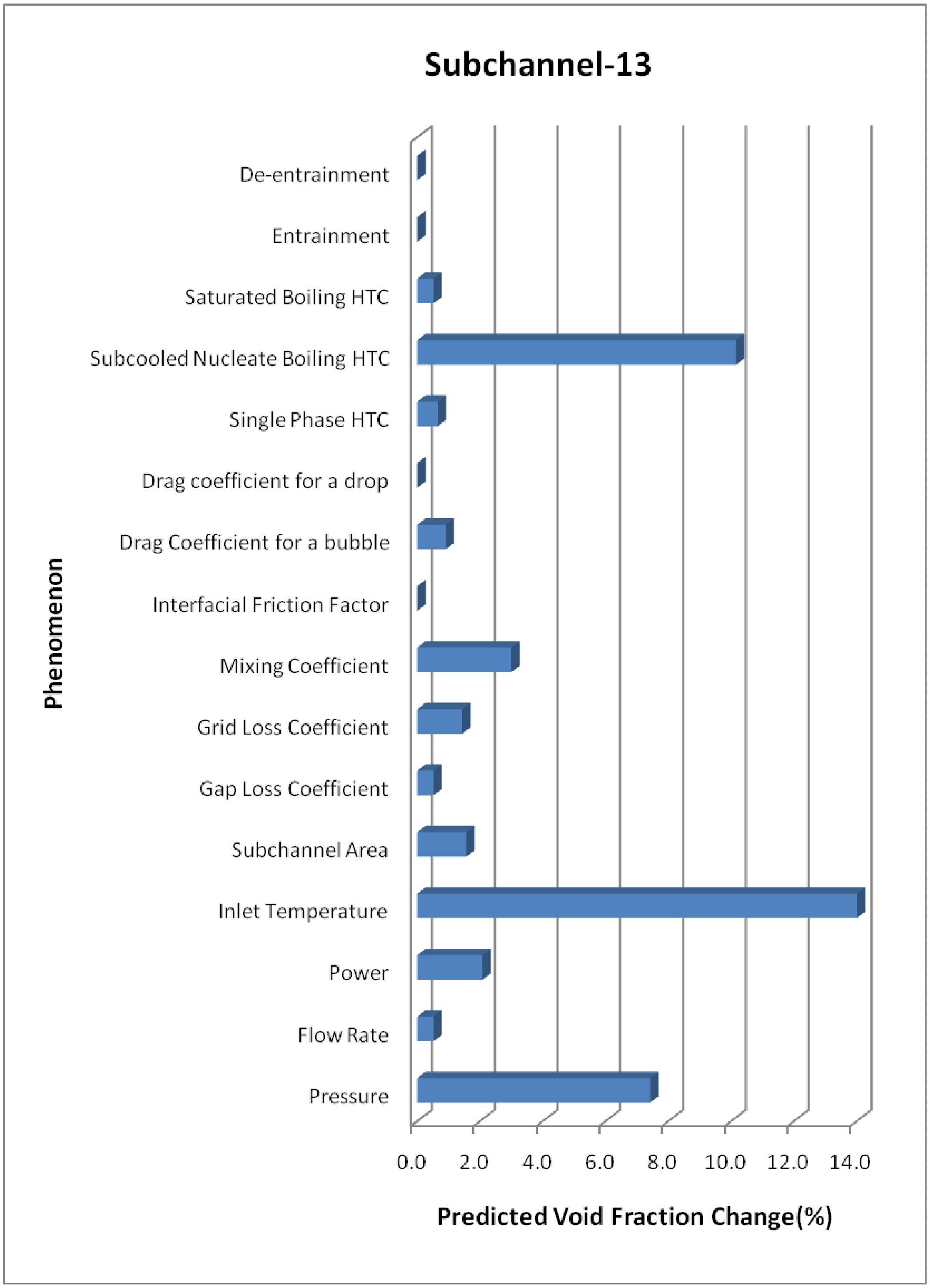

Figure 6.84. Predicted 13th Subchannel Void Fraction Change versus Phenomenon for Test 4101-69

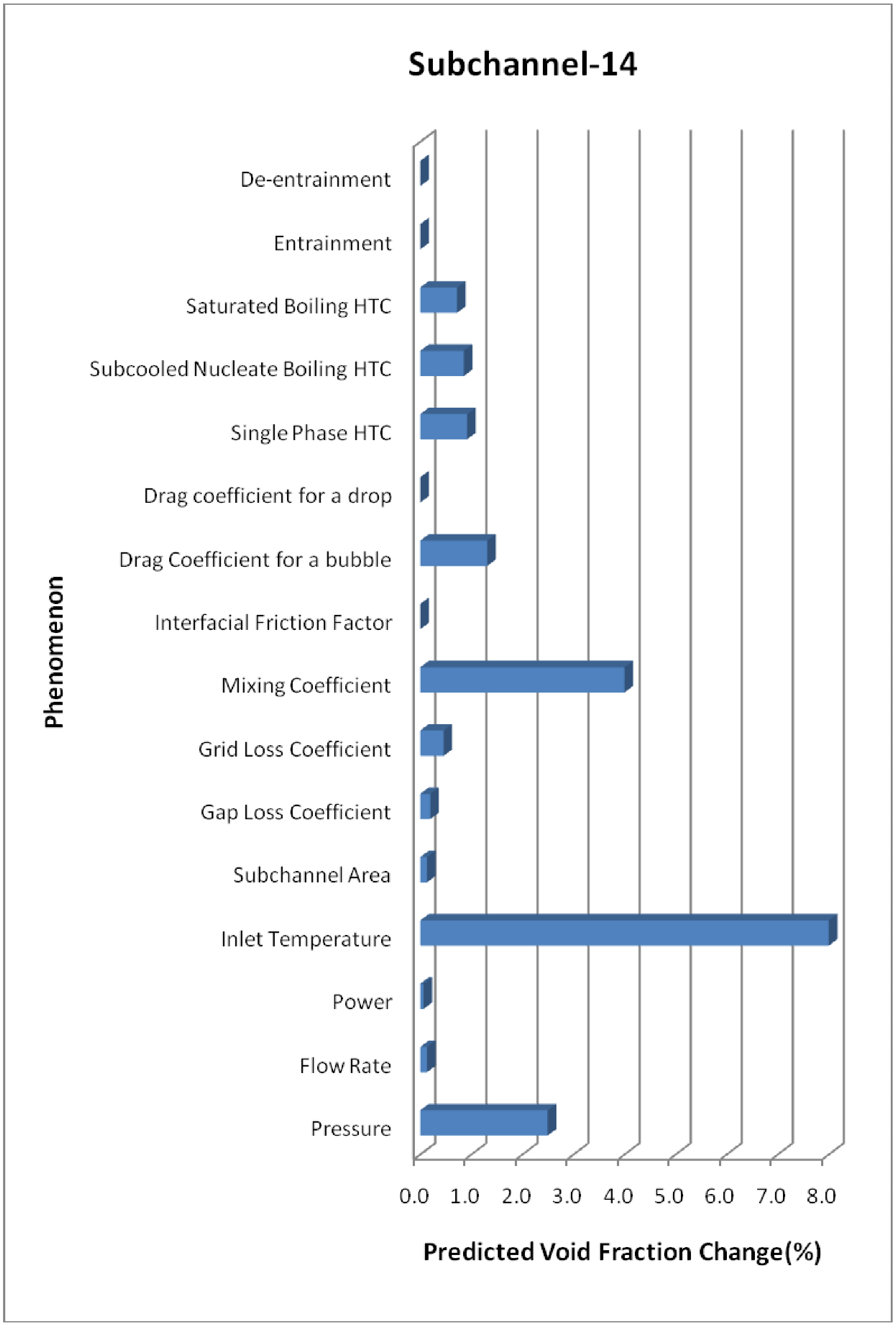

Figure 6.85. Predicted 14th Subchannel Void Fraction Change versus Phenomenon for Test 4101-69

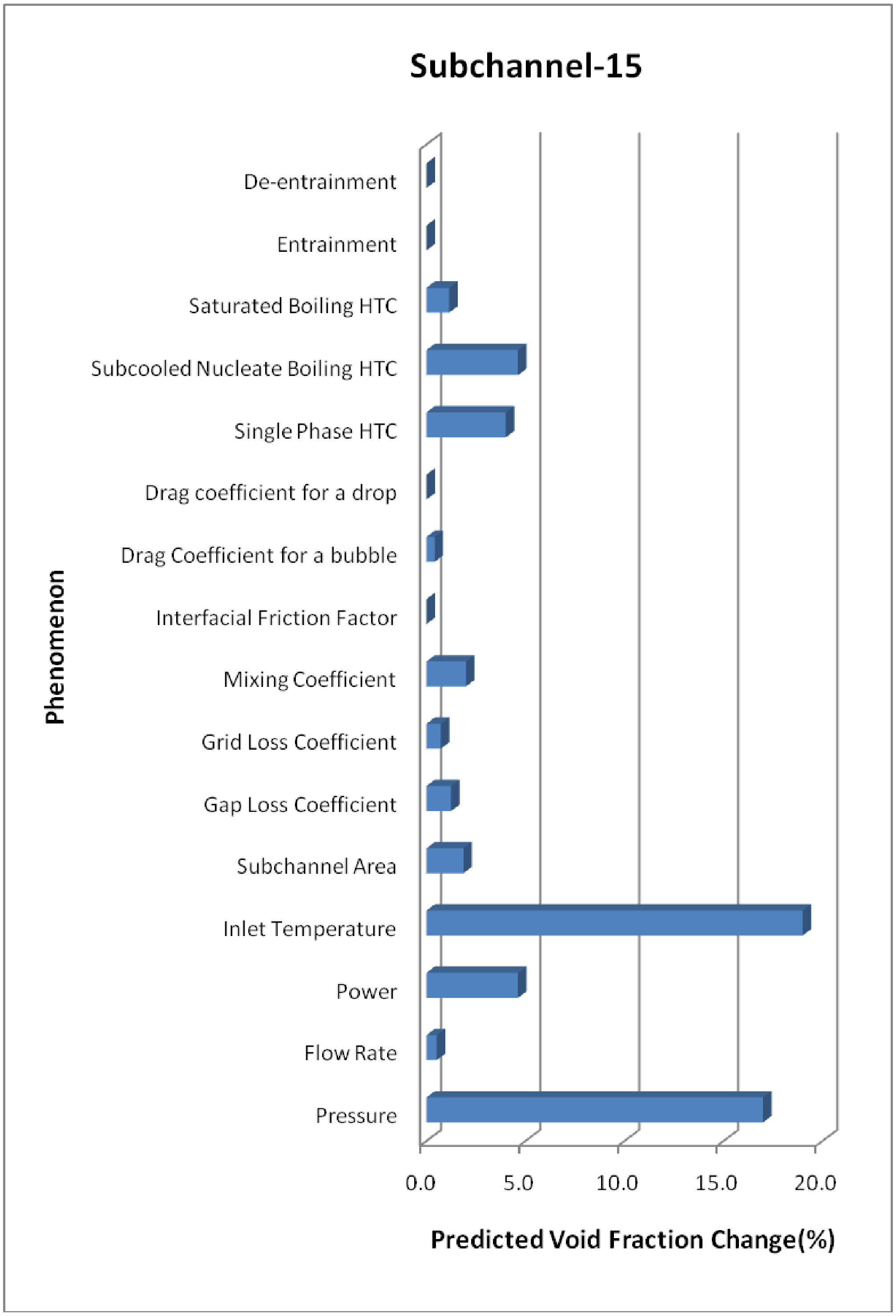

Figure 6.86. Predicted 15th Subchannel Void Fraction Change versus Phenomenon for Test 4101-69

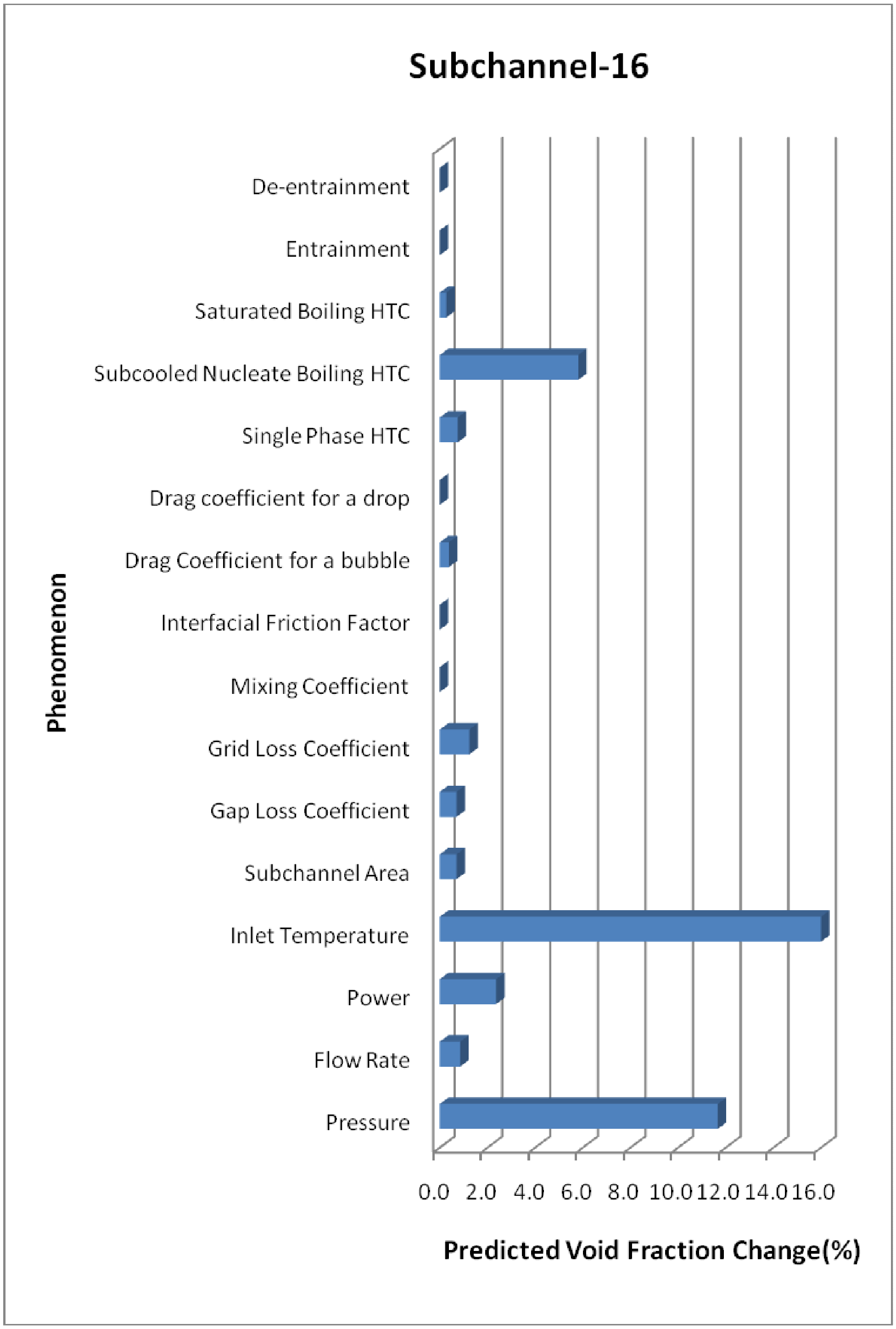

Figure 6.87. Predicted 16th Subchannel Void Fraction Change versus Phenomenon for Test 4101-69

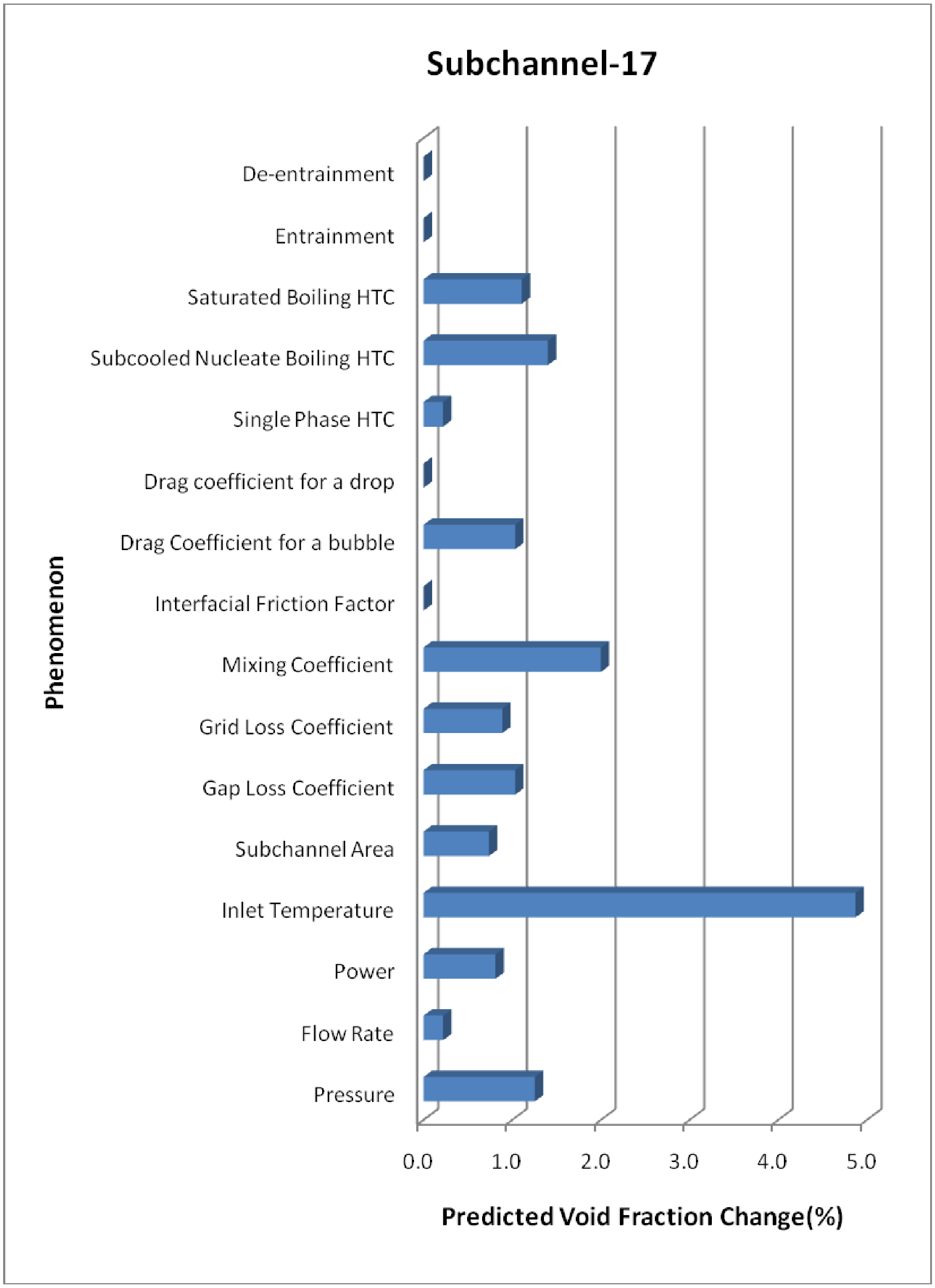

Figure 6.88. Predicted 17th Subchannel Void Fraction Change versus Phenomenon for Test 4101-69

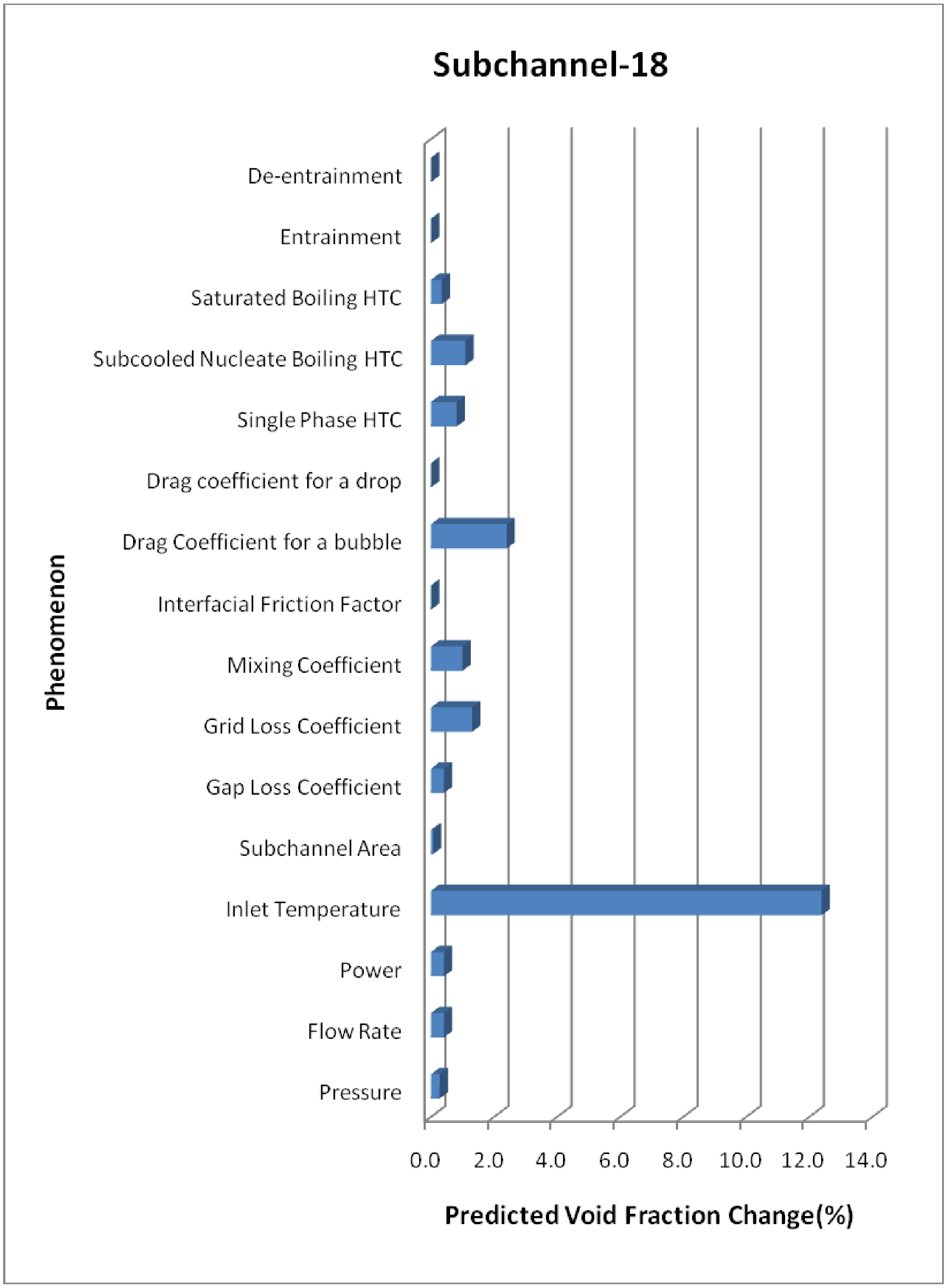

Figure 6.89. Predicted 18th Subchannel Void Fraction Change versus Phenomenon for Test 4101-69

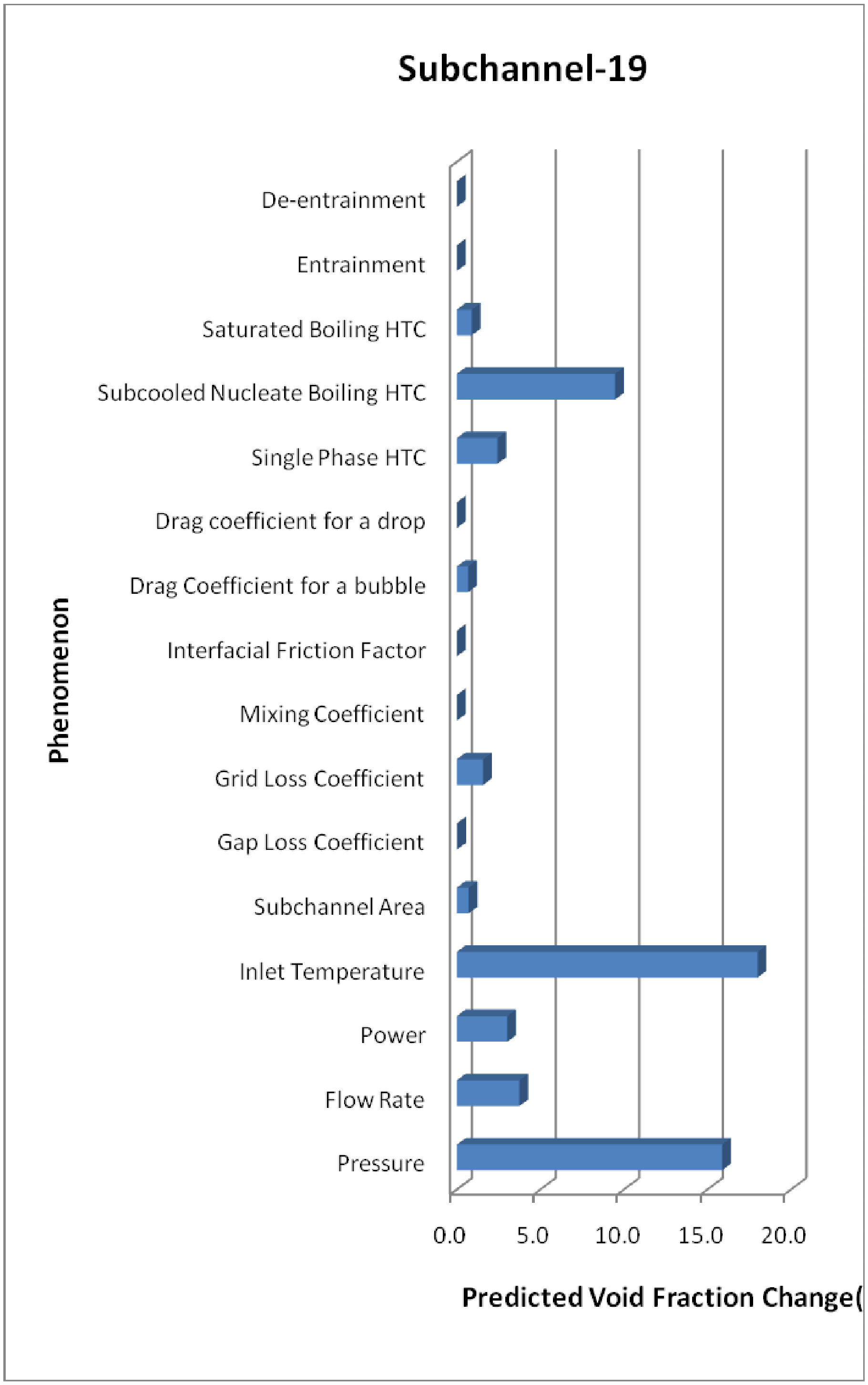

Figure 6.90. Predicted 19th Subchannel Void Fraction Change versus Phenomenon for Test 4101-69

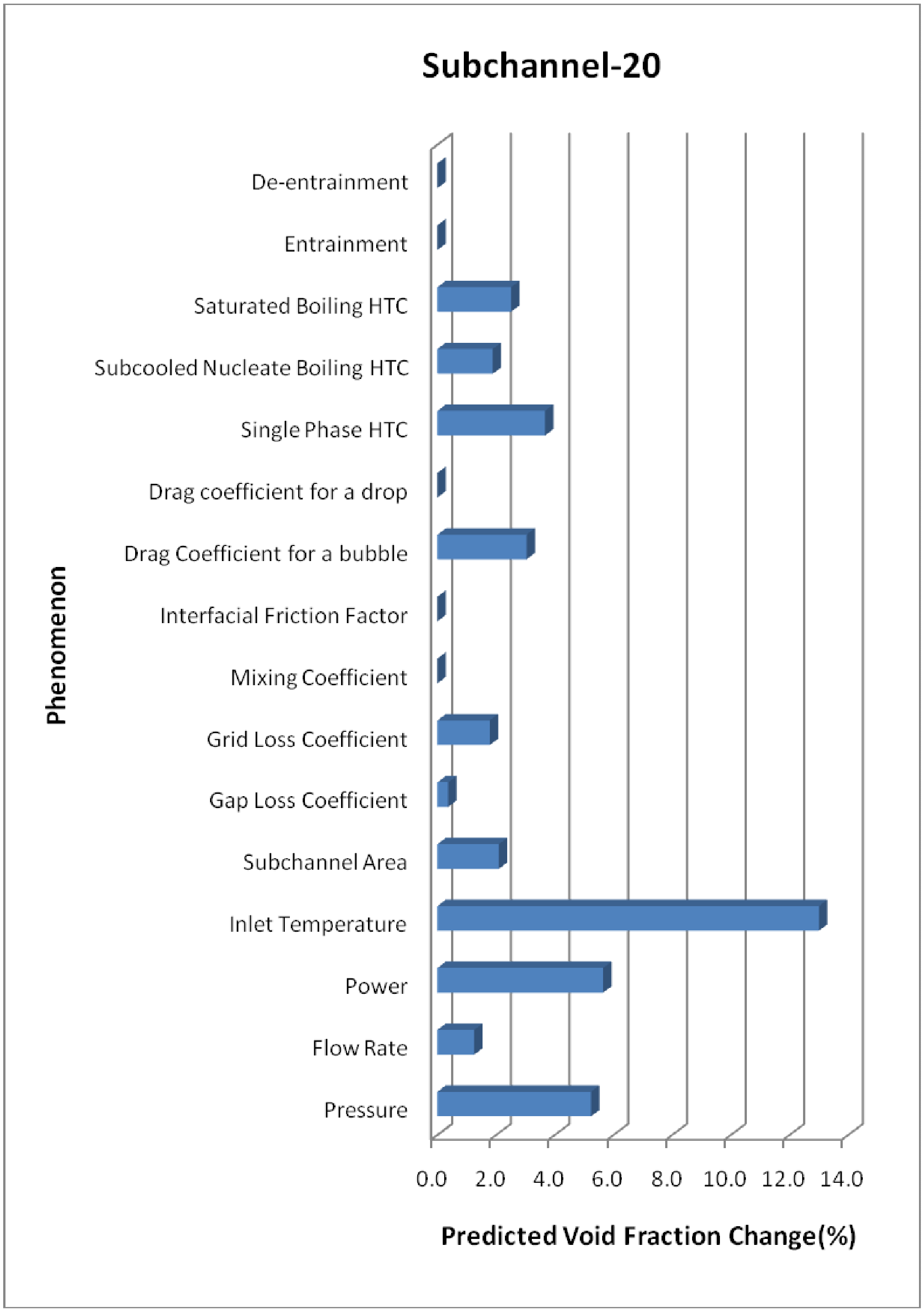

Figure 6.91. Predicted 20th Subchannel Void Fraction Change versus Phenomenon for Test 4101-69

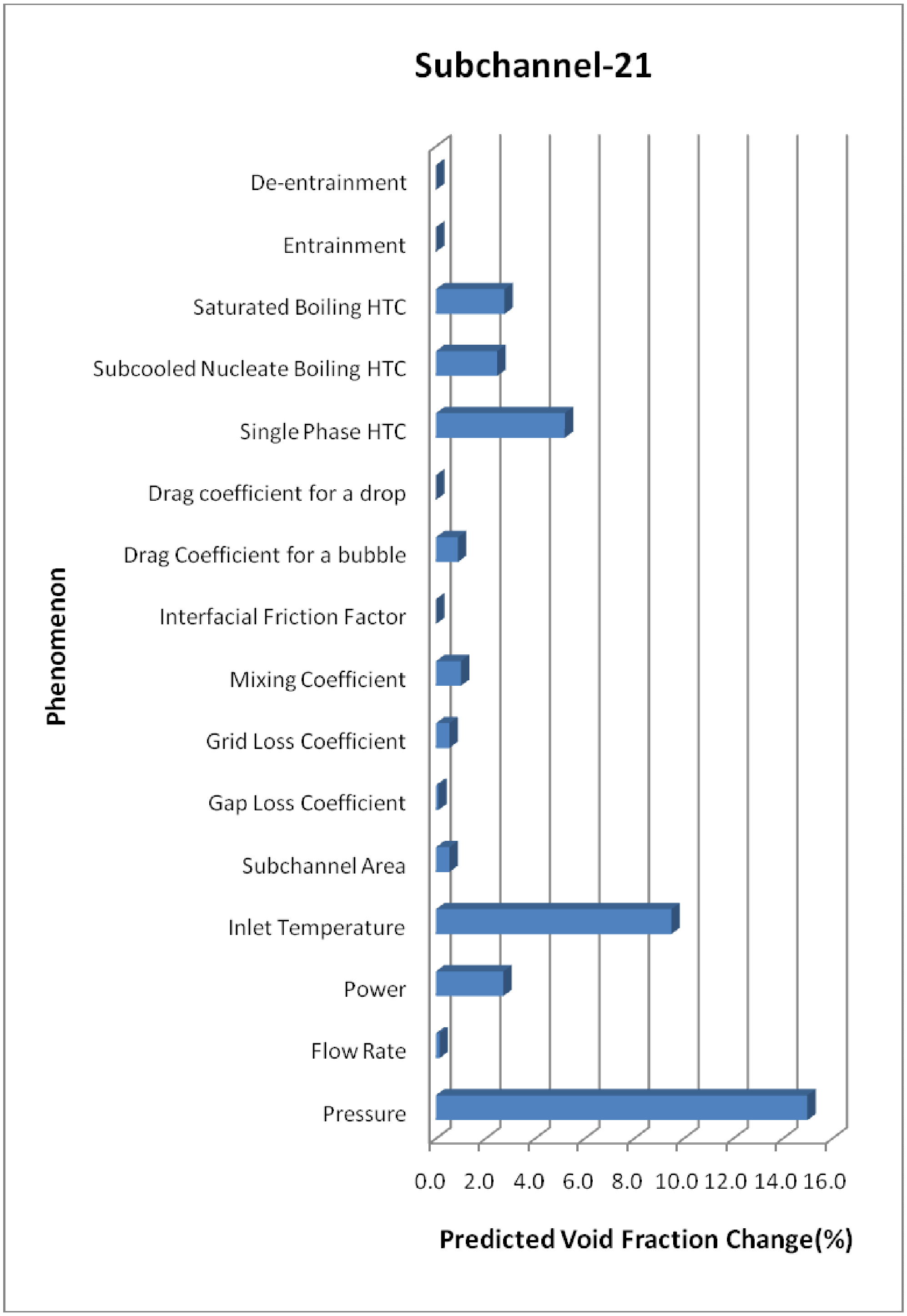

Figure 6.92. Predicted 21st Subchannel Void Fraction Change versus Phenomenon for Test 4101-69

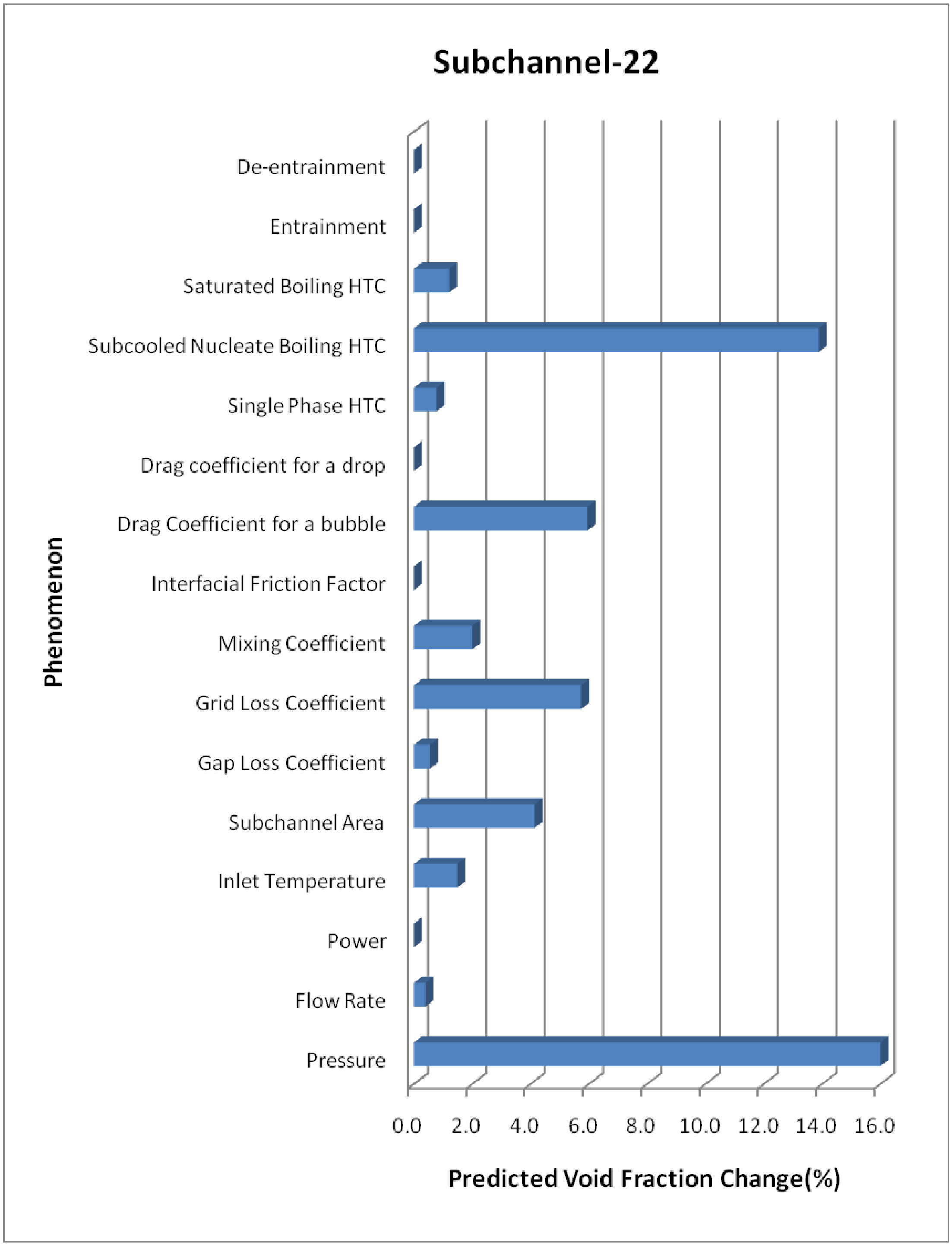

Figure 6.93. Predicted 22nd Subchannel Void Fraction Change versus Phenomenon for Test 4101-69

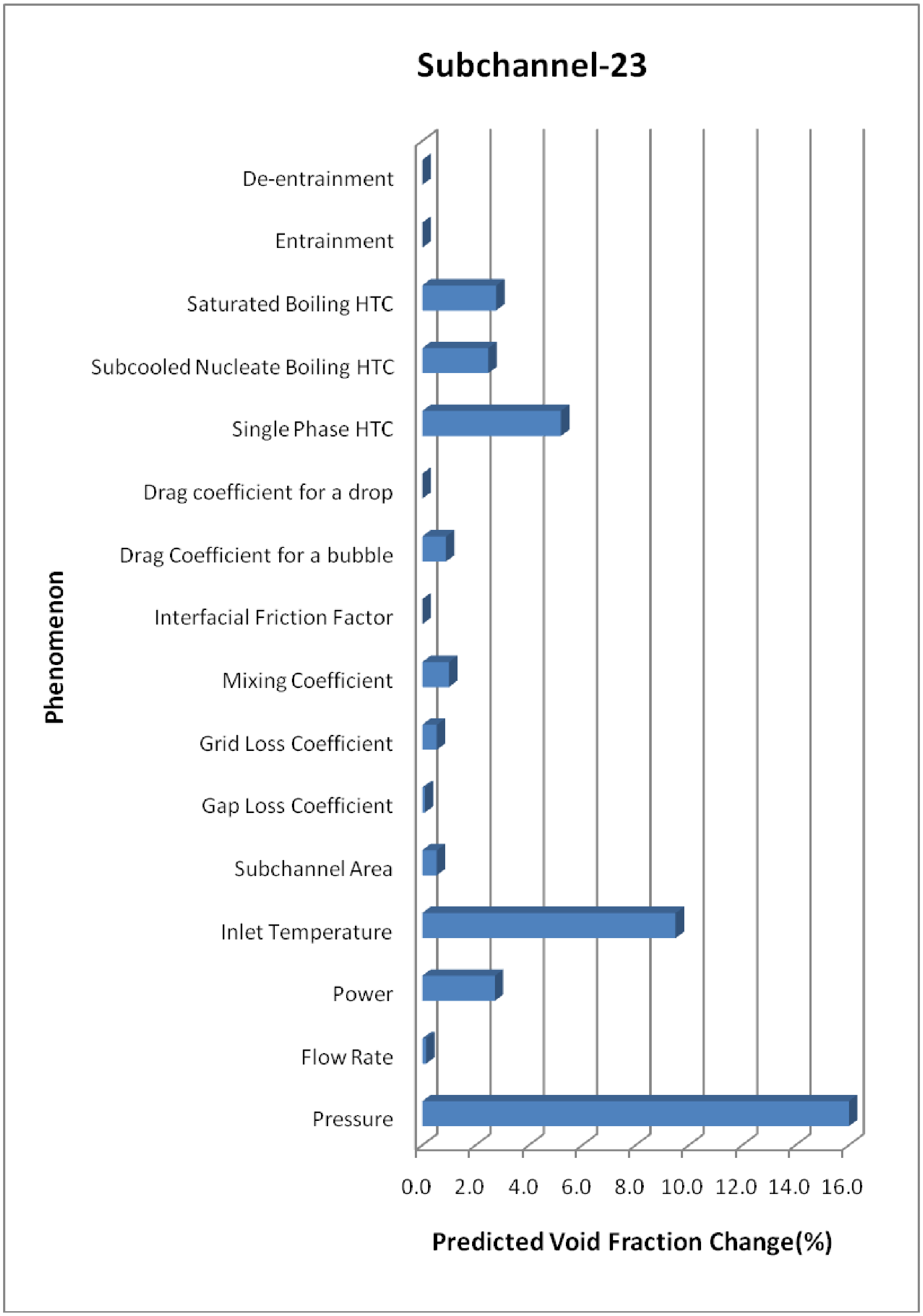

Figure 6.94. Predicted 23th Subchannel Void Fraction Change versus Phenomenon for Test 4101-69

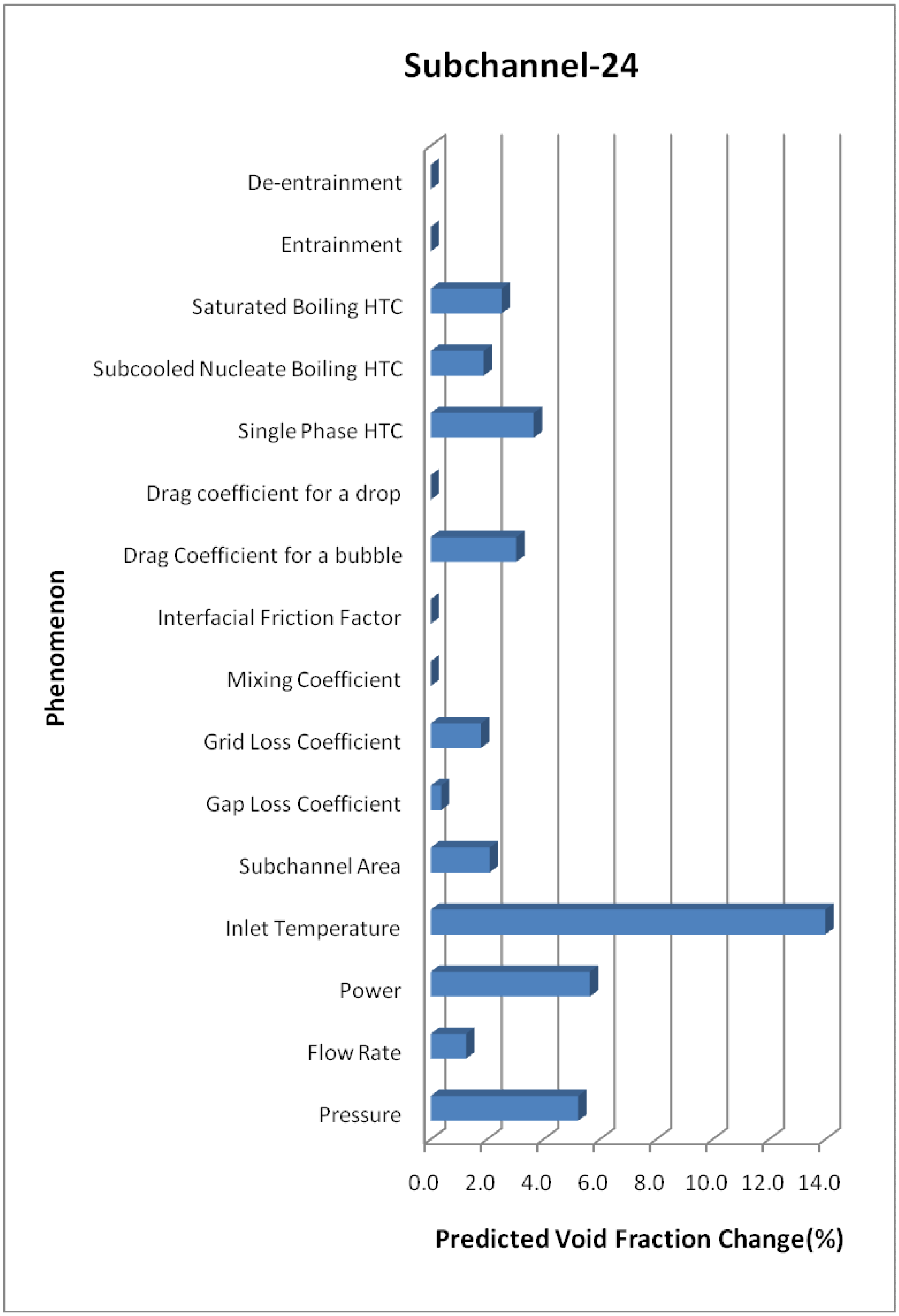

Figure 6.95. Predicted 24th Subchannel Void Fraction Change versus Phenomenon for Test 4101-69

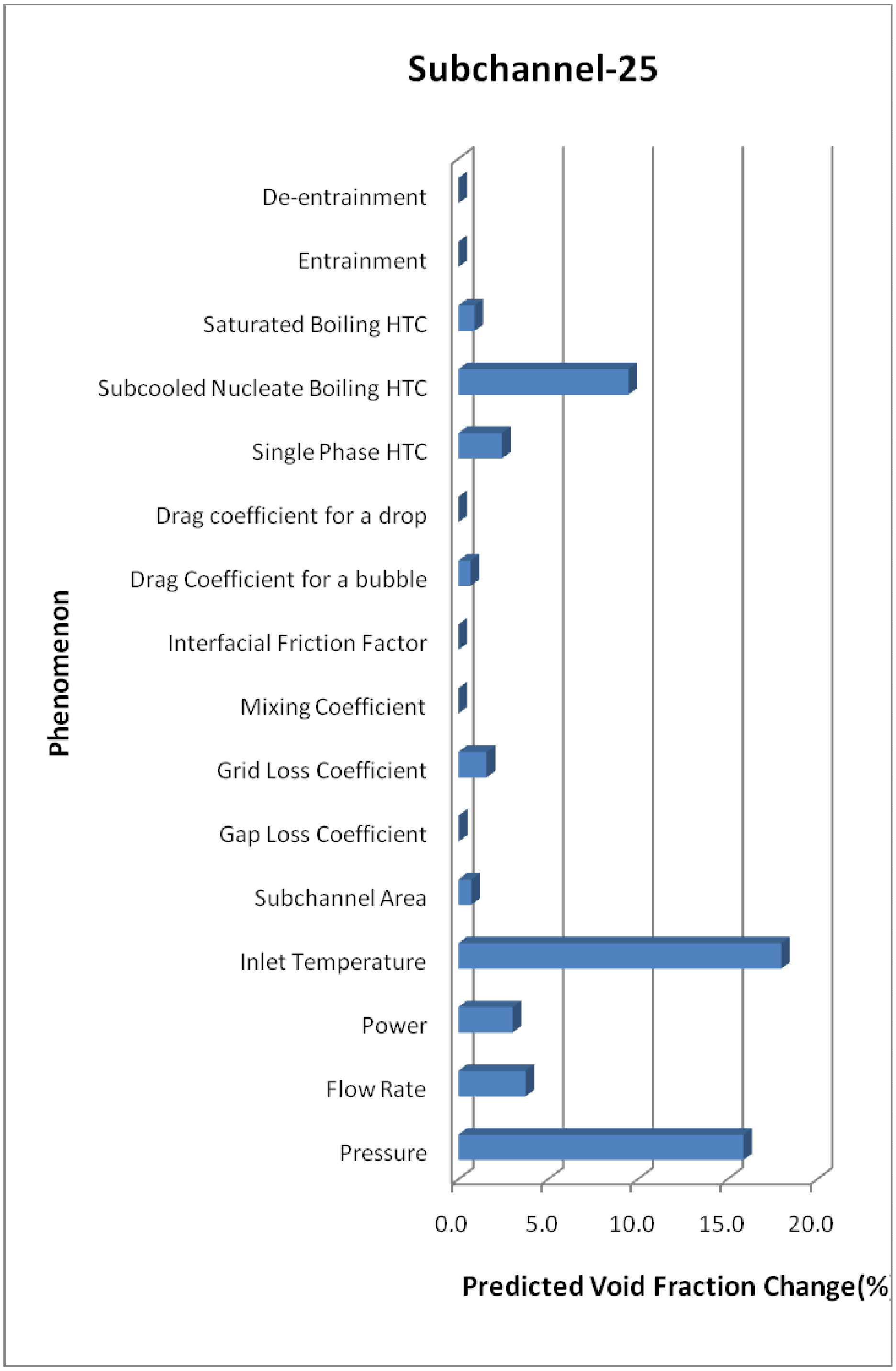

Figure 6.96. Predicted 25th Subchannel Void Fraction Change versus Phenomenon for Test 4101-69

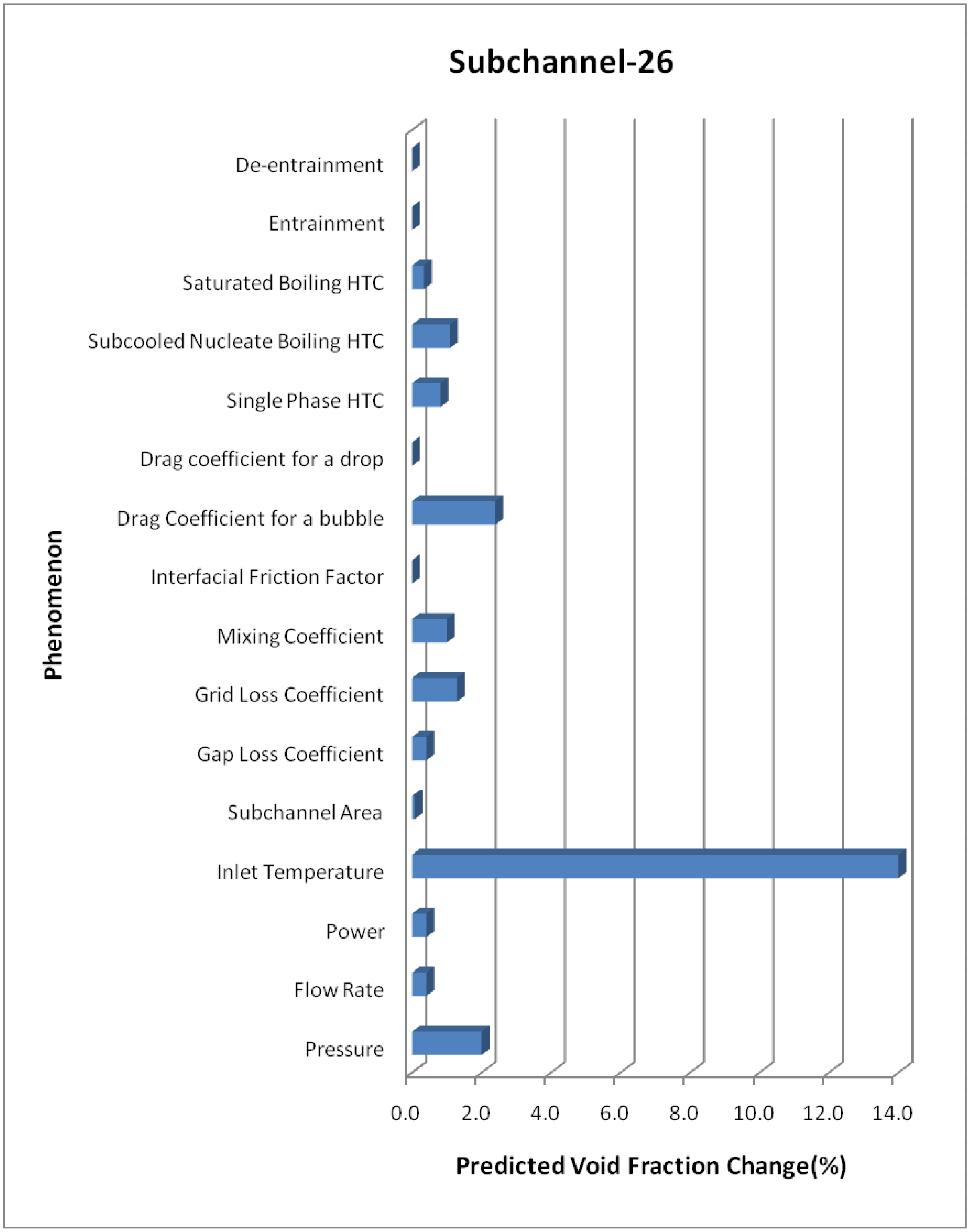

Figure 6.97. Predicted 26th Subchannel Void Fraction Change versus Phenomenon for Test 4101-69

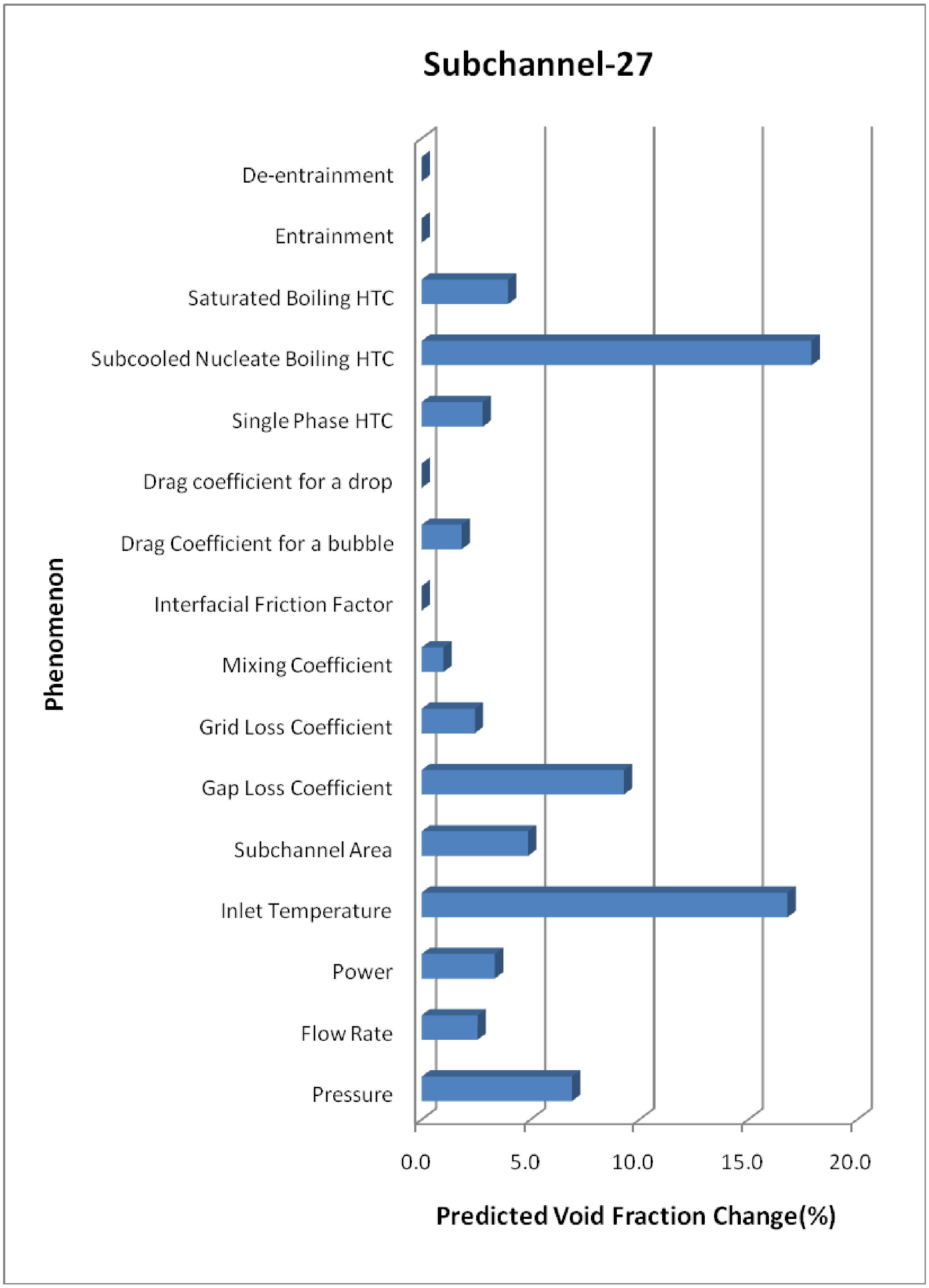

Figure 6.98. Predicted 27th Subchannel Void Fraction Change versus Phenomenon for Test 4101-69

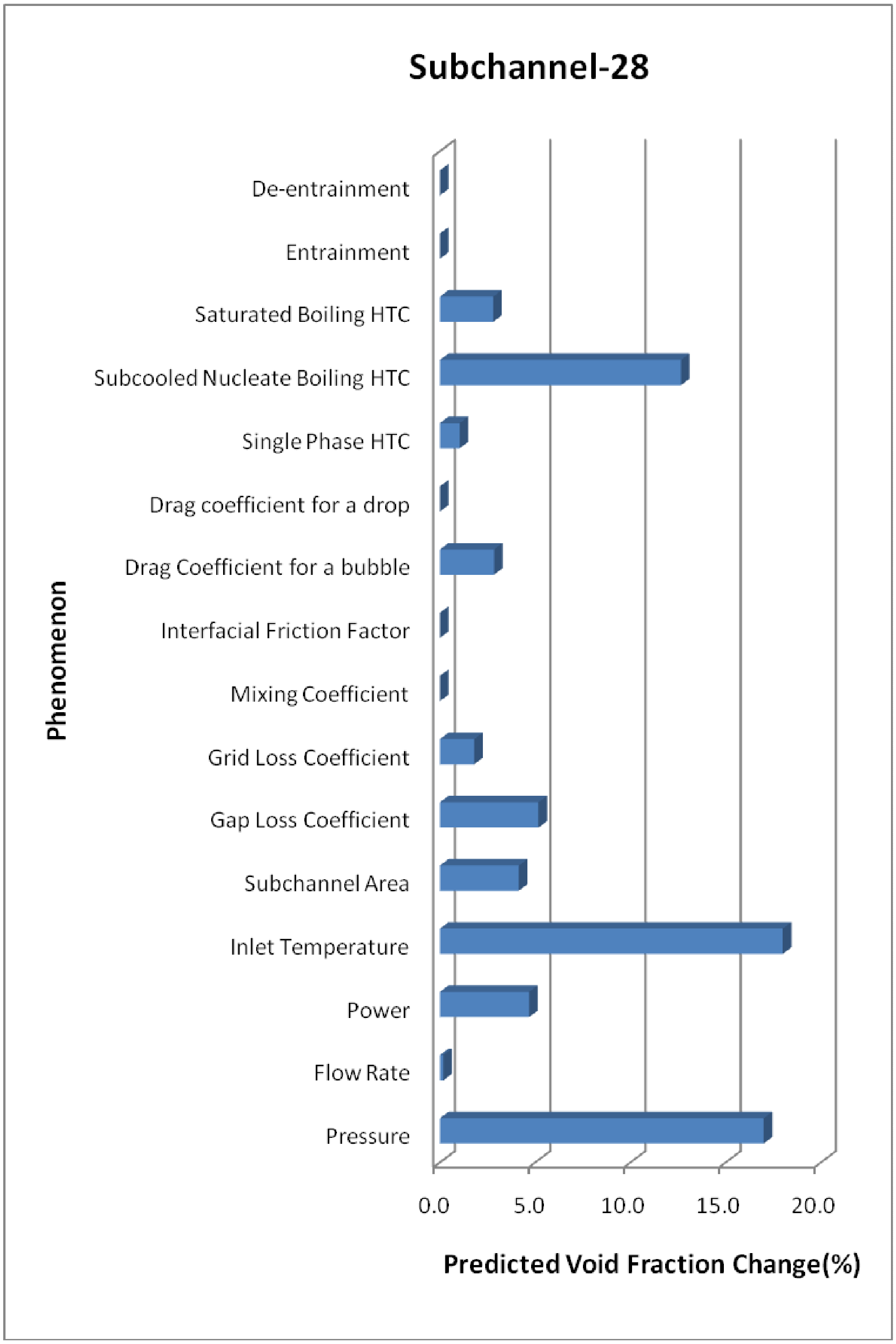

Figure 6.99. Predicted 28th Subchannel Void Fraction Change versus Phenomenon for Test 4101-69

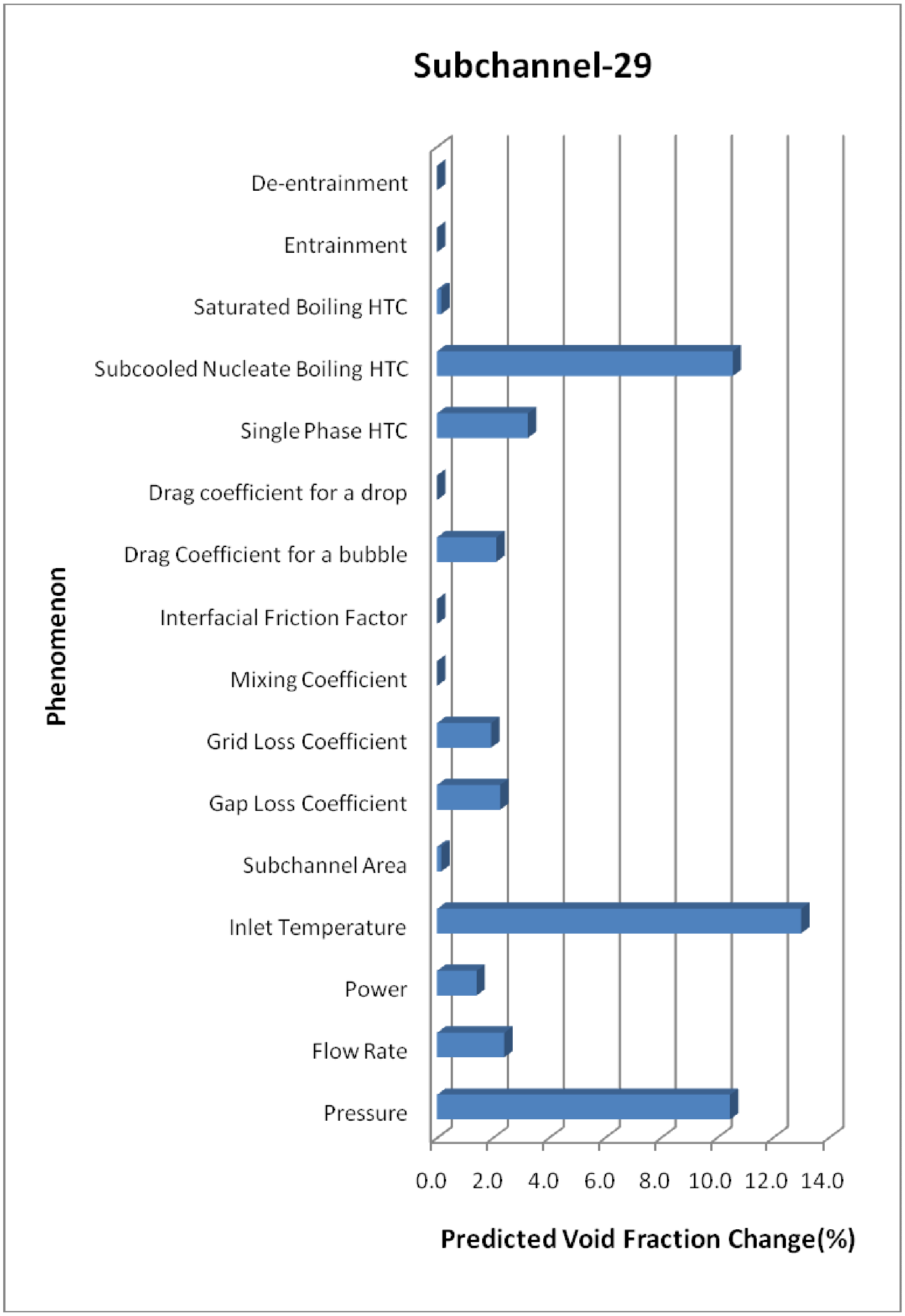

Figure 6.100. Predicted 29th Subchannel Void Fraction Change versus Phenomenon for Test 4101-69

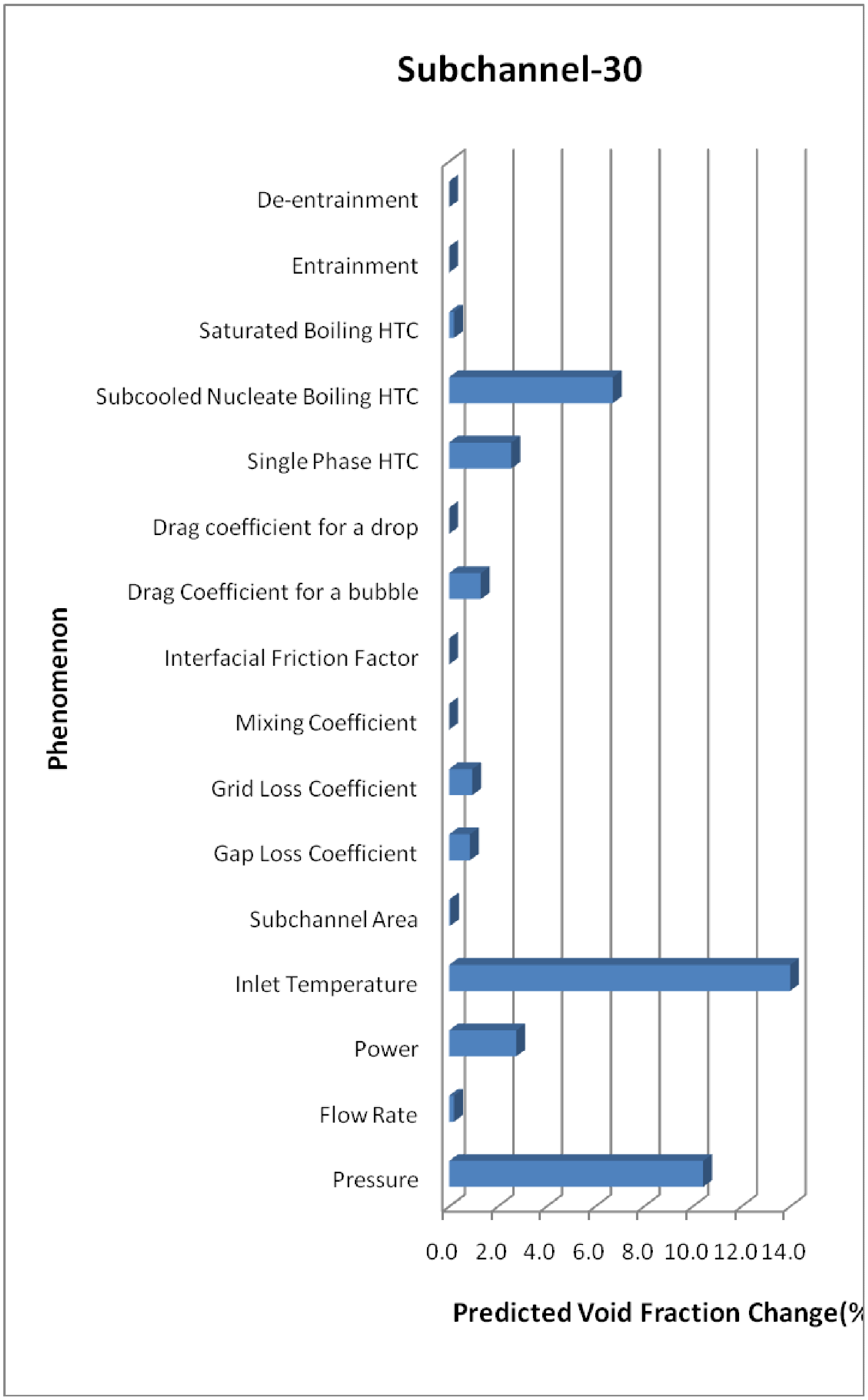

Figure 6.101. Predicted 30th Subchannel Void Fraction Change versus Phenomenon for Test 4101-69

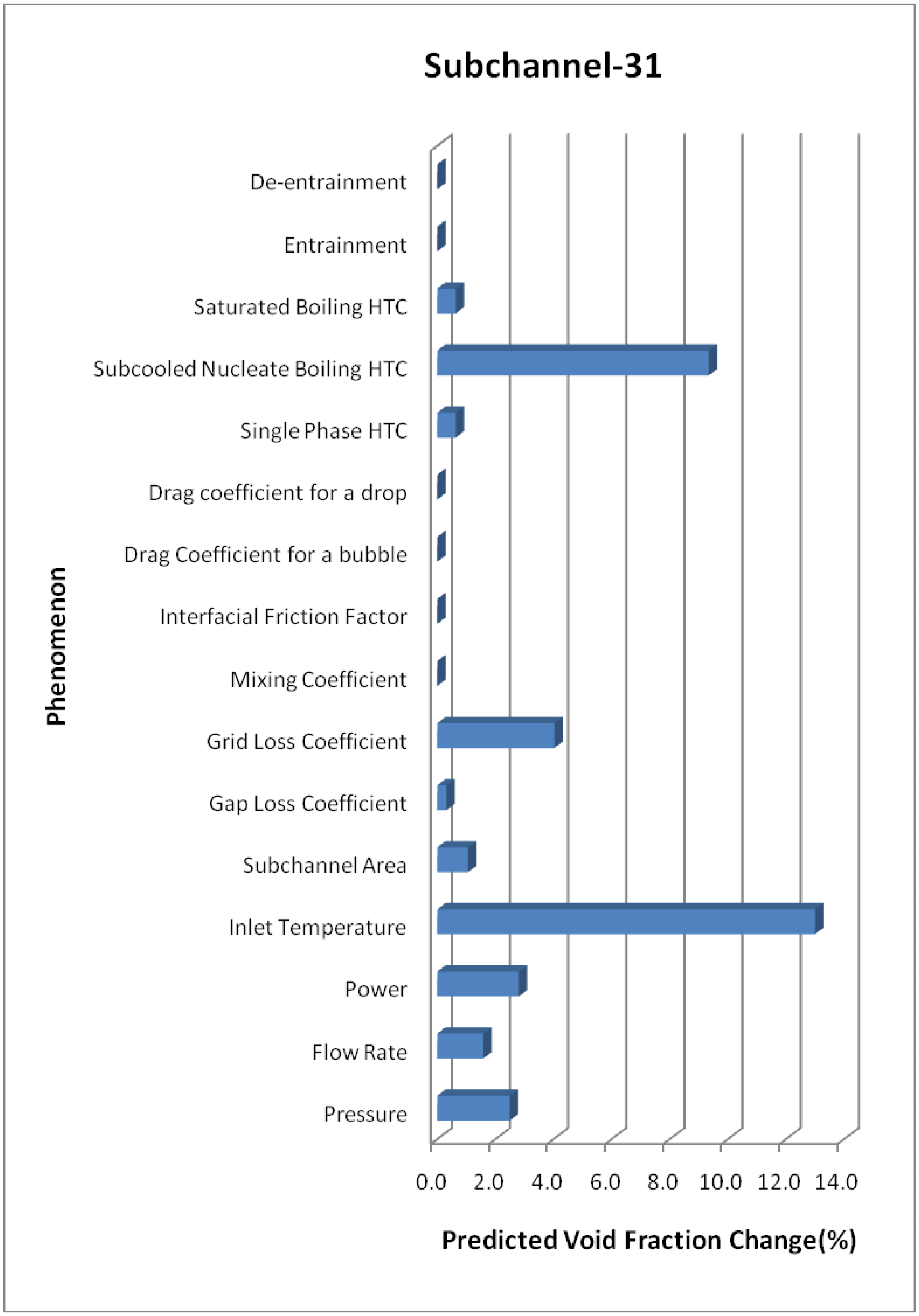

Figure 6.102. Predicted 31st Subchannel Void Fraction Change versus Phenomenon for Test 4101-69

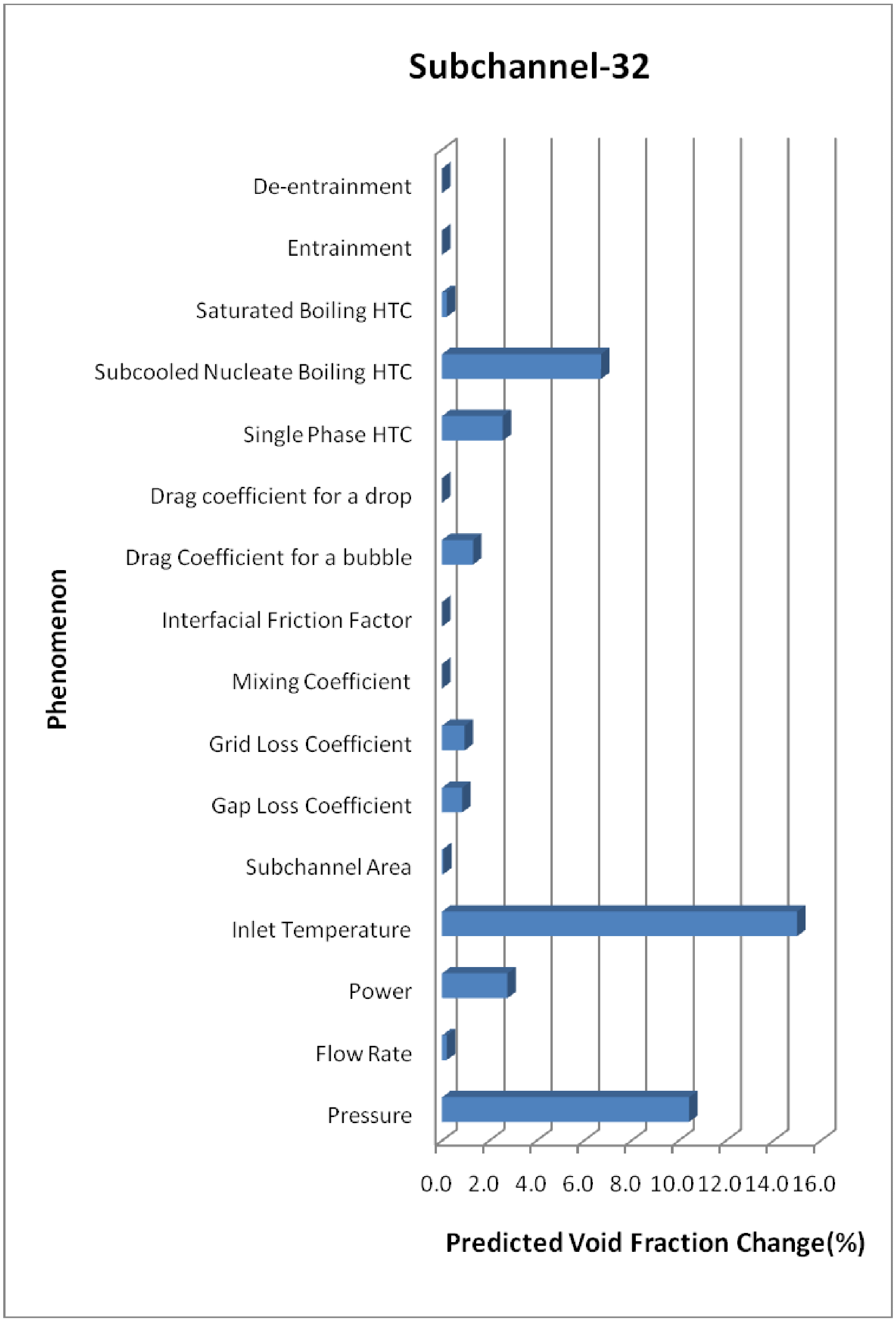

Figure 6.103. Predicted 32nd Subchannel Void Fraction Change versus Phenomenon for Test 4101-69

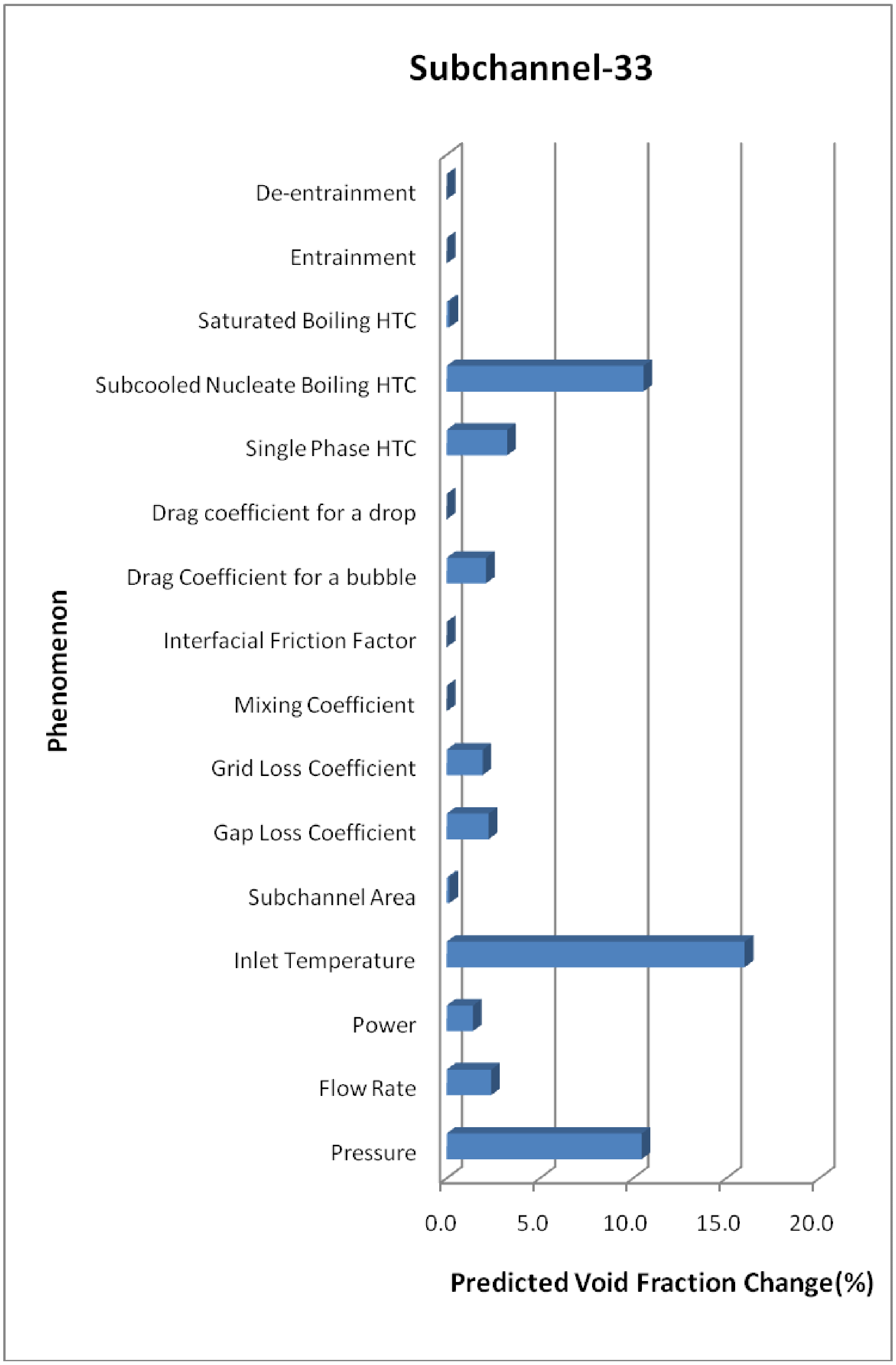

Figure 6.104. Predicted 33th Subchannel Void Fraction Change versus Phenomenon for Test 4101-69

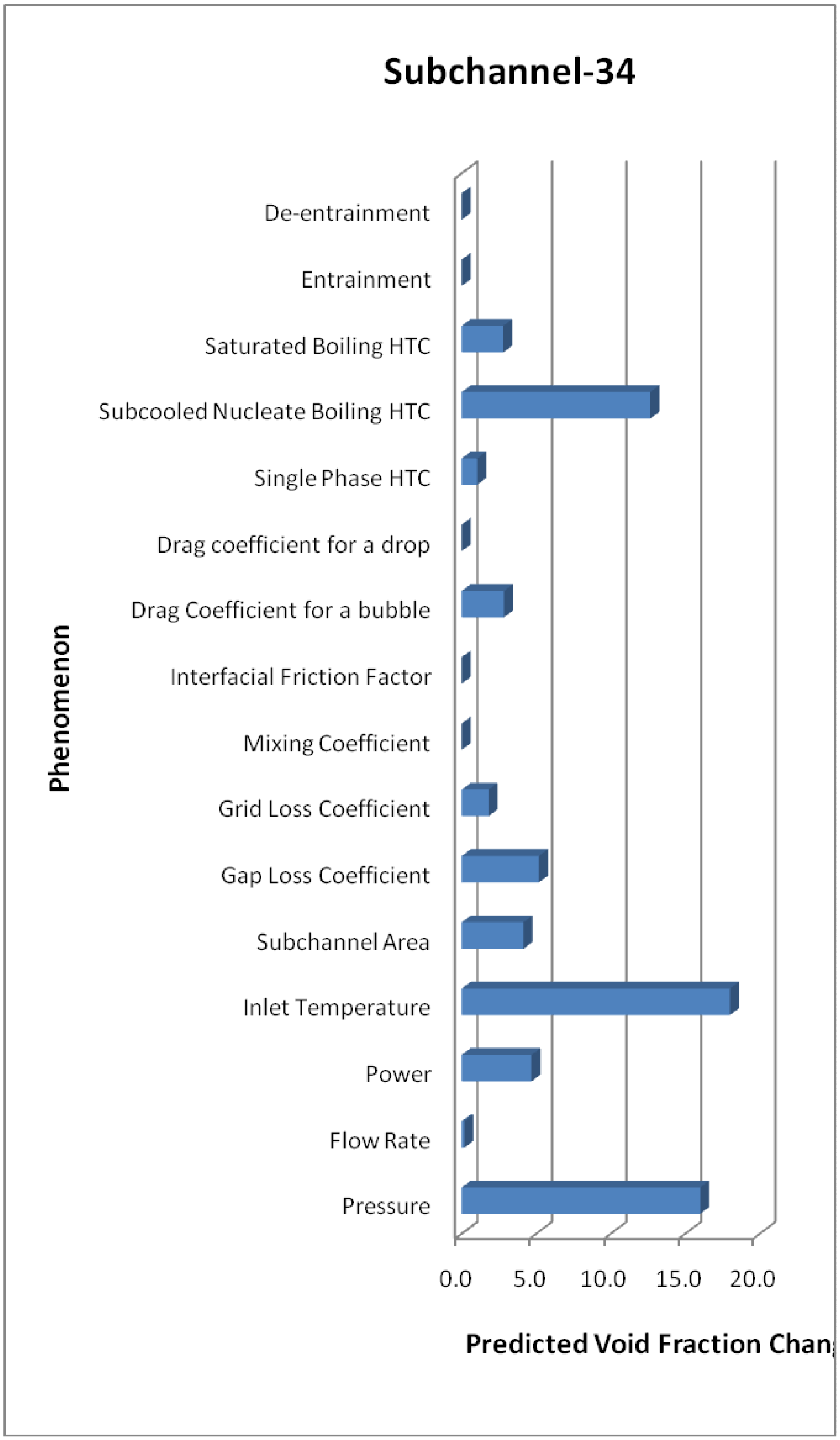

Figure 6.105. Predicted 34th Subchannel Void Fraction Change versus Phenomenon for Test 4101-69

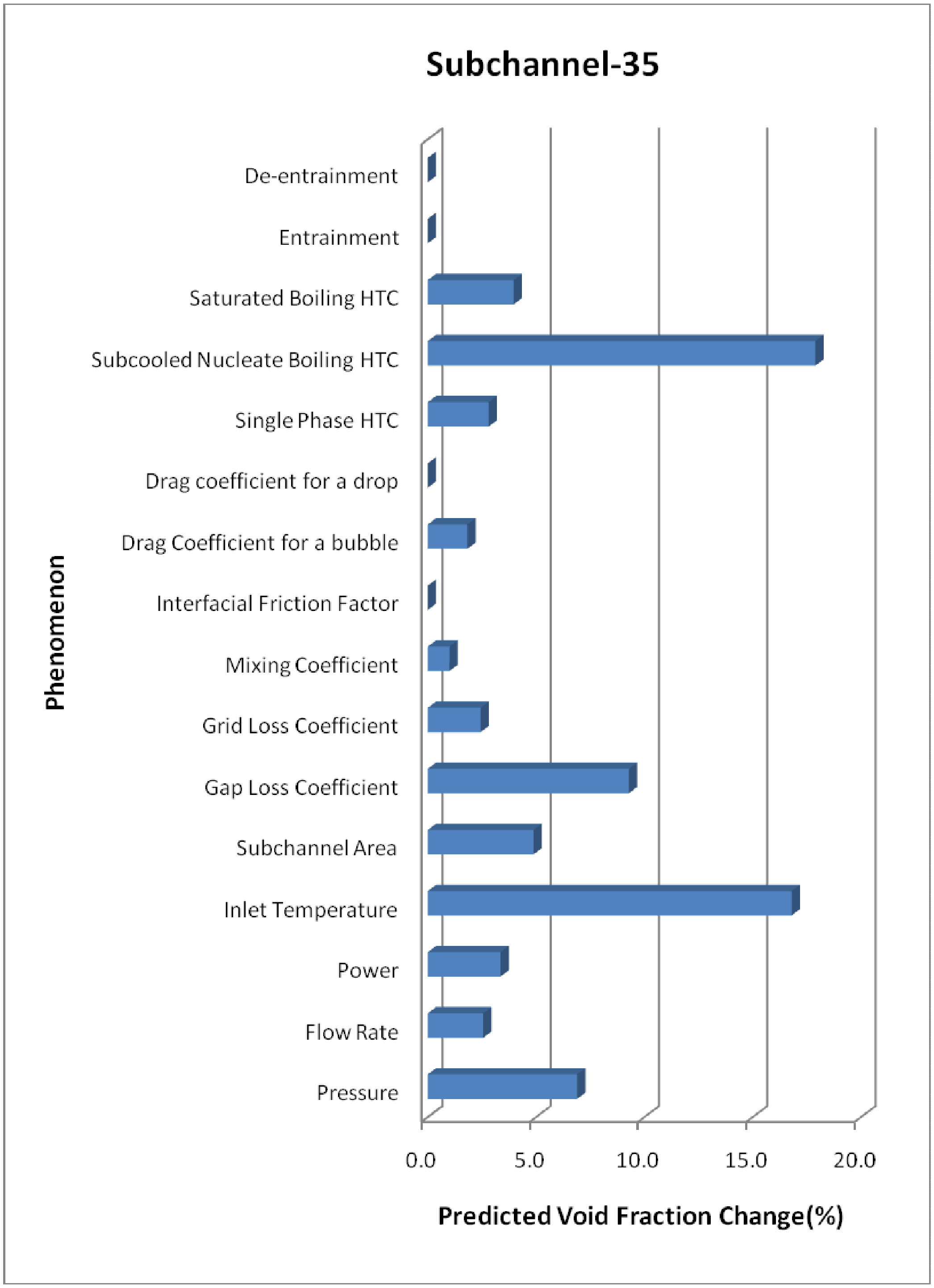

Figure 6.106. Predicted 35th Subchannel Void Fraction Change versus Phenomenon for Test 4101-69

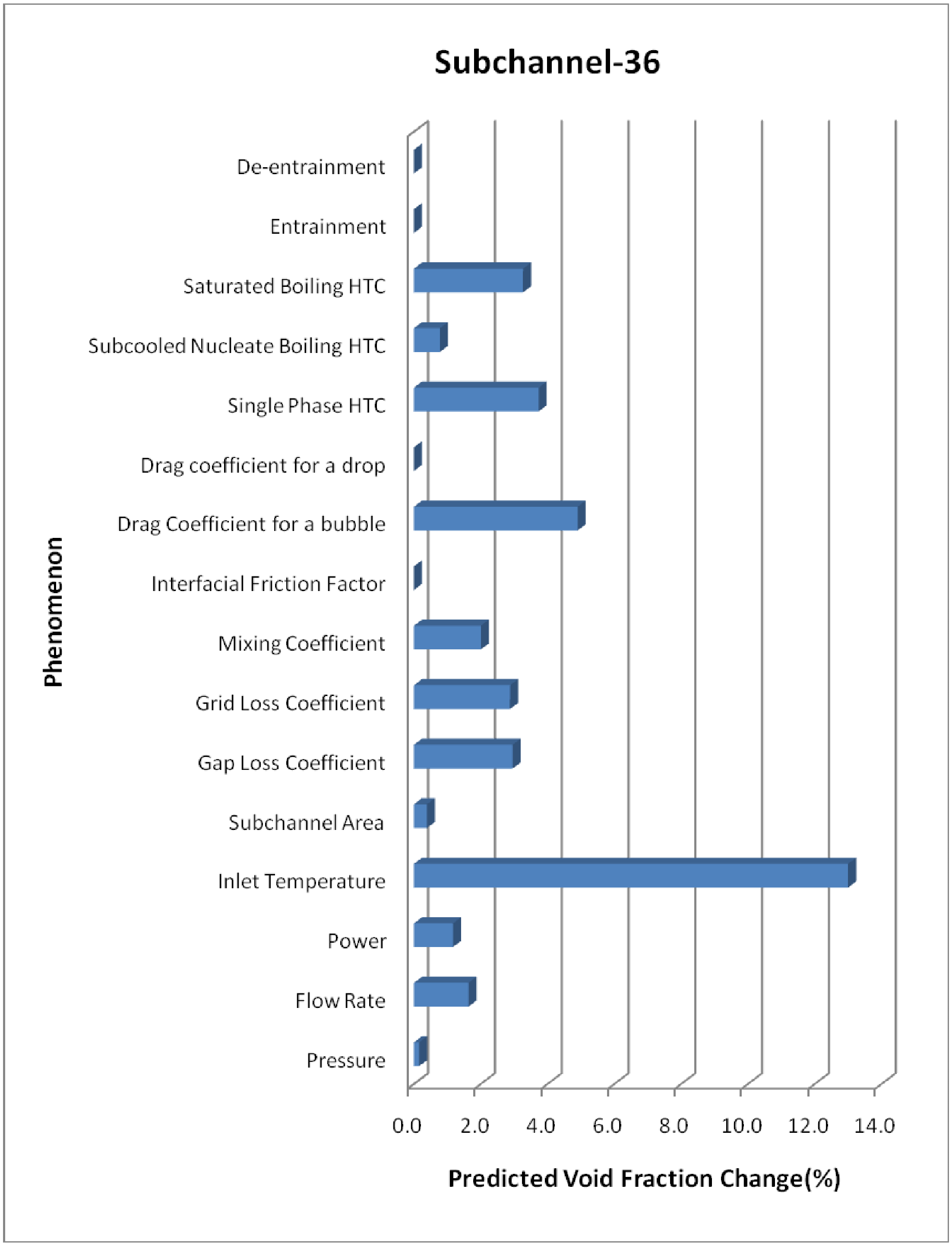

Figure 6.107. Predicted 36th Subchannel Void Fraction Change versus Phenomenon for Test 4101-69

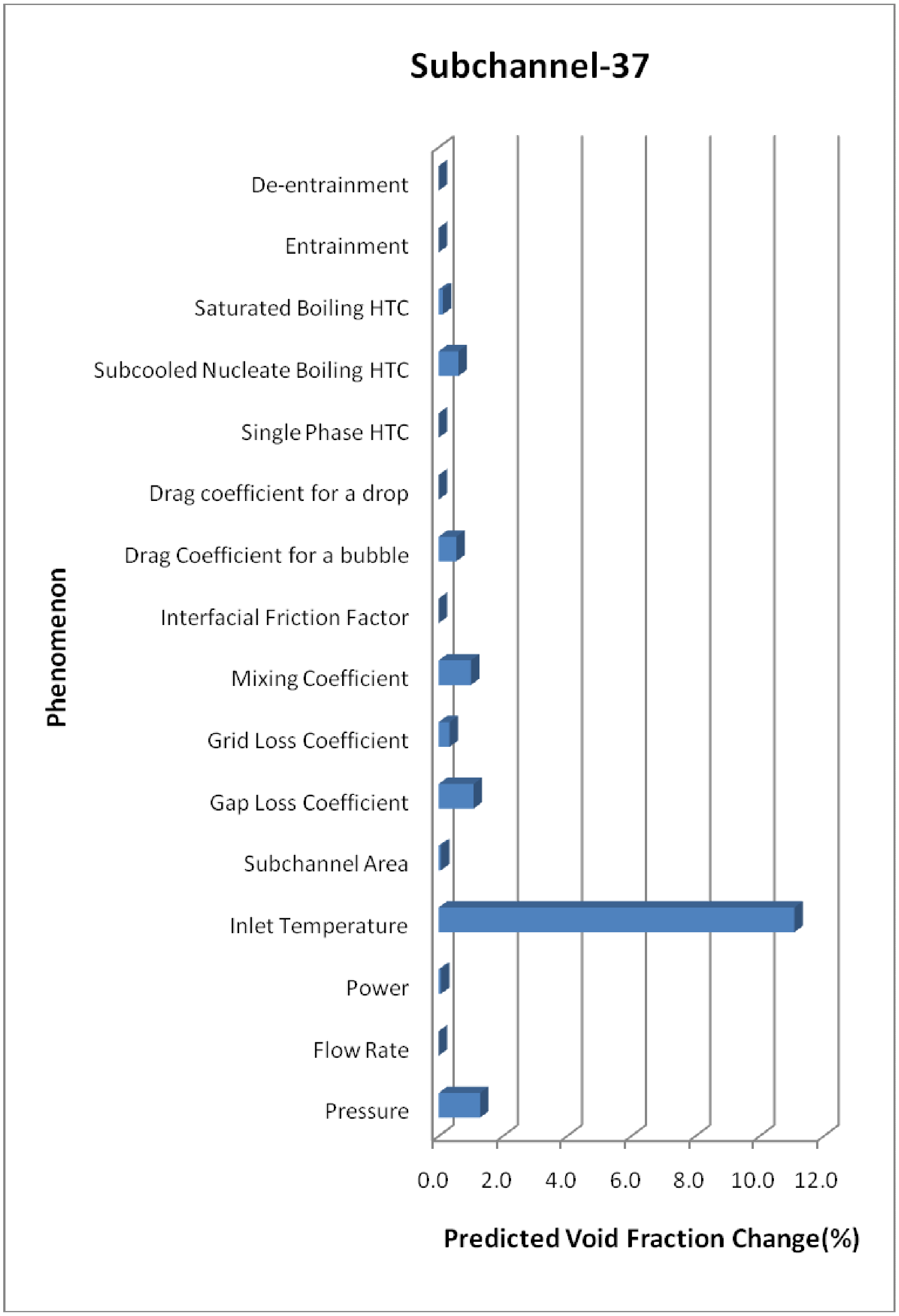

Figure 6.108. Predicted 37th Subchannel Void Fraction Change versus Phenomenon for Test 4101-69

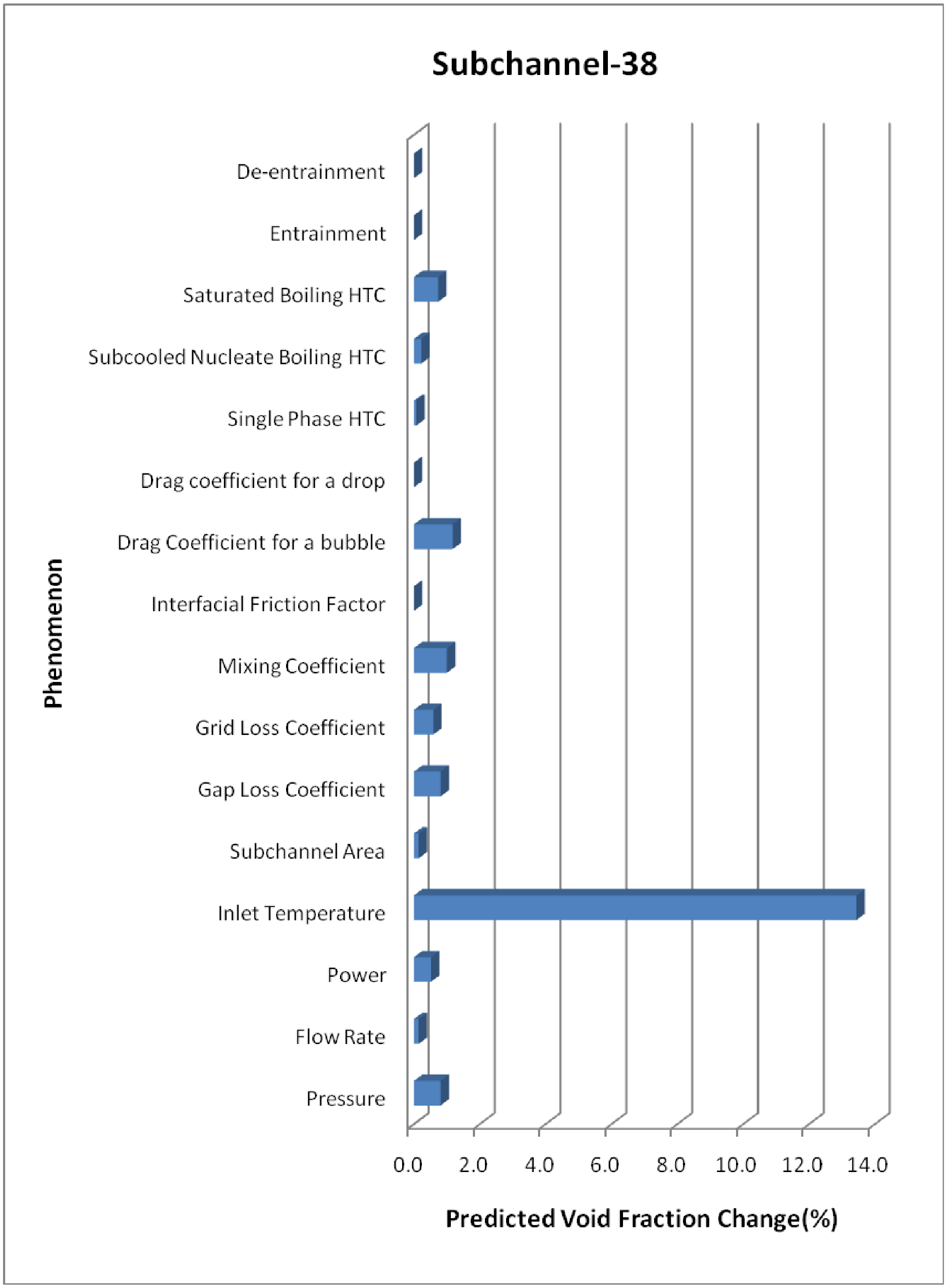

Figure 6.109. Predicted 38th Subchannel Void Fraction Change versus Phenomenon for Test 4101-69

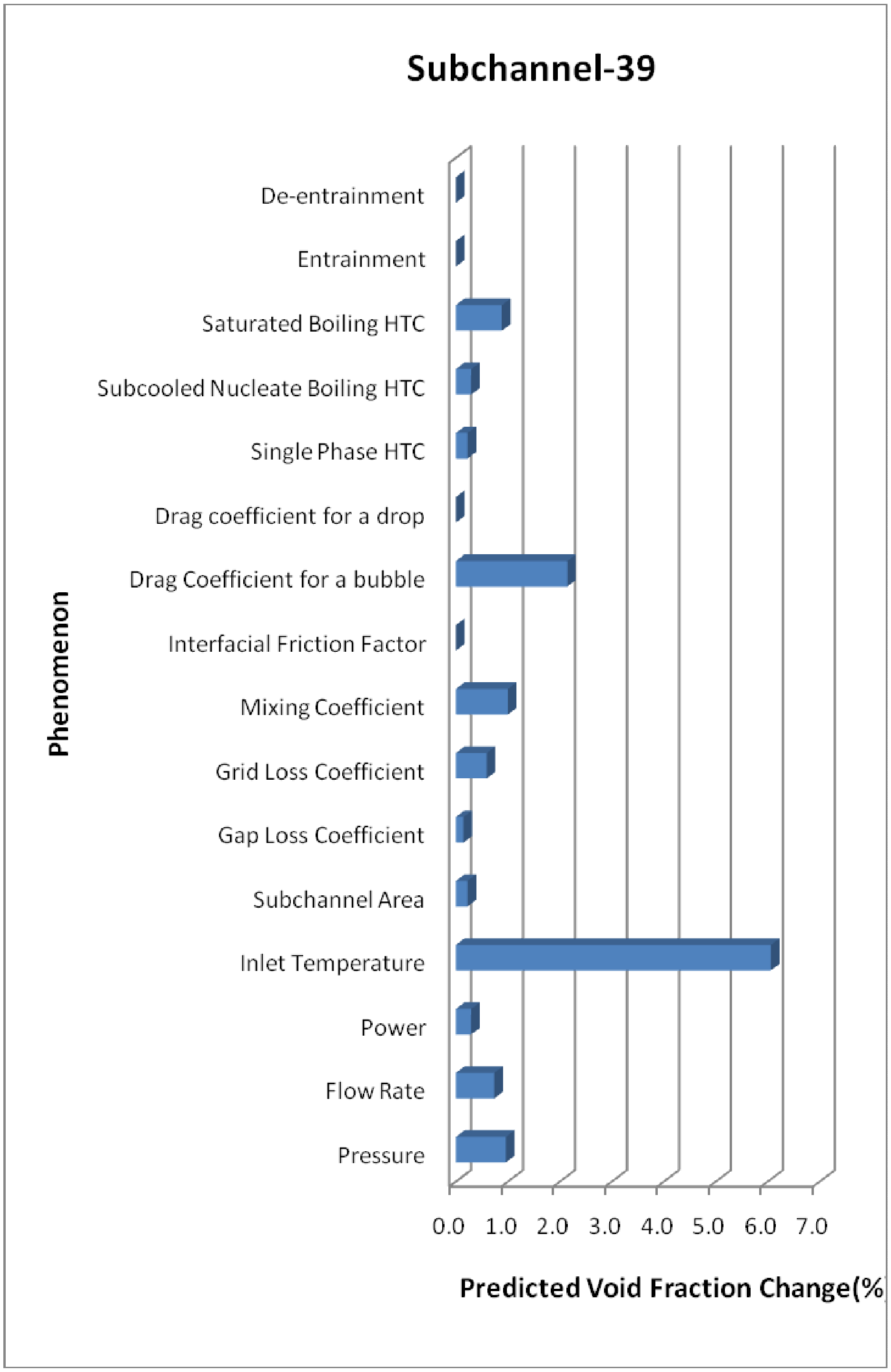

Figure 6.110. Predicted 39th Subchannel Void Fraction Change versus Phenomenon for Test 4101-69

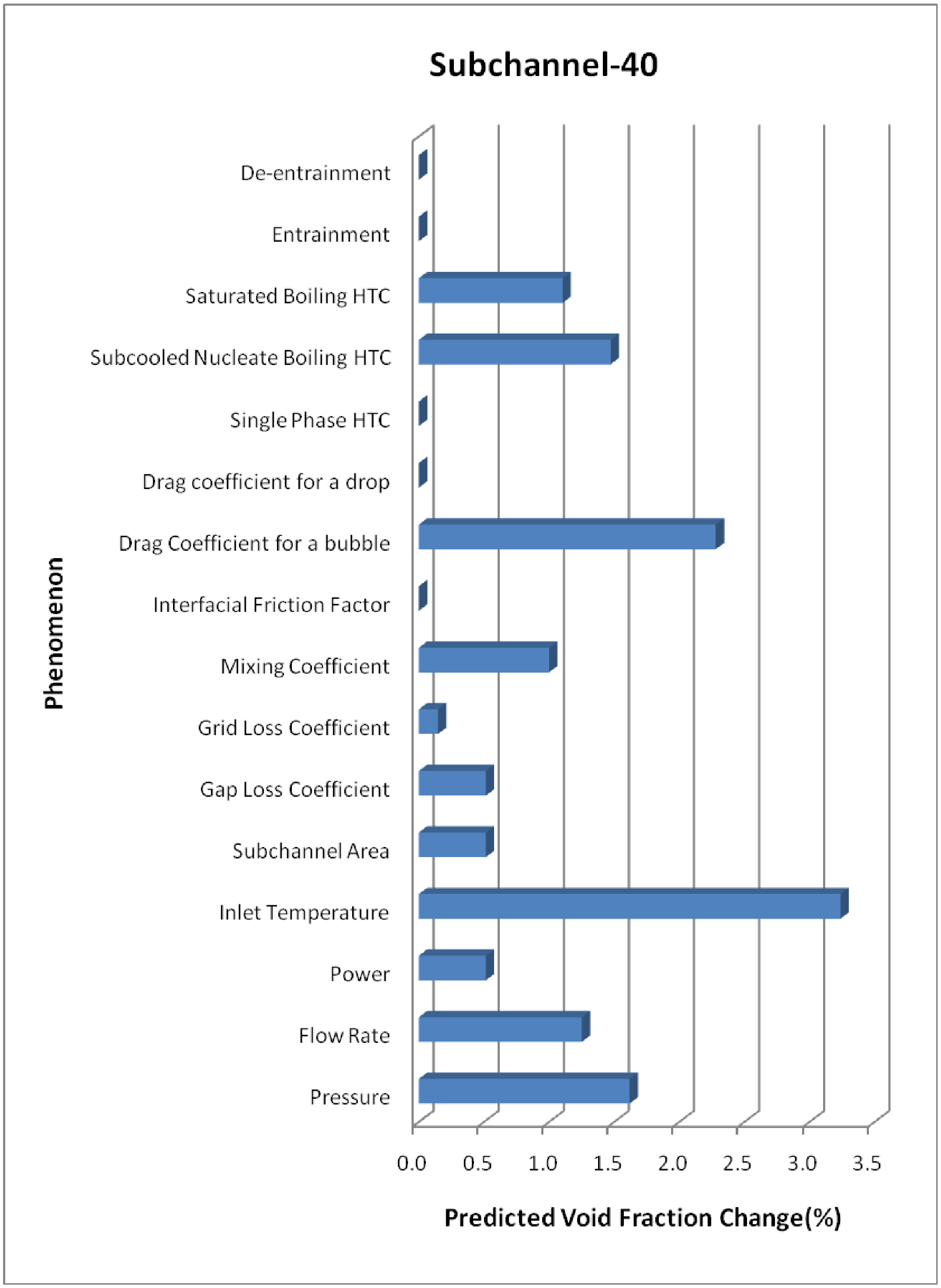

Figure 6.111. Predicted 40th Subchannel Void Fraction Change versus Phenomenon for Test 4101-69

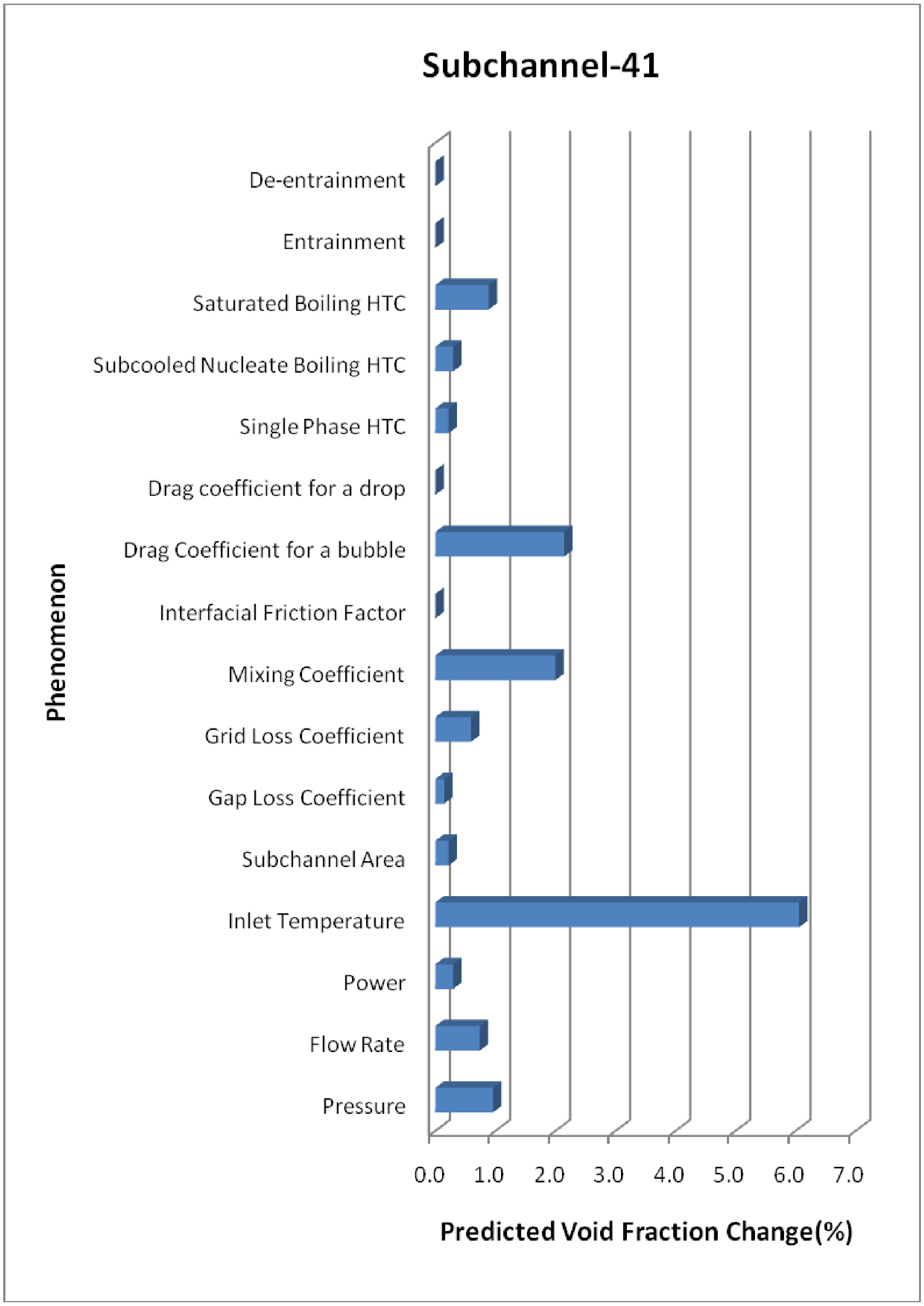

Figure 6.112. Predicted 41st Subchannel Void Fraction Change versus Phenomenon for Test 4101-69

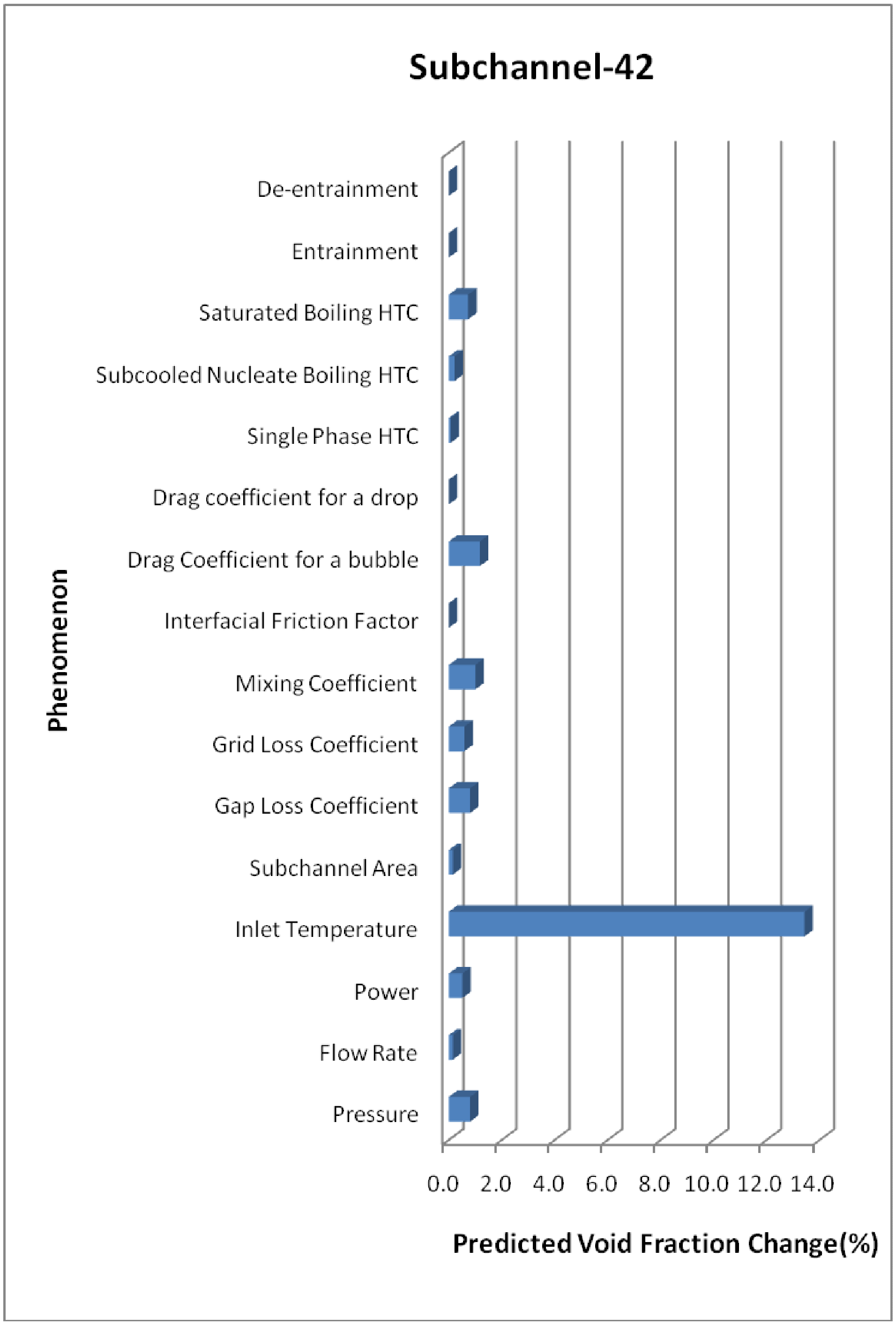

Figure 6.113. Predicted 42th Subchannel Void Fraction Change versus Phenomenon for Test 4101-69

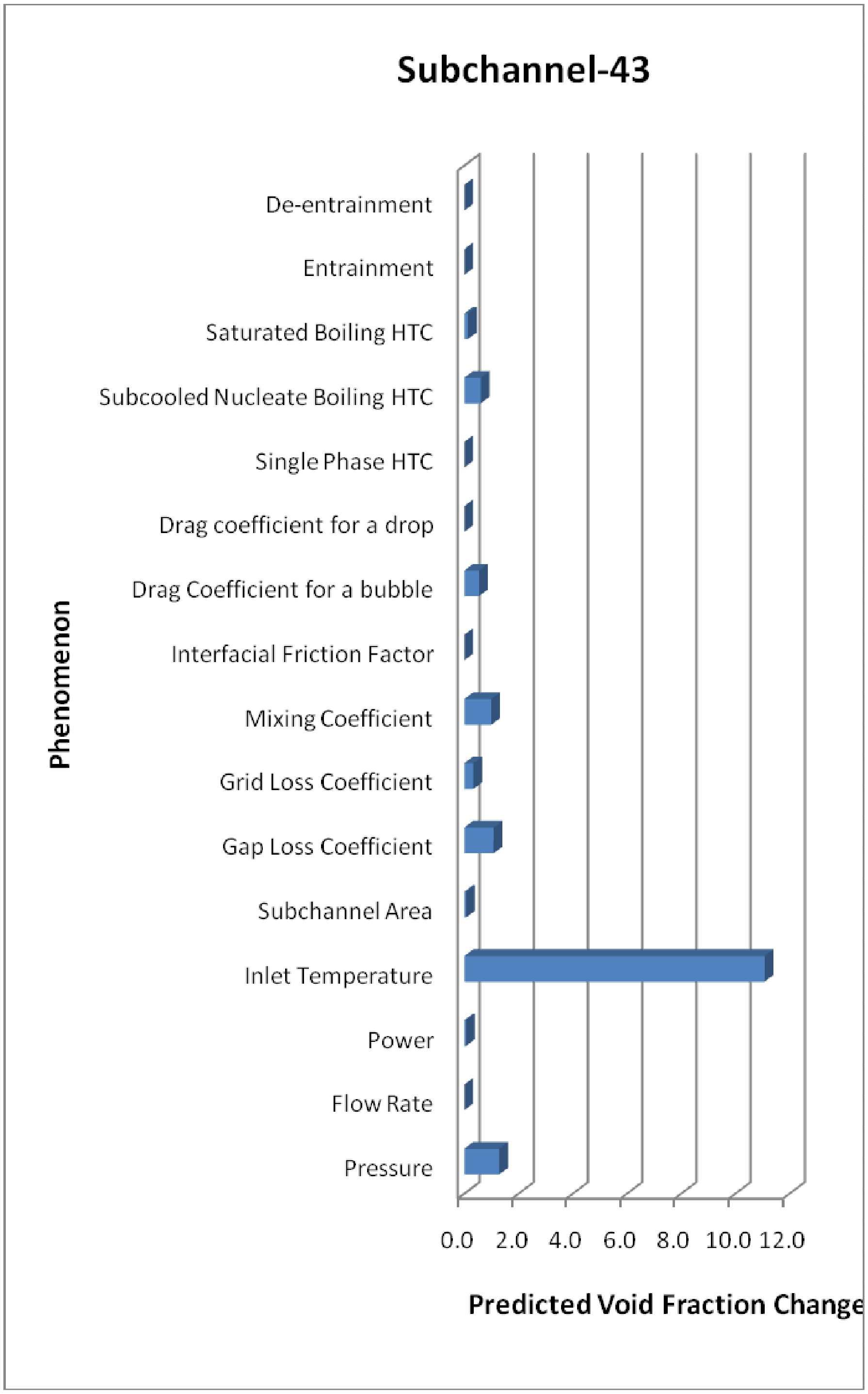

Figure 6.114. Predicted 43th Subchannel Void Fraction Change versus Phenomenon for Test 4101-69

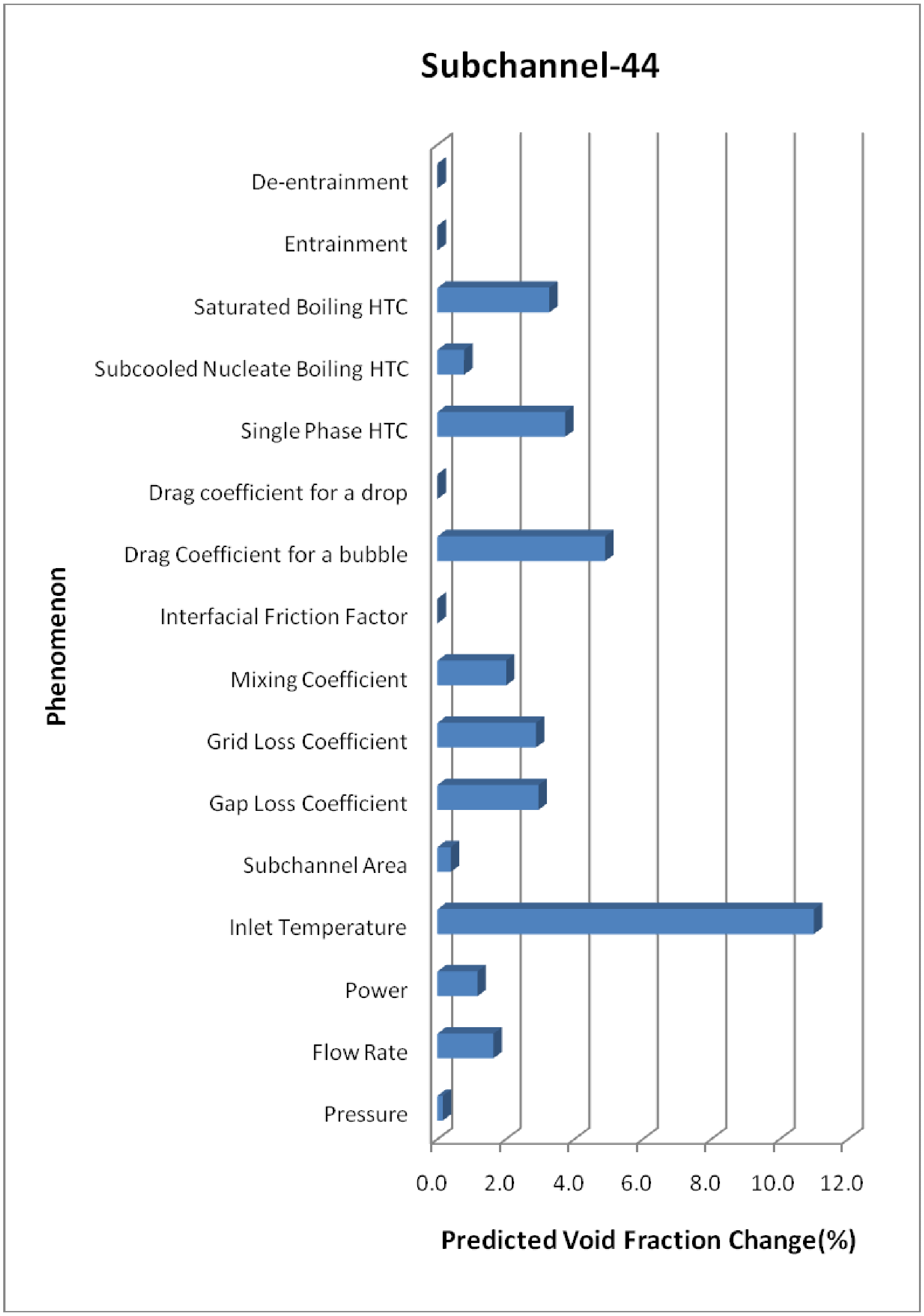

Figure 6.115. Predicted 44th Subchannel Void Fraction Change versus Phenomenon for Test 4101-69

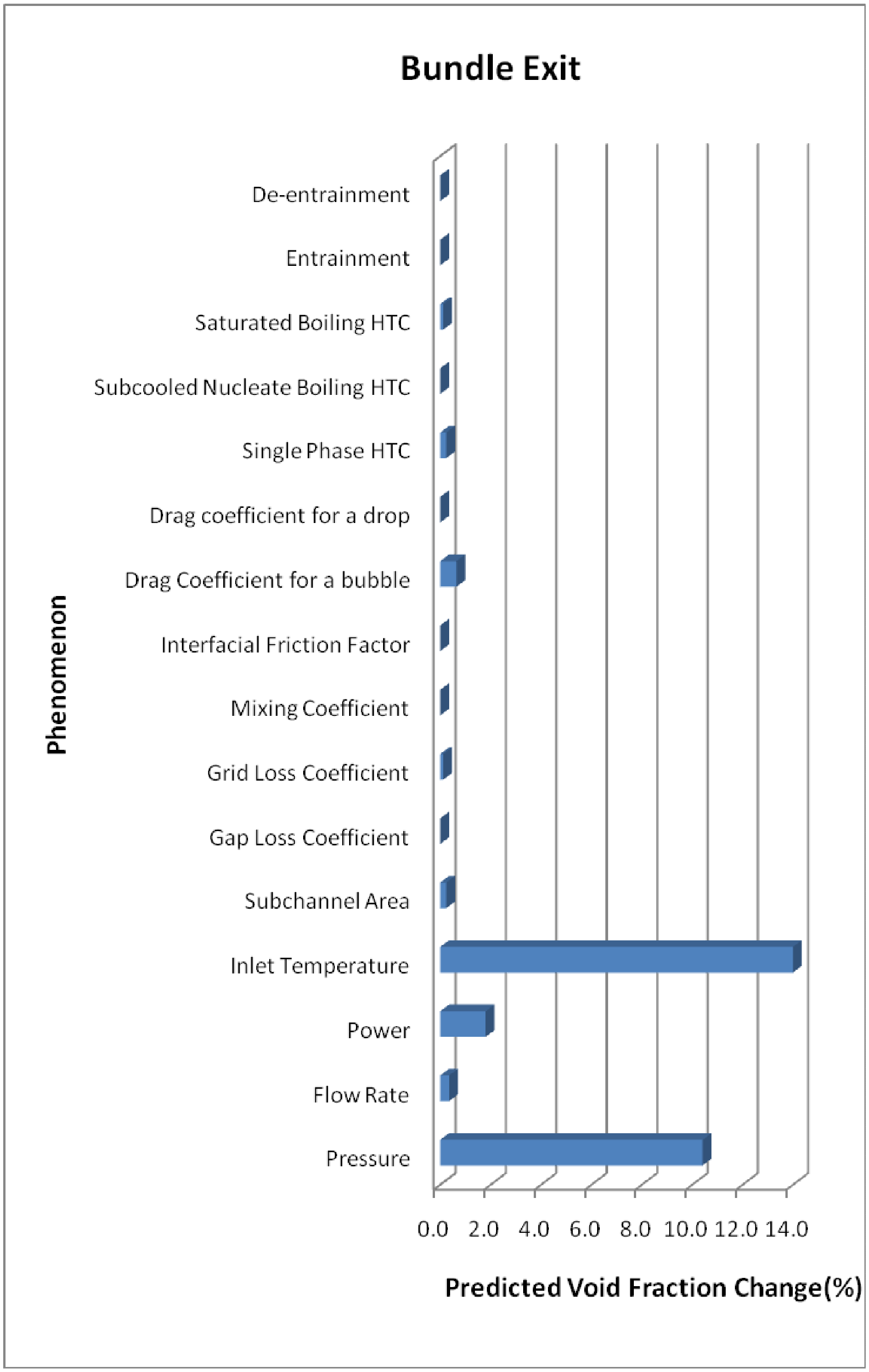

Figure 6.116. Predicted Bundle Void Fraction Change versus Phenomenon for Test 4101-69

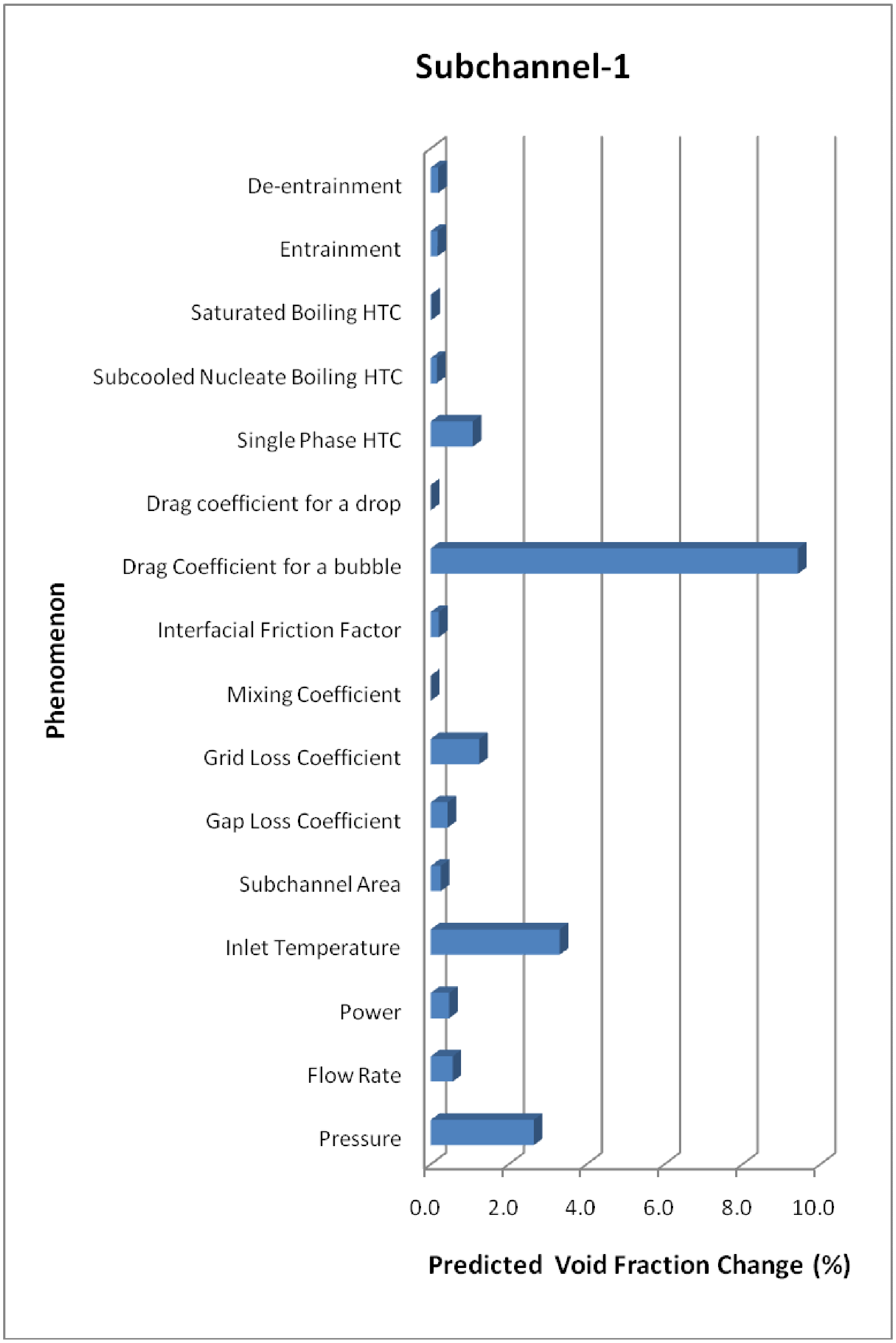

Figure 6.117. Predicted 1st Subchannel Void Fraction Change versus Phenomenon for Test 4101-55

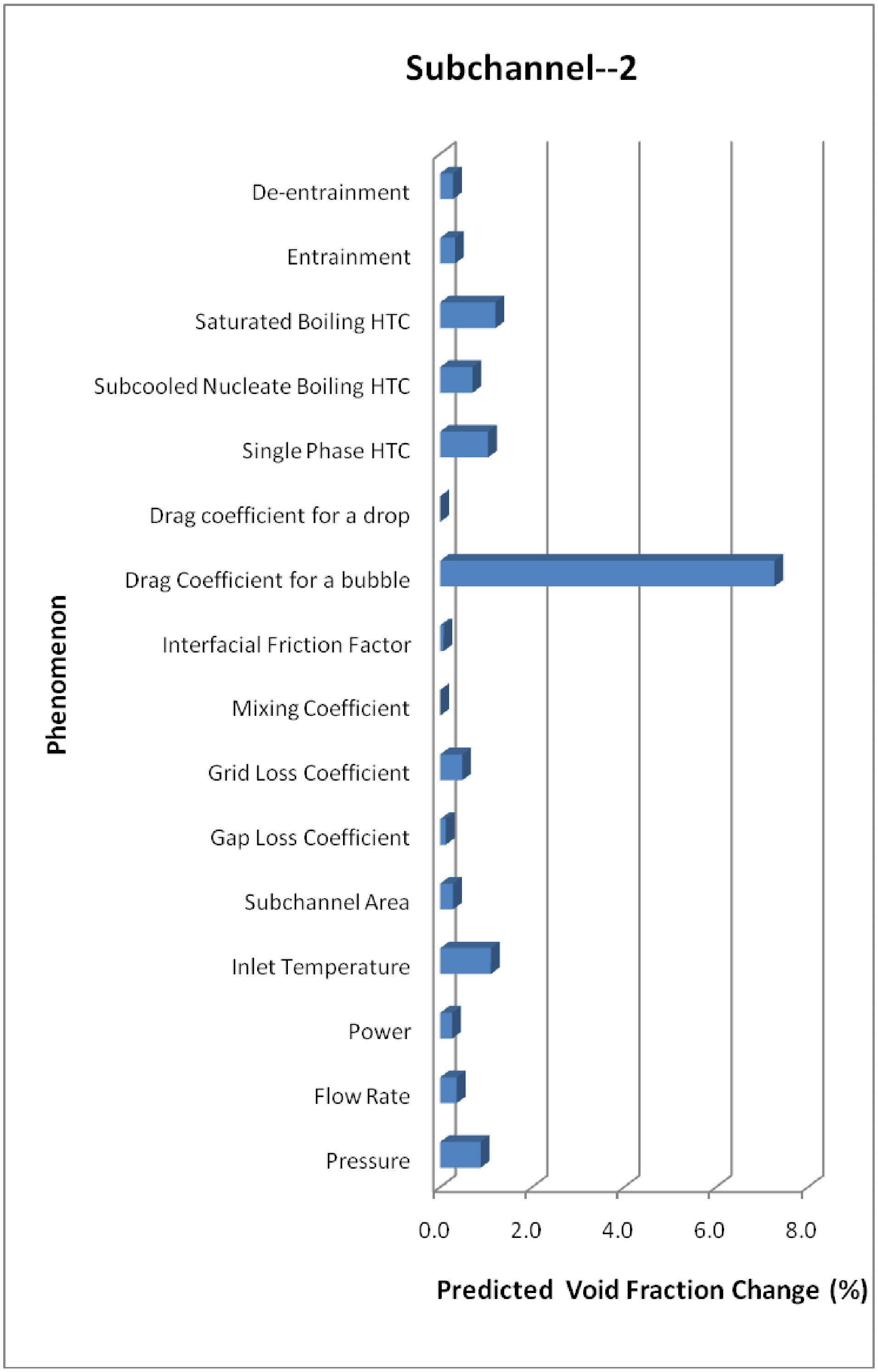

Figure 6.118. Predicted 2nd Subchannel Void Fraction Change versus Phenomenon for Test 4101-55

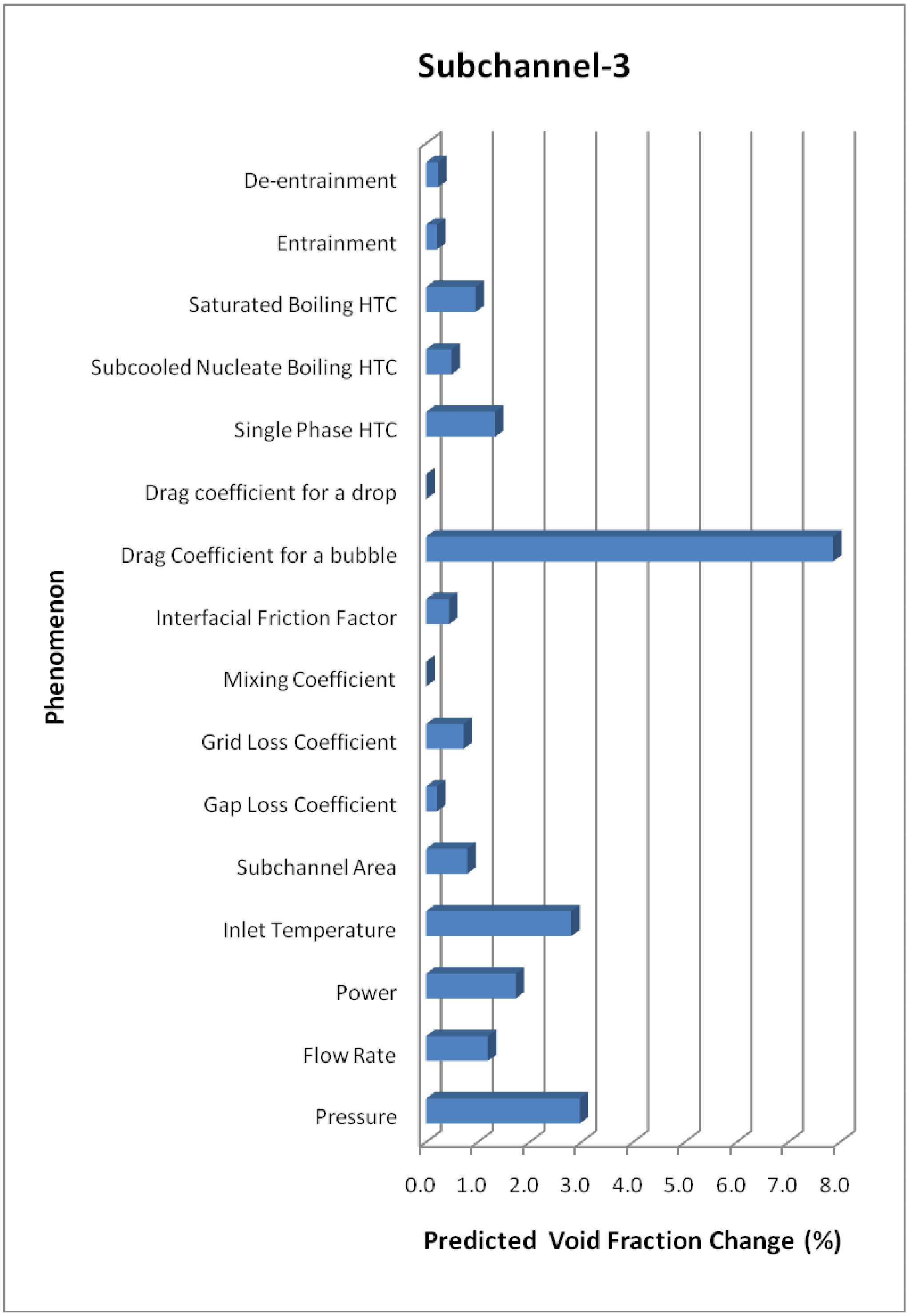

Figure 6.119. Predicted 3rd Subchannel Void Fraction Change versus Phenomenon for Test 4101-55

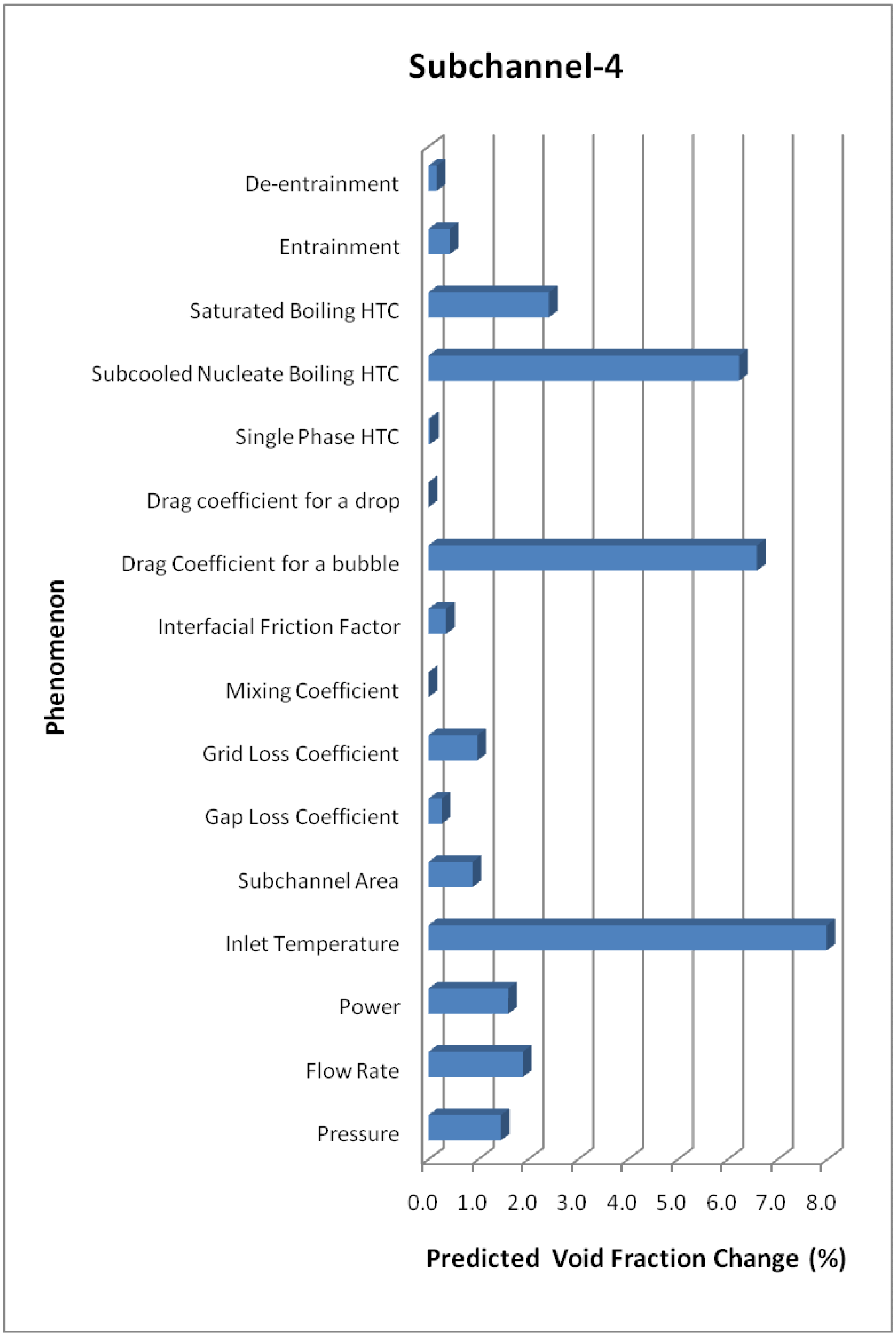

Figure 6.120. Predicted 4th Subchannel Void Fraction Change versus Phenomenon for Test 4101-55

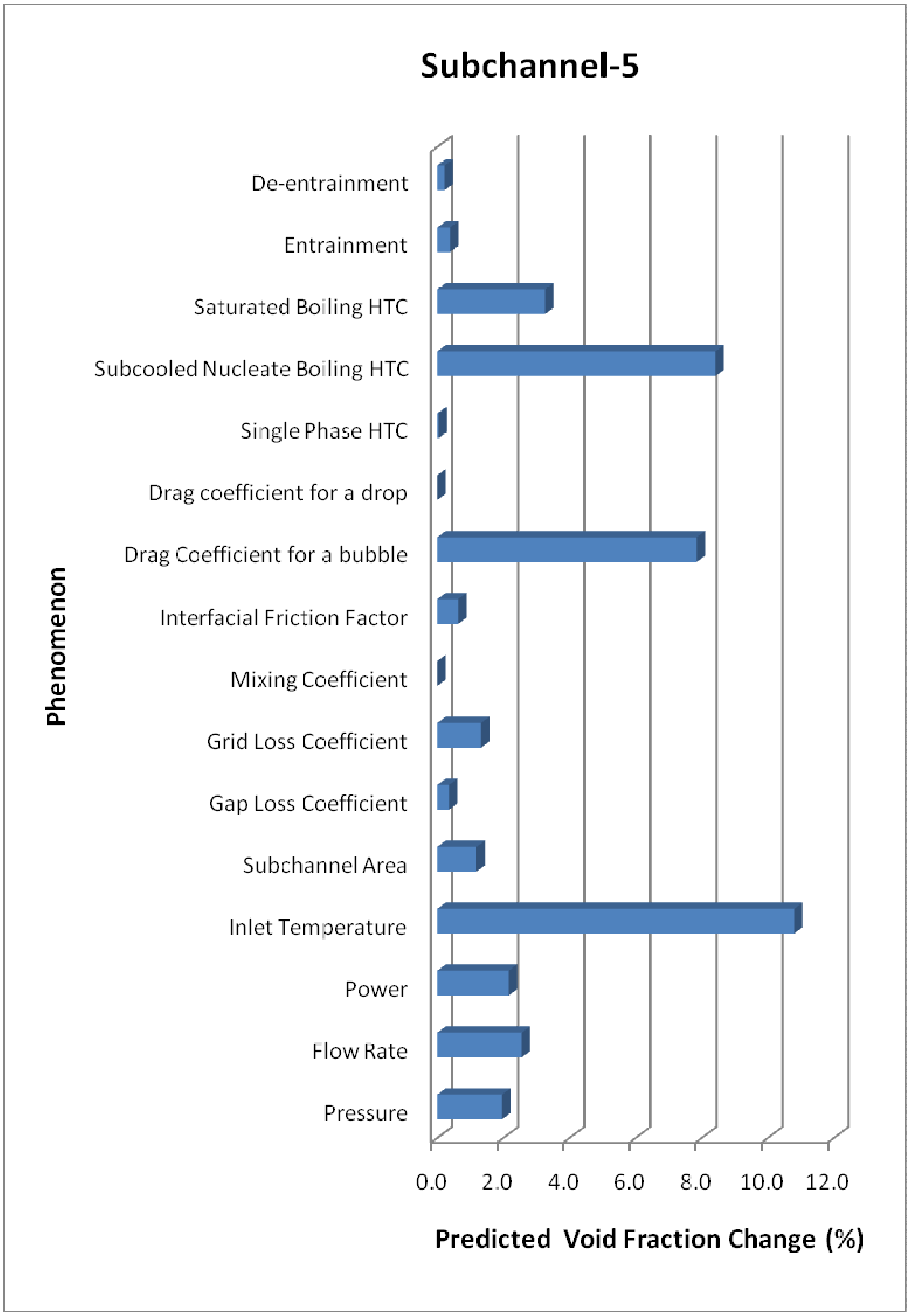

Figure 6.121. Predicted 5th Subchannel Void Fraction Change versus Phenomenon for Test 4101-55

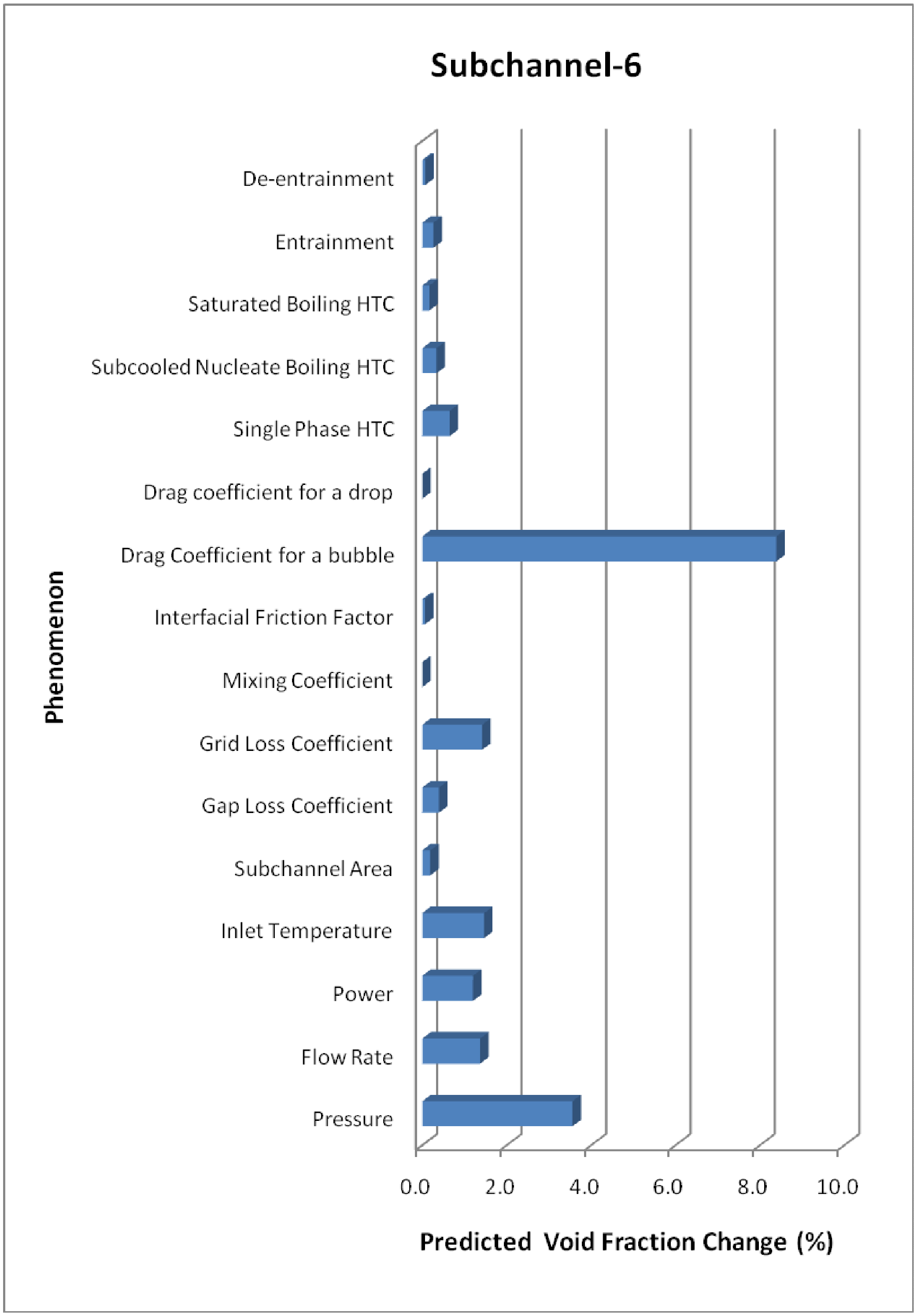

Figure 6.122. Predicted 6th Subchannel Void Fraction Change versus Phenomenon for Test 4101-55

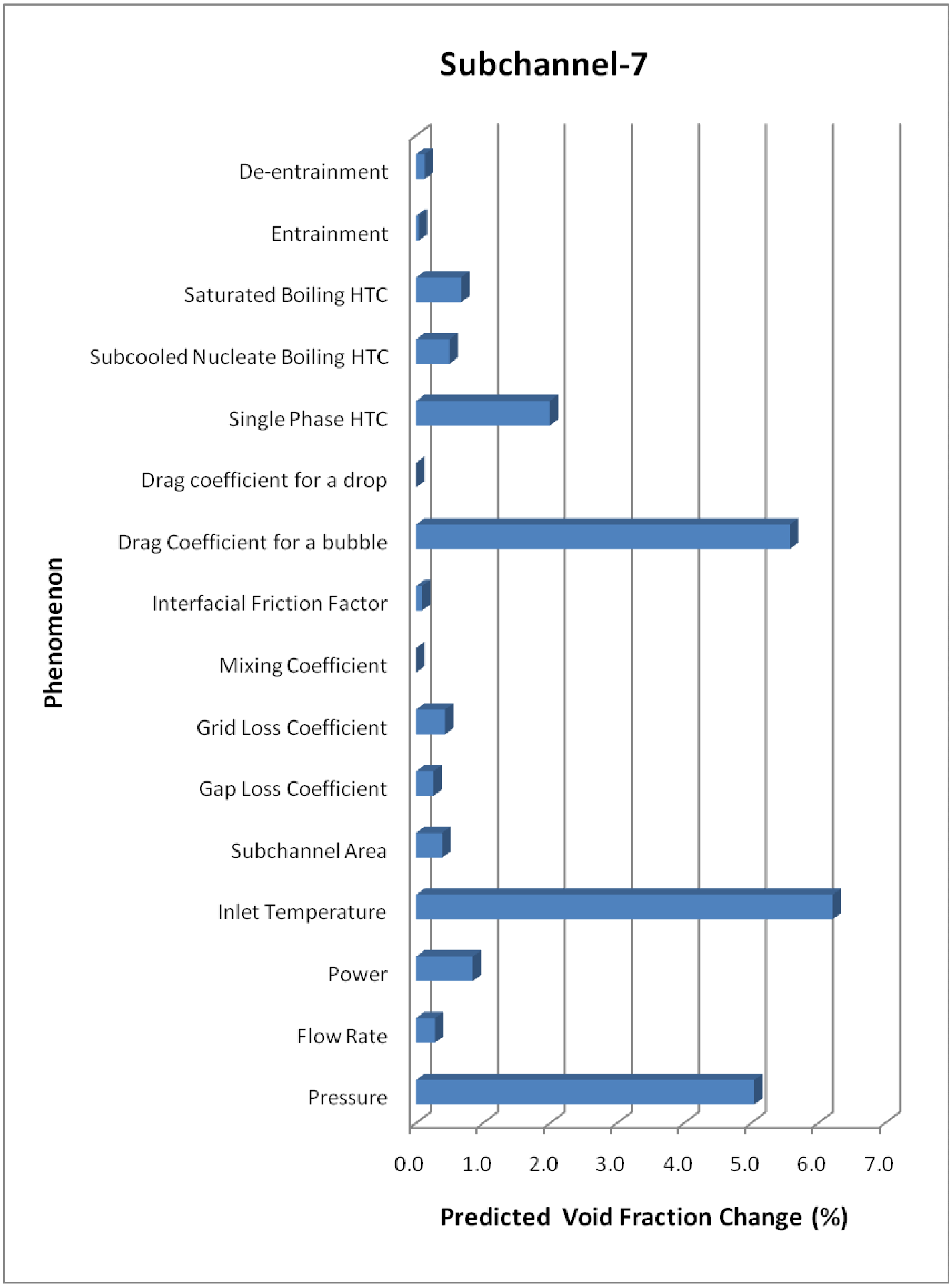

Figure 6.123. Predicted 7th Subchannel Void Fraction Change versus Phenomenon for Test 4101-55

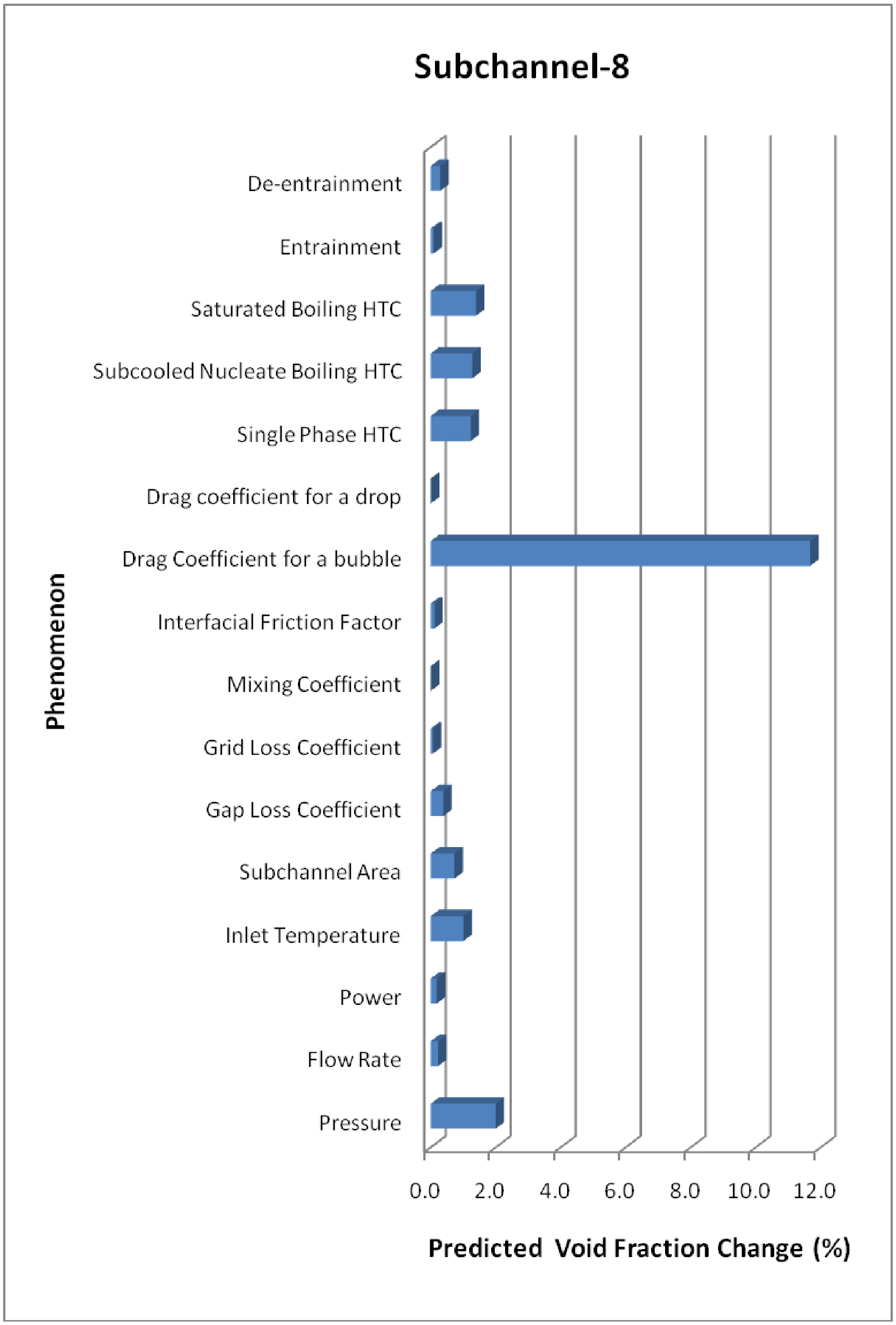

Figure 6.124. Predicted 8th Subchannel Void Fraction Change versus Phenomenon for Test 4101-55

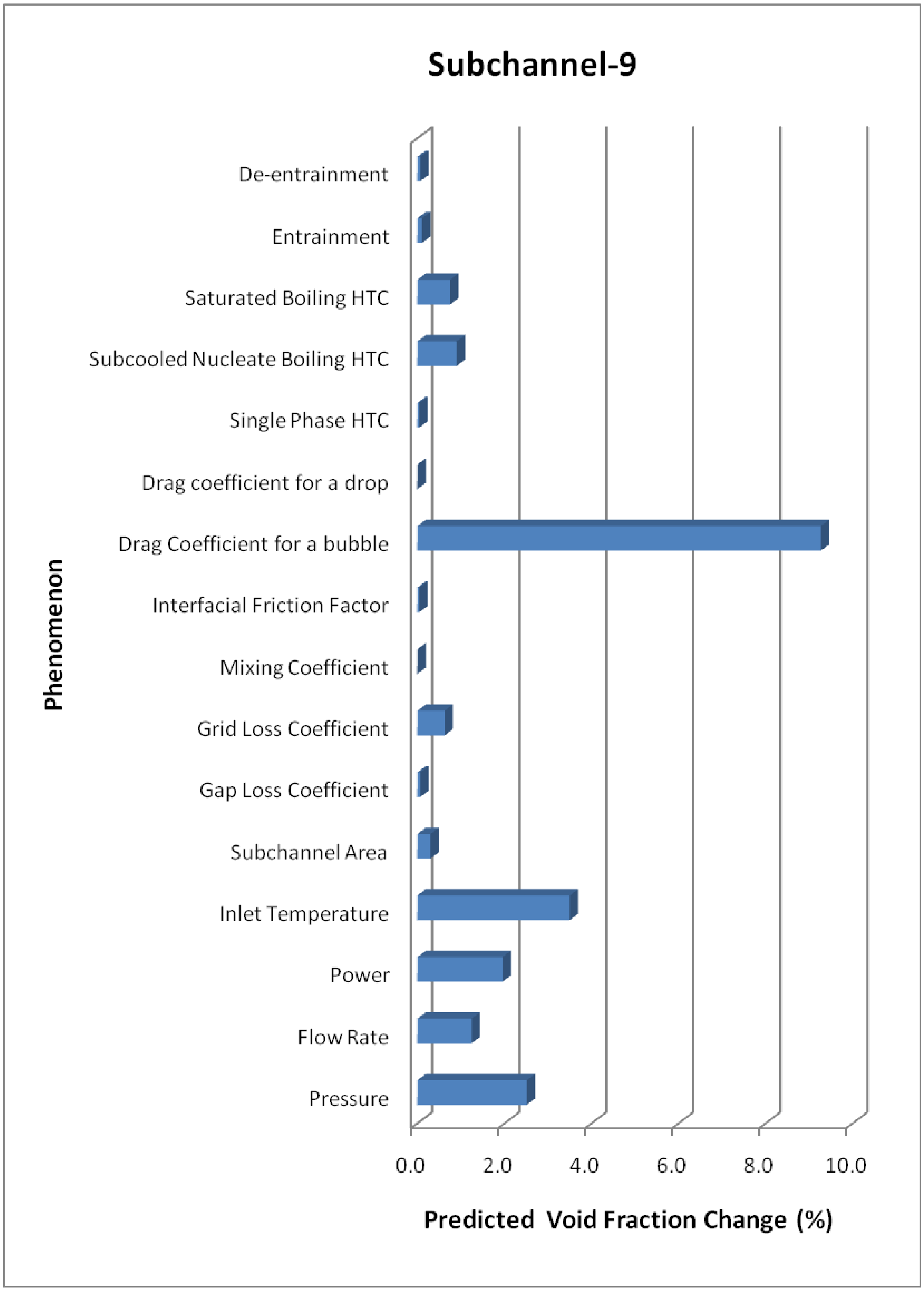

Figure 6.125. Predicted 9th Subchannel Void Fraction Change versus Phenomenon for Test 4101-55

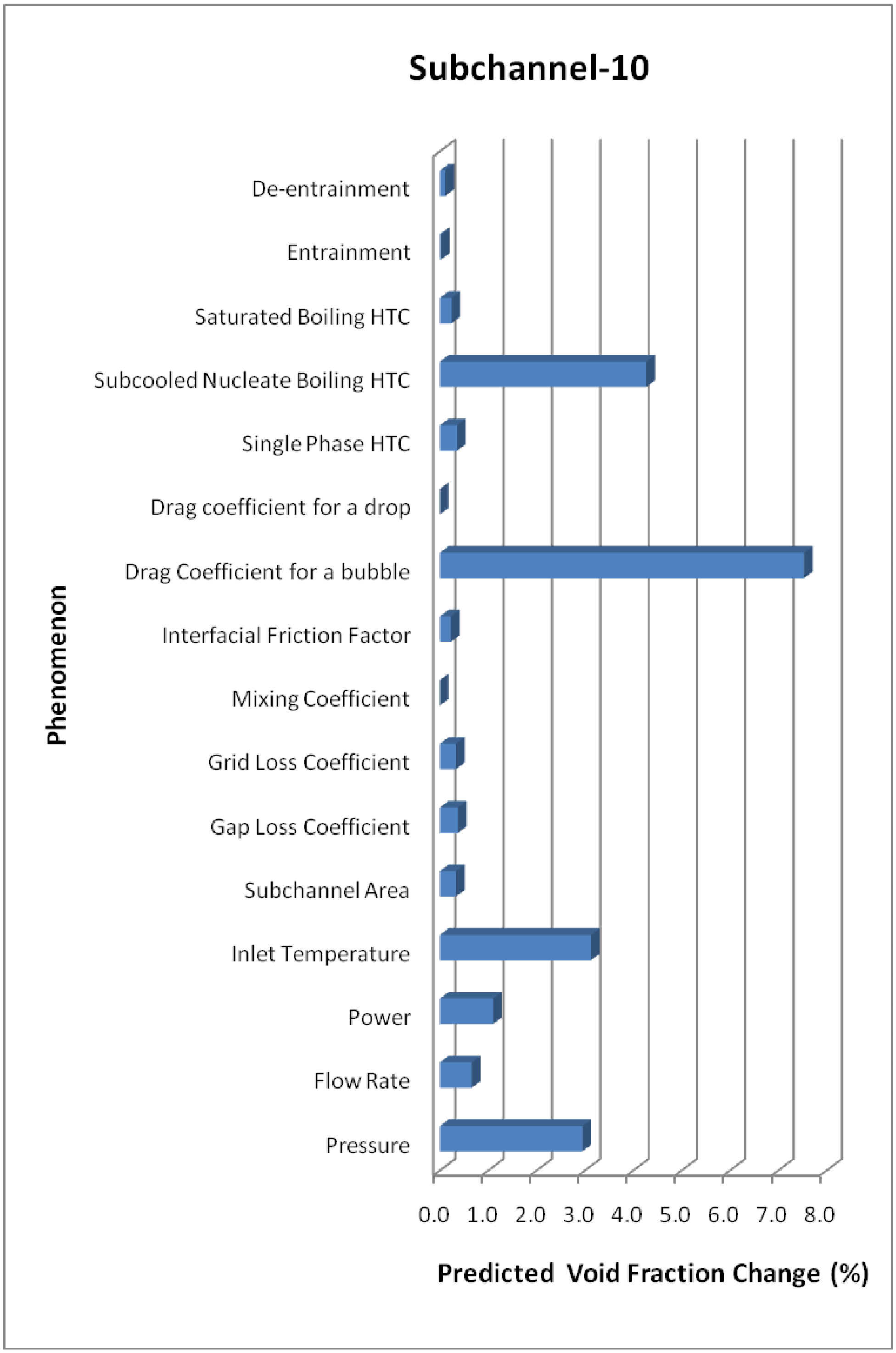

Figure 6.126. Predicted 10th Subchannel Void Fraction Change versus Phenomenon for Test 4101-55

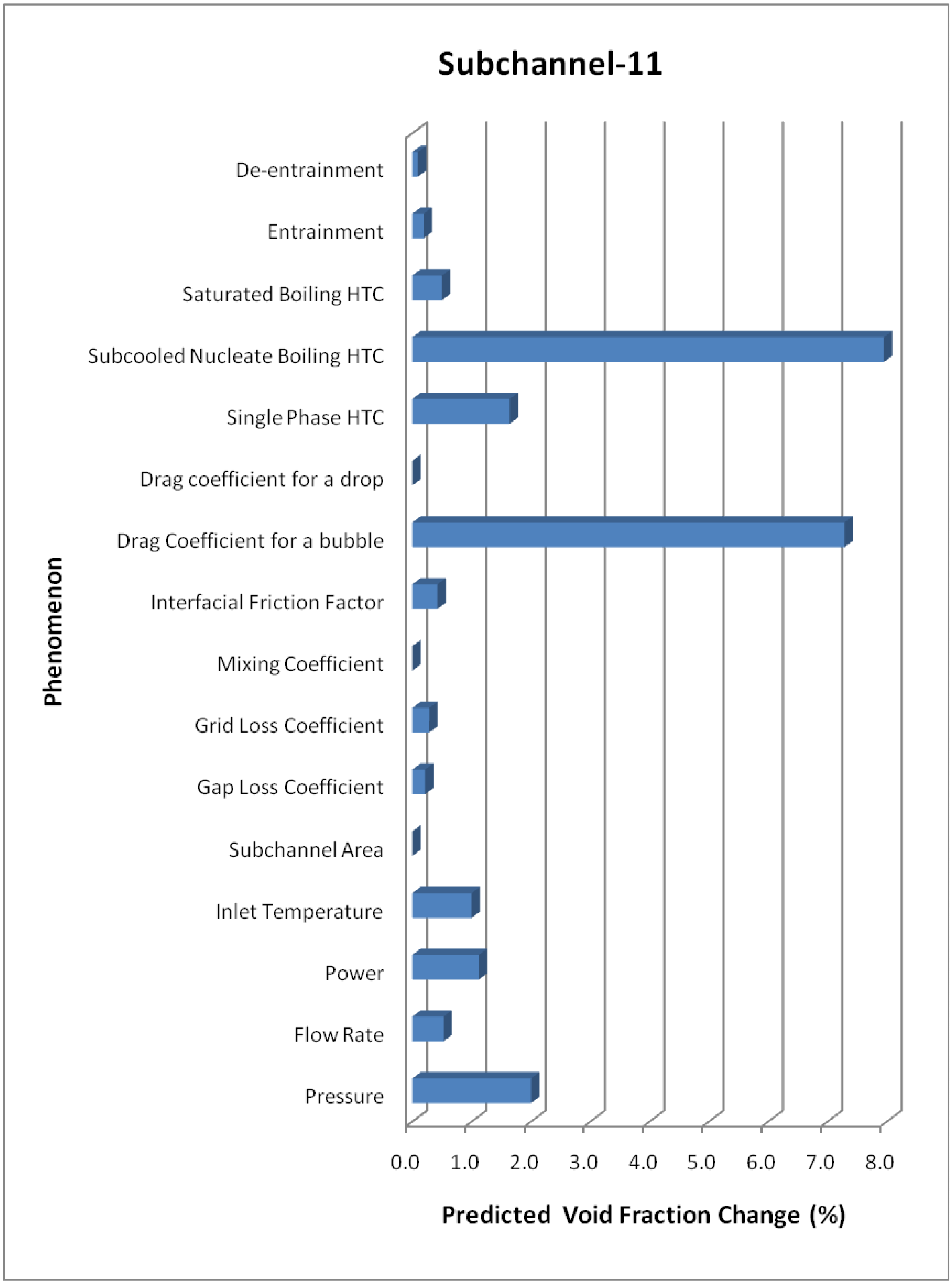

Figure 6.127. Predicted 11th Subchannel Void Fraction Change versus Phenomenon for Test 4101-55

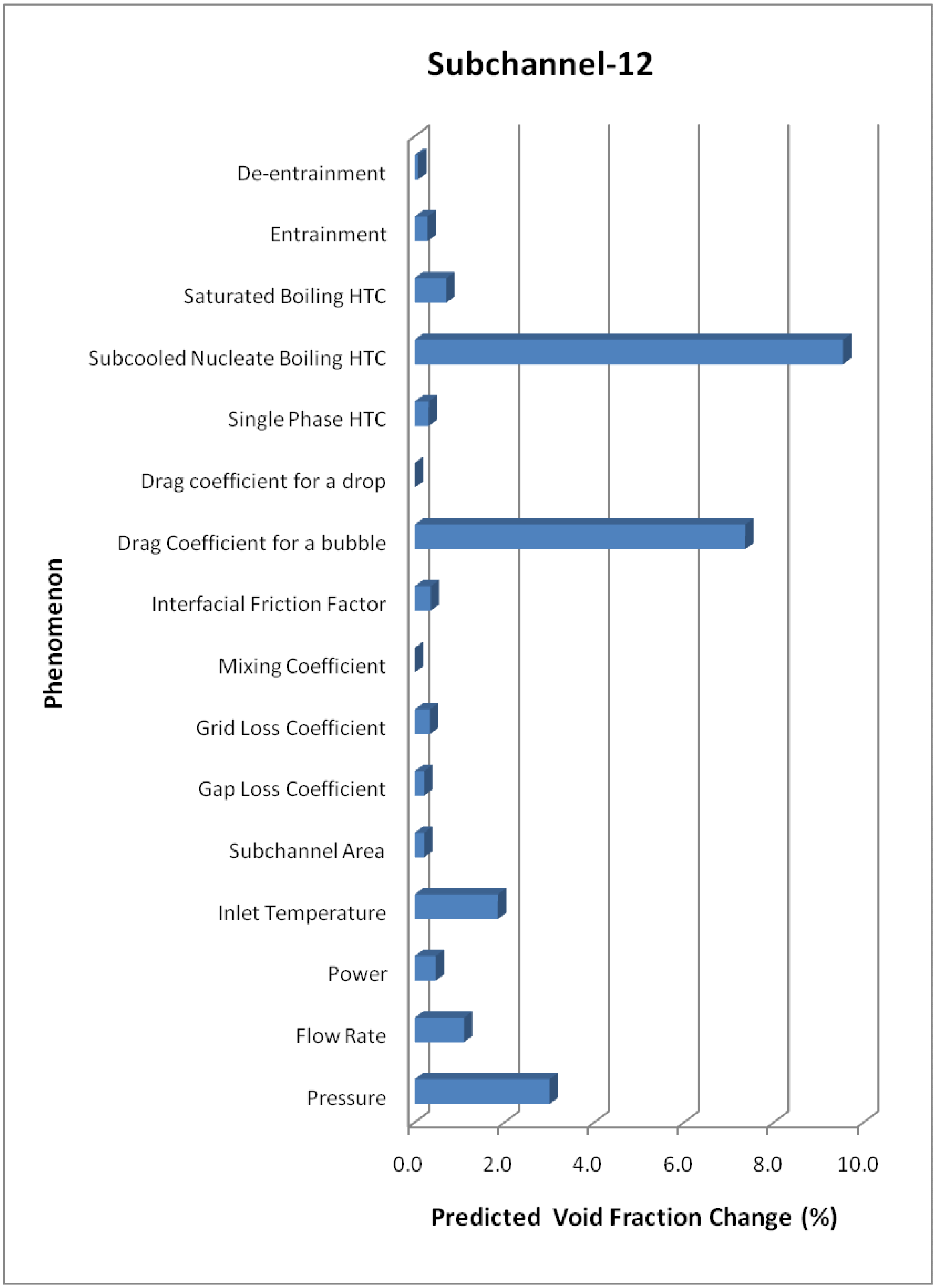

Figure 6.128. Predicted 12th Subchannel Void Fraction Change versus Phenomenon for Test 4101-55

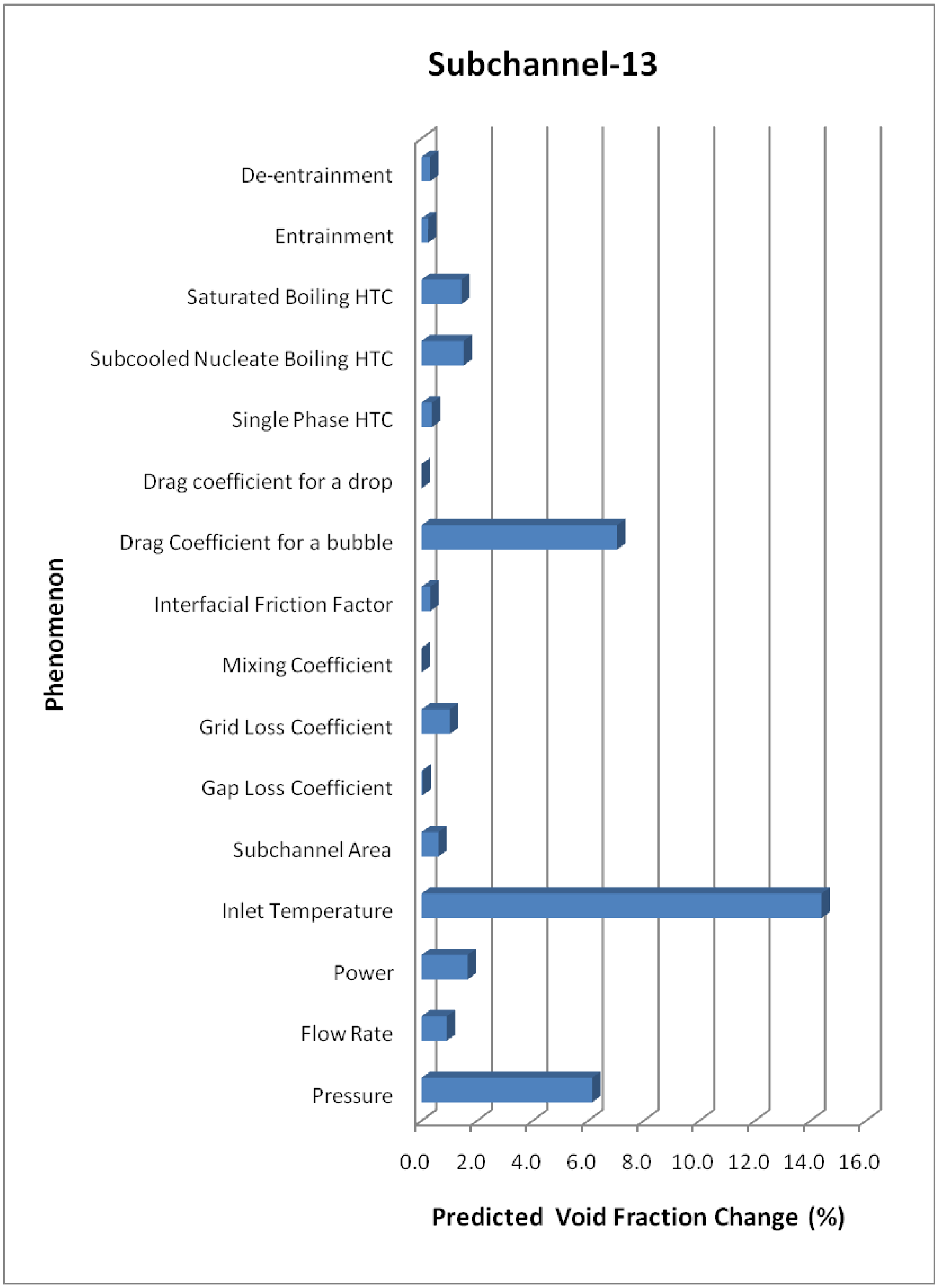

Figure 6.129. Predicted 13th Subchannel Void Fraction Change versus Phenomenon for Test 4101-55

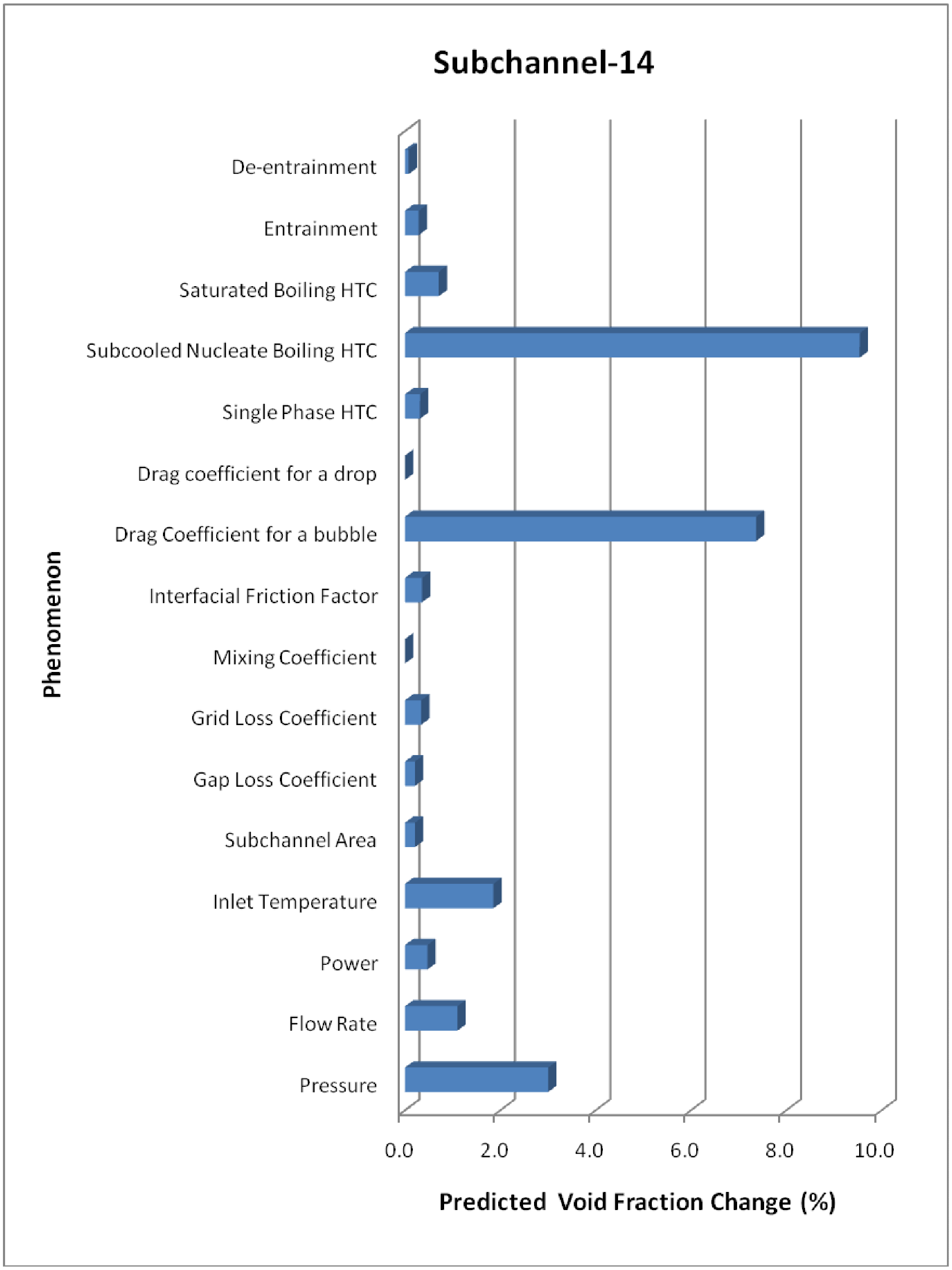

Figure 6.130. Predicted 14th Subchannel Void Fraction Change versus Phenomenon for Test 4101-55

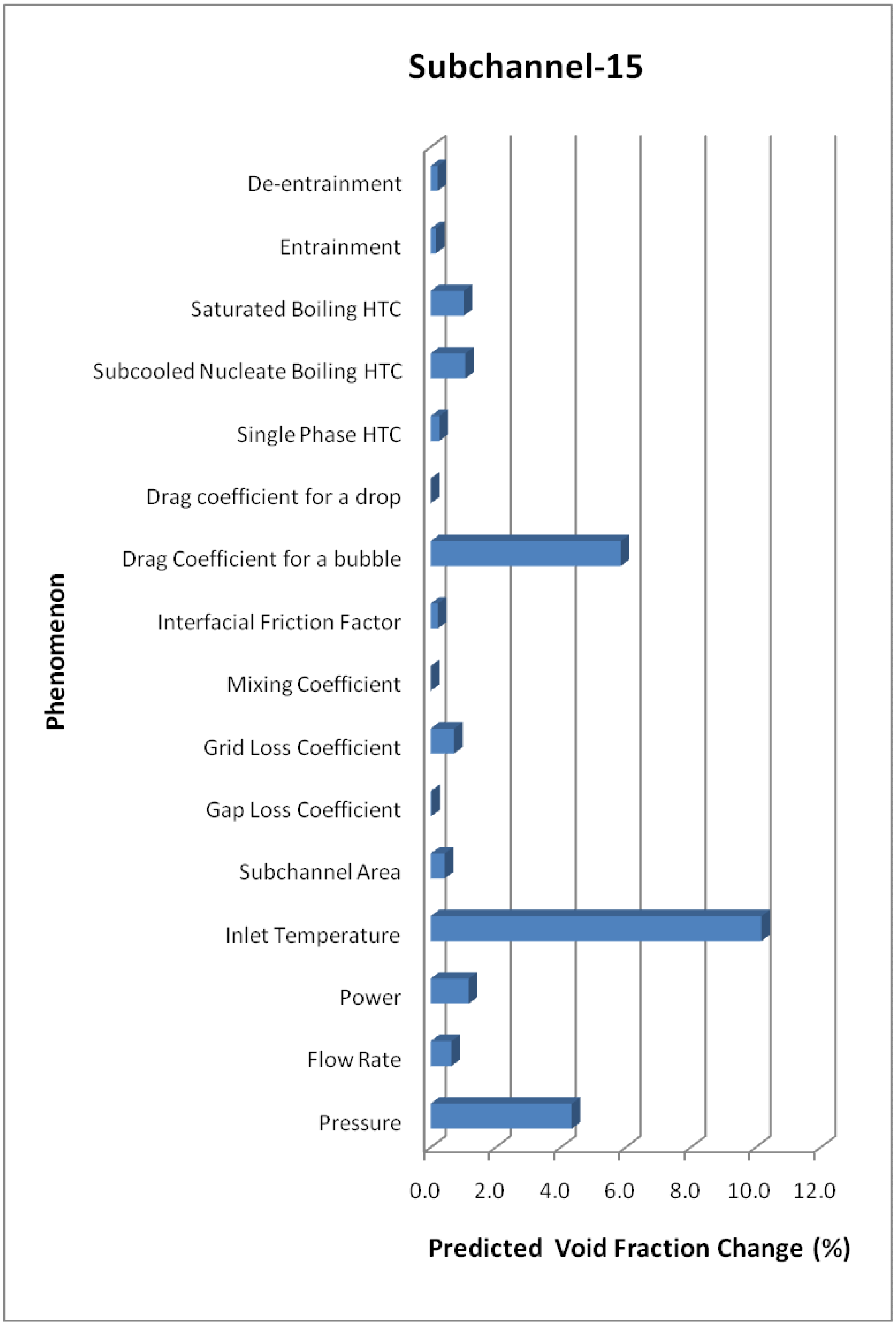

Figure 6.131. Predicted 15th Subchannel Void Fraction Change versus Phenomenon for Test 4101-55

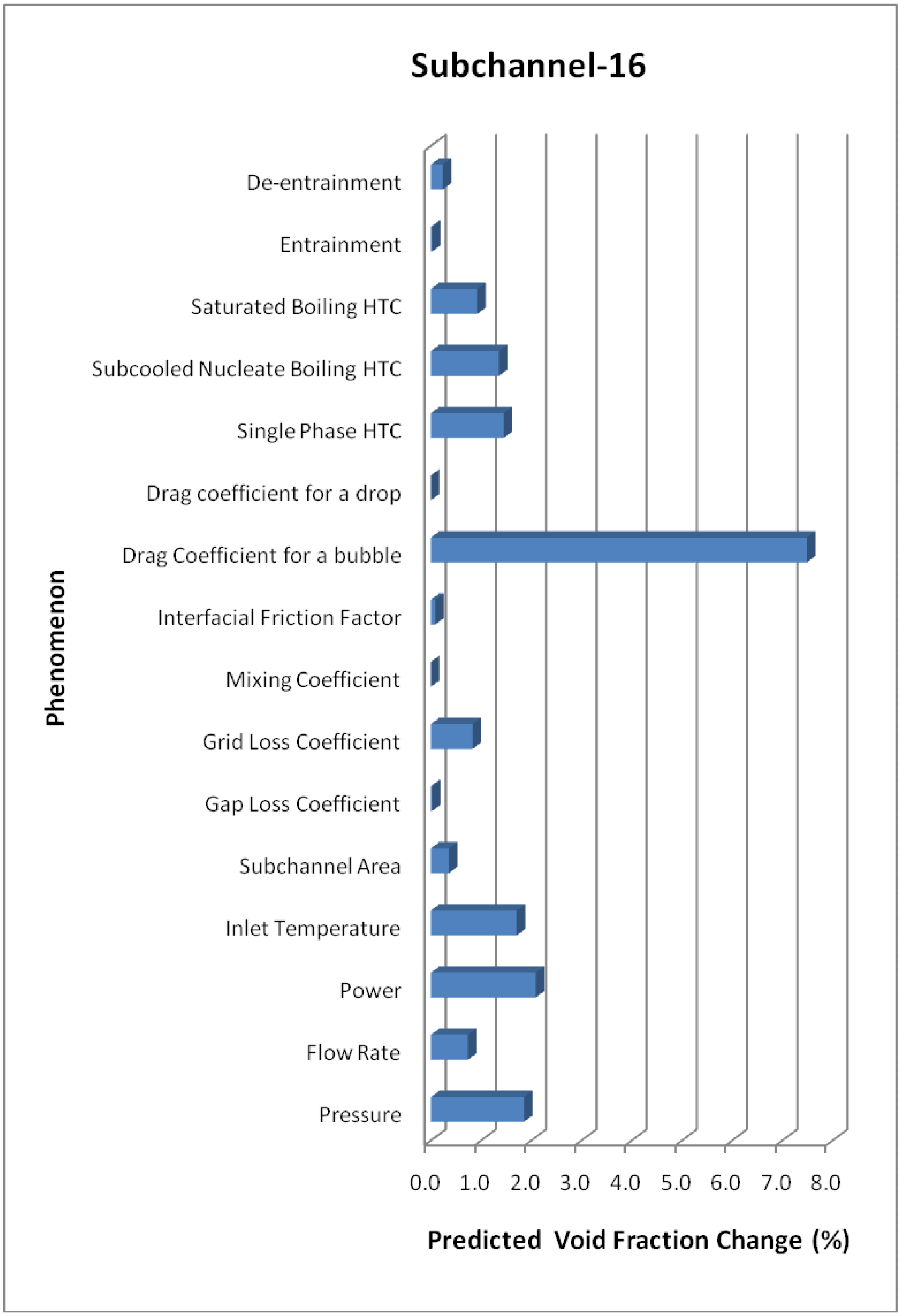

Figure 6.132. Predicted 16th Subchannel Void Fraction Change versus Phenomenon for Test 4101-55

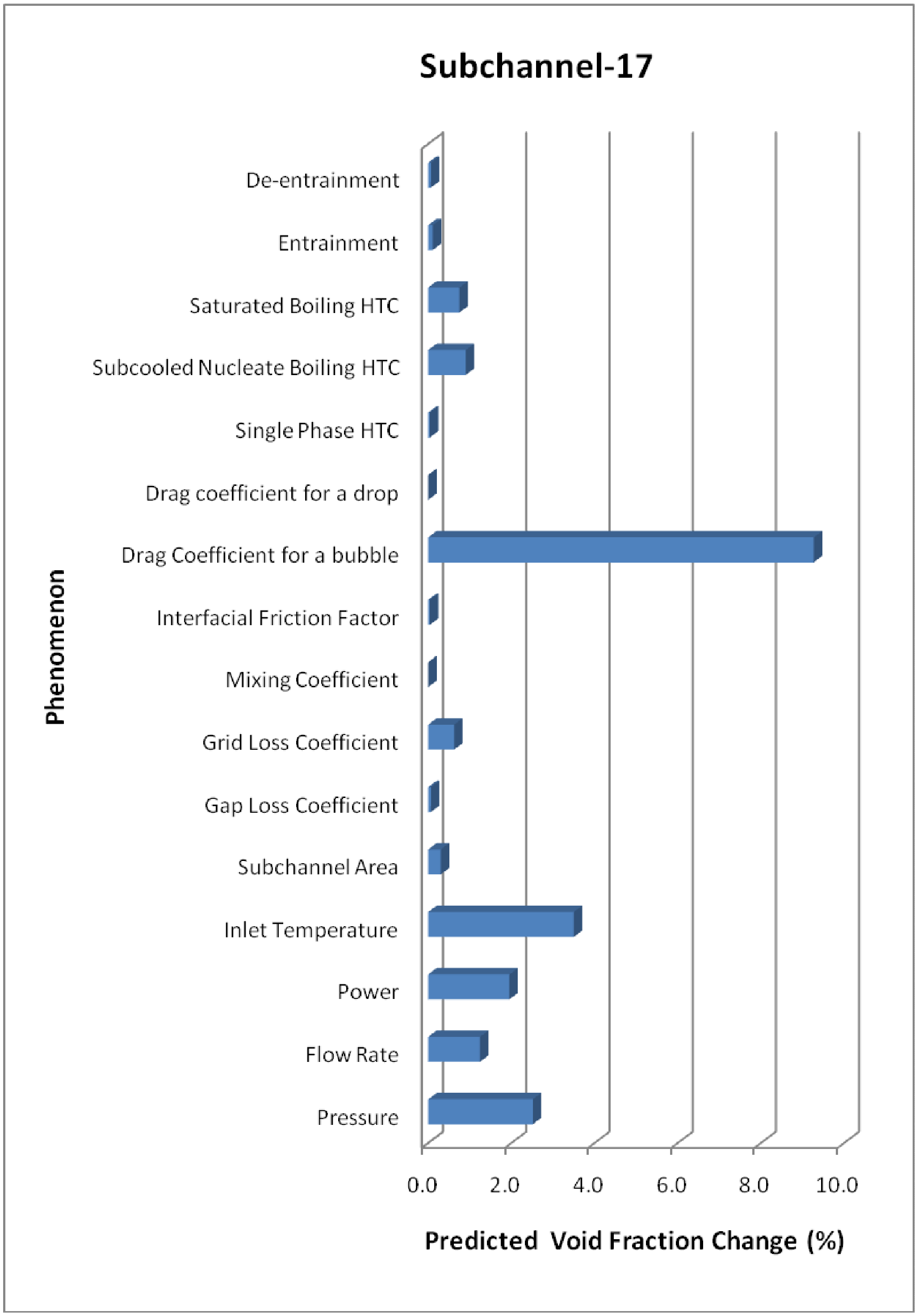

Figure 6.133. Predicted 17th Subchannel Void Fraction Change versus Phenomenon for Test 4101-55

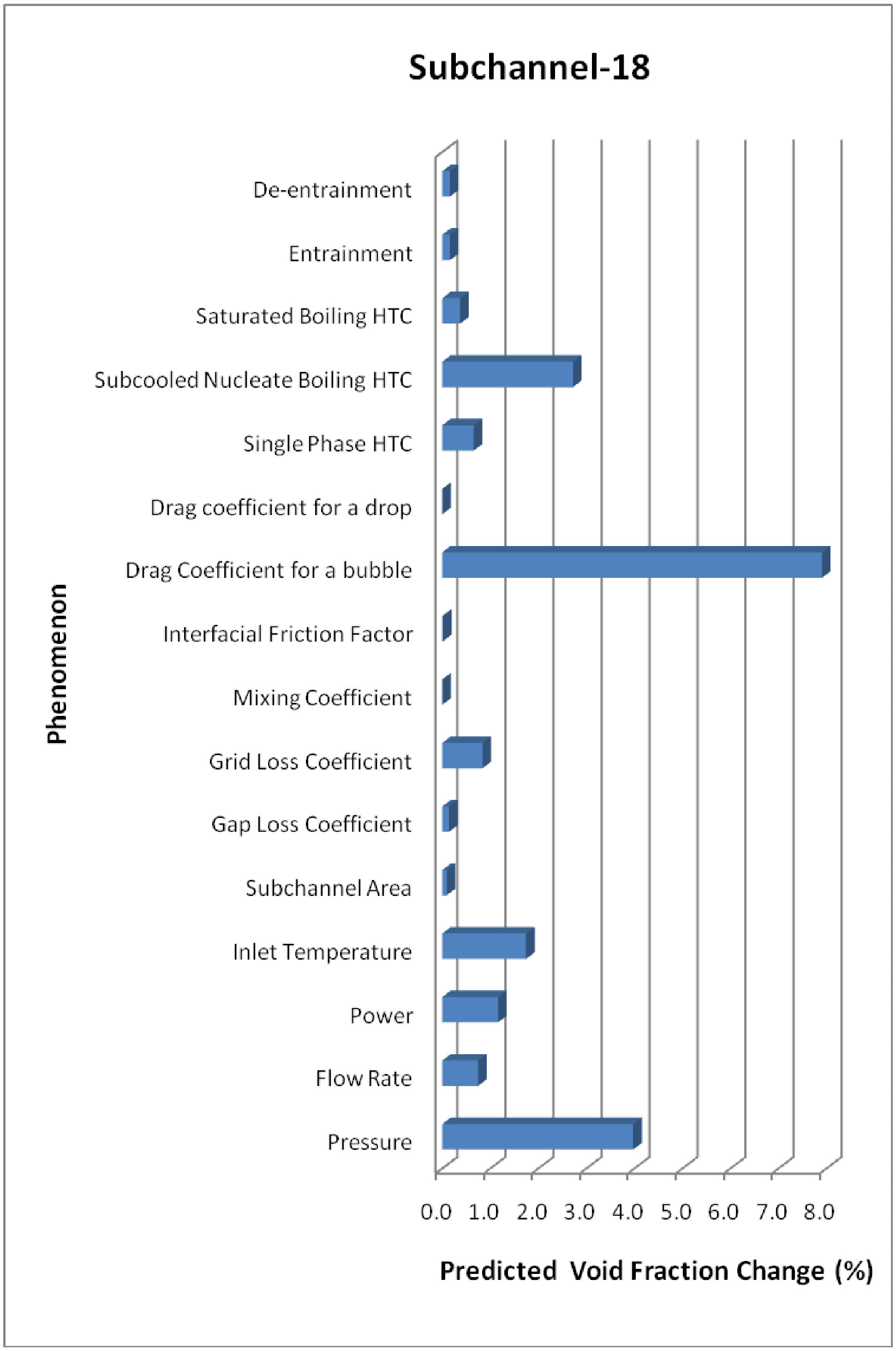

Figure 6.134. Predicted 18th Subchannel Void Fraction Change versus Phenomenon for Test 4101-55

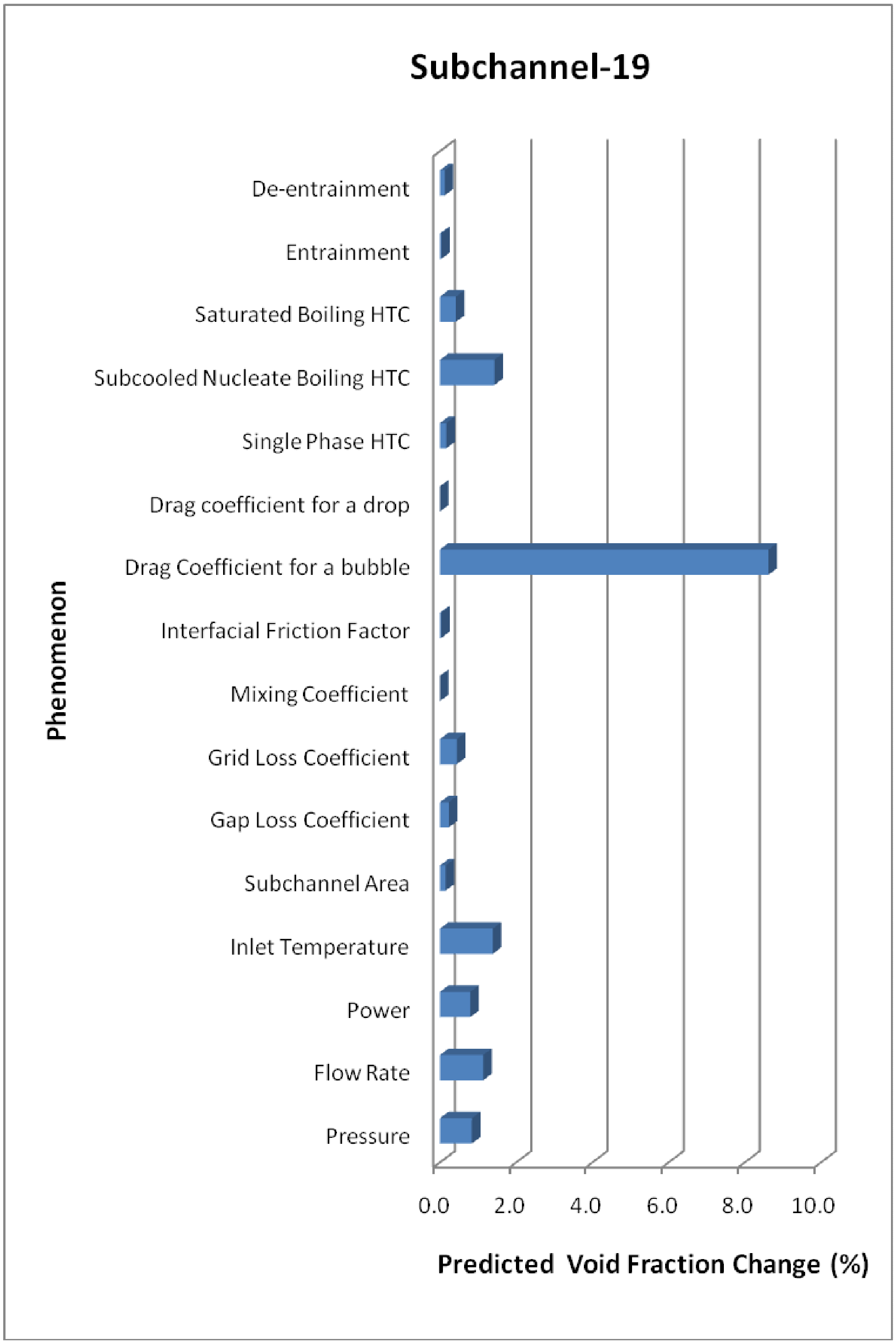

Figure 6.135. Predicted 19th Subchannel Void Fraction Change versus Phenomenon for Test 4101-55

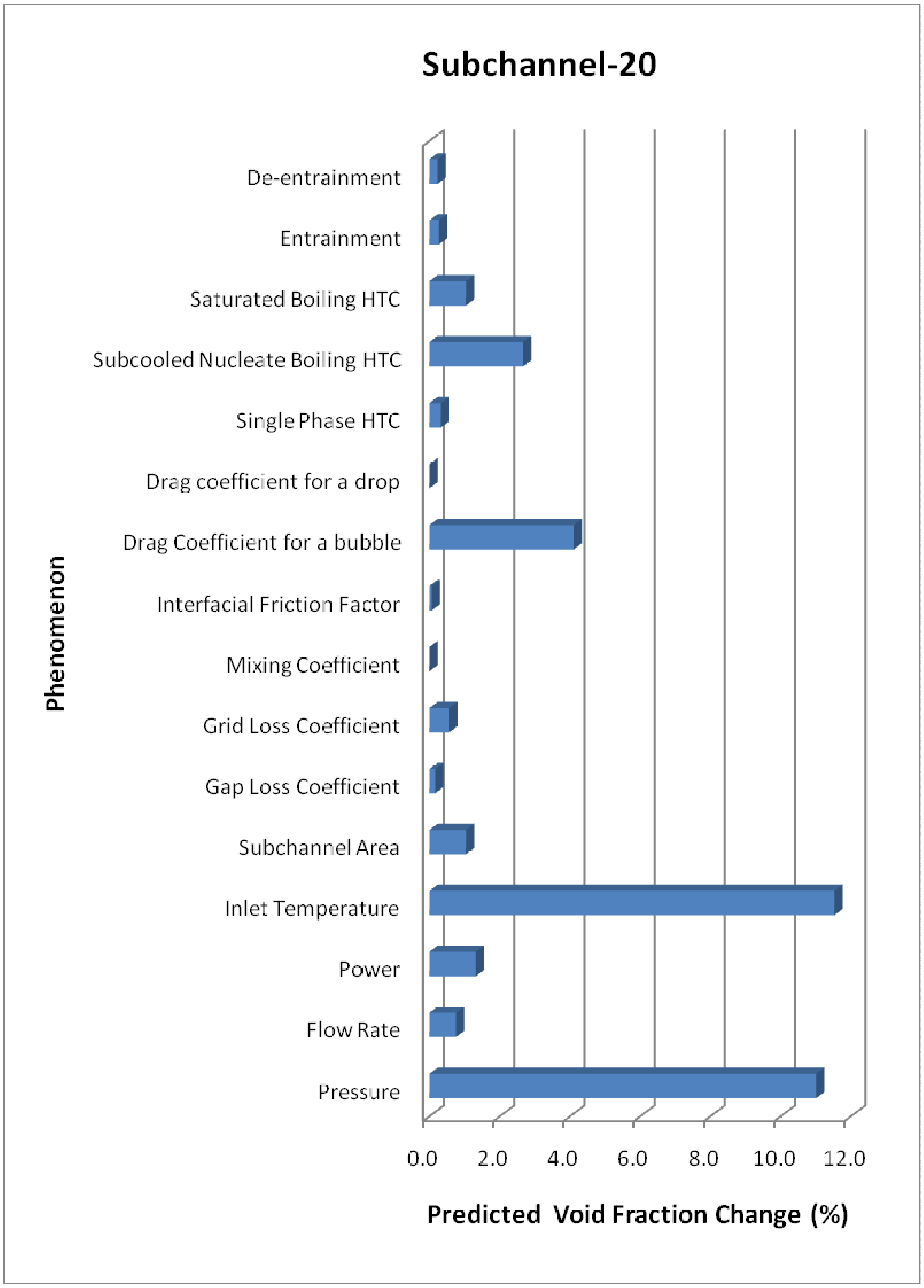

Figure 6.136. Predicted 20th Subchannel Void Fraction Change versus Phenomenon for Test 4101-55

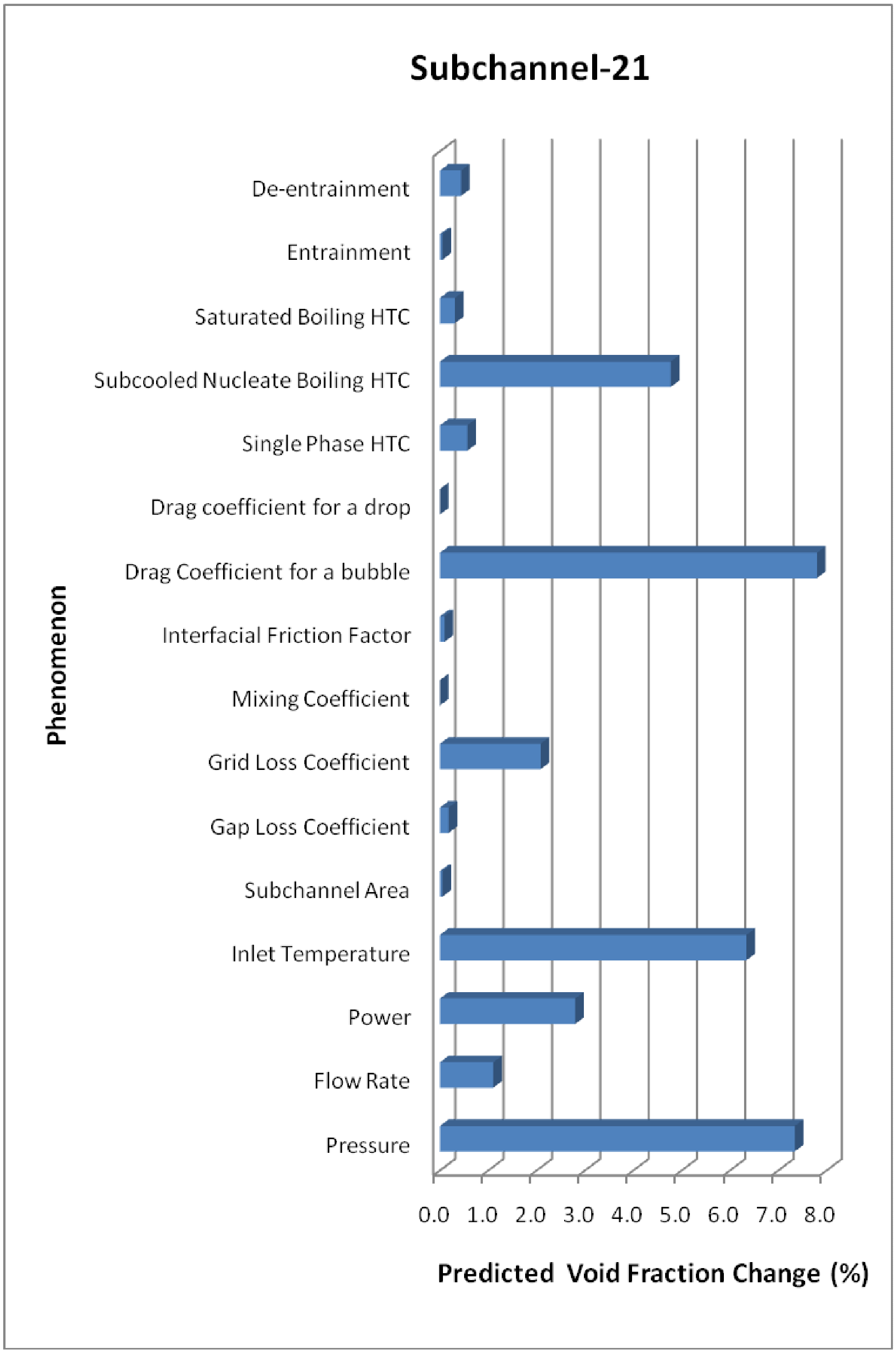

Figure 6.137. Predicted 21st Subchannel Void Fraction Change versus Phenomenon for Test 4101-55

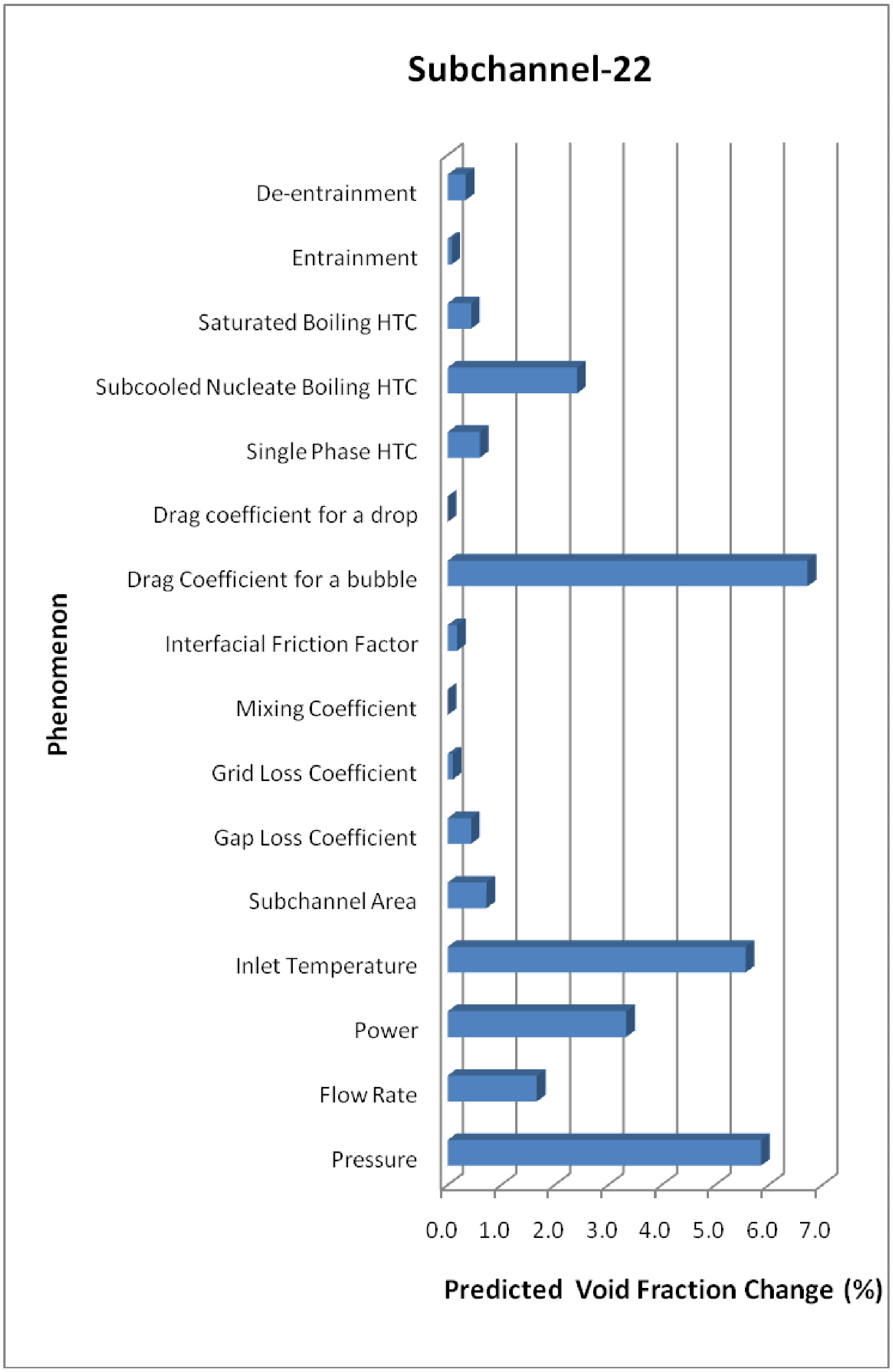

Figure 6.138. Predicted 22nd Subchannel Void Fraction Change versus Phenomenon for Test 4101-55

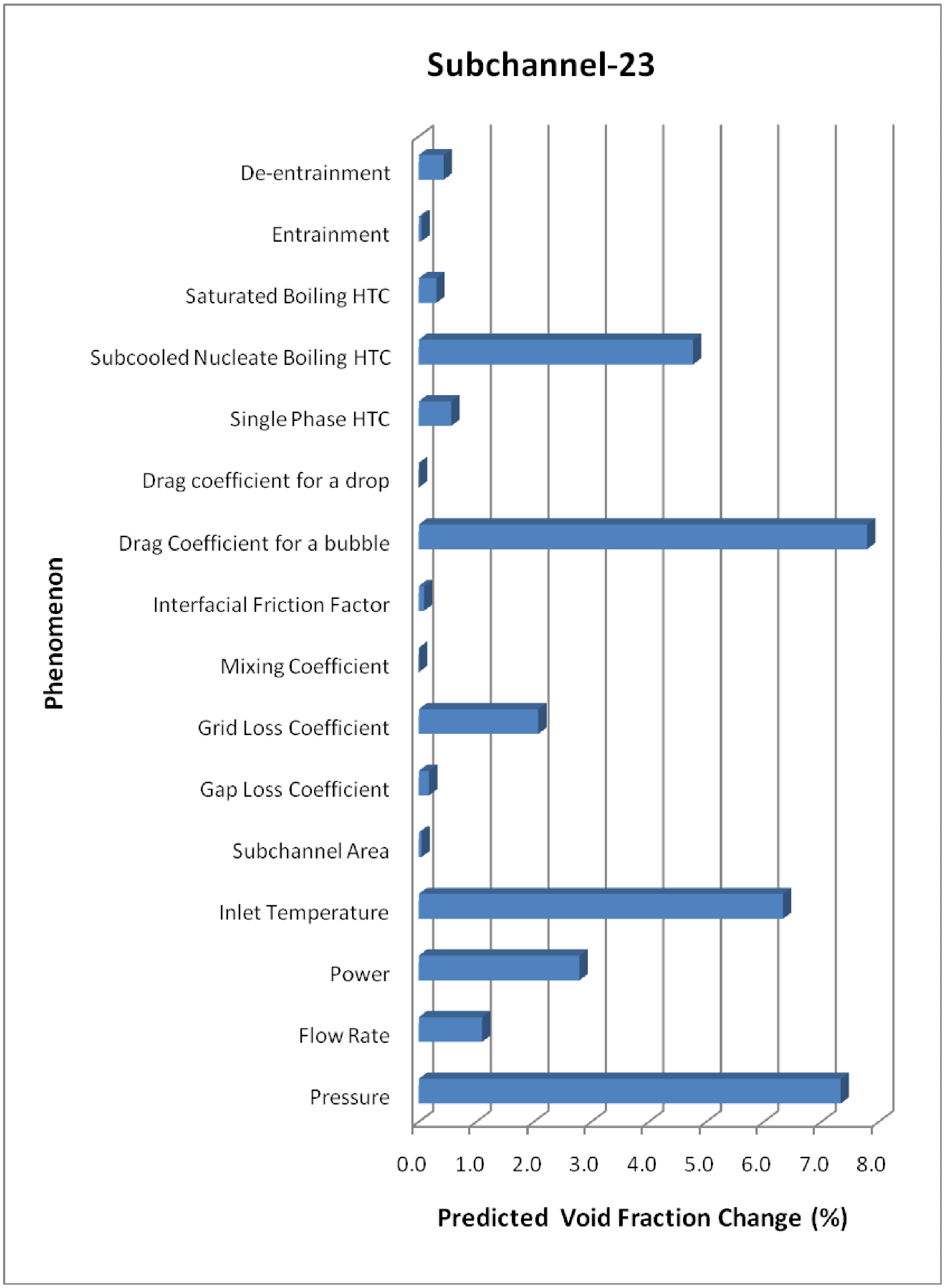

Figure 6.139. Predicted 23th Subchannel Void Fraction Change versus Phenomenon for Test 4101-55

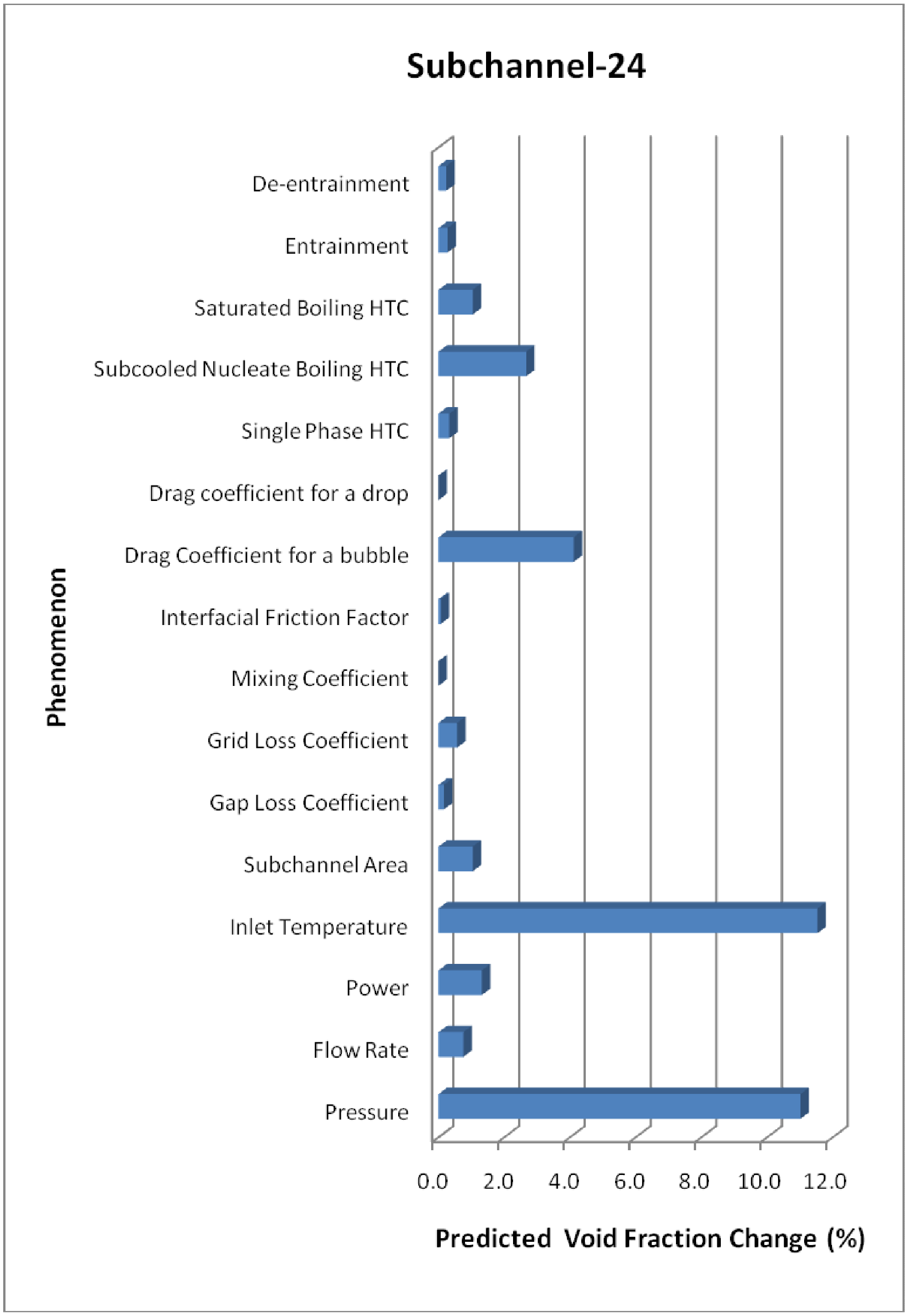

Figure 6.140. Predicted 24th Subchannel Void Fraction Change versus Phenomenon for Test 4101-55

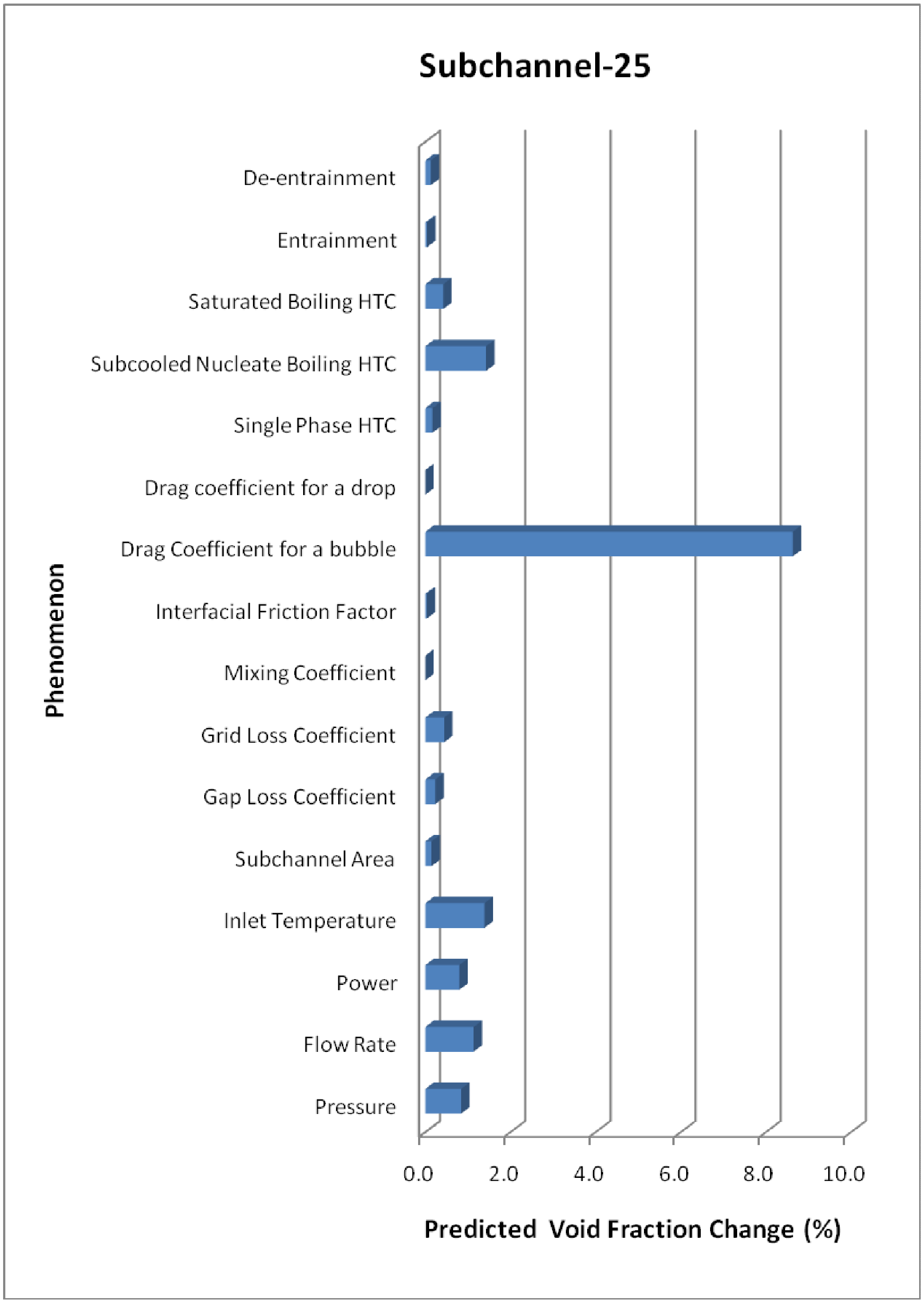

Figure 6.141. Predicted 25th Subchannel Void Fraction Change versus Phenomenon for Test 4101-55

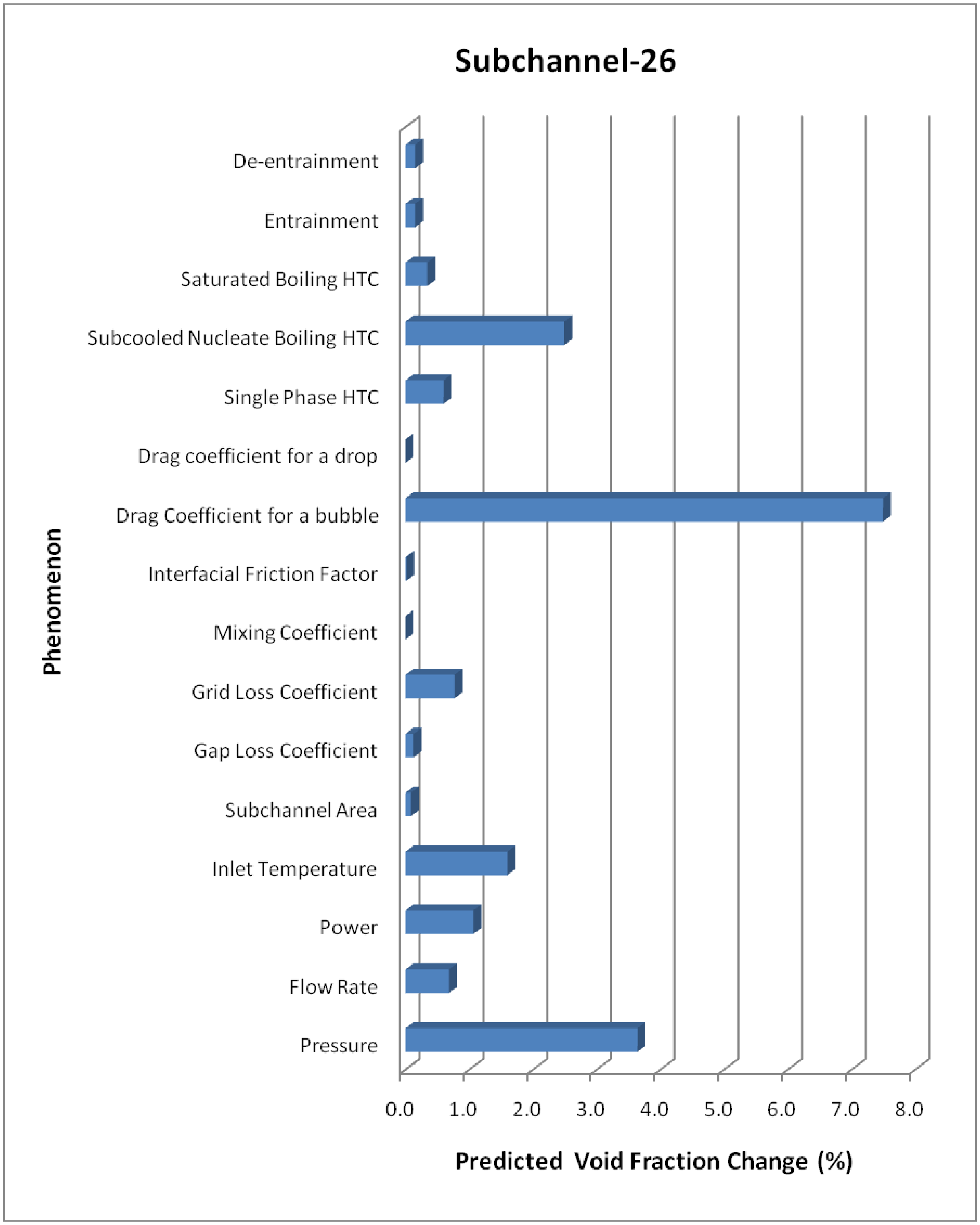

Figure 6.142. Predicted 26th Subchannel Void Fraction Change versus Phenomenon for Test 4101-55

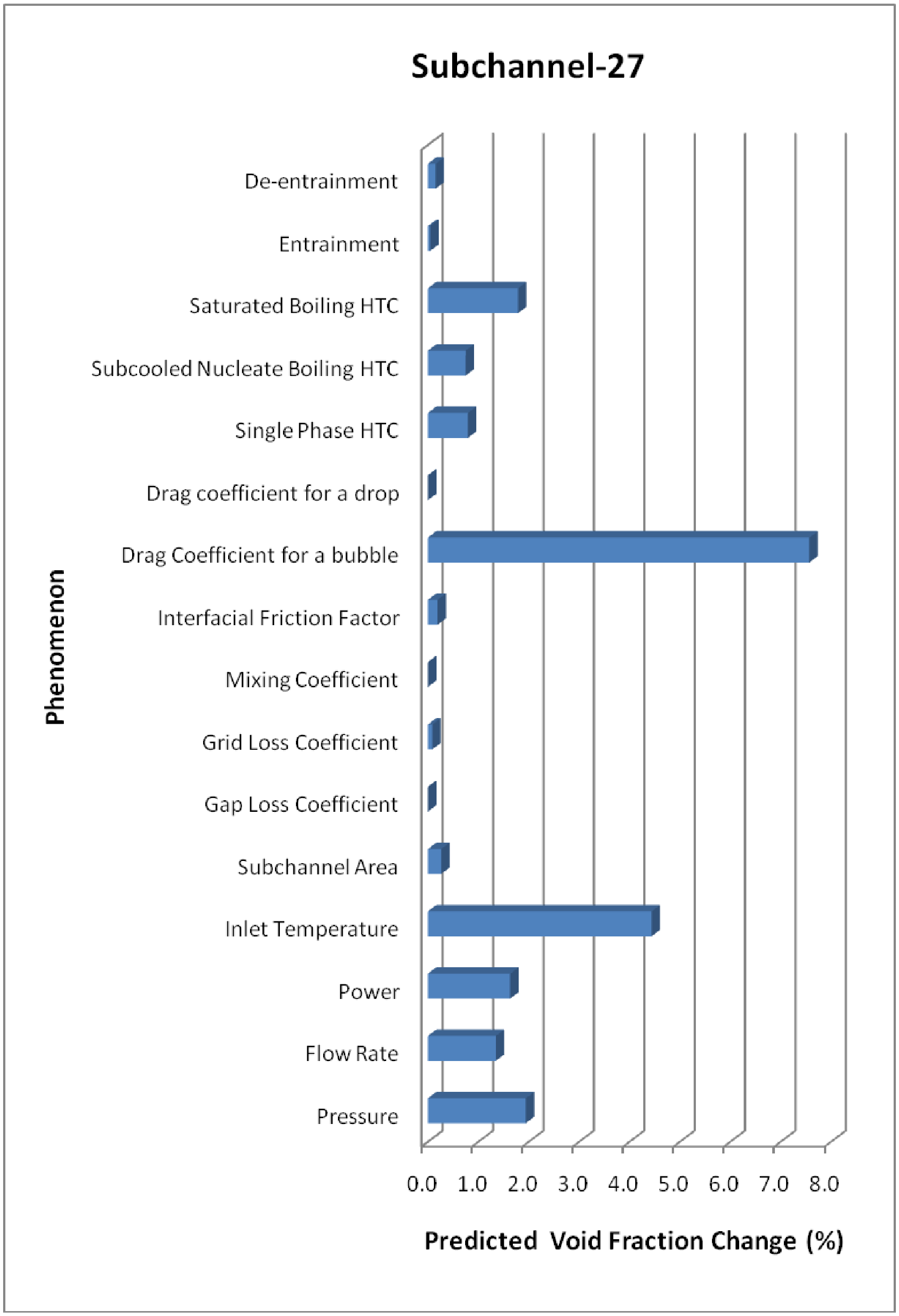

Figure 6.143. Predicted 27th Subchannel Void Fraction Change versus Phenomenon for Test 4101-55

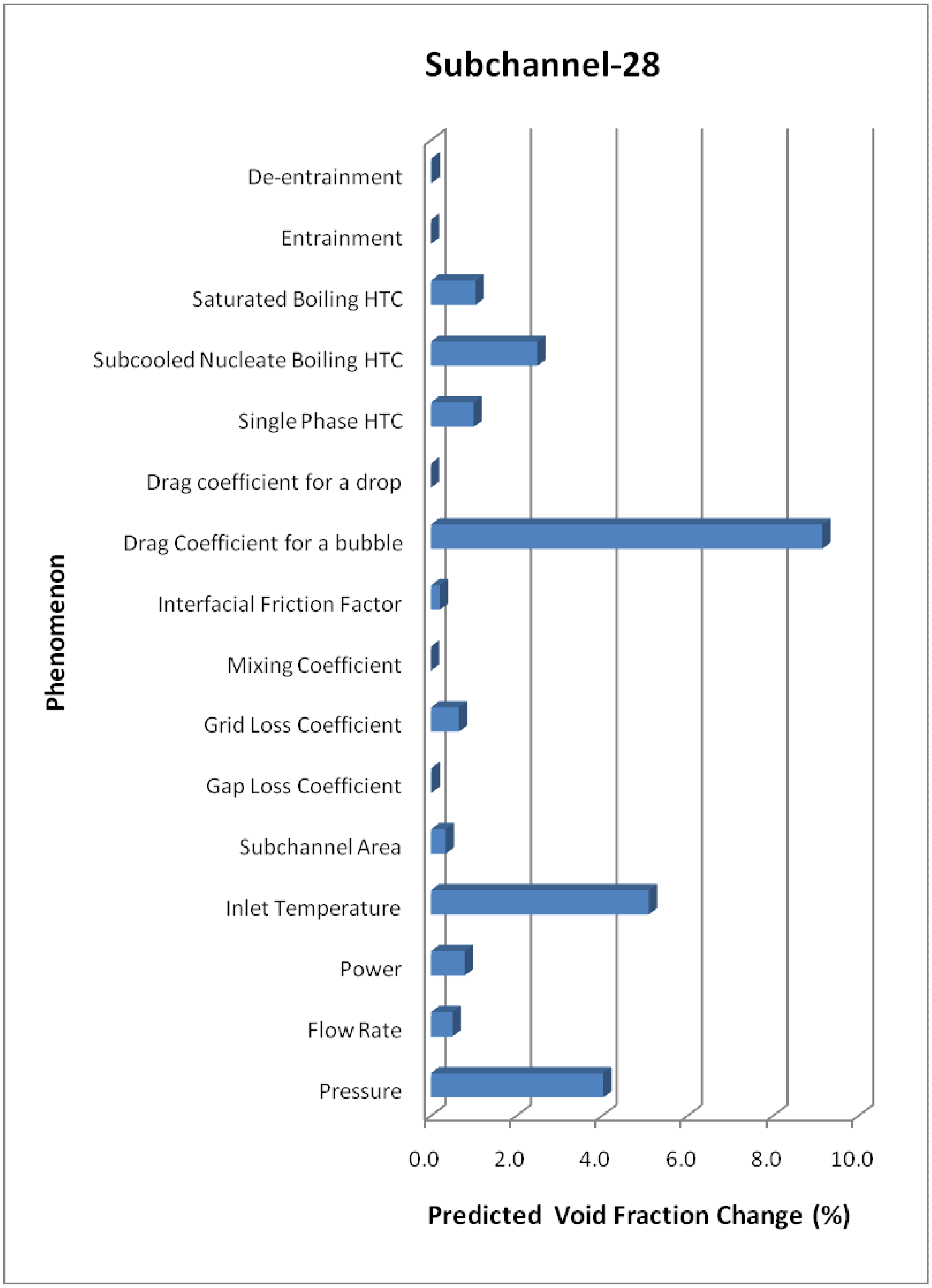

Figure 6.144. Predicted 28th Subchannel Void Fraction Change versus Phenomenon for Test 4101-55

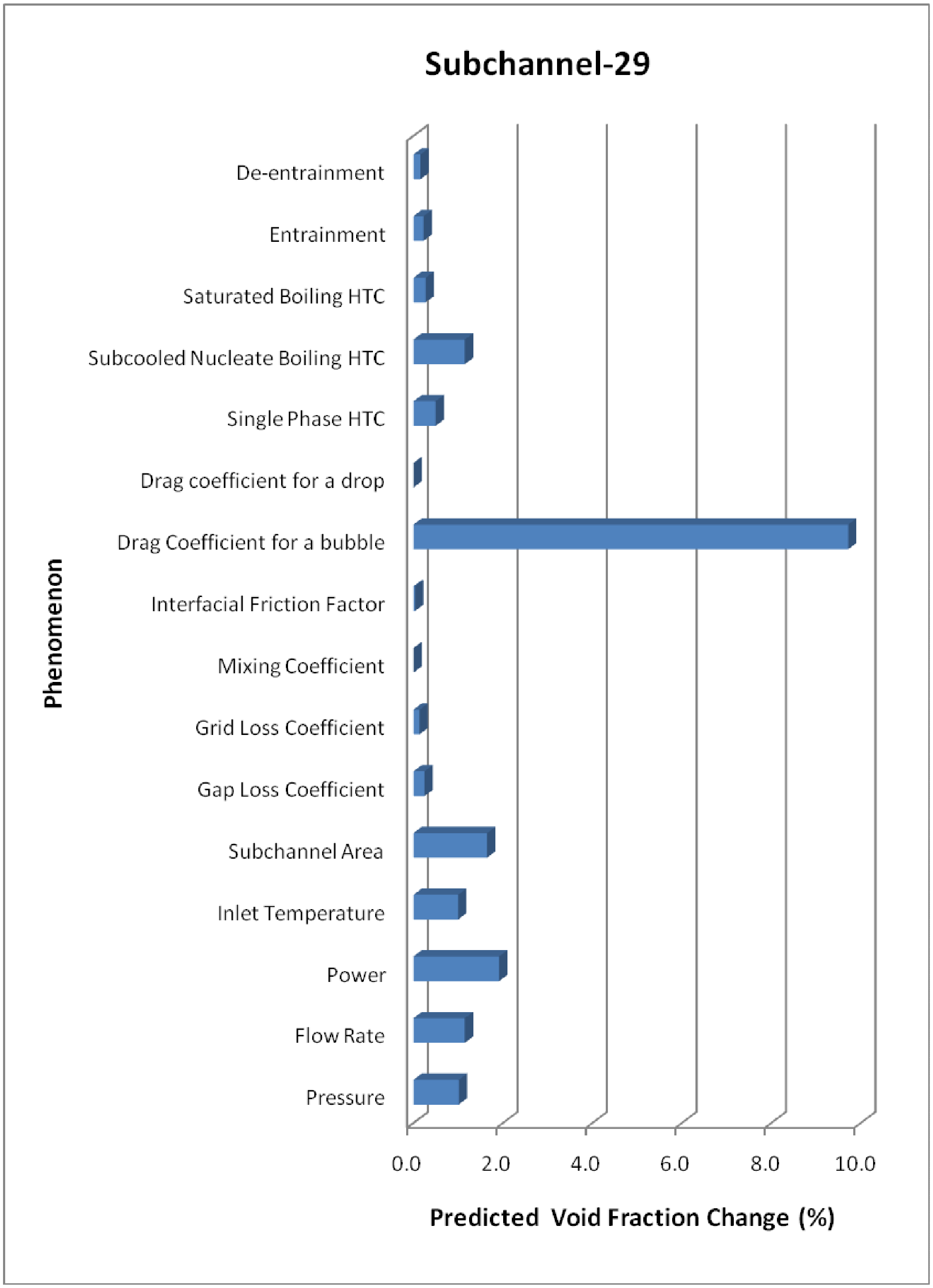

Figure 6.145. Predicted 29th Subchannel Void Fraction Change versus Phenomenon for Test 4101-55

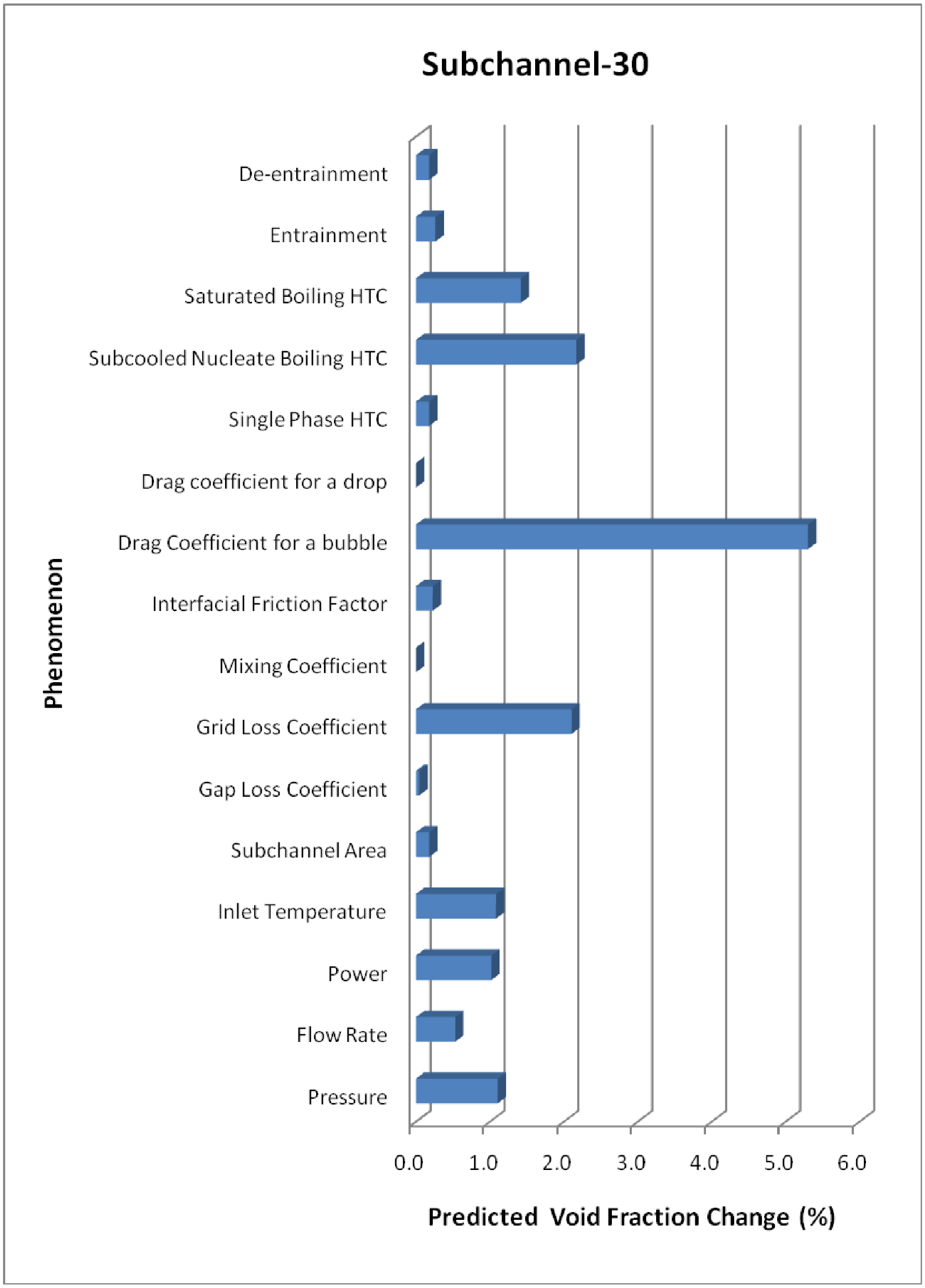

Figure 6.146. Predicted 30th Subchannel Void Fraction Change versus Phenomenon for Test 4101-55

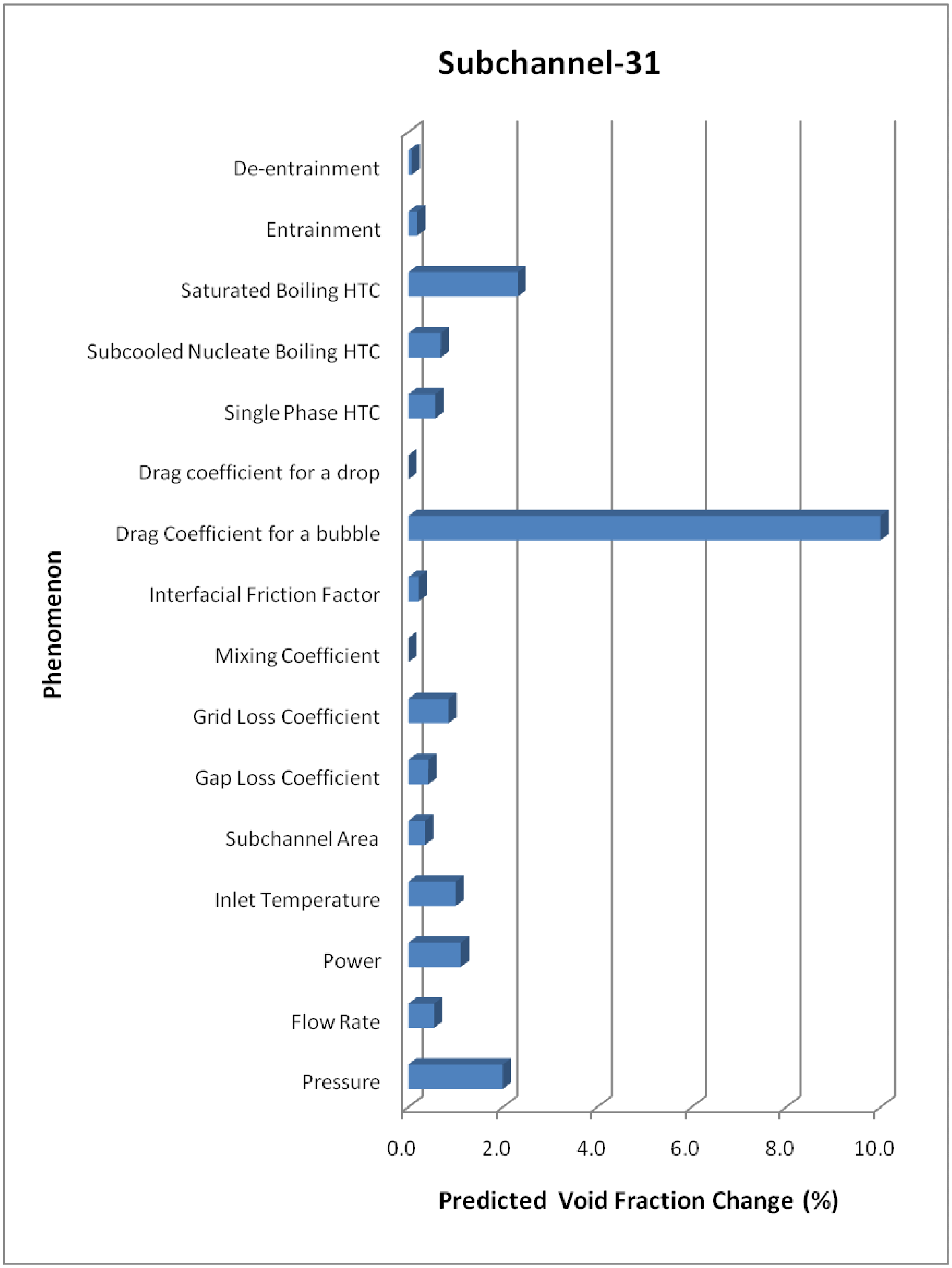

Figure 6.147. Predicted 31st Subchannel Void Fraction Change versus Phenomenon for Test 4101-55

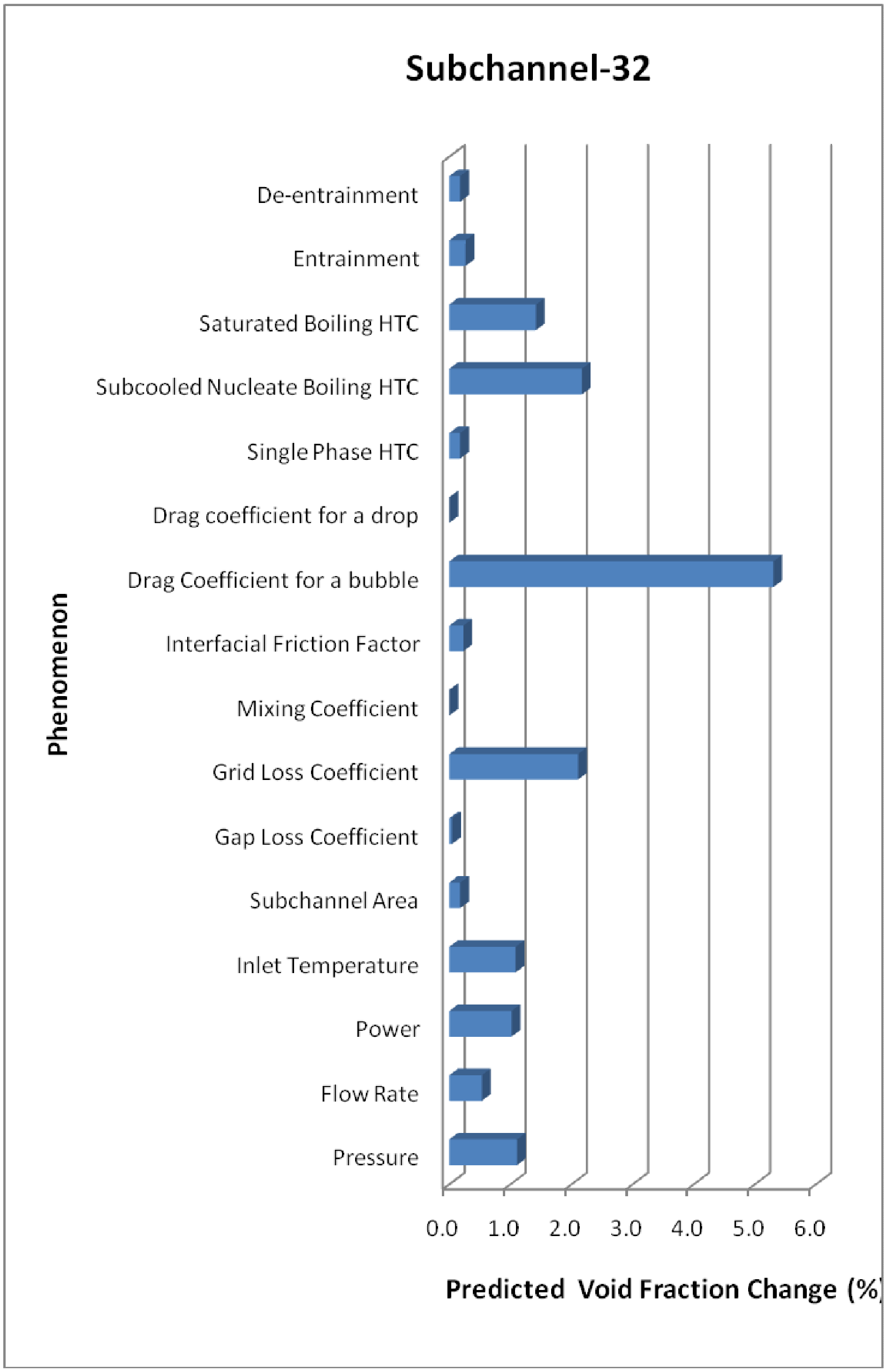

Figure 6.148. Predicted 32nd Subchannel Void Fraction Change versus Phenomenon for Test 4101-55

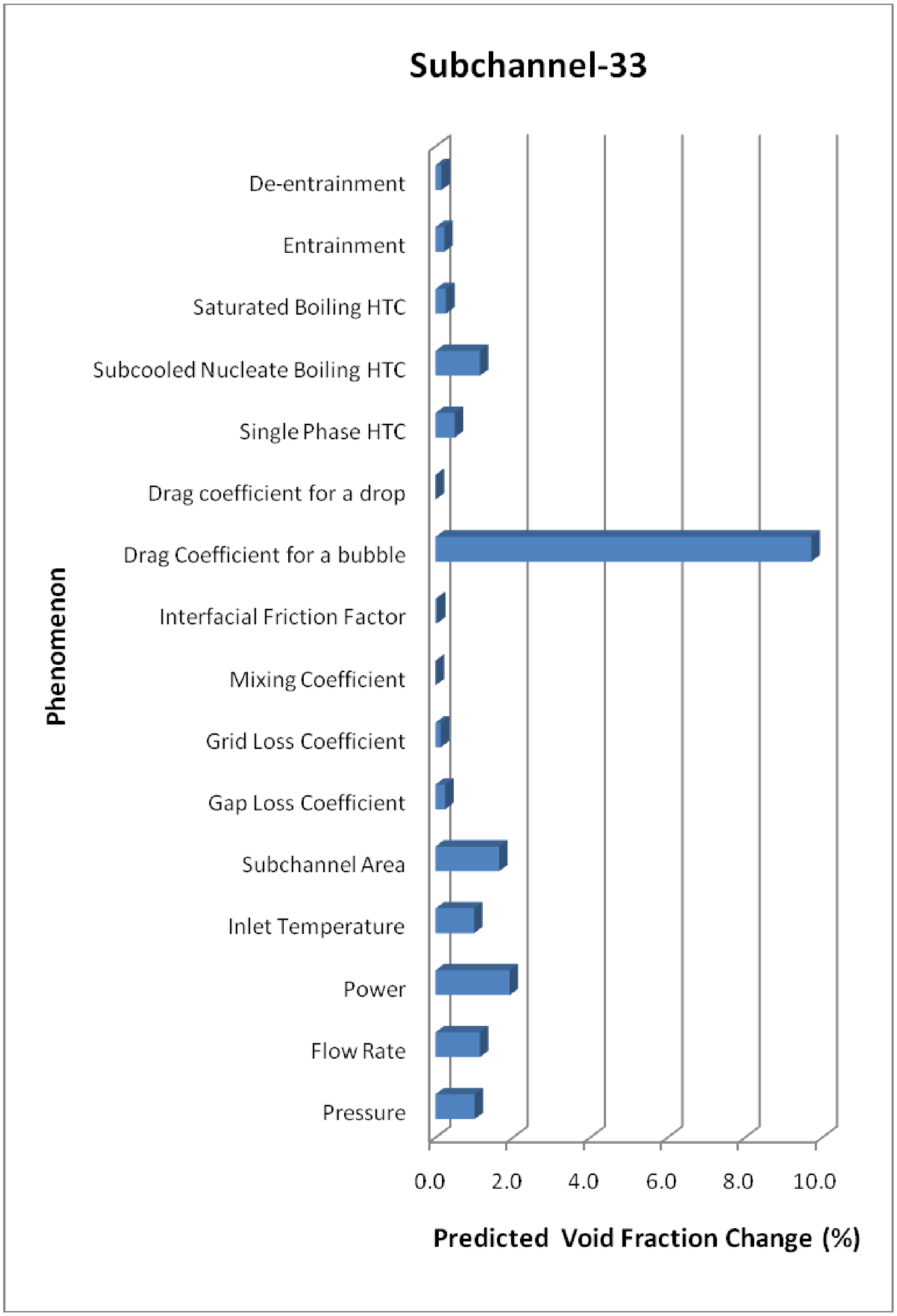

Figure 6.149. Predicted 33th Subchannel Void Fraction Change versus Phenomenon for Test 4101-55

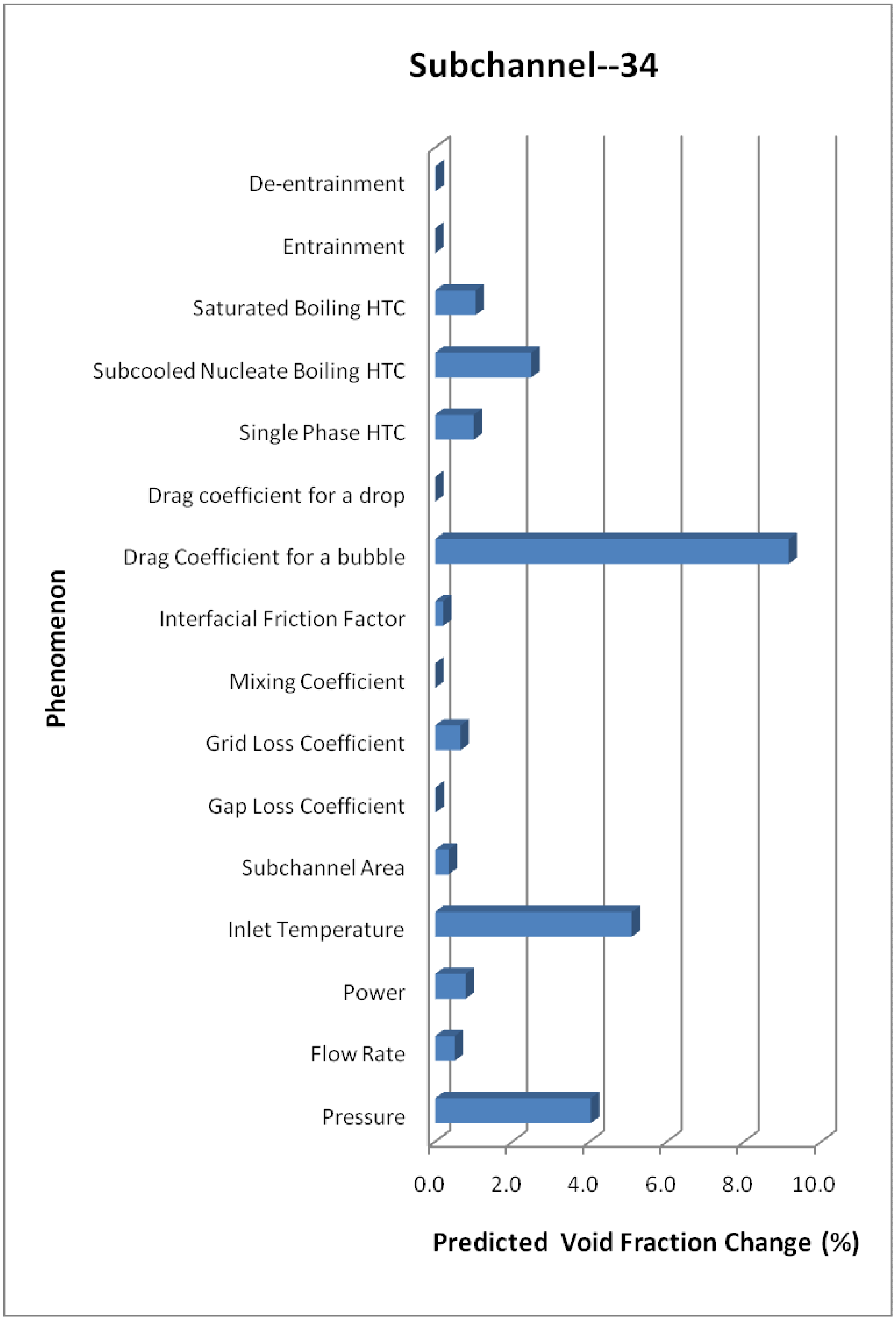

Figure 6.150. Predicted 34th Subchannel Void Fraction Change versus Phenomenon for Test 4101-55

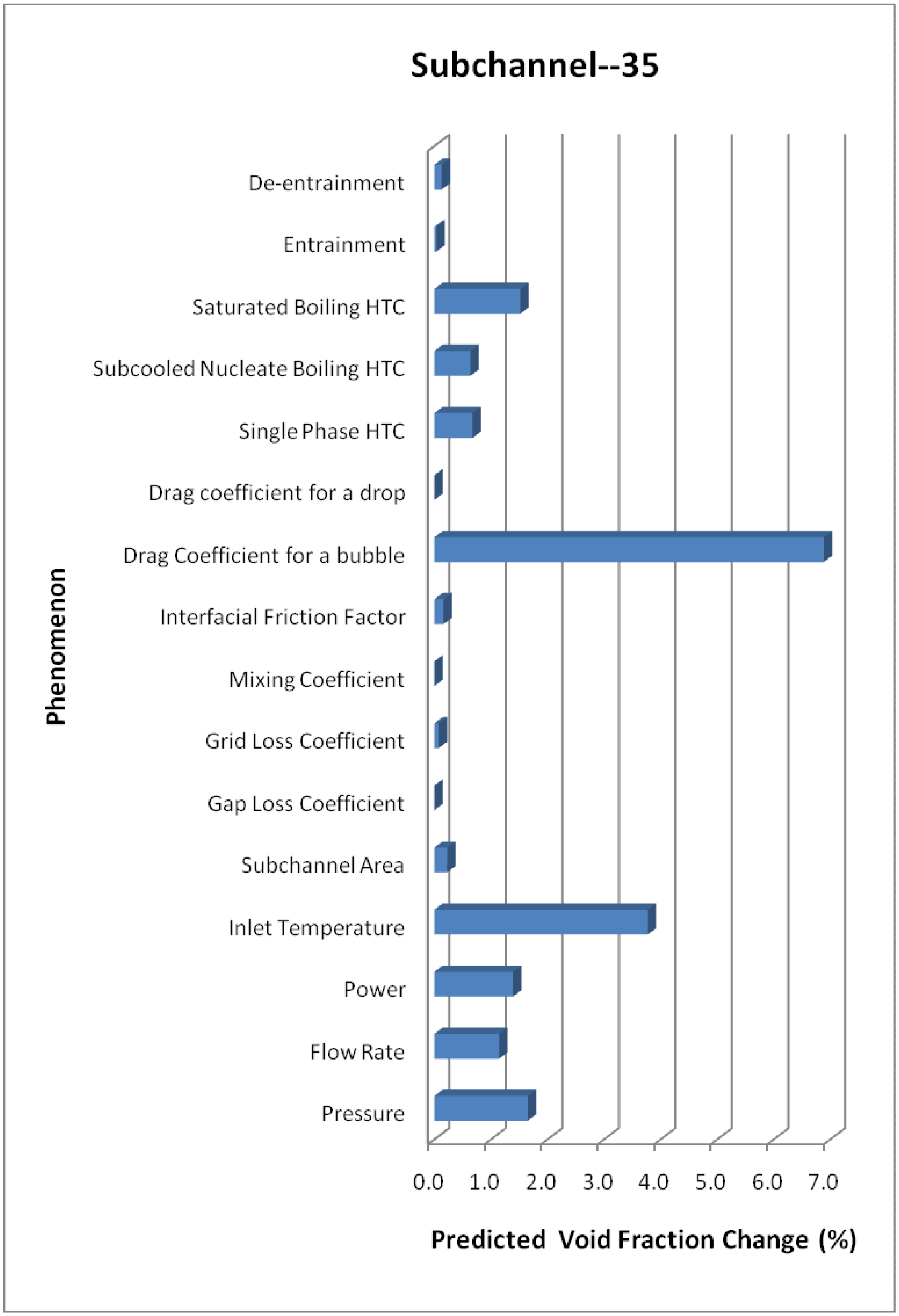

Figure 6.151. Predicted 35th Subchannel Void Fraction Change versus Phenomenon for Test 4101-55

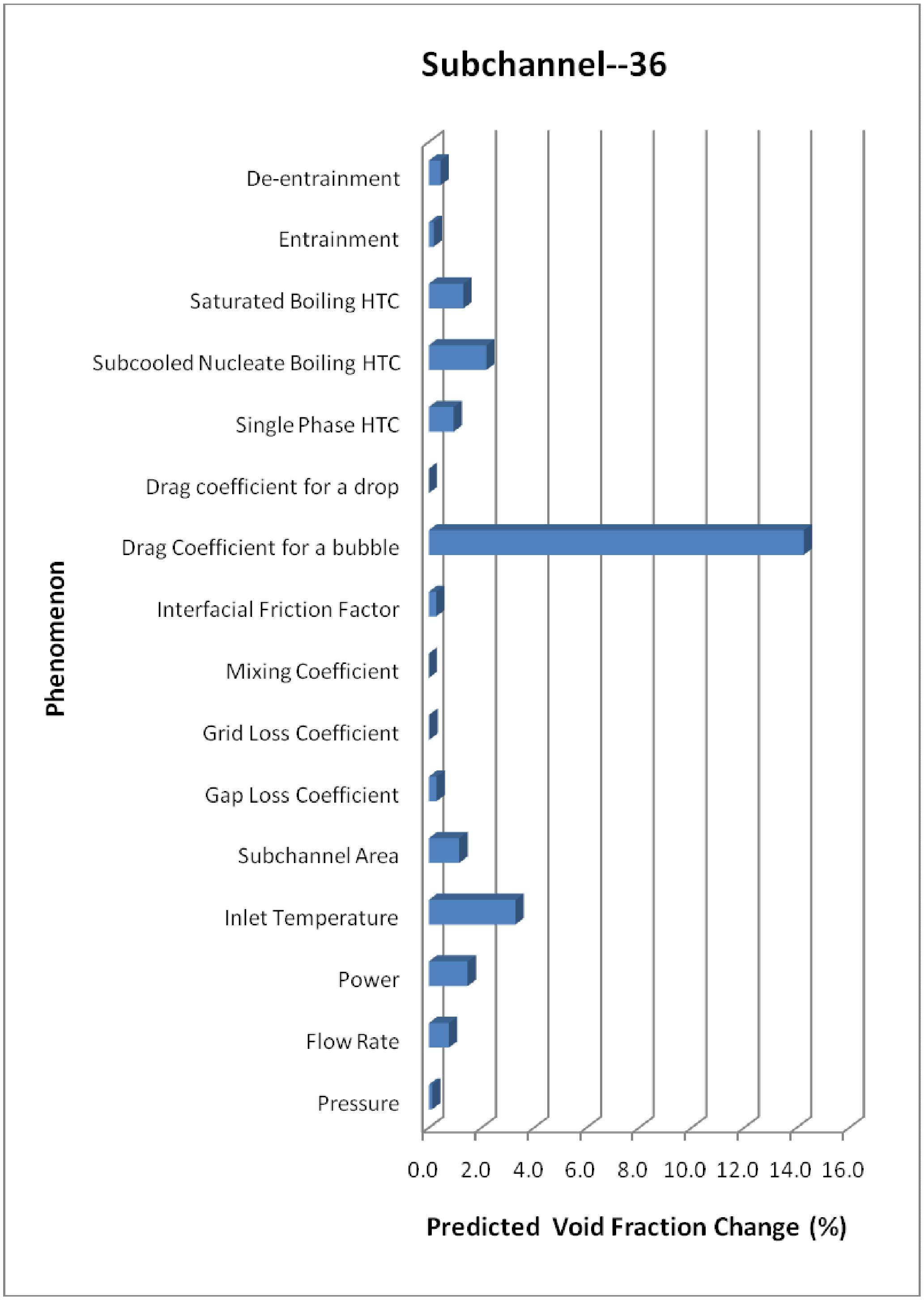

Figure 6.152. Predicted 36th Subchannel Void Fraction Change versus Phenomenon for Test 4101-55

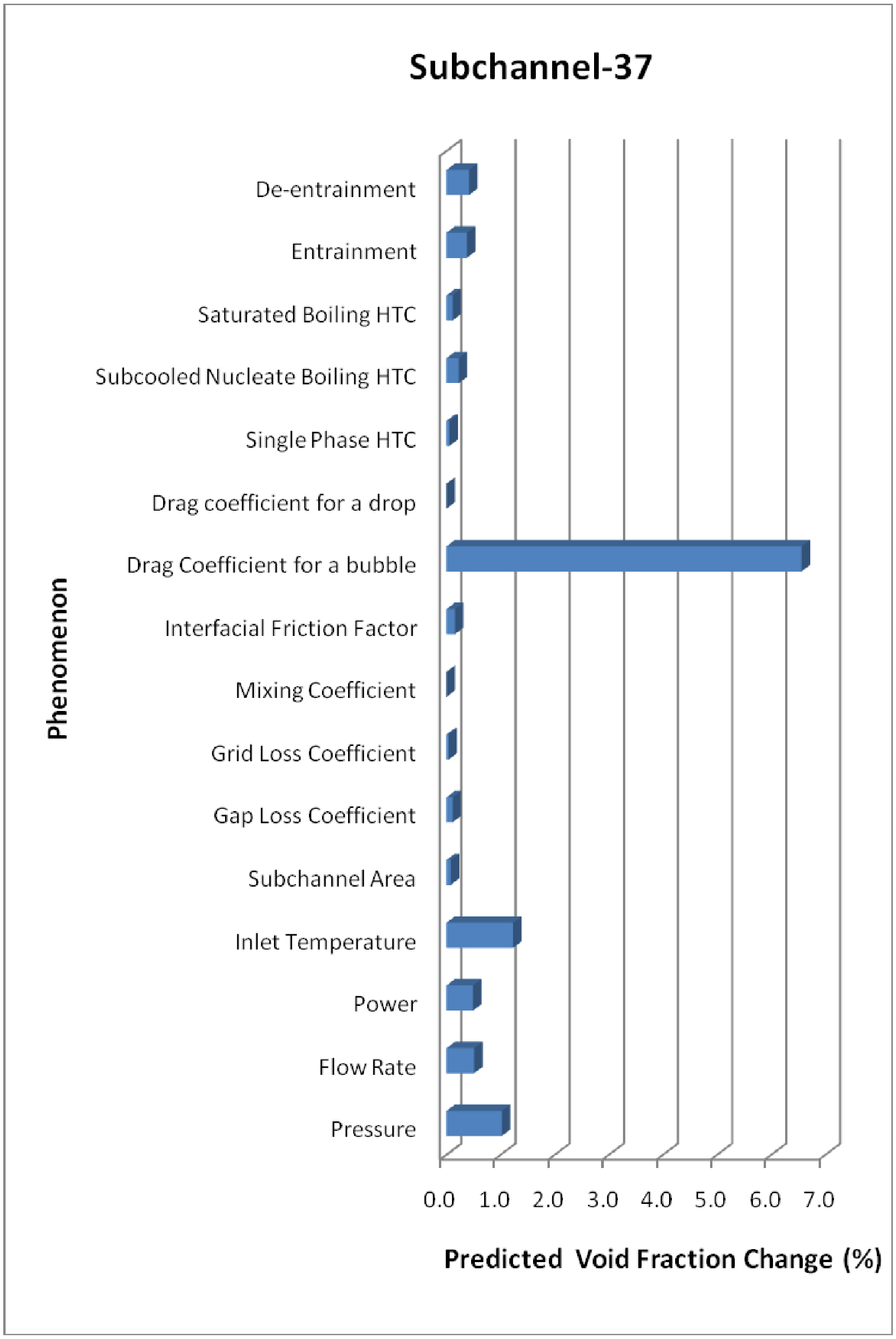

Figure 6.153. Predicted 37th Subchannel Void Fraction Change versus Phenomenon for Test 4101-55

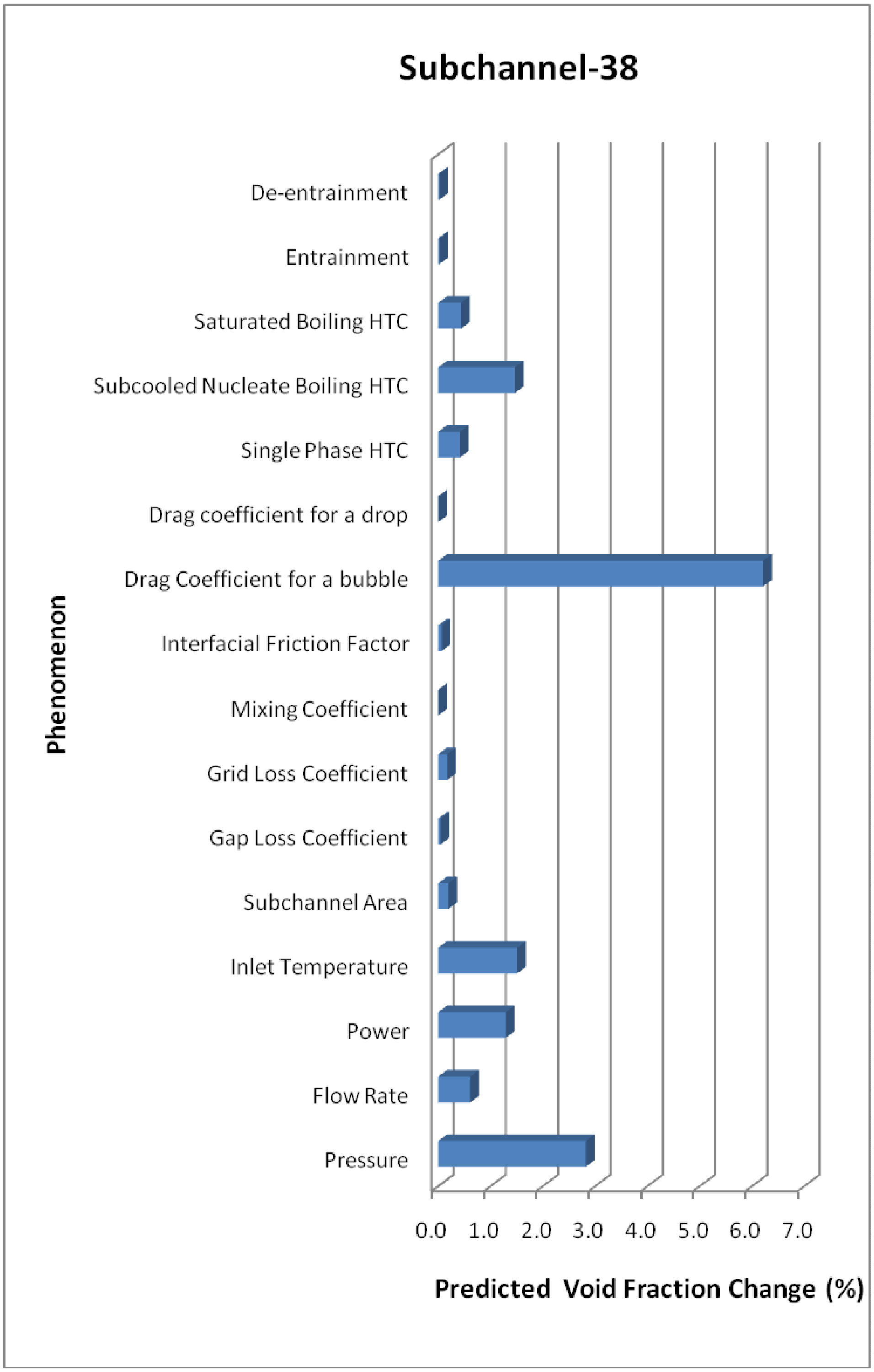

Figure 6.154. Predicted 38th Subchannel Void Fraction Change versus Phenomenon for Test 4101-55

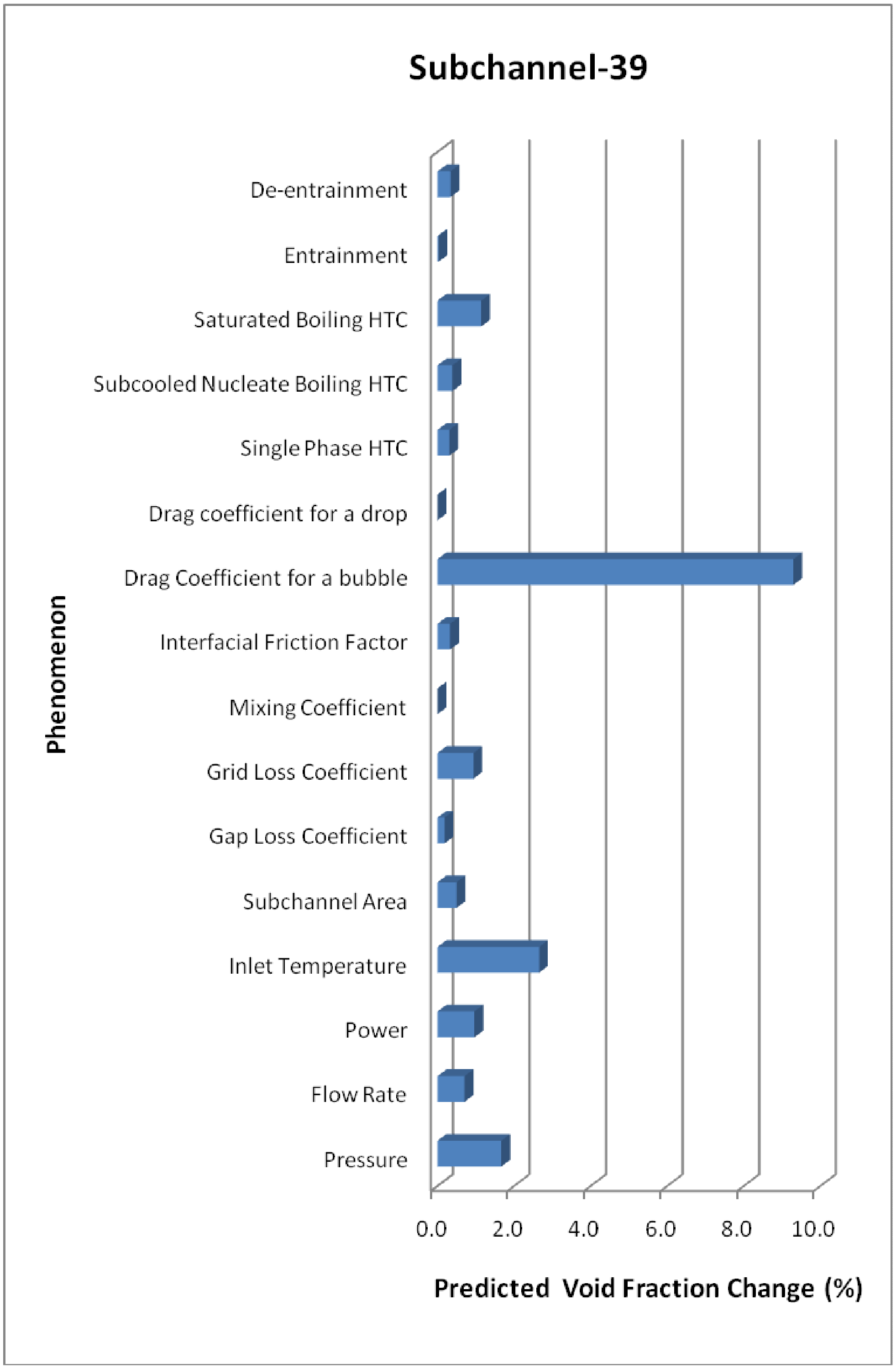

Figure 6.155. Predicted 39th Subchannel Void Fraction Change versus Phenomenon for Test 4101-55

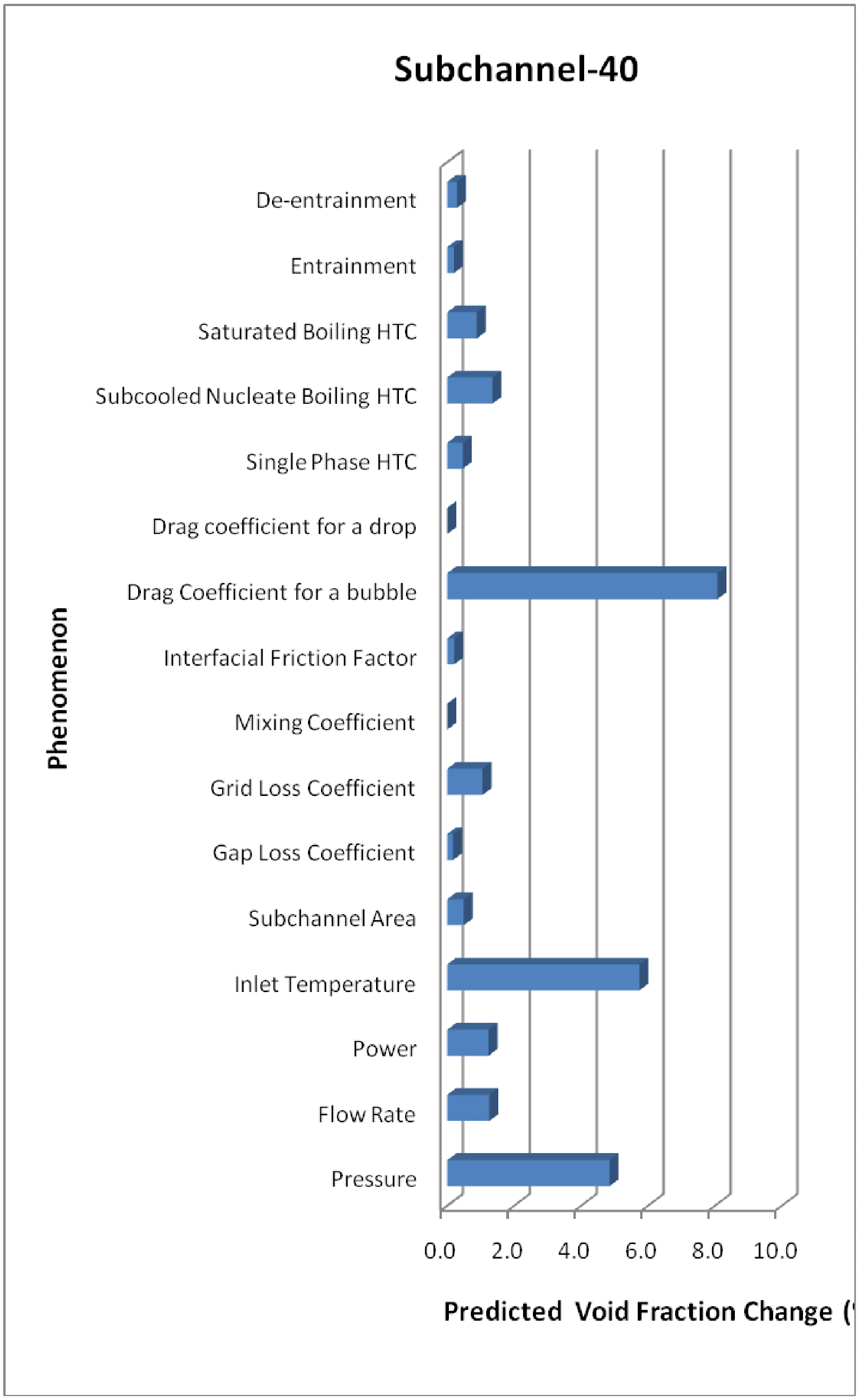

Figure 6.156. Predicted 40th Subchannel Void Fraction Change versus Phenomenon for Test 4101-55

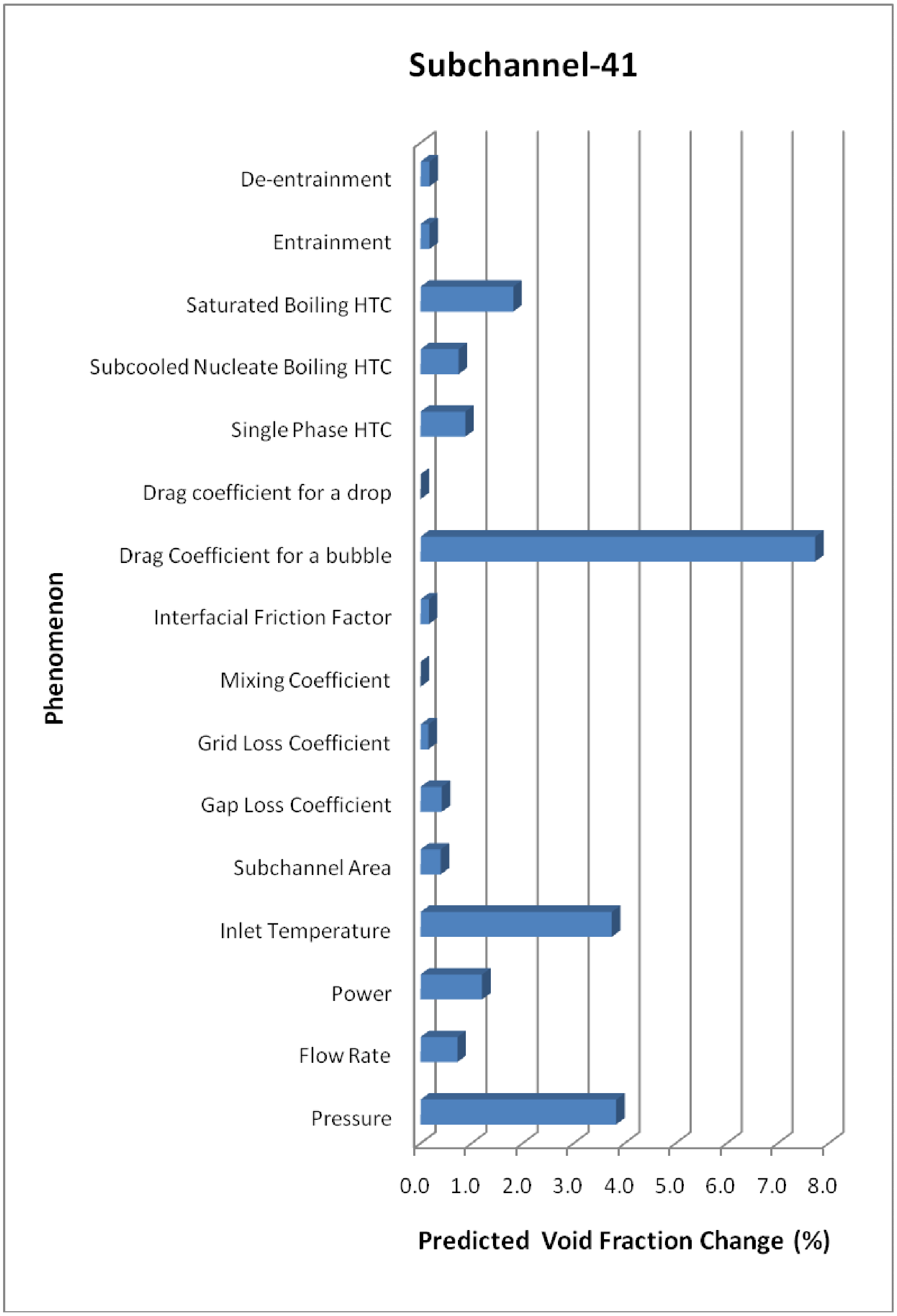

Figure 6.157. Predicted 41st Subchannel Void Fraction Change versus Phenomenon for Test 4101-55

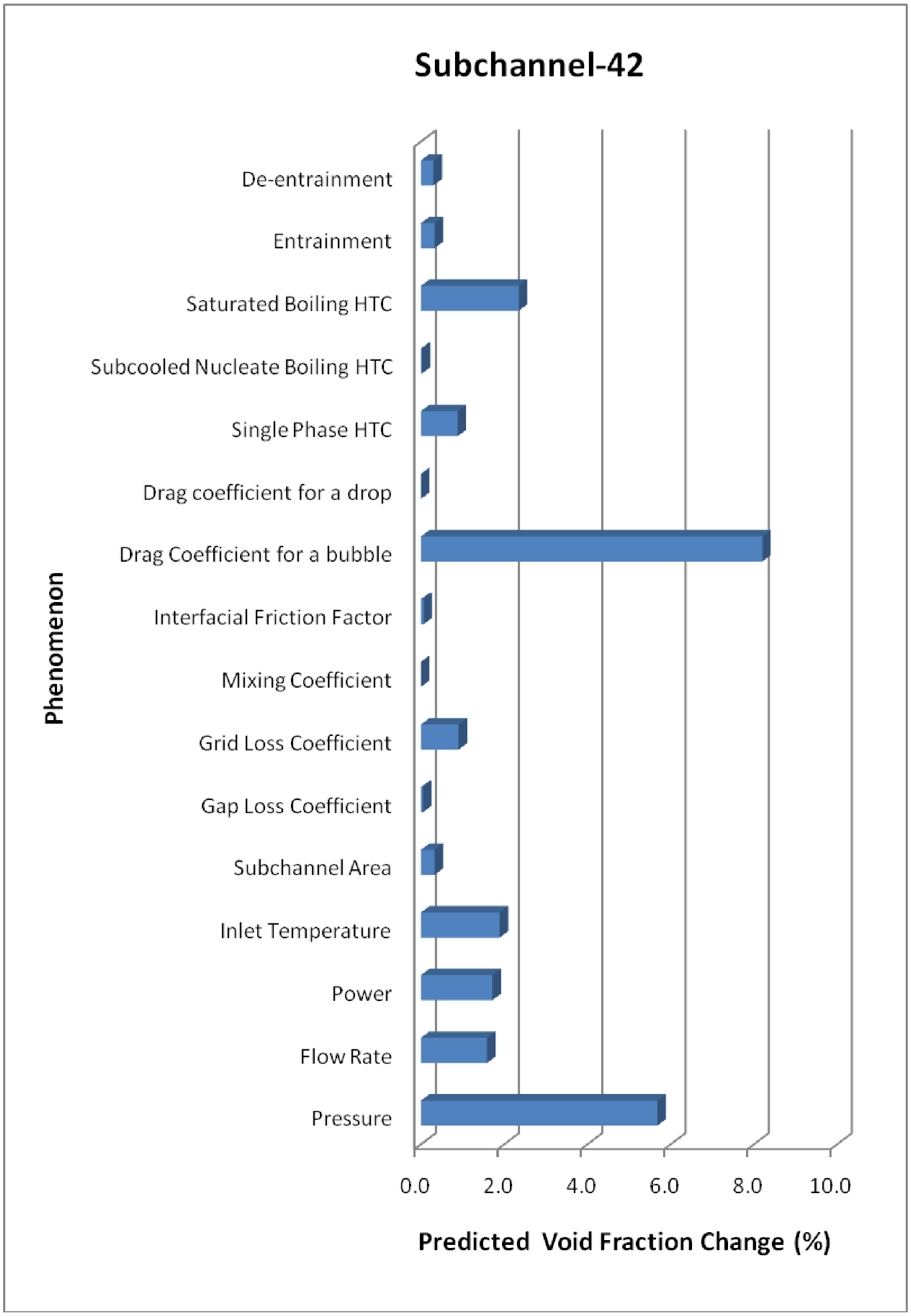

Figure 6.158. Predicted 42nd Subchannel Void Fraction Change versus Phenomenon for Test 4101-55

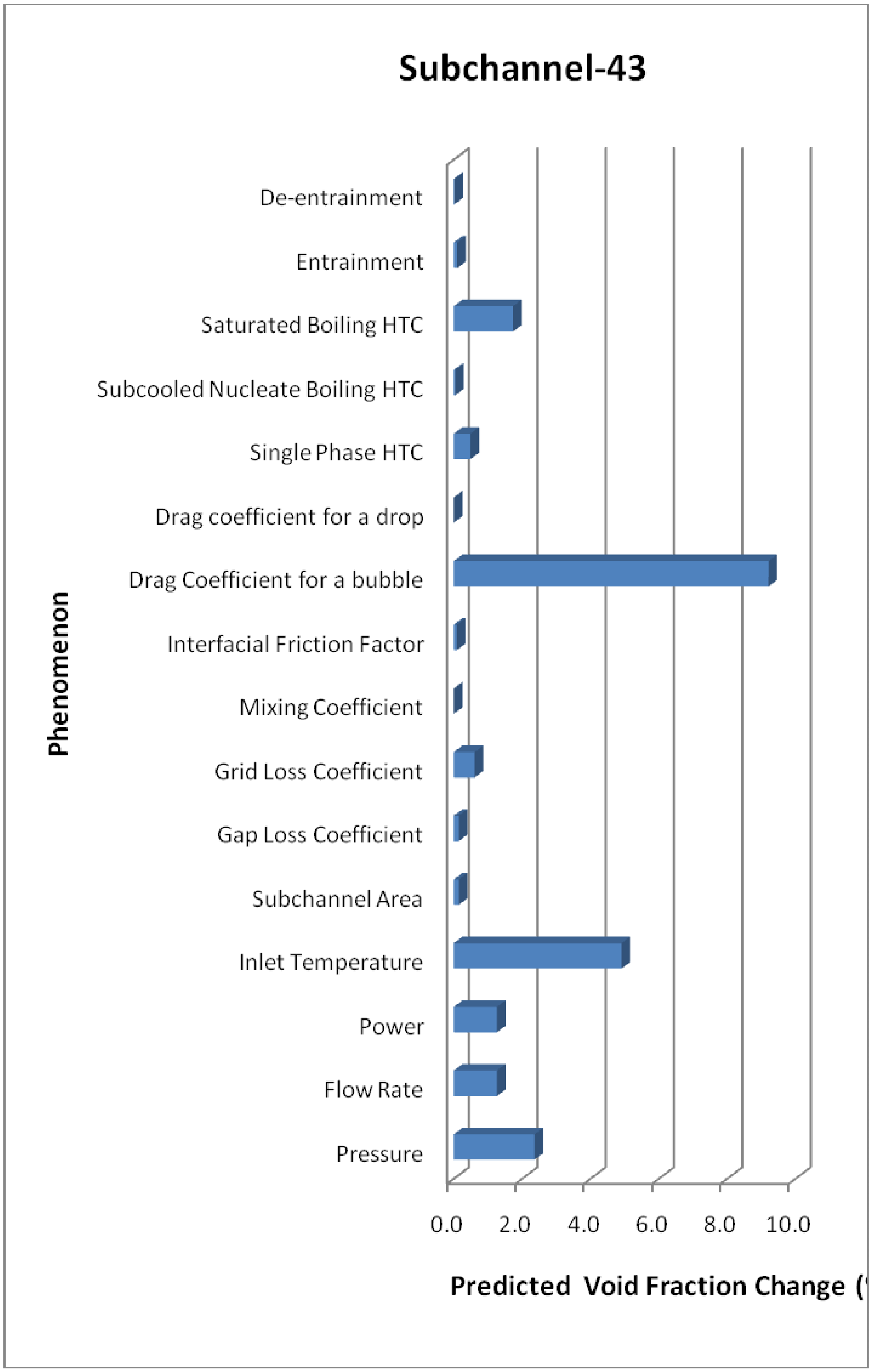

Figure 6.159. Predicted 43th Subchannel Void Fraction Change versus Phenomenon for Test 4101-55

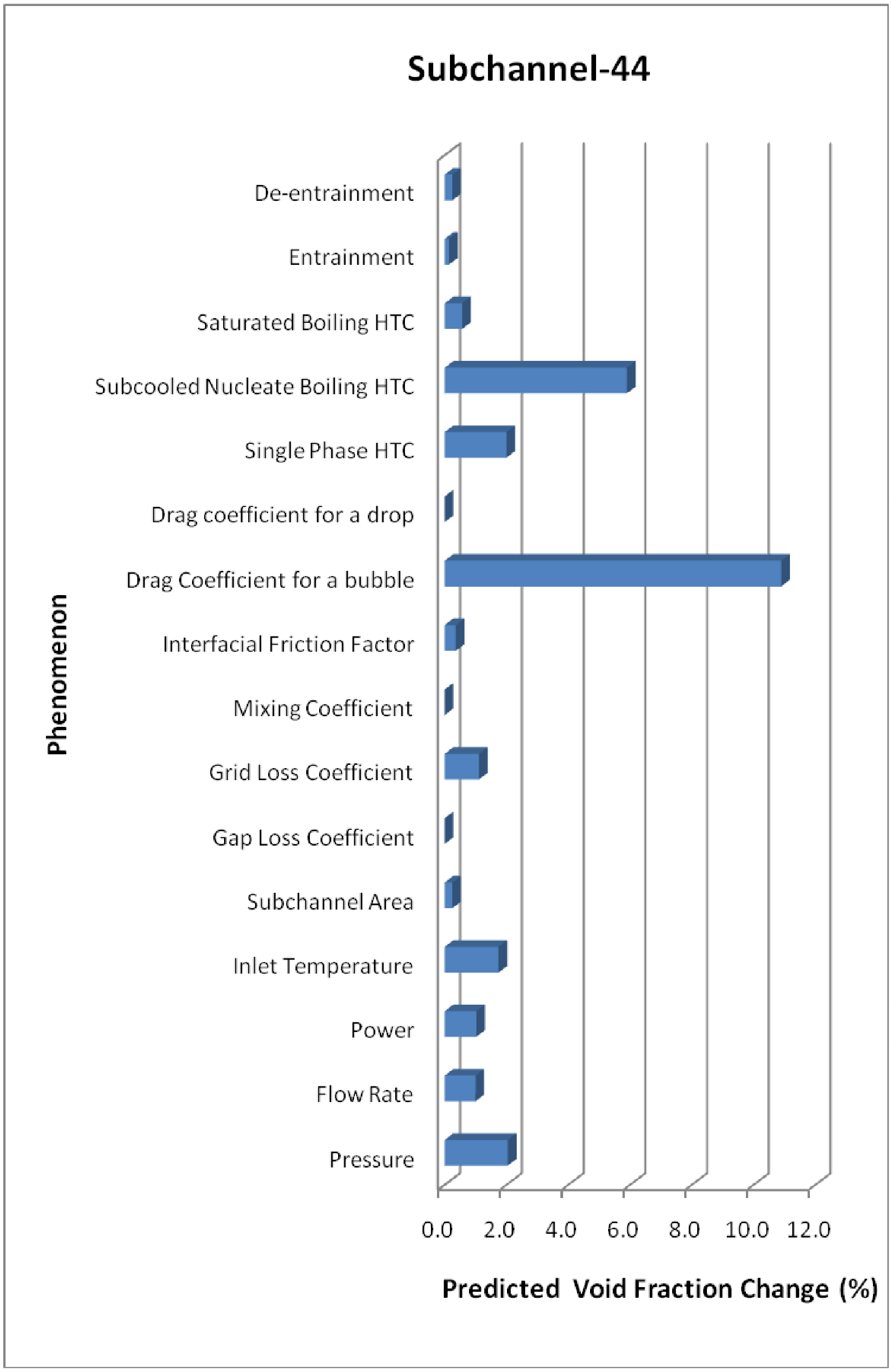

Figure 6.160. Predicted 44th Subchannel Void Fraction Change versus Phenomenon for Test 4101-55

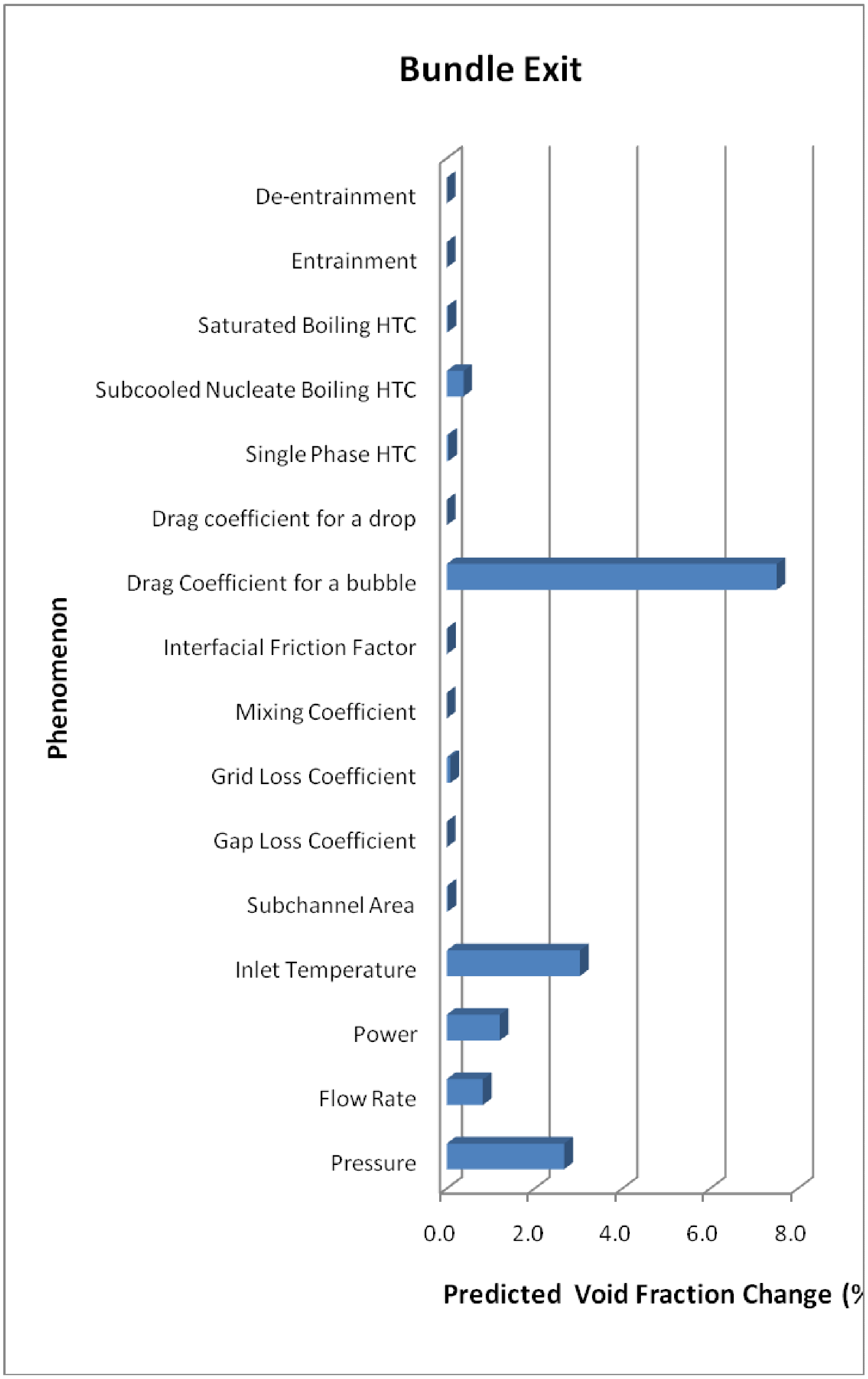

Figure 6.161. Predicted Bundle Void Fraction Change versus Phenomenon for Test 4101-55

6.2. Implementation of Particular Methodology to Steady State Critical Power in the BWR Bundle

Critical power is the power that demonstrates the dry-out occurrence of the liquid film on the heated rod. Thus, critical power is an important factor for the safety margin. This section of the chapter includes the application of the particular uncertainty methodology to the steady state critical power scenario/case.

6.2.1. Step-1

1. **Specify Scenario**: The scenario/case is steady state critical power. This scenario/case was limited with the steady state critical power and dry-out elevation for the BWRs.
2. **PIRT**: The PIRT of this case was given in Table 6.29.

Table 6.29. PIRT for Steady State Critical Power

Boundary Condition Effect			
ID	Parameter	Ranking	Basis for Ranking
1	Initial vessel operating pressure	M	This parameter affects the saturation temperature. The ranking of this parameter has to be determined with sensitivity analysis
2	Flow rate in the bundle	H	This parameter is in the energy equation
3	Power	H	This parameter is in the energy equation
4	Inlet Flow Temperature	M	This parameter changes the inlet boundary condition. The ranking of this parameter has to be determined with sensitivity analysis

where L: Low, M: Medium, H: High

Table 6.29. PIRT for Steady State Critical Power (Cont.)

Geometry Effect			
ID	Parameter	Ranking	Basis for Ranking
1	Wetted perimeter	L	This perimeter affects the friction factor
2	Sub-channel area	H	This parameter affects the mass flow rate
3	Nominal gap width	L	This parameter affect the lateral flow
4	The distance between the centers of channels	L	This parameter affect the lateral flow
5	Fraction of channel area blocked by grid	M	This parameter affects the pressure drop and the heat transfer. The ranking of this parameter has to be determined with sensitivity analysis
6	Grid Perimeter	M	This parameter is used to calculate spacer loss coefficient. The ranking of this parameter has to be determined with sensitivity analysis
7	Heated perimeter	H	This perimeter affects the heat flux and void distribution
8	Housing wetted perimeter	L	This perimeter affects the friction factor

where L: Low, M: Medium, H: High

Table 6.29. PIRT for Steady State Critical Power (Cont.)

Model Parameter Effect – Hydraulics			
ID	Parameter	Ranking	Basis for Ranking
1	The loss coefficient for a gap -lateral-	L	This parameter affects the lateral flow in a bundle. The ranking of this parameter has to be determined with sensitivity analysis
2	The wall friction factor for the gap	L	This affects the pressure drop
3	The grid loss coefficient -axial-	M	This parameter affects the pressure drop in the bundle. The ranking of this parameter has to be determined with sensitivity analysis
4	The mixing coefficient	H	This parameter affects the lateral void distribution in the bundle and void distribution affects the critical power.
5	Equilibrium distribution weighing factor in void drift	H	This parameter affects the lateral void distribution and void distribution affects the critical power.
Interfacial Mass Transfer			
6	Interfacial Friction Factor	H	This parameter affects the pressure drop
Interfacial Drag Force			
7	Drag Coefficient for bubble flow regime	L	The ranking of this parameter has to be determined with sensitivity analysis
8	Drag Coefficient for drop flow regime	M	The ranking of this parameter has to be determined with sensitivity analysis
9	Interfacial friction factor for film flow regime	H	This parameter affects the mass transfer between film flow and vapor.
Friction Factor in Wall Drag Force			
10	Single Phase Friction Factor in Wall Drag Force	L	This affects the pressure drop
11	Two Phase Friction Factor in Wall Drag Force	M	This affects the pressure drop. Because two phase pressure drop models have higher uncertainty, this parameter is ranked as M. The ranking of this parameter has to be determined with sensitivity analysis.

where L: Low, M: Medium, H: High

Table 6.29. PIRT for Steady State Critical Power (Cont.)

Model Parameter Effect – Thermal			
ID	Parameter	Ranking	Basis for Ranking
Wall Heat Transfer Coefficient			
1	Single phase liquid	M	This parameter affects the heat transfer from wall to the fluid. The ranking of this parameter has to be determined with sensitivity analysis.
2	Subcooled nucleate boiling	M	This parameter affects the heat transfer from wall to the fluid. The ranking of this parameter has to be determined with sensitivity analysis.
3	Saturated boiling region	M	This parameter affects the heat transfer from wall to the fluid. The ranking of this parameter has to be determined with sensitivity analysis.
Entrainment/Deposition			
Entrainment in film flow			
4	Entrainment rate	H	The ranking of this parameter has to be determined with sensitivity analysis. This parameter has more importance in the post-CHF scenario.
De-Entrainment in film flow			
5	De-entrainment rate for film flow	H	The ranking of this parameter has to be determined with sensitivity analysis.
Critical Heat Flux			
6	Critical Heat Flux Correlation	H	This affects the critical power.

where L: Low, M: Medium, H: High

Table 6.30. Comparison of Two Independent Expert Groups' Decisions about the PIRT Tables for the Critical Power

Effect	Parameter(s)	First group's Decision	Second Group's Decision	Final Decision	Comments
Boundary Condition Effect	Inlet Temperature	L	M	M	Second group commented that if the inlet temperature is increased, exit temperature of the coolant changes for a fixed power.
Geometry Effect	All	Agreement	Agreement	-	-
Hydraulic Effect	Interfacial friction factor in mass transfer and interfacial drag force	M	H	H	2nd group's suggested to change this parameter's ranking to high..
Thermal effect	All	Agreement	Agreement	-	-

3. **Select Code**: COBRA-TF (RBHT) was selected for this analysis because this code is capable of predicting critical power and dry-out elevation.

4. **Provide Complete Documentation**: Two NUREG's documents were provided about COBRA-TF (RBHT):

    a. COBRA/TRAC- A Thermal-Hydraulics Code for Transient Analysis of Nuclear Reactor Vessels and Primary Coolant Systems [2]

    b. Analysis of FLECHT-SEASET 163-Rod Blocked Bundle Data Using COBRA-TF [1]

5. **Determine Code Applicability:** COBRA-TF (RBHT) is capable of predicting crtical power and dry-out elevation [1, 2].

6.2.1. Step-2

6. **Experimental Database**: This database consists of the critical power as well as the dry-out elevation data. All the experimental information was provided in Chapter 4.

7. **Code Assessment Matrix:** Code assessment matrix is the same matrix selected for the uncertainty analysis. This matrix was obtained with the Spanning Algorithm in the 11th element.

8. **Define Nodalization**: The nodalization results are same as given in Table 6.3 and 6.4.

9. **Evaluate the Results with Richardson Extrapolation**: This element is the same with the corresponding element of the steady state void distribution.

10. **Noding Change**: There is no need to change the nodes.

6.2.3. Step-3

11. Filter: This element has two components: selection of the bundle and selection of the experimental cases with Spanning Algorithm.

a. **Selection of Bundle Type**: C2A is selected for the critical power case. The reasons are same reason as given in the 11th element of the void distribution case.

b. **Selection of the Experimental Cases:** Spanning algorithm was used to obtain the experimental cases. For the critical power case, the output (dependent) uncertain parameter is critical power and independent parameters in the database are pressure, flow rate and inlet sub-cooling. The selected cases (as shown in Table 6.31) were obtained with spanning algorithm. Different colors were used to highlight the selected cases in Figure 6.162-6.164.

Table 6.31. The selected cases for the critical power

Experiment	Output Pressure	Flow Rate	Inlet Subcooling	Critical Power	Elevation Level	Positions of the Selected Points in the Plots
	MPa	ton/h	kJ/kg	MW	-	-
SA603901	7.18	10.01	25.82	3.2	A	Left
SA505900	5.49	20.14	26.04	5.98	A	Bottom
SA812800	8.67	65.27	135.52	8.9	B	Top
SA512800	5.5	65.52	133.75	11.09	A	Right

where A and B: Dry-out elevation levels. The descriptions of them were provided in Chapter 4.

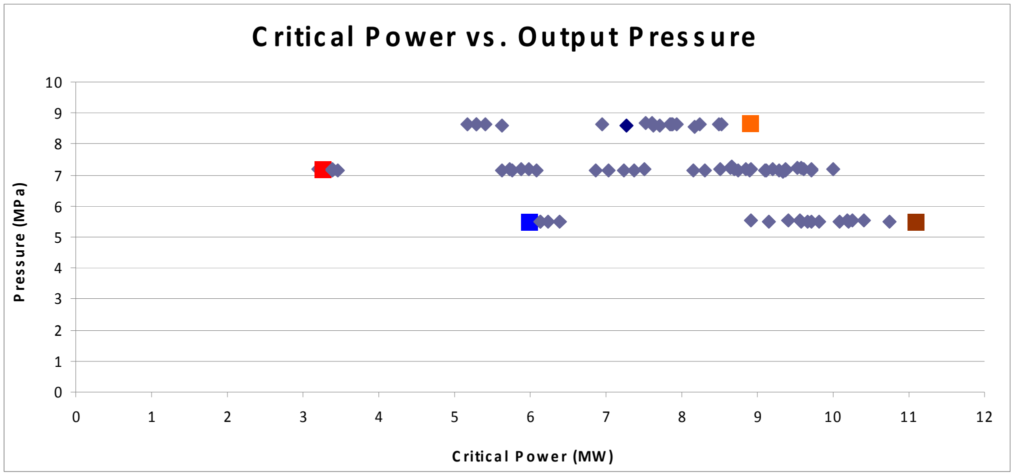

Figure 6.162. Critical Power vs. Output Pressure

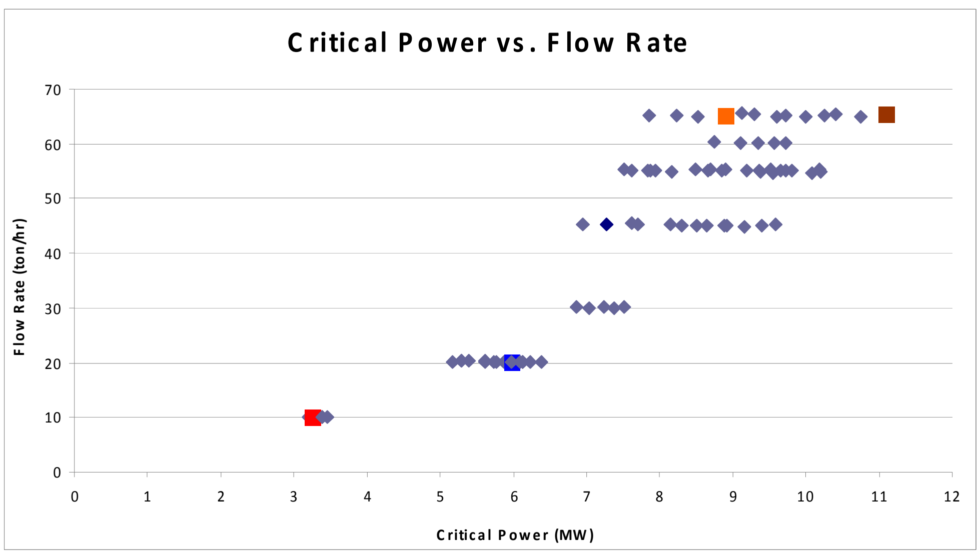

Figure 6.163. Critical Power vs. Flow Rate

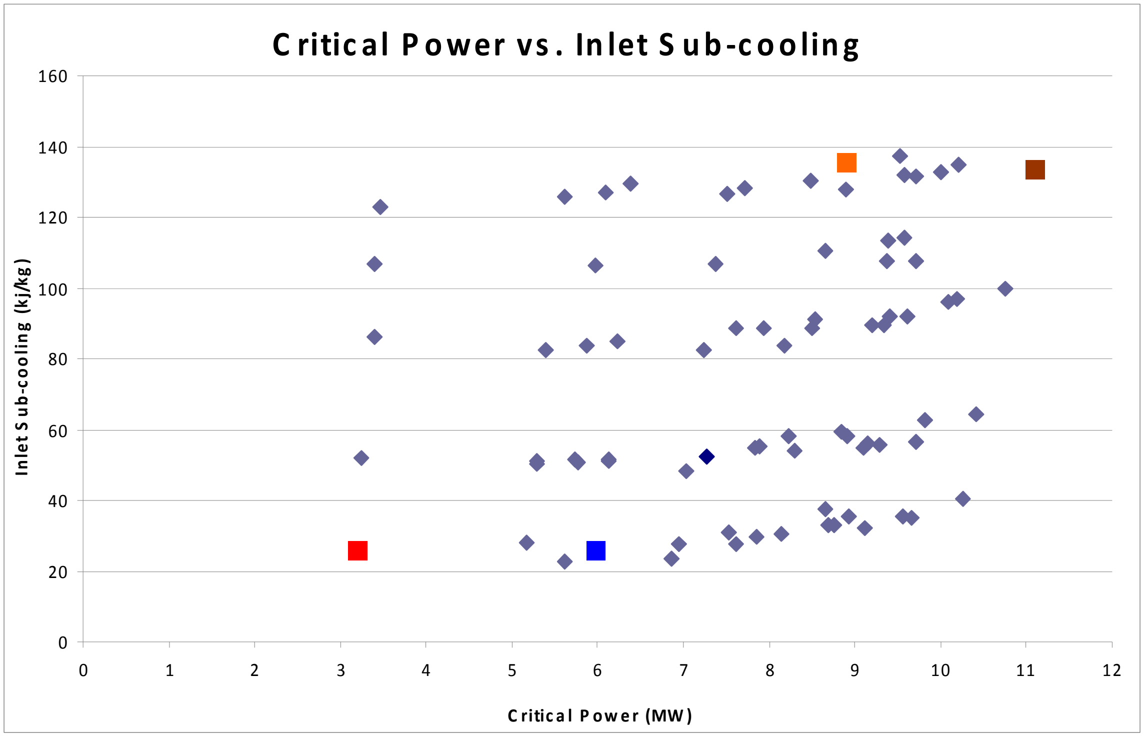

Figure 6.164. Critical power vs. inlet sub-cooling

12. **Finding the number of the run-cases:** There is only one phenomenon for this case and it is dry-out phenomenon. Therefore, Wilks formula was used (with the β=95/100 and γ= 95/100) and sample number was calculated as 59.

13. **Uncertain parameters and corresponding CDFs/SCDFs:** Low ranked and inappropriate uncertainty parameters are eliminated in this element of the uncertainty system. All the uncertainty parameters in the boundary condition effect were selected. The output parameter is critical power. In other words, power was not selected because one parameter cannot be input and output parameter at the same time. Therefore, power was not shown as input uncertainty parameter in the results.

Geometry effect phenomenon includes only two medium ranked uncertain parameters. These are fraction of channel area blocked by grid and grid perimeter. Because spacer loss coefficient includes these parameters, spacer loss coefficient is used instead of these parameters. Heated perimeter is not used in the COBRA-TF model so that this was eliminated. Subchannel flow area was selected from geometry effect. Void drift is accounted in COBRA-TF. When mixing coefficient is changed, both void drift and mixing coefficient are changed essentially. Two phase friction factor in wall drag force is not used in the COBRA-TF (RBHT). Thus, the grid loss coefficient, mixing coefficient, interfacial friction factor and drag coefficient for drop flow regime were selected in hydraulics effect. Single phase heat transfer coefficient, subcooled nucleate heat transfer coefficient, and saturated heat transfer coefficient, entrainment rate for film flow, de-entrainment rate in for film flow and critical heat flux were selected in thermal effect.

Figure 6.6, 6.7, 6.9, 6.10, 6.12, 6.13, 6.14, 6.16, 6.17-6.21 and 6.165 demonstrate the CDFs/SCDFs of pressure [10, 11, 12], mass flow rate [10, 11, 12], inlet temperature [10, 11, 12], flow area [13], grid loss coefficient [15, 16], mixing coefficient [9], interfacial friction factor [17], drag coefficient for a droplet [20], single phase heat transfer coefficient [21, 22, 23], subcooled nucleate boiling heat transfer coefficient [24], saturated boiling heat transfer coefficient [24], entrainment [25, 26], de-entrainment [25, 27] and critical heat flux [31] respectively.

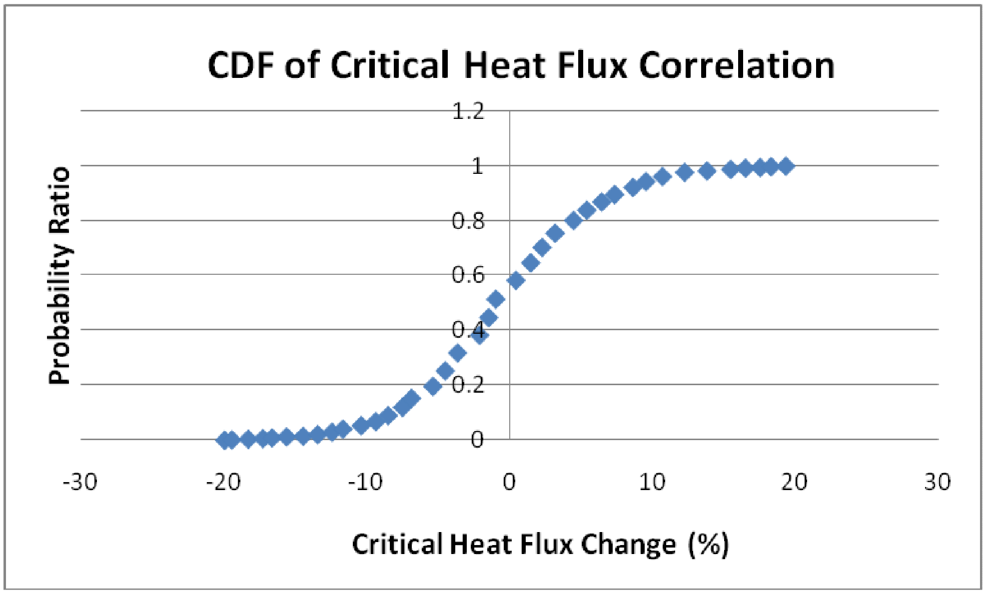

Figure 6.165. CDF/SCDF of Critical Heat Flux

14. **Determine Random Numbers with SRS:** 59 random numbers (between 0 and 1) were generated for each medium and high ranked uncertainty parameters. Each number's generation was independent than the others. These numbers are the inputs to the Order Statistics Method.

15. **Random Number Table**: The results of 14th element, pre-samples, were recorded into the random number table (Table 6.32).

Table 6.32. Pre-sample Table for Critical Power

ID	Pressure	Flow Rate	Inlet Temperature	Flow Area	Grid Loss Coefficient	Mixing	fi	CDd	HTCsingle	HTCsub	HTCsat	Entrainment Rate	De-entrainment	Critical Heat Flux
1	0.88	0.38	0.76	0.45	0.52	0.10	0.75	0.41	0.50	0.92	0.71	0.86	0.36	0.61
2	0.35	0.94	0.60	0.48	0.17	0.12	0.44	0.13	0.00	0.74	0.61	0.71	0.55	0.16
3	0.36	0.11	0.25	0.55	0.62	0.62	0.81	0.15	0.99	0.64	0.70	0.41	0.73	0.54
4	0.20	0.30	0.50	0.46	0.51	0.80	0.76	0.80	0.98	0.46	0.60	0.08	0.33	0.86
5	0.66	0.57	0.13	0.57	0.53	0.36	0.49	0.85	0.40	0.12	0.63	0.37	0.59	0.07
6	0.72	0.85	0.02	0.56	0.23	0.54	0.08	0.51	0.60	0.85	0.65	0.52	0.69	0.83
7	0.88	0.91	0.99	0.20	0.78	0.24	0.48	0.88	0.56	0.68	0.53	0.78	0.97	0.06
8	0.33	0.54	0.70	0.16	0.51	0.46	0.73	0.50	0.57	0.12	0.76	0.40	0.05	0.85
9	0.64	0.21	0.26	0.21	0.23	0.45	0.62	0.75	0.24	0.70	0.85	0.42	0.47	0.94
10	0.54	0.57	0.97	0.47	0.75	0.03	0.43	0.21	0.33	0.41	0.75	0.25	0.29	0.30
11	0.89	0.65	0.98	0.83	0.30	0.07	0.77	0.74	0.42	0.47	0.39	0.70	0.51	0.22
12	0.37	0.45	0.99	0.51	0.63	0.36	0.70	0.60	0.70	0.45	0.67	0.40	0.98	0.54
13	0.74	0.50	0.45	0.90	0.25	0.12	0.00	0.35	0.61	0.72	0.47	0.06	0.02	0.00
14	1.00	0.80	0.51	0.67	0.07	1.00	0.45	0.41	0.41	0.25	0.30	0.64	0.02	0.50
15	0.17	0.19	0.47	0.13	0.30	0.38	0.66	0.93	0.82	0.55	0.48	0.68	0.19	0.30
16	0.48	0.02	0.98	0.47	0.78	0.46	0.80	0.51	0.47	0.69	0.19	0.99	0.79	0.64
17	0.79	0.69	0.53	0.89	0.66	0.22	0.78	0.47	0.38	0.76	0.50	0.87	0.77	0.69
18	0.21	0.50	0.98	0.98	0.76	0.69	0.79	0.60	0.72	0.63	0.37	0.60	0.55	0.30
19	0.93	0.68	0.29	0.85	0.72	0.61	1.00	0.77	0.83	0.98	0.50	0.38	0.48	0.57
20	0.66	0.62	0.99	0.99	0.23	0.95	0.14	0.16	0.31	0.68	0.57	0.65	0.13	0.80
21	0.23	0.21	0.18	0.32	0.21	0.44	0.48	0.62	0.94	0.30	0.44	0.60	0.36	0.08
22	0.24	0.56	0.52	0.06	0.47	0.31	0.93	0.65	0.32	0.55	0.51	0.65	0.23	0.56
23	0.47	0.81	0.83	0.76	0.75	0.53	0.53	0.63	0.70	0.17	0.70	0.71	0.39	0.60
24	0.50	0.21	0.19	0.67	0.31	0.37	0.41	0.69	0.60	0.44	0.60	0.61	0.69	0.14
25	0.27	0.99	0.67	0.43	0.20	0.27	0.70	0.42	0.76	0.55	0.96	0.87	0.17	0.78
26	0.53	0.07	0.74	0.70	0.75	0.46	0.11	0.99	0.33	0.41	0.70	0.69	0.57	0.50
27	0.01	0.74	0.05	0.96	0.57	0.65	0.60	0.00	0.49	0.83	0.47	0.49	0.65	0.68
28	0.38	0.92	0.40	0.33	0.67	0.23	0.50	0.64	0.86	0.45	0.72	0.15	0.57	1.00
29	0.50	0.64	0.32	0.12	0.44	0.20	0.41	0.77	0.62	0.17	0.00	0.88	0.92	0.95
30	0.05	0.46	0.01	0.24	0.31	0.60	0.61	0.23	0.53	0.23	0.47	0.65	0.81	0.47
31	0.61	0.54	0.25	0.34	0.73	0.12	0.79	0.71	0.50	0.35	0.31	0.71	0.86	0.50
32	0.53	0.65	0.05	0.65	0.40	0.05	0.45	0.89	0.36	0.20	0.74	0.68	0.45	0.44
33	0.50	0.30	0.21	0.62	0.88	0.62	0.93	0.71	0.39	0.36	0.65	0.43	0.43	0.44

where fi: interfacial friction factor, CDd: Drag Coefficient for a Droplet, HTCsingle: Single Phase Heat Transfer Coefficient, HTCsub: Subcooled Nucleate Boiling Heat Transfer Coefficient, HTCsat: Saturated Boiling Heat Transfer Coefficient

Table 6.32. Pre-sample Table for Critical Power (Cont.)

ID	Pressure	Flow Rate	Inlet Temperature	Flow Area	Grid Loss Coefficient	Mixing	fi	CDd	HTCsingle	HTCsub	HTCsat	Entrainment Rate	De-entrainment	Critical Heat Flux
34	0.66	0.88	0.72	0.59	0.89	0.61	0.33	0.52	0.56	1.00	0.31	0.43	0.88	0.34
35	0.81	0.30	0.16	0.15	0.25	0.58	0.52	0.54	0.70	0.51	0.82	0.32	0.56	0.63
36	0.92	0.37	0.48	0.66	0.93	0.20	0.70	0.47	0.88	0.17	0.56	0.17	0.46	0.58
37	0.70	0.28	0.69	0.30	0.96	0.61	0.73	0.06	0.45	0.73	0.99	0.55	0.55	0.99
38	0.62	0.91	0.89	0.79	0.96	0.24	0.80	0.21	0.47	0.22	0.72	0.94	0.73	0.30
39	0.80	0.62	0.26	0.05	0.28	0.84	0.49	0.48	0.55	0.34	0.63	0.56	0.95	0.31
40	0.23	0.41	0.34	0.39	0.33	0.29	0.20	0.49	0.54	0.46	0.33	0.00	0.74	0.58
41	0.70	0.17	0.35	0.65	0.92	0.37	0.84	0.14	0.55	0.85	0.59	0.14	1.00	0.78
42	0.89	0.30	0.58	0.65	0.40	0.01	0.81	0.53	0.68	0.29	0.26	0.41	0.36	0.66
43	0.62	0.43	0.09	0.22	0.36	0.77	0.10	0.83	0.34	0.99	0.81	0.28	0.70	0.78
44	0.21	0.53	0.27	0.22	0.57	0.37	0.44	0.45	0.50	0.58	0.04	0.04	0.06	0.74
45	0.51	0.89	0.65	0.32	0.03	0.59	0.56	0.98	0.42	0.26	0.76	0.78	0.56	0.16
46	0.55	0.86	0.05	0.87	0.22	0.52	0.17	0.25	0.82	0.43	0.35	0.82	0.46	0.17
47	0.72	0.70	0.99	0.47	0.07	0.69	0.13	0.32	0.77	0.71	0.71	0.32	0.27	0.88
48	0.62	0.24	0.83	0.71	0.62	0.56	0.56	0.41	0.19	0.74	0.65	0.55	0.58	0.55
49	0.59	0.86	0.44	0.58	0.43	0.76	0.72	0.66	0.23	0.92	0.73	0.85	0.65	0.24
50	0.12	0.53	0.12	0.63	0.19	0.67	0.70	0.74	0.50	0.16	0.84	0.95	0.58	0.77
51	0.44	0.44	0.77	0.88	0.56	0.27	0.28	0.84	0.87	0.14	0.82	1.00	0.67	0.53
52	0.12	0.73	0.65	0.73	0.40	0.00	0.94	0.46	0.90	0.12	0.78	0.26	0.50	0.82
53	0.90	0.96	0.18	0.24	0.72	0.55	0.43	0.54	0.36	0.21	0.40	0.42	0.21	0.39
54	0.93	0.24	0.63	0.40	0.63	0.24	0.51	0.43	0.46	0.00	1.00	0.92	0.92	0.69
55	0.24	0.99	0.94	0.39	0.65	0.82	0.90	0.25	0.34	0.25	0.37	0.35	0.92	0.15
56	0.37	0.95	0.86	0.92	0.74	0.46	0.82	0.67	0.52	0.22	1.00	0.52	0.81	0.19
57	0.41	0.32	0.59	0.75	0.18	0.72	0.73	0.83	0.90	0.72	0.51	0.86	0.15	0.73
58	0.34	0.71	0.38	0.46	0.65	0.41	0.75	0.22	0.75	0.93	0.80	0.50	0.74	0.34
59	0.60	0.56	0.61	0.47	0.46	0.82	0.96	0.98	0.95	0.76	0.54	0.89	0.81	0.21

where fi: interfacial friction factor, CDd: Drag Coefficient for a Droplet, HTCsingle: Single Phase Heat Transfer Coefficient, HTCsub: Subcooled Nucleate Boiling Heat Transfer Coefficient, HTCsat: Saturated Boiling Heat Transfer Coefficient

16. **Sampling with Order Statistics:** Samples were selected by using pre-samples and interpolation and shown in Table 6.33. Inlet temperature was converted to the inlet

enthalpy to make the sample matrix appropriate to the COBRA-TF (RBHT) input deck.

Table 6.33. Sample Table for Critical Power

ID	Pressure	Flow Rate	Inlet Enthalpy	Flow Area	Grid Loss Coefficient	Mixing	fi	CDd	HTCsingle	HTCsub	HTCsat	Entrainment Rate	De-entrainment	Critical Heat Flux
1	0.57	-0.15	0.21	-0.03	-9.83	-40.91	2.13	-2.88	0.52	12.59	-6.89	28.07	-2.39	0.81
2	-0.20	0.74	0.08	-0.01	-6.60	-38.63	-8.57	-14.76	-5.74	-4.99	-9.61	18.86	10.24	-6.66
3	-0.18	-0.60	-0.20	0.03	-11.79	7.47	5.02	-13.40	9.78	-8.95	-7.52	3.49	20.42	-0.41
4	-0.41	-0.27	0.00	-0.03	-9.78	21.15	2.43	10.94	9.46	-13.14	-9.70	-21.69	-6.57	6.05
5	0.20	0.09	-0.29	0.05	-10.02	-22.43	-6.26	13.44	-0.66	-28.43	-9.16	-1.21	12.12	-9.65
6	0.29	0.53	-0.38	0.04	-7.16	-0.78	-31.07	0.33	2.15	2.07	-8.67	8.48	18.00	5.21
7	0.57	0.67	0.39	-0.21	-13.63	-31.70	-6.47	14.89	1.29	-7.90	-11.43	23.72	37.06	-10.25
8	-0.22	0.05	0.16	-0.25	-9.74	-8.74	1.45	0.00	1.53	-28.73	-4.03	2.83	-22.67	5.61
9	0.18	-0.41	-0.20	-0.20	-7.22	-10.09	-1.38	8.77	-2.86	-7.57	1.57	3.97	5.45	9.54
10	0.05	0.09	0.37	-0.02	-13.40	-59.87	-8.84	-10.50	-1.81	-14.42	-4.51	-10.16	-8.04	-3.93
11	0.60	0.19	0.38	0.23	-7.81	-43.53	3.63	8.19	-0.42	-12.88	-14.83	18.48	8.18	-5.09
12	-0.17	-0.06	0.39	0.01	-11.88	-22.05	0.63	3.45	2.75	-13.40	-8.24	1.89	38.29	-0.49
13	0.33	0.00	-0.04	0.32	-7.40	-38.45	-47.26	-5.00	2.22	-6.50	-12.88	-22.39	-27.25	-20.00
14	0.97	0.42	0.01	0.11	-5.31	92.66	-6.58	-2.91	-0.32	-16.37	-12.86	14.18	-28.92	0.47
15	-0.48	-0.44	-0.02	-0.28	-7.83	-20.20	-0.09	19.01	5.65	-10.88	-12.68	17.18	-13.09	-3.93
16	-0.02	-0.92	0.38	-0.02	-13.64	-8.82	4.66	0.33	0.22	-7.79	-21.83	41.04	23.90	1.34
17	0.40	0.25	0.02	0.31	-12.56	-32.73	3.90	-1.14	-0.81	-3.94	-12.11	28.50	23.25	2.01
18	-0.40	0.00	0.38	0.45	-13.48	12.24	4.27	3.29	2.87	-9.03	-15.26	12.36	10.35	-3.93
19	0.72	0.24	-0.17	0.26	-13.24	5.91	17.95	9.52	5.89	18.60	-12.14	-0.04	6.02	0.17
20	0.21	0.15	0.39	0.47	-7.19	58.07	-20.60	-12.65	-1.84	3.99	-7.88	15.55	-19.96	5.94
21	-0.38	-0.39	-0.26	-0.12	-6.96	-11.93	-7.20	3.97	8.01	-16.78	-13.76	12.50	-1.68	-9.05
22	-0.35	0.08	0.02	-0.38	-8.96	-27.23	9.20	5.01	-1.95	-10.85	-11.76	15.70	-10.81	0.04
23	-0.03	0.44	0.27	0.17	-13.39	-1.98	-3.75	4.31	2.71	-23.73	-7.52	19.18	1.41	0.65
24	0.00	-0.40	-0.25	0.11	-7.92	-21.28	-9.07	6.35	2.15	-13.76	-9.76	12.81	17.81	-7.18
25	-0.30	0.95	0.14	-0.05	-6.87	-29.83	0.70	-2.46	3.99	-10.88	16.12	28.69	-13.86	3.73
26	0.04	-0.71	0.19	0.13	-13.42	-8.86	-23.55	24.86	-1.85	-14.39	-7.52	17.83	11.29	-1.09
27	-0.94	0.32	-0.36	0.41	-10.87	10.19	-2.16	-25.69	0.39	0.91	-12.88	6.59	15.93	1.99
28	-0.15	0.69	-0.08	-0.11	-12.70	-32.18	-4.85	4.66	6.77	-13.43	-6.14	-16.12	10.95	19.35
29	0.00	0.18	-0.14	-0.29	-8.79	-33.83	-9.13	9.68	2.26	-24.97	-32.76	29.40	31.87	9.93
30	-0.79	-0.05	-0.39	-0.17	-7.91	4.82	-1.87	-9.63	0.92	-18.30	-12.88	15.70	25.47	-1.29
31	0.14	0.05	-0.20	-0.10	-13.27	-38.65	4.12	7.11	0.57	-15.69	-16.45	19.17	28.12	-1.06
32	0.03	0.19	-0.36	0.10	-8.55	-49.51	-8.43	15.81	-1.16	-20.33	-5.19	17.66	4.86	-1.52
33	-0.01	-0.26	-0.23	0.08	-14.72	7.25	8.65	7.11	-0.73	-15.41	-8.68	4.15	4.18	-1.59
34	0.20	0.58	0.18	0.06	-14.86	6.80	-11.69	0.65	1.22	39.68	-16.49	4.33	29.16	-3.27
35	0.44	-0.26	-0.27	-0.26	-7.33	2.76	-4.01	1.35	2.74	-11.91	-0.08	-7.01	10.70	1.22
36	0.68	-0.17	-0.02	0.10	-15.64	-33.76	0.65	-0.96	7.01	-23.81	-10.63	-13.51	5.07	0.33
37	0.26	-0.30	0.15	-0.13	-16.22	6.28	1.34	-19.84	-0.02	-6.00	33.98	9.94	10.35	14.70

where fi: interfacial friction factor, CDd: Drag Coefficient for a Droplet, HTCsingle: Single Phase Heat Transfer Coefficient, HTCsub: Subcooled Nucleate Boiling Heat Transfer Coefficient, HTCsat: Saturated Boiling Heat Transfer Coefficient

Table 6.33. Sample Table for Critical Power (Cont.)

ID	Pressure	Flow Rate	Inlet Enthalpy	Flow Area	Grid Loss Coefficient	Mixing	fi	CDd	HTCsingle	HTCsub	HTCsat	Entrainment Rate	De-entrainment Rate	Critical Heat Flux
38	0.15	0.66	0.31	0.20	-16.33	-31.53	4.65	-10.46	0.20	-19.31	-6.36	32.91	20.01	-3.93
39	0.43	0.15	-0.19	-0.40	-7.68	25.61	-5.71	-0.67	1.21	-15.86	-9.01	10.48	34.31	-3.79
40	-0.37	-0.12	-0.13	-0.07	-8.11	-28.40	-16.19	-0.27	1.07	-13.05	-16.17	-28.96	20.67	0.41
41	0.27	-0.47	-0.12	0.10	-15.50	-21.14	6.22	-14.14	1.22	1.86	-9.96	-16.91	43.54	3.83
42	0.62	-0.26	0.06	0.09	-8.50	-59.87	5.02	0.98	2.61	-17.05	-17.63	3.64	-2.53	1.70
43	0.15	-0.09	-0.33	-0.20	-8.26	18.33	-25.79	12.20	-1.56	25.66	-0.57	-8.40	18.40	3.86
44	-0.40	0.03	-0.19	-0.20	-10.74	-22.03	-8.64	-1.57	0.58	-10.16	-32.76	-22.99	-22.53	2.91
45	0.01	0.61	0.12	-0.12	-17.00	4.16	-3.27	23.87	-0.33	-17.67	-3.74	23.48	10.47	-6.86
46	0.06	0.55	-0.36	0.28	-7.09	-2.31	-17.94	-8.68	5.77	-13.79	-15.65	26.23	5.22	-6.17
47	0.29	0.27	0.39	-0.02	-5.35	12.43	-20.37	-6.24	4.65	-6.84	-7.13	-6.85	-9.13	6.72
48	0.15	-0.36	0.26	0.14	-11.77	0.97	-3.20	-3.02	-3.83	-4.99	-8.63	9.96	11.37	-0.36
49	0.11	0.55	-0.05	0.05	-8.70	17.34	1.17	5.46	-2.97	12.36	-5.73	27.68	15.46	-4.72
50	-0.58	0.04	-0.31	0.08	-6.85	10.97	0.63	8.55	0.57	-25.61	1.26	34.18	11.55	3.46
51	-0.08	-0.07	0.21	0.30	-10.73	-29.92	-13.88	12.99	6.85	-27.53	0.15	43.57	17.02	-0.65
52	-0.58	0.31	0.12	0.15	-8.52	-59.87	9.36	-1.25	7.31	-28.92	-2.75	-9.72	7.53	4.96
53	0.62	0.82	-0.25	-0.18	-13.21	-0.04	-8.82	1.41	-1.17	-19.92	-14.67	3.92	-11.85	-2.06
54	0.71	-0.36	0.11	-0.07	-12.02	-31.56	-4.22	-2.26	0.14	-32.76	39.68	31.89	31.98	2.05
55	-0.35	0.94	0.35	-0.07	-12.34	23.10	7.29	-8.79	-1.67	-17.77	-15.30	-4.60	31.82	-6.99
56	-0.17	0.80	0.29	0.35	-13.34	-8.79	5.39	5.60	0.81	-18.63	39.78	8.38	25.18	-5.64
57	-0.11	-0.24	0.07	0.17	-6.74	14.11	1.55	12.46	7.27	-6.64	-11.98	28.03	-16.34	2.68
58	-0.20	0.28	-0.10	-0.03	-12.30	-15.93	2.13	-10.06	3.72	13.04	-1.13	7.82	21.58	-3.07
59	0.13	0.07	0.09	-0.02	-8.91	23.23	10.91	23.07	8.40	-3.54	-11.01	29.92	25.55	-5.27

where fi: interfacial friction factor, CDd: Drag Coefficient for a Droplet, HTCsingle: Single Phase Heat Transfer Coefficient, HTCsub: Subcooled Nucleate Boiling Heat Transfer Coefficient, HTCsat: Saturated Boiling Heat Transfer Coefficient

17. **Uncertainty Parameter Table:** Uncertainty parameter table shows the ratio of the uncertainty parameters' change in Table 6.34.

Table 6.34. Uncertainty Parameter Table for Critical Power

ID	Pressure	Flow Rate	Inlet Enthalpy	Flow Area	Grid Loss Coefficient	Mixing	fi	CDd	HTCsingle	HTCsub	HTCsat	Entrainment Rate	De-entrainment Rate	Critical Heat Flux
1	1.006	0.998	1.002	1.000	0.902	0.591	1.021	0.971	1.005	1.126	0.931	1.281	0.976	1.008
2	0.998	1.007	1.001	1.000	0.934	0.614	0.914	0.852	0.943	0.950	0.904	1.189	1.102	0.933
3	0.998	0.994	0.998	1.000	0.882	1.075	1.050	0.866	1.098	0.910	0.925	1.035	1.204	0.996
4	0.996	0.997	1.000	1.000	0.902	1.211	1.024	1.109	1.095	0.869	0.903	0.783	0.934	1.060
5	1.002	1.001	0.997	1.000	0.900	0.776	0.937	1.134	0.993	0.716	0.908	0.988	1.121	0.903
6	1.003	1.005	0.996	1.000	0.928	0.992	0.689	1.003	1.021	1.021	0.913	1.085	1.180	1.052
7	1.006	1.007	1.004	0.998	0.864	0.683	0.935	1.149	1.013	0.921	0.886	1.237	1.371	0.898
8	0.998	1.001	1.002	0.998	0.903	0.913	1.014	1.000	1.015	0.713	0.960	1.028	0.773	1.056
9	1.002	0.996	0.998	0.998	0.928	0.899	0.986	1.088	0.971	0.924	1.016	1.040	1.055	1.095
10	1.000	1.001	1.004	1.000	0.866	0.401	0.912	0.895	0.982	0.856	0.955	0.898	0.920	0.961
11	1.006	1.002	1.004	1.002	0.922	0.565	1.036	1.082	0.996	0.871	0.852	1.185	1.082	0.949
12	0.998	0.999	1.004	1.000	0.881	0.779	1.006	1.034	1.027	0.866	0.918	1.019	1.383	0.995
13	1.003	1.000	1.000	1.003	0.926	0.616	0.527	0.950	1.022	0.935	0.871	0.776	0.728	0.800
14	1.010	1.004	1.000	1.001	0.947	1.927	0.934	0.971	0.997	0.836	0.871	1.142	0.711	1.005
15	0.995	0.996	1.000	0.997	0.922	0.798	0.999	1.190	1.057	0.891	0.873	1.172	0.869	0.961
16	1.000	0.991	1.004	1.000	0.864	0.912	1.047	1.003	1.002	0.922	0.782	1.410	1.239	1.013
17	1.004	1.002	1.000	1.003	0.874	0.673	1.039	0.989	0.992	0.961	0.879	1.285	1.232	1.020
18	0.996	1.000	1.004	1.005	0.865	1.122	1.043	1.033	1.029	0.910	0.847	1.124	1.103	0.961
19	1.007	1.002	0.998	1.003	0.868	1.059	1.179	1.095	1.059	1.186	0.879	1.000	1.060	1.002
20	1.002	1.002	1.004	1.005	0.928	1.581	0.794	0.873	0.982	1.040	0.921	1.155	0.800	1.059
21	0.996	0.996	0.997	0.999	0.930	0.881	0.928	1.040	1.080	0.832	0.862	1.125	0.983	0.909
22	0.997	1.001	1.000	0.996	0.910	0.728	1.092	1.050	0.980	0.891	0.882	1.157	0.892	1.000
23	1.000	1.004	1.003	1.002	0.866	0.980	0.962	1.043	1.027	0.763	0.925	1.192	1.014	1.007
24	1.000	0.996	0.997	1.001	0.921	0.787	0.909	1.063	1.021	0.862	0.902	1.128	1.178	0.928
25	0.997	1.009	1.001	1.000	0.931	0.702	1.007	0.975	1.040	0.891	1.161	1.287	0.861	1.037
26	1.000	0.993	1.002	1.001	0.866	0.911	0.764	1.249	0.982	0.856	0.925	1.178	1.113	0.989
27	0.991	1.003	0.996	1.004	0.891	1.102	0.978	0.743	1.004	1.009	0.871	1.066	1.159	1.020
28	0.999	1.007	0.999	0.999	0.873	0.678	0.951	1.047	1.068	0.866	0.939	0.839	1.109	1.194
29	1.000	1.002	0.999	0.997	0.912	0.662	0.909	1.097	1.023	0.750	0.672	1.294	1.319	1.099
30	0.992	1.000	0.996	0.998	0.921	1.048	0.981	0.904	1.009	0.817	0.871	1.157	1.255	0.987
31	1.001	1.000	0.998	0.999	0.867	0.614	1.041	1.071	1.006	0.843	0.835	1.192	1.281	0.989
32	1.000	1.002	0.996	1.001	0.915	0.505	0.916	1.158	0.988	0.797	0.948	1.177	1.049	0.985
33	1.000	0.997	0.998	1.001	0.853	1.072	1.087	1.071	0.993	0.846	0.913	1.042	1.042	0.984
34	1.002	1.006	1.002	1.001	0.851	1.068	0.883	1.007	1.012	1.397	0.835	1.043	1.292	0.967
35	1.004	0.997	0.997	0.997	0.927	1.028	0.960	1.014	1.027	0.881	0.999	0.930	1.107	1.012
36	1.007	0.998	1.000	1.001	0.844	0.662	1.007	0.990	1.070	0.762	0.894	0.865	1.051	1.003

where fi: interfacial friction factor, CDd: Drag Coefficient for a Droplet, HTCsingle: Single Phase Heat Transfer Coefficient, HTCsub: Subcooled Nucleate Boiling Heat Transfer Coefficient, HTCsat: Saturated Boiling Heat Transfer Coefficient

Table 6.34. Uncertainty Parameter Table for Critical Power(Cont.)

ID	Pressure	Flow Rate	Inlet Enthalpy	Flow Area	Grid Loss Coefficient	Mixing	fi	CDd	HTCsingle	HTCsub	HTCsat	Entrainment Rate	De-entrainment Rate	Critical Heat Flux
37	1.003	0.997	1.002	0.999	0.838	1.063	1.013	0.802	1.000	0.940	1.340	1.099	1.104	1.147
38	1.002	1.007	1.003	1.002	0.837	0.685	1.046	0.895	1.002	0.807	0.936	1.329	1.200	0.961
39	1.004	1.002	0.998	0.996	0.923	1.256	0.943	0.993	1.012	0.841	0.910	1.105	1.343	0.962
40	0.996	0.999	0.999	0.999	0.919	0.716	0.838	0.997	1.011	0.870	0.838	0.710	1.207	1.004
41	1.003	0.995	0.999	1.001	0.845	0.789	1.062	0.859	1.012	1.019	0.900	0.831	1.435	1.038
42	1.006	0.997	1.001	1.001	0.915	0.401	1.050	1.010	1.026	0.829	0.824	1.036	0.975	1.017
43	1.001	0.999	0.997	0.998	0.917	1.183	0.742	1.122	0.984	1.257	0.994	0.916	1.184	1.039
44	0.996	1.000	0.998	0.998	0.893	0.780	0.914	0.984	1.006	0.898	0.672	0.770	0.775	1.029
45	1.000	1.006	1.001	0.999	0.830	1.042	0.967	1.239	0.997	0.823	0.963	1.235	1.105	0.931
46	1.001	1.005	0.996	1.003	0.929	0.977	0.821	0.913	1.058	0.862	0.844	1.262	1.052	0.938
47	1.003	1.003	1.004	1.000	0.947	1.124	0.796	0.938	1.046	0.932	0.929	0.931	0.909	1.067
48	1.001	0.996	1.003	1.001	0.882	1.010	0.968	0.970	0.962	0.950	0.914	1.100	1.114	0.996
49	1.001	1.005	1.000	1.001	0.913	1.173	1.012	1.055	0.970	1.124	0.943	1.277	1.155	0.953
50	0.994	1.000	0.997	1.001	0.931	1.110	1.006	1.086	1.006	0.744	1.013	1.342	1.115	1.035
51	0.999	0.999	1.002	1.003	0.893	0.701	0.861	1.130	1.069	0.725	1.001	1.436	1.170	0.994
52	0.994	1.003	1.001	1.002	0.915	0.401	1.094	0.987	1.073	0.711	0.973	0.903	1.075	1.050
53	1.006	1.008	0.997	0.998	0.868	1.000	0.912	1.014	0.988	0.801	0.853	1.039	0.882	0.979
54	1.007	0.996	1.001	0.999	0.880	0.684	0.958	0.977	1.001	0.672	1.397	1.319	1.320	1.021
55	0.996	1.009	1.003	0.999	0.877	1.231	1.073	0.912	0.983	0.822	0.847	0.954	1.318	0.930
56	0.998	1.008	1.003	1.003	0.867	0.912	1.054	1.056	1.008	0.814	1.398	1.084	1.252	0.944
57	0.999	0.998	1.001	1.002	0.933	1.141	1.015	1.125	1.073	0.934	0.880	1.280	0.837	1.027
58	0.998	1.003	0.999	1.000	0.877	0.841	1.021	0.899	1.037	1.130	0.989	1.078	1.216	0.969
59	1.001	1.001	1.001	1.000	0.911	1.232	1.109	1.231	1.084	0.965	0.890	1.299	1.256	0.947

where fi: interfacial friction factor, CDd: Drag Coefficient for a Droplet, HTCsingle: Single Phase Heat Transfer Coefficient, HTCsub: Subcooled Nucleate Boiling Heat Transfer Coefficient, HTCsat: Saturated Boiling Heat Transfer Coefficient

18. Code Inputs: Code inputs were already discussed in 18th element of the void distribution uncertainty analysis section.

19. Code: This section was already described in the 19th element of the void distribution uncertainty analysis section.

20. Outputs: A special critical output file was designed and implemented into COBRA-TF (RBGHT). This output file's name is Deck.fth_cp. This special file extracts the information of critical power (MW), dry-out elevation (inches) and uncertainty parameter ratios from the COBRA-TF results. Figure 6.166 shows the format of this file.

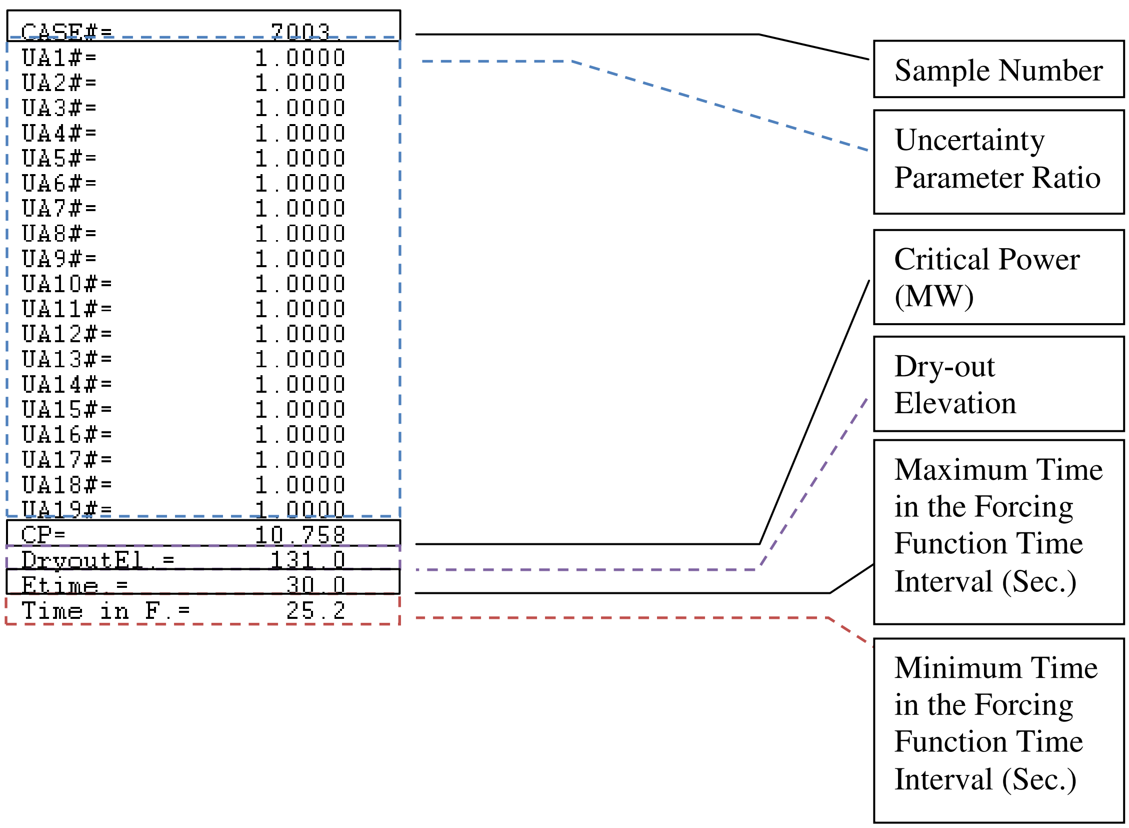

Figure 6.166. The Format of Critical Power Output File (Deck.fth_cp)

21-23. Master Program, UA Database and Uncertainty Comparison Methods: These three elements have been already discussed in the implementation of void distribution uncertainty analysis. For the uncertainty comparison methods, the accuracy of the critical power was obtained from the experimental database. The absolute accuracies of the critical power is 1.5%.

24. **Uncertainty Comparison Tables:** This table includes the comparison between predicted and measured values (whose output are given in Appendix-4 in section 6.4.4) of critical power (Table 6.35) as well as the dry-out elevation (Table 6.36). Table 6.36 does not include coverage ratio because the experimental uncertainty is such a high value (512mm as shown in Figure 4.8) that the coverage ratio covers all the predicted uncertainties. Therefore, coverage ratio was not calculated for the dry-out elevation.

Table 6.35. Uncertainty Comparison Tables of Critical Power

Test Number	Mean Value of Predicted Critical Power (MW)	Mean Relative Bias of Critical Power	Maximum Bias of Critical Power	Standard Deviation of Predicted Critical Power (MW)	Coverage Ratio of Critical Power	Measured Critical Power (MW)
SA 603901	2.81	-0.12	0.254	0.194	0.034	3.2
SA 505900	5.14	-0.14	0.292	0.41	0.051	5.98
SA 512800	10.52	-0.05	0.127	0.17	0.136	11.09
SA 812800	10.3	0.15	0.205	0.15	0.017	8.9

Table 6.36. Uncertainty Comparison Tables of Dry-out Elevation

Test Number	Mean Value of Predicted Dry-out Elevation (inches)	Mean Relative Bias of Dry-out Elevation	Maximum Bias of Dry-out Elevation	Standard Deviation of Predicted Dry-out Elevation (inches)	Measured Dry-out Elevation (inches)
SA 603901	126.13	-0.09	0.229	7.44	138.62
SA 505900	128.23	-0.075	0.264	11.79	138.62
SA 512800	130.59	-0.06	0.091	1.47	138.62
SA 812800	100.4	0.16	0.203	21.05	118.47

25. **Sensitivity Parameter Table:** Sensitivity parameter table (Table 6.37) contains the uncertainty parameters and corresponding input uncertainties. Input uncertainties are determined with taking the maximum and minimum of each column in Table 6.34. This table is used to perform sensitivity analysis by changing one parameter at a time. This allows the analyst to see which uncertainty parameter significantly affects the output uncertainty parameter (or ranking of the input uncertainty parameters).

Table 6.37. Sensitivity Parameter Table for Critical Power

ID	Pressure	Flow rate	Inlet Enthalpy	Flow Area	Grid Loss Coefficient	Mixing Coefficient	fi	CDd	HTCsingle	HTCsub	HTCsat	Entrainment	De-entrainment	Critical Heat Flux
Max	1.01	1.01	1.004	1.005	0.95	1.93	1.18	1.25	1.10	1.40	1.40	1.44	1.44	1.19
Min	0.99	0.99	0.996	0.996	0.83	0.40	0.53	0.74	0.94	0.67	0.67	0.71	0.71	0.80

where fi: interfacial friction factor, CDb: Drag Coefficient for a Bubble, CDd: Drag Coefficient for a Droplet, HTCsingle: Single Phase Heat Transfer Coefficient, HTCsub: Subcooled Nucleate Boiling Heat Transfer Coefficient, HTCsat: Saturated Boiling Heat Transfer Coefficient, Entrainment: Entrainment rate, De-entrainment: De-entrainment rate

26. **Sensitivity Comparison Results**: This element shows the sensitivity analysis results. The uncertainty parameter was changed based on sensitivity parameter table. The

absolute maximum change on the critical power and dry-out elevation are demonstrated in this comparison results. Figure 6.167 - 6.170 demonstrate the critical power change from the nominal predicted critical power for the cases SA-603901, SA-505900, SA-512800 and SA-812800 respectively. Figure 6.171-6.174 demonstrate the dry-out elevation change from the nominal predicted dry-out elevation for the cases SA-603901, SA-505900, SA-512800 and SA-812800 respectively.

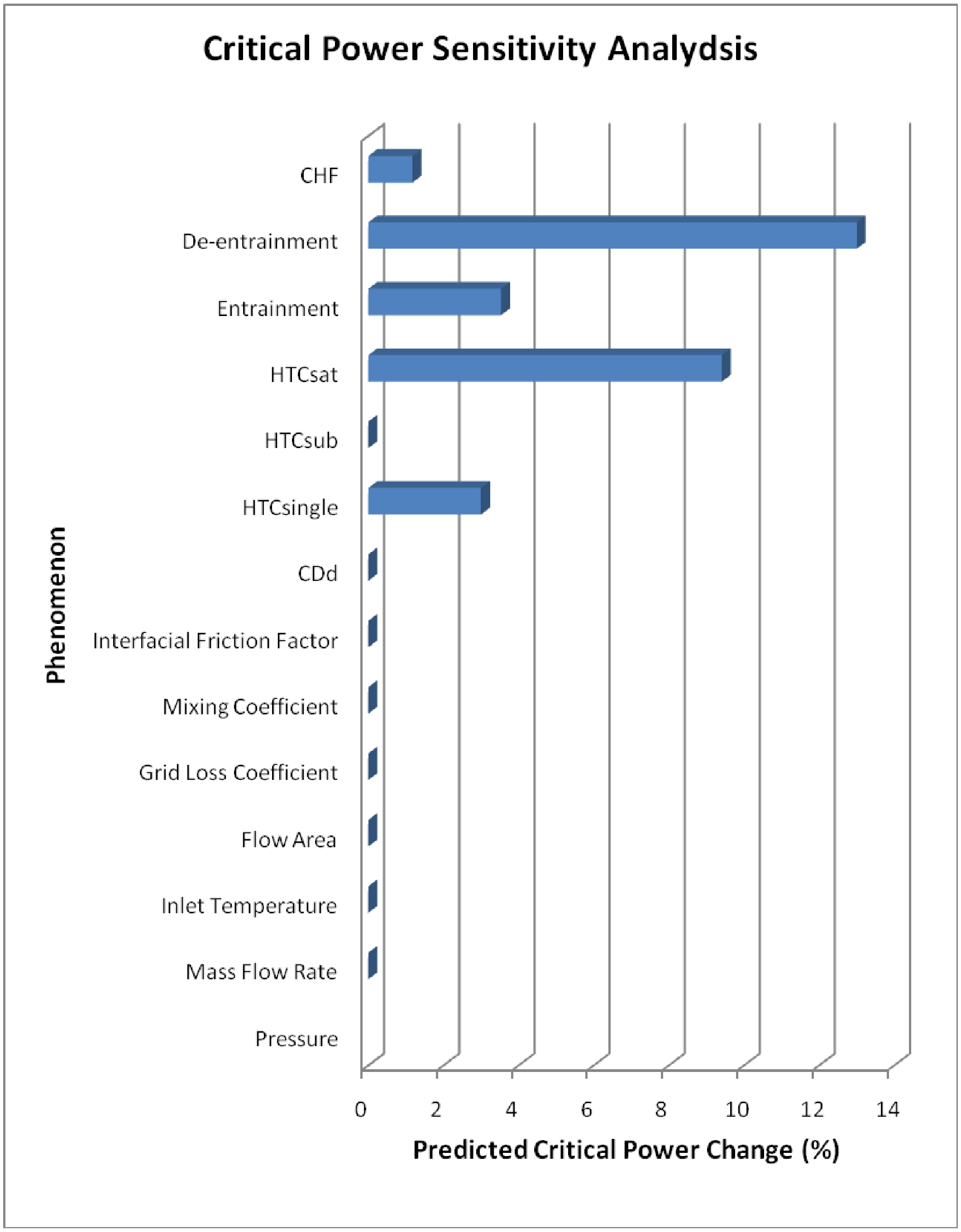

Figure 6.167. Sensitivity Result of Critical Power for the Test Case SA-603901

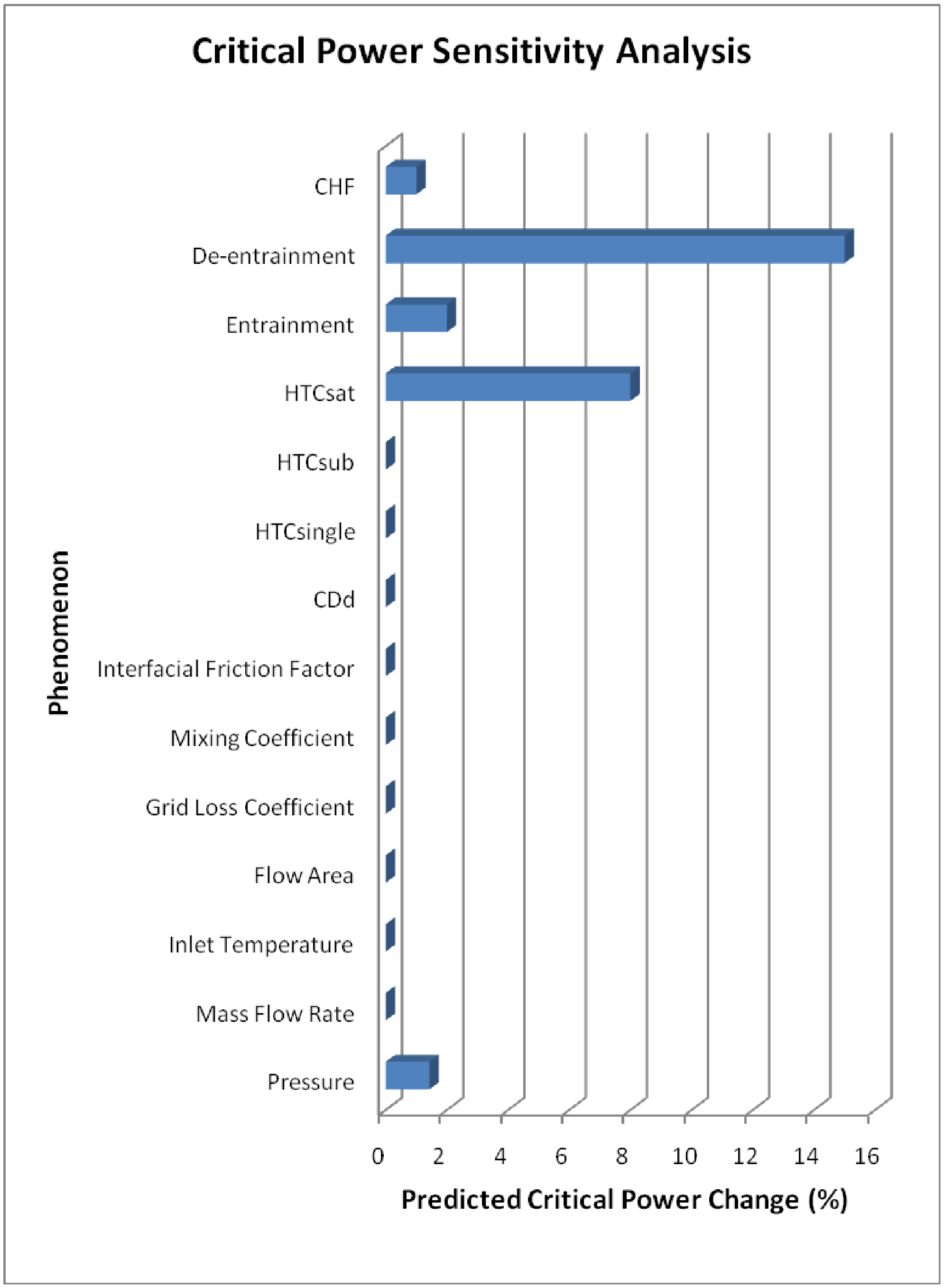

Figure 6.168. Sensitivity Result of Critical Power for the Test Case SA-505900

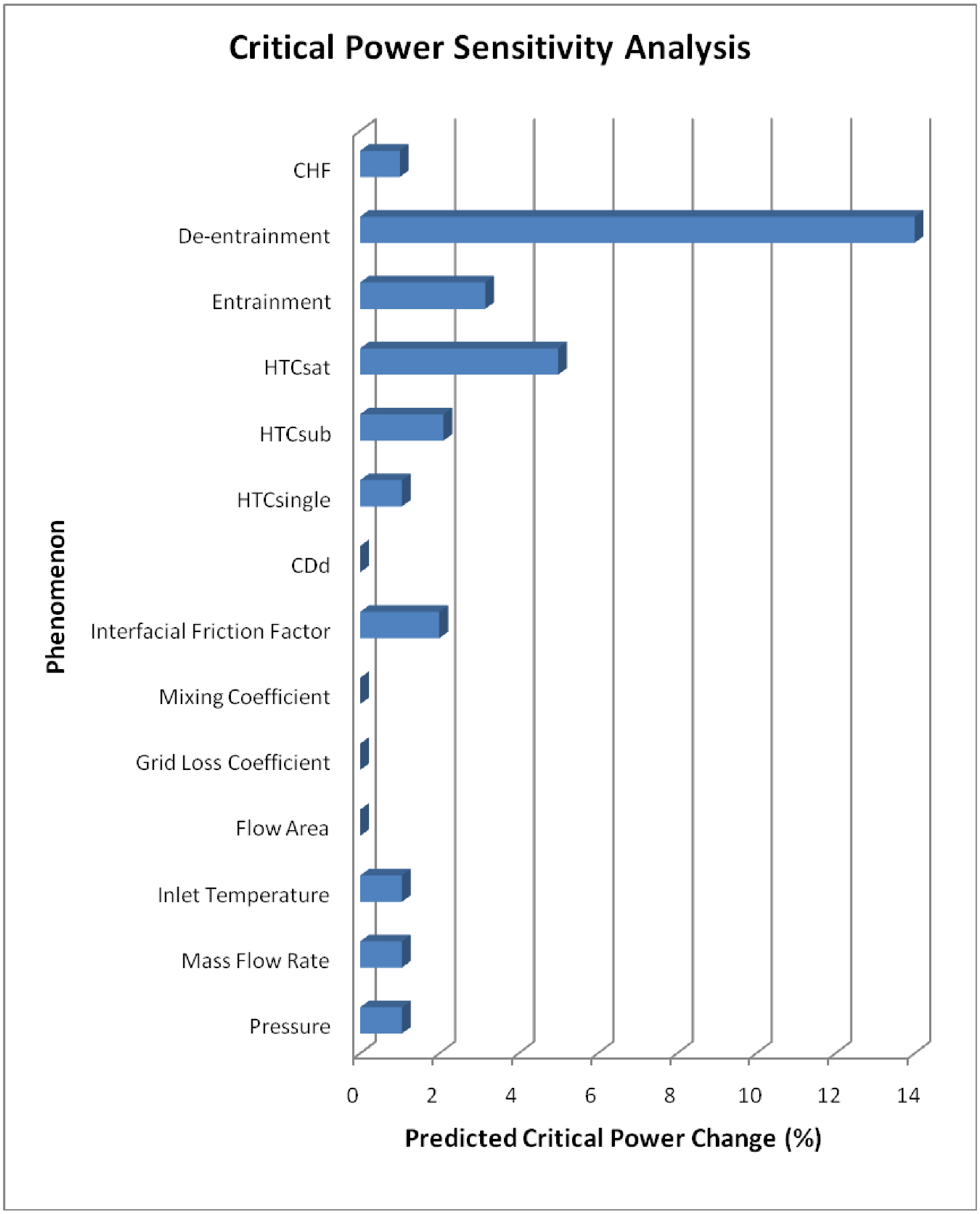

Figure 6.169. Sensitivity Result of Critical Power for the Test Case SA-512800

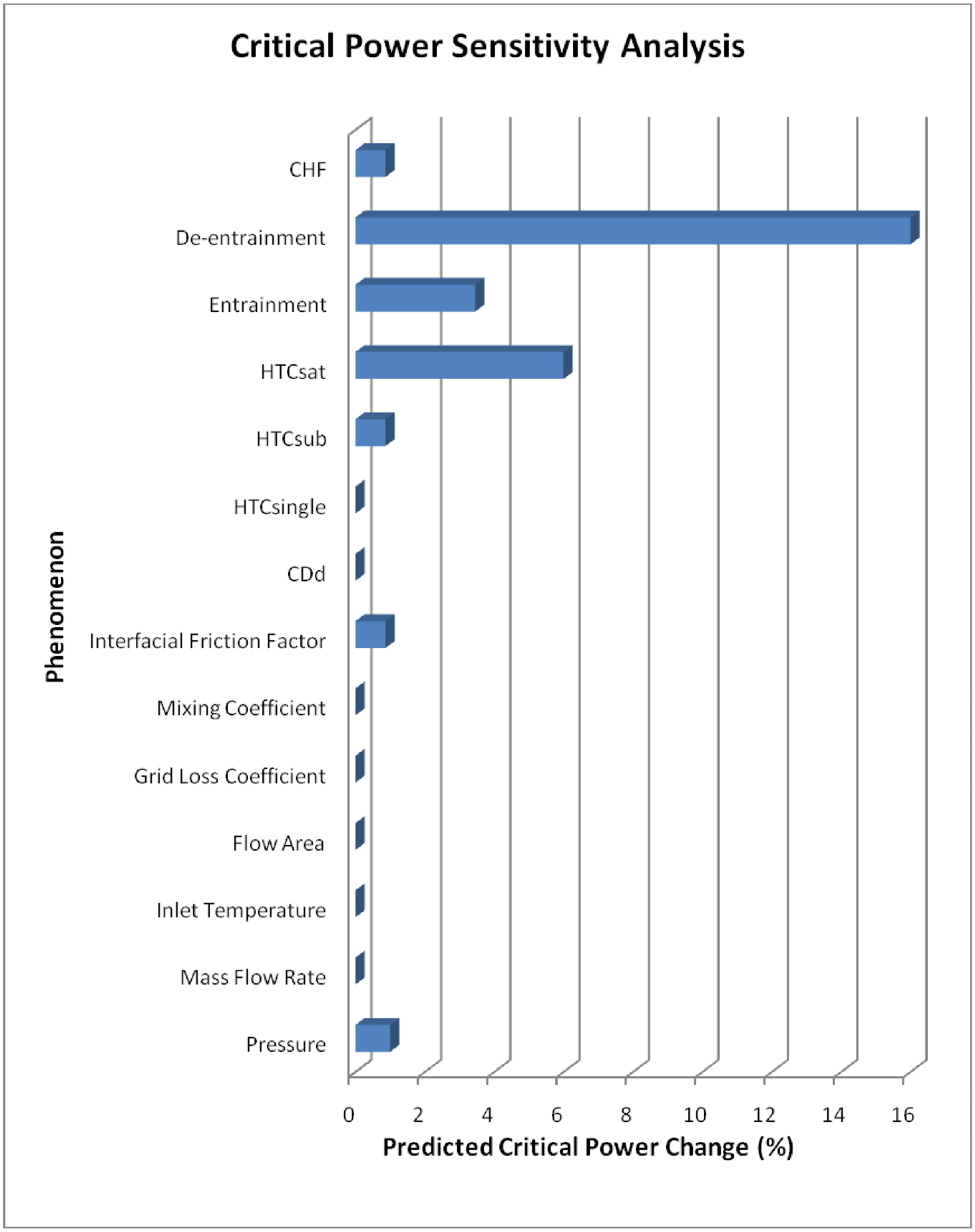

Figure 6.170. Sensitivity Result of Critical Power for the Test Case SA-812800

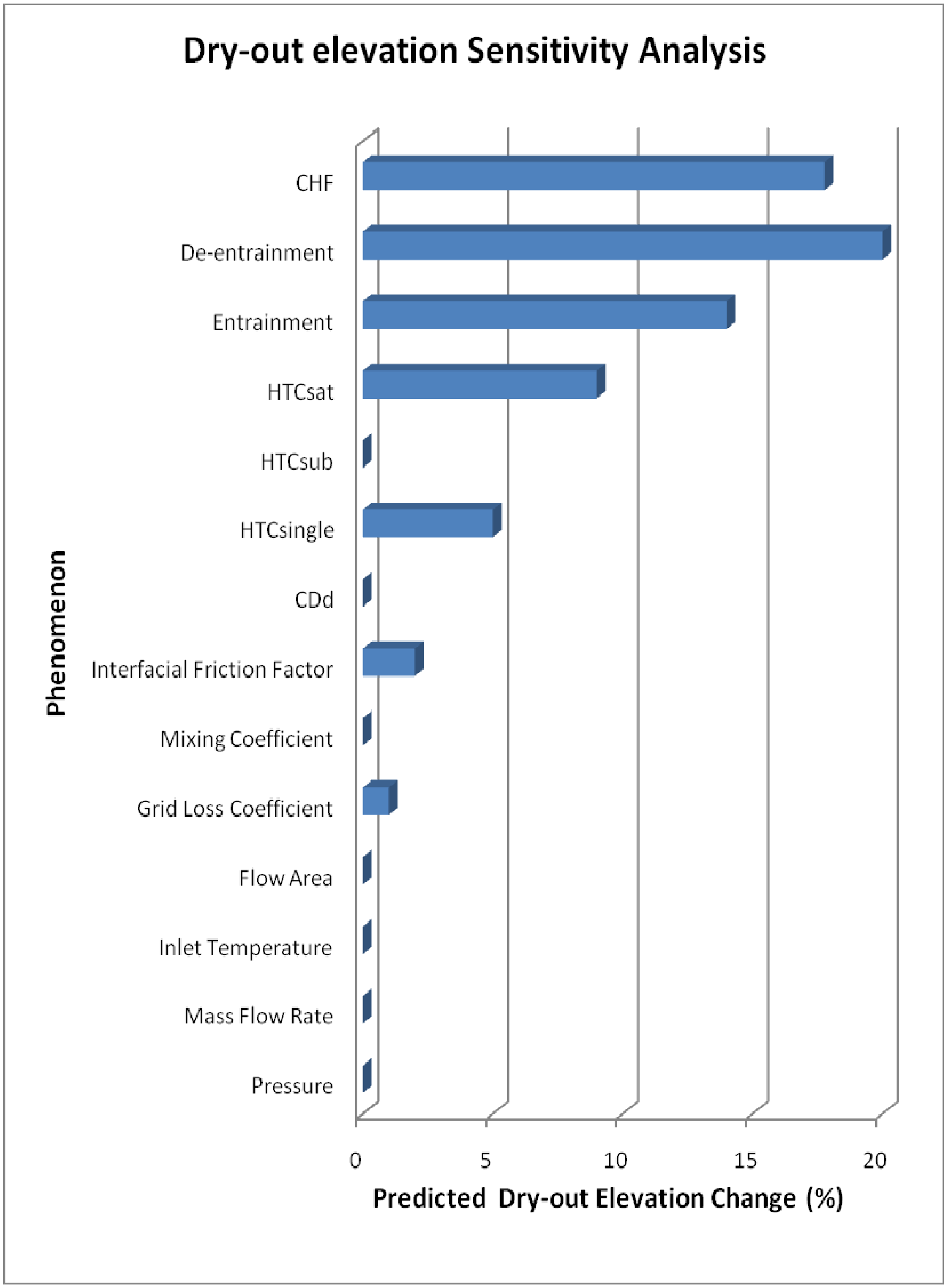

Figure 6.171. Sensitivity Result of Dry-out Elevation for the Test Case SA-603901

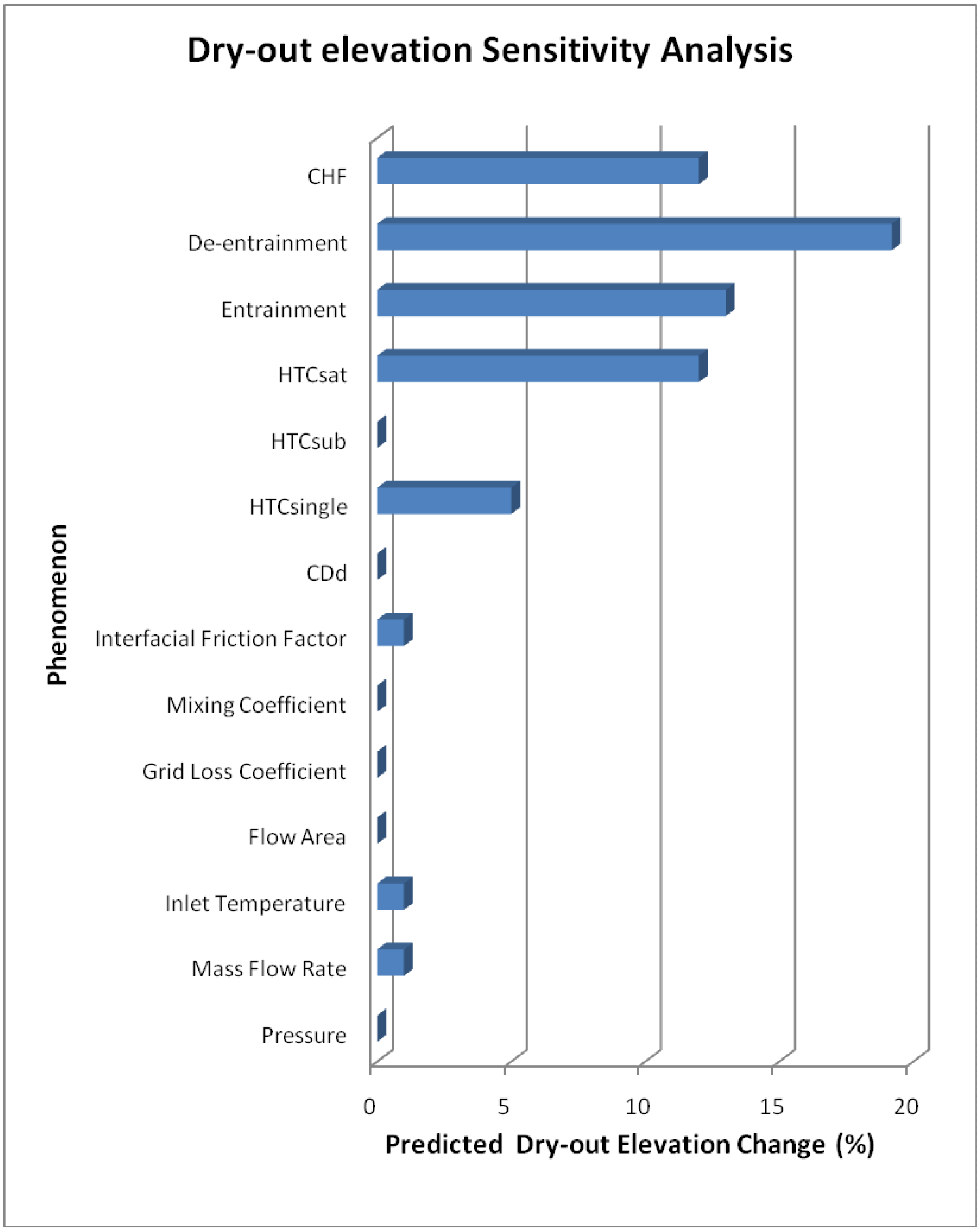

Figure 6.172. Sensitivity Result of Dry-out Elevation for the Test Case SA-505900

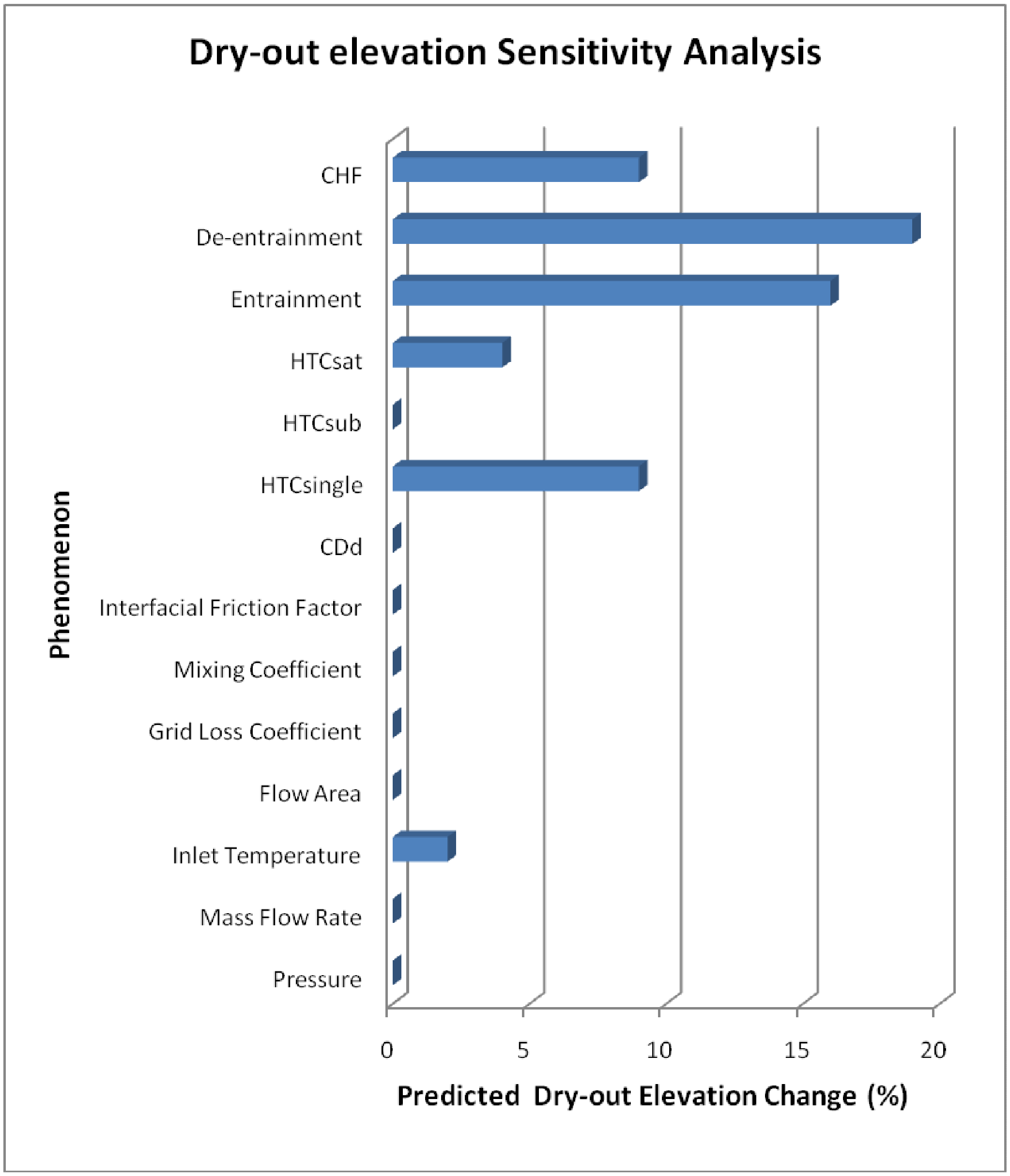

Figure 6.173. Sensitivity Result of Dry-out Elevation for the Test Case SA-512800

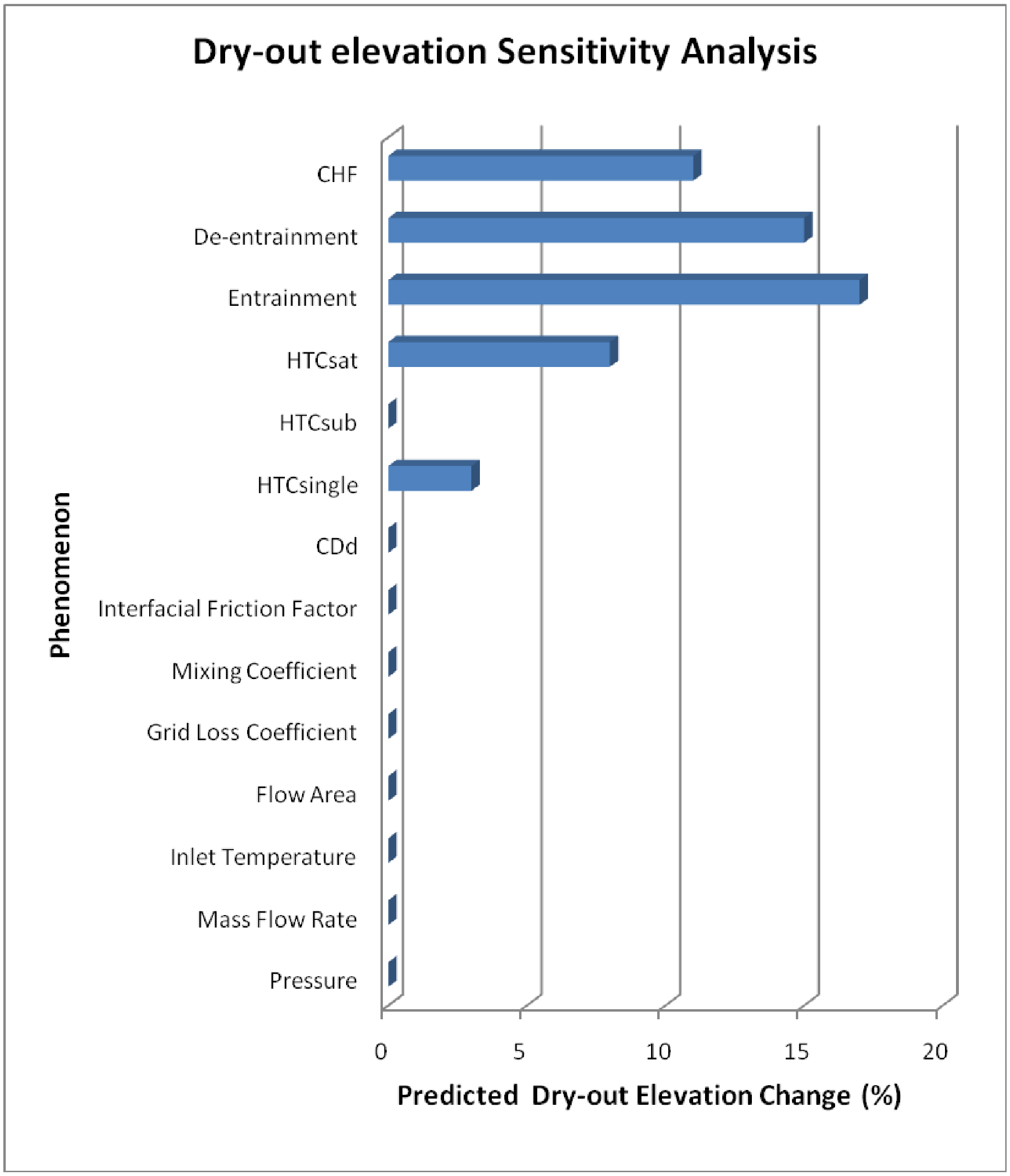

Figure 6.174. Sensitivity Result of Dry-out Elevation for the Test Case SA-812800

The uncertainty and sensitivity analyses of the steady state void distribution and critical power were completed with these plots. Next chapter discuses the results of the uncertainty and sensitivity analyses results.

All the comparisons tables and figures (including the effects of dominant phenomena on each subchannel and bundle void fractions, critical power as well as dry-out elevation) were provided in Chapter 6. According to these figures and tables, the following conclusions were observed:

- The mean bias of most of the subchannels around the water rod and corner subchannels are higher than the others.

- The maximum bias of most of the corner and side subchannels, subchannels near water rod and their adjacent subchannels, are higher than others.

- Standard deviation of most of the subchannels around water rod and corner subchannels are higher than the other ones.

- Coverage ratio of most of the subchannels which are adjacent to the side, corner and central (near the water rod) subchannels are higher than the others.

- The dominant phenomena for all of the subchannels are the de-entrainment of droplets and entrainment rate. Besides, drag coefficient for bubble flow regime can be countable as the third dominant phenomenon. These ranking is similar for the bundle void fraction as well.

- Average bias is smaller than 16% for both critical power and dry-out elevation.

- De-entrainment, saturated heat transfer coefficient, entrainment and critical heat flux phenomena are the dominant phenomena for the critical power predictions.

De-entrainment, entrainment saturated heat transfer coefficient, single heat transfer coefficients and critical heat flux are the dominant phenomena for the dry-out elevation prediction.

6.3. Phenomena Identification Ranking Table Finalization

PIRT tables are developed by using expert groups. However, the dominant phenomena could be different at the end of the uncertainty analysis. This section discusses the differences between the dominant phenomena obtained by the uncertainty analysis and the dominant phenomena developed by the expert groups with PIRT. This comparison is called as finalization of the PIRT.

6.3.1. Finalization of the PIRT for the Void Distribution

The highly ranked phenomena selected for the steady state void distribution are flow rate, power, sub-channel flow area, mixing coefficient and interfacial friction factor.

- Flow Rate: Because it has a small accuracy (1%), this parameter is not dominant at the sensitivity analysis.
- Power: Because it has a small accuracy (1.5%), this parameter is not dominant at the sensitivity analysis.
- Sub-channel flow area: Because it has a small accuracy (0.5%), this parameter is not dominant at the sensitivity analysis.

- Mixing Coefficient: Mixing coefficient has a small uncertainty (standard deviation is 13%) and it is a small constant value for high void fractions. Therefore, it is not dominant at the sensitivity analysis.
- Interfacial friction factor: Since interfacial friction factor has a small uncertainty (~20%), it is as dominant as de-entrainment and entrainment.

Finally, the results of the uncertainty and sensitivity results show whether an uncertainty parameter is dominant or not depends on the accuracy of the individual uncertainty parameter's accuracy.

6.3.2. Finalization of the PIRT for the Critical Power

The highly ranked phenomena selected for the steady state void distribution are flow rate, power, sub-channel flow area, mixing coefficient, interfacial friction factor, entrainment and de-entrainment rate and critical heat flux.

- Flow Rate: Because it has a small accuracy (1%), this parameter is not dominant at the sensitivity analysis.
- Power: Because his parameter was not used as input parameter in the COBRA-TF to predict steady state critical power.
- Sub-channel flow area: Because it has a small accuracy (0.5%), this parameter is not dominant at the sensitivity analysis.

- Mixing Coefficient: Mixing coefficient has a small uncertainty (standard deviation is 13%) and it is a small constant value for high void fractions. Therefore, it is not dominant at the sensitivity analysis.
- Interfacial friction factor: Since interfacial friction factor has a small uncertainty (~20%), it is as dominant as de-entrainment and entrainment. However, it is 6th dominant phenomena on the critical power.
- Entrainment rate: This parameter is dominant at the sensitivity analysis.
- De-entrainment rate: This parameter is dominant at the sensitivity analysis.
- Critical heat flux: This parameter is dominant at the sensitivity analysis.

Finally, the results of the uncertainty and sensitivity results show that whether an uncertainty parameter is dominant or not depends on the accuracy of the individual uncertainty parameter's accuracy.

6.4. References

1. Analysis of FLECHT-SEASET 163-Rod Blocked Bundle Data Using COBRA-TF, NRC/EPRI/ Westinghouse Report No:15, NUREG/CR-4166 EPRI NP-4111 WCAP-10375

2. COBRA/TRAC- A Thermal-Hydraulics Code for Transient Analysis of Nuclear Reactor Vessels and Primary Coolant Systems, NUREG/CR-3046 PNL-4385 Vol.1

3. Aydogan, F. et al., 2007, Phenomena Idenditification Ranking Table for BWR Steady State Void Distribution, (254), Nureth-12 International Conference

4. Richardson, L. F., 1910, The approximate arithmetical solution by finite differences of physical problems including differential equations, with an application to the stresses in a masonry dam". Philosophical Transactions of the Royal Society of London, Series A 210: 307–357

5. Bousbia, A., Kliem, S., Rohde, U., D'Auria, F. and Petruzzi, A., 2006, Uncertainty and sensitivity analyses of the Kozloduy pump trip test using coupled thermal–hydraulic 3D kinetics code, , Nuclear Engineering and Design 236 (2006) 1240–1255

6. Frepoli C. AP1000, 2005, Best Estimate Large Break LOCA Analysis Performed with the Westinghouse Automated Statistical Treatment of Uncertainty Method, ICONE13-50115

7. Report of Uncertainty Analysis Methods Study for Advanced Best Estimate Thermal Hydraulic Code Applications, NEA/CSNI/R(97)35

8. U.S. Nuclear Regulatory Commission, Regulatory Guide 1.157 (Task RS 701-4), Best Estimate Calculations of Emergency Core Cooling Performance

9. Rogers, J.T. and Rosehart, R.G., 1972, mixing by turbulent interchange in fuel bundles. Correlations and inferences, AIChE-ASME Heat Transfer Conference, 72-HT-53

10. Neykov, B., Aydogan, F., Hochreiter, L., Ivanov, K. , Utsuno, H. , Fumio, K., Sartori, E., Martin, M., 2005, NUPEC BWR Full-Size Fine-Mesh Bundle Test (BFBT) Benchmark Volume I: Specifications, NEA/NSC/DOC(2005)5

11. Aydogan, F., Hochreiter, L., Ivanov, K., Martin, M., Utsuno, H., Sartori, E., 2007, NUPEC BWR FULL_SIZE FINE-MESH BUNDLE TEST (BFBT) BENCHMARK Volume II: Uncertainty and Sensitivity Analyses of Void Distribution and Critical Power-Specification, NEA/NSC/DOC(2007)21

12. Gaudier, F. and Martin, M., 2006, Uncertainty Analysis: Application to Void Fraction Model, 3rd BFBT Workshop, University of Pisa, Italy

13. Special communication with Dr. Kurshad Muftuoglu in General Electric Company

14. Gilbert, J. S., Williams, K. A., 1983, 2d/3d Program Technical Note Rod Bundle Cross-Flow Study, Energy Division, Los Alamos National Laboratory, Los Alamos, (LA-2D/3D-TN-83-13)

15. Utsuno, H., 2007, Procedure to Calculate a Spacer Loss Coefficient using NUPEC BFBT Data, Presentation in the 4th BFBT Workshop, Paris, France

16. http://www.nea.fr/html/science/egrsltb/BFBT

17. Wallis, G., 1969, One Dimensional Two Phase Flow, McGraw-Hill Book Company

18. Sun, X., Liu, Y., Ozar, B., Ishii, M., Kelly, J. M., 2004, Study on Drag Coefficientsfor Two Groups of Bubbles, ICONE12-49231, Proceedings of ICONE12, 12th International Conference on Nuclear Engineering, Virginia USA

19. Ishii, M., Zuber, N., 1979, Drag Coefficient and Relative Velocity in Bubbly, Droplet or Particulate Flows, AIChE Journal (Vol. 25, No, 5), p. 843-855

20. Crowe, C., Sommerfeld, M. and Tsuji, Y.,1998, Multiphase Flows with Droplets and Particles, CRC Press, ISBN: 0-8493-9469-4, p. 67

21. Spring, J. P., McLaughlin, D. M., 2006, Rod Bundle Heat Transfer- Steady State Steam Cooling Experiments, ICONE14-89734, Proceedings of ICONE 14: International Conference on Nuclear Engineering, Florida

22. Weisman, J., 1959, Heat transfer to water flowing parallel to tube bundles, Nucl. Sci. Eng.. 6:79

23. Special communication with James Spring in the Pennsylvania State University

24. CHEN, J., 1966, Correlation for boiling heat transfer to saturated fluids in convective flow, I&EC Process Design and development, Vol 5 No. 3

25. Cousins, L. B., Denton, W. H. and Hewitt, G. F., 1965, Liquid mass transfer in annular two phase flow, Paper C4 presented at the Symposium on two-phase flow volume 2, Exeter, England, p. (401-430)

26. Ishii, M. and Mishima, K., 1982, Liquid transfer and entrainment correlation for droplet-annular flow, 7th International Heat Transfer Conference, Munich

27. Ishii, M. and Mishima, K., 1982, Two Fluid Model and Hydrodynamic Constitutive Relations, Nuclear Engineering and Design 82 (1984) 107-126, North Holland, Amsterdam

28. Wickett, T. , et al., 1998, Report of the uncertainty methods study for advanced best estimate thermal hydraulic code applications, NEA/CSNI/R(97)35

29. Wickett, A.J. and Yadigaroglu, G., 1994, Report of a CSNI workshop on uncertainty analysis methods, NEA/CSNI/R(1994)20/VOL1

30. Avramova, M., 2003, Cobra-TF development, qualification, and application to light water reactor analysis, Msc Thesis, The Pennsylvania State University

31. Biasi, L., et. al., 1967, Studies on burnout part 3. A new correlation for round ducts and uniform heating and its comparison with world data, Energia Nucleare, vol. 14. N.9. September

6.5. Appendix

6.5.1. Appendix-1

BFBT Steady State Void Distribution Data

```
****************************************************************************
EXPERIMENT NUMBER:      4101-01
EXPERIMENT DATE:        91/05/29
EXPERIMENT NAME:        Steady_State_Void_Fraction_Test
M/T FILE :              V02100
EXPERIMENT_CONDITION
Pressure    MPa         0.981
Flow Rate   t/h         10.0
Inlet Subcooling        kJ/kg       50.2
Outlet Quality          %           1.0
EQUIPMENT CONDITION
X-ray_Voltage:          kV          DEN.    160     CT      120
X-ray_Current:          mA          DEN.    19      CT      400
DEN.Beam Width:         mm          1.0
DEN.Sampling Time:      mS          20.0
CT.Sampling Time:       mS          15.0
PROCESS CONDITION(mean value in time)
Pressure    MPa         0.995
Flow Rate   t/h         10.12
Inlet Subcooling        kJ/kg       54.1
Power       MW          0.22
Process data
CH.-No      Name of Process data            TagNo   value
1           Flow of circular system(A)      m^3/h   FT001   11.05
2           Flow of circular system(B)      m^3/h   FT002   0.08
```

3	Flow of circular system(C)	m^3/h	FT003	0.1	
4	Pressure of circular pump-outlet	MPa	PT002	2.83	
5	Temperature at filter-outlet	deg-C	TE003A	167.0	
6	Pressure at inlet	MPa	PT007	1.04	
7	Pressure at outlet	MPa	PT010	1.02	
8	Temperature at inlet	deg-C	TEN007	166.9	
9	Leakage flow through blind alley	m^3/h	FT301	0.000	
10	Local fluid-Temperature(CH1)	deg-C	TE460	167.4	
11	Local fluid-Temperature(CH2)	deg-C	TE461	167.7	
12	2ndary total current	kA	AZ510	2.76	
13	Voltage on heated length(1)	V	VE313A	81.1	
14	Local pressure-difference at inlet	MPa	PT019	0.931	
15	Local pressure-difference at outlet		MPa	PT020	0.894
16	Temperature at outlet	deg-c	TEN010	176.9	
17	Current at inlet(A)	kA	AI511	2.72	
18	Current at inlet(B)	kA	AI512	2.75	
19	Voltage on heated length(2)	V	VE313B	81.4	

RESULT(DEN.)(mean value in time)

DEN.Rod position (mm)

DEN.No	ROD1	ROD2	ROD3	ROD4	ROD5	ROD6	ROD7	ROD8	ROD9
DEN.#1	-65.60	-49.80	-33.50	-17.50	-1.20	15.00	31.20	47.30	63.40
DEN.#2	-64.20	-48.50	-32.20	-16.00	0.20	16.40	32.30	48.70	64.60
DEN.#3	-69.20	-53.30	-37.20	-20.80	-4.70	11.40	27.50	43.80	59.90

DEN.Chordal Averaged void Fraction (%)

DEN.No	ROD1	ROD2	ROD3	ROD4	ROD5	ROD6	ROD7	ROD8	ROD9
DEN.#1	18.0	12.5	3.9	4.1	4.7	3.3	2.9	13.5	13.0
DEN.#2	-0.9	-0.8	-1.1	-1.4	-1.6	-0.3	-1.0	0.0	-1.0
DEN.#3	-1.5	-0.5	-0.4	-2.1	-2.7	0.1	-1.2	-0.6	-0.9

DEN.Cross-sectional Averaged void Fraction(%)

DEN.#1	8.4
DEN.#2	-0.9
DEN.#3	-1.1

RESULT(CT)(mean value in time)

CT Subchannel Averaged void Fraction(%)

y/x	1	2	3	4	5	6	7	8	9
1	12.8	21.9	25.8	26.4	22.2	21.0	21.3	20.2	19.6
2	16.1	34.2	42.5	44.8	41.2	39.6	41.6	42.2	30.1
3	19.9	38.1	49.4	53.1	49.8	48.4	50.7	51.2	32.8
4	20.3	38.7	50.7	47.9	26.5	38.9	49.9	48.5	30.7
5	21.2	37.9	48.0	26.2	0.0	21.4	44.6	45.1	26.9
6	24.0	38.8	50.8	42.7	26.5	38.7	49.0	45.0	25.1
7	28.3	43.1	54.0	48.4	48.9	47.7	52.8	48.5	27.4
8	24.8	41.1	50.0	44.3	40.0	41.5	48.8	44.0	26.5
9	16.0	25.6	27.2	26.7	26.2	26.0	28.7	28.8	20.0

CT Cross-sectional Averaged void Fraction(%)

38.3

Flow area (mm^2)

9463

CT Pixel-void fraction(%)

* This section includes 512x512 pixels void fractions measured by the CT-Scanner

6.5.2. Appendix-2

Source Code of COBRA-TF Changes

Uncertainty Modules were implemented by using Compaq Visual Fortran (Professional Edition 6.1.0)

Defining the Uncertainty Module in Module.f

```
cfth------------------------------------------
cfth  I am defining new module for card-0
cfth
      module fth_module
           include "respar.h"
      real*8 :: fth1, fth2, fth3, fth4, fth5, fth6, fth7, fth8, fth9,
     $         fth10,fth11,fth12,fth13,fth14,fth15,fth16,fth17,fth18,
     $         fth19,fth20  !! UA parameters
      end module fth_module
cfth------------------------------------------
```

Reading Card-0 **in Input.f**

```
cfth  UA parameters module
      use fth_module
 read(iin,10045) fth1,fth2,fth3,fth4,fth5,fth6,fth7,fth8,fth9,fth10
           read(iin,10045) fth11,fth12,fth13,fth14,fth15,fth16,fth17,
     $           fth18,fth19,fth20
           write (*,*) "UA Parameters -Fatih Aydogan-",fth1, fth2,fth3,fth4,
     $         fth5,fth6,fth7,fth8,fth9,fth10,fth11,fth12,fth13,
     $         fth14,fth15,fth16,fth17,fth18,fth19,fth20
10045 format(10f7.5)
```

Changing the values of Pressure, Mass Flow Rate, Flow Area and Inlet Enthalpy with Uncertainty Parameter Ratio in Setin.f

<u>Changing the pressure</u>

```
            pref = pref*fth1  //vessel pressure in card 1

            pvalue(n) = pvalue(n)*fth1 //inlet pressure in card 13

            cfth    changing the pres-xvalue(n)-card13- with the UA       ***

            xvalue(n) = xvalue(n)*fth1 /output pressure in card 13
```

<u>Changing the inlet enthalpy</u>

```
            hin = hin*fth4     //changing inlet enthalpy in card 1

            hvalue(n) = hvalue(n)*fth4 //inlet enthalpy in card 13
```

<u>Changing the power</u>

```
aflux = aflux*fth3  //changing power in card 1
```

<u>Changing the mass flow rate in card 13</u>

```
     if(ispec(n).eq.2) then  !! for the initial condition

cfth    changing the flowrate-pvalue in card13- with the UA  ***

     pvalue(n) = pvalue(n)*fth2
```

<u>Changing the flow area in card 2</u>

```
do 250 l=1,nchanl

     read (i2,10030) i,(zdum(k),k=1,4),izdum(5),zdum(6),zdum(7),zdum(8)

cfth  changing the flow area -AN- or here zdum(1) with the UA           ***

              zdum(1) = zdum(1)*fth5 //changing the flow area

…
```

<u>Changing the gap loss coefficient in card 3</u>

```
                do 350  i=1,nk

                  read (i2,10060) k,ik(k),jk(k),gapn(k),length(k),zdum(1),zdum(2),

    +             igapb(k),igapa(k),zdum(3),(igap(k,n),jgap(k,n),

    +             n =1,3)

                 cfth  changing the gaplosscoeff-wkr- with the UA           ***OK

                 write(*,*) "original wkr=", zdum(1),"with fth6=",fth6

                 zdum(1) = zdum(1)*fth6  //changing the gap loss coefficient

                …
```

<u>Changing the grid loss coefficient in card 7</u>

```
 do 730 icd=1,ncd
 read(i2,10035) cdl,j,(izdum(m),m=1,12)
cdl = cdl*fth7
…
```

Changing the Mixing Coefficient in VDRIFT.f

```
…
beta_sp = beta_sp*fth8
…
```

Changing the Single Phase Heat Transfer Coefficient in HCOOL.f

```
…
        htcl = htcl*fth14
        …
```

Changing the Interfacial Friction Factor in Holintfr.f and Intfr.f

```
        …
        fi = fi*fth13
        …
```

Changing the Entrainment Rate in Holintfr.f

```
        …
        se = se_sp*fth17
        …
```

Changing the De-Entrainment Rate in Holintfr.f

```
…
sde = sde*fth18
…
```

Changing the Drag Coefficient for a Bubble in Holintfr.f

```
        …
        cdb = cdb*fth11
        …
```

Changing the Drag Coefficient for a Droplet in Holintfr.f and Intfr.f

```
…
```

```
cdd = cdd*fth12
        …
```

Changing the Subcooled heat transfer coefficient in Hcool.f

```
        …
        hnb = hnb*fth15
…
```

Changing the Saturated heat transfer coefficient in Hcool.f

```
…
        chen3 = chen3*fth16
…
```

Changing the critical heat flux in boiling.f

```
        …
        qchf= qchf* fth19
        …
```

Printing the Subchannel and Bundle Void Distribution in Result.f

```
cfth---------------------------
        use setupd, only: an
   real bundle_vf1,bundle_vf2,bundle_vf3
cfth---------------------------
…
cfth  bundle_vf initilization-------------
   bundle_vf1=0.
   bundle_vf2=0.
        bundle_vf3=0.
cfth  -----------------------------------
…
   write(i3,10005) j,x(jx),(output(ix),ix=1,4),aliq(i,j),
  $  al(i,j),ae(i,j),flml,fgml,feml,isij(i,j),
  2    qliq(i,j),qvap(i,j),gama(i,j)
```

```
cfth  printing void fraction to the deck.fth_o -------------------------
      if(j.eq.30)          then     !!if icine  (.and.etime.gt.0) ekle
                write (111,99901) i,al(i,j),etime
99901    format(1x,'ch#=',i2,3x,'VF=',f6.4,4x,'time=',f5.1)

cfth      calculation of the bundle VF ------------------
          bundle_vf1=bundle_vf1+ al(i,j)* an(i)      !! VF*FA summation
          bundle_vf2=bundle_vf2+ an(i)               !! FA  summation
                 if(i.eq.nout1) then
            bundle_vf3=bundle_vf1/bundle_vf2   !! sum(VF*FA)/sum(FA)
            write (111,99902) bundle_vf3,etime
99902        format(1x,'BU  -1   VF=',f6.4,4x,'time=',f5.1)
          endif
                endif
cfth--------------------------------------------------------------------

cfth  printing UA parameters into the deck.fth_o ----------------------
      if(etime.eq.0)     then   !! it prints out at the beginning
      write (111,99903) fth20,fth1, fth2,fth3,fth4,fth5,fth6,fth7,fth8,
     &       fth9,fth10,fth11,fth12,fth13,fth14,fth15,fth16,fth17,
     $       fth18,fth19

99903 format(/
     &       1x,'CASE#=     ',3x,f6.0/
     &       1x,'UA1#=      ',3x,f6.4/
     &       1x,'UA2#=      ',3x,f6.4/
     &       1x,'UA3#=      ',3x,f6.4/
     &       1x,'UA4#=      ',3x,f6.4/
     &       1x,'UA5#=      ',3x,f6.4/
     &       1x,'UA6#=      ',3x,f6.4/
```

```
     &      1x,'UA7#=      ',3x,f6.4/
     &      1x,'UA8#=      ',3x,f6.4/
     &      1x,'UA9#=      ',3x,f6.4/
     &      1x,'UA10#=     ',3x,f6.4/
     &      1x,'UA11#=     ',3x,f6.4/
     &      1x,'UA12#=     ',3x,f6.4/
     &      1x,'UA13#=     ',3x,f6.4/
     &      1x,'UA14#=     ',3x,f6.4/
     &      1x,'UA15#=     ',3x,f6.4/
     &      1x,'UA16#=     ',3x,f6.4/
     &      1x,'UA17#=     ',3x,f6.4/
     &      1x,'UA18#=     ',3x,f6.4/
     &      1x,'UA19#=     ',3x,f6.4/)
            endif
cfth  ---------------------------------------------------------------
```

Printing the Critical Power Results in Result.f

```
cfth  I added the use quen below for CHF---
            use quen, only: chf_fth
real temp_diff, cp_power, time_fth
            real*4 dryelev
            integer ii_fth, ii_fth2,ii_fth3,ii_fth4,ii_fth5


cfth *******************CP************************
cfth  rod temperatures are written here ***
cfth  I will use this temperature for critical power ***
      cp_power=0.                                   !!initilization //fth
            dryelev=999.                            !!initilization //fth
cfth       write (112,*) "deneme"
```

```
cfth---------------------------------------------------------------calculation of power---------------------------
      if(etime.ne.(0.0)) then
       DO 98909 ii_fth3 = 1,(nq-1)
                   if((etime.ge.yq(ii_fth3)).and.                   !!calculation of the power according to forcing table
     &      (etime.le.yq(ii_fth3+1))) then                          !!yq(x) is the time of pair x in the in the forcing table
                cp_power=aflux_fth*12.16521*60/1000                 !!height of the BFBT heated rod is 12.16521 and power is
in MW and 60 is the rod number
                      cp_power=cp_power*fq(ii_fth3)                 !!which forcing func. intervial that we are using.
                                 time_fth=yq(ii_fth3)
                  endif
98909  continue
      endif
cfth---------------------------------------------------------------calculation of power---------------------------



cfth---------------------------------------------------------------calculation of dryout elevation----------------
      DO 90909 ii_fth = 1, (jnodes)                                          !!axial node number
               DO  90909 ii_fth2 = 0, 29                                     !!rod number-1 , there are 30rods in my model
                DO  90909 ii_fth4 = 1, 4                                     !!120=30*4=30:rod#, 4:surface number for my
calc
                  ii_fth5= ii_fth2*4+ii_fth4                                 !!surface number according to rod number
         temp_diff= trod(2,ii_fth+1,ii_fth5)                                 !!temperature difference between axial nodes
     &                  -trod(2,ii_fth,ii_fth5)
                    if(temp_diff.gt.( 72.)) then
                    dryelev= 12.0*xc(ii_fth,(ii_fth2+1))                     !!dryout elevation
                    goto 99199                                               !!if there is a temperature increase goto printing
option

         endif
90909 continue
```

```
cfth-----------------------------------------------------------------calculation of dryout elevation----------------


cfth-----------------------------------------------------------------printing results-------------------------------

99199      if(dryelev.ne.999.) then                                        !!if there is a dryout then print out results to the
file
cfth  printing UA parameters and CP data into the deck.fth_o ------------
       write (112,99904) fth20,fth1, fth2,fth3,fth4,fth5,
     &      fth6,fth7,fth8,fth9,fth10,fth11,fth12,fth13,
     $      fth14,fth15,fth16,fth17,fth18,fth19,
     &      cp_power,dryelev,etime,time_fth
99904   format(/
     &      1x,'CASE#=      ',3x,f6.0/
     &      1x,'UA1#=       ',3x,f6.4/
     &      1x,'UA2#=       ',3x,f6.4/
     &      1x,'UA3#=       ',3x,f6.4/
     &      1x,'UA4#=       ',3x,f6.4/
     &      1x,'UA5#=       ',3x,f6.4/
     &      1x,'UA6#=       ',3x,f6.4/
     &      1x,'UA7#=       ',3x,f6.4/
     &      1x,'UA8#=       ',3x,f6.4/
     &      1x,'UA9#=       ',3x,f6.4/
     &      1x,'UA10#=      ',3x,f6.4/
     &      1x,'UA11#=      ',3x,f6.4/
     &      1x,'UA12#=      ',3x,f6.4/
     &      1x,'UA13#=      ',3x,f6.4/
     &      1x,'UA14#=      ',3x,f6.4/
     &      1x,'UA15#=      ',3x,f6.4/
     &      1x,'UA16#=      ',3x,f6.4/
     &      1x,'UA17#=      ',3x,f6.4/
     &      1x,'UA18#=      ',3x,f6.4/
```

```
    &      1x,'UA19#=      ',3x,f6.4/
    &      1x,'CP=         ',3x,f6.3/
    &      1x,'DryoutEl.=  ',3x,f6.1/
    &      1x,'Etime.=     ',3x,f6.1/
    &      1x,'Time in F.= ',3x,f6.1/)
cfth  ----------------------------------------------------------------


           stop '!!! DRYOUT !!!'
                                                          !!if there is a CP, goto the END of the
program
           endif
cfth----------------------------------------------------------------printing results-------------------------------
cfth ********************CP**************************
ROGERS MIXING MODEL
!~~~~~~~~~~~~~~~~~~~~~~~~~~~~~~~~~~~~~~~~~~~~~~~~~~~~~
!      This subroutine performs the calculations
!     for the turbulent mixing and the void drift
!~~~~~~~~~~~~~~~~~~~~~~~~~~~~~~~~~~~~~~~~~~~~~~~~~~~~~
      subroutine vdrift(j)
      use gapdat2
      use drop
      use gasvar
      use mcmx
      use momntd2
      use propdat, only: pref, ul, ufilm
      use spltdat
      use turbvar
      use twophas
cfth  use respar
      use veldat1
```

```
cfth  my UA parameter module is below
      use fth_module


      real maseqv,maseql,maseqg
      real eneqv, eneql, momeqv, momeql
      real dmomv, dmoml, dmasv, dmasl, dmasg
      real dnrgv, dnrgl


cfth  new parameters for rogers---------------------
      real beta_sp, beta_tp, lambda, fliq, hvap, ppsia, vismii,vismjj
     &     ,rliqbar, rvapbar,dhydbar,xflii,xfljj,grav, a1, a2, x, x0
     &    ,theta1, thetam
      integer, intent(in) :: j
cfth  ---------------------------------------------


      isec=isect
      dx = dxs(isec,j)
      jbot = isects(isec,4)
      jabs = j+jbot
      ichn=isects(isec,2)
      jnodes=isects(isec,1)+1
      bta=beta(isec)
      aak=aaak(isec)

        imx=imix(isec)
        dfrodd = dfrod(isec)

      do 20 ig=1,nk
      k=idgap(ig)
      ii=ik(k)
```

```
      jj=jk(k)
      if(lchan(ii).ne.isec) go to 20

      giiv=fgm(ii,j)/amom(ii,j)
      giil=(flm(ii,j))/amom(ii,j)
      gjjv=fgm(jj,j)/amom(jj,j)
      gjjl=(flm(jj,j))/amom(jj,j)
      giiv=abs(giiv)
      giil=abs(giil)
      gjjv=abs(gjjv)
      gjjl=abs(gjjl)
      gii=giiv+giil
      gjj=gjjv+gjjl
cfth
      gbar=(gii*amom(ii,j)+gjj*amom(jj,j))/(amom(ii,j)+amom(jj,j))
      gbar = amax1(0.0,gbar)

c     densities of mixture for subchannels ii and jj
      rmixii = al(ii,j) * (rv(ii,j)+rmgas(ii,j))
     &        + (1.-al(ii,j))*rl(ii,j)
      rmixjj = al(jj,j) * (rv(jj,j)+rmgas(jj,j))
     &        + (1.-al(jj,j))*rl(jj,j)
c     density of mixture averaged over subchannels ii and jj
      rmixbar = (rmixii*amom(ii,j)+rmixjj*amom(ii,j))
     &          / (amom(ii,j) + amom(jj,j))

      if (imx.eq.1) then
        wp(k)=bta*gbar*gap(k,j)

        area=gap(k,j)*dx
```

```
      rm1=al(ii,j)*(rv(ii,j)+rmgas(ii,j))+aliq(ii,j)*rl(ii,j)
      rm2=al(jj,j)*(rv(jj,j)+rmgas(jj,j))+aliq(jj,j)*rl(jj,j)
      rmbar=0.5*(rm1+rm2)
      epsol=wp(k)/(gap(k,j)*rmbar)
     elseif (imx. eq. 2) then

cfth-  FINAL IMPLEMENATATION OF THE MIXING AND VD for ROGERS MODEL

cfth-  Dynamic viscosity of mixture in subchannel ii
      hliq= hl(ii,j)
      hvap= hl(ii,j)
           rfilm=rv(ii,j)
           ppsia =pref + p(ii,j)/(12.**2) - pmgas(ii,j)
           call prop(ppsia,hliq,hvap,1)
           vismii=(1.-al(ii,j)) * ul + al(ii,j)*ufilm
cfth-  Dynamic viscosity of mixture in subchannel ii
      hliq= hl(jj,j)
      hvap= hl(jj,j)
           rfilm=rv(jj,j)
           ppsia =pref + p(jj,j)/(12.**2) - pmgas(jj,j)
           call prop(ppsia,hliq,hvap,1)
           vismjj=(1. - al(jj,j)) * ul + al(jj,j)*ufilm

cfth   single phase turbulent mixing coefficient beta_sp
cfth   according to correlation of Rogers and Rosehart
      lambda= 0.0058 * (gap(k,j) / dfrodd ** (-1.46))
      if (dhyd(ii,j).le. dhyd(jj,j)) then
       re = gii * dhyd(ii,j) / (vismii/3600.)
       if (re.eq.0.0) then
        beta_sp=0.0
```

```
        else
          beta_sp = 0.5 * lambda * re ** (-0.1)
     &              * (1. + (dhyd(jj,j) / dhyd(ii,j)) ** 1.5)
        endif
       else
          re = gjj*dhyd(jj,j) / (vismjj/3600.)
        if (re.eq.0.0) then
          beta_sp=0.0
        else
          beta_sp=0.5 * lambda * re ** (-0.1)
     &            * (1.+ (dhyd(ii,j) / dhyd(jj,j))**1.5 )
     &            * (dhyd(jj,j)/dfrodd)
        endif
       endif

c     density of liquid averaged over subchannels ii and jj
      rliqbar = (rl(ii,j) * amom(ii,j) + rl(jj,j) * amom(jj,j))
     &            / (amom(ii,j) + amom(jj,j))
c     density of vapor averaged over subchannels ii and jj
      rvapbar = (rv(ii,j) * rmgas(ii,j) * amom(ii,j)
     &            + (rv(jj,j) + rmgas(jj,j) ) * amom(jj,j))
     &            / (amom(ii,j) + amom(jj,j))
c     average hydraulic diameter
      dhydbar = 0.5 * (dhyd(ii,j) + dhyd(jj,j))
c     flow qualities for subchannels ii and jj
      xflii = fgm(ii,j) / (flm(ii,j) + fem(ii,j) + fgm(ii,j))
      xfljj = fgm(jj,j) / (flm(jj,j) + fem(jj,j) + fgm(jj,j))
c     flow quality averaged over subchannels ii and jj
      x= (xflii * amom(ii,j) + xfljj * amom(jj,j))
     &   / (amom(ii,j)) + (amom(jj,j))
```

```
c     accelaration due to gravity
      grav = 32.185   ! ft/s^2 = 9.81m/s^2
c     quality at which the two phase mixing reaches its maximum
      a1 = 0.4
          a2 = 0.6
          xmax=(a1*sqrt(grav * rliqbar*(rliqbar-rvapbar)*dhydbar)
     &     / gbar + a2)
     &     / (sqrt(rliqbar/rvapbar) + a2)
          x0 = xmax * 0.57 * re**0.0417
c     two phase multiplier theta
      thetam = 5.0
      if (x.le.0.0) then
            theta1 = 1.0
          elseif (x.le.xmax) then
            theta1 = 1.0 + (thetam - 1.0) * x / xmax
          elseif (x.lt.1.0) then
            theta1 = 1.0 + (thetam - 1.0) * (xmax - x0)/(x - x0)
          else
            theta1 = 1.0
          endif
c     two phase turbulent mixing coefficient beta_tp


cfth  UA-parameter
cfth  for mixing coefficient beta_sp


cfth   ***
cfth  changing the beta_sp with the UA   ***
      write(*,*) "original beta_sp=", beta_sp,"with fth8=",fth8
          beta_sp = beta_sp*fth8
          write(*,*) "beta_sp after UA change=", beta_sp
```

```
      beta_tp = theta1 * beta_sp
      epsol = beta_tp * gbar / rmixbar
              endif
C---------------------------------------------------------------------
      if ( isij(ii,j).gt.4.or.isij(jj,j).gt.4) go to 15

c     .... compute momentum terms due to mixing

      dmomv=epsol*(giiv-gjjv)*area
      dmoml=epsol*(giil-gjjl)*area

c       ....compute momentum terms due to void drift.

      z1=aak*(gii-gjj)/(gii+gjj+1.0e-08)
      momeqv=z1*(giiv+gjjv)
        momeql=-z1*(giil+gjjl)
      dmomv = dmomv-momeqv*epsol*area
      dmoml = dmoml-momeql*epsol*area
        tmomv(ii)=tmomv(ii)+dmomv
      tmomv(jj)=tmomv(jj)-dmomv
      tmoml(ii)=tmoml(ii)+dmoml
      tmoml(jj)=tmoml(jj)-dmoml

c     ....compute mass terms due to void drift

      maseqv=z1*(al(ii,j)*rv(ii,j)+al(jj,j)*rv(jj,j))
      maseql=-z1*(al(ii,j)*rl(ii,j)+al(jj,j)*rl(jj,j))
      maseqg=z1*(al(ii,j)*rmgas(ii,j)+al(jj,j)*rmgas(jj,j))

c     ....compute mass terms due to mixing
```

```
      dmasv=epsol*(al(ii,j)*rv(ii,j)-al(jj,j)*rv(jj,j)-maseqv)*area
      dmasl=epsol*(aliq(ii,j)*rl(ii,j)-aliq(jj,j)
     $      *rl(jj,j)-maseql)*area
      dmasg=epsol*(al(ii,j)*rmgas(ii,j)-al(jj,j)*rmgas(jj,j)-maseqg)
     $ *area

      tmasv(ii,j)=tmasv(ii,j)+dmasv
      tmasv(jj,j)=tmasv(jj,j)-dmasv
      tmasl(ii,j)=tmasl(ii,j)+dmasl
      tmasl(jj,j)=tmasl(jj,j)-dmasl
      tmasg(ii,j)=tmasg(ii,j)+dmasg
      tmasg(jj,j)=tmasg(jj,j)-dmasg

c     ....compute energy terms due to mixing
      dnrgv=epsol*(al(ii,j)*(rv(ii,j)*hv(ii,j)+rmgas(ii,j)*hmgas(ii,j))
     +      -al(jj,j)*(rv(jj,j)*hv(jj,j)-rmgas(jj,j)*hmgas(jj,j)))*area
      dnrgl = epsol*(aliq(ii,j)*rl(ii,j)*hl(ii,j)-aliq(jj,j)
     +        *rl(jj,j)*hl(jj,j))*area

c     ....compute energy terms due to void drift

        eneqv=z1*(al(ii,j)*rv(ii,j)*hv(ii,j)+al(jj,j)*rv(jj,j)*hv(jj,j))
        dnrgv = dnrgv-eneqv*epsol*area
      eneql=-z1*(al(ii,j)*rl(ii,j)*hl(ii,j)+al(jj,j)*rl(jj,j)*hl(jj,j))
      dnrgl = dnrgl-eneql*epsol*area

      tnrgv(ii,j)=tnrgv(ii,j)+dnrgv
      tnrgv(jj,j)=tnrgv(jj,j)-dnrgv
      tnrgl(ii,j)=tnrgl(ii,j)+dnrgl
```

```
      tnrgl(jj,j)=tnrgl(jj,j)-dnrgl

      go to 20

c     hot wall flow regime - single phase vapor mixing only.

c     .... compute momentum terms due to mixing

 15   dmomv=epsol*(giiv-gjjv)*area
      dmoml=epsol*(giil-gjjl)*area
      tmomv(ii)=tmomv(ii)+dmomv
      tmomv(jj)=tmomv(jj)-dmomv
      tmoml(ii)=tmoml(ii)+dmoml
      tmoml(jj)=tmoml(jj)-dmoml
c     ....compute mass terms due to mixing

      dmasv=epsol*(al(ii,j)*rv(ii,j)-al(jj,j)*rv(jj,j))*area
      dmasl=epsol*(aliq(ii,j)*rl(ii,j)-aliq(jj,j)
     $      *rl(jj,j))*area
      dmasg=epsol*(al(ii,j)*rmgas(ii,j)-al(jj,j)*rmgas(jj,j))
     $      *area

      tmasv(ii,j)=tmasv(ii,j)+dmasv
      tmasv(jj,j)=tmasv(jj,j)-dmasv
      tmasl(ii,j)=tmasl(ii,j)+dmasl
      tmasl(jj,j)=tmasl(jj,j)-dmasl
      tmasg(ii,j)=tmasg(ii,j)+dmasg
      tmasg(jj,j)=tmasg(jj,j)-dmasg

c     ....compute energy terms due to mixing
```

```
      dnrgv=epsol*(al(ii,j)*(rv(ii,j)*hv(ii,j)+rmgas(ii,j)*hmgas(ii,j))
     +     -al(jj,j)*(rv(jj,j)*hv(jj,j)-rmgas(jj,j)*hmgas(jj,j)))*area
      dnrgl = epsol*(aliq(ii,j)*rl(ii,j)*hl(ii,j)-aliq(jj,j)
     +       *rl(jj,j)*hl(jj,j))*area


      tnrgv(ii,j)=tnrgv(ii,j)+dnrgv
      tnrgv(jj,j)=tnrgv(jj,j)-dnrgv
      tnrgl(ii,j)=tnrgl(ii,j)+dnrgl
      tnrgl(jj,j)=tnrgl(jj,j)-dnrgl

   20 continue
      return
      end
```

6.5.3. Appendix-3

MASTER CODE

MASTER program was coded with Visual C++ 2005 (Express Edition – version 8.0)

```
/*  Fatih Aydogan, Master Program to run Multiple COBRA-TF inputs
              June 2007
    Runs COBRA-TF with Windows XP Command Line Execution
               Inputs: *.inpx (executes all .inpx extension files in current directory)
                Outputs: *.out, *.gph,*.run,*.fth,*.inp
                 COBRA_RB_V1.exe must also be present at the same folder
*/

#include <stdlib.h>                                    // Allows execution of system commands
#include <stdio.h>                                     // Allows sprintf -> Stores char* into first char
arg.
#include <iostream>
```

```
#include <fstream>
#define DEBUG 0
using namespace std;

int main()
{
   string oldExten  = "inpx";                                   //1.inpx   -before running-
            string oldExten2  = "inpxx";                        //1.inpxx  -after running-
   string exe      = "COBRA_RB_V1.exe";
   string execDir   = "";
   string inputDir  = "";
   string outputDir = "";
            string dirCmd    = "dir /B";                        // linux = "cp "
            string copyCmd   = "copy /B";                       // cp
            string moveCmd   = "move /Y";
            string strTemp;
            string baseInput = "deck.inp";
            string baseOut   = "deck.out";
            string baseOut2  = "deck.fth_o";           //this output will be on when I change the cobra-f source and it starts
to produce the utilized output for VD
   string baseOut4  = "deck.fth_cp"; //this output will be on when I change the cobra-f source and it starts to produce
the utilized output for CP
            string baseOut3  = "deck.run";   //this output will be on when I change the cobra-f source and it starts to
produce the utilized output for VD and CP
            string graphOut  = "deck_grf";
            string tempF     = "temp.txt";
            char command[1024];

  system("del deck.inp"); system("del deck.run"); system("del deck.out"); system("del deck_grf"); /* cleaning the
previous files         */
  cout << "COBRA-TF Batch Run All *.inpx (Batch Execution Program)" <<endl;  system("date /t"); system ("dir
path");                                                         // to be sure which director we are working

// dir .inpx
  sprintf(command, "dir /b *%s", oldExten.c_str());  system(command);

// copy list of .inpx into temp.txt
  sprintf(command, "dir /b *%s > temp.txt", oldExten.c_str());  system(command);

  #if DEBUG
    system("Pause");
  #endif

  ifstream infile ("temp.txt", ios_base::in);

  char c_strLine[1024];
  int lineNum = 1;
  while (infile.getline(c_strLine,1024))
  {
    string strLine (c_strLine);
    int charLoc = 0;
    charLoc = strLine.find(oldExten);

    if ( charLoc == string::npos )                              // Insure that no other inputs are run.
    {
                    cout << "Line: " << c_strLine << " skipped on Line Number: " << lineNum << endl;
    }
    else
    {
```

```
        string word;
        word = strLine.substr(0,charLoc);
        cout << "Running Case: " << lineNum << " Case Name: "<< word.c_str() << endl;
                        system(command);

        sprintf(command, "echo on"); system(command);

//      Move first case *.inpx to deck.inp
        sprintf(command, "%s %s %s", copyCmd.c_str(), c_strLine, baseInput.c_str()); system(command);

//      Execute cobra-tf
        sprintf(command, "%s", exe.c_str()); system(command);

//      Rename 1.inpx to *.inpxx   -if one file is run, this file's extension will be changed to *.inpxx-
        sprintf(command, "%s %s %sinpxx", moveCmd.c_str(), c_strLine, word.c_str());
                        system(command);

//      Rename deck.out to *.out
        sprintf(command, "%s %s %sout", moveCmd.c_str(), baseOut.c_str(), word.c_str()); system(command);

//      Rename deck_grf to *.gph
                         sprintf(command, "%s %s %sgph", moveCmd.c_str(), graphOut.c_str(), word.c_str());
system(command);

//      Rename deck.run to *.run
        sprintf(command, "%s %s %srun", moveCmd.c_str(), baseOut3.c_str(), word.c_str()); system(command);

//      Rename deck.fth_o to *.fth_o
        sprintf(command, "%s %s %sfth_o", moveCmd.c_str(), baseOut2.c_str(), word.c_str()); system(command);

//                      Rename deck.fth_cp to *.fth_cp
        sprintf(command, "%s %s %sfth_cp", moveCmd.c_str(), baseOut4.c_str(), word.c_str()); system(command);

//        sprintf(command, "mkdir %s", neminBin.c_str()); system(command);

// Cleanup Neminsteady files
//                      sprintf(command, "del ", inputDir.c_str(), word.c_str(), neminBin.c_str());
//        system("del deck.inp"); system("del deck.run"); system("del deck.out"); system("del deck_grf");
    }
    lineNum ++;
  }

  system("date /t");   cout << "Program Terminated" << endl;     system("Pause");
  return 0;
}
```

6.5.4. Appendix-4

An example Critical Power Data from BFBT

Steady State Critical Power Tests Data
Test Assembly C2B
Experiment Number T/S OUTLET PRES Flow Rate Inlet Subcooling Critical Power BT Location
MPa ton/h kJ/kg MW

SA505500	5.49	20.16	50.95	6.13	04-A240
SA505501	5.49	20.10	51.35	6.13	04-A240
SA505600	5.51	20.12	84.79	6.23	04-A240
SA505800	5.50	20.19	129.38	6.39	04-A240
SA505900	5.49	20.14	26.04	5.98	04-A240
SA510500	5.48	55.06	56.41	9.72	53-A150
SA510501	5.51	55.11	62.48	9.81	59-B45
SA510600	5.51	54.70	96.16	10.09	59-B45
SA510601	5.52	55.34	96.79	10.19	53-A150
SA510800	5.51	54.81	134.97	10.20	53-A150
SA510900	5.52	54.70	35.33	9.56	59-B45
SA510901	5.51	55.05	35.02	9.66	25-B315
SA512500	5.54	65.48	64.36	10.41	53-A150
SA512600	5.51	64.97	99.60	10.75	53-A150
SA512800	5.50	65.52	133.75	11.09	53-A150

…

Chapter 7

CONCLUSIONS AND RECOMMENDATIONS FOR FUTURE WORK

Thermal hydraulic codes (such as, COBRA-TF [1, 2]) are commonly used tools in licensing processes for the evaluation of various thermal hydraulic scenarios. The results of code predictions are generally subjected to uncertainties due to model limits, approximations in the numerical solution, nodalization, homogenization approaches and imperfect knowledge of boundary and initial conditions. Uncertainty analysis predicts uncertainty bands of an output. Most of the uncertainty analyses are based on Loss of Coolant Accident (LOCA) scenario in order to determine the performance of the Emergency Core Cooling Systems (ECCS) according to Nuclear Regulatory Commission (NRC) Regulatory Guide 1.157 [3]. This dissertation focuses on the uncertainty analysis of steady state void distribution and critical power of COBRA-TF predictions. Therefore, an uncertainty methodology was developed and implemented for these particular scenarios/cases.

This dissertation provides a unique development and analysis of the NUPEC BFBT void distribution and critical power databases and associated model uncertainties using the COBRA-TF subchannel computer code. The main contributions and uniqueness of the dissertation are given as,

- The development and analysis of the void distribution uncertainty predictions based on BWR subchannels and bundle,

- The development and analysis of the critical power uncertainty predictions based on critical power and dry-out elevation,

- The developed and implemented uncertainty analyses methodology includes the assessment of the uncertainties with the detailed BFBT void distribution and critical power database from the NUPEC Benchmark Program.

- Assessment of the model uncertainties in the COBRA-TF computer code and determination of the effects of these model uncertainties on the subchannel and bundle void predictions as well as on the critical power and the dry-out elevation predictions.

The work presented in this dissertation had the goal of development and implementation of a particular uncertainty methodology specific for a particular problem. This was achieved by developing of the particular uncertainty methodology based on the uncertainties of the BWR rod, bundle, subchannel void fraction, critical power and dry-out elevation data. In addition, the uncertainty analysis also considered the COBRA-TF model uncertainties, which were used to analyze these experiments. Elements of CSAU and GRS uncertainty approaches were used to develop the uncertainty methodology. An element of CSAU method is the PIRT and an element of the GRS method is the subjective probability distribution (SPDF). They were both utilized for this uncertainty methodology. The following alternative ways can also be used in the uncertainty methodology for the future work:

- Another experimental case selection algorithm can be used instead of spanning algorithm. This algorithm was developed to span the experimental database but one can use another algorithm to select the experimental cases due to any other user defined criteria. Therefore, more, less or different experimental cases may be selected so that the uncertainty ranges may be compared with the presented results.

- In addition to BFBT database, another experimental database may be used. Because the boundary condition of experimental cases and their corresponding accuracies affect the uncertainty results, uncertainty results of both experimental databases may be observed and compared.

- The sampling number was determined as 59 by using WILKS approach. This sampling number may be increased to see its effect on the uncertainties.

- Random numbers were generated with Simple Random Sampling (SRS). Different combinations of random numbers can be generated with SRS and the results can be compared.

- Sensitivity analysis used to determine the dominant phenomena and their rankings. In this analysis, one parameter was changed at a time. Another phenomena ranking method using uncertainty results may be used instead of sensitivity analysis.

- Instead of SRS and Order Statistics, other methods (such as, Monte Carlo, Latin Hypercube, etc) can be used and the results can be compared.

- Other uncertainty methodologies, such as, CSAU, could be used instead of the particular uncertainty methodology. However, they may be more bounding.

7.1. References

1. Analysis of FLECHT-SEASET 163-Rod Blocked Bundle Data Using COBRA-TF, NRC/EPRI/ Westinghouse Report No:15, NUREG/CR-4166 EPRI NP-4111 WCAP-10375

2. COBRA/TRAC- A Thermal-Hydraulics Code for Transient Analysis of Nuclear Reactor Vessels and Primary Coolant Systems, NUREG/CR-3046 PNL-4385 Vol.1

3. U.S. Nuclear Regulatory Commission, Regulatory Guide 1.157 (Task RS 701-4), Best Estimate Calculations of Emergency Core Cooling Performance

VITA

Fatih Aydogan

EDUCATION

2008 The Pennsylvania State University, University Park, PA.
Ph.D. in Nuclear Engineering
2004 Hacettepe University, Ankara, Turkey
M.S. in Computer Engineering
2000 Hacettepe University, Ankara, Turkey
B.S. in Nuclear Engineering

ARCHIVAL PUBLICATIONS

- *"Evaluation of the Subchannel Code COBRA-TF for the Prediction of BWR Fuel Assembly Void Distribution and Pressure Drop",* NURETH-12, 2007,
- *"Overview and status of the OECD/NRC BFBT BENCHMARK activities",* NURETH-12, 2007,
- *"OECD-NEA/US-NRC BFBT Uncertainty Analysis of void distribution and critical power for BWRs, Volume II"*, OECD, 2007, NEA/NSC/DOC(2007)21,
- *"The Phenomena Identification Ranking Table of Steady State BWR Void Distribution",* NURETH-12, 2007,
- *"The Phenomena Identification Ranking Table of Steady State BWR Critical Power",* NURETH-12, 2007,
- *"Correlation for Void Fraction Measurements of the BFBT X-Ray Densitometers"*, ANS/ENS, Washington-DC, 2007,
- *"Evaluation of Thermal Time Constant for the BFBT Heater Rods"*, ANS/ENS, Washington-DC, 2007,
- *"Evaluation of Subchannel Code for BWR Type Bundles, COBRA-TF, for the BWR Fuel Assembly and Void Fraction Distribution in BWR",* ASME/ICONE14, ICON14/89174, 2006,
- *"OECD-NEA/US-NRC BFBT Specification"*, OECD 2006, NEA No. 6212, NEA/NSC/DOC(2005)5, ISBN 92-64-01088-2, 2006,
- *"BFBT International Subchannel Computer Code Benchmark Program",* ANS, RIO, 2006,
- *"Derivation of Subchannel Loss Coefficients and COBRA-TF Model for BFBT Bundles",* F. Aydogan, L. Hochreiter, K. Ivanov, BFBT Workshop in University Park, US, 2005,
- *"COBRA-TF Modeling Issues for BFBT Void Distribution",* F. Aydogan, L. Hochreiter, K. Ivanov, BFBT Workshop in University Park, US, 2005,
- *"Modeling and Implementation of Data mining Modules for E-Commerce",* F. Aydogan, Master Dissertation, Hacettepe University, Ankara, Turkey, 2004.